Trinity College Dublin

The University of Dublin

Development and characterization of corneal substitutes from decellularized tissues

Julia Fernández Pérez, B.Sc., M.Sc.

A thesis submitted to the University of Dublin
in partial fulfilment of the requirements for the degree of
Doctor in Philosophy

2020

Supervisor: Prof. Mark Ahearne

Internal Examiner: Prof. David Hoey
External examiner: Prof. Heli Skottman

Declaration

I declare that this thesis has not been submitted as an exercise for a degree at this or any other university and it is entirely my own work.

I agree to deposit this thesis in the University's open access institutional repository or allow the Library to do so on my behalf, subject to Irish Copyright Legislation and Trinity College Library conditions of use and acknowledgement.

I consent to the examiner retaining a copy of the thesis beyond the examining period, should they so wish (EU GDPR May 2018).

_____

Julia Fernández-Pérez

Dublin 2020

Summary

The cornea is crucial for vision since it is the first structure to allow light into the eye. Diseases affecting the cornea can lead to vision impairment and ultimately to blindness. It is estimated that 45 million people worldwide suffer from corneal blindness. In cases of extensive damage and non-responsiveness to pharmacological treatment, patients will be treated with a corneal transplant, or keratoplasty. The cornea is the most commonly transplanted organ worldwide. Rejection in high-risk patients and a shortage of donors are the main triggers for the development of alternative therapies to treat corneal blindness. The use of decellularized tissues is gaining interest for corneal tissue engineering as it can replicate the biochemical and structural characteristics of the native tissue. However, there is a lack of knowledge on the culture conditions, recellularization and effect of further processing when using decellularized corneas.

The aim of the first study in this thesis was to identify biochemical cues that could promote a keratocyte-like phenotype in human corneal stromal cells that had become fibroblastic when expanded in serum-supplemented media while also examining the effect on cell proliferation and migration. Results showed that ascorbic acid (AA), retinoic acid (RA), insulin-transferrin-selenium (ITS), insulin-like growth factor 1 (IGF-1) and 3-isobutyl-1-methylxanthine (IBMX) promoted a dendritic morphology, increased the expression of keratocyte markers, such as keratocan, ALDH3A1 and CD34, and prevented myofibroblast differentiation, while in some cases increasing proliferation. Transforming growth factor β1 and β3 (TGF-β1 and TGF-β3) promoted the differentiation toward myofibroblasts, with increased expression of α-smooth muscle actin (α-SMA). Fibroblast growth factor 2 (FGF-2) supported a fibroblastic phenotype while platelet-derived growth factor homodimer B (PDGF-BB) induced a pro-migratory fibroblastic phenotype. A combination of all the pro-keratocyte factors was also compared to the serum-free only, which significantly increased CD34 and keratocan expression.

Next, I investigated the possibility of recellularizing decellularized porcine corneas with human stromal cells. Three culturing regimes were evaluated: 2 weeks in serum supplemented medium, 4 weeks in serum supplemented medium, and 2 weeks in serum-supplemented followed by 2 weeks in a serum-free medium supplemented with

AA and ITS. Repopulated scaffolds that were cultured in the third condition displayed an *in vivo*-like phenotype, by up-regulating ALDH3A1, CD34, keratocan, lumican, decorin and collagen I. Despite the dense extracellular matrix (ECM) of the cornea, cells seeded on the surface of the decellularized corneas were able to migrate into deeper areas, with culturing regime not playing a critical role. Recellularized and acellular scaffolds were implanted in a rabbit anterior lamellar keratoplasty (ALK) model and were well tolerated. H&E staining showed that in both groups the implanted scaffolds were repopulated by surrounding stromal cells. Underlying the epithelium some scar tissue was present that was collagen III, fibronectin and α-SMA positive. The *in vitro* recellularization did not seem to have a significant role in the overall implant success.

In the next study, a different approach was used to improve the overall cellularity of corneal substitutes. Since the cornea is composed of densely packed collagen lamellae, recellularization is slow both *in vivo* and *in vitro*. I developed constructs based on the use of decellularized corneas but using a bottom up approach by layering sheets of decellularized tissue with cell-laden hydrogels. Hydrogels can be used to encapsulate cells but lack mechanical strength. I hypothesized that better tissue engineered constructs could be obtained by combining the advantages of both materials. In this study, the aim was to fabricate a corneal substitute by using sheets of decellularized porcine cornea and cell-laden collagen hydrogels. These constructs presented high transparency, easy handling after fabrication, high viability and *in vivo*-like phenotype after a culture period of 3 weeks. Furthermore, constructs containing both stromal and epithelial cells were fabricated. Constructs were sutured onto an *ex vivo* model of ALK, which was re-epithelialized by host cells by day 7 and integrated with the host stroma.

Finally, cornea ECM-derived hydrogels were obtained by decellularizing porcine corneas using several decellularizing methods. The aim of this study was to examine the impact of decellularization protocols in hydrogel characteristics. Porcine corneas were isolated and decellularized with SDS, Triton X-100 or by freeze-thaw cycles. All decellularization methods decreased DNA significantly measured by PicoGreen and visually assessed by the absence of cell nuclei. Collagen and other ECM components were highly retained, as quantified by hydroxyproline content and sGAG, by histological analysis and by SDS-PAGE. Hydrogels obtained by freeze-thaw decellularization were the most transparent. The method of decellularization impacted gelation kinetics assessed by turbidimetric analysis. All hydrogels showed a fibrillary and porous structure

determined by cryoSEM. Human corneal stromal cells were embedded in the hydrogels. SDS decellularization rendered cytotoxic gels, while the other decellularization methods produced highly cytocompatible hydrogels. The main finding of this study was that freeze-thaw decellularization produced gels with the overall best properties.

In conclusion, this thesis shows the versatility of using decellularized porcine corneas for the biofabrication of corneal substitutes and highlights the importance of culture conditions in the maintenance or recovery of native cell phenotype.

Acknowledgements

I would like to start acknowledging my supervisor Prof Mark Ahearne for giving me the opportunity to pursue a PhD in his lab. I have learnt a lot during this period at Trinity College Dublin.

A tremendous amount of appreciation goes to all colleagues at the Trinity Center for Biomedical Engineering, who have helped me navigate through my project and who ended up being good friends. Special thanks goes to (Dr) Jenny, who has been a great lab mate, house mate and dear friend! Long hours were spent in the kitchen “complaining” about failed experiments. I am very thankful to the Spanish-speaking gang with (Dr) Tommy, (Dr) Dinorath, (Dr) Pedro, Xavi and Cristina, because having your language and culture close when living abroad is important. My Ahearne lab fellow Sophia has been a very supportive and fun friend. (Dr) Jess and (Dr) Rossana have been the best buddies to share this adventure, we’ve grown so much together! Special thanks go to Ahearne lab PostDocs Karl, Peter and Promita for their help and knowledge. Plenty of other lab colleagues have made this journey memorable (I am for sure missing lots of people): Pierluca, Mathieu, Susan, Grá, Simon, Dave, Olwyn, Matteo, Kiara, Kian, Fiona, Ian, Michelle, Farhad, Emma, Leyla. Students I have had over the years have tought me how to be patient and to appreciate the mentors I have had before.

My family has always been by my side even if from afar back in Spain. Their inconditonal love and support has been essential in my life. Un beso grande!

Last, and for sure not least, I would like to express my gratitude and love to (Dr) Stefan, house mate, lab partner, and, most importantly, life companion. The future is ahead of us, let’s go reach our dreams!

Table of Contents

List of Figures

List of Tables

Nomenclature

AA	Ascorbic acid
AB	Alcian blue
ACTA	Alpha smooth muscle actin (gene)
ALDH	Aldehyde dehydrogenases
ALK	Anterior lamellar keratoplasty
BSA	Bovine serum albumin
DALK	Deep anterior lamellar keratoplasty
DAPI	4′,6-diamidino-2-phenylindole
DCN	Decorin (gene)
DMEM	Dulbecco's modified eagle medium
ECM	Extracellular matrix
EDTA	Ethylenediaminetetraacetic acid
EGF	Epithelial growth factor
FBS	Fetal bovine serum
FGF	Fibroblast growth factor
FN	Fibronectin
GAG	Glycosaminoglycans
GAPDH	Glyceraldehyde-3-phosphate dehydrogenase
GF	Growth factor
GMP	Good manufacturing practices
H&E	Haematoxylin and eosin
HA	Hyaluronic acid
hCSSCs	Human corneal stromal stem cells
IBMX	3-isobutyl-1-methylxanthine
IGF	Insulin-like growth factor
IOP	Intraocular pressure
iPSCs	Induced pluripotent stem cells
ITS	Insulin-transferrin-selenium
KERA	Keratocan (gene)
KPro	Keratoprosthesis
KSPG	Keratin sulphated proteoglycans
LSCD	Limbal stem cell deficiency

LUM	Lumican (gene)
MMP	Matrix metalloproteinase
MSC	Mesenchymal stromal cell
OCT	Optical coherence tomography
PBS	Phosphate buffered saline
PDGF	Platelet-derived growth factor
PFA	Paraformaldehyde
PHEMA	Poly-2-hydroxyethyl methacrylate
PLA_2	Phospholipase a_2
PMMA	Poly(methyl methacrylate)
PR	Picrosirius red
RA	Retinoic acid
SD	Standard deviation
SDC	Sodium deoxycholate
SDS	Sodium dodecyl sulphate
SEM	Scanning electron microscopy
sGAG	Sulphated glycosaminoglycans
TEM	Transmission electron microscopy
TGF	Transforming growth factor
TNFα	Tumor necrosis factor alpha
VEGF	Vascular endothelial growth factor
ZO-1	Zonula occludens-1
α-Gal	Galactose-alpha-1,3-galactose
α-SMA	Alpha smooth muscle actin

Publications

Journal articles published during candidacy and that are part of this thesis

1. Fernández-Pérez J & Ahearne M. Influence of biochemical cues in human corneal stromal cell phenotype. Current Eye Research. 2018; 43(13). doi: 10.1080/02713683.2018.1536216.
2. Fernández-Pérez J & Ahearne M. Decellularization and recellularization of cornea: Progress towards a donor alternative. Methods. doi: 10.1016/j.ymeth.2019.05.009.
3. Fernández-Pérez J & Ahearne M. The impact of decellularization methods on cornea extracellular matrix-derived hydrogels. Scientific Reports. 2019; 9(1). doi: 10.1038/s41598-019-49575-2.
4. Ahearne M, Fernández-Pérez J, Masterton S, Madden PW & Bhattacharjee P. Designing scaffolds for corneal regeneration. Advanced Functional Materials. 2019, 1908996. doi: 10.1002/adfm.201908996.
5. Fernández-Pérez J, Madden PW & Ahearne M. Engineering a corneal stromal equivalent using a novel multi-layered fabrication assembly technique. TissueEngineering Part A. 2020. doi: 10.1089/ten.TEA.2020.0019.

Journal articles published during candidacy and that are not part of this thesis

1. Fernández-Pérez J, Binner M, Werner C, Bray LJ. Limbal stromal cells derived from porcine tissue demonstrate mesenchymal characteristics in vitro. Scientific Reports. 2017; 7(1):6377. doi: 10.1038/s41598-017-06898-2.
2. Fernández-Pérez J*, Kador K*, Lynch A, Ahearne M. Characterization of extracellular matrix modified poly(e-caprolactone) electrospun scaffolds with differing fiber orientations for corneal stroma regeneration. Materials Science & Engineering C. 2020; 108. doi: 10.1016/j.msec.2019.110415
3. Bhattacharjee P, Fernández-Pérez J, Ahearne M. Potential for combined delivery of riboflavin and all-trans retinoic acid, from silk fibroin for corneal bioengineering. Materials Science & Engineering C. 2019; 105. doi: 10.1016/j.msec.2019.110093

Conference abstracts

1. 22nd Annual Bioengineering in Ireland Conference, Galway, Ireland, January 2016 (oral and poster)
2. European Vision and Eye Research Congress, Nice, France, September 2016 (oral)
3. 23rd Annual Bioengineering in Ireland Conference, Belfast, UK, January 2017 (oral)
4. TERMIS European Chapter Meeting 2017, Davos, Switzerland, June 2017 (oral)
5. Matrix Biology Ireland, November 2017 (oral and poster)
6. 24th Annual Bioengineering in Ireland Conference, Maynooth, Ireland, January 2018 (oral)
7. 8th World Congress of Biomechanics, Dublin, Ireland, July 2018 (poster)
8. XXIII Biennial Meeting of the International Society for Eye Research, Belfast, UK, September 2018 (oral)
9. 25th Annual Bioengineering in Ireland Conference, Limerick, Ireland, January 2019 (oral)
10. Mi Tesis en 3 Minutos (Thesis in 3 in Spanish). Organized by Spanish Research Society in Ireland, March 2019 (oral)
11. TERMIS European Chapter Meeting 2019, Rhodes, Greece, May 2019 (oral)
12. Gordon Research Conferences: Biomaterials and Tissue Engineering, Castelldefels, Spain, July 2019 (poster)

CHAPTER 1

Introduction

The cornea is the window through which we see our world. Deep and severe injuries can lead to scar formation and corneal haze, resulting in blindness. Corneal blindness affects more than 45 million people worldwide, being surpassed one of the major causes of blindness together with other conditions such as cataracts, age-related macular degeneration or glaucoma (Flaxman et al., 2017; Pascolini and Mariotti, 2012; Whitcher et al., 2001). In severe cases when pharmacological treatment has been insufficient, the gold standard treatment is keratoplasty, the transplantation of a donor cornea to replace the damaged one. It has been recently estimated that only one patient is treated for every 70 that are in need of a transplant (Gain et al., 2016). By implementing policies to increase donations, improving storage conditions and logistics to transport the tissues from the banks to the hospitals, tissue shortages could be reduced. However, donor shortage will continue to be an issue with the increase in demand due to population growth and ageing. Therefore, alternatives to donor allografts are necessary and are being developed, such as cell-based therapies and tissue engineering strategies (Ghezzi et al., 2015; Griffith et al., 2016).

Artificial implants (keratoprostheses) are made from biologically inert materials, such as poly-2-hydroxyethyl methacrylate (PHEMA) or poly(methyl methacrylate) (PMMA), which only restore visual acuity and integrate poorly with the host tissue. These implants do not allow for re-epithelialization, re-innervation, migration of surrounding keratocytes, nor recellularization by endothelial cells. These devices are currently offered to patients that present poor prognosis for a traditional keratoplasty, and have been associated with numerous complications (Crawford, 2016; Srikumaran et al., 2014). It is clear materials that promote integration and endogenous repair are desirable in the corneal field.

Tissue engineering is based on the interplay between cells, scaffolds and stimuli, including mechanical, chemical or biological cues. In the field of corneal tissue engineering, multiple biomaterials are being investigated (Matthyssen et al., 2018). Biomaterials developed for corneal tissue engineering range from purely synthetic

polymers such as polyethylene glycol (Tan et al., 2013), polyglycolic acid (Hu et al., 2006), or polycaprolactone (Kim et al., 2018); to natural ones, such as collagen (Islam et al., 2018; Koulikovska et al., 2015; Liu et al., 2009), chitosan (Rafat et al., 2008; Zhu et al., 2006), silk fibroin (Bray et al., 2012; Fernández-Pérez et al., 2017; Ghezzi et al., 2017), fibrin (Alaminos et al., 2006; Rama et al., 2001) and self-assembling peptides (Uzunalli et al., 2014). Scaffold-free approaches where cells secrete their own extracellular matrix (ECM) and create a tissue *in vitro* have been reported too (Boulze Pankert et al., 2014; Gouveia et al., 2015; Guo et al., 2007) but these are costly and take months to obtain. Recently, research has focused on developing strategies to decellularize human corneas unsuitable for traditional transplantation or from animal origin to be used as transplantable tissue (Lynch et al., 2016b; Wilson et al., 2015). This process aims to remove the donor's cells so that only the extracellular matrix (ECM) is left. Ideally, the obtained matrices are biochemically and structurally identical to the original tissue. Such features are very difficult to recreate using other biomaterials. There is a lack of knowledge on the recellularization, culture conditions and effect of further processing when using decellularized corneas.

1.1. Aims and objectives

The main aim of this thesis is to develop tissue engineering strategies for corneal implant alternatives based on decellularized porcine corneas. To achieve this aim, several objectives have been identified.

The optimal method of cultivating isolated human stromal cells has to be defined. To obtain a large enough number of stromal cells required for cell-based therapies or tissue engineering, they must be expanded *in vitro* normally using serum-supplemented media. When keratocytes are exposed to serum, they become fibroblastic recapitulating the *in vivo* process of wound healing. In the first study, a comprehensive analysis will aim to identify medium supplements that promote the recovery of a keratocyte-like phenotype in human corneal stromal cells that have become fibroblastic when expanded in serum-supplemented media.

The use of decellularized corneas as scaffolds for corneal tissue engineering is attractive since both the fibril architecture and corneal composition can be accurately mimicked. The next objective is to recellularize decellularized porcine corneas. The repopulation will be analysed in terms of cell penetration, phenotype and fate after implantation in a rabbit model. Non-recellularized scaffolds will be used as controls.

Recellularizing decellularized whole corneas with stromal cells can be difficult due to the high density of collagen fibers in the tissue. Therefore, another aim of this thesis is to explore other fabrication methods to use decellularized corneas, rather than the whole tissue ones. A multi-layered approach will be developed in order to ensure the presence of stromal cells throughout the whole construct.

Decellularized tissues can be used to form hydrogels which can encapsulate cells in a biochemically native-like environment. As a final objective, cornea ECM-derived hydrogels will be fabricated using several decellularization methods to evaluate their impact on the gel characteristics. The potential of these hydrogels as ocular adhesives will be evaluated using an *ex vivo* corneal wound model.

Overall, the objectives of this thesis can be summarized as follows:

- Elucidate the role of media supplements to promote a keratocyte-like phenotype in serum-expanded stromal cells
- Repopulate whole decellularized corneas with stromal cells and evaluate their benefit in a rabbit anterior lamellar keratoplasty model
- Explore alternative methods to fabricate cornea-like tissues using decellularized cornea as starting materials to obtain highly cellular constructs
- Compare decellularization methods to obtain cornea ECM-derived hydrogels and their use as wound healing treatments

CHAPTER 2

Literature Review

2.1. Introduction

In this section, the following aspects of corneal tissue engineering will be reviewed. First, an overview of the cornea, its main components, structure and function will be given. Then, the wound healing process and main key growth factors and biochemical cues will be discussed with a focus on the culture of isolated stromal cells for cell-based therapies. Furthermore, the main pathologies affecting the cornea and current treatments will be described. Finally, corneal tissue engineering will be reviewed with a clear focus on the use of decellularized corneal tissues.

2.2. Anatomy of the cornea

The cornea, together with the sclera, forms the ocular surface. Due to its transparency and refractive power of 40 diopters, it has a light focusing function as well as a protective role against infections. Therefore, alterations to the corneas homeostasis can lead to blindness. The cornea has 5 layers (from anterior to posterior): epithelium, Bowman's layer, stroma, Descemet's membrane and endothelium. The corneal epithelium consists of stratified epithelial cells whose main function is to act as a barrier to protect the inner corneal layers (DelMonte and Kim, 2011). Human limbal epithelial stem cells that reside in the Palisades of Vogt, between the sclera and the cornea, replenish the epithelial cell population (Li et al., 2007). The stroma is the thickest part of the cornea, it is populated by keratocytes and is comprised of extracellular matrix (ECM) consisting of collagen I and lesser amounts of collagen V, glycosaminoglycans (GAGs) and proteoglycans, such as the small leucine-rich proteoglycans decorin, lumican and keratocan (Birk et al., 1986; Chakravarti et al., 1995; Corpuz et al., 1996; Lee and Davison, 1984; Li et al., 1992). The endothelium consists of a monolayer of hexagonal cells with limited regenerative capabilities and is separated from the stroma by the Descemet's membrane. These cells pump fluids from the stroma to the aqueous humour to maintain water homeostasis and are responsible for transporting nutrients to the

avascular cornea (Bonanno, 2012; Dikstein and Maurice, 1972). A general schematic view of the eye and a histological section of the central cornea are depicted in Figure 2-1.

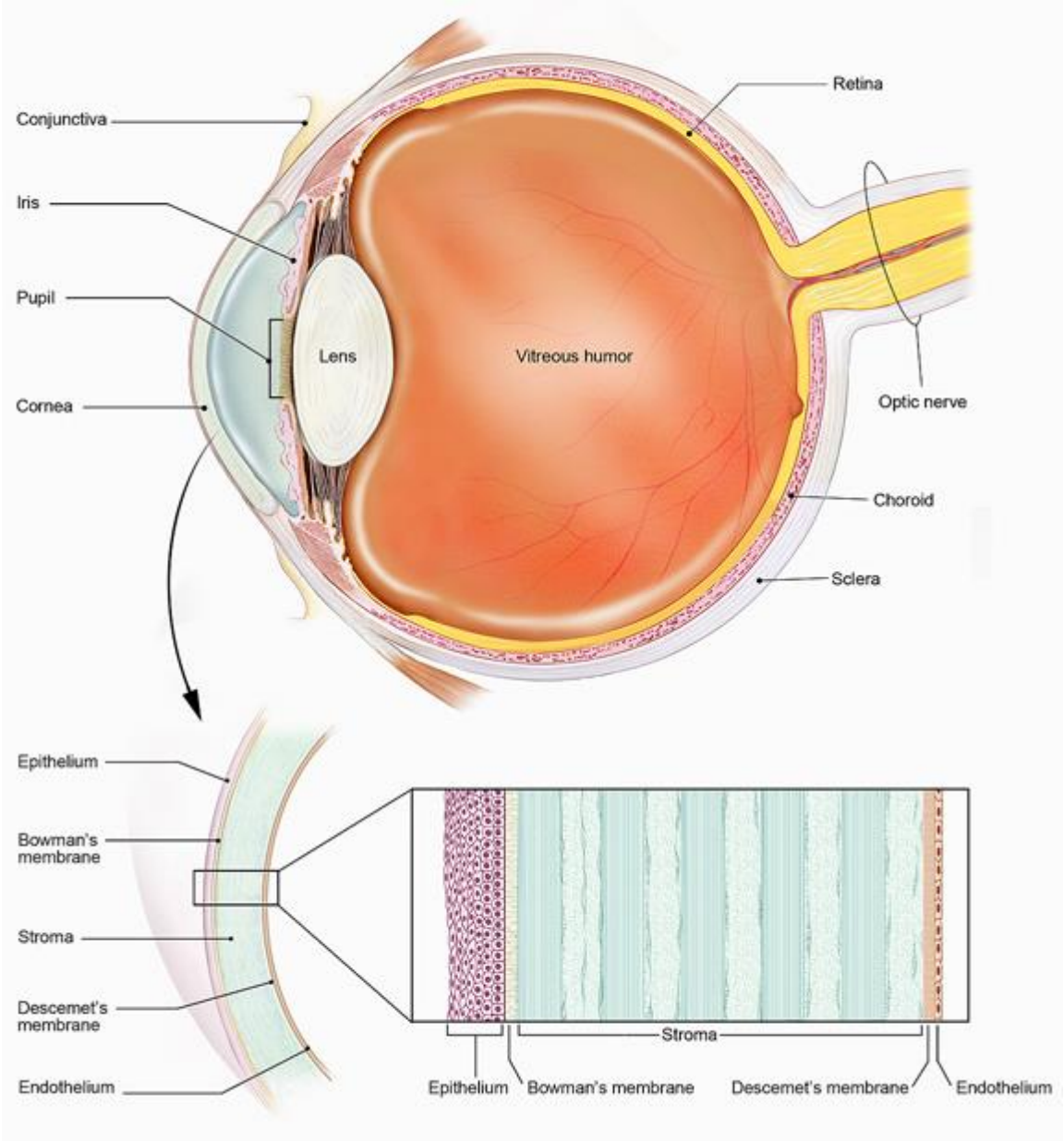

Figure 2-1. Anatomy of the human eye and cornea. From National Eye Institute, National Institutes of Health.

2.3. Wound healing in the corneal stroma: one cell, three phenotypes

Upon injury deep enough to involve the stroma, the first event is keratocyte cell death in the immediate surroundings of the damage (Wilson and Kim, 1998). It is thought to be a benign response in order to minimize inflammation. Next to follow is "keratocyte activation" which commences 6 hour post-injury. Keratocytes enter the cell cycle, losing their quiescence and start migrating towards the injury site (Fini and Stramer, 2005).

These cells become bigger in size, with multiple nucleoli, adopt a spindle shape and lose their cytoplasmic granules. There are also changes in gene expression with increased expression of fibronectin and the fibronectin-binding integrin heterodimer α5β1 (Welch et al., 1990), and several matrix metalloproteinases (MMPs) such as MMP-1 (collagenase), MMP-3 (stromelysin) and MMP-9 (gelatinase B) (Fini et al., 1992; Girard et al., 1993; Matsubara et al., 1991b, 1991a). This ECM-remodelling-phenotype is accompanied by the loss of corneal crystallins, such as ALDH3A1 (Jester et al., 1999). A subpopulation of activated keratocytes can transition to a myofibroblast phenotype. These cells are large and express alpha smooth muscle actin (α-SMA). They are responsible of wound contraction and further ECM remodelling. A trigger of differentiation is the release of TGF-β1 by corneal epithelial cells (Torricelli et al., 2016). Usually ECM deposited by activated fibroblasts and myofibroblasts alters the cornea's composition and organization, resulting in opacification. The provisional ECM deposited by myofibroblasts is rich in fibronectin, collagen III and tenascin (Fini, 1999; Tervo et al., 1991).

These two distinct phenotypes can be obtained *in vitro* from isolated keratocytes via the supplementation of medium with FBS (activated keratocytes) and addition of TGF-β1 (myofibroblasts). Myofibroblasts can transition into activated keratocytes, which indicates that these are not terminally differentiated phenotypes (Maltseva et al., 2001). A native keratocyte phenotype is difficult to maintain *in vitro* and required serum free medium. To maintain cell viability other biomolecules may be incorporates in the medium. In the following section, the effect that several of these biomolecules have on cultured corneal stromal-derived cells will be reviewed, and the findings are summarized in Table 2-1.

2.3.1 Fibroblast Growth Factor

The Fibroblast Growth Factor (FGF) family comprises 22 members, and FGF-2, also called basic FGF (bFGF) has been the most studied in the cornea. This growth factor is a single chain of 155 amino acids and weighs 17.2 kDa. The gene encoding for this protein is located in chromosome number four in humans. It interacts with four receptors (FGFR1, FGFR2, FGFR3 and FGFR4) (Xu, 1996). It has a heparin-binding domain that

increases its affinity to the receptors. It is expressed by the epithelium in the human cornea and by cultured stromal fibroblasts (Wilson et al., 1992).

In simple *in vitro* 2D monolayer experiments, most studies agree that FGF-2 has an effect on keratocyte proliferation (Jester et al., 1996; Long et al., 2000; Maltseva et al., 2001). In early studies by Jester and colleagues in 1996, it was stated that incubation with 10 ng/ml of FGF-2 maintained the typical stellate morphology of keratocytes, there was no up-regulation of α-SMA and there was almost no increase in fibronectin deposition (Jester et al., 1996). These findings suggest that FGF-2 does not promote myofibroblast differentiation. However, later studies by the same group reported a change of morphology to a fibroblastic, spindle-shaped (activated keratocyte) (Jester and Ho-Chang, 2003). Later studies have demonstrated the increase of ECM component deposition by FGF-2-treated corneal stromal cells, especially typical corneal keratin sulphated proteoglycans (KSPG) core proteins such as lumican, mimecan and keratocan (Long et al., 2000). Other components such as chondroitin and decorin are also increased (Etheredge et al., 2009). Contradictions arise when measuring collagen synthesis; Etheredge and colleagues claim that collagen synthesis is inhibited, while Borderie et al. report enhanced synthesis of Collagen V (Borderie et al., 1999). However, the culture conditions (2D vs 3D) should be taken into account. FGF-2 has chemotactic effects as seen in experiments using Boyden chamber (Grant et al., 1992) and increases cell migration in collagen gels (Andresen et al., 1997). Boyden chamber assays consist of a well insert with a polycarbonate substrate onto which cells are seeded. To study if one component is chemotactic, it is added to the medium on the bottom well and after some time the cells on the bottom side of the membrane are counted.

2.3.2 Insulin-like Growth Factor

Insulin-like Growth Factors (IGF) have a similar structure than that of Insulin but have higher activity. The family is comprised of two members: IGF-1 and IGF-2. The gene for IGF-1 is found on chromosome 12 in humans and encodes for a protein 195 aminoacids in length and a mass of 21.8 kDa. IGF-1 binds to tyrosine kinase receptor IFG1R, specifically to the alpha subunit, which activates signalling cascades of the PI3K-AKT/PKB and Ras-MAPK pathways. The binding of IGF-1 to integrins on the cells is necessary to form a ternary complex with the receptor to activate it (Saegusa et al., 2009).

IGF-1 increases collagen production and proteoglycans such as chondroitin and keratan sulphate (Etheredge et al., 2009; Hassell et al., 2008). The effect on proliferation is not clear as some studies claim that IGF-1 has no effect on proliferation (Etheredge et al., 2009) while others report a significant increase in H-thymidine incorporation as well as an anti-apoptotic effect of IGF-1, together with PDGF-BB, insulin, IGF-2 and EGF (Yanai et al., 2002). Absence of a migratory effect was stated by Andresen (Andresen et al., 1997). IGF-1 participates in the maintenance of typical dendritic keratocyte morphology at 50 ng/ml (Jester and Ho-Chang, 2003).

2.3.3 Platelet-Derived Growth-Factor

Platelet-derived Growth Factor (PDGF) acts as a dimer of four isoforms PDGF: A, B, C, and D. The two chains form homo- or heterodimers via two disulphide bonds and bind to two monomeric receptor subunits (PDGFR-α and PDGFR-β), which are tyrosine kinase receptors (Andrae et al., 2008). It is released by platelets upon wounding (as indicated by its name) but it is also secreted by activated macrophages, smooth muscle cells, endothelial cells and epidermal keratinocytes (Heldin and Westermark, 1999). In the cornea, PDGF isoforms A and B, and receptors α and β have been detected in cultured epithelial, fibroblasts and endothelial cells (Kim et al., 1999) and in tear fluid after photorefractive keratectomy (Vesaluoma et al., 1997).

Although other isoforms have been used in some studies, most research has been focused on PDGF-BB. At fairly high concentrations 25-100 ng/ml (but also at lower 10 ng/ml), PDGF-BB has mitogenic activity, increasing corneal fibroblast proliferation (Borderie et al., 1999; Etheredge et al., 2009; Gallego-Muñoz et al., 2017b; Hoppenreijs et al., 1993; Kim et al., 1999). An influence in migration, stimulating chemotaxis, has been reported for PDGF-BB in experiments using Boyden chambers (Kamiyama et al., 1998), in compressed collagen gels (Kim et al., 2010) and in scratch assays (Gallego-Muñoz et al., 2017b). Cell morphology changes when keratocytes are exposed to PDGF-BB in compressed collagen gels, adopting an elongated shape but with processes (Kim et al., 2010); a phenotype between quiescent and activated keratocytes.

2.3.4 Transforming Growth Factor

The Transforming Growth Factor beta (TGF-β) family is composed by TGF-β1, TGF-β2 and TGF-β3, found in chromosome 19, 1 and 14, respectively. The most studied of them is TGF-β1, which has positive and negative effects in the regulation of proliferation, growth and differentiation in multiple cell types, ranging from osteoblasts to regulatory T-cells. It is secreted and stored in the extracellular matrix as a 290 kDa complex which is inactive until cleavage by the matrix metalloproteinase 3 that releases the growth factor from the latency-associated peptide (LAP) (Shi et al., 2011). In the human cornea, mRNA and protein of TGF-β receptor types I, II and III were found in limbal basal cells and in the endothelium (Joyce and Zieske, 1997); while TGF-β2-LAP have been reported in the epithelium and stroma, and TGF-β3-LAP in the subepithelial region (Nishida et al., 1994).

TGF-β1 appears widely in the literature and it is accepted as a growth factor that promotes myofibroblast differentiation. Cells grown in serum-free medium supplemented with TGF-β1 develop stress fibres and a contractile phenotype with the expression of smooth muscle actin (α-SMA) and increased fibronectin deposition. These findings from early studies in 1996 by Jester and colleagues (Jester et al., 1996) have been confirmed by other researchers who have also shown an increase of other fibrotic markers such as collagen III upon treatment with TGF-β1, not only in human cells but also from rabbit and bovine cell sources (Andresen et al., 1997; Etheredge et al., 2009; Jester and Ho-Chang, 2003; West-Mays et al., 1999). Migration studies show that TGF-β1 inhibits migration at physiologic concentrations (10 ng/ml) (Andresen et al., 1997) while having a chemokinetic effect at extremely low concentrations (0.5 pg/ml) (Grant et al., 1992). TGF-β2 has not been studied as much as TGF-β1 but has been proven to have very similar effect on cultured corneal keratocytes and fibroblasts (Karamichos et al., 2011a; Kim et al., 2010). Recently, Karamichos and colleagues have claimed the anti-scarring effect of TGF-β3, showing a down-regulation of α-SMA and collagen III, and increased ECM deposition (Karamichos et al., 2013, 2011a). In another study they show the potential of TGF-β3 to revert a scar phenotype (myofibroblasts) into a scar-less wound-healing one, resembling that occurring during development (Karamichos et al., 2014b). In a recent study Sidney and Hopkinson confirmed these findings and report restored expression of keratocyte markers CD34, ALDH3A1 and keratocan, increase in collagen I and lumican

deposition, but with no down-regulation of MSC markers CD90, CD73 and CD105 (Sidney and Hopkinson, 2016).

2.3.5 Ascorbic Acid

Ascorbic acid has been shown to increase proliferation, synthesis of collagen I and III, stratification (self-assembly constructs) in rabbit, bovine and human keratocytes (Grobe and Reichl, 2013; Guo et al., 2007; Musselmann et al., 2006; Phu and Orwin, 2009; Saika et al., 1992, 1991). In 1991 and 1992, Saika and colleagues demonstrated the increase in proliferation (Saika et al., 1991) and production of type I and type III collagen peptides (Saika et al., 1992) by cultured rabbit keratocytes when cultured in serum-free medium containing 0.1 mM ascorbic acid. The authors suggest the increase in proliferation is related to the increase of collagen production, rather than a direct enhancement of mitosis, as the addition of a proline analog (AzC) which reduces the production of procollagen reduced proliferation. The authors also introduce the use of L-ascorbic acid 2-phosphate as it is more stable in culture than ascorbic acid alone (Saika, 1993). Musselmann and colleagues showed that 1 mM ascorbic acid did not increase proliferation unless 10 µg/ml insulin was also added. Ascorbic acid stabilized the folded triple helix of collagen and increased the accumulation of lumican and keratocan in the medium (Musselmann et al., 2006). Studies by Guo et al. examined the morphology of deposited ECM of human corneal fibroblasts (i.e. cultured in 10% FBS) upon treatment with 1 mM ascorbic acid (Guo et al., 2007). The authors showed cell stratification and aligned collagen deposition in a "lamellar" arrangement similar to that seen in the developing cornea. After 4 weeks in culture, constructs had an average thickness of 36.3 µm with multiple parallel layers of cells. Phu and Orwin showed cell stratification and an increase in non-organized ECM deposition coupled with expression of contractile proteins, such as α-SMA, when rabbit corneal fibroblasts were treated with 0.5 mM glucopryranosyl-L-ascorbic acid. However, when the cells were seeded on aligned electrospun collagen constructs, the addition of AA led to an increase in aligned ECM deposition and a decrease in α-SMA (Phu and Orwin, 2009). Grobe and Reichl studied the effect of ascorbic acid on primary human corneal stromal cells and on immortalized human corneal keratocytes (Grobe and Reichl, 2013). They showed an increment in cell viability in primary cells but not in the cell line upon treatment with 50 µg/ml (ca. 0.3 mM) of vitamin C. Secretion of collagen, especially type I, was enhanced and

stratification was observed which improved the mechanical properties and increased the percentage of light transmission.

2.3.6 Retinoic Acid

In 1986 Kenney and colleagues (Kenney et al., 1986) studied the effect of retinol and retinoic acid on cultured rabbit corneal fibroblasts. They quantified labelled thymidine incorporation, synthesis of collagens, sulphated glycosaminoglycans and fibronectin, and collagenase activity. They demonstrated a decrease in proliferation by reduction of thymidine incorporation. Collagen synthesis was reduced but the ratio of collagen types was maintained, collagen I being the 90% of collagen synthesised and collagen III roughly making up for the remaining 10%. The synthesis of fibronectin was greatly increased by 2.5-fold. Soluble sGAGs were shown to be increased by treatment with retinol and retinoic acid, while sGAGs associated with the cell layer where reduced. The concentrations used by these researchers (1-2 x 10^{-7} M) was two orders of magnitude lower than the ones used by Gouveia and Connon 27 years later (Gouveia and Connon, 2013). In their studies, retinoic acid increased cell proliferation and stratification, elevated the expression of keratocyte markers such as keratocan, lumican, decorin, ALDH1 and collagen I, while decreasing fibrosis and proteolytic markers such as α-SMA and MMP-1, MMP-3 and MMP-9. They also demonstrated impaired keratocyte migration using a scratch assay. Similar results were shown by the same group when keratocytes where cultured in compressed collagen gels (Abidin et al., 2015).

Table 2-1. Biochemical cues and their effects on corneal stromal cells. S = species, R = rabbit, H = human, B = bovine.

Factor	Concentration	Effects of Factor	S	2D/3D	Other culture conditions	Reference
FGF-2	10 ng/ml	Increased proliferation, No increase in FN deposition, No α-SMA staining, Maintenance of stellate morphology	R	2D	Serum-free supplemented with RPMI, gluthatione, non-essential AA, pyruvic acid and 1% glutamine	(Jester et al., 1996)
	10 ng/ml	Fibroblastic morphology, No α-SMA staining Increased ECM contraction	R	2D	Serum-free supplemented with RPMI, gluthatione, non-essential AA, pyruvic acid, 1% glutamine, 100 µg/ml ascorbic acid	(Jester and Ho-Chang, 2003)
	80 ng/ml	Positive migratory effects (chemotactic) in Boyden chamber	H	2D	M199 +10% FCS for expansion DMEM + 1% albumin (BSA) for experiments	(Grant et al., 1992)
	10 ng/ml	Increased migration in collagen gels	H	2D	Isolated in 10% FBS, experiments in serum-free DME-F12 + 0.1% HAS on collagen gels for migration	(Andresen et al., 1997)
	10 ng/ml	Increased proliferation, Inhibition of collagen production, Increased chondroitin synthesis and decorin (low tensile strength)	B	2D	Serum-free, experiments last 13 days, radiolabeled ^{3}H-thymidine for DNA synthesis or ^{3}H-glycine for protein/collagen synthesis	(Etheredge et al., 2009)
	10 ng/ml	Increased organized matrix deposition, Differentiate human corneal stromal stem cells into keratocyte-like (down-regulate α-SMA)	H	2D	hCSSCs on highly aligned fibrous substrate experiments include conditions +TGF-β3 (synergistic effect)	(Wu et al., 2013)
	10 ng/ml	Increased proliferation, No influence on matrix synthesis	B	2D	Serum-free with AA, Monolayer covered with 3% agarose	(Etheredge et al., 2010)
	10 ng/ml	Stimulation of expression of KSPG core proteins (lumican, mimecan, and keratocan), Increased mRNA pools of keratocan	B	2D	Medium contained ITS and 0.1% platelet-poor horse serum. Determination of proteoglycan synthesis by radiolabelled [^{35}S]methionine/cysteine	(Long et al., 2000)
	10 ng/ml	Enhanced gel contraction	H	3D	Experiments in normal collagen gels (1.4 mg/ml)	(Assouline et al., 1992)
	10 ng/ml	Enhanced Collagen VI synthesis No presence of α-SMA	H	3D	Collagen gel (1.5 mg/ml) contraction test +/- FCS and +/- GFs	(Borderie et al., 1999)
IGF-1	50 ng/ml	Maintenance of keratocyte phenotype (dendritic/stellate morphology)	R	2D	Serum-free supplemented with RPMI, gluthatione, non-essential AA, pyruvic acid, 1% glutamine, 100 µg/ml ascorbic acid	(Jester and Ho-Chang, 2003)
	10-30 ng/ml	No effect on migration	H	2D	Human. See same reference	(Andresen et al., 1997)

	10 ng/ml	No proliferation effect, Increase in collagen production and chondroitin and keratin sulphate	B	2D	Serum-free, experiments last 13 days, radiolabeled ^{3}H-thymidine for DNA synthesis or ^{3}H-glycine for protein/collagen synthesis	(Etheredge et al., 2009)
	10 ng/ml	Increased deposition of collagen and proteoglycans (possibly due to the trapping between cells and agarose)	B	2D	Serum-free with AA, Culture on dishes with a 3% agarose layer	(Hassell et al., 2008)
	10 ng/ml	Inhibit gel contraction in combination with FGF-2 (10 ng/ml) & PDGF-BB (10 ng/ml), and increase in gel contraction in combination with EGF (1 ng/ml)	H	3D	Experiments in normal collagen gels (1.4 mg/ml)	(Assouline et al., 1992)
PDGF-BB	30 ng/ml	Enhanced corneal fibroblast migration (chemotaxis)	R	2D	Isolated in TCM-199 +20% FBS Expanded in TCM-199 +5% FBS Experiments in TCM-199 serum-free	(Kamiyama et al., 1998)
	10 ng/ml	Increased invasion in gel	H	2D	See same reference	(Andresen et al., 1997)
	10 ng/ml	Increased proliferation, Increased ECM deposition (chondroitin and keratin sulphate, less increase in HA)	B	2D	Serum-free, experiments last 13 days, radiolabeled ^{3}H-thymidine for DNA synthesis or ^{3}H-glycine for protein/collagen synthesis	(Etheredge et al., 2009)
PDGF-AB	100 ng/ml	Increase proliferation, Differentiate into fibroblastic-like cells with loss of dendritic cell processes and elongation of the cell body No α-SMA expression	R	2D	See same reference	(Jester and Ho-Chang, 2003)
PDGF-BB	10, 25, 50 ng/ml	Increased corneal fibroblast proliferation Stimulate positive chemotaxis	H	2D	EMEM with 10% FBS, experiments with 0.5% FBS	(Kim et al., 1999)
	10 ng/ml	Increased proliferation when covered with agarose	B	2D	Monolayer covered with 3% agarose	(Etheredge et al., 2010)
	25-100 ng/ml	Increased proliferation	H	2D	Human corneal fibroblasts in 2% FBS	(Hoppenreijs et al., 1993)
	10 ng/ml	High gel contraction	H	3D	Experiments in normal collagen gels (1.4 mg/ml)	(Assouline et al., 1992)
PDGF (AA, BB, AB?)	50 ng/ml	PDGF stimulated significant keratocyte migration Morphology: more elongated and developed less convoluted cell, without inducing stress fiber formation, elongated with branching processes	R	3D	On and in compressed collagen gels (~133mg/ml) DMEM supplemented with 1% RPMI vitamin mix, 100 µM nonessential amino acids, 100 µg/mL ascorbic acid and 1% penicillin/streptomycin amphotericin B	(Kim et al., 2010)

TGF-β1	0.1, 1, 10 ng/ml	Increased cell proliferation, Increased α-SMA expression and FN deposition, stress fibres, Loss of stellate morphology towards spindle-shaped fibroblasts, higher dose larger cells.	R	2D	Serum-free supplemented with RPMI, gluthatione, non-essential AA, pyruvic acid and 1% glutamine	(Jester et al., 1996)
	1 ng/ml	Large and spread morphology Increased α-SMA expression	R	2D	Serum-free supplemented with RPMI, gluthatione, non-essential AA, pyruvic acid, 1% glutamine, 100 µg/ml ascorbic acid	(Jester and Ho-Chang, 2003)
TGF-β1 & TGF-β2	0.1 ng/ml	Stimulation of matrix production Fibrotic markers up-regulated (Col-III, α-SMA)	H	2D	EMEM + 10% FBS + ascorbic acid	(Karamichos et al., 2011b)
TGF-β3	0.1 ng/ml	Matrix deposition (high level of alignment and organization)	H	2D	+10% FBS (fibroblasts) vs. +1% FBS +AA (keratocytes)	(Karamichos et al., 2013)
TGF-β3	0.1 ng/ml	Up-regulation of keratocyte markers, Down-regulation of α-SMA, Orthogonal collagen deposition	H	2D	hCSSCs on highly aligned fibrous substrate in serum-free +AA +ITS. Long culturing periods (9 weeks) Experiments include conditions +FGF-2 (synergistic effect)	(Wu et al., 2013)
TGF (β1?)	0.5 pg/ml	Chemokinetic effect	H	2D	M199 +10% FCS for expansion DMEM + 1% albumin (BSA) for experiments	(Grant et al., 1992)
TGF-β1	2 ng/ml	Not much influence in proliferation, Increased deposition of collagens but also fibronectin (scar-like)	B	2D	Serum-free, experiments last 13 days, radiolabeled ^{3}H-thymidine for DNA synthesis or ^{3}H-glycine for protein/collagen synthesis	(Etheredge et al., 2009)
TGF (β1?)	10 ng/ml	Inhibition of collagenase in early passage corneal fibroblasts	R	2D	Treatment with CytochalasinB and phorbol myristate acetate (PMA), which promote collagenase expression, radiolabelling of synthesized products	(West-Mays et al., 1999)
TGF-β1	10ng/ml	Increase in proliferation Inhibition of migration	H	3D	Isolated in 10% FBS, experiments in serum-free DME-F12 + 0.1% HAS on collagen gels (1.75 mg/ml) for migration	(Andresen et al., 1997)
Ascorbic Acid	1 mM P-Asc or 0.5 mM G-Asc	ECM assembly in parallel arrays of fibrils	H	2D	Fibroblasts were cultured in EMEM with 10% FBS and 1 mM P-Asc or 0.5 mM G-Asc, on transwell six-well plates with membrane inserts with 3.0 µm pores (Boyden chamber)	(Guo et al., 2007)
	0.1 mM	Increase in proliferation	R	2D	Rabbit keratocytes	(Saika et al., 1991)
	0.1 mM	Increased production of Collagen I and III peptides	R	2D	Rabbit keratocytes	(Saika et al., 1992)

	1 mM	Increased proliferation only if insulin (10 µg/ml) also present	B	2D	Bovine at p0 DMEM/F12 no FBS	(Musselmann et al., 2006)
Retinoic Acid	10×10^{-6} M	Increased cell proliferation Increased keratocyte marker expression (keratocan, decorin and lumican) Decreased expression of fibrotic markers (MMP1, MMP9 and α-SMA) Impaired migration	H	2D	Serum-free +ITS +AA	(Gouveia and Connon, 2013)
	10^{-6} M	Inhibition of collagenase in early passage corneal fibroblasts	R	2D	See same reference	(West-Mays et al., 1999)
	$1\text{-}2 \times 10^{-7}$ M	Reduced cell proliferation Reduced collagen synthesis, increase in FN and soluble GAGs, No change in morphology	R	2D	Rabbit cells, expanded in 20% FBS medium, experiments in serum-free DMEM	(Kenney et al., 1986)
	10×10^{-6} M	Inhibit the contractility of keratocytes while allowing the build-up of corneal stromal extracellular matrix	H	3D	Serum-free +ITS +AA. Experiments in compressed collagen matrices (~2.5 kPa)	(Abidin et al., 2015)

2.4. Pathology of the cornea

Corneal diseases are one of the most prevalent causes of blindness, which affect more than 45 million people worldwide (Whitcher et al., 2001). Furthermore, it is estimated that 10 million people worldwide have bilateral corneal blindness (Pascolini and Mariotti, 2012). Other major pathologies leading to blindness include cataracts, age-related macular disease, glaucoma or diabetic retinopathy (Flaxman et al., 2017). While minor injuries to the corneal surface can heal easily, deeper injuries can lead to scarring and corneal haze. Untreated keratitis (cornea inflammation) can also lead to corneal scarring. Keratitis can be non-infectious caused by injuries or contact lens misuse; or infectious caused by bacteria, such as *Chlamydia trachomatis*, viruses, such as *Herpes zoster* and *Herpes simplex*, and fungi and protozoa (Reinhard and Larkin, 2006). Corneal dystrophies including Fuch's dystrophy (deterioration of the endothelium), keratoconus (thinning of the cornea), lattice dystrophy (amyloid deposits in the stroma) and map-dot-fingerprint dystrophy (folding of the Bowman's membrane) can result in vision loss (Reinhard and Larkin, 2006; Schorderet, 2015). Other diseases affecting the cornea are iridocorneal endothelial syndrome, in which the endothelial cells migrate towards the iris; Steven-Johnson syndrome, in which the patient presents painful blisters; or dry eye, in which the surface of the eye is not properly lubricated due to reduced tear film production (Reinhard and Larkin, 2006).

2.4.1 Treatment of severe corneal diseases

Infectious corneal keratitis are treated with the corresponding antibiotics or antiviral drugs. Main symptomatology is treated with anti-inflammatory drugs, i.e. corticosteroids, such as dexamethasone. Many other corneal diseases reduced the ocular surface lubrication, requiring artificial tears to be prescribed. Since one of the common denominators of severe corneal disease is neovascularization, anti-angiogenic treatments, including anti-VEGF therapies, are used (Jeng, 2014).

When the abovementioned treatments are not sufficient and the cornea has become hazy or opaque, the treatment offered to patients is keratoplasty, i.e. the transplantation of a donor's cornea. Although the predominant technique is penetrating keratoplasty, which replaces the full-thickness of the cornea, new approaches are being performed. Other types of keratoplasties include: anterior lamellar keratoplasty and deep anterior lamellar keratoplasty (which replaces the damaged stroma) or Descemet's

stripping automated endothelial keratoplasty and Descemet's membrane endothelial keratoplasty (which replaces only the endothelium) (Tan et al., 2012). Exemplifying drawings of these techniques can be seen in Figure 2-3.

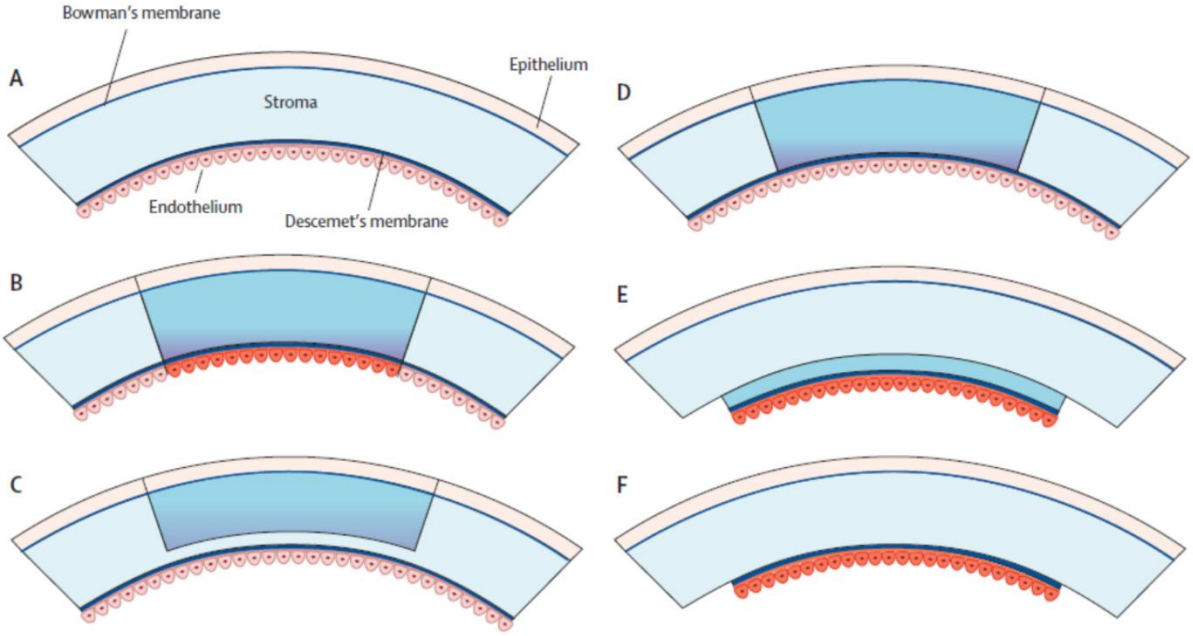

Figure 2-2. Types of keratoplasties. A) General structure of the cornea. B) Penetrating keratoplasty. C) Anterior lamellar keratoplasty (D) Deep lamellar endothelial keratoplasty. (E) Descemet's stripping automated endothelial keratoplasty. (F) Descemet's membrane endothelial keratoplasty. From Tua et al., 2012.

Around 185.000 corneal transplants are performed yearly, making it the most common type of transplant worldwide (Gain et al., 2016). Grafts in "low risk" patients, such as those suffering from keratoconus, have high survival rates of 95% at 5 years (Hjortdal et al., 2013). On the other hand, graft failure is reported to be higher than 35% at 3 years in "high risk" patients, in which the "immune privileged" status of the cornea has been compromised by neovascularization, for example (Bartels et al., 2003). In a recent global survey it was determined that there is only one cornea available for every 70 needed, which highlights the severe donor shortage of such a tissue (Gain et al., 2016). It is clear that alternatives to this approach need to be developed.

Keratoprostheses such as the Boston KPro or the AlphaCor^{TM}, made from methacrylated synthetic non-resorbable polymers, can be an option for patients with high risk of graft failure. However, these artificial corneas do not promote tissue regeneration and are frequently associated with glaucoma (Chew et al., 2009; Hicks et al., 2006; Jirá et al., 2011). It is for these reasons that there has been a lot of interest in corneal bioengineering as an approach to generate transplantable tissues.

2.5. Corneal tissue engineering

Tissue bioengineering aims to overcome donation shortages and immune rejection by fabricating organs in the lab with patient-specific cells. Traditional tissue engineering is based on the interplay between cells, the fabrication of biocompatible scaffolds and the application of external stimuli including mechanical, chemical or biological stimuli. In the field of corneal tissue engineering, multiple biomaterials are being investigated (Matthyssen et al., 2018). Optimal corneal scaffold materials should be transparent, biocompatible, and biodegradable, and have sufficient mechanical strength to be sutured. Collagen-based materials are the most common as collagen is the most abundant component of the corneal stroma. These have been fabricated as highly-hydrated hydrogels (Fagerholm et al., 2010; Liu et al., 2008), plastically compressed matrices (Kureshi et al., 2015; Levis et al., 2010) and membranes by vitrification (McIntosh Ambrose et al., 2009). Other natural polymers such as chitosan (Rafat et al., 2008; Zhu et al., 2006), silk fibroin (Bray et al., 2012; Fernández-Pérez et al., 2017; Wang et al., 2017), fibrin (Alaminos et al., 2006; Rama et al., 2001) and self-assembling peptides (Uzunalli et al., 2014) have also been investigated. 3D bioprinting, a revolutionary technique, has also been used to fabricate corneas using bioinks (Isaacson et al., 2018; Sorkio et al., 2018). While these studies have produced some promising results, these materials lack the biochemical composition of the real cornea and fail to replicate the cornea fibril arrangements and ECM architecture. Techniques such as 3D bioprinting (Isaacson et al., 2018; Sorkio et al., 2018) or electrospinning (Tonsomboon and Oyen, 2013; Wilson et al., 2012) have the potential to generate scaffolds with similar shape and structure to real cornea but these still do not replicate the composition. Hydrogels derived from corneal ECM have also been developed that maintain much of the cornea's ECM but often lack its fibril organization (Ahearne and Coyle, 2016; Ahearne and Lynch, 2015; Kim et al., 2019b). Scaffold-free approaches where cells secrete their own ECM and create a tissue *in vitro* have also been reported (Boulze Pankert et al., 2014; Gouveia et al., 2017; Guo et al., 2007) but these are costly and require long culture periods. Therefore, the use of decellularized corneas as a scaffold for corneal engineering is attractive since both the fibril architecture and corneal composition can be accurately mimicked. In the following sections, corneal tissue engineering based on corneal decellularization will be reviewed,

which usually involves the following: isolating the donor tissue, removing cells, adding new healthy cells and implanting into a patient, as depicted in Figure 2-3.

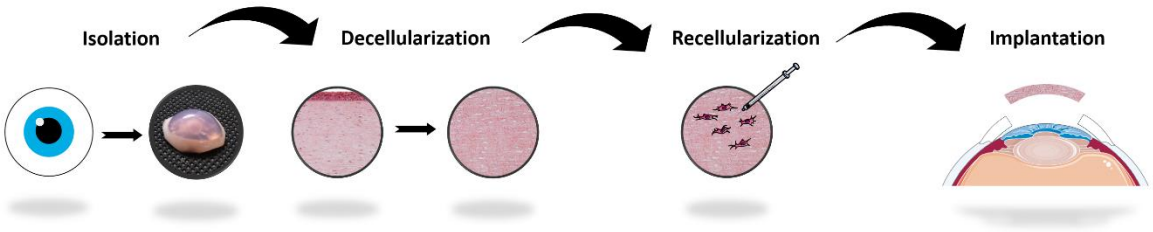

Figure 2-3. General workflow for the use of decellularized corneas as donor alternatives.

2.5.1 Decellularization of the cornea

Organ decellularization consists of removing cells and their debris to obtain an acellular scaffold composed of the organ's extracellular matrix (ECM). By removing the cells, major histocompatibility complexes are depleted thus reducing the risk of graft rejection. The main advantage of using decellularized corneas is that the obtained scaffold is biochemically identical to original tissue. Furthermore, the exquisite collagen arrangement in the corneal stroma can be maintained, which is difficult to replicate using other biomaterials. Cell removal reduces graft rejection by depleting the scaffolds from major histocompatibility complexes. Insufficient decellularization has been shown to illicit polarization of macrophages to an M1-phenotype *in vivo* and *in vitro* (Keane et al., 2012). Furthermore, cellular components that have not been removed can be bound by immunoglobulins and complement proteins which will activate macrophages and B lymphocytes (Nagata et al., 2010). In the last decade a wide range of organs have been decellularized including heart (Guyette et al., 2014; Ott et al., 2008), kidney (Orlando et al., 2013), liver (Barakat et al., 2012; Kajbafzadeh et al., 2013; Yagi et al., 2013), lung (Booth et al., 2012; Gilpin et al., 2014; Nichols et al., 2013; O'Neill et al., 2013) or pancreas (Goh et al., 2013). In this section different techniques used to remove cells and cellular components from the cornea will be explored. All decellularization techniques can be categorized into three types of methods: physical, chemical and biological methods. However, it should be noted that most decellularization protocols combine several methods and techniques. A summary of these methods used in the cornea can be found in Table 2-2.

Physical methods

Some form of mechanical agitation is present in most decellularization protocols and mostly carried out using orbital shakers or rotators to promote the flow of decellularizing agents through the ECM. For example, Nara and colleagues have described the use of a direct perfusion chamber that applied detergents in a continuous unidirectional flow (Nara et al., 2016). The use of automatized devices that allow both mechanical agitation and fluid exchange, such as the one described by Pellegata and colleagues to decellularize blood vessels, offers great promise to speed up the process and ensure sterility (Pellegata et al., 2012).

A simple method of decellularization is using repeated freeze-thaw cycles where cells are lysed due to the formation of ice crystals. This is usually followed by rinsing or the addition of another decellularization method to ensure removal of cell debris (Ahearne and Lynch, 2015; Diao et al., 2015; Li et al., 2017; Oh et al., 2009; Proulx et al., 2009). Temperatures used for the freeze-thawing cycles range from -20 °C to -197 °C with the use of liquid nitrogen. Another method is the use of electrophoresis, which has been reported in the literature as a final step to remove debris (Shao et al., 2015, 2012) but is not a widespread method. The use of high hydrostatic pressure has been shown to reduce DNA and maintain glycosaminoglycan (GAG) levels in decellularized porcine corneas (Hashimoto et al., 2016, 2010; Sasaki et al., 2009). This method is not used commonly as the equipment needed is expensive (Lynch and Ahearne, 2013). Li and colleagues have recently reported on the use of ultrasound in conjunction with freeze-thawing and nucleases for the decellularization of porcine corneas (Li et al., 2017).

Decellularization using supercritical CO_2 was first used by Sawada and colleagues for vascular tissues (Sawada et al., 2008). This technique is based on the high permeability and transfer rate characteristic of supercritical fluids. Carbon dioxide can be used as a critical fluid under moderate conditions (T_C = 32 °C, P_C = 7.38 MPa) and after the procedure there are no remnants as the gas can diffuse out easily. Bovine (Guler et al., 2017) and porcine (Huang et al., 2017) corneas have also been recently decellularized using this method with good initial results. Furthermore, this technique can be used to sterilize the tissue simultaneously (Wehmeyer et al., 2015).

While not strictly a decellularization method, lyophilisation has been used by researchers to obtain more porous scaffolds as water in the decellularized cornea becomes

frozen and then removed by sublimation once a vacuum is applied. With this approach the repopulation by neighbouring cells is thought to increase although the process would likely disrupt the cornea's collagen architecture (Lin et al., 2008; Pang et al., 2010; Xiao et al., 2011).

Chemical agents

The use of detergents is the most common method for corneal decellularization. The most widely used is the ionic detergent sodium dodecyl sulphate (SDS) (Alió del Barrio et al., 2018, 2015; Du and Wu, 2011; Pang et al., 2010; Yam et al., 2016; Yoeruek et al., 2012a; Zhou et al., 2011). While extremely effective, SDS can disrupt the ECM as it is a denaturing agent. Therefore other milder detergents are being explored such as sodium deoxycholate (Diao et al., 2015; Xu et al., 2017). Non-ionic detergents, such as Triton X-100, are less effective but in turn less disruptive (Choi et al., 2010; Du et al., 2011; Fu et al., 2010; Luo et al., 2013; Xu et al., 2008). Zwitteronic detergents have characteristics of ionic detergents, as they have positive and negative functional groups, and non-ionic detergents, as their net charge is zero. However, these detergents have been used unsuccessfully for cornea decellularization (Du et al., 2011).

Organic acids have also been used to decellularize corneas. Peracetic acid has widely been used to decellularize and terminally sterilize urinary bladder and small intestine submucosa by the Badylak lab (Freytes et al., 2008; Gilbert et al., 2008; Mase et al., 2010), and Ponce Márquez reported the use of it for the cornea with suboptimal results (Ponce Márquez et al., 2009). Mild acids commonly found in nature, such as acetic, formic and citric acids, have been recently employed for porcine cornea decellularization. Formic acid at a 30% concentration showed the best results in terms of DNA removal, and sulfated GAG (sGAG) and collagen retention (Lin et al., 2019). Bases are less used than acids and only ammonium hydroxide appears in the literature for corneal decellularization (Choi et al., 2010; Z. Zhang et al., 2015) while sodium hydroxide has been used to decellularize lungs and heart valves (Sengyoku et al., 2018; van Steenberghe et al., 2018).

Hypertonic solutions, especially sodium chloride at concentrations of 1.5 or 2 M, have been used by multiple research groups with positive outcomes in terms of transparency, cell removal and retention of ECM components (González-Andrades et al.,

2011; He et al., 2016; Huang et al., 2017; Luo et al., 2013; Ma et al., 2015; Oh et al., 2009; Wilson et al., 2016; Yam et al., 2016; M.-C. Zhang et al., 2015). When combined with a washing step using 0.2 % Triton X-100 the best results were achieved (Luo et al., 2013; M.-C. Zhang et al., 2015).

Other chemicals used to decellularize corneas include alcohols, such as ethanol, and chelating agents, such as Ethylenediaminetetraacetic acid (EDTA). Ponce Márquez and colleagues used 75% ethanol following a protocol originally described to decellularize arteries (McFetridge et al., 2004; Ponce Márquez et al., 2009). EDTA is commonly used in conjunction with trypsin as it helps disrupt cell-cell interactions by sequestering calcium present in cadherin junctions (Oh et al., 2009; Xu et al., 2008; Yoeruek et al., 2012a).

Biological agents

Several enzymes have been used in the literature to decellularize corneas. Trypsin and Dispase II are cell dissociating proteins commonly used for cell isolation. If used for longer periods or at higher concentrations, they can result in cell lysis (González-Andrades et al., 2011; Hong et al., 2018; Huh et al., 2018; Lin et al., 2008; Oh et al., 2009; Xu et al., 2008; Zhang et al., 2007). Phospholipase A_2 (PLA_2) is an esterase that breaks the phospholipids present in the cell membrane and has been shown to remove cell components successfully with minimal ECM disruption (Li et al., 2011; Wu et al., 2009; Z. Wu et al., 2014; Xiao et al., 2011). Another biological agent is human serum which has been used to decellularize blood vessels (Gui et al., 2010) and corneas alongside the use of electrophoresis (Shao et al., 2015, 2012). Most studies include an additional step of incubation with nucleases to assist with the degradation of DNA released following cell lysis (Alió del Barrio et al., 2015; Diao et al., 2015; Hashimoto et al., 2015; Lynch et al., 2016b; Shafiq et al., 2012; Xu et al., 2017; Yoeruek et al., 2012b).

Table 2-2. Summary of the decellularization methods reviewed, all used in the cornea.

Decellularization methods	References
Physical methods	
Agitation	n.a.
Freeze-thawing	(Ahearne and Lynch, 2015; Diao et al., 2015; Li et al., 2017; Oh et al., 2009; Proulx et al., 2009)
Electrophoresis	(Shao et al., 2015, 2012)
High hydrostatic pressure	(Hashimoto et al., 2016, 2010; Sasaki et al., 2009)
Supercritical CO_2	(Guler et al., 2017; Sawada et al., 2008)
Lyophilization	(Lin et al., 2008; Pang et al., 2010; Xiao et al., 2011)
Chemical agents	
Sodium dodecyl sulphate (SDS)	(Alió del Barrio et al., 2018, 2015; Du and Wu, 2011; Pang et al., 2010; Yam et al., 2016; Yoeruek et al., 2012a; Zhou et al., 2011)
Sodium deoxycholate	(Diao et al., 2015; Xu et al., 2017)
Triton X-100	(Choi et al., 2010; Du et al., 2011; Fu et al., 2010; Luo et al., 2013; Xu et al., 2008)
Peracetic acid	(Ponce Márquez et al., 2009)
Formic acid	(Lin et al., 2019)
Ammonium hydroxide	(Choi et al., 2010; Z. Zhang et al., 2015)
Sodium chloride (hypertonic)	(González-Andrades et al., 2011; He et al., 2016; Huang et al., 2017; Luo et al., 2013; Ma et al., 2015; Oh et al., 2009; Wilson et al., 2016; Yam et al., 2016; M.-C. Zhang et al., 2015)
Ethylenediaminetetraacetic acid (EDTA)	(Oh et al., 2009; Xu et al., 2008; Yoeruek et al., 2012a)
Biological agents	
Trypsin	(González-Andrades et al., 2011; Hong et al., 2018; Huh et al., 2018; Lin et al., 2008; Oh et al., 2009; Xu et al., 2008; Zhang et al., 2007)
Dispase	(González-Andrades et al., 2011; Oh et al., 2009; Xu et al., 2008; Zhang et al., 2007)
Phospholipase A_2	(Li et al., 2011; Wu et al., 2009; Z. Wu et al., 2014; Xiao et al., 2011)
Human serum	(Shao et al., 2015, 2012)
Nucleases (DNAse and RNAse)	(Alió del Barrio et al., 2015; Diao et al., 2015; Hashimoto et al., 2015; Lynch et al., 2016b; Shafiq et al., 2012; Xu et al., 2017; Yoeruek et al., 2012b)

Confirmation of decellularization

There is no current consensus to validate the success of a decellularization protocol. In general, the decellularization procedure should remove exogenous cells, and

cell debris, including DNA, RNA and other cell remnants such as mitochondria, while minimally disrupting the ECM. To verify the removal of nuclei and cellular components three parameters should be examined (Scarritt et al., 2019). The first parameter involves staining with Haematoxylin and Eosin (H&E) and/or 4′,6-diamidino-2-phenylindole (DAPI) to demonstrate absence of intact cell nuclei. Next dsDNA is quantified via Hoechst 33342 binding or via PicoGreen™ (Invitrogen) assay. This should give values of below 50 ng of dsDNA per mg of dry weight (Crapo et al., 2011). Finally the maximum length of DNA remnants should be 200 bp determined via agarose gel electrophoresis (Crapo et al., 2011; Nagata et al., 2010).

While these parameters will determine the presence of cellular components, it is important that the decellularization process also maintains the cornea's structure, composition and transparency to allow the scaffold to retain its function. ECM can be analysed using standard histological stains such as Picrosirius Red, to stain collagen fibers, or Alcian Blue, to visualize GAGs. These parameters can also be quantified using biochemical assays such as hydroxyproline reagent to quantify collagen (Ignat'eva et al., 2007; Kafienah and Sims, 2004) or dimethylmethylene blue assay to quantify GAGs (Farndale et al., 1982). Immunohistochemistry can be used to identify specific ECM components such as the type of collagen present or specific proteoglycans and GAGs. Second harmonic generation imaging can be used as a non-destructive technique to give information on collagen fiber orientation and identify damage to the collagen during decellularization (Bueno et al., 2011). Electron microscopy offers a great deal of ultrastructure detail, especially in the cornea where the precise arrangement of collagen bundles determines the optical properties of the tissue. Both SEM and TEM require highly specialized and expensive equipment, only available in big universities and research centres.

Unlike most other tissues and organs, the transparency of scaffolds is an important parameter that needs to be considered for corneal tissue engineering. The optical characteristics of decellularized corneal scaffolds can be easily quantified using a simple spectrophotometer (or plate reader). The absorbance at different wavelengths in the visual spectrum of light provides information on the clarity or opacity of a scaffold. The mechanical properties of decellularized cornea also need to be sufficient to allow suturing and withstand any applied forces. Minimizing disruption to the ECM during decellularization should allow the mechanical characteristics of the cornea to be

maintained. Furthermore, the use of osmoregulators such as dextran or glycerol can aid on palliating swelling and thus recovering transparency and increasing tissue stiffness and strength (Lynch et al., 2016b; Murab and Ghosh, 2016).

Species used for corneal decellularization

Porcine corneas have been the most extensively studied for decellularization mainly due to their availability and anatomical similarities with the human cornea. However, porcine cells present several epitopes that are extremely immunogenic to humans such as Galactose-alpha-1,3-galactose (α-Gal) and N-glycolylneuraminic acid (Neu5Gc). Insufficient cell removal could elicit an immune response that could lead to graft rejection. It is therefore recommended to perform immunostaining against these epitopes to ensure their absence in the scaffolds. As reviewed by Kim and Hara (Kim and Hara, 2015), the thickness of the porcine cornea varies greatly with age and breed, which highlights the need of standardisation. By breeding animals specifically for organ decellularization and transplantation in quarantined animal facilities, heterogeneity from batches can be monitored and brought to a minimum. In addition, with the advent of genetic engineering, pure xenogenic transplantation could become a reality, with the use of so-called "humanized" pigs. Two main hurdles have to be overcome in order to use pig corneas for transplantation as if they were human: the removal of multiple xenoreactive cell surface molecules and porcine endogenous retroviruses (PERV). The use of CRISPR-Cas9 has been shown to be successful in obtaining triple knockout strains of pigs lacking GGTA1, CMAH, and β4GalNT2, genes important for the presence of immunogenic surface glycans (Estrada et al., 2015; Wang et al., 2018; Zhang et al., 2018). This same genome editing technique has been used to remove PERVs *in vitro* to obtain PERV-inactivated pigs (Niu et al., 2017). Other species that have been used to fabricate decellularized corneal scaffolds include cat (Li et al., 2011), ostrich (Liu et al., 2016), bovine (Ponce Márquez et al., 2009; Zheng et al., 2018) goat (Nara et al., 2016) or dog (Feng and Wang, 2015).

Human corneas have been used in decellularization experiments (Alió del Barrio et al., 2018, 2015; Yam et al., 2016; Z. Zhang et al., 2015). While the use of human tissue does not have to face the same challenges of xenogenic tissues, the availability of such tissues is scarce. However, corneas deemed unsuitable for corneal transplantation due to

low endothelial cell count could be used to obtain decellularized scaffolds (Wilson et al., 2013). Furthermore, recent studies have focused on the use of discarded tissue after refractive surgeries as an alternative source (Yam et al., 2016; Yin et al., 2016). In this case, thinner tissues are decellularized which facilitate the removal of cellular components, compared to whole corneas.

Optimal parameters for decellularization

It is difficult to determine the optimal technique for decellularizing cornea due to the different researchers obtaining differing results despite using similar protocols. A number of papers have directly compared different decellularization techniques on cornea to determine the optimal technique. Shafiq et al., (2011) compared several different techniques and found that a combination of sodium chloride and nucleases was the best option for removing cellular components while still supporting the growth of new cells (Shafiq et al., 2012). Wilson et al., (2016) compared hyperionic, ionic and non-ionic detergents and concluded that increasing the efficiency of cell removal led to increased ECM damage (Wilson et al., 2016). For this reason it is still difficult to identify one specific methods that is closer to use in clinical practice.

In addition to the decellularization efficiency of these techniques, issues associated with gaining regulatory approval for clinical translation of corneas subjected to each technique has to be considered. For example, the use of detergents and nucleases may provide a barrier to the cornea's clinical use since there is a risk that any residual chemical could have a negative effect post-implantation. Non-chemical techniques may be more beneficial for gaining clinical approval but can be more expensive to operate.

2.5.2 Recellularization of the cornea

Once the removal of exogenous cells has been confirmed, it may be beneficial to repopulate these matrices with human cells to generate a viable cornea. The origin of the cells used for scaffold recellularization is an important issue to take into account. For every cell type found in the cornea, there are several potential sources, with benefits and drawbacks associated to each of them. There are reports of decellularized matrices being repopulated using immortalized cell lines (Diao et al., 2015; He et al., 2016; Xu et al., 2017) and while such cell types are acceptable for *in vitro* studies as a proof of concept, these should not be acceptable for transplantation. Cells modified to be passaged *ad*

infinitum pose the risk of tumour formation (Ramboer et al., 2014). Therefore, it is advisable to only use primary cultivated cells. This requires the initial isolation of cells from the patient or donor, further expansion in the laboratory, seeding of these cells onto the scaffold, culture/maturation of the newly cellularized organ and implantation into the patient. Recellularization of perfused organs such as the heart or the lungs have used the endogenous vasculature to reintroduce cells (Moser and Ott, 2014), however the cornea, being an avascular organ, relatively thin and containing 3 different cell types needs to be recellularized using other approaches. Potential cell sources for corneal recellularization are discussed in the following sections and are summarized in Table 2-3.

Table 2-3. Potential cell sources for cornea recellularization.

Cornea layer and cell source	**References**
Epithelium	
Limbal stem cells from unaffected contralateral eye biopsy	(Rama et al., 2010)
Oral mucosa	(Kolli et al., 2014; Nishida et al., 2004)
iPSCs	(Hayashi et al., 2012; Mikhailova et al., 2014; Vattulainen et al., 2019)
Stroma	
Keratocytes/Corneal Fibroblasts	(Diao et al., 2015; González-Andrades et al., 2011; Ma et al., 2015; Shafiq et al., 2012; Xu et al., 2017)
Adipose-derived MSC	(Alió del Barrio et al., 2018; Alió Del Barrio et al., 2017; Arnalich-Montiel et al., 2008; Du et al., 2010; Espandar et al., 2012; Lynch and Ahearne, 2017; S. Zhang et al., 2013)
iPSCs	(Naylor et al., 2016)
Endothelium	
Human endothelial cells	(Choi et al., 2010)
Human immortalized endothelial cells	(He et al., 2016)
iPSCs	(Wagoner et al., 2018)

Stroma

For the repopulation of the corneal stroma, autologous corneal stromal cells can be obtained from a small biopsy from the contralateral eye. Since these cells are from the patient, they are less likely to illicit an immune response. If both eyes are compromised, alternatives have to be found. Since the cornea is avascular, it is often considered to be an "immune privileged" organ so allogenic cells could be used with less risk of rejection compared to other organs. Alternatively a number of studies have examined the use of autogenic cells but from an extraocular source. Since keratocytes originate from the neural crest mesenchyme, other mesenchymal tissues have the potential to be differentiated into keratocytes. Mesenchymal stem cells derived from adipose tissues have been successfully induced to express corneal keratocyte markers such as ALDH3A1, keratocan, lumican and decorin (Arnalich-Montiel et al., 2008; Du et al., 2010; Espandar et al., 2012; Lynch and Ahearne, 2017; S. Zhang et al., 2013). Adipose-derived MSC have been used clinically as a cell therapy without a scaffolding material (Alió Del Barrio et al., 2017) and seeded onto decellularized human corneal stroma sheets (Alió del Barrio et al., 2018). The differentiation of induced pluripotent stem cells (iPSC) into keratocyte-like cells has been reported in the literature (Naylor et al., 2016). iPSCs were differentiated into neural crest cells and cultured on cadaveric human corneas into which the cells migrated and adopted a similar phenotype to keratocytes. This technique offers the opportunity for autogenic cell transplantation. There have been reports of oncogenic transformation of iPSCs (Gutierrez-Aranda et al., 2010) so the use of such cells for the treatment of low risk corneal diseases might not be recommended.

The stroma is the thickest layer of the cornea consisting of densely packed collagen fibrils. This structure makes it difficult for cells to penetrate and recellularize after decellularization. One approach to overcome this problem is to inject cells directly into the stroma, however the optimal procedure for doing this is unclear. Cell seeding densities, volume per injection and number of injections vary between publications with values for the final injected volume ranging from 12 µl in 2 µl injections (Xu et al., 2017) to 1 full ml in a single injection (Fu et al., 2010; Pang et al., 2010; Zhang et al., 2016). In addition, during decellularization tissues swell significantly making it difficult to inject more liquid (Lynch et al., 2016b). The number of cells seeded ranges in the literature from only 1200 and 4500 cells per construct (Diao et al., 2015; Xu et al., 2017) up to $1x10^5$, $4x10^5$ and $5x10^5$ cells (Fu et al., 2010; Shafiq et al., 2012; Zhang et al., 2016). It

is noteworthy that in multiple publications the final number of seeded cells is difficult to determine (Alió del Barrio et al., 2015; Yoeruek et al., 2012a). Furthermore, injections can disrupt the stromal fibril architecture and result in permanent damage (Moser and Ott, 2014).

The simplest method to recellularize the stroma is to seed cells directly on the surface of the decellularized scaffold. This approach relies on the capacity of the cells to migrate into deeper regions of the stroma. Gravity might also have an effect (i. e. the cells sink deep into the stroma). González-Andrades and colleagues showed repopulation of NaCl-decellularized porcine corneas with human keratocytes which were distributed similarly to the native counterparts (González-Andrades et al., 2011). More recently, Alió del Barrio *et al*. reported recellularization of 120 µm thick decellularized laminas with adipose-derived MSCs for 24 hours before implantation (Alió del Barrio et al., 2018). The authors did not shown the distribution of these cells on the scaffold. In addition, freeze-drying have been use to induce the formation of pores to increase the depth that cells can penetrate and repopulated the corneas *in vitro* (Pang et al., 2010).

While not commonly used for cornea, there are reports of bioreactors being used to aid in repopulating decellularized corneas with cells or as a culture method after initial seeding. Fu and colleagues used a magnetic stirrer to keep the construct in suspension during the culture period (Fu et al., 2010). The use of a rotary cell culture system for repopulating purposes has also been described in the literature, whereby the cells are encouraged to colonize the scaffold as they cannot attach elsewhere (Dai et al., 2012). A more sophisticated bioreactor system has been reported for the repopulation of the epithelium which mimicked and *in vivo* air-liquid interface (Z. Wu et al., 2014).

Another strategy is to recellularize the scaffolds *in situ* during transplantation. Ma and colleagues describe a method by which cells were seeded on thin sheets of decellularized porcine cornea as they were being placed on the bed of a lamellar keratoplasty (Ma et al., 2015). The procedure was repeated so that five layers had been deposited. When compared to the sheets without cells or a thicker acellular tissue, the recellularized sheets showed better results in terms of transparency and overall transplant success.

Epithelium

The corneal epithelium is constantly undergoing renewal from limbal epithelial stem cells (Li et al., 2007). If the limbus is damaged and the stem cells are lost, the patient can develop Limbal Stem Cell Deficiency (LSCD), resulting in conjunctivalization and neovascularization of the cornea (Dua et al., 2000). If the contralateral eye is not affected, a small biopsy can be taken and limbal stem cells can be isolated and expanded. These cells can then be transplanted onto the diseased cornea and replenish the stem cell niche (Rama et al., 2010). An alternative method has also been used in which there is no *in vitro* expansion and the small biopsies are fixed with fibrin glue around the edges of the cornea, away from the visual axis (Sangwan et al., 2012). This technique named Simple Limbal Epithelial Transplantation (SLET) is gaining use in developing countries as it is more economical (Basu et al., 2016). If both eyes are affected, allogenic cells or cells from the same patient but from an extraocular source, such as the oral mucosa, can be used (Kolli et al., 2014; Nishida et al., 2004). An alternative allogenic cell source are iPSCs differentiated into limbal epithelial stem cell-like cells (Hayashi et al., 2012; Mikhailova et al., 2014; Vattulainen et al., 2019). A first in human clinical trial has been performed in Japan using these cells (Cyranoski, 2019).

Decellularized corneas have been repopulated *in vitro* with epithelial cells, which rapidly attach and form a multi-layered epithelium, typically expressing cytokeratin 3 and 12 (Pang et al., 2010; Xu et al., 2008; Zhang et al., 2016). Better results have been reported when using a construct based on a decellularized porcine cornea repopulated with stromal and epithelial cells compared to the acellular construct in a one year anterior corneal transplant model in dogs (Xu et al., 2017). However, in this study a group with only stromal cells was not included and the implanted cells were not labelled, therefore the healthy epithelium was probably from the host. It is noteworthy, however, that results in the literature are inconclusive as to *in vitro* re-epithelialization of decellularized matrices before implantation in defects of the central cornea. Luo and colleagues seeded amniotic epithelial cells onto decellularized scaffolds and implanted them into an alkali burn rabbit model (Luo et al., 2013). When compared to an acellular scaffold, the pre-epithelialized construct was accepted better, probably due to the anti-angiogenic and anti-inflammatory factors secreted by the amniotic epithelial cells.

Endothelium

Corneal endothelial cells do not proliferate *in vivo* as they are arrested in the G_1 phase (Joyce et al., 1996b, 1996a). *In vitro*, however, endothelial cells can be isolated and expanded, and seeded onto carrier materials for transplantation. Multiple studies have investigated the optimization of culture conditions to promote proliferation and avoid endothelial-to-mesenchymal transition (Soh et al., 2017). The use of these cells relies on donor corneas and can only be done with allogenic cells. As for keratocytes and epithelial cells, human corneal endothelial-like cells have been obtained from iPSCs that could potentially be used for implantation (Wagoner et al., 2018).

Attempts have been made to use decellularized corneas as carriers for endothelial cell transplantation (Bayyoud et al., 2012; Choi et al., 2010; He et al., 2016; Ju et al., 2012a; Proulx et al., 2009; Xu et al., 2008). Choi and colleagues decellularized 110 µm-thick sections of human corneas with Triton X-100 and NH_4OH and seeded them with human endothelial cells for 14 days (Choi et al., 2010). The constructs expressed zonula occludens-1 (ZO-1), gap junction protein connexin-43 and Na^+/K^+-ATPase, markers of mature and functional corneal endothelium. Another study obtained decellularized sections using a femtosecond laser, seeded an endothelial cell-line and performed an *ex vivo* transplantation, demonstrating the potential for translation into the clinic (He et al., 2016). An alternative approach has been to use trypsin-decellularized crystalline lens capsules as it is a tissue usually discarded during cataract surgeries (Van den Bogerd et al., 2018).

Further remarks

While one would think that *in vitro* recellularization prior to implantation would be essential for positive outcome, there are several examples where the implantation of an acellular anterior cornea (i.e. host endothelium remained intact) has been successful (Amano et al., 2008; Hashimoto et al., 2015; Huang et al., 2017; Lin et al., 2008; Pang et al., 2010; Sasaki et al., 2009; Wu et al., 2009; Xu et al., 2008; Yam et al., 2016; M.-C. Zhang et al., 2015; Zhou et al., 2011). Most of these studies evaluate their success in terms of low immune reaction, little or no vascularization and transparency recovery. It is important to note that the surgical procedure in these studies was an intrastromal pocket or an anterior lamellar keratoplasty, i.e. the endothelium remained undamaged. The

repopulation of the acellular graft by host stromal cells is usually only assessed by simple histological staining and claims of infiltrating keratocytes are often inconclusive. Generally the epithelium is able to grow over the scaffolds with no major differences to the control, especially at the longer time-points. Other studies, however, show better results when comparing cell-containing scaffolds versus their acellular counterparts (Alió del Barrio et al., 2015; Diao et al., 2015; Luo et al., 2013; Ma et al., 2015; Xu et al., 2017). More studies need to be done to determine the necessity of recellularization, although eliminating the need for cells makes its potential translation to the clinic easier, with reduced costs and decreased risk of infection and disease transmission.

2.5.3 *In vivo* studies

While there has been considerable *in vitro* research undertaken to demonstrate the potential of decellularized and recellularized corneas as an alternative donor corneas for keratoplasties, the ultimate goal is to translate this research into the clinic to benefit patients. Prior to their use with patients, the cornea need to be tested in animal models *in vivo* to evaluate the host response to the implants. Following the successful outcome of animal models, a number of studies have recently entered clinical trials. This section will focus on the progress of decellularized corneas as transplants with the most up-to-date results of animal experiments and clinical data, which are summarized in Table 2-4.

Techniques used to assess outcome

Multiple techniques are used in *in vivo* experiments to assess the progress of an implant. These can be mainly divided into two groups: non-disruptive techniques used during the experiment and while the animal or patient is still alive, and terminal techniques, performed after the sacrifice of the animal (or in case of failure and the patient is re-transplanted).

Most of the techniques used during experiments to assess the implanted decellularized corneas are the same of those routinely by ophthalmologists after a real corneal transplant. Intraocular pressure (IOP) is routinely measured using a tonometer since increased IOP post transplantation can lead to glaucoma. Slit lamp biomicroscopy can be used to evaluate the thickness and transparency of the cornea. Optical coherence tomography (OCT) can also be used to measure thickness for all the cornea and obtain a

pachymetric map, i.e. a topographical map (Hurmeric et al., 2012). To assess health of the epithelium, the anterior surface is stained with fluorescein and imaged using blue light. Areas of debrided or damaged epithelium will appear fluorescent. Other parameters such as neovascularization, inflammation, infection are usually determined visually by trained personnel using a grading scheme (Faraj et al., 2016). A technique that is becoming popular in the recent times is laser scanning *in vivo* confocal microscopy. As it is a contact technique, in patients it is done under local topical anaesthesia while in animal models it is performed under total anaesthesia. This method allows the visualization with high resolution at all depths of the cornea without the aid of any enhancing contrast agents. It is the only technique that can be used to quantify nerve regeneration (Lagali et al., 2013a, 2013b).

Terminal techniques require the excision of the cornea. Despite being quite an old technique, histological staining with H&E provides useful information about the implant. This technique can assess epithelial health by allowing the number of cell layers and their morphology to be visualized, quantifying the repopulation of the implant by the surrounding stromal cells and identifying the presence of inflammatory cells in addition to examining other parameters. Other standard histological stains can also provide information about the ECM composition, such as Alcian Blue for GAGs and Picrosirius Red for collagens. Another method to obtain more information on the corneas is immunohistochemistry. The phenotype of quiescent keratocytes can be determined by positive staining of crystalline protein aldehyde dehydrogenase 3A1 (ALDH3A1) or transmembrane phosphoglycoprotein CD34. Presence of myofibroblasts, typical of fibrosis, can be detected by positive staining for alpha smooth muscle actin (α-SMA). Blood vessels can be identified staining for Platelet endothelial cell adhesion molecule (PECAM-1), also known as CD31, or for von Willebrand factor (vWF). The presence of Integrin alpha M ($\alpha_M\beta_2$), also known as CD11b, is a hallmark of the activity of the innate immune system. The fate of implanted cells can be determined by several different methods. Cells can be fluorescently labelled before implantation and this staining is still visible even after 12 weeks, as reported by Alió del Barrio and colleagues (Alió del Barrio et al., 2015). Another approach is to stain for species-specific markers when implanting cells from one species into a recipient of a different species. An example of this is the human nuclear antigen, which is located in human nucleoli but not in rodent nucleoli. The possibility of implanted cells undergoing apoptosis can be determined by the Terminal

deoxynucleotidyl transferase dUTP nick end labeling (TUNEL) assay which detects DNA fragmentation. On the other hand, proliferating cells can be detected by Bromodeoxyuridine (BrdU) labelling one hour prior to animal sacrifice. Cells synthesising new DNA will incorporate this synthetic nucleoside which can be detected with specific antibodies. By using electron microscopy more detailed information about the arrangement of the collagen fibrils can be obtained. Serial block face-scanning electron microscopy (SBF-SEM) and 3D reconstruction of the sections allows the visualization of cell distribution and lamellae arrangement with great resolution (Islam et al., 2018). X-ray scattering is another method to analyse the structure of the cornea and the orientation of fibrillar collagens (Aghamohammadzadeh et al., 2004).

Selection of animal models

The most common used animal model in research is the mouse. This is due to the relative low cost, short gestation period, large litter size and overall ease of housing. Furthermore, the abundance of genetically defined strains offers the possibility of studying immune responses in a mechanistic way (Yin et al., 2014). However, the size of the mouse ocular globe is rather small, hence it is rarely used for corneal studies. Rat models have been developed to study corneal rejection and immunomodulation with cell therapy, such as MSCs infusion (Maenz et al., 2011; Murphy et al., 2016; Treacy et al., 2014). Shafiq and colleagues have described the use of decellularized human cornea as a limbal graft in a rat laser induced limbal injury model (Shafiq et al., 2014).

While corneal transplants can be performed using mice and rats as experimental animal models, they are difficult surgeries and poorly model human corneas. For this reason, the rabbit remains the most commonly used animal model for corneal studies (Gwon, 2008). Rabbit eyes have a very similar anatomy to human eyes and are big enough to be operated with standard human surgical techniques. As a proof of concept many early studies using decellularized corneal tissue for transplantation were used in intrastromal pocket surgeries (Alió del Barrio et al., 2015; Amano et al., 2008; Du and Wu, 2011; Hashimoto et al., 2010; Ma et al., 2015; Pang et al., 2010; Sasaki et al., 2009; Xu et al., 2008; Yam et al., 2016; Yoeruek et al., 2012b; Zhou et al., 2011). This technique can give a good insight into the immune response generated by the scaffold and some information about the neighbouring cells' behaviour and migration into the implanted matrix. However, these surgeries are not routinely performed in the clinic, so for a more

translational approach anterior or deep anterior lamellar keratoplasties are more suitable. One of the first experiments in rabbits using decellularized corneal tissues was performed by Wu and colleagues in 2009 (Wu et al., 2009). They reported the use of PLA_2 decellularized porcine corneas on an anterior lamellar keratoplasty model in rabbits. The acellular grafts were re-epithelialized in one week, transparency recovered in less than 3 months and with no presence of neovascularization. Luo and colleagues decellularized corneas using 2 M NaCl and seeded amniotic epithelial cells (Luo et al., 2013). Tissue-engineered constructs implanted in rabbits showed better integration and transparency than the acellular counterparts. Detergent decellularized corneas were implanted intrastromally with no major signs of rejection or neovascularization and recovering transparency before 6 months post-implantation (Pang et al., 2010). Hashimoto and colleagues decellularized porcine corneas with high hydrostatic pressure and implanted them in a deep anterior lamellar keratoplasty model (Hashimoto et al., 2015). Scaffolds integrated completely into the host cornea, recovered transparency and showed no signs of inflammation or neovascularization. Re-epithelialization was slow and some keratocytes migrated into the scaffold. Porcine corneas decellularized using supercritical carbon dioxide have shown very promising results after grafting into rabbits (Huang et al., 2017). Transparency was achieved within 2 weeks and epithelium re-grew in a month. While these studies demonstrate the promise of decellularized corneas for use in transplantations, differences in the regenerative capacities of rabbit and human corneas should also be considered.

In addition to rabbits, other species have been used as animal models for corneal transplantation such as mini-pigs (Jangamreddy et al., 2018; Liu et al., 2009), cats (Boulze Pankert et al., 2014) and dogs (Xu et al., 2017). However, only one study has used the dog as a model for implantation of decellularized matrices as an alternative to human cadaveric donor corneas. Porcine corneas were decellularized using sodium deoxycholate and sodium orthovanadate and seeded with stromal and epithelial cells. Constructs were implanted in dogs and followed during a one year period. Recellularized scaffolds showed improved re-innervation, epithelial integrity and central corneal thickness.

Human studies

Despite being a recent approach, clinical studies have been carried out with decellularized corneal tissues. Alió del Barrio and colleagues recently reported the use of thin sections (laminas) of decellularized human corneas as intrastromal implants for advanced keratoconus patients (Alió del Barrio et al., 2018). Some of the laminas where seeded with autologous adipose-derived MSCs. Initial reports show improved visual acuity, corneal shape and topography, and patients recovered normal corneal thickness. The implanted tissue remained visible with OCT after 6 months and some signs of recellularization by host keratocytes detected by confocal biomicroscopy. The authors identified no positive effect from the recellularized tissues versus the acellular tissues.

Chinese company China Regenerative Medicine International Limited (CRMI) was granted a medical device registration certificate by the China Food and Drug Administration (CFDA) in 2015. Their product consists of a porcine cornea decellularized with 2 M NaCl, washed with 0.2% Triton X-100, dehydrated with glycerol, and irradiated with Co^{60} to ensure sterility (Luo et al., 2013). In a first study in 2015, Zhang and colleagues reported the outcome of 47 patients with fungal corneal ulcers treated with such product (M.-C. Zhang et al., 2015). Irritation and neovascularization scores improved as did the transparency of the graft, originally hazy. Another short-term study using this product has been reported for the treatment of herpes simplex keratitis with generally positive results, albeit some patients needing re-grafting of human allograft transplantation due to scaffold dissolution (Zheng et al., 2019). Another recent study used this product in 27 patients suffering from different infectious keratitis (Li et al., 2019). Graft transparency and patient's visual acuity improved. Some repopulating keratocytes were identified via in vivo confocal microscopy at 3 and 6 months post-implantation. The company has also recently reported the implantation of scaffolds obtained via a different decellularization method that better preserves transparency and fibril architecture (Shi et al., 2019). When implanted in patients suffering from infectious keratitis, their visual acuity improved.

Being a relatively new field, there is still much research and optimization needed before these corneas can be accepted as valid alternatives to real corneas for keratoplasty. Most of the decellularization techniques discussed can only be done in small batches, at a laboratory scale. Efforts are required to automate the optimized decellularization protocols under sterile conditions at a larger scale. Furthermore, an international

consensus is required to assess the quality of these scaffolds in terms of xenogenic or allogenic cell removal and ECM preservation. It would be beneficial to identify the most appropriate cell source for specific corneal transplants and how best to deliver these cells to recellularize the scaffolds. Good manufacturing practices (GMP) should be ensured in all steps and correct storage and transportation organized in a similar fashion as in current eye banking. If recellularization is not necessary for a specific application, then off-the-shelf scaffolds can be developed. In all cases, these alternative scaffolds should show similar if not improved efficacy to keratoplasties.

Table 2-4. Summary of *in vivo* studies using decellularized corneas (SDS: sodium dodecyl sulfate, SDC: sodium deoxycholate, ALK: anterior lamellar keratoplasty, Y: recellularized, N: not recellularized).

Origin of cornea	Decellularization type	Details of decellularization	Surgical procedure	Recipient species	Cells (Y/N)	Details about cells	Reference
Porcine	Physical	Nitrogen gas	Intrastromal pocket	Rabbit	N	-	(Amano et al., 2008)
Porcine	Chemical + Physical	SDS + sodium orthovanadate	ALK	Rabbit	Y	Human immortalized stromal cells injected and cultured for 3 days prior to implantation	(Diao et al., 2015)
Porcine	Chemical + Biological	Triton + Dispase + Trypsin	Intrastromal pocket	Rabbit	N	-	(Xu et al., 2008)
Porcine	Physical	High hydrostatic pressure	Intrastromal pocket	Rabbit	N	-	(Sasaki et al., 2009)
Porcine	Chemical	SDS	Intrastromal pocket	Rabbit	N	-	(Pang et al., 2010)
Porcine	Chemical	SDS	Intrastromal pocket	Rabbit	N	-	(Du and Wu, 2011)
Porcine	Chemical	Phospholipase A2	Interlamellar keratoplasty	Rabbit	N	-	(Xiao et al., 2011)
Porcine	Chemical	SDS	Intrastromal pocket	Rabbit	N	-	(Zhou et al., 2011)
Porcine	Chemical	SDS	Intrastromal pocket	Rabbit	N	-	(Yoeruek et al., 2012b)
Porcine	Chemical	NaCl + Triton X-100	Intrastromal pocket and ALK	Rabbit	Y	Rabbit amniotic epithelial cells for ALK cultured for 1 week before implantation	(Luo et al., 2013)
Human	Chemical	SDS	Intrastromal pocket	Rabbit	Y	Human adipose-derived MSC injected into the stroma and cultured 5 days before implantation	(Alió del Barrio et al., 2015)
Porcine	Physical	High hydrostatic pressure	ALK	Rabbit	N	-	(Hashimoto et al., 2015)
Porcine	Chemical	NaCl	Intrastromal pocket	Rabbit	Y	Keratocytes in suspension sandwiched between sheets of	(Ma et al., 2015)

						decellularized tissue during surgery (species not stated)	
Human	Chemical	SDS	Intrastromal pocket	Rabbit	N	-	(Yam et al., 2016)
Porcine	Physical	High hydrostatic pressure	Intrastromal pocket	Rabbit	N	-	(Hashimoto et al., 2016)
Porcine	Chemical	SDC + sodium orthovanadate	ALK	Dog	Y	Human epithelial and stromal cells	(Xu et al., 2017)
Human	Chemical	SDS	Intrastromal pocket (indication: advanced keratoconus)	Human	Y	Human adipose-derived MSC cultured for 24h prior to implantation	(Alió del Barrio et al., 2018)
Porcine	Physical	High hydrostatic pressure	Intrastromal pocket	Rabbit	N	-	(Hashimoto et al., 2010)
Porcine	Chemical	NaCl + Triton X-100	ALK (indication: fungal ulcers)	Human	N	-	(M.-C. Zhang et al., 2015)
Porcine	Biological	Phospholipase A2	ALK	Rabbit	N	-	(Wu et al., 2009)
Cat	Chemical + Biological	Phospholipase A2 + SDC	Tectonic ALK	Rabbit	N	-	(Li et al., 2011)
Porcine	Chemical	Glycerol + EDC/NHS crosslinking	ALK in infectious keratitis model	Rabbit	N	-	(Lin et al., 2017)
Porcine	Biological + Physical	Human serum + electrophoresis	Intrastromal pocket	Rabbit	N	-	(Shao et al., 2015)
Porcine	Biological + Physical + Chemical	Trypsin + freeze-thawing + NaOH	ALK	Rabbit	N	-	(Lin et al., 2008)
Porcine	Chemical	NaCl + Triton X-100	ALK (indication: herpes simplex keratitis)	Human	N	-	(Zheng et al., 2019)
Porcine	Chemical	NaCl + Triton X-100	ALK (indication: infectious keratitis)	Human	N	-	(Li et al., 2019)
Porcine	Physical + Chemical	High hydrostatic pressure + sodium lauroylglutamate	ALK (indication: infectious keratitis)	Human	N	-	(Shi et al., 2019)

2.5.4 Further approaches for the use of decellularized cornea in tissue engineering

There have been a few novel approaches to generating corneal scaffolds that combine decellularization with other material fabrication techniques. For example, one approach has been to embed a decellularized lenticule in a compressed collagen I hydrogel to improve the hydrogel's mechanical properties, susceptibility to degradation and suturability, while maintaining its excellent cytocompatibility in a LESC deficiency model in rabbits (Hong et al., 2018).

Hydrogels obtained from the solubilisation of ECM obtained from decellularized organs has been pioneered by the group led by Stephen Badylak. To form these hydrogels, organs are decellularized, lyophilized, ground into a powder and digested in acidic pepsin to form a solubilized ECM. By neutralizing the pH of the solution and raising the temperature to 37 °C fibrillation is induced. Hydrogels following this method have been obtained from many organs including urinary bladder matrix (Freytes et al., 2008), dermis (Wolf et al., 2012), pancreas (Gaetani et al., 2018; Odorico et al., 2018), myocardium (Johnson et al., 2011; Ungerleider et al., 2015), skeletal muscle (Ungerleider et al., 2015), demineralized bone (Sawkins et al., 2013), small intestinal submucosa (Voytik-Harbin et al., 1998), liver (Lee et al., 2017), cartilage (Pati et al., 2014), adipose tissue (Pati et al., 2014) and kidney (Magno et al., 2017). This approach allows for the injection of these hydrogels into the diseased site due to their shear thinning properties and opens the door for their use in 3D bioprinting. Hydrogels obtained from decellularized corneas have been reported in the literature (Ahearne and Coyle, 2016; Ahearne and Lynch, 2015; Kim et al., 2019b; Lu et al., 2015). Since these hydrogels are quite weak, post-gelation cross-linking can be performed, for example using a UVA-riboflavin technique similar to the technique used clinically on patients suffering from with keratoconus (Ahearne and Coyle, 2016). The decellularization technique used also needs to be considered as this can a significant effect on the hydrogels final physical and biological characteristics (as will be seen in Chapter 6). Kim and colleagues recently reported 3D bioprinting of decellularized cornea ECM (Kim et al., 2019b), which were more transparent than their collagen I counterpart. Furthermore, they have described a way of aligning the collagen fibrils during the printing process (Kim et al., 2019a). Cells in the aligned constructs presented increased expression of keratocyte markers keratocan and ALDH. Collagen and ECM-derived hydrogels are usually highly hydrated, which makes them mechanically

weak and less resembling the native tissue. Therefore, some researchers have developed strategies to increase the protein concentration, for example plastic compression. In a recent report, Hong and colleagues presented scaffolds formed from the plastic compression of different mixtures of type I collagen and decellularized cornea ECM hydrogels (Hong et al., 2019). Increasing the content of the cornea ECM fraction resulted in increased transparency and light transmittance due to the reduced fibril diameter, but also reduced mechanical strength. They also fabricated a construct with embedded keratocytes and further seeded epithelial cells on the surface, obtaining an anterior cornea model.

ECM in the form of particles has been incorporated into different biomaterials to generate scaffolds for several different types of tissue. In these scaffolds the ECM is used to provide biochemical cues and support biological functions rather than construct a 3D environment (Brown et al., 2012; Edgar et al., 2018; Kruper et al., 2013; LeCheminant and Field, 2012). Recently tissue-derived microparticles from the lymph nodes, cartilage and cornea were compared for their potential to improve corneal wound healing (Yin et al., 2019a). *In vitro* these particles decreased TNFα and MMP9 expression by keratocytes induced by exogenous IL-1β. *In vivo* experiments were performed using the lymph node particles as they showed better in vitro effects on epithelial and conjunctival cells, in terms of tear protein production and reduction of inflammation. The particles were applied on an anterior lamellar keratoplasty model in a rabbit using fibrin glue as a carrier. In a subsequent study, the particles were applied to an *ex vivo* model of keratoconus, obtained by weakening the stroma with Chondroitinase ABC (Yin et al., 2019b). The treatment improved mechanical properties, increased collagen fibril density and promoted the expression of several keratocyte markers.

2.6. Summary

Alternatives to current gold standard of severe corneal diseases need to be found due to the severe donor shortage. Tissue engineering approaches can offer a solution to this issue by fabricating corneal substitutes. Tissue engineering strategies are based on the interplay between cells, materials and modulators, such as physical and biochemical cues. Growth factors and other biomolecules have an important role during wound healing and during *in vitro* culture. Therefore, knowing the effect of these cues on human

keratocytes is crucial to modulating cell behaviour in scaffolds. As was described in the literature review, many growth factors have been studied but very few studies have investigated the role of each of them individually in a basic basal medium. Therefore, the first study of this thesis is a thorough investigation of biochemical cues influencing serum-expanded stromal cells into recovering quiescence and expression of keratocyte markers. Decellularized corneas have enormous potential to be used as alternatives to traditional donor corneas and could help alleviate the shortage of donor corneas suitable for transplantation worldwide. However, it is important to identify a good recellularization protocol, as reports in the literature are quite varied. For that reason, in the second study of this thesis, *in vitro* recellularization of decellularized thick sections of cornea is investigated and further analysed in an *in vivo* model in rabbits. Alternative techniques for using decellularized tissues need to be explored in order to expand the repertoire of options for corneal tissue engineering. The third study focuses on the fabrication of a layered corneal construct based of thin sheets of decellularized corneal tissue and cell-laden collagen hydrogels. Hydrogels are widely used in tissue engineering and can be obtained by the solubilisation of decellularized tissues. However, the influence that detergents used for decellularization have on the final gels has not been widely studied. Therefore, the fourth study describes the impact of decellularization methods on the characteristics of ECM-derived hydrogels.

CHAPTER 3

Influence of biochemical cues in human corneal stromal cell phenotype

3.1. Introduction

As described in the Literature Review, due to a shortage of donor corneas for transplantation, alternatives to donor allografts are being developed such as cell-based therapies and tissue engineering strategies (Ghezzi et al., 2015; Griffith et al., 2016). To successfully develop new cell-based therapies, a suitable cell source is required. For injuries or diseases affecting the corneal stroma, keratocytes, the main cell type in the stroma that has characteristics associated with mesenchymal stromal cells, are the logical choice of cells for corneal regeneration. To obtain a large enough number of stromal cells required for cell-based therapies or tissue engineering, the cells must be expanded *in vitro* normally using serum-supplemented media. When keratocytes are exposed to serum, they become fibroblastic recapitulating the *in vivo* process of wound healing. Upon serum activation there is a change in morphology from a dendritic shape to an elongated spindle morphology and markers associated with the native keratocyte phenotype such as crystalline ALDH3A1 and keratin sulphate proteoglycans such as keratocan are lost (Jester et al., 1999). When treated with TGF-β1 corneal fibroblasts transition to a myofibroblast phenotype, becoming larger and expressing α-SMA. These two distinct phenotypes are fairly easy to obtain *in vitro* from isolated corneal stromal cells via the supplementation of medium with FBS for fibroblasts and addition of TGF-β1 for myofibroblasts. Although some studies have reported a partial reversal to a keratocyte-like phenotype using serum-free media (Berryhill et al., 2002; Lynch et al., 2016a; Sidney and Hopkinson, 2016; Wilson et al., 2012), there is still a lack of information on how individual media supplements such as vitamins or growth factors affect this process.

The aim of this study was to examine the effect of several biochemical reagents, ranging from small molecules to proteins, on the phenotype and activity of serum-expanded human corneal stromal cells when switched to a serum-free media. By doing

this, the role of individual biochemical cues on the ability to restore a keratocyte phenotype *in vitro* can be examined.

3.2. Material and Methods

3.2.1 Cell isolation

Cells were isolated from the healthy donor's corneal-scleral ring remaining after a corneal transplant in accordance with the Declaration of Helsinki. The use of human cornea tissue with donor consent for isolating cells received ethical approval from the Trinity College Dublin, University of Dublin, School of Medicine Research Ethics Committee. The corneal-scleral rings were rinsed with sterile Phosphate Buffered Saline (PBS) and the sclera, epithelium and endothelium were carefully removed using a scalpel blade. After a brief wash with sterile PBS, the corneal stroma was diced into small pieces, transferred into 25cm^2 culture flasks and let attach to the plastic. Media consisting of low-glucose Dulbecco's Modified Eagle Medium (DMEM, Hyclone) supplemented with 10% Foetal Bovine Serum (FBS, Gibco) and 2% Pen/Strep (Invitrogen) was added and the stromal pieces were cultured at 37 °C and 5% CO_2 in a humidified incubator. Media was changed regularly until cells had migrated from the tissue and reached 80-90% confluence, then they were passaged to allow further expansion. Cells in this study were used at passage 4 from cryopreserved expanded cells from one single donor.

3.2.2 Cell culture conditions

Cells from a single donor were harvested and seeded at 10,000 cells per cm^2 using low-glucose DMEM +10% FBS and let attach overnight. The following day media was switched to DMEM/F12 (glucose concentration: 3.15 mg/ml, Hyclone) for a 3 day serum-starvation period, after which one of the following biochemical factors was added with the following concentrations: 100 µg/ml ascorbic acid (AA, Sigma); 0.1 µM retinoic acid (RA, Sigma); 10 ng/ml fibroblast growth factor 2 (FGF-2, R&D); 50 ng/ml platelet derived growth factor BB (PDGF-BB, Preprotech); 50 ng/ml Insulin-like Growth Factor 1 (IGF-1, ProSpec); 10 ng/ml transforming growth factor β1 (TGF-β1, ProSpec); 0.1 ng/ml transforming growth factor β3 (TGF-β3, R&D); 1x insulin-transferrin-selenium (ITS, Gibco) and 10^{-5} M 3-isobutyl-1-methylxanthine (IBMX, Sigma). Control groups were cells cultured in serum-free DMEM/F12 only and cells cultured in DMEM/F12 supplemented with 10% FBS. Medium was changed every two days for culture periods

of 1, 7 and 14 days. Images of the cells were recorded over the culture period using an Olympus IX83 microscope.

3.2.3 Metabolic activity

Metabolic activity was assessed by the PrestoBlue assay (Invitrogen) following the manufacturer's instructions. 96-well plates were seeded separately for each time-point (day 1, 3, 7 and 14). Media was removed and 100 µl PrestoBlue working solution (1x from a 10x stock) was added and incubated at 37 °C for 1 hour. The plates were analysed on a plate reader (BioTek™ Synergy HTX) by measuring the absorbance at 570 nm and 600 nm. Metabolic activity was calculated relative to the serum-free medium condition.

3.2.4 Gene expression

RNA from cultures was isolated using Trizol, according to the manufacturer's instructions (Invitrogen). Briefly, 1 ml of Trizol was added to the monolayer and a cell scrapper was used to detach the cells. 200 µl of chloroform were added, vortexed and centrifuged at 12000g at 4 °C. The supernatant was transferred to a new RNAse-free tube to which the same volume of isopropanol and 4 µl of Glycoblue (Applied Biosystems) were added. After an overnight incubation at -20 °C, tubes were centrifuged at 12000g for 15 minutes at 4 °C. The supernatant was discarded and 1 ml 70% ethanol was added and vortexed to wash the pellet. After a second centrifugation step of 12000g for 15 minutes at 4 °C, the ethanol was removed, the pellet was air dried and dissolved in 11 µl of RNAse-free water. RNA yield and purity was quantified using a NanoDrop-1000 (ThermoFisher).

A high capacity cDNA reverse transcription kit (Invitrogen) was used to reverse transcribe 500 ng of RNA using a thermocycler. Real-time PCR of the resultant cDNA was performed using TaqMan gene expression assay primers and TaqMan Universal Master Mix II (all Applied Biosystems). The primers examined were glyceraldehyde-3-phosphate dehydrogenase (*GAPDH*, Hs02758991_g1), aldehyde dehydrogenase 3A1 (*ALDH3A1*, Hs00964880_m1), alpha smooth muscle actin (*ACTA2*, Hs00426835_g1), keratocan (*KERA*; Hs00559942_m1) and collagen 1a1 (COL1; Hs00164004_m1). Each gene of interest was normalized against *GAPDH* using the ΔΔCt method. Calculated values were expressed as a power of $2^{-\Delta\Delta Ct}$. For this study, all values were normalized to the serum-free controls at each time-point.

3.2.5 Immunochemistry

Cells were fixed with 4% Paraformaldehyde (PFA) for 15 minutes, followed by three washes with PBS and stored at 4 °C until further staining. Blocking and permeabilization were carried out in a single step using 2% FBS and 0.5% Triton X-100 diluted in PBS for 30 minutes at room temperature, followed by three washing steps with PBS. Primary antibodies were incubated overnight at 4 °C. Concentrations were used as follows: ALDH3A1 (Abcam) 1:250, keratocan (Santa Cruz) 1:100, α-SMA (Abcam) 1:250. After three washes with PBS, samples were incubated with the secondary antibody and phalloidin-rhodamine for 1 hour at room temperature. Samples were washed three times with PBS and incubated for 10 minutes with DAPI. Images were obtained using an Olympus IX83 microscope.

3.2.6 Flow cytometry

Cell phenotype was further assessed by flow cytometry. Data was acquired using an LSRFortessa (BD Biosciences) flow cytometer and then analysed using FlowJo software (Tree Star Inc.). Cells were trypsinized and resuspended in 150 µl of 2% FBS in PBS and 50 µl of cell suspension was used for the staining. 1 µl of each of the following fluorophore-coupled antibodies was added to the cell suspension: CD34-allophycocyanin (APC), CD44-eFluor450, CD45-fluorescein isothiocyanate (FITC), CD73-PerCP-eFluor710, CD90-phycoerythrin (PE) and CD105-PE-Cy7 (all eBiosciences), and the final volume was adjusted to 100 µl (so that antibodies were used at 1:100 dilution). Samples were vortexed and incubated at 4 °C for a minimum of 30 minutes. Unstained controls were treated the same way. Compensation beads (eBiosciences) were stained with each fluorophore-coupled antibody. Two washing steps were performed to remove unbound antibodies. The remaining pellet was resuspended in 300 µl of buffer and 5 µl of propidium iodide was added to recognize and exclude dead cells.

3.2.7 Wound healing assay

To assess the influence of biochemical cues in migration of human corneal keratocyte-like cells a scratch assay was performed. Cells were seeded in 6 well plates at a density of 10,000 cells per cm^2 in expansion media, which was changed regularly until confluent. Cells were then serum-starved using DMEM/F12 for 3 days. A “scratch” was applied to the monolayer with a 200 µl pipette tip, which resulted in a cell-free area. Cells were then cultured in media containing each of the molecules to be tested, having 2 controls: one serum-free only and one containing 10% FBS. Cells were imaged on the

same area every day for 7 days using phase contrast imaging in an inverted microscope (Olympus IX83) coupled to a digital camera. The cell-free area at each time-point was calculated using ImageJ (NIH) by finding the edges, adjusting the threshold, binarizing the images and selecting the cell-free areas with the tracing tool. The wound closure was calculated using the following formula:

$$\frac{cell\ free\ area\ t_0 - cell\ free\ area\ t_x}{cell\ free\ area\ t_0} \times 100$$

3.2.8 Statistical analysis

All experiments were performed three times using a minimum of three replicates, unless otherwise stated. Statistical analyses were performed using GraphPad Prism Software 5.0 (GraphPad Software, Inc. La Jolla, CA). All data are presented as the mean ± SD. To determine statistical significance one-way ANOVA with Dunnet post-hoc analyses were performed. Differences were considered to be statistically significant at $p \leq 0.05$.

3.3. Results

3.3.1 Effect of biochemical cues on metabolic activity

Metabolic activity under the induction of each biochemical cue was analysed using the PrestoBlue® assay and used as an estimate for cell proliferation (Figure 3-1). The addition of FBS to the medium had a remarkable effect on proliferation, increasing 591% ± 131% (average ± SD) at day 7 compared to the serum-free control. TGF-β1 increased proliferation significantly from day 3 onwards, achieving values of 199% ± 29% by day 14. A similar trend was observed when cells were treated with TGF-β3, which increased proliferation at day 7 (164% ± 31%) and day 14 (203% ± 74%). IGF-1 increased proliferation significantly at day 3 (136% ±19%) and day 7 (144% ± 25%) but then the effect appeared to stagnate. ITS promoted proliferation after one (156% ± 20%) and two weeks in culture (181% ± 94%). The rest of treatments did not have a positive nor negative effect on cell metabolic activity when compared to the control. Another way of assessing proliferation, instead of relying on metabolic activity, could be quantifying Ki67-positive cells via immunocytochemistry.

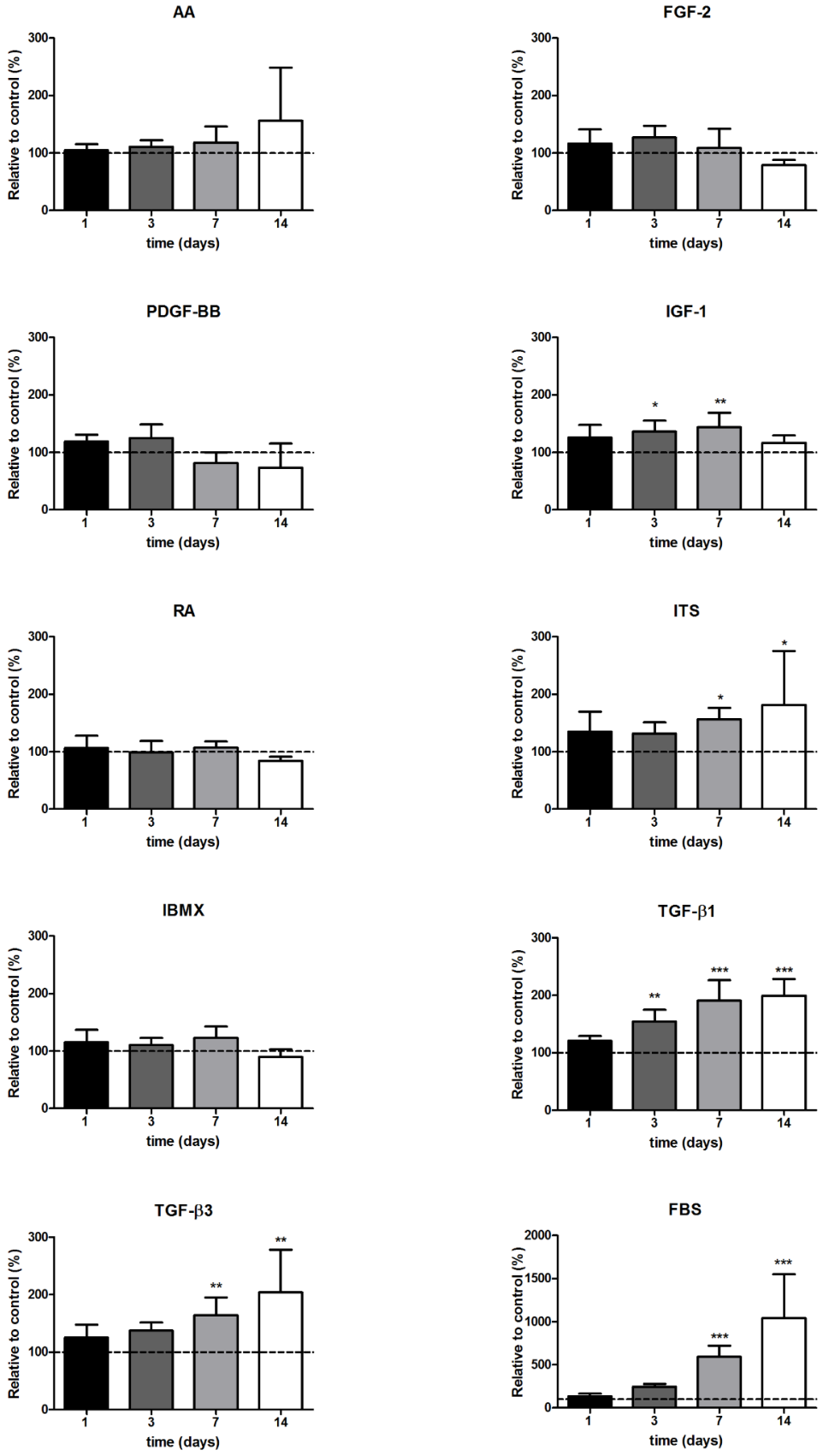

Figure 3-1. Effect of treatment on metabolic activity of human corneal stromal-derived cells (n = 6). Dotted line indicated control (* $p < 0.05$, ** $p < 0.01$, *** $p < 0.001$).

3.3.2 Effect of biochemical cues on cell morphology

Removal of serum from the medium had an effect on cell morphology, with the cells becoming smaller and the appearance of dendrites (Figure 3-2). This morphology resembles that of quiescent keratocytes *in vivo*. More cells adopt this morphology upon the addition of IGF-1, AA, RA, ITS or IBMX. The addition of PDGF-BB induced the cells to cluster and adopt a very elongated spindle shape. FGF-2 maintained a fibroblastic-like morphology, with very few sparse cells having processes. TGF-β1 and TGF-β3 induced cells to adopt a spread-out shape with some cells becoming polygonal and stress fibres visible. Cells cultured with FBS maintained a spindle shape.

3.3.3 Effect of biochemical cues on cell phenotype

Removal of serum from the medium led to an increased expression of keratocyte markers ALDH3A1 and keratocan when compared to cells cultured in serum-supplemented media (Figure 3-3). None of the biochemical reagents had a significantly positive effect on *ALDH3A1* expression when compared to the serum-free control. TGF-β1, PDGF-BB and FBS down-regulated the expression of this gene. The expression of keratocan was significantly up-regulated upon treatment with AA and IBMX after 14 days of induction (3.82 ± 1.87 and 3.99 ± 4.58, respectively; average ± SD). RA, ITS and IGF-1 also up-regulated this marker, but to a limited extent ($p > 0.05$). FGF-2, PDGF-BB, TGF-β1 and TGF-β3 did not have a significant effect, while FBS down-regulated the expression of keratocan. Expression of collagen I (*COL1*) was increased significantly at time-point day 1 with the addition of IGF-1, TGF-β1 and TGF-β3 (1.74 ± 0.28, 1.54 ± 0.34, 1.73 ± 0.11, respectively; average ± SD). At later time-points only AA and ITS increased significantly this gene's expression (3.82 ± 0.20, 3.00 ± 0.44, respectively; average ± SD). TGF-β1 up-regulated significantly the expression of *ACTA2* at all time-points tested (8.74 ± 2.29 at day 1, 7.55 ± 2.46 at day 7 and 4.33 ± 1.87 at day 14; average ± SD). TGF-β3 had the same effect as TGF-β1, with very similar fold changes compared

with the serum-free control (8.42 ± 4.78 at day 1, 4.36 ± 3.43 at day 7 and 3.26 ± 2.14 at day 14; average ± SD). Levels of myofibroblastic marker *ACTA2* did not change much over time, for all other treatments.

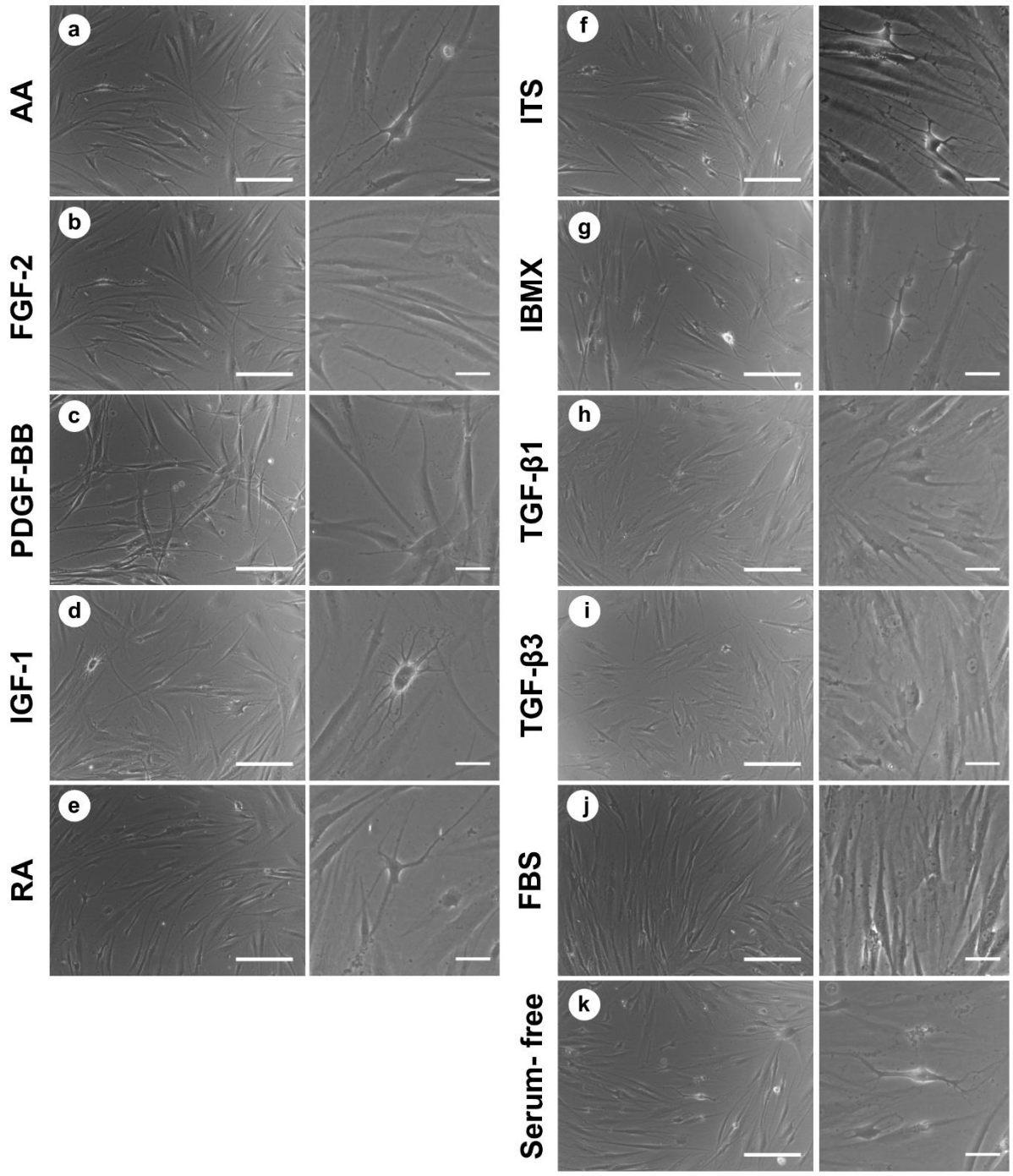

Figure 3-2. Morphology of cultured cells under the induction of studied biochemical cues after 14 days in culture: (a) ascorbic acid; (b) FGF-2; (c) PDGF-BB; (d) IGF-1; (e) retinoic acid; (f) insulin-transferrin-selenium; (g) IBMX; (h) TGF-β1; (I) TGF-β3; (J) foetal bovine serum; (k) serum-free control. Low magnification scale bar = 200 µm, high magnification scale bar = 50 µm.

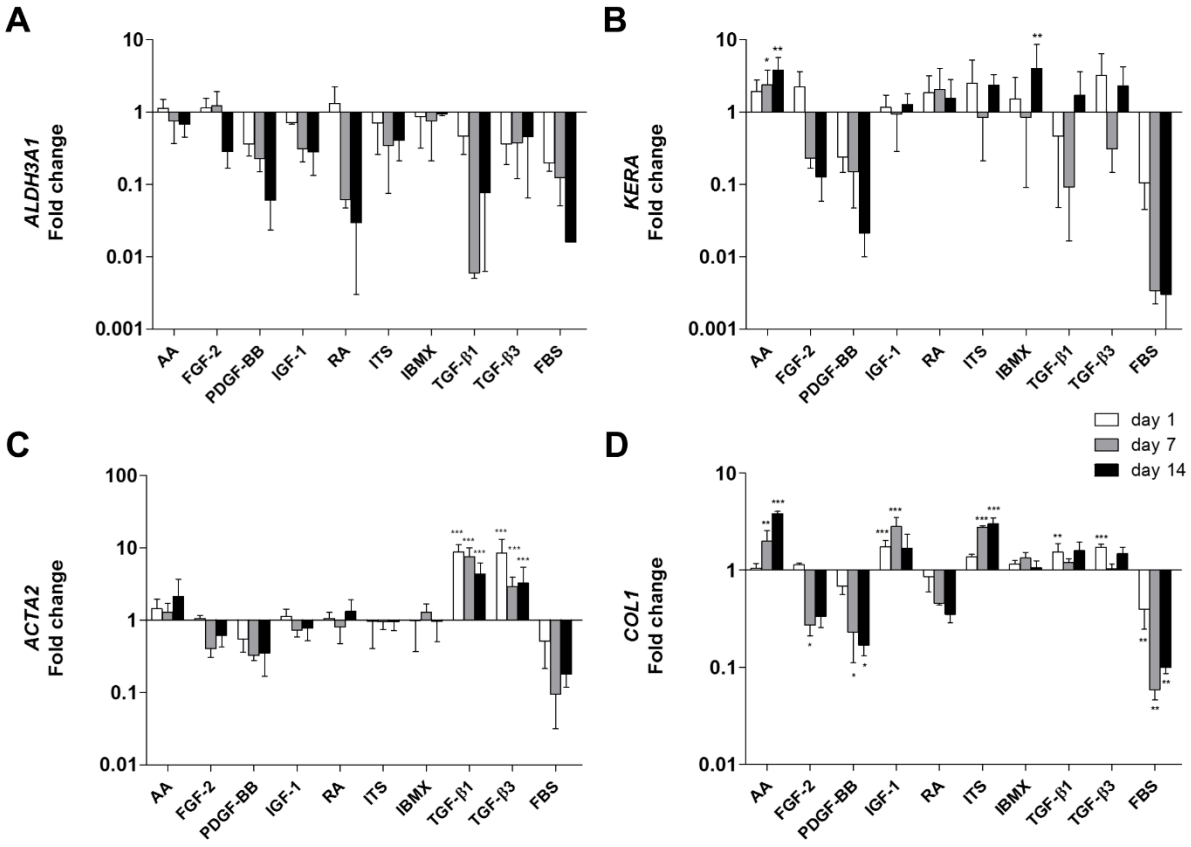

Figure 3-3. Effect of tested treatments on the expression of a) ALDH3A1, b) KERA, c) ACTA2 and d) COL1 as determined by qPCR relative to serum-free control at each time-point (n =5–10). p* < 0.05, p** < 0.01, p*** < 0.001.

Expression of these markers was further analysed qualitatively with immunochemistry. While expression of ALDH3A1 was down-regulated at the mRNA level, staining showed positive cells in some conditions. Cells with a dendritic morphology showed more intense staining, especially when treated with ITS, IGF-1, IBMX, RA and in the serum-free control. Very low staining was seen in cultures treated with PDGF-BB, FBS, TGF-β1 and TGF-β3 (Figure 3-4 A). Immunostaining of keratocan showed faint cytosolic staining in all conditions. When cells were treated with IGF-1, IBMX, ITS and RA, bright perinuclear staining was observed (Figure 3-4 B). However, keratocan is a keratin sulphated proteoglycan that is deposited as ECM, hence was probably washed away during cell feedings. Expression of α-SMA correlated with expression of its gene *ACTA2*. Bright α-SMA stress fibers can be observed in cells treated with TGF-β1 and TGF-β3. Very sparse α-SMA^{+} cells were seen in treatments with AA and ITS (Figure 3-4 C).

After 7 and 14 days in culture, cell surface markers were analysed and quantified by flow cytometry (Table 3-1). Typical markers used for the identification of

mesenchymal stromal cells were employed. CD34 was found to change the most for each treatment. After 7 days of treatment, the serum-free controls presented 9.13% of the population positive for this marker, while treatment with AA, IBMX, IGF-1, ITS and RA increased this percentage considerably (14.03, 10.81, 9.52, 13.55 and 31.75%, respectively). This trend was maintained and increased after 14 days. However, only treatment with RA increased the $CD34^+$ population significantly. Other biochemical cues led to a reduction in the percentage of positive CD34 cells by day 7 (FBS: 0.08%, PDGF-BB: 0.47%, TGF-β1: 1.62% and TGF-β3: 2.09%) and day 14 (FBS: 1.47%, PDGF-BB: 1.49%, TGF-β1: 5.15% and TGF-β3: 5.03%). CD73 remained >90% positive and was only reduced when treated with FBS and PDGF-BB (78.23% and 86.90%, respectively at day 7). After 14 days in culture, this marker remained positive (>90%) in all conditions. CD90 was >95% positive in all conditions, and most conditions induced an expression of >99%. Expression of CD90 remained positive after 14 days (>90%). Expression of CD105 also remained positive (>88%) at culture time 7 days and 14 days. CD45 was <2% in all conditions at day 7 and <3.5% at day 14. CD44 was highly expressed (>95% positive) in all conditions at day 7 without any noticeable difference among groups and remained positive after 14 days of treatment.

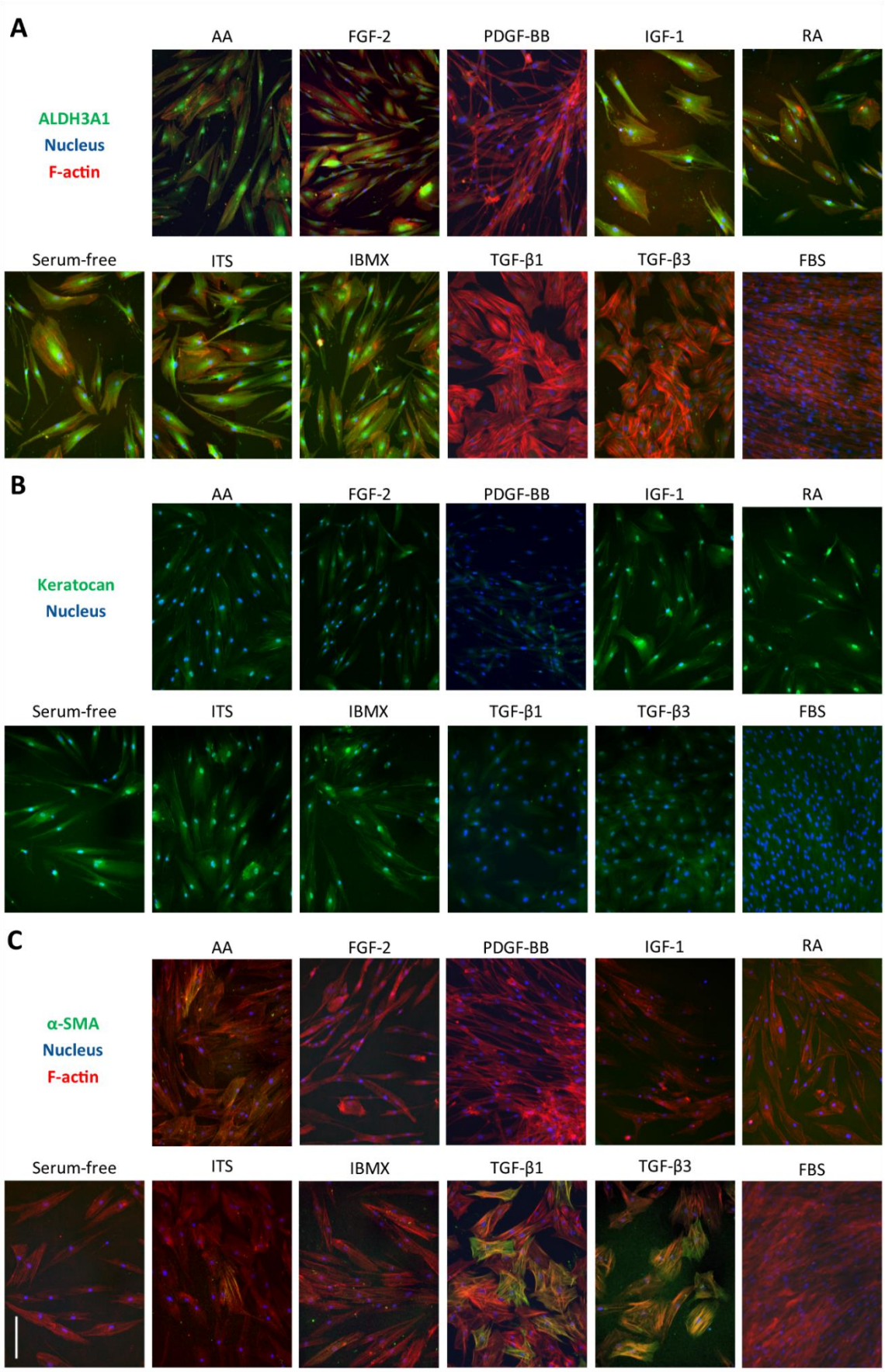

Figure 3-4. Effect of biochemical cues on the expression of markers determined by immunofluorescence after 14 days of treatment. a) ALDH3A1 (green), nuclei (blue) and F-actin (red). b) Keratocan (green), nuclei (blue). c) α-SMA (green), nuclei (blue) and F-actin (red). Scale bar = 200 µm.

Table 3-1. Cell surface marker expression after 7 and 14 days of treatment (n = 4). Data shown as average ± standard deviation. *** p < 0.001.

DAY 7	CD34	CD44	CD45	CD73	CD90	CD105
Serum-free	9.13% ± 0.05	95.15% ± 0.03	1.21% ± 0.01	92.05% ± 0.04	97.98% ± 0.02	88.20% ± 0.04
AA	14.03% ± 0.10	97.60% ± 0.03	0.79% ± 0.01	91.93% ± 0.06	99.10% ± 0.01	90.23% ± 0.08
FGF-2	8.09% ± 0.08	98.58% ± 0.01	1.48% ± 0.01	95.15% ± 0.03	99.50% ± 0.01	93.13% ± 0.05
PDGF-BB	0.47% ± 0.01	97.58% ± 0.04	0.68% ± 0.01	86.90% ± 0.07	98.50% ± 0.02	89.60% ± 0.06
IGF-1	9.52% ± 0.03	98.43% ± 0.01	0.80% ± 0.01	91.00% ± 0.06	99.03% ± 0.01	95.20% ± 0.03
RA	31.75% ± 0.08 (***)	98.23% ± 0.01	0.91% ± 0.01	93.58% ± 0.05	99.40% ± 0.00	92.75% ± 0.04
ITS	13.55% ± 0.07	98.83% ± 0.01	1.58% ± 0.02	91.15% ± 0.08	99.30% ± 0.01	95.95% ± 0.02
IBMX	10.81% ± 0.05	98.18% ± 0.01	1.21% ± 0.01	89.58% ± 0.12	99.48% ± 0.01	88.43% ± 0.11
TGF-β1	1.62% ± 0.02	98.43% ± 0.01	0.39% ± 0.00	90.83% ± 0.06	99.58% ± 0.00	93.48% ± 0.04
TGF-β3	2.09% ± 0.02	97.83% ± 0.01	0.43% ± 0.00	90.90% ± 0.06	99.68% ± 0.00	92.50% ± 0.03
FBS	0.08% ± 0.00	97.95% ± 0.02	0.05% ± 0.00	78.23% ± 0.03	96.78% ± 0.03	89.65% ± 0.14
DAY 14	CD34	CD44	CD45	CD73	CD90	CD105
Serum-free	11.39% ± 0.10	95.83% ± 0.04	1.36% ± 0.02	96.70% ± 0.03	96.55% ± 0.03	94.83% ± 0.04
AA	20.08% ± 0.11	94.85% ± 0.07	1.19% ± 0.02	94.75% ± 0.06	95.60% ± 0.07	92.98% ± 0.08
FGF-2	12.11% ± 0.13	96.48% ± 0.05	2.31% ± 0.02	96.23% ± 0.04	94.38% ± 0.05	91.48% ± 0.06
PDGF-BB	1.49% ± 0.02	95.53% ± 0.05	3.02% ± 0.03	94.60% ± 0.03	92.73% ± 0.06	81.68% ± 0.13
IGF-1	15.10% ± 0.09	96.33% ± 0.04	2.76% ± 0.03	97.00% ± 0.03	97.30% ± 0.03	96.55% ± 0.04
RA	35.35% ± 0.14	94.33% ± 0.07	3.16% ± 0.03	94.70% ± 0.07	95.08% ± 0.07	92.43% ± 0.08
ITS	13.67% ± 0.10	90.45% ± 0.15	1.51% ± 0.01	90.70% ± 0.14	91.23% ± 0.15	90.45% ± 0.14
IBMX	12.42% ± 0.09	94.00% ± 0.09	1.86% ± 0.02	94.73% ± 0.08	94.75% ± 0.08	92.35% ± 0.09
TGF-β1	5.15% ± 0.06	87.93% ± 0.16	0.55% ± 0.01	96.20% ± 0.03	89.28% ± 0.16	84.63% ± 0.16
TGF-β3	5.03% ± 0.09	96.23% ± 0.06	0.51% ± 0.01	95.70% ± 0.04	96.80% ± 0.05	94.27% ± 0.04
FBS	1.47% ± 0.03	97.40% ± 0.03	0.12% ± 0.00	93.63% ± 0.01	95.60% ± 0.03	94.30% ± 0.04

3.3.4 Effect of biochemical cues on wound healing ability

The influence of biochemical cues on the ability of wound healing was studied with a scratch assay (Figure 3-5). Seven days after the scratch was performed, only cells fed with serum-supplemented medium (100% ± 0%; average ± SD) or medium with PDGF-BB were able to fully close the wound gap (93% ± 3%; average ± SD). Supplementation with IGF-1 and ITS increased the closing of the scratch significantly when compared to the serum-free control (73% ± 8% and 69% ± 8%, respectively; average ± SD). Addition of AA, FGF-2 and IBMX slightly increased cell migration but not significantly. RA, TGF-β1 and TGF-β3 reduced cell migration to some extent. Only PDGF-BB can be described to have a positive migration effect as the wound closure is only due to cell migration since this growth factor had little effect on cell proliferation.

3.3.5 Combinatorial effect of pro-keratocyte cues

A final experiment was conducted where the biochemical cues that showed a promotion of the keratocyte phenotype were used in combination with the basal medium and compared to serum-free conditions. Cells cultured for two weeks in medium containing AA, ITS, RA and IBMX presented a higher number of dendritic cells, $CD34^+$ population was highly increased and keratocan gene expression was particularly up-regulated. However, expression of ALDH3A1 was down-regulated and expression of COL1 did not increase. α-SMA remained negative at the gene and protein level. Cells were positive for CD44, CD90 and CD105 and negative for CD45 in both media conditions, while CD73 decreased slightly, yet significantly. These results are depicted in Figure 3-6.

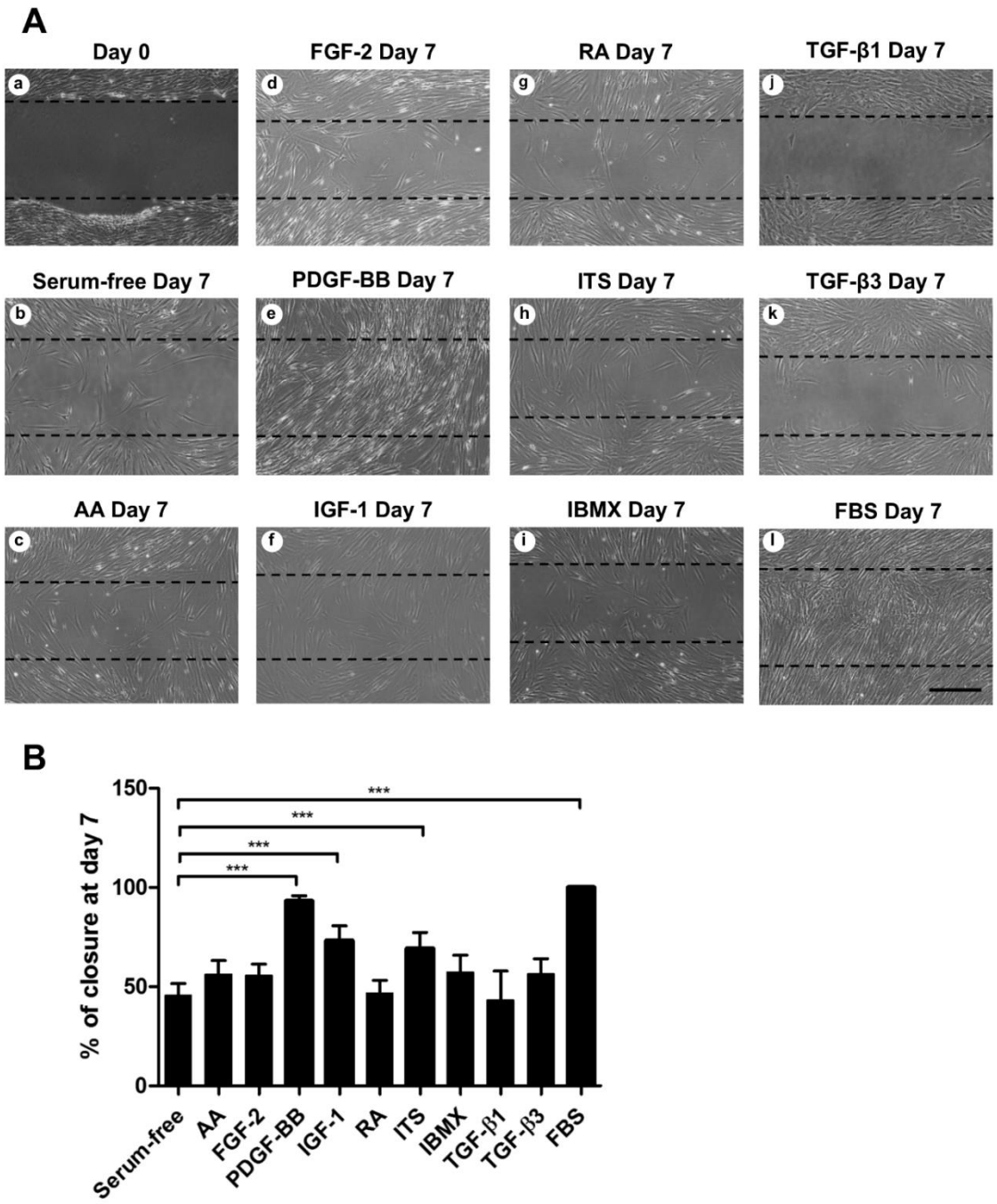

Figure 3-5. Effect of tested biochemical cues on cell migration. a) Phase contrast micrographs of wound closure at day 0 and day 7. Dashed line represents scratch at day 0. Scale bar = 200 µm. b) Quantification of wound closure by day 7 (n = 6); p*** < 0.001.

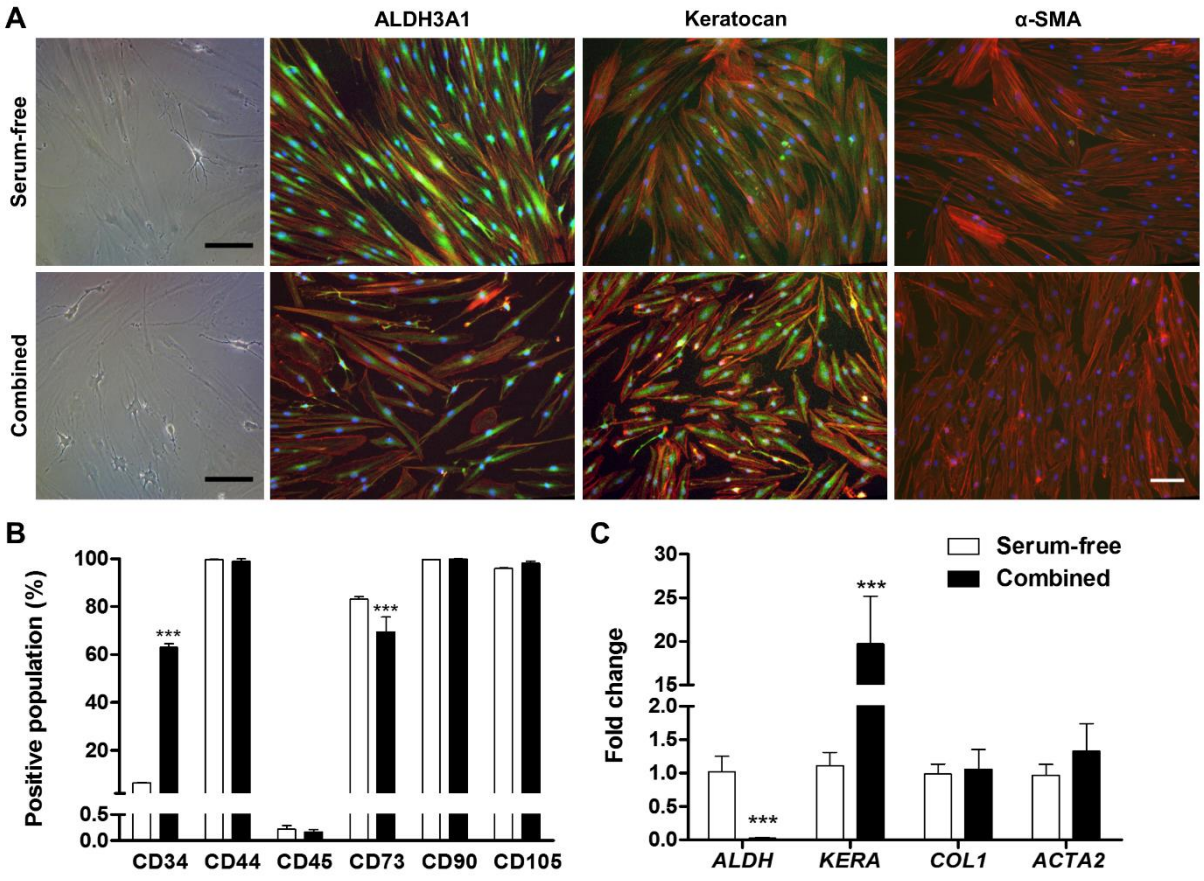

Figure 3-6. Effect of combined pro-keratocyte cues. a) Bright field images and immunofluorescence against ALDH3A1, Keratocan and α-SMA (all green, F-actin is shown in red and nuclei in blue). Scale bar = 100 µm. b) Flow cytometry profiling of cells cultured in serum-free medium or with the combination of pro-keratocyte cues (n = 3). c) Gene expression of cells cultured in serum-free medium or with the combination of pro-keratocyte cues (n = 6). p *** < 0.001.

3.4. Discussion

Understanding the effect of different biochemical cues on cultured human corneal stromal cells is key to understanding their physiological and pathological behaviour. A deep knowledge of cell culture conditions is essential when developing *in vitro* models of corneal diseases, as well as developing cell-based therapies and tissue engineering corneal substitutes. Here a thorough study of how human corneal stromal-derived cells, initially expanded in serum-containing medium, react to a range of biochemical cues under serum-free conditions is presented. A summary showing the overall effect of each cue on the cell behaviour is shown in Table 3-2.

Expansion of corneal stromal cells in FBS is known to result in a fibroblastic phenotype (Fini, 1999). While alternatives to FBS such as bovine pituitary extract, show a lot of promise as an approach for expanding keratocytes while maintaining the native phenotype (Xu et al., 2013), most researchers still use FBS in the expansion phase. When

compared to cells where FBS was removed, the cells in FBS proliferated rapidly, maintained a spindle morphology, and displayed low levels of keratocan and ALDH3A1 at both mRNA and the protein level as reported previously by other researchers (Beales et al., 1999; Espana et al., 2003). Despite the activated nature, the cells did not differentiate into myofibroblasts as very little α-SMA could be detected, either at the mRNA or the protein level. Similar results have been shown in our group and in others, especially when seeded at high densities (Guerriero et al., 2007; Lynch et al., 2016a; Masur et al., 1996; Pot et al., 2010). MSC markers were expressed in the same pattern as the serum-free control, except no increase in CD34 was observed. Cells treated with FBS closed fully the wound in the scratch assay, although this could be due to proliferation.

Both AA and RA are antioxidant vitamins commonly used as culture media supplements to support cell growth. In this study both regents supported a dendritic morphology, had little effect on cell proliferation, inhibited α-SMA formation and promoted an increase in keratocan gene expression although only AA was statistically significant. The findings for AA agree with previous studies that show increased keratocan expression (Musselmann et al., 2006) and no significant change in MSC markers (Sidney and Hopkinson, 2016) associated with this molecule. There are conflicting reports on the effect of AA on proliferation with both increases in proliferation or no alterations in cell number having been shown (Musselmann et al., 2006; Saika et al., 1991). It has long been known that AA stabilizes the triple helix of collagen as it is a co-substrate of peptidyl-prolyl hydroxylase which converts proline into hydroxyproline (Stone and Meister, 1962). In this study AA increased expression of COL1 gene, similar as reported for other cell types such as skin fibroblasts and avian tendon cells (Lyons and Schwarz, 1984; Tajima and Pinnell, 1982). RA has also been associated with both increases and decreases in cell number although this is dependent on the concentration of RA used (Gouveia and Connon, 2013; Kenney et al., 1986). RA has also been associated with increases in the expression of keratocyte markers in both ordinary cell culture (Gouveia and Connon, 2013) and in collagen hydrogels (Abidin et al., 2015). RA had a significant effect in increasing the $CD34^+$ population, while not modifying the expression of the other MSC markers, in a similar way as reported by Sidney and Hopkinson (Sidney and Hopkinson, 2016). The observed reduction in migration of cells treated with RA also matches previous findings that used keratocytes (Gouveia and Connon, 2013) and adipose-derived stem cells in a keratocyte differentiation medium (Lynch and Ahearne,

2017). Gouveia and Connon showed that promoter regions of keratocyte marker genes did not have RARE sequences, and therefore RA should signal via alternative pathways. However, the gene encoding for CD34 has an enhancer region (GeneHancer identifier GH01I207846) with RARα binding domains which could explain the increase in $CD34^+$ cells when treated with RA. These results indicate that both AA and RA may assist in inducing a partial restoration of the keratocyte phenotype.

FGF-2 did not have a significant effect on cell proliferation, contrary to some reports in the literature (Jester et al., 1996; Long et al., 2000) although these studies used media formulations containing additional supplements. However, our FGF-2 proliferation data did agree with findings that used bovine keratocytes (Etheredge et al., 2009). FGF-2 did not have an effect in changing cell morphology after serum-starvation as cells maintained their spindle shape, similar to some previously reported studies (Jester and Ho-Chang, 2003). Expression of ALDH3A1, keratocan and α-SMA were not up-regulated. It has been postulated that the reduced expression of keratan sulfate proteoglycans such as Lumican or Keratocan by FGF-2 is mediated by the Rho and JNK pathways (Chen et al., 2011, 2009). Furthermore, FGF-2 supplementation led to a reduction in the number of $CD34^+$ cells. The loss of CD34 in the cornea is associated with keratoconus where cells also become more fibroblastic (Toti et al., 2002). Overall these findings suggest that FGF-2 induces a fibroblastic phenotype of cultured stromal cells.

PDGF-BB did not promote cell proliferation in this study, conflicting with some published research. However, in those studies the media used was supplemented with 0.5% FBS (Kim et al., 1999) or 2% FBS (Hoppenreijs et al., 1993). In the current study, cells treated with PDGF-BB show a fibroblastic-like shape but with a more elongated cell body than when treated with FBS, a similar finding to that previously described (Jester and Ho-Chang, 2003). However, when cells treated with PDGF-BB were embedded in compressed collagen gels they presented branching processes indicating that the physical surroundings may play a role in how the cells react to the growth factor (Kim et al., 2010). In our study, expression of keratocyte markers was down-regulated, while no up-regulation of myofibroblastic markers was detected. As seen with FGF-2, treatment with PDGF-BB also reduced the number of $CD34^+$ cells. This growth factor also displayed a strong chemotactic effect as has been previously demonstrated in 2D using Boyden chambers (Kamiyama et al., 1998) and in 3D compressed collagen gels (Kim et al., 2010). It is believed that PDGF influences cell migration via Erk, which phosphorylates FAK

and paxillin regulating dynamics of focal adhesions (Huang et al., 2004). Decrease in actin stress fibers can me mediated by N-WASP after downstream signalling via PI3K and Cdc42, a Rho GTPase (Jiménez et al., 2000). Hence we can conclude that PDGF-BB promotes a motile fibroblastic phenotype.

In this study the roles of IGF-1 and ITS supplementation were examined. Insulin is a commonly used cell culture supplement that regulates the uptake of glucose and amino acids. Insulin binds to insulin receptor (INSR) through the alpha subunit, which produces a conformational change that will induce the phosphorylation of tyrosine residues in the beta subunit of the insulin receptor. This triggers a downstream signalling cascade through the MAPK pathway, inducing cell proliferation, and through the PI3K/Akt pathway leading to cell growth, and lipid, glycogen and protein synthesis (Haeusler et al., 2017; LeRoith and Roberts, 2003; Saltiel and Kahn, 2001). IGF-1 led to an early positive increase in cell proliferation, a dendritic morphology, increases in keratocan gene expression, ALDH3A1 staining and $CD34^+$ cells. Etheredge and colleagues reported no effect on corneal fibroblast proliferation at a concentration of 10 ng/ml, while Yanai and colleagues showed increase in proliferation and inhibition of apoptosis at 305 nM, which corresponds to 2 µg/ml (Etheredge et al., 2009; Yanai et al., 2002). Maintenance of a dendritic morphology in rabbit stromal cells when treated with IGF-1 has also previously been shown (Jester and Ho-Chang, 2003). ITS had a positive effect in cell survival similar to that seen by other authors (Musselmann et al., 2006), promoted a dendritic morphology with multiple processes and led to a significant increase in *COL1* gene expression, ALDH3A1 immunofluorescence and more $CD34^+$ cells. Similar to IGF-1, ITS promoted the closure of the wound in the scratch assay but the increase in proliferation renders the chemotactic effect elusive. No up-regulation of *ACTA2* or expression of α-SMA was detected for either IGF-1 or ITS. In fact, recent studies suggest that IGF-1 inhibits fibrosis initiated by TGF-β (Sarenac et al., 2016). Taking these findings together, it can be said that both IGF-1 and ITS partially induce a quiescent keratocyte phenotype.

IBMX is a competitive non-selective inhibitor of phosphodiesterase that raises intracellular cAMP levels, which activate protein kinase A, phosphorylating in turn cAMP response element-binding proteins (CREB) in the nucleus which act as transcription factors (Parsons et al., 1988). Researchers have used IBMX to emulate the effects of low glucose conditions (Foster et al., 2015). Upon treatment with IBMX, cells

with multiple dendrite-like structures were observed similar to that reported previously (Foster et al., 2015). A significant increase in keratocan gene expression was observed and bright perinuclear staining was observed for this marker. The increase of this marker could be due the presence of CRE sequences in the promoter of this gene (Foster et al., 2015). ALH3A1 was highly expressed in cells with processes, similar to observations by Foster and colleagues for ALDH1 (Foster et al., 2015). These authors reported an increase of CD34 at the transcriptional level, while our study showed an increase in the $CD34^{+}$ population via flow cytometry. IBMX did not induce changes in any other MSC markers and did not show a chemotactic effect. The addition of this chemical did not influence expression of *COL1* or *ACTA2*. This data indicates that treatment with IBMX promoted the restoration of a keratocyte-like phenotype.

Both TGF-β1 and TGF-β3 had a similar effect on all the parameters examined in this study, particularly the up-regulation and immunochemical staining of α-SMA, a known myofibroblast marker. It has previously been well established that TGF-β1 induces a myofibroblastic phenotype (Andresen et al., 1997; Etheredge et al., 2009; Jester et al., 1996; Jester and Ho-Chang, 2003; West-Mays et al., 1999). Transcription of α-SMA is induced by the translocation to the nucleus of phosphorylated Smad2/3/4 complex. These proteins are activated by ALK5, which is phosphorylated by TGFβ Receptor I and II upon ligand binding (Massagué 2000). Fibroblasts expressing α-SMA display a retarded motility using a scratch assay (Rønnov-Jessen and Petersen, 1996) which coincides with the current findings where α-SMA positive cells were unable to bridge the gap during the scratch assay. In fact, the edge of the wound was always clear and straight, and the whole front would move together, suggesting that any apparent migration was due to cell proliferation. Despite an initial up-regulation of *COL1* by both TGFs, at later time-points the expression was similar to that of the serum-free control. The effect of TGF-β3 in this study was interesting since it contradicts some other studies that suggest TGF-β3 has an antifibrotic effect (Karamichos et al., 2014b, 2011a). One possible explanation is that the authors used a self-assembled culture, medium containing 10% FBS and AA and cultured their cells for 4 weeks, hence multiple factors may be contributing to the cell behaviour. Sidney and Hopkinson showed that TGF-β3 led to lower levels of ALDH3A1 and vimentin and higher levels α-SMA gene expression when compared to cells cultured under serum and growth factor free conditions (Sidney and Hopkinson, 2016). Another study recently showed positive α-SMA staining resulting

from the addition of TGF-β3 although the amount of staining was significantly less than at the same concentration of TGF-β1 (Sriram et al., 2017). From our results it would appear that both TGF-β1 and TGF-β3 promote a myofibroblastic phenotype.

When AA, ITS, RA and IBMX were used in combination, keratocyte markers CD34 and keratocan were up-regulated, while ALDH3A1 was down-regulated and COL1 remained unchanged. Since RA individually decreased these two markers one could speculate that RA is the main responsible and that the other cues could not synergistically overcome this.

As discussed throughout, multiple signalling pathways are involved after supplementation with the factors studied here. Although outside of this study's scope, investigating the expression of some of the key down-stream proteins is key to understanding the mechanisms of keratocyte activation and return to quiescence. The use of advanced molecular techniques with high-throughput potential, such as microarrays, would be extremely beneficial for this.

This study reveals once more the importance of biochemical cues to promote the reversal of activated keratocytes towards a quiescent keratocyte phenotype *in vitro*. However, biochemical supplementation of the medium is unlikely to lead to a full phenotype reversal. Other environmental cues such as substrate stiffness, material topography and 3D culture play an important role as multiple studies have demonstrated (Lakshman and Petroll, 2012; Lynch et al., 2016a; Wilson et al., 2012). Furthermore, factors such as the donor's age and health, the number of population doublings of the cells and the time in culture are among other variables that need to be considered. Since tissue remodelling and wound healing are long lasting processes in the corneal stroma (Wilson et al., 2001), it is therefore logical to suspect that phenotype reversal *in vitro* can only be achieved after longer culture periods.

Table 3-2. Summary of results from this study.

Reagent	Proliferation	Morphology	Phenotype	Migration	Final cell type
AA	/	Dendritic	General expression of keratocyte markers (significant up-regulation of keratocan) Significant up-regulation of COL1 No α-SMA	/	Keratocyte-like
FGF-2	/	Spindle	No up-regulation of keratocyte markers No α-SMA	/	Fibroblast (activated keratocyte)
PDGF-BB	/	Elongated spindle	No up-regulation of keratocyte markers No α-SMA	+	Fibroblast (activated keratocyte)
IGF-1	+	Dendritic	General expression of keratocyte markers Significant up-regulation of COL1 No α-SMA	+	Keratocyte-like
RA	/	Dendritic	General expression of keratocyte markers (significant increase of $CD34^+$ cells) No α-SMA	-	Keratocyte-like
ITS	+	Dendritic	General expression of keratocyte markers Significant up-regulation of COL1 No α-SMA	+	Keratocyte-like
IBMX	/	Dendritic	General expression of keratocyte markers (significant up-regulation of keratocan) No α-SMA	/	Keratocyte-like
TGF-β1	+	Spread and polygonal	No expression of keratocyte markers Significant up-regulation of COL1 Significant up-regulation of α-SMA	-	Myofibroblast
TGF-β3	+	Spread and polygonal	No expression of keratocyte markers Significant up-regulation of COL1 Significant up-regulation of α-SMA	-	Myofibroblast
FBS	+	Spindle	Down-regulation of keratocyte markers No α-SMA	+	Fibroblast (activated keratocyte)

3.5. Concluding remarks

In this Chapter, several biochemical cues have been investigated for their influence in cell proliferation, morphology, phenotype and migration of serum-expanded corneal stromal cells. It has been demonstrated that human corneal stromal-derived cells

originally expanded in serum-containing medium can partially recover a quiescent keratocyte-like phenotype by the removal of serum and the addition of AA, IGF-1, RA, ITS and IBMX to a basal medium. The keratocyte-like phenotype was demonstrated by a dendritic morphology and up-regulation keratocyte markers such as keratocan, ALDH3A1, COL1 and CD34. For further studies, AA and ITS will be used to supplement serum-free DMEM/F12 since these components increased cell proliferation, partially recovered a keratocyte phenotype and promoted cell migration. In the next chapter, these cells will be used to repopulate decellularized porcine corneas *in vitro* and their implantation *in vivo* in a rabbit ALK model will be studied.

CHAPTER 4

Decellularized and recellularized porcine corneas in an Anterior Lamellar Keratoplasty rabbit model

4.1. Introduction

As discussed in the Literature Review, there is an important need to develop tissue engineered construct to overcome donor shortage for corneal transplantation. Decellularized tissues and organs can replicate the native tissue, at the composition and structure level, making them ideal materials for tissue engineering.

The feasibility of implanting decellularized corneas of both porcine and human origin *in vivo* has been demonstrated previously, mainly using rabbit models (Table 2-4). Despite low immune reaction, some transparency recovery and little neovascularization, very few keratocytes repopulate the implant, even in experiments lasting 12 months, both in interlamellar grafts and in anterior or deep lamellar keratoplasty models (Alió del Barrio et al., 2015; Du and Wu, 2011; Hashimoto et al., 2015, 2010; Pang et al., 2010). In those studies, the stroma was barely repopulated while the epithelium successfully covered the implants in the anterior lamellar models. Keratocytes are needed for the homeostasis of the corneal stroma as they remodel the ECM. They can also influence re-innervation as they secrete neuro-regulatory factors (Yam et al., 2017). Therefore, it can be assumed that recellularized scaffolds should be superior to acellular scaffolds. In a study by Diao and colleagues, it was shown that decellularized porcine corneas recellularized by injection of human stromal cells recovered transparency faster than their acellular counterpart and presented a more native-like ultrastructure (Diao et al., 2015). In one study, amniotic epithelial cells were seeded onto decellularized porcine corneas and implanted in rabbits. These recellularized scaffolds performed better, presumably due to the anti-inflammatory and anti-angiogenic properties of amniotic cells (Luo et al., 2013). In a long term study in dogs, decellularized porcine corneas recellularized with human epithelial and stromal cells showed improved re-innervation, epithelial integrity

and central corneal thickness than cell free scaffolds (Xu et al., 2017). There has been some recent reports of implantation of decellularized porcine corneas into humans with relative positive results, i.e. no graft rejection, gradual recovery of transparency and some improvement in visual acuity (Li et al., 2019; M.-C. Zhang et al., 2015; Zheng et al., 2019) although again there is no evidence of cells infiltrating the stroma in these studies. In a recent study, thin sections of human decellularized corneas were implanted in patients with advanced keratoconus (Alió del Barrio et al., 2018). Some patients were implanted with scaffolds seeded with their own adipose-derived MSCs. The authors identified no positive effect from the recellularized tissues versus the acellular tissues.

The first aim of the current study was to explore *in vitro* recellularization of scaffolds obtained from decellularized porcine corneas in order to obtain highly cellular constructs prior to implantation. The extent of recellularization and cell phenotype was analysed. The second aim was to test if recellularized scaffolds are superior to cell free ones in an *in vivo* ALK model in rabbits.

4.2. Materials and Methods

4.2.1 Isolation and decellularization of porcine corneas

Porcine ocular globes were obtained from a local slaughterhouse an abattoir (Rosderra Meats, Edenderry, Ireland) and transported refrigerated. The remaining pieces of flesh were removed and under aseptic conditions. The eyes were immersed in 2 % iodine solution (Videne®, Ecolab, Belgium) in sterile phosphate buffer saline (PBS) for five minutes, gently rocking throughout. The eyes were subsequently washed twice in sterile PBS. After the epithelium had been debrided with ethanol, the recipient cornea was trephined to 250 µm depth using a 6.5 mm diameter adjustable vacuum trephine (Moria Surgical, Antony, France) and the stromal tissue excised by blunt dissection with a pre-blunted crescent blade (2.5 mm crescent, Beaver Visitec, Waltham, MA. USA) and transferred into a sterile vessel for decellularization.

Decellularization was performed as described elsewhere (Lynch et al., 2016b). Briefly, corneal buttons were immersed in decellularization solution containing 0.5 % (w/v) Sodium dodecyl sulphate (SDS, Sigma) and 1 % (v/v) Triton X-100 (Sigma) in distilled water. To promote removal of debris, samples were placed in an orbital shaker

for 72 hours at room temperature, changing the solution every 24 hours. Corneal lenticules were then treated with 10 U/ml of RNAse and DNAse (both Sigma) in 10 mM $MgCl_2$ solution for 1 hour at 37 °C rotating at 15 RPM. Afterwards samples were washed with PBS containing antibiotics and antimycotics for another 72 hours, changing the solution daily, on a rotator at 15 RPM. Samples were stored until used in PBS supplemented with 200 U/ml penicillin (Gibco), 200 µg/ml streptomycin (Gibco) and 2.5 µg/ml Amphotericin B (Sigma) in PBS at 4 °C. Samples were then placed in medium for 24 hours in a humidified incubator at 37 °C for recellularization studies, stored at -80 °C for biochemical analysis or fixed for 30 minutes with 4 % PFA at room temperature for histology.

4.2.2 Corneal transparency and light transmittance

The macroscopic appearance and transparency of decellularized corneas and scaffolds was assessed by placing them over printed text before and after immersion into 100 % glycerol for 2 hours. Subsequently, light transmittance was quantified. The absorbance of light at several different wavelengths ranging from 350 to 700 nm was determined with a microplate reader (BioTek™ Synergy HTX). Ultrapure water was used as a baseline control. The transmittance of light was calculated using the following formula:

$$\%\, Transmittance = 10^{2-Absorbance}$$

4.2.3 Biochemical analysis

DNA content. Native and decellularized corneas were freeze dried using standard protocols and weighed to obtain the dry weight values. Freeze-dried samples were digested in 3.88 U/ml of papain solution rotating at 60°C for 18 hours. Immediately after, the DNA assay was performed. DNA content was quantified with the Quant-iT™ PicoGreen® dsDNA Kit (Molecular Probes, Biosciences) following the manufacturer's instructions. Standards were prepared from DNA solutions to perform a calibration curve. 10 µl of sample or standard were mixed with 190 µl of working die solution and incubated at room temperature for 5 minutes. The plates were read using a spectrophotometer (BioTek™ Synergy HTX) at 480 nm of excitation wavelength and 520 nm of emission wavelength. Furthermore, DNA fragment size was assessed by 3% agarose gel electrophoresis after extraction of the DNA using a DNeasy kit (Qiagen) and following manufacturer's instructions.

GAG content. Determination of glycosaminoglycans (GAG) was done via the 1, 9 dimethylmethylene blue dye (DMMB) assay (Blyscan™, Biocolor, UK). Briefly, 10 µl of papain digested samples were incubated with DMMB in rotation for 30 minutes at room temperature, then centrifuged at 15000 G for 10 minutes and supernatant removed. The pellet was then treated with dye dissociation reagent and the mixture was read in a spectrophotometer at 656 nm excitation wavelength (BioTek™ Synergy HTX). GAG standards were treated equally to obtain a standard curve.

Collagen content. The collagen content in the samples was determined via the hydroxyproline assay (Kafienah and Sims, 2004). This assay quantifies the amount of hydroxyproline which is related to the amount of collagen with the ratio 1:7.69 (Ignat'eva et al., 2007). Briefly, 10 µl of papain digested pellet sample was incubated with 38 % HCl at 110 °C for 18 hours. After drying for 48 hours at 50 °C, samples were dissolved in 500 µl H_2O, and then a further 1:10 dilution. Serial dilutions of trans-4-Hydroxy-Lproline (Fluka) in Papain Buffer Extract were made to obtain a standard curve. Samples and standards were incubated 20 minutes at room temperature with assay buffer (containing n-propanol) and chloramine-T reagent to oxidize hydroxyproline. DMBA reagent (which contains perchloric acid and 4- (Dimethylamino) benzaldehyde) was then added, mixed and incubated for 20 minutes at 60 °C, previously sealing the plate. After cooling down, the plate was read at 570 nm excitation wavelength using a spectrophotometer (BioTek™ Synergy HTX).

4.2.4 Cell culture

Human corneal stromal cells were isolated from the healthy corneo-scleral rims remaining after corneal surgeries as described in Chapter 3. In this study cells were expanded from cryopreserved stocks and used at passages 4 and 5. Expansion medium consisted of low glucose DMEM (HyClone) supplemented with 10% FBS (Gibco).

Scaffolds were recellularized by seeding 0.1 $x10^6$ stromal cells in small volumes (10-15 µl), allowing cell attachment for 30 minutes in a humidified incubator. Scaffolds were then flipped and cells were seeded on the opposite side for another 30 minutes. Scaffolds were placed on polytetrafluoroethylene (PTFE) disks to avoid cells attaching to the tissue culture plate and promote their attachment to the scaffolds. Finally, 0.3 $x10^6$ cells in medium containing FBS (Expansion medium) were added and scaffolds were cultured for 14 days changing media every second day. Some samples were cultured for

further two weeks in the same conditions or switched to serum-free DMEM/F12 (HyClone) medium supplemented with 50 µg/ml Ascorbic Acid (Sigma) and 1x ITS (Gibco) (Keratocyte medium).

Limbal epithelial cells were isolated as follows. The remnants of corneo-scleral rings from healthy donors were collected after surgery. The remaining limbus was cut into four pieces and incubated with 2.5 mg/ml dispase (Life Technologies) at 37 °C for 1 hour. Limbal epithelial sheets were collected by scraping the limbal surface with a scalpel blade and pipette tip. The collected cells were pooled and centrifuged at 170 G for 5 min. The cells were then resuspended in epithelial medium (described below) and seeded on gelatin-coated plates or directly onto the scaffolds. A 0.1 % (w/v) solution of gelatin was prepared, autoclaved and sterile filtered. The culture surfaces were covered with the solution for 1 hour in a humidified incubator. Solution was removed and surfaces rinsed twice with PBS.

Epithelial medium used was based on Rheinwald and Green formulation (Rheinwald and Green, 1977, 1975) with some modifications (Fernández-Pérez et al., 2017). The medium was composed of a 3:1 mixture of DMEM (Hyclone) and Ham F12 medium (Gibco) supplemented with 10% FBS (Gibco), 5 µg/ml human recombinant insulin (Sigma), 0.4 µg/ml hydrocortisone (Sigma), 2 pM triiodo-L-thyronine (T3, Sigma), 10^{-5} M isoprenaline hydrochloride (Sigma), 5 µg/ml transferrin (Sigma), 10 ng/ml human epithelial growth factor (EGF, Source BioScience), 180 µM adenine (Sigma), 2 mM L-glutamine (Gibco), 100 U/ml penicillin (Gibco) and 100 µg/ml streptomycin (Gibco).

100.000 cells/cm^2 were seeded in a small volume (15 µl) and carefully pipetted on the surface of the scaffolds, and let attach in the incubator for 1 hours. Fresh medium was then added. Scaffolds were cultured for one week and were then fixed and stained to identify the cytoskeleton and cell nuclei.

4.2.5 qPCR

Following manufacturer's instructions, (Invitrogen) Trizol was used to extract RNA from cells in the scaffolds. Samples were triturated using a tissue homogenizer (IKA T10 basic) to increase lysis and release of the genetic material. Chloroform was then added, samples thoroughly vortexed and centrifuged for 15 minutes at 12000 G and at 4 °C. Supernatant was transferred into a new tube and the same volume of isopropanol and

3 µl of Glycoblue (Life Technologies). Samples were kept overnight at -20 °C and then centrifuged at 12000 G for 15 minutes at 4 °C. The supernatant was discarded and 70 % ethanol in RNAse free water was added to wash the pellet. Samples were centrifuged again, ethanol removed and pellet air dried. Finally, the pellet was dissolved in RNAse free water. RNA yield and purity quantified by the use of a NanoDrop-1000 (ThermoFisher). All steps were performed on ice. A high capacity cDNA reverse transcription kit (Invitrogen) was used to convert RNA into cDNA. Real-time PCR was performed using TaqMan Universal Master Mix II and the following TaqMan primers: glyceraldehyde-3- phosphate dehydrogenase (GAPDH, Hs02758991_g1), aldehyde dehydrogenase 3A1 (ALDH3A1, Hs00964880_m1), alpha smooth muscle actin (ACTA2, Hs00426835_g1), keratocan (KERA; Hs00559942_m1), collagen 1a1 (COL1; Hs00164004_m1), lumican (LUM, Hs00929860_m1), decorin (DCN, Hs00754870_s1) and CD34 (Hs00990732_m1). The genes of interest were normalized against GAPDH using the $\Delta\Delta C_t$ method. Calculated values were expressed as a power of $2^{-\Delta\Delta C_t}$. For this study, all values were normalized to the serum-expanded cells before seeding onto the scaffolds.

4.2.6 Histology, immunostaining and imaging

Samples were fixed in 4% PFA, blocked and permeabilized with 2% FBS and 0.5 % Triton X-100, and stained with 4',6-diamidino-2-phenylindole (DAPI) and phalloidin-conjugated to tetramethylrhodamine (TRITC), to visualize cell nuclei and cytoskeleton, respectively. Scaffolds were imaged using a confocal microscope (Leica SP8). Afterwards they were wax embed, 6 µm thick slices were obtained using a microtome (Leica RM2125) and mounted on glass slides (Superfrost® Plus, Thermo Scientific). Native porcine corneas and decellularized samples were stained with Haematoxylin and Eosin (H&E), Alcian Blue and Picrosirius Red using standard procedures. Recellularized constructs were stained with H&E and DAPI. Immunofluorescence was carried out with the conditions indicated in Table 4-1. Slides were imaged using a laser scanning confocal microscope (Leica SP8).

Table 4-1. Details of immunofluorescence methods.

Primary antibody	Catalogue number (brand)	Dilution	Antigen retrieval method	Secondary antibody (dilution)
ALDH1A1	Ab9883 (Abcam)	1:200	Heat-mediated citrate buffer pH 6 (30 minutes at 95 °C)	Donkey anti-goat AlexaFluor®488 (1:200)
ALDH3A1	Ab76976 (Abcam)	1:200	Heat-mediated citrate buffer pH 6 (30 minutes at 95 °C)	Donkey anti-rabbit-AlexaFluor®488 (1:200)

Aquaporin 1	Ab9566 (Abcam)	1:100	Heat-mediated citrate buffer pH 6 (30 minutes at 95 °C)	Goat anti-mouse AlexaFluor®488 (1:200)
α-SMA	Ab7817 (Abcam)	1:100	Heat-mediated citrate buffer pH 6 (30 minutes at 95 °C)	Goat anti-mouse AlexaFluor®488 (1:200)
Collagen III	GTX26310 (GeneTex)	1:2000	Heat-mediated citrate buffer pH 6 (30 minutes at 95 °C)	Goat anti-mouse AlexaFluor®488 (1:200)
Keratocan	HPA039321 (Atlas Antibodies)	1:50	Heat-mediated citrate buffer pH 6 (30 minutes at 95 °C)	Donkey anti-rabbit-AlexaFluor® 488 (1:200)
Fibronectin	Ab6328 (Abcam)	1:200	Proteinase K (15 minutes at 37 °C)	Goat anti-mouse AlexaFluor®488 (1:200)

4.2.7 Axonal outgrowth compatibility test

Dorsal root ganglia (DRG) were isolated from adult rats (as described by (Tukmachev et al., 2016)), placed directly on the scaffolds and let attach for 1 hour, when 1 ml of DMEM supplemented with 10% FBS and 10 ng/ml NGF was added. Media was changed every three days. After 14 days in culture, scaffolds were fixed and immunostained against neural marker βIII-tubulin (Sigma) at a 1:100 concentration.

4.2.8 Corneal transplantation in rabbits

Eight female New Zealand rabbits (21-23 weeks old, 2.75-4.0 kg) were used for the experiment, randomly divided into 2 groups of 4 each. Additional rabbits were used to establish the model. Animal welfare and surgery was approved by Research Ethics Committees of both Trinity College Dublin (301107-1001) and Dublin City University (DCUREC/2018/253). The project was authorised by the Health Products Regulatory Authority (AE19136/PO93).

Decellularized porcine corneas, either recellularized with human stromal cells (condition: 2 weeks Expansion + 2 weeks Keratocyte) or not recellularized, were transplanted into the right eye of each rabbit via deep anterior lamellar keratoplasty (DALK), while the left eye was left as control. For the surgery the rabbits were first pre-medicated with subcutaneous buprenorphine (0.03mg/kg) (Buprecare, Animalcare Group, York, UK) and then anesthetized with intravenous ketamine (10 mg/kg) (Hameln pharmaceuticals Gloucester, UK) and xylazine (3 mg/kg) (Sedaxylan, Dechra, Shrewsbury, UK) whilst oxygen was administered through a face mask to maintain oxygen saturation. To extend anaesthesia, 0-5.0 % gaseous isoflurane (Isoflurin, Vetpharma Animal Health, Barcelona, Spain) was used and additional intravenous ketamine and xylazine given as a bolus, as necessary.

After the epithelium had been debrided with ethanol over the operating site, the recipient cornea was trephined to 250 µm depth using a 6.0 mm diameter Barron radial vacuum trephine (Barron Precision Instruments, Grand Blanc, MI, USA) and the stromal tissue excised by blunt dissection with a pre-blunted crescent blade (2.5 mm crescent, Beaver Visitec, Waltham, MA. USA). Scaffolds were sutured into the rabbit defect with 16 interrupted 10–0 nylon sutures (Serag Wiessner, Naila, Germany or Ethicon) and the knots buried to reduce irritation. Immediately after surgery the eye was irrigated with the broad-spectrum antibiotic, cefuroxime (Aprok, Biopharma S.R.L., Roma, Italy). For the entire length of the experiment, postoperative topical corticosteroid, (Betnesol 0.1% w/v, RPH Pharmaceuticals AB) drops or ointment, and topical antibiotic chloramphenicol drops (Minims chloramphenicol 0.5%, Bausch Health, Dublin, Ireland) or ointment were applied three to four times daily.

Eye examinations were performed at the following time-points after operation: 1 day, 3 days, 7 days, 14 days, 1 month, 2 months and 3 months. At these times, slit lamp biomicroscopy (Portable Slit Lamp, Reichert, Buffalo, NY, USA) was used for the general assessment of the health of the anterior segment of the eye and intraocular pressure was monitored by contact tonometry measurement (Tonovet Plus, Icare, Vantaa, Finland). After 14 days, the extent of re-epithelialization of the implants was confirmed by fluorescein staining (Minims Fluorescein Sodium 1%, Bausch Health, Ireland).

At 3 months post-operative, the rabbits were euthanized with an overdose of intravenous sodium pentobarbital (250 mg/kg, Dolethal, Vetoquinol Ireland, Towcester, UK). Eye globes were removed, photographed and examined by optical coherence tomography (OCT). They were then fixed in 10 % formalin for 24 hours at room temperature, the corneas were then excised and embedded in paraffin for histological and immunohistochemical analysis, as described previously.

4.3. Results

4.3.1 Scaffold characterization

The decellularization was successful as seen by DAPI and H&E staining (Figure 4-1 A and B), where no traces of basophile nuclei could be identified. Quantification with PicoGreen confirmed that DNA was extensively removed. Decellularized corneas presented an average of 30.97 ng of DNA per mg of dry weight, while native corneas had an average of 728.9 ng/mg (Figure 4-1 C). Sulphated glycosaminoglycans were

significantly reduced during the decellularization process, as seen by the reduction of Alcian Blue staining (Figure 4-1 A and B) and by quantification with biochemical assays (Figure 4-1 D). In the native cornea levels of sGAG were 450.6 ± 34.5 µg/mg of dry weight, mean ± SD), while in the decellularized porcine corneas these levels were lower 86.9 ± 58.7 µg/mg of dry weight (mean ± SD). Collagen abundance was maintained during decellularization, as seen by Picrosirius Red staining (Figure 4-1 A and B) and quantified by hydroxyproline assay (Figure 4-1 E). Native cornea had an average content of collagen of 0.54 ± 0.07 mg per mg of dry material (mean ± SD), while decellularized corneas had an average content of 0.63 ± 0.07 mg of collagen per mg of dry material (mean ± SD). Bright bands > 1500 base pairs (supercoiled DNA) were seen for the native tissue, while only some faint smear could be observed for the decellularized tissue lanes below 200 bp in the electrophoresis gel (Figure 4-1 F). Second harmonic generation of collagen imaged by two-photon microscopy indicated minor disruptions of fibre arrangement after decellularization (Figure 4-2).

As seen in Figure 4-3, the obtained scaffolds had excellent optical properties when examined macroscopically. Light transmittance from the scaffolds ranged from 0.95 % at a wavelength of 300 nm to 43.72 % at 700 nm. As a comparison, native porcine corneas transmitted from 9.86 % of 300 nm light to 92.79 % of 700 nm wavelength. However, when treated with glycerol, their original light transmittance recovered.

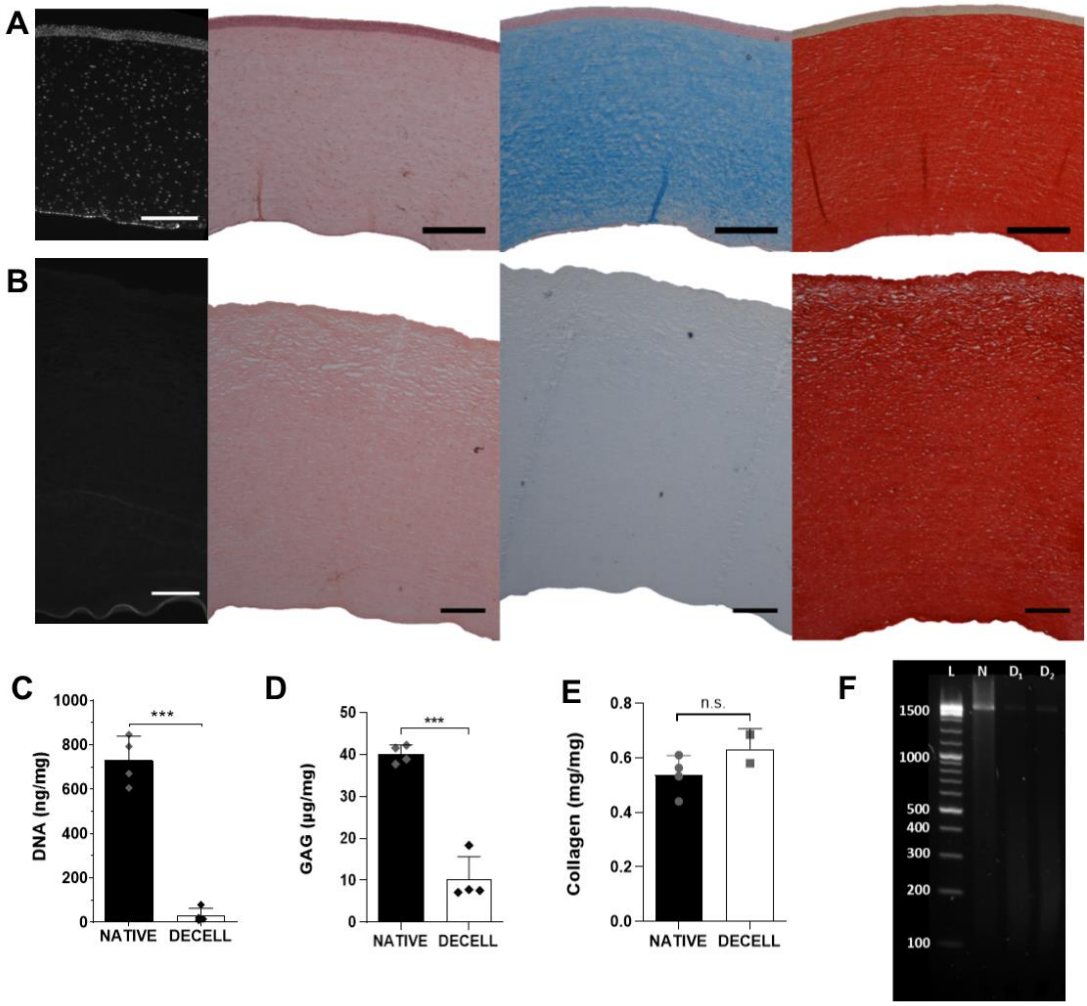

Figure 4-2. Evaluation of decellularization efficacy. A) Native porcine cornea stained with DAPI, H&E, Alcian Blue and Picrosirius Red (from left to right). B) Decellularized porcine cornea stained with DAPI, H&E, Alcian Blue and Picrosirius Red C) DNA quantification of native and decellularized porcine corneas (n=4). D) Quantification of sulphated glycosaminoglycans in native and decellularized porcine corneas (n=4). E) Total collagen quantification in native and decellularized porcine corneas (n=2-4). F) Agarose gel electrophoresis of DNA extracted from native tissue (N) and decellularized tissues (D1 and D2), L = ladder. White scale bar = 500 µm, black scale bar = 250 µm. p * < 0.05, p ** < 0.01, p *** < 0.001

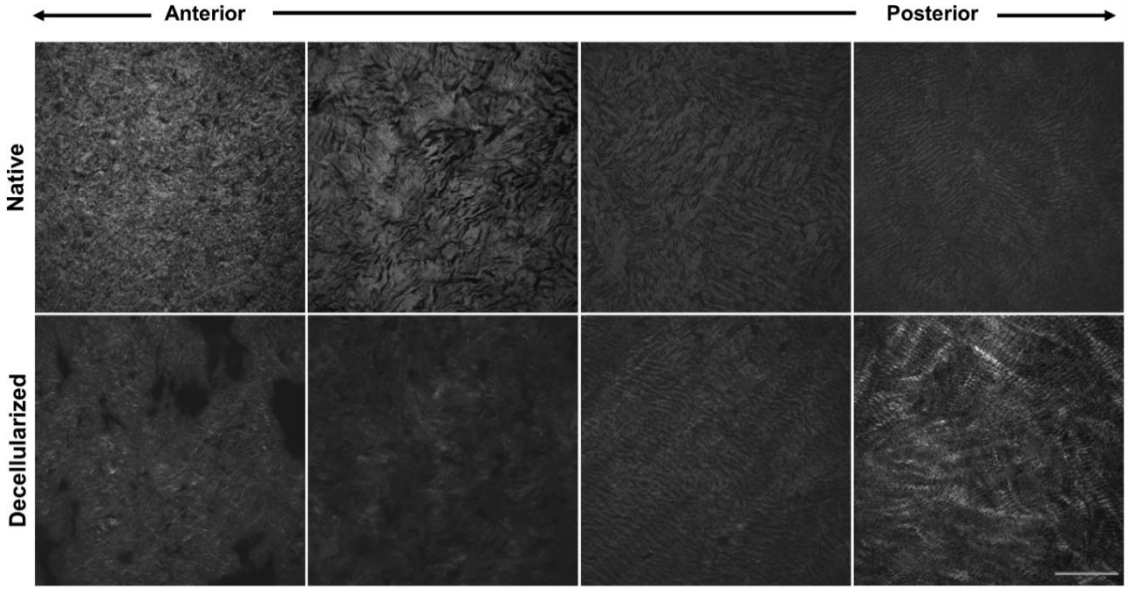

Figure 4-1. Two-photon imaging of native and decellularized porcine corneas (scale bar = 100 µm).

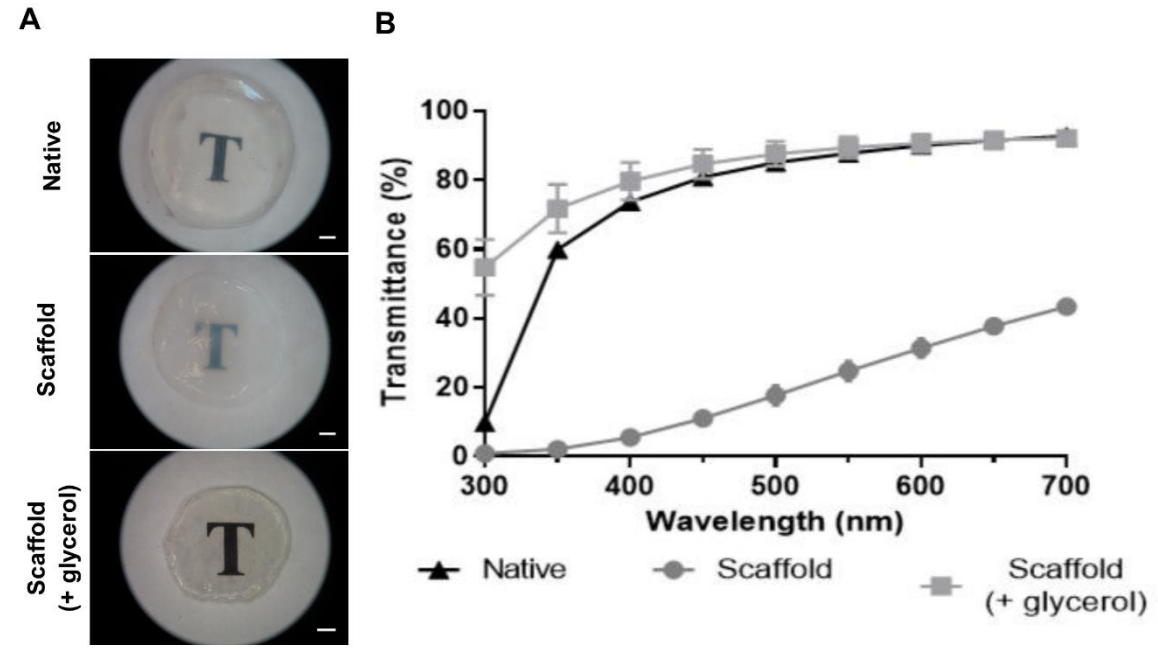

Figure 4-3. Scaffolds from decellularized porcine corneas before and after immersion in glycerol. A) Macroscopic appearance of native porcine cornea and scaffold. Scale bar = 1 mm. B) Light transmittance at different wavelengths of native porcine cornea and scaffold (n=3).

4.3.2 Stromal repopulation

To assess stromal repopulation, scaffolds were fixed, stained with phalloidin and imaged via confocal microscopy. On the most superficial areas, densely packed cells could be seen, while in deeper areas cells were scarcer but seemed to be forming a network similar to that seen *in vivo* (Figure 4-4). Since the tissue is very dense, standard confocal microscopy did not allow imaging deeper than 100 µm. Therefore, samples were embedded in paraffin, sliced transversally and nuclei stained with DAPI. The distance of each nuclei to the surface was measured to quantify the depth that cells had been able to migrate inside the scaffold. While most of the cells remained on the surface, there was an important number of cells migrating towards deeper areas of the scaffold (Figure 4-5 A). There was no statistical significance between the distance migrated by cells in all three conditions tested. The medians were 66 µm for the 2 weeks expansion medium and coincidentally 71 µm for both 4 weeks in expansion medium and for 2 weeks in expansion and 2 weeks in keratocyte medium (Figure 4-5 B). DNA levels did not vary significantly throughout the culture periods indicating that an equilibrium of proliferation and death was reached (Figure 4-4 C). Simple seeding on the surface was chosen as the recellularization method since other recellularization methods had been tested in a pilot study and were less successful (Appendix Figure A-2).

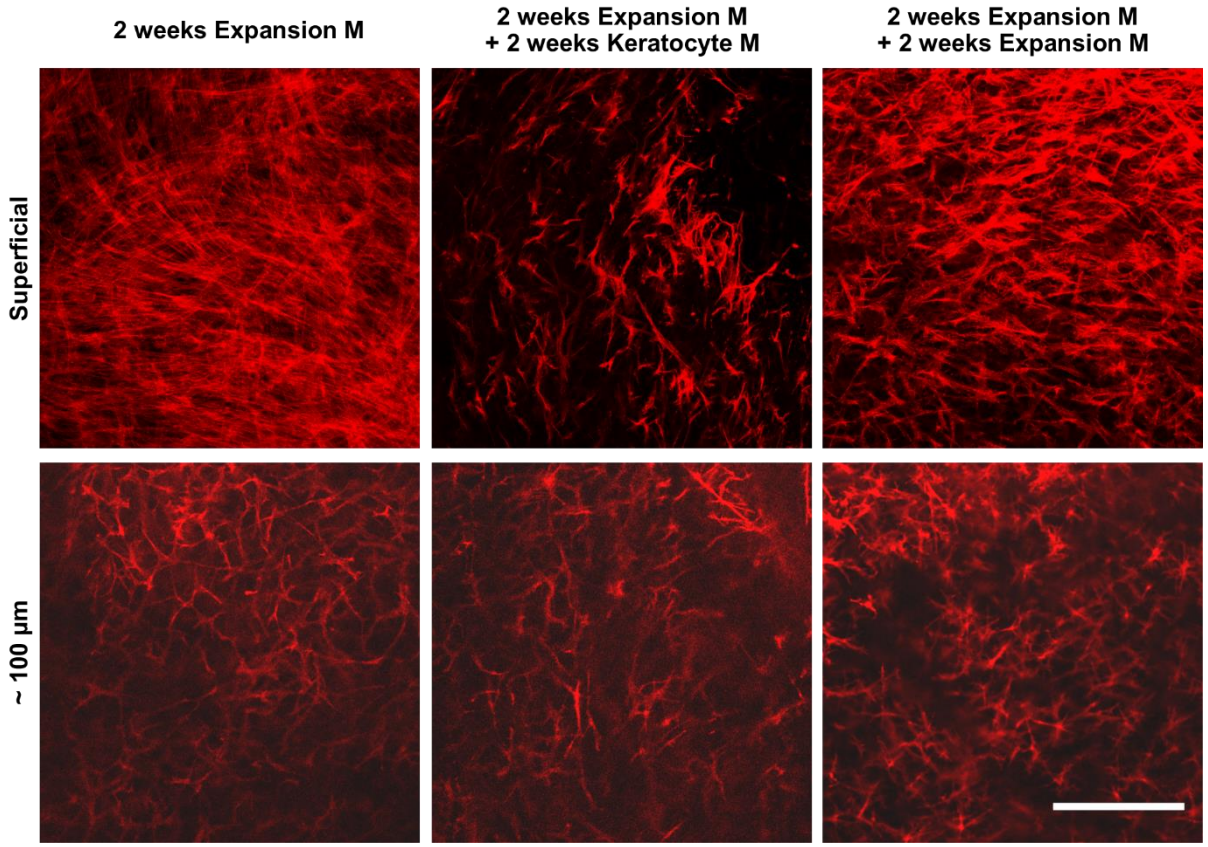

Figure 4-5. Stromal repopulation. Repopulated scaffolds imaged with confocal microscopy at superficial and deep areas. Scale bar = 200 µm.

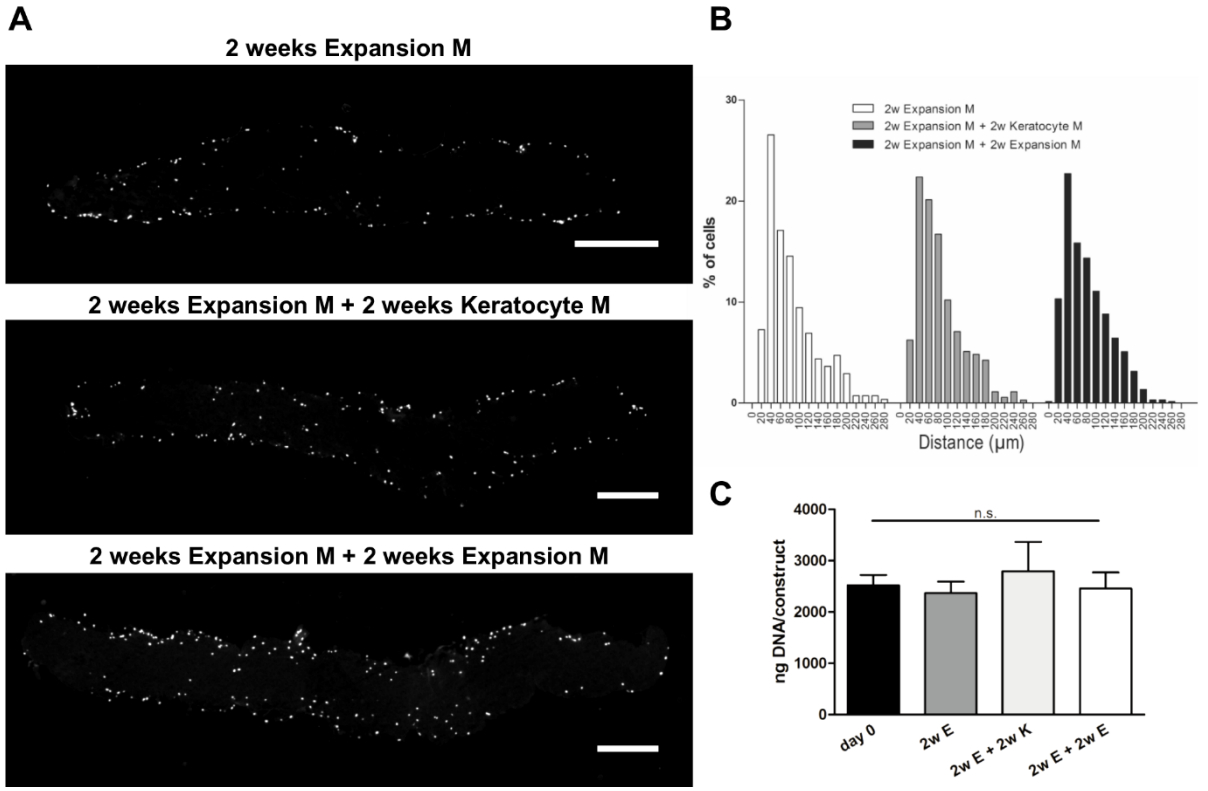

Figure 4-4. Analysis of migrated stromal cells into the scaffold. A) Histological sections of repopulated scaffolds stained with DAPI. Scale bar = 500 µm. B) Quantification of distance migrated by the cells from the surface of the scaffold. C) DNA quantification of repopulated scaffolds (n.s. = not significant).

The phenotype of cells in the repopulated scaffolds was assessed by quantitative

PCR (Figure 4-6). Keratocyte markers ALDH3A1 and CD34 were significantly up-regulated in the 2w Expansion + 2w Keratocyte medium group. Small leucine-rich proteoglycans keratocan, decorin and lumican were also up-regulated in this group. These extracellular matrix components are typically found in the corneal stroma. The expression of collagen I was up-regulated as well. There was a slight, yet significant increase in the expression of fibrotic marker α-SMA (ACTA) in the 2w Expansion + 2w Keratocyte medium group.

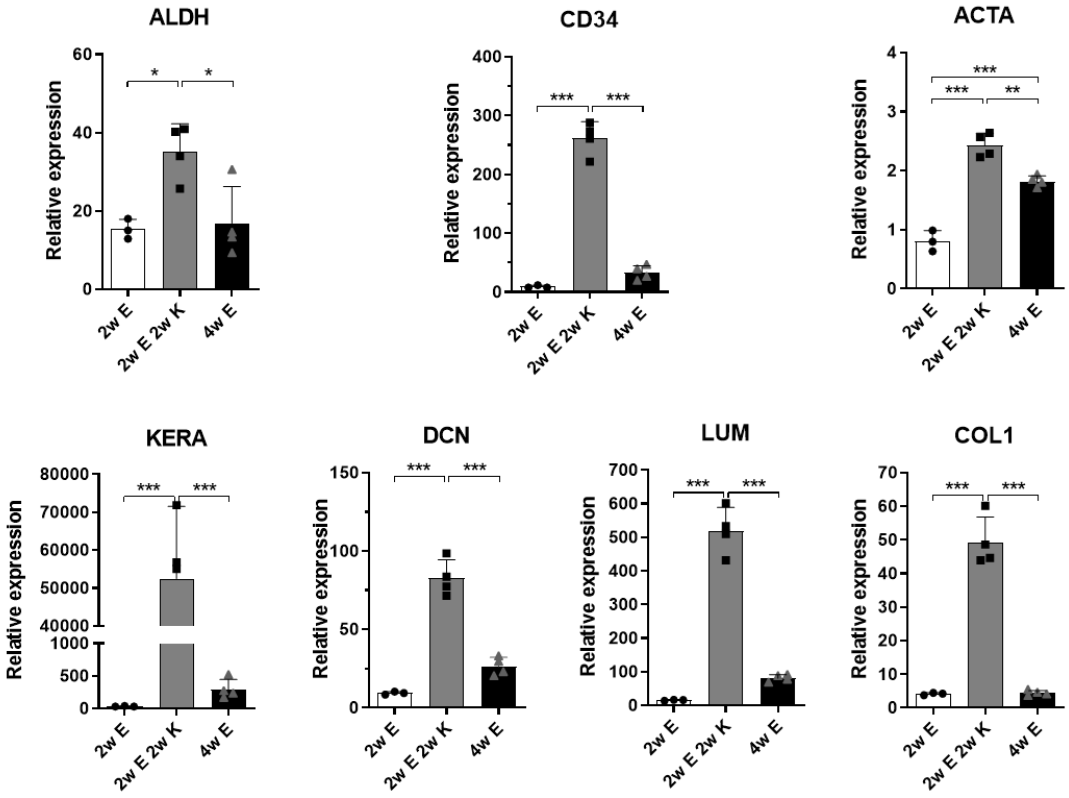

Figure 4-6. Gene expression analysis of stromal cells on scaffolds (n = 3-4). * $p < 0.05$, ** $p < 0.01$, *** $p < 0.001$.

Cell phenotype was further analysed via immunohistochemistry (Figure 4-6). Human central cornea and limbus were used as controls. Cells cultured for 2 weeks in Expansion medium followed by 2 weeks in Keratocyte medium recovered expression of ALDH3A1, but were negative for keratocan. In addition, no staining was visible for myofibroblastic marker α-SMA. Cells cultured for 4 weeks in Expansion medium showed faint ALDH3A1 staining and were negative for keratocan and α-SMA. Cells cultured for 2 weeks in Expansion medium only were negative for all three markers.

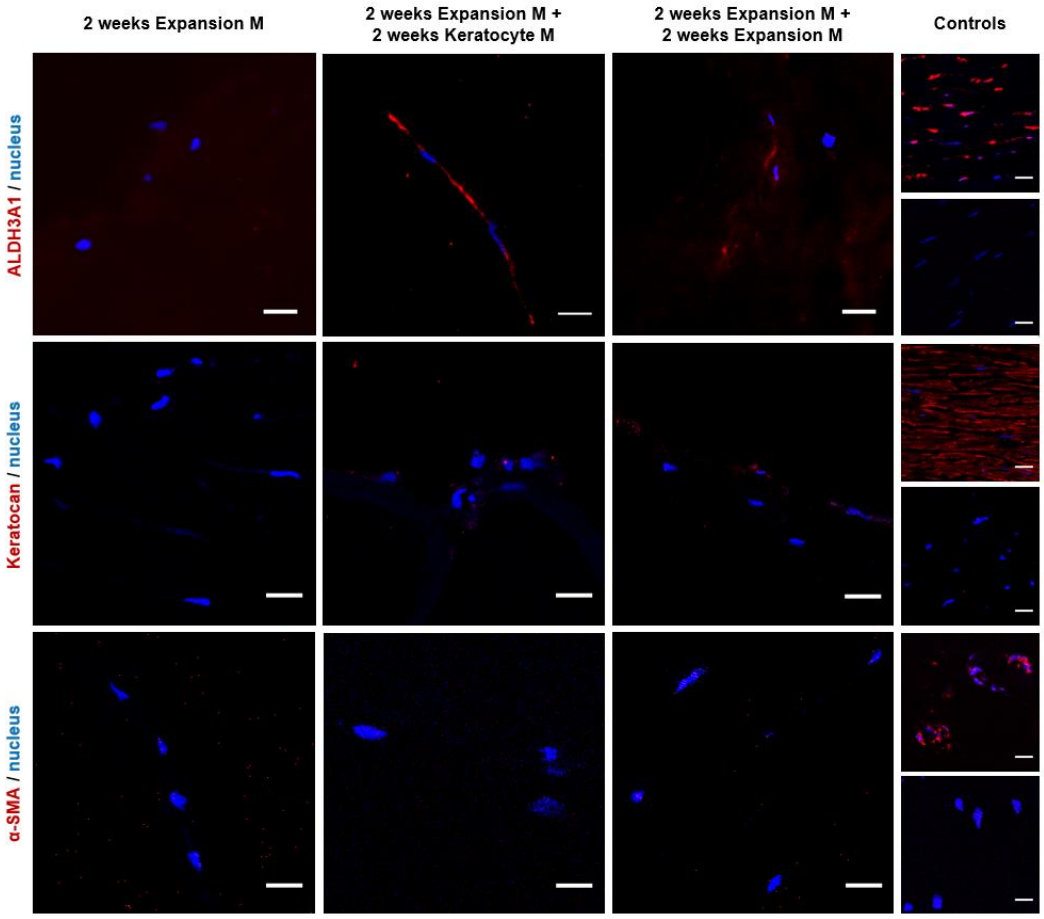

Figure 4-7. Phenotype of migrated cells. Keratocyte markers ALDH3A1 and keratocan, fibrotic marker α-SMA (scale bar = 20 µm). Positive controls for ALDH3A1 and Keratocan are taken from human central corneas and from the limbal area for α-SMA (top rows). Negative controls consisted of secondary antibody only (bottom rows).

4.3.3 Epithelial repopulation

Freshly isolated human limbal epithelial cells were seeded onto the scaffolds and colonized the surface of the scaffold. Cells adopted the typical cobblestone morphology with a high nucleus-cytoplasm ratio (Figure 4-8).

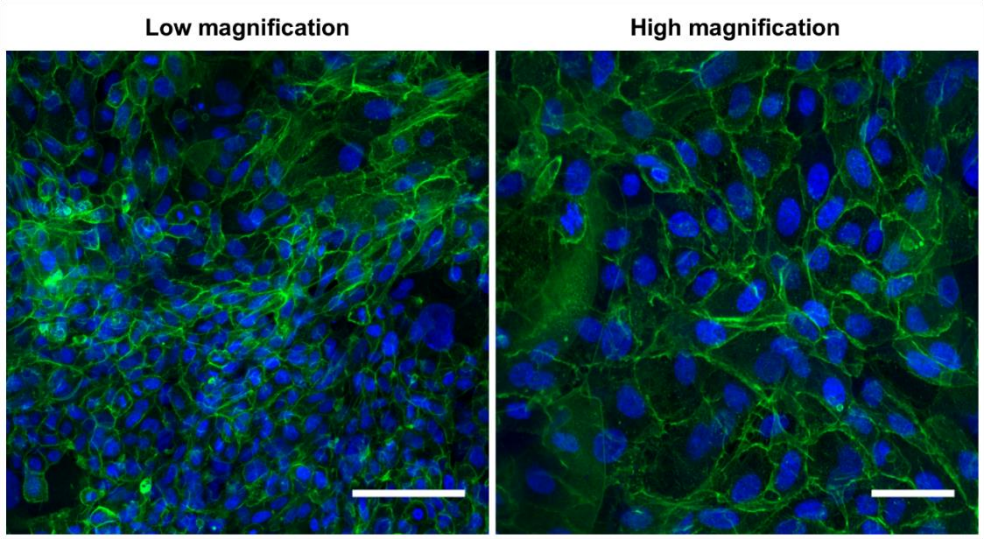

Figure 4-8. Repopulation of scaffolds with epithelial cells. F-actin (green) and cell nuclei (blue). Scale bar = 100 µm (low magnification) and 50 µm (high magnification).

4.3.4 Scaffolds show axonal regrowth potential

Neurites sprouted out from the rat DRGs and grew throughout the scaffolds after a two week culture period (Figure 4-9). This indicates that axon regrowth into the scaffolds is possible.

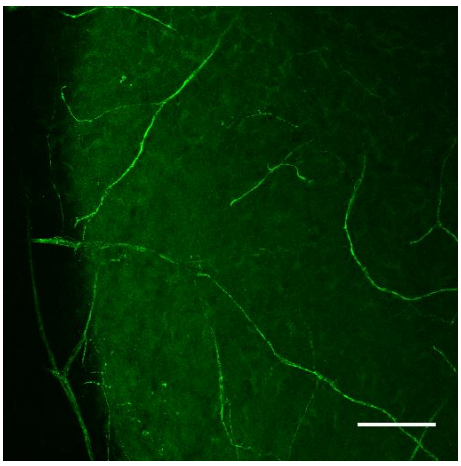

Figure 4-9. Potential of axonal regrowth into scaffolds. βIII-tubulin-positive neurites from rat DRG sprouted throughout the scaffold. Scale bar = 100 µm.

4.3.5 *In vivo* implantation of scaffolds

The scaffolds were successfully implanted with 16 10-0 sutures (Figure 4-10). Over the experimentation period, the scaffolds appeared to decrease in diameter. While some neovascularization was present, other strong evidence of rejection was absent, such as oedema or increase in intraocular pressure. Fluorescein staining demonstrated regeneration of the epithelium over the scaffold surface three weeks post-implantation (Figure 4-10 e). There was no indication of transparency returning to the implanted scaffolds by 3 months.

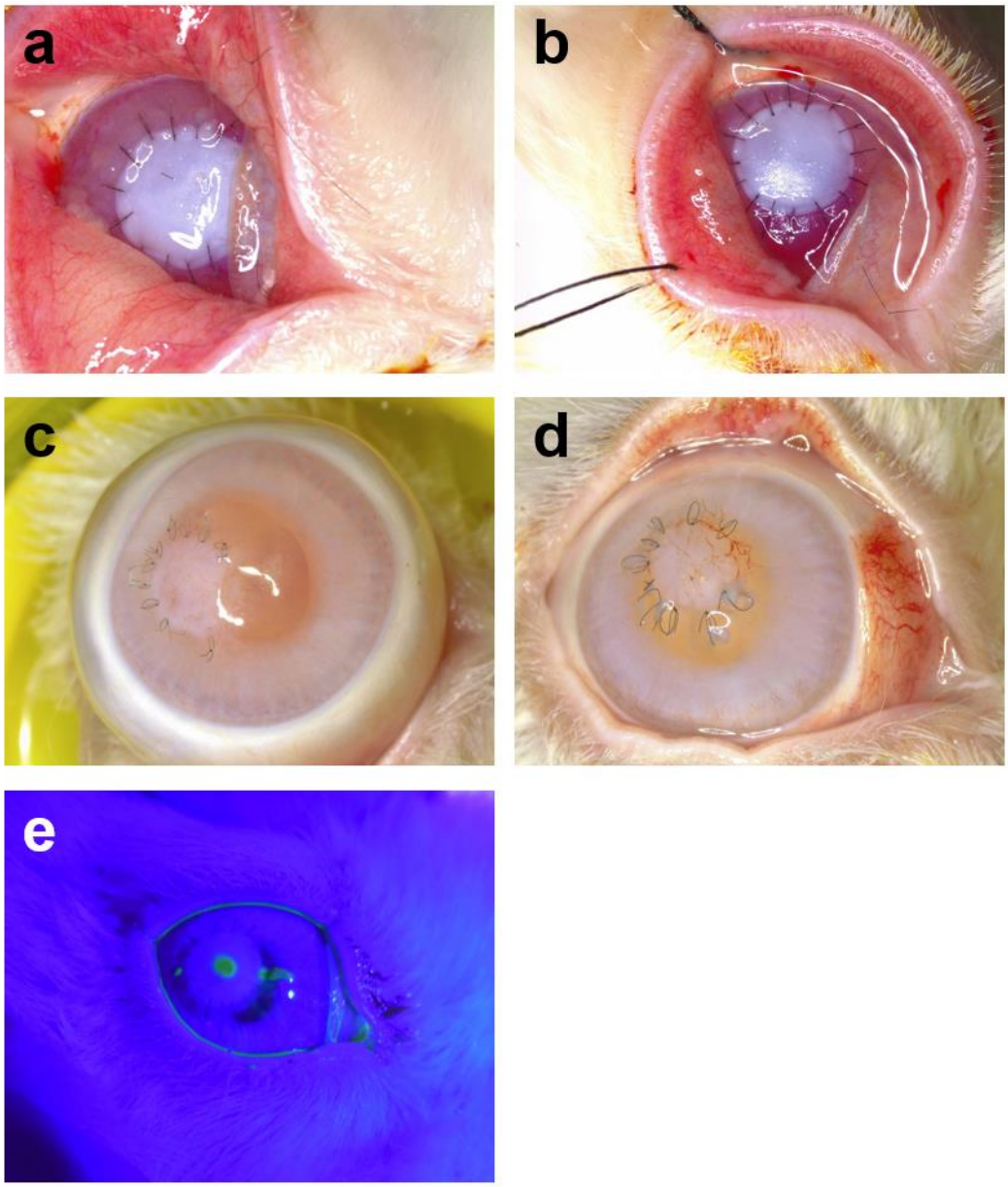

Figure 4-10. Macroscopic appearance of implants right after surgery (a, b) and after three months (c, d) of recellularized scaffolds (a, c) and non recellularized scaffolds (b, d); fluorescein staining 3 weeks post-surgery (e).

Three months after implantation animals were euthanized and the corneas retrieved for histological analysis. Epithelium was present in all corneas. Underlying the epithelium some scar tissue was present. H&E staining showed the presence of cells repopulating the implanted scaffolds (Figure 4-11). Immunostaining against ALDH1A1 showed positive cells in the epithelium, the host stroma and endothelium. Some ALDH1A1 positive cells could be observed in some scaffolds, both in the recellularized and non-recellularized groups. A vast amount of α-SMA positive were found in the underlying scar tissue, indicating the presence of myofibroblasts, α-SMA positive cells could also be observed at the walls of blood vessels.

Extracellular matrix arrangement was analysed by picrosirius red, collagen I, collagen III and fibronectin (Figure 4-12). Picrosirius red staining showed a dense tissue, somehow different than the underlying stroma, which stained positive for porcine collagen I, indicating unequivocally the implanted scaffold. The scar tissue was further characterized and resulted being fibronectin and collagen III positive. Some collagen III staining could also be observed at the underlying stroma surrounding the bottom of the scaffold. Furthermore, endothelium was intact in all cases with AQP1 expression and a thin layer of fibronectin in the Descemet's membrane (Figure 4-13).

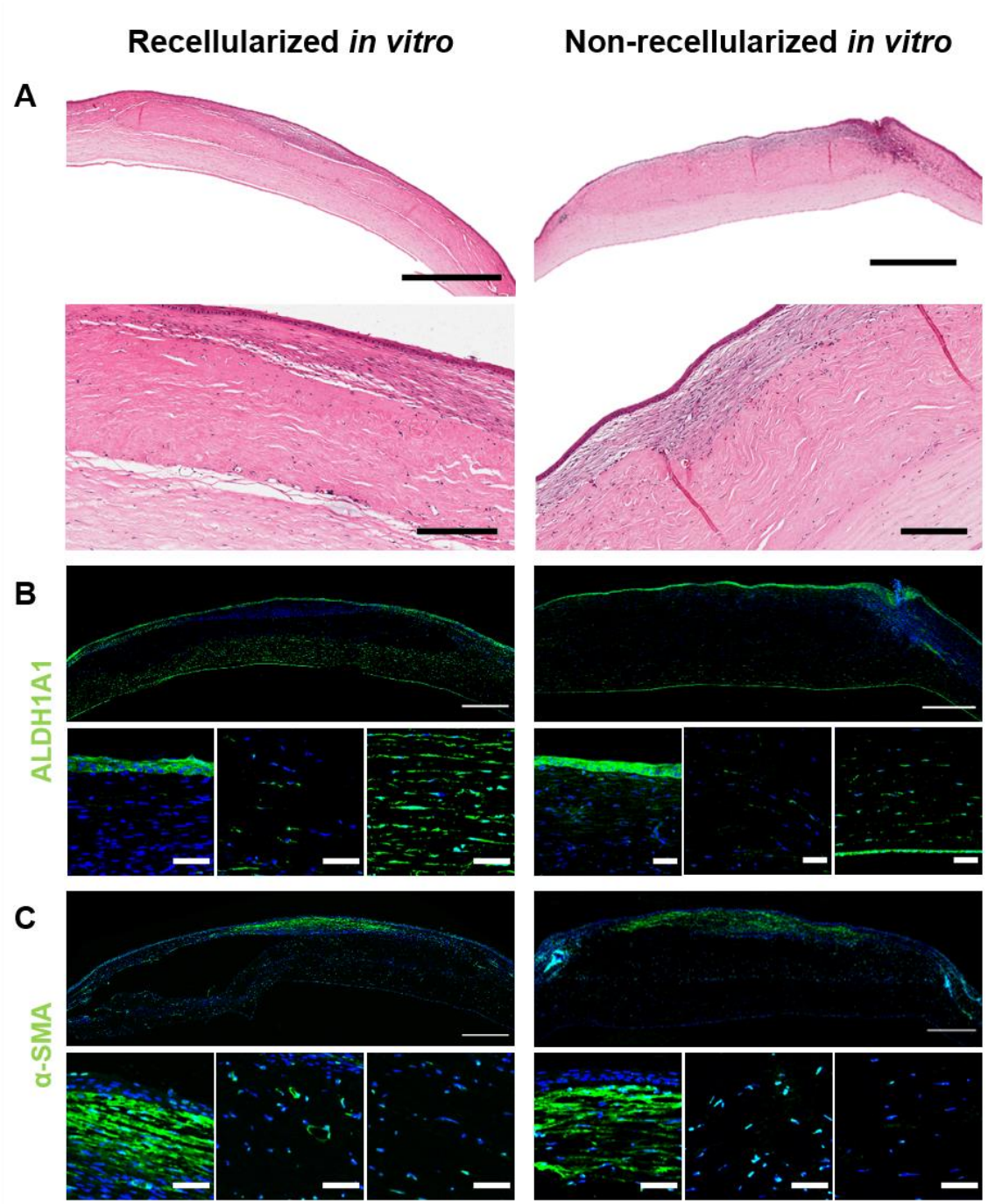

Figure 4-11. Cellular distribution and phenotype at 3 months post-implantation, representative images of an *in vitro* recellularized implant (left) and a non-recellularized one (right). A) H&E staining (low magnification scale bar = 1 mm, high magnification scale bar = 200 µm); B) immunostaining against ALDH1A1; C) immunostaining against α-SMA. B and C) overview and close-ups at top (left), centre (middle) and bottom (right) of the cornea (low magnification scale bar = 500 µm, high magnification scale bar = 50 µm).

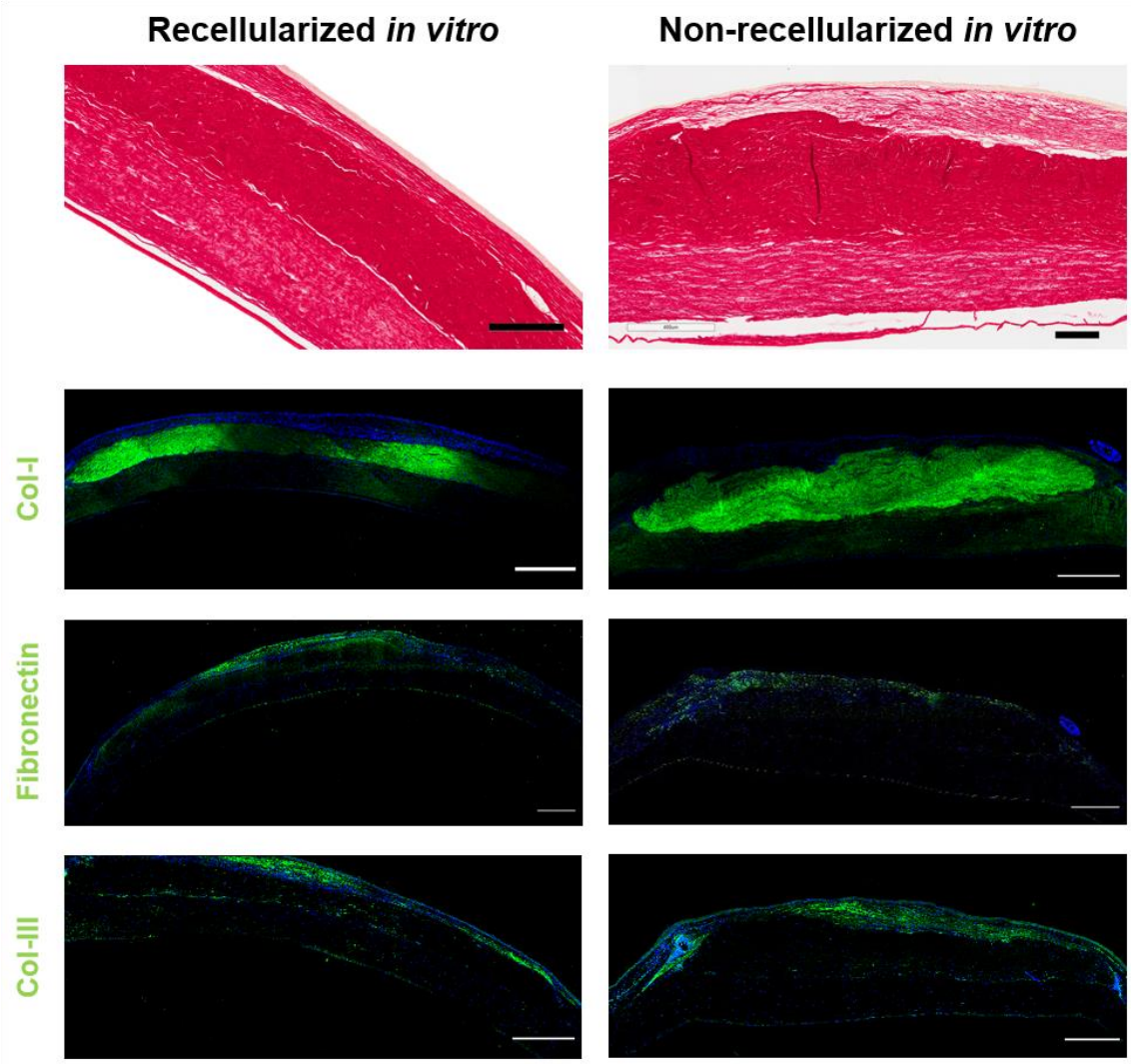

Figure 4-12. ECM analysis at 3 months post-implantation, representative images of an in vitro recellularized implants (left) and a non-recellularized one (right). Picrosirius red staining (scale bar = 200 µm) and immunostaining against collagen I, fibronectin and collagen III (scale bar = 500 µm).

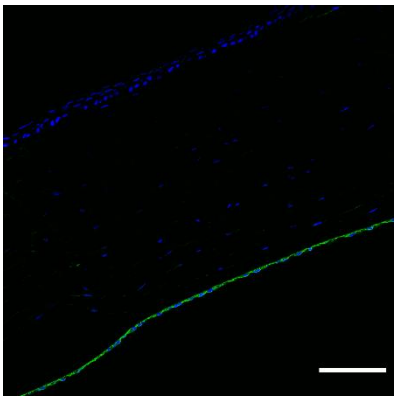

Figure 4-13. Immunostaining against AQP1 (scale bar = 100 µm).

4.4. Discussion

In this study, a scaffold obtained by decellularization of porcine corneas is presented that supported the repopulation by both epithelial and stromal cells. Cells colonized the scaffolds and retained *in vivo*-like morphology and phenotype. However, recellularization prior to implantation did not appear to have much effect on the scaffolds survival or functionality over 3 months.

Multiple decellularization methods have been reported in the literature that use physical, chemical, and enzymatic processes, or combinations. In the present study, detergents and nucleases were employed and successfully removed 96 % of dsDNA, achieving levels below the recommended 50 ng/mg of dry weight (Crapo et al., 2011). The effectiveness of cell removal was accompanied by the loss of sGAG. Similar loss of sGAG has been reported in the literature for other organs such as heart (Ott et al., 2008), liver (Uygun et al., 2010), lung (Petersen et al., 2010) and kidney (Nakayama et al., 2010), and also specifically for cornea (Pang et al., 2010; Sasaki et al., 2009). Collagen content remained constant and no disruption of the fibril architecture was apparent after decellularization.

In this study, human keratocytes have been used as the cell source for stroma repopulation. These cells can be expanded in medium containing FBS, which activates them to become more fibroblastic. To recover quiescence, i.e. *in vivo*-like phenotype, serum needs to be removed from the medium and be supplemented with ascorbic acid and insulin, as seen in Chapter 3 (Beales et al., 1999; Berryhill et al., 2002; Lynch et al., 2016a; Sidney and Hopkinson, 2016; Wilson et al., 2012). Cells repopulating the scaffolds expressed keratocyte cellular markers ALDH3A1 and CD34, and extracellular markers KERA, DCN and LUM, when cultured under serum-free conditions. González-Andrades and colleagues reported the recovery of keratocyte phenotype after repopulation of porcine corneas using hypertonic solutions (González-Andrades et al., 2011).

Corneal scarring is not uncommon after surgery, and the appropriate epithelial repopulation and basement membrane regeneration is key to minimize this scarring (Torricelli et al., 2016). In this study, all scaffolds were covered with epithelium by week 3, which is in accordance to other reports (Hashimoto et al., 2019, 2015; Huang et al., 2017). The basement membrane acts as a barrier limiting the access of pro-scarring and

inflammatory cytokines, such as TGF-β1 and IL-1β , from the epithelium and tears into the stroma (Stramer et al., 2003). This is achieved by the several ECM components other than collagens, such as nidogens, perlecan or laminin, that are part of the basement membrane of the corneal epithelium and can bind TGF-β1 (Medeiros et al., 2018). Decellularization might have impacted the composition of the basement membrane, by reducing sGAG and other components and thus compromising its barrier function. Once the basement membrane is fully regenerated, no more activation of myofibroblasts occurs, and these undergo apoptosis, reverting the scar (Mohan et al., 2003). Furthermore, despite the decellularization process not disrupting vastly the ECM, the surface topography of the scaffolds might have been altered. It is known that stromal surface irregularities can induce stromal haze and promotion of myofibroblast transformation (Netto et al., 2006).

The phenotype of the cells in the scaffolds differed from the cells in the scar tissue and the surrounding stroma. The phenotype of cells in the scaffold varied with some cells staining positive for keratocyte marker ALDH, some for myofibroblastic marker α-SMA and others for neither marker potentially indicating fibroblastic phenotype. The infiltration of other cell types such as immune cells could be identified by immunohistochemistry, for example against CD11b a marker for monocytes, neutrophils, natural killer cells, granulocytes and macrophages (Gallego-Muñoz et al., 2017a).

It remains unclear if the human cells present in the scaffolds before implantation remained viable. Labelling of the cells prior to seeding and implantation could have been used to identify them, as staining against human nucleolar antibody did not offer a conclusive answer. Reports in the literature vary widely on the repopulation of surrounding keratocytes into implanted biomaterials. Acellular porcine corneas implanted in humans showed very little repopulation at 3 months (Li et al., 2019), but multiple stromal cells were present at only 2 months in a separate study (Shi et al., 2017). The depth of the tissue removed and, consequentially, the amount of host stroma left could play a role supporting scaffold repopulation *in vivo*. In more porous materials such as the recombinant collagen III hydrogels cross-linked with 2-methacryloyloxyethyl phosphorylcholine (a synthetic phospholipid), described by May Griffith's group, multiple cells can be observed in the stroma by *in vivo* confocal imaging (Buznyk et al., 2015). These cells, however, these cells were highly reflective, indicating an activated keratocyte or myofibroblast phenotype.

The promotion of endogenous nerve regeneration is believed to be an important factor in corneal health after transplantation, when the nerves are severed (Shtein et al., 2012). While it was not evaluated in this study, re-innervation of the grafts is not expected to have occurred in the timeframe of our study. In a recent study by Li and colleagues, the presence of nerves was reported only after 6 months post-implantation in 2 out of 27 cases (Li et al., 2019). In normal allografts some stromal nerves can appear after 2 months, but basal epithelium re-innervation might not occur until 2 years post-surgery, with corneal sensitivity being recovered no earlier than 3 years (Darwish et al., 2007; Richter et al., 1996). Similar to repopulation by surrounding stromal cells, the porosity of the implant can influence re-innervation; making hydrogels much easier to re-innervate (Islam et al., 2018; Jangamreddy et al., 2018). As seen by the *in vitro* test, rat DRGs were able to sprout over the scaffolds, showing that re-innervation should not be impeded. Similar *in vitro* validations have been used before using embryonic mice DRGs (Boulze Pankert et al., 2014) and embryonic chick DRGs (Liu et al., 2008).

4.5. Concluding remarks

In this Chapter we successfully obtained scaffolds from decellularized porcine corneas that could be recellularized with stromal cells which recovered keratocyte-like phenotype. These scaffolds supported the growth of epithelial cells and the sprouting of DRGs *in vitro*. When implanted *in vivo* in an ALK rabbit model, both recellularized and non-recellularized scaffolds were tolerated and not rejected, despite some neovascularization occurring. In the following Chapter modifications to the fabrication of these scaffolds will be made in order to obtain constructs with high cellularity.

CHAPTER 5

Anterior cornea tissue equivalents based on decellularized stromal sheets and cell-laden collagen hydrogels

5.1. Introduction

As seen in Chapter 4, it is possible to recellularize decellularized corneas by simple seeding. However, to achieve sufficient repopulation, a minimum of two weeks in proliferation conditions was needed. Lengthy culture periods could hinder the translation of these therapies as it can increase their cost and delay the treatment of the patient. Therefore, strategies to enable the immediate incorporation of cells throughout the scaffold would be desirable to reduce time and costs.

An origin of corneal tissue available for decellularization are lenticules extracted from myopia correction surgeries, known as small incision lenticule extraction (SMILE). Otherwise discarded, these thin sections of tissue can provide an excellent material (Hong et al., 2018; Yam et al., 2016; Yin et al., 2016). The use of decellularized lenticules sandwiched with fibrin glue has been reported in a rabbit model of ALK (Yin et al., 2016). These fully acellular constructs were fully re-epithelialized 4 weeks post-implantation and at 3 months the fibrin gel had fully dissolved and the construct had engrafted with the stromal bed. While some sparse cells could be seen in the decellularized lenticules, the phenotype of these was not characterized. In another study, thin sheets of decellularized porcine cornea were implanted intrastromally in a layered fashion seeding stromal cells on top of each sheet (Ma et al., 2015). After six months the corneas had the same thickness as unoperated eyes and some cells were visible in between engrafted sheets. However, it was unclear if those cells were the implanted ones or came from the host. The first study showed the feasibility of binding the decellularized lenticules without using cells, while the second study showed the possibility of recellularizing each layer *in situ*. The combination of both approaches set the basis for this study.

The aim of this study was to develop a corneal substitute by using sheets of decellularized porcine cornea and cell-laden collagen hydrogels. These constructs

presented high transparency, easy handling after fabrication, high viability and *in vivo*-like phenotype after a culture period of 3 weeks. Furthermore, constructs containing both stromal and epithelial cells were fabricated, and remained viable when sutured into an *ex vivo* model of ALK.

5.2. Materials and Methods

5.2.1 Fabrication of acellular matrix sheets

Porcine eyes were obtained within 24 hours from abattoir death. After trimming and under sterile conditions, the eye globes were washed twice with phosphate buffered saline (PBS), immersed in 2% iodine solution (Videne®, Ecolab, Belgium) for 4 minutes under gentle agitation and then rinsed three times with PBS for 2 minutes. The central corneal button from each eye was excised using a 10 mm biopsy punch. Corneal buttons were embedded in optimal cutting temperature medium (OCT, Thermo-Scientific, Ireland), snap-frozen in liquid nitrogen and cryosectioned on a cryostat (Leica, Germany) to obtain 60 µm-thick slices. Slices were washed in PBS to remove OCT and then transferred into a decellularization solution of 0.5% (w/v) sodium dodecyl sulphate (SDS) and 1% (v/v) Triton X-100 (both Sigma-Aldrich, Ireland) in distilled water for 24 hours at room temperature. To promote penetration of the solution and removal of debris, this and further processing was carried out on an orbital shaker. The samples were treated with 10 U/ml of RNAse and DNAse in 10 mM $MgCl_2$ solution for 1 hour at 37 °C (all Sigma), then decontaminated by washing in PBS supplemented with 100 U/ml penicillin, 100 mg/ml streptomycin (both Gibco, Ireland) and 250 ng/ml amphotericin B (Sigma) for another 24 hours at room temperature, followed by washing in sterile distilled water 3 times. The acellular sheets were air-dried in a sterile biohazard cabinet and stored in a sealed container at room temperature until use. Native, decellularized, and decellularized, dehydrated and rehydrated sheets were fixed in 4% paraformaldehyde for 15 minutes at room temperature. They were then embedded in paraffin wax and sectioned on a microtome (Leica). Slides were de-paraffinized, rehydrated and coverslipped using DAPI-containing aqueous mounting medium (Sigma). Slides were imaged with an epifluorescence microscope (Olympus IX83). The thickness of the sheets was measured

in ImageJ from those images (n = 20-30). Additionally, the macroscopic appearance and transparency of the dried acellular sheets was assessed by placing them over printed text.

5.2.2 DNA content

Native and decellularized porcine cornea sheets were freeze dried and digested in 3.88 U/ml of papain solution rotating at 60 °C for 18 hours. DNA content was then quantified using a Quant-iT™ PicoGreen® dsDNA Kit (Invitrogen, Ireland) following the manufacturer's instructions. The plates were read using a spectrophotometer (BioTek™ Synergy HTX) using 480 nm excitation wavelength and 520 nm emission wavelength.

5.2.3 Degradation test

In vitro enzymatic digestion was performed to determine the resistance to biodegradation. Single decellularized sheets and 100 µl collagen gels (cast as described later) were tested by being incubated with 1 ml 20 U/ml collagenase I (Gibco) in PBS at 37 °C. Photographs were taken periodically, before the supernatant was collected and fresh collagenase solution added. Collagen content in the supernatant was quantified by measuring the hydroxyproline content via a dimethylaminobenzaldehyde (DMBA) assay (Kafienah and Sims, 2004). Briefly, 200 µl of supernatant at each time-point was digested with 12 M HCl for 18 hours at 110 °C. These samples were then allowed to evaporate for 48 hours at 50 °C in a fume hood. After evaporation, the dry samples were resuspended in deionized water and incubated for 20 minutes at room temperature with Chloramine T and an oxidizing buffer. DMBA reagent was added and incubated for 20 minutes at 60 °C. After cooling the reactants were read at 570 nm in a plate reader (BioTek™ Synergy HTX).

5.2.4 Cell culture

Human corneal stromal cells were isolated from the healthy corneo-scleral rims remaining after corneal surgeries as described in Chapter 3. In this study cells were expanded from cryopreserved stocks and used at passages 4 and 5 from a single donor. Expansion medium consisted of low glucose DMEM (HyClone) supplemented with 10% FBS (Gibco).

Human telomerase immortalized corneal epithelial cells (hTCEpi, Evercyte, Austria) were expanded and cultured using Keratinocyte Growth medium (PromoCell, Germany), following manufacturer's instructions. A cell line was used in this study for its availability.

5.2.5 Construction of an engineered corneal stroma

Collagen hydrogels were prepared from rat tail collagen I (Corning, USA) as previously described (Ahearne et al., 2008). A 3.5 mg/ml solution was prepared from stock, salt concentration adjusted using 10x PBS and pH raised to neutral by addition of 1 N NaOH. After this neutralisation, 10,000 cells/µl gel were embedded in the solution. 25 µl of solution was deposited on a decellularized corneal sheet and a second sheet placed on top. This process was repeated until there were 4 gels and 5 sheets. This construct was then incubated for 30 minutes at 37 °C in a humidified incubator, before being submerged in a media of DMEM/F12 (1:1, Hyclone) supplemented with 1x insulin-transferrin-selenium (ITS, Gibco) and 100 µg/ml L-ascorbic acid-2-phosphate (Sigma). This medium was chosen as it has been shown to promote a keratocyte-like phenotype (Chapter 3). Constructs were fed every second day for 3 weeks.

50.000 hTCEpi cells were seeded on the construct after 2 weeks and cultured for another week in Keratinocyte growth medium. A cell line was used in this study for their availability compared to primary cells from donor tissue.

5.2.6 Cell viability

Constructs were incubated with 2 µM Calcein-AM and 4 µM EthD-1 (both Biotium) for 1 hour at 37 °C in a humidified incubator. Samples were washed three times in PBS and imaged by laser scanning confocal imaging (Leica SP8).

5.2.7 Transparency and light transmittance

The macroscopic appearance of the constructs was assessed by placing them over printed text. Additionally, light transmittance through the constructs after three weeks of culture was quantified by measuring the absorbance of light at different wavelengths ranging from 300 to 700 nm that pass through each sample using a microplate reader (BioTek™ Synergy HTX, USA). The absorbance of light passing through ultrapure water was used as a control to represent 100% transmittance and this absorbance reading was subtracted from the measured absorbance of each sample to give the change in absorbance due to the sample being present (*A*). The transmittance of light was calculated using the following formula as described elsewhere (Kim et al., 2019b):

$$Transmittance\ (\%) = \frac{1}{10^{A}} \times 100$$

5.2.8 qPCR

RNA from constructs was extracted using Trizol, following the manufacturer's instructions (Invitrogen). To increase lysis and release of the genetic material, samples were triturated using a tissue homogenizer (IKA T10 basic, Germany). Chloroform was added, the samples were vortexed and then centrifuged for 15 minutes at 12,000 g at 4 °C. The supernatant was transferred into a new tube and an equal volume of isopropanol added, along with 3 µl of GlycoBlueTM (Invitrogen) to improve precipitation. Samples were kept overnight at -20 °C and then centrifuged at 12,000 g for 15 minutes at 4 °C. The supernatant was discarded and 70% ethanol in RNAse-free water used to wash the pellet. Samples were centrifuged again, and the supernatant removed before the pellets were air dried. The pellets were dissolved in RNAse-free water and RNA yield and purity quantified using a NanoDrop-1000 (Thermo-Scientific). All steps were performed on ice. RNA was converted into cDNA using a high capacity cDNA reverse transcription kit (Invitrogen). Real-time PCR was performed using TaqMan Universal Master Mix II and the following TaqMan primers: glyceraldehyde-3- phosphate dehydrogenase (GAPDH, Hs02758991_g1), aldehyde dehydrogenase 3A1 (ALDH3A1, Hs00964880_m1), alpha smooth muscle actin (ACTA2, Hs00426835_g1), keratocan (KERA; Hs00559942_m1), collagen 1a1 (COL1; Hs00164004_m1), lumican (LUM, Hs00929860_m1), decorin (DCN, Hs00754870_s1) and CD34 (Hs00990732_m1). The genes of interest were normalized against GAPDH using the ΔΔCt method. Calculated values were expressed as a power of $2^{-\Delta\Delta Ct}$. For this study, all values were normalized to the serum-expanded cells.

5.2.9 Histological analysis and immunohistochemistry

After culture, samples were fixed with 4% paraformaldehyde for 15 minutes at room temperature. Afterwards they were embedded in paraffin and sectioned using a microtome. Routine Haematoxylin & Eosin, Alcian Blue and Picrosirius Red staining were performed. Slides were stained with Harris Haematoxylin (Sigma-Aldrich) for 4 minutes, followed by a 10-minute wash with running tap water. Then slides were immersed in acid alcohol for 30 seconds and washed with tap water for 5 minutes. Finally, slides were stained with Eosin Y (Sigma-Aldrich) for 2 minutes. Alcian blue was used to assess sGAG content. Slides were stained with 1% Alcian Blue 8GX (Sigma-Aldrich) in 0.1 M HCl for 5 minutes followed by three 30-second washes in dH_2O. Picro-sirius red

was used to assess collagen distribution. Slides were stained with Sirius Red (Sigma-Aldrich) in a saturated aqueous solution of picric acid for one hour and then for one minute in 0.5% acetic acid. After staining, all slides were dehydrated and coverslipped using DPX.

Immunofluorescent staining was performed as follows. Slides were rehydrated followed by an antigen retrieval step. Samples were then blocked with 1% BSA and 10% donkey serum in 0.5% Triton X-100 for one hour at room temperature. The following primary antibodies were used: Collagen I (ab90395, Abcam), Decorin (ab189364, Abcam), Keratocan (HPA039321, Sigma), ALDH3A1 (ab76976, Abcam), Lumican (ab168348, Abcam), CD34 (ab81289, Abcam) and α-SMA (ab7817, Abcam), and incubated overnight at 4 °C. Afterwards, three 5-minute washes with 1 % BSA in PBS were performed. Secondary antibody was then incubated for 1 hour at room temperature. Samples were then washed three times for 5 minutes with 1% BSA in PBS. Slides were then coverslipped using DAPI-containing aqueous mounting medium (Sigma). Slides were imaged using laser scanning confocal microscopy (Leica SP8).

Constructs containing epithelial and stromal cells were fixed for 15 minutes in 4 % paraformaldehyde, subsequently stained with Phalloidin-TRITC (Sigma) and DAPI, and imaged using laser scanning confocal microscopy (Leica SP8).

5.2.10 Implantation of constructs onto an *ex vivo* porcine cornea

Porcine eyes were obtained within 24 hours from abattoir death. A 6 mm diameter defect of approximately half of the depth of the cornea was made using a trephine. Lamellar dissection was performed using a blunt crescent knife (Beaver-Visitec International, UK). Constructs after 3 weeks of culture (without epithelial cells) were sutured in place with 4 or 8, 10-0 nylon sutures. The corneas were resected with 5 mm of scleral rim and placed onto a hemispherical agarose mould (2% agarose w/v). Corneas were cultured for 7 days in a humidified chamber in 4 ml of serum-free DMEM/F12, supplemented with 4% dextran (MW 450,000-650,000, Sigma) to limit swelling. The media was added to the level of the limbus, leaving the cornea at the air-liquid interphase. Medium was changed daily, with 3 drops added onto the corneal surface to limit drying. To determine re-epithelialization from the host tissue fluorescein staining was performed. Four-five drops of 1% fluorescein sodium salt (Sigma) in PBS solution were added to cover the surface of the corneas, after one minute of incubation at room temperature,

sterile PBS was used to wash the corneas until no more dye was visibly leaching. In the dark, samples were exposed to blue light from a handheld slit lamp (15090 – PSL, Reichert) and imaged with a cell phone. This was performed at 2 and 7 days after implantation. After culture, corneas were fixed overnight in formalin and processed for wax embedding and H&E staining, as previously described.

5.2.11 Statistical analysis

All experiments were performed three times with a minimum of three replicates. Unpaired two-tailed t-test and 2-way ANOVA were employed. Statistical significance was accepted at a level of $p < 0.05$.

5.3. Results

The decellularized sheets obtained were highly transparent (Figure 5-1 A). Sections stained with DAPI presented no cell nuclei after decellularization (Figure 5-1 B). Thickness measurements showed that the decellularization procedure had a swelling effect on the sections and that, when sections were air dried and rehydrated, they did not recover their original thickness. Figure 5-1 C). Quantification of dsDNA showed successful decellularization, with significantly lower levels of DNA remnants than the native tissue (Figure 5-1 D). Native sheets had 982.8 ± 286 ng/mg of DNA per dry tissue (average ± standard deviation), while decellularized sheets presented 13 ± 1.2 ng/mg of DNA per dry tissue (average ± standard deviation).

Degradation was slower in the decellularized sheets than the collagen hydrogels. After 4 hours of incubation in collagenase solution, hydrogels appeared to completely degrade, while decellularized sheets were still visible (Figure 5-2A). Even after 24 hours, remnants of the sheets were still present. When quantified (Figure 5-2 B), 57% of the hydrogels was degraded by 2 hours, 87% by 4 hours and 100% after 24 hours. In comparison, 39%, 73% and 92% of the decellularized sheets were degraded after 2, 4 and 24 hours, respectively. After 48 hours, sheets had degraded completely.

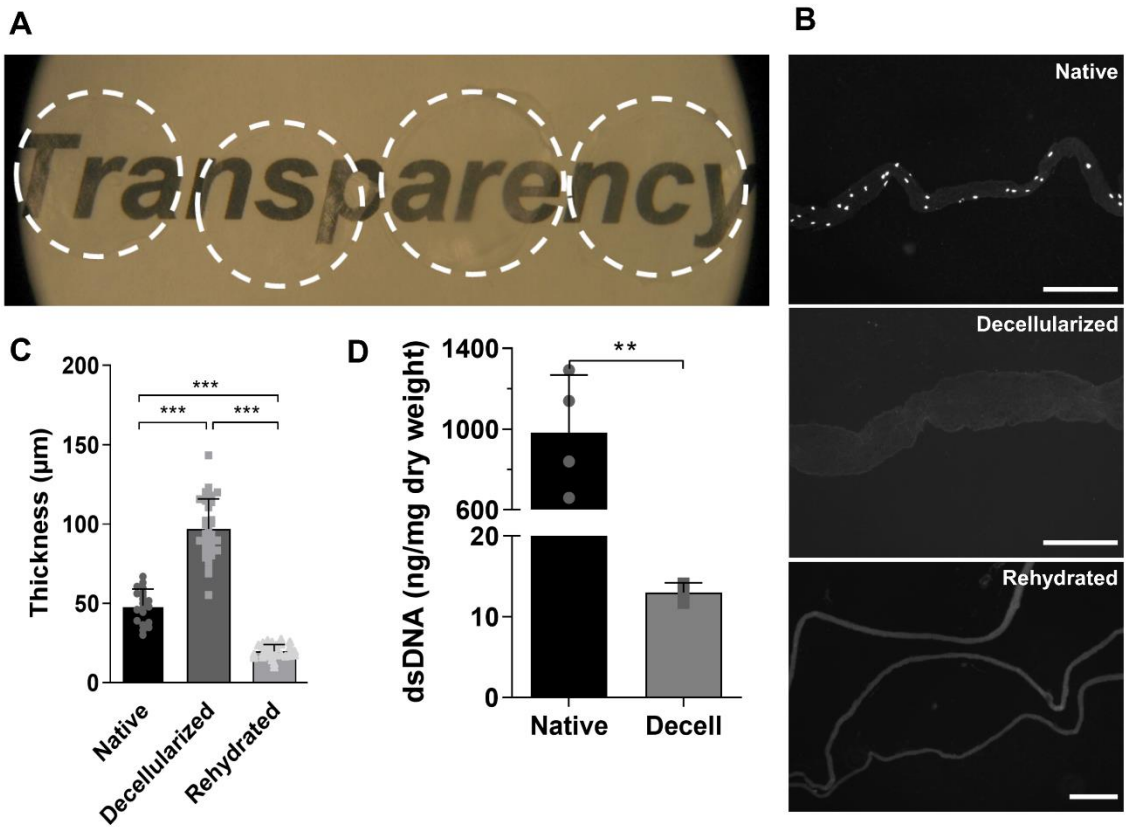

Figure 5-1. Characterization of decellularized sheets. A) Macroscopic appearance of the sheets, which were highly transparent. B) DAPI staining of wax embed sheets showing the absence of cell nuclei after decellularization (scale bar = 200 µm). C) Thickness measurements of sheets: native, after decellularization, and after dehydration and rehydration (n=20-30). D) dsDNA quantification of native and decellularized sheets (n=3-4). * $p \leq 0.05$, ** $p \leq 0.001$, *** $p \leq 0.0001$.

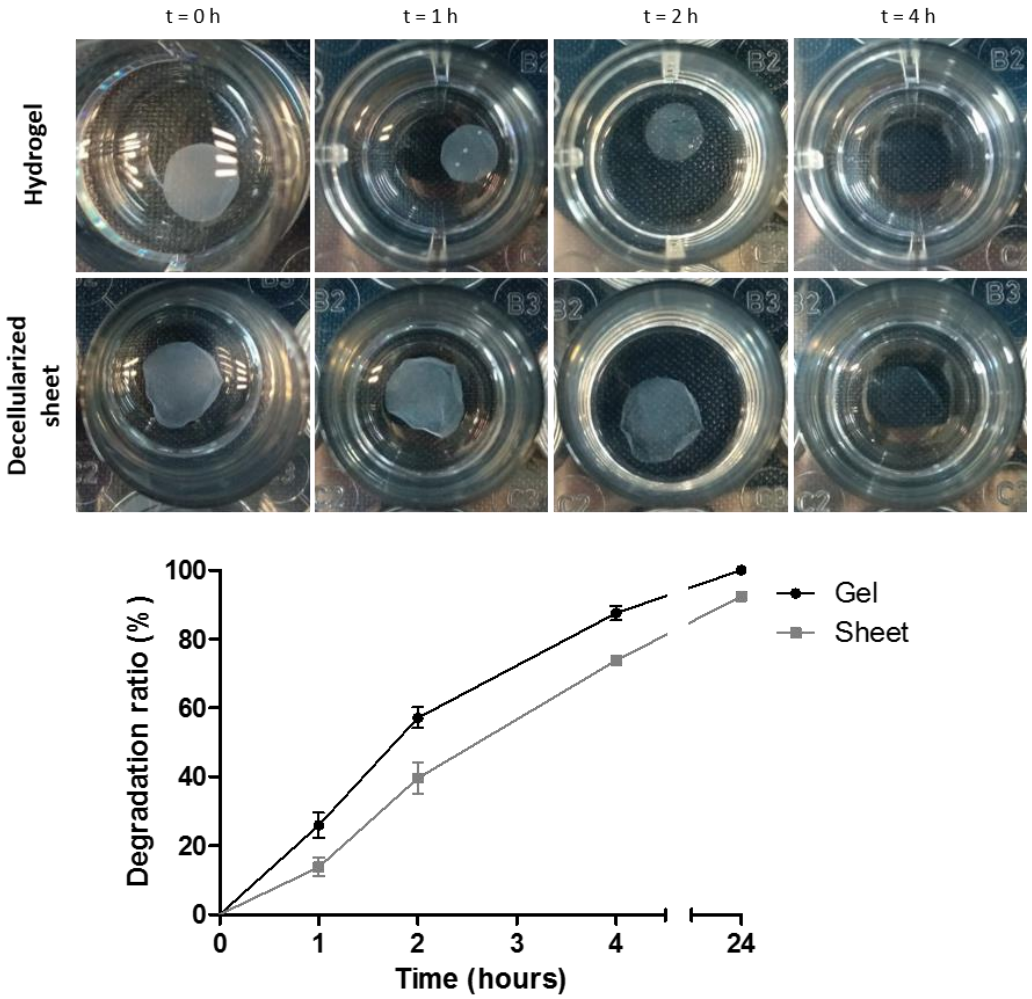

Figure 5-2. Resistance to biodegradation. Macroscopic visualization and quantitative analysis of degradation (n=4).

Tissue constructs were obtained by stacking dried sheets with cell-laden collagen hydrogels between sheets. Human corneal stromal cells remained highly viable in the constructs throughout the culturing period, even in serum-deprived conditions (Figure 5-3). After one day in culture, some cell spreading could be detected within the scaffold. After the culture period, most cells presented an elongated morphology with visible processes. Furthermore, constructs presented good optical properties when assessed macroscopically (Figure 5-4 A). When quantified, constructs allowed for >40% of transmittance in the longer wavelengths of the visible spectrum (Figure 5-4 B).

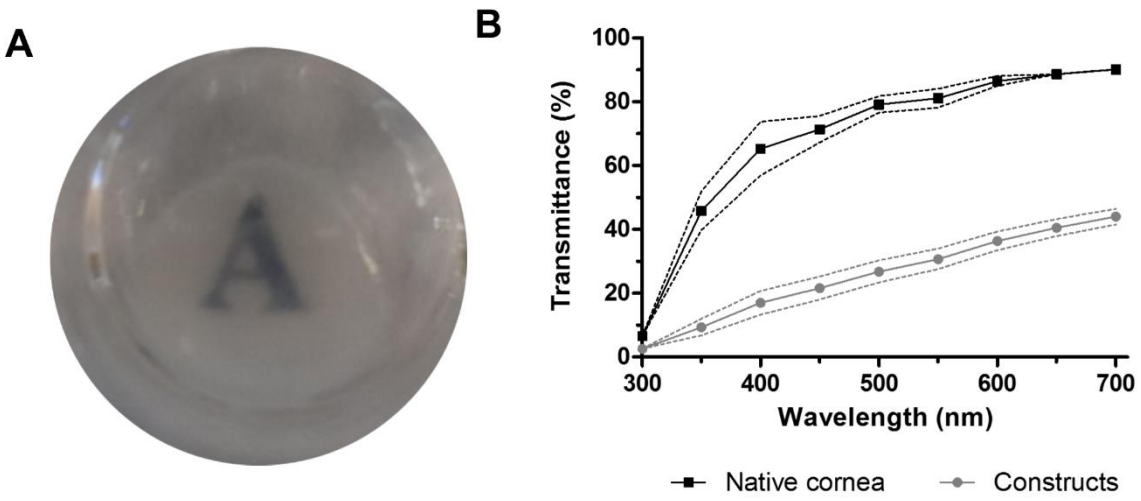

Figure 5-4. Macroscopic appearance of constructs after 3 weeks of culture (A) and quantification of light transmittance (B) (n=5-25).

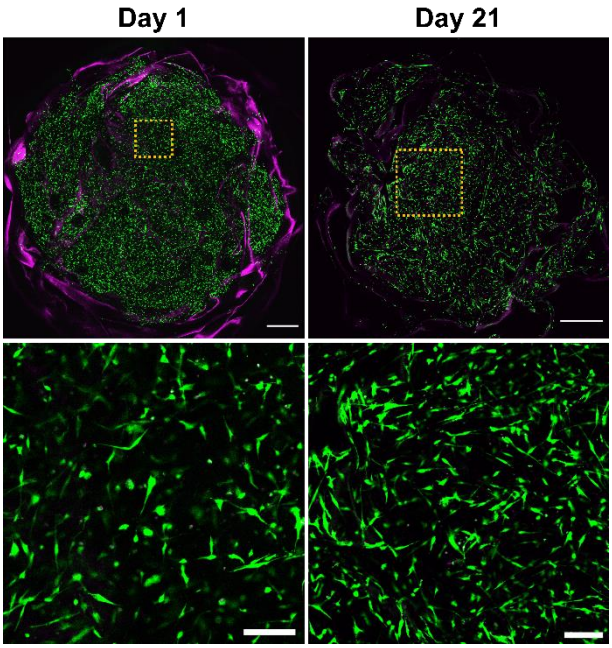

Figure 5-3. Cell viability in constructs after fabrication and after 3 weeks in culture (live = green, dead = magenta, top scale bar = 1 mm, bottom scale bar = 200 µm).

Characteristic markers of cornea ECM and stromal cell phenotype were analysed by qPCR (Figure 5-5). Keratocyte markers ALDH3A1 and CD34 were significantly up-regulated when compared to the constructs cultured for one day in serum-free conditions. This shows the plasticity of these cells to recover keratocyte markers upon serum starvation. All ECM components analysed were highly up-regulated. Typical small leucine-rich proteoglycans found in the cornea keratocan, lumican and decorin were

expressed significantly higher. The expression of collagen I, the most common collagen in the corneal stroma, was significantly up-regulated. Furthermore, fibrotic marker ACTA was not significantly up-regulated.

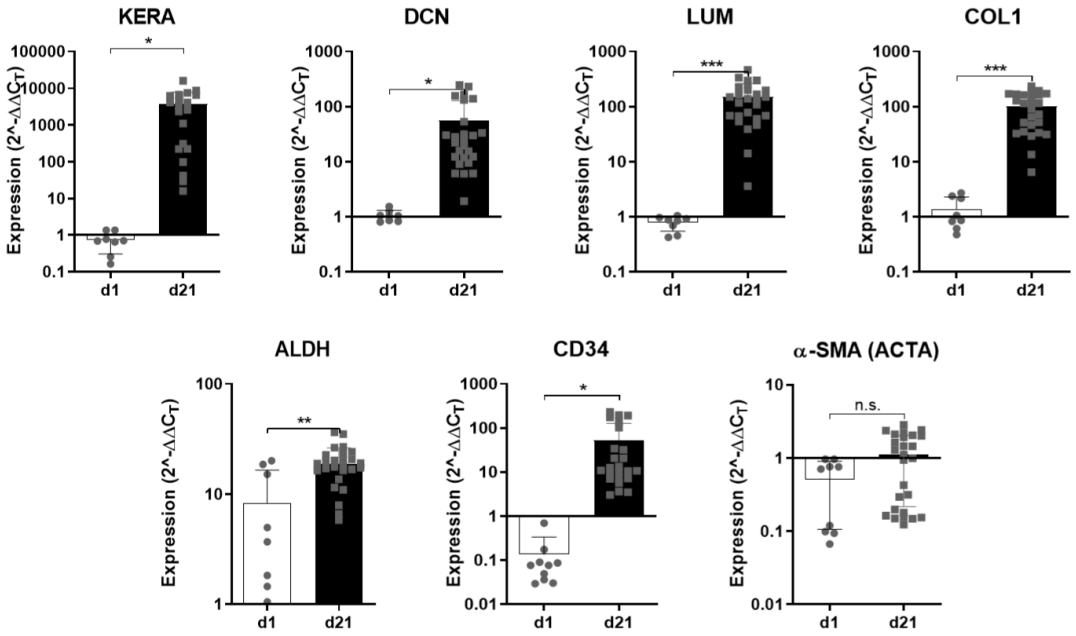

Figure 5-5. Phenotypic analysis of stromal cells in the constructs by qPCR. Relative expression of Keratocan (KERA), Decorin (DCN), Lumican (LUM), Collagen I (COL1), ALDH3A1, CD34 and α-SMA (ACTA). (n=5-18) * $p \leq 0.05$, ** $p \leq 0.001$, *** $p \leq 0.0001$.

Constructs were further analysed via histology and immunohistochemistry (Figure 5-6). The thickness of the constructs decreased significantly during the culturing period, from 245.2 ± 66.50 µm to 187.9 ± 27.44 µm, presumably due to the cells remodelling the collagen hydrogel. Constructs presented cells distributed evenly in all hydrogel layers, as seen by H&E staining (Figure 5-6 A). Picrosirius red staining for collagen showed differential staining in the hydrogel portion and the decellularized sheets (Figure 5-6 B). Despite the loss of sGAG during decellularization, upon subsequent culture, cells produced their own ECM in the hydrogel sections (Figure 5-6 C). Immunohistostaining corroborated the results obtained from qPCR with constructs staining positive for ALDH3A1, CD34, keratocan, lumican, decorin and collagen I, while α-SMA remained negative (Figure 5-6 D).

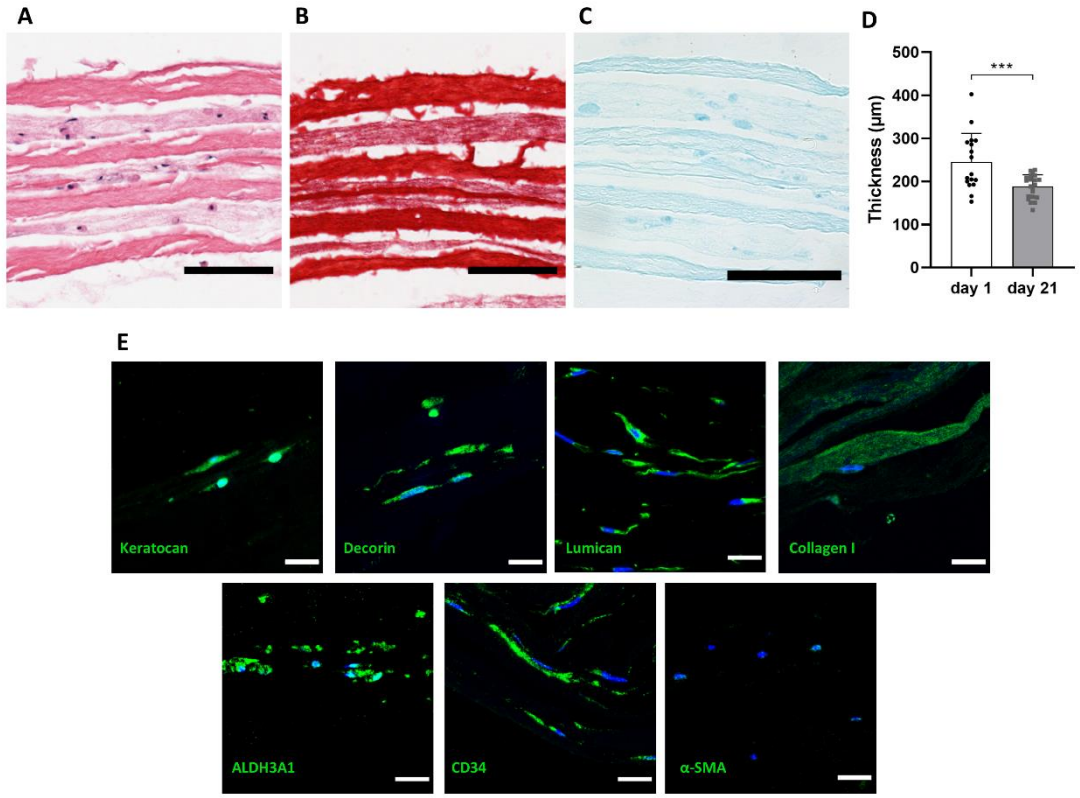

Figure 5-6. Histological examination of constructs at day 21, staining with A) haematoxylin and eosin, B) picrosirius red and C) alcian blue (scale bar = 100 µm). D) Thickness measurements of constructs at day 1 and day 21. E) Immunohistofluorescent staining of Keratocan, Lumican, Decorin, Collagen I, ALDH3A1, CD34 and α-SMA (green), and cell nuclei (blue), scale bar = 20 µm.

Corneal epithelial cells were cultured on the top layer of the constructs (Figure 5-7). A co-culture was successfully obtained using this method with stromal cell detected in the middle and lower layers. Epithelial cells attached easily to the construct surface and formed a tight epithelium with cells presenting a typical cobblestone morphology (Figure 5-7 E). Some degree of stratification was visible in H&E stained sections (Figure 5-7 F&G).

Constructs were successfully implanted onto porcine corneas in an *ex vivo* ALK model (Figure 5-8). Constructs were amenable to surgical handling and suturing without tearing (Figure 5-8 A). Fluorescein staining is commonly used to assess corneal epithelial wounds. If the staining is positive (yellow), that indicates an area with damaged or absent epithelium (barrier function compromised); whereas a negative staining is an indication of a healthy epithelium as its barrier does not allow the penetration of the dye. In this study, positive staining was seen on the constructs after two days of implantation, while the presence of only small islands of positive fluorescein staining at day 7 indicated that neighbouring epithelial cells colonized the surface of the scaffold (Figure 5-8 B).

Histological analysis via H&E showed good integration of the construct onto the host bed and at its periphery, while the surface was covered in a neo-epithelium (Figure 5-8 C).

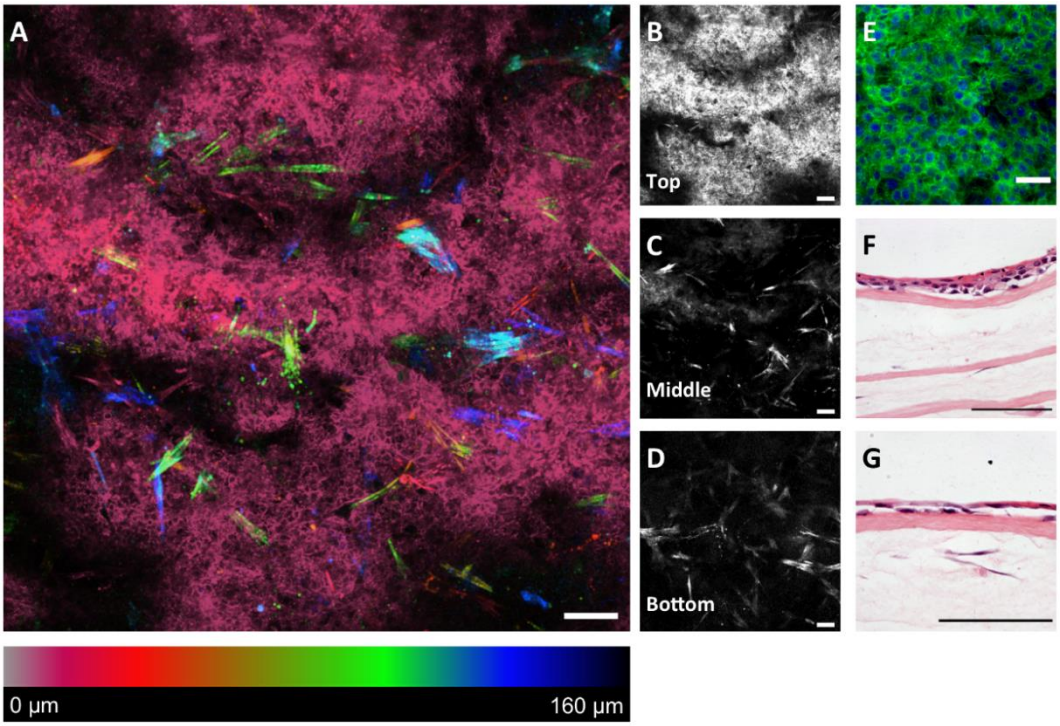

Figure 5-7. Anterior cornea constructs containing epithelium. A) Depth color-coded Z-stack, cells at the surface (epithelium) appear pink/read, while stromal cells in deeper areas appear from orange to blue; B-D) single images of the z-stack (scale bar = 100 µm); E) higher magnification of the epithelium F-actin (green) and nuclei (blue), scale bar = 10 µm; F-G) haematoxylin and eosin stained sections (scale bar = 100 µm).

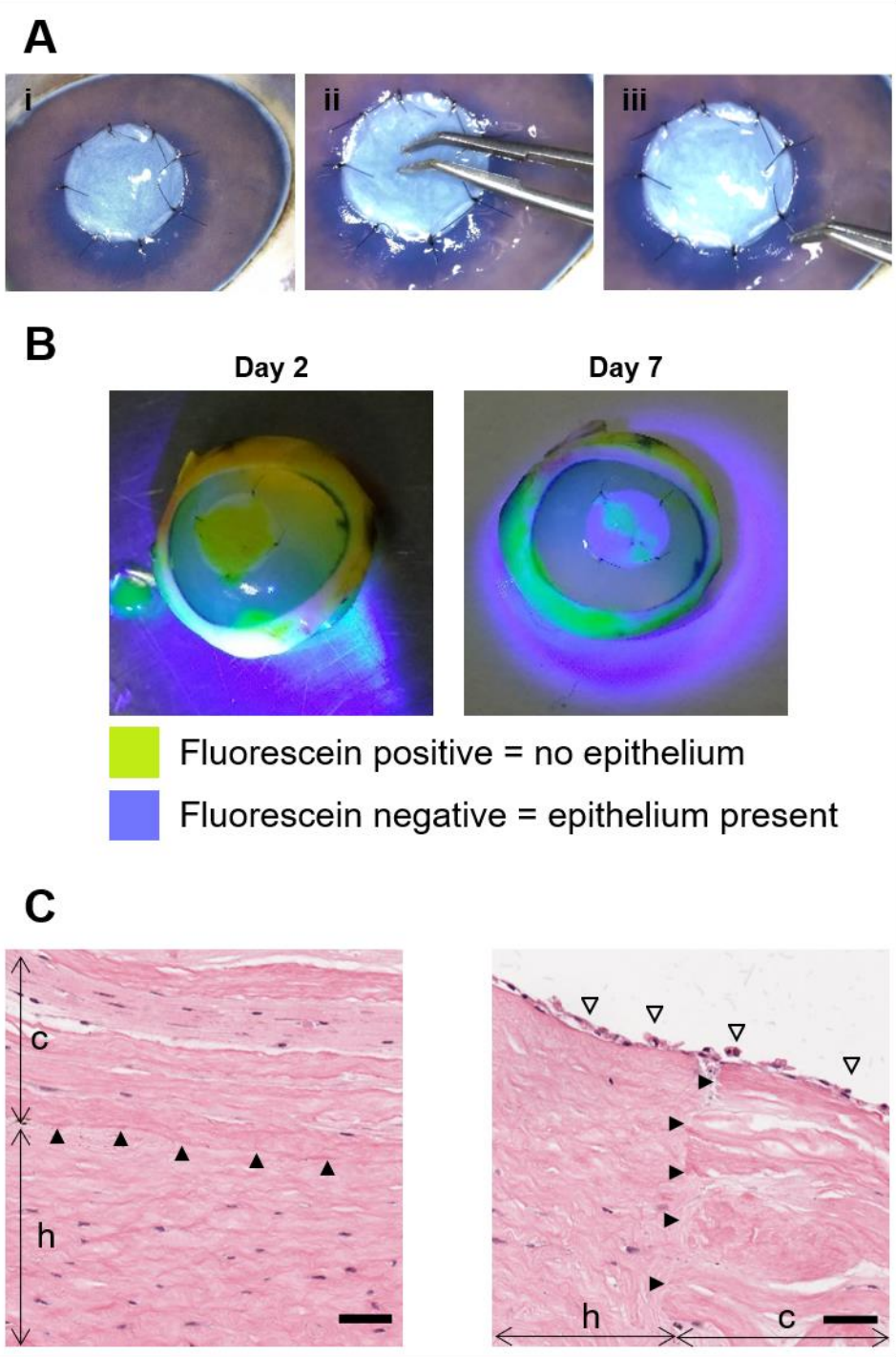

Figure 5-8. Implantation of constructs without epithelium onto an ex vivo porcine cornea (n=3). A) Surgical procedure: (i) implant sutured in place using 10-0 nylon sutures, (ii) pressing onto the implant to show strength of construct and suture points and (iii) pulling of sutures to demonstrate construct does not tear. B) Fluorescein staining of operated porcine corneas after implantation and culture. C) H&E analysis of implanted constructs, showing good integration of construct (c) with the host (h) (arrowheads) at the centre and the edge of the construct. Epithelium (empty arrowheads) from the host has grown onto the construct (scale bar = 50 µm).

5.4. Discussion

To overcome the severe worldwide shortage of donor corneal tissue for transplantation, tissue engineering approaches are being developed. Here a multi-layered construct fabricated with decellularized cornea sheets and cell-laden collagen hydrogels is described. These corneal stroma tissue equivalents presented high cell viability, transparency, expression of stromal cell markers and supported epithelial regeneration.

Decellularization of the stromal sheets was successful, with values of dsDNA remaining well below the recommended maximum concentration of 50 ng/mg of dry tissue to minimise adverse host reactions (Crapo et al., 2011). While a shorter decellularization protocol to that previously described was used in this study, levels of DNA were lower (Lynch et al., 2016b). This is probably due to the thinner tissue allowing improved penetration of the detergents. Swelling occurred during the decellularization process, which has been previously reported (Dong et al., 2019; Du and Wu, 2011; Lin et al., 2017; Pang et al., 2010; Wu et al., 2009). Once the endothelium is damaged or removed, the cornea swells. Furthermore, SDS is an aliphatic molecule and it binds to proteins by its hydrophobic domain which results in increased negative charge which attracts water and leads to swelling (Courtman et al., 1994). To counteract this, osmoregulators such as dextran (Lynch et al., 2016b; Murab and Ghosh, 2016), glycerol (Murab and Ghosh, 2016), gelatin and sodium chloride (Shi et al., 2019) can be used to reduce swelling. Unsurprisingly, dehydration resulted in a reduction in thickness, however, the thickness only partially recovered upon rehydration. This could be attributed to the loss of GAGs during the decellularization process that would normally attract water molecules into the tissue (Han et al., 2011; Wang et al., 2016).

In this study, the sheets were dehydrated by air-drying in a laminar flow hood and did not fully recover their thickness after rehydration. This would lead to a denser collagen network than found in the native tissue. Alternative dehydration techniques such as freeze-drying or critical point drying could be used but these also introduce new limitations. While freeze-drying has been previously used to obtain dried sheets of decellularized cartilage (Gong et al., 2011), preliminary investigations by our group using stromal sheets showed that freeze-drying did not affect the thickness but inhibited the transmission of light through the tissue. Critical point drying was not used as it could lead to degradation of the extracellular matrix following exposure to ethanol. The addition of a protecting agent to limit shrinkage was not explored in this study but could potentially

assist in controlling the sheet thickness (Allen et al., 2013). While other researchers have used freshly decellularized lenticules (Alió del Barrio et al., 2018; Yam et al., 2016; Yin et al., 2016), in this study, dried lenticules were used because of their ease in handling, room temperature storage and possibility of terminal sterilization, such as gamma irradiation.

We hypothesized that cell delivery via a gel would be a gentle, but effective, way to allow the inclusion of cells at all depths. Collagen I was chosen since it is the primary type of collagen found in the corneal stroma (Lee and Davison, 1984). Our approach showed homogeneous cell distribution throughout the construct. In addition, the collagen hydrogel proved to be an excellent binding agent of the dehydrated decellularized sheets, which were attracted by the moisture of the hydrogel.

The use of the decellularized sheets provided stability to the construct, making it more robust and easier to handle than a gel alone. Hong et al, 2018 reported a carrier for limbal epithelial stem cells based on embedding a single sheet of decellularized human cornea in a collagen gel that was further plastically compressed (Hong et al., 2018). With this approach they increased the suturability and resistance to biodegradation of the construct. In our study, the sheets resisted degradation more than the hydrogels, giving an advantage for the strength and retention of an implant. Furthermore, when corneal stromal cells are embedded in collagen gel alone and cultured under free-floating conditions, they contract greatly (Miotto et al., 2019). By removing the serum from the medium this phenomenon can be diminished (Miotto et al., 2019), but the present study shows that contraction can be controlled by anchoring the collagen gel to a stronger material (Ahearne et al., 2010), in this case, the decellularized sheets. The differences in construct thickness reported during the culture period could indicate remodelling or compaction of the collagen hydrogel, conferring the constructs more mechanical stability. Moreover, additional cross-linking, such as UV-riboflavin, genipin or transglutaminase, could further improve mechanical properties.

Layer-by-layer is an approach that has been used for stromal replacement constructs, since it aims to replicate the lamellar structure of the corneal stroma. Wilson and colleagues fabricated a stromal model by orthogonal stacking of layers of cell-seeded, aligned, electrospun PLDLA mesh, using collagen gel to bind them together (Wilson et al., 2012). Ghezzi et al., 2017 reported constructs based on orthogonally stacked cell-

seeded patterned silk films, without the aid of any binding material (Ghezzi et al., 2017). Che and colleagues have recently described the fabrication of stromal equivalents by stacking cell-seeded ultrathin amniotic membrane (Che et al., 2019). In this case, an extended culture period of 8 weeks allowed the stromal cells to produce extracellular matrix to bind the layers. The constructs reported in our present study were fabricated with materials found in the native stroma, which might present advantages for clinical translation. Decellularized porcine corneas have been used to treat patients suffering from corneal ulcers (Shi et al., 2019; M.-C. Zhang et al., 2015; Zheng et al., 2019) showing the feasibility of employing xenogeneic material. The use of discarded tissue from myopia correction procedures is an option to use human material (Yam et al., 2016; Yin et al., 2016) as well as donated corneas unsuitable for transplantation due to low endothelial cell count, for example (Alió del Barrio et al., 2018).

In the present study, the keratocytes were primarily found in the gel. It is known that *in vivo* remodelling of thin decellularized stromal tissue is faster than that of thicker tissues (Ma et al., 2015). In the present study, the 3 weeks of culture might not have been enough time to allow the cells to repopulate the sheets by migrating from the gels. However, the reduction in construct thickness observed can be an indication of cells remodelling the collagen hydrogel. It is necessary to remark that the non recovery of sheet thickness after dehydration could have led to collagen fiber compaction, which might make the sheets more dense and, therefore, more difficult for the cells to penetrate. Moreover, the culture conditions used here have been optimized for the recovery of a keratocyte phenotype and these cells are known to migrate slowly (Fernández-Pérez and Ahearne, 2019). We would therefore expect that given enough time, once the keratocytes have remodelled the collagen gel, they would migrate to the decellularized sheets as a suitable substrate. In the future, using corneal stromal stem cells (CSSCs) instead of corneal fibroblasts in serum-free conditions might improve the outcome further since CSSCs present a more keratocyte-like phenotype (J. Wu et al., 2014), produce a more natural ECM (Karamichos et al., 2014a) and possess anti-scarring activity (Basu et al., 2014). These cells have also been shown to support limbal epithelial stem cells in a compressed collagen I stromal model (Kureshi et al., 2015).

Several studies have developed hydrogels as corneal substitutes, which required implantation using overlying sutures as they are not sufficiently strong to be implanted using running sutures (Fagerholm et al., 2014, 2010; Liu et al., 2009; Rafat et al., 2008)

or relied on the use of fibrin glue (Massie et al., 2015). Alternative strategies such as the one reported by Hong and colleagues increased suturability by embedding a decellularized human corneal lenticule in a compressed collagen gel (Hong et al., 2018). These authors also report the fabrication of anterior stromal equivalents by embedding keratocytes in a plastically compressed gel, composed of a collagen I and decellularized corneal ECM mixture, with epithelial cells on the surface (Hong et al., 2019). In the approach we took, stacking the decellularized sheets with the normally unsuturable collagen gels provided a construct that could be sutured with conventional interrupted 10-0 sutures.

Constructs at the time of implantation had a thickness of approximately 190 µm, suitable for ALK and superficial ALK. These procedures are employed to treat anterior stromal defects, such as scarring, opacification or ulceration resulting from infection, inflammation, trauma or inadequate healing after surgical refractive procedures (Espandar and Carlson, 2013; Ganger et al., 2016). Patients suffering from lattice, granular or Reis-Bückler corneal dystrophies could also benefit from the use of these constructs (Espandar and Carlson, 2013; Ganger et al., 2016). If thicker or thinner constructs would be needed, more or less layers, respectively, should be stacked when fabricating the constructs. The optical properties of the presented constructs were suboptimal. However, studies report a recovery of transparency upon implantation, once the hydration state of the construct matches the native rather dehydrated nature (Hashimoto et al., 2015; Wu et al., 2009). Furthermore, decellularized cornea ECM-derived hydrogels could be employed in future studies since these are more transparent than rat-tail collagen hydrogels (Ahearne and Lynch, 2015).

Decellularized stromal lenticules similar to the ones described here have been used to culture corneal endothelial cells (Arnalich-Montiel et al., 2019; Choi et al., 2010; He et al., 2016; Ju et al., 2012b). Whilst not in the scope of this study, the constructs described could also be seeded with endothelial cells to obtain a full thickness laboratory-grown corneal substitute.

In summary, the feasibility of fabricating an anterior cornea equivalent using only tissue-derived materials was demonstrated, with good cell viability, optical properties and cell phenotype. These were assembled in a rapid process that allowed regular and dense cell distribution, independent of cell migration. These corneal substitutes show

translatability since they can be sutured and support regeneration of the epithelium in an *ex vivo* model.

5.5. Concluding remarks

In this Chapter, the feasibility of fabricating an anterior cornea equivalent using only tissue-derived materials was demonstrated, with good cell viability, optical properties and cell phenotype. These were assembled in a rapid process that allowed for good cell distribution independent of cell migration. These corneal substitutes show translatability since they are suturable and allow re-epithelialization in an *ex vivo* model. In the following chapter hydrogels will be obtained from decellularized corneas and the impact of each decellularization method will be analysed.

CHAPTER 6

The impact of decellularization methods on extracellular matrix derived hydrogels

6.1. Introduction

The extracellular matrix (ECM) is primarily composed of structural and regulatory proteins and polysaccharides and is generated and maintained by cells. Many cellular functions, such as proliferation, migration or differentiation are regulated by the ECM (Frantz et al., 2010). Each organ and tissue is composed of a distinctive ECM, in its biochemical composition and structural organization. The properties of ECM are important in the fields of tissue engineering and regenerative medicine, which often aim to replicate the composition and structure of the ECM. By using synthetic or natural materials, three-dimensional scaffolds can be fabricated to repair or restore damaged organs and tissues.

One popular approach to generating scaffolds that try to imitate the tissues or organs ECM characteristics is to use decellularization. This technique involves the removal of cellular components from a tissue so that only the ECM remains. Many methods have been examined for performing decellularization and these can be divided into three main categories: physical, chemical and biological (Crapo et al., 2011). Physical methods include freeze-thawing cycles (Ide et al., 1983; Proulx et al., 2009; Rahman et al., 2018; Utomo et al., 2015), high hydrostatic pressure (Funamoto et al., 2010; Hashimoto et al., 2016; Santoso et al., 2014) or supercritical CO_2 (Guler et al., 2017; Seo et al., 2018; White et al., 2018). Chemical agents can involve ionic detergents, such as sodium dodecyl sulphate (SDS) (Lynch et al., 2016b; Zilic et al., 2016) or sodium deoxycholate (Price et al., 2015); non-ionic detergents, such as Triton X-100 (Choi et al., 2010); hypertonic or hypotonic salt solutions, such as sodium chloride (González-Andrades et al., 2011; Luo et al., 2013); and acids and bases, such as peracetic acid (Wolf et al., 2012) or ammonium hydroxide (Baptista et al., 2011). Enzymes such as trypsin, dispase and phospholipase A2 have been used as biological methods for decellularization

(Chen et al., 2004; Wu et al., 2009). Furthermore, nucleases, such as DNAse, are used to promote the fragmentation of residual DNA into <200bp fragments in order to minimize immunological responses (Crapo et al., 2011). Extensive research has been completed to optimize these decellularization procedures to allow for maximal cell removal and minimal ECM damage for each tissue/organ.

One difficulty associated with some decellularized tissues is their limited potential for recellularization. For many tissue-engineering applications, healthy cells need to be embedded into the ECM to generate a functional and viable tissue. To overcome this problem decellularized organs and tissues can be transformed into hydrogels that allow cells to be encapsulated throughout their structure. These hydrogels can then be used as injectables for minimally invasive delivery into irregular spaces (Chaimov et al., 2017; Lin et al., 2016; Singelyn et al., 2009; Ungerleider et al., 2015; Wang et al., 2013; L. Zhang et al., 2013) and for 3D printing of scaffolds (Choi et al., 2016; Jang et al., 2017, 2016; Pati et al., 2015, 2014; Skardal et al., 2015). Since the first report of ECM-derived hydrogels in 1998 (Voytik-Harbin et al., 1998), over 70 papers have appeared in the literature describing the use of ECM-derived hydrogels from a wide variety of organs (Saldin et al., 2017). ECM-derived hydrogels have been under investigation to treat several medical conditions. These include type 1 diabetes, where the hydrogel provided a matrix to delivery cells to the pancreas (Chaimov et al., 2017); myocardial infarction by replacing damaged cardiac tissue (Singelyn et al., 2009), skin wounds (Engel et al., 2015), and keratoconus by using the ECM to 3D bioprint a corneal stromal substitute (Kim et al., 2019a). Despite the increasing interest in such hydrogels, the effect of different decellularization methods on the final hydrogel characteristics has not been widely studied.

The aim of this study was to examine the impact of three different decellularization protocols on ECM-derived hydrogels obtained from porcine corneas. Two detergent-based techniques (SDS and Triton X-100) and a freeze-thaw cycling technique were used to decellularize corneas and hydrogels were fabricated from the resulting ECM. The impact of these decellularization protocols were evaluated in terms of biochemical composition, transparency, gelation kinetics, mechanical properties and cytocompatibility.

6.2. Materials and Methods

6.2.1 Decellularization of porcine corneas Porcine ocular globes were obtained from a local slaughterhouse. The remaining pieces of flesh were removed and, under aseptic conditions, the eyes were immersed in 2% iodine solution (Videne®, Ecolab, Belgium) in sterile phosphate buffer saline (PBS) for one minute, gently rocking throughout. The eyes were subsequently washed twice in sterile PBS and the central corneal button was excised using scissors and cut into small pieces (2 mm x 2 mm, approximately). Three decellularization methods were tested:

a) SDS (anionic detergent): each corneal button was immersed in 3 ml of 0.1% (w/v) sodium dodecyl sulphate (SDS, Sigma-Aldrich) solution for 72 hours under rotation. Solution was exchanged every 24 hours.

b) Triton (non-ionic detergent): each corneal button was immersed in 3 ml of 1% (v/v) Triton X-100 (Sigma) solution for 72 hours under rotation. Solution was exchanged every 24 hours.

c) Freeze-thaw (mechanical procedure): each corneal button was immersed in 5 ml sterile deionized H_2O and placed in a -80 °C freezer for a minimum of 5 hours. Thereafter, they were let to thaw at room temperature. Once thawed, the solution was exchanged and the procedure repeated until 5 freeze-thaw cycles had been completed.

Afterwards, all corneas where subjected to a DNAse treatment for 1 hour at 37 °C under rotation. DNAse (Sigma-Aldrich) was used at a concentration of 10 U/ml prepared in 10 mM magnesium chloride buffer at pH 7.5. Corneas where extensively washed with sterile deionized water for 72 hours, with solution exchanged every 24 hours, under gentle rotation. Finally, decellularized corneas where dehydrated using a freeze drier and turned into powder by cryomilling (SPEX SamplePrep Freeze/Mill). Non-decellularized corneas were lyophilized and cryomilled to be used as controls (native).

6.2.2 Hydrogel formation

ECM hydrogels were prepared as previously described (Ahearne and Lynch, 2015). Briefly, ECM powder was dissolved in 1 mg/ml pepsin solution in 0.1 M hydrochloric acid at a concentration of 20 mg/ml and incubated for 72 hours at room temperature under slow rotation. Hydrogels were formed by neutralizing the solution with 1 N NaOH, balancing salt concentration using 10x PBS and incubating at 37 °C for one hour to induce fibrillation. Hydrogels had a final ECM concentration of 16 mg/ml. This process is depicted in Figure 6-1. Rat-tail collagen I (Corning) hydrogels were fabricated as described previously (Ahearne and Lynch, 2015) and used as a control for some studies.

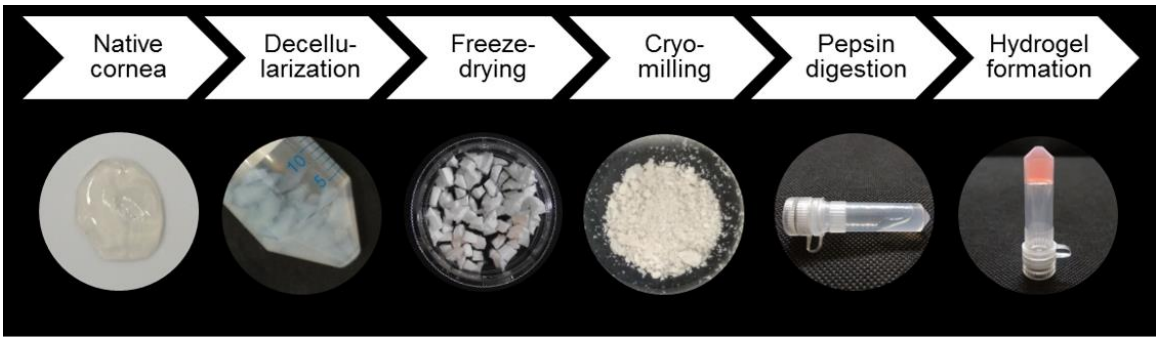

Figure 6-1. Main steps in the fabrication of cornea ECM-derived hydrogels.

6.2.3 Biochemical quantification

Quantification of dsDNA, sGAG and collagen was performed after papain digestion of 100 µl hydrogels. DNA was quantified with the Quant-iT™ PicoGreen™ dsDNA Assay Kit (Invitrogen), following manufacturer's specifications. sGAG quantification was performed using dimethylmethylene blue dye-binding assay (Blyscan, Biocolor). Collagen content was inferred by measuring the content of hydroxyproline using a chloramine T assay (Ignat'eva et al., 2007; Kafienah and Sims, 2004).

6.2.4 Histology

Hydrogels were fixed in 4% paraformaldehyde and processed for wax embedding. 6 µm-thick slices of each sample were cut, attached to a glass slide, dewaxed, rehydrated and stained as follows. Haematoxylin & eosin was used to visualize any nuclei still present after decellularization. Slides were stained with Harris Haematoxylin (Sigma-Aldrich) for 4 minutes, followed by a 10-minute wash with running tap water. Then slides were immersed in acid alcohol for 30 seconds and washed with tap water for 5 minutes. Finally, slides were stained with Eosin Y (Sigma-Aldrich) for 2 minutes. Picro-sirius red

was used to assess collagen distribution. Slides were stained with Sirius Red (Sigma-Aldrich) in a saturated aqueous solution of picric acid for one hour and then for one minute in 0.5% acetic acid. Alcian blue was used to assess sGAG content. Slides were stained with 1% Alcian Blue 8GX (Sigma-Aldrich) in 0.1 M HCl for 5 minutes followed by three 30-second washes in dH_2O. After staining, all slides were dehydrated and coverslipped using DPX.

6.2.5 SDS-PAGE and western blot

7.5% polyacrylamide gels were cast and loaded with 50 µg of sample mixed with Laemmli buffer (1:1) that was previously boiled for 5 minutes. Gels were run for 90 minutes at 120 V. Gels were then stained with GelCode (Thermo-Fisher) following manufacturer's directions. For western blot, 100 µg were loaded into precast 12% SDS-PAGE gels (Biorad) and run at 200V for 45 minutes. Gels were transferred to a PVDF membrane using a semi-dry transfer system (Thermo-Fisher) with Pierce 1-step transfer buffer (Thermo-Fisher). The membrane was activated with methanol and then blocked overnight at 4 °C with 3% BSA. Primary antibody (keratocan, sc-66941, Santa Cruz) was used at a dilution of 1:200 in 3% BSA and incubated overnight at 4 °C. Three 5-minute washes with TBST were performed under agitation, and then the HRP-linked secondary antibody (A0545, Sigma-Aldrich) at a dilution of 1:1000 was incubated for an hour at room temperature. Another set of washing steps was carried out and then membranes were developed with Western Chemiluminescent HRP Substrate (Fisher Scientific). Membranes were imaged with GelDoc (Biorad).

6.2.6 Transparency

The macroscopic appearance and transparency of the gels was assessed by placing them over printed text. Subsequently, light transmittance was quantified. The absorbance of light at several wavelengths ranging from 350 to 700 nm was determined with a microplate reader (BioTekTM Synergy HTX). Deionized water was used as a baseline control. The transmittance of light was calculated using the following formula:

$$\%\, Transmittance = 10^{2-Absorbance}$$

6.2.7 Gelation kinetics

Gelation kinetics was determined via turbidimetric spectrophotometric analysis, as described elsewhere (Freytes et al., 2008). Briefly, 100 µl hydrogels were casted into

96-well plates at 4 °C and inserted in a plate reader pre-heated at 37 °C (BioTekTM Synergy HTX). Absorbance at 405 nm wavelength was measured every 3 minutes for 90 minutes. Absorbance values were normalized with the following formula:

$$NA = {(A - A_0)}\Big/{(A_{max} - A_0)}$$

where NA is the normalized absorbance, A is the absorbance at any given time, A_0 is the initial absorbance and A_{max} is the maximal absorbance.

The lag phase (t_{lag}) was calculated by obtaining the linear portion of the curve and extrapolating the time value at which the normalized absorbance is 0. Similarly, $t_{1/2}$ was determined as the time at which the normalized absorbance is 0.5. The slope of the linear portion of the curve determined the gelation speed (S).

6.2.8 Rheology

All rheological experiments were performed using a MCR 102 rheometer (Anton Paar, Austria) equipped with temperature controlling systems and using a 25 mm diameter parallel plate. Viscosity of pre-gel solutions was measured by performing a frequency sweep, from 0.1 to 1000 Hz, at 5% strain at 15 °C. Viscosity constants can be found in Supplementary Table S1. Storage and loss moduli were calculated with fixed frequency of 1 rad/s and 5% strain. Pre-gel solutions were applied at 4 °C and left equilibrate during 10 minutes, after which temperature was raised to 37 °C to induce gelation. Measurements where stopped once G' values plateaued.

6.2.9 CryoSEM

Hydrogels were snap-frozen in nitrogen for 5 seconds, sublimated for 40 minutes at -100 °C and 10^{-5} Pa, freeze fractured and sputter coated with platinum for 20 seconds. These were then imaged with a scanning electron microscope at 5 kV (Ultra2 Zeiss, Germany, with a Quorum Technologies CryoSEM Preparation System, UK).

6.2.10 Cell culture

Human corneal stromal cells were isolated and cultured as described in Chapter 3. 100,000 cells were embedded in each 100 µl hydrogel and cast in the wells of a 96-well plate. After gelation, hydrogels were released from the wells and transferred to 24-well plates. Constructs were fed every second day with low glucose DMEM (Hyclone) supplemented with 10% FBS, 100 U/ml Penicillin 100 µg/ml Streptomycin (both Gibco).

Cell viability was assessed at day 1 and day 5 by staining the constructs with 2 µM calcein-acetoxymethyl ester and 4 µM ethidium homodimer-1 in PBS for 1 hour at 37 °C in a humidified incubator. Cells were then imaged via laser scanning confocal microscopy (Leica SP8). Furthermore, the shape of the hydrogels was monitored and images were taken daily over 5 days. The area of the hydrogels was calculated using Image J (NIH) and was plotted as the percentage of change of area with time.

6.2.11 Methylene blue active substances (MBAS) assay

MBAS assay was performed with some modifications from previously described methods (Mathapati et al., 2010). A methylene blue (Sigma-Aldrich) solution was prepared in water to a final concentration of 250 µg/ml. 1 mg of cryomilled powder from each experimental group was mixed with 1 ml of distilled water and vortexed thoroughly for 1 minute and spun down for 30 seconds on a mini-centrifuge. 250 µl of this supernatant was mixed with 250 µl methylene blue solution and vortexed. Then 1 ml of chloroform was added, vortexed 3 times for 30 seconds and centrifuged for 1 minute using a benchtop centrifuge. A negative control was obtained using 250 µl distilled water and a positive control using 250 µl of 0.5% SDS solution. A phase separation was evident in all tests and visually the SDS group had a blue coloration in the organic (bottom) phase. This was further quantified by measuring the absorbance of the bottom phase at 665nm using a plate reader (BioTekTM Synergy HTX).

6.2.12 *Ex vivo* testing of ECM-derived hydrogels as ocular adhesives

Porcine ocular globes were obtained from a local butcher within 24 hours of sacrifice. Only eyes with no evident epithelial or stromal damage were used. Remaining eyelid and surrounding muscle was trimmed off. The eyes were then disinfected by submerging them into a 2% iodine solution for 1 minute followed by 2 rinses in sterile PBS. Following Castro *et al.*'s protocol, a corneal defect was created with a 5 mm biopsy punch rotating clockwise and anticlockwise three times (Castro et al., 2019). The stromal piece was resected using a blunt crescent knife (Beaver-Visitec International, Inc.). The cornea was then dissected from the globe with 2-3 mm of corneo-scleral ring. The corneas were placed on an artificial chamber epithelial side down and 1 ml of sterile warm 1% agarose was poured on the endothelial side. Upon polymerization, the cornea was placed epithelial side up in a 6-well plate. 500 µl of acellular hydrogel (freeze-thawing decellularization method) were prepared (as described above) and 10-20 µl were pipetted into the created defect. The plate was then closed and placed into a humidified incubator

at 37 °C for 30 minutes. Once the hydrogel had polymerized, 3-4 ml of medium (DMEM low glucose + 10% FBS) were added so that the level arrived to the limbal region. Three drops of media were added to the surface of the cornea to keep it moist. Media was changed daily and fresh drops were added to the surface twice a day. Re-epithelialization was assessed by fluorescein staining after 2 and 5 days. A fresh solution of 2% (w/v) fluorescein sodium salt (Sigma-Aldrich) solution was prepared in PBS. Corneas were stained with this solution for 30 seconds and then washed 3 times with PBS. They were immediately imaged under a blue light. After 5 days, corneas were examined via fluorescein staining and fixed overnight in 4% PFA. They were then embedded in paraffin and sliced using a microtome. Haematoxylin and eosin staining was performed as described above.

6.2.13 Statistical analysis

GraphPad Prism Software 5.0 (GraphPad Software, Inc. La Jolla, CA, USA) was used to perform statistical analyses. All data are presented as the mean ± SD. One-way ANOVA with Tuckey post-hoc analyses were performed to determine statistical significance. Differences were considered to be statistically significant at $p \leq 0.05$.

6.3. Results

6.3.1 Biochemical characterization of decellularized material

The biochemical composition of the fabricated ECM hydrogels was analysed. PicoGreen™ was used to quantify DNA remnants, collagen content was measured by hydroxyproline quantification and sulphated glycosaminoglycans (sGAG) were quantified by dimethylmethylene blue assay (DMMB). All decellularization methods led to a significant reduction in DNA when compared to the non-decellularized control, i.e. hydrogels from native corneas (Figure 6-2A). Collagen levels remained constant in all treatments (Figure 6-2B). sGAG levels were maintained when decellularization was performed with Triton or the freeze-thaw methods, while SDS resulted in significant loss of sGAG (Figure 6-2C). Furthermore, histological examination appeared to validate these results (Figure 6-2D). Staining with haematoxylin & eosin confirmed the absence of cell nuclei after decellularization. Dense collagen was observed after picro-sirius red staining across all samples. Alcian blue staining showed the presence of sGAG in all hydrogels with a noticeable reduction in staining for the SDS treated group.

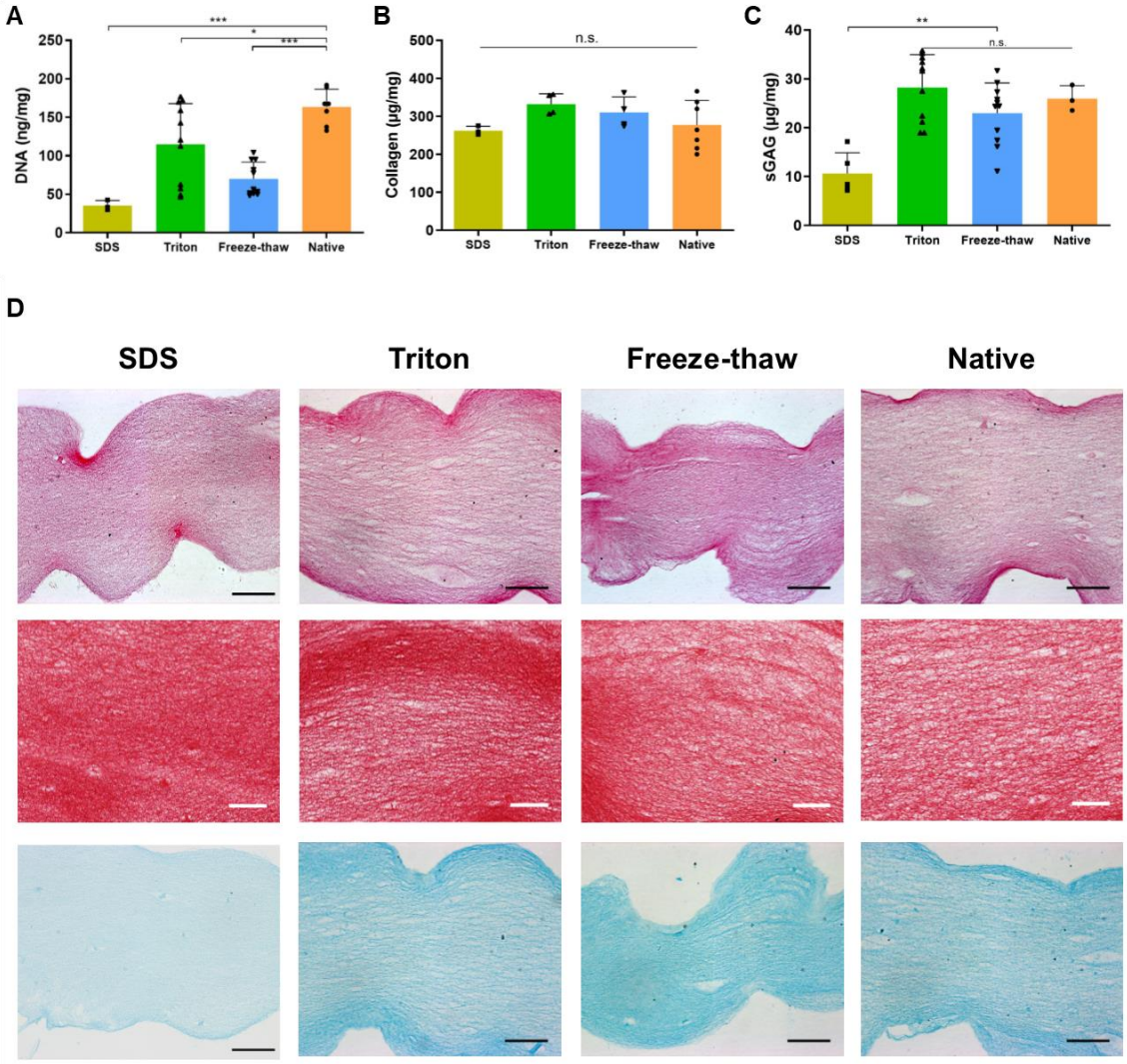

Figure 6-2. Evaluation of decellularization of ECM-derived hydrogels: A) Quantification of dsDNA (n=3-11), B) Collagen (n=3-7), and C) sGAG (n=3-11); * $p < 0.05$, ** $p < 0.01$, *** $p < 0.001$; D) histological examination of hydrogels, stained with haematoxylin and eosin, picro-sirius red and Alcian blue; black scale bar = 100 µm, white scale bar = 50 µm.

Further analysis of the composition of ECM-derived hydrogels was performed using SDS-PAGE and western blotting. SDS-PAGE showed the presence of collagen chains β, α1 and α2 for all conditions. Gamma chains were too heavy to be detected in a 7% polyacrylamide gel. Other lighter proteins were detected in the ECM-derived material lanes but not in a pure collagen I control isolated from rat-tail (Figure 6-3). Immunodetection via western blot detected the presence of the corneal proteoglycan keratocan in all ECM-derived materials, independent of decellularization method, but not in rat-tail derived collagen. Other proteoglycans such as decorin or lumican might also be present, but the lack of good antibodies against porcine antigens did not allow their detection.

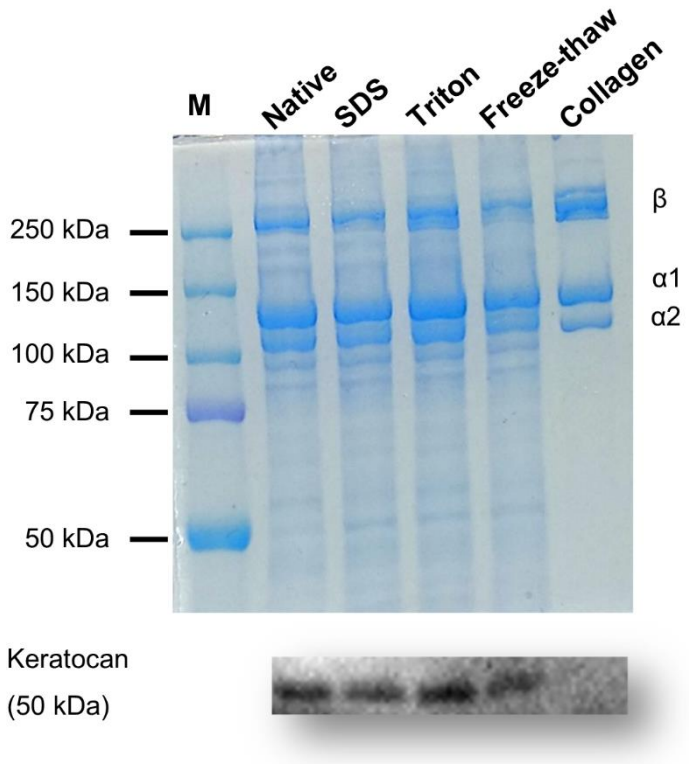

Figure 6-3. Biochemical composition of ECM-derived hydrogels via SDS-PAGE (7%) and western blot against keratocan; M = molecular weight ladder.

6.3.2 Light transmittance

Since ECM from cornea was used to fabricate the hydrogels in this study, it is necessary to examine the transparency of the hydrogels since this is required for corneal tissue engineering. Transparency was measured by quantifying the light absorbed by the material and from this calculating the amount of light transmitted through each sample. As seen in Figure 6-4, all hydrogels allowed light to pass through them, although hydrogels decellularized using SDS and the native hydrogels were cloudier in appearance. Quantitatively, all hydrogels presented at least 50% light transmittance at the end of the visible spectrum. Hydrogels decellularized using the freeze-thaw method were the most transparent with transmittance values above 70%. These values are only slightly lower than full thickness porcine corneas.

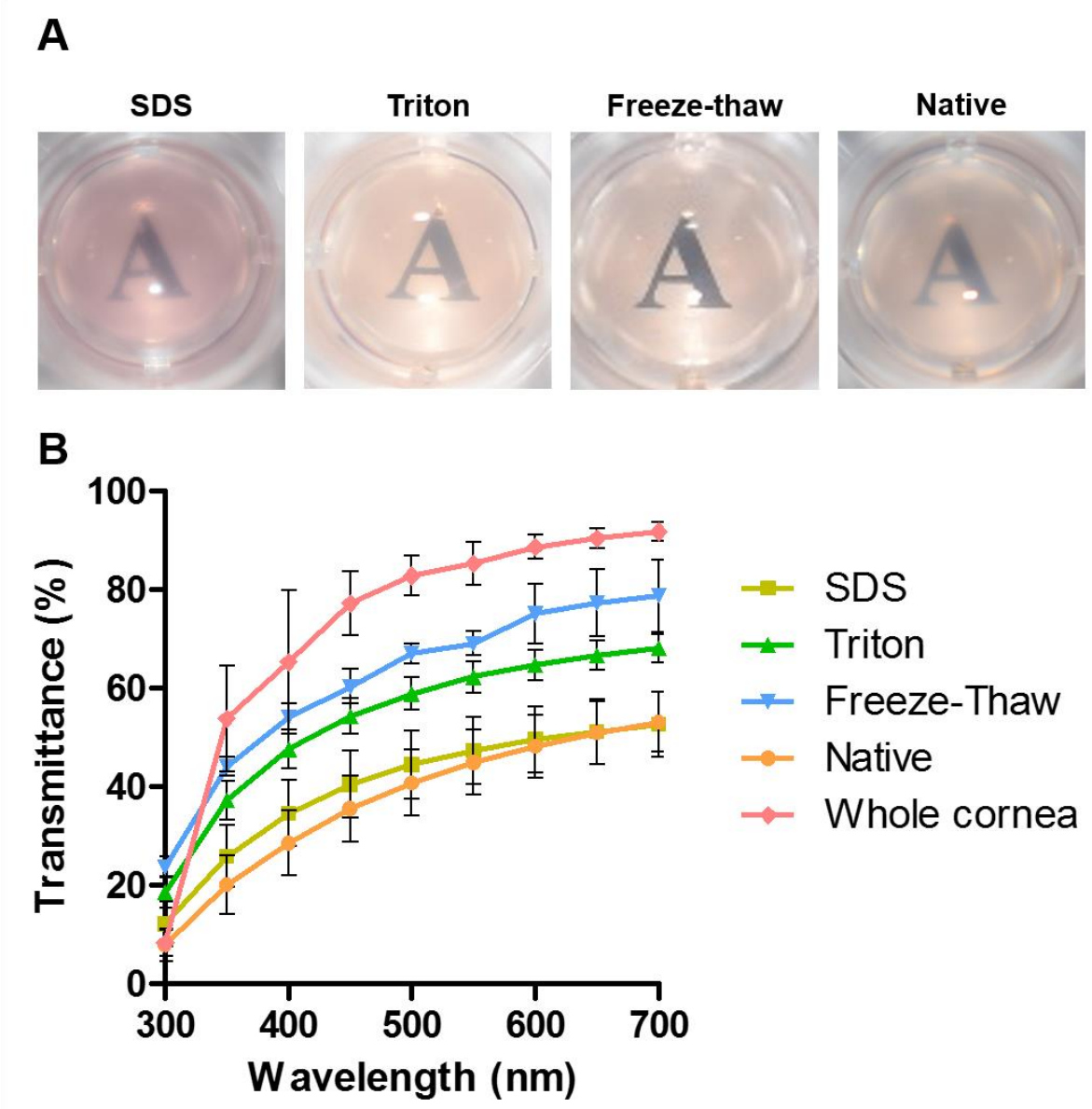

Figure 6-4. Transparency analysis of ECM-derived hydrogels: A) Macroscopic appearance with hydrogels placed over printed text; B) light transmittance quantification over the visible spectrum of light (n=4).

6.3.3 Gelation kinetics

Gelation kinetics of ECM hydrogels were analysed by turbidimetric analysis. This technique is based on the increased in turbidity, and thus absorbance, experienced during collagen self-assembly. All samples presented a sigmoidal profile and gelled after a lag period or t_{lag} (Figure 6-5). All treatments yielded hydrogels which started gelling after a longer lag phase than pure rat-tail collagen (t_{lag} 7.93 ± 0.55 minutes). Freeze-thawing produced the earliest gelling material of all treatments (t_{lag} 16.43 ± 0.37 minutes), while SDS treated hydrogels took the longest to gel (t_{lag} 27.53 ± 1.36 minutes). However, there

was no statistically significance difference between the different speeds at which the ECM-derived materials gelled. All values are displayed in Table 6-1.

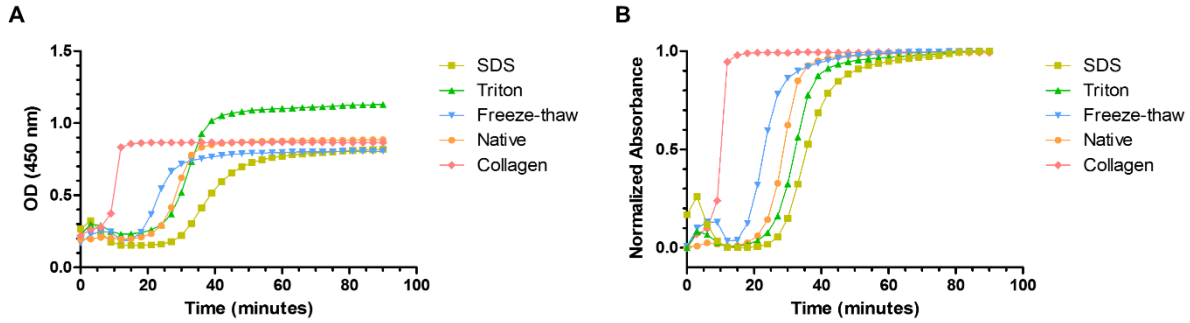

Figure 6-5. Gelation kinetics of ECM-derived hydrogels via turbidimetric analysis (n=4): A) Raw values; B) normalized data.

Table 6-1. Turbidimetric analysis results of ECM-derived hydrogels. Average ± SD.

Condition	*S*	$t_{1/2}$ *(min)*	t_{lag} *(min)*
SDS	0.061 (± 0.006)	35.75 (± 1.86)	27.53 (± 1.36)
Triton	0.070 (± 0.003)	32.14 (± 0.33)	24.94 (± 0.28)
Freeze-thaw	0.075 (± 0.002)	23.11 (± 0.35)	16.43 (± 0.37)
Native	0.090 (± 0.002)	28.04 (± 1.51)	22.51 (± 1.37)
Collagen	0.235 (± 0.026)	10.08 (± 0.33)	7.93 (± 0.55)

6.3.4 Rheology of ECM hydrogels

Rheology was utilized to assess mechanical characteristics of the hydrogels. Increasing shear rates were used to calculate the viscosity at 15 °C, quite below gelling temperature. Shear thinning properties were observed in all pre-gel solutions, regardless of decellularization treatment (Figure 6-5 A). Storage modulus (*G'*) and loss modulus (*G''*) were determined by following the gelation kinetics at 37 °C over time at a fixed frequency of 1 rad/s and 5% strain. All hydrogels had similar moduli values with no statistical significance among decellularization treatments (Figure 6-6 B). Only the Triton and the freeze-thaw groups were significantly weaker than the rat-tail collagen hydrogels.

6.3.5 Evaluation of hydrogel ultrastructure

CryoSEM was employed to study the structure of the hydrogels in the least disruptive way. Samples were snap frozen in nitrogen, sublimated, freeze-fractured and coated for SEM imaging. SEM confirmed the porous and fibrillar structure of the

hydrogels, without evident differences between treatments (Figure 6-7). Some areas displayed inhomogeneity in the density of fibres.

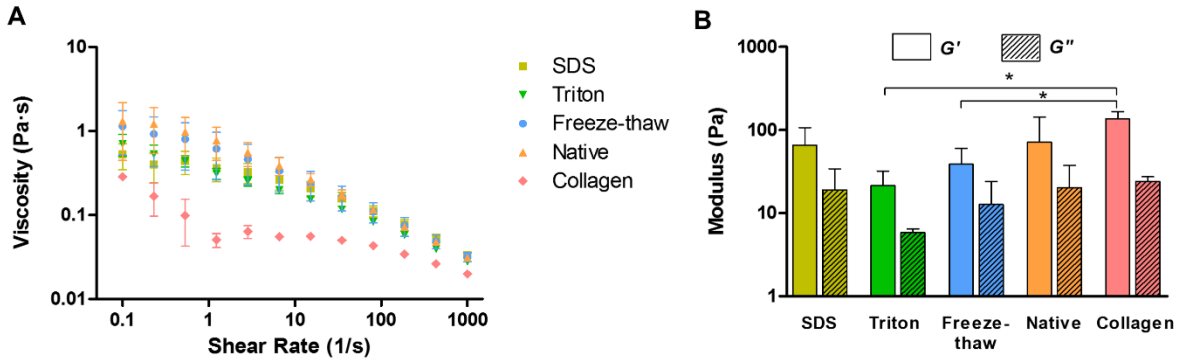

Figure 6-6. Rheology analysis of ECM-derived hydrogels: A) Viscosity measurements at increasing shear rates (n=3); B) storage modulus (G') and loss modulus (G''); n=4-7, * $p < 0.05$.

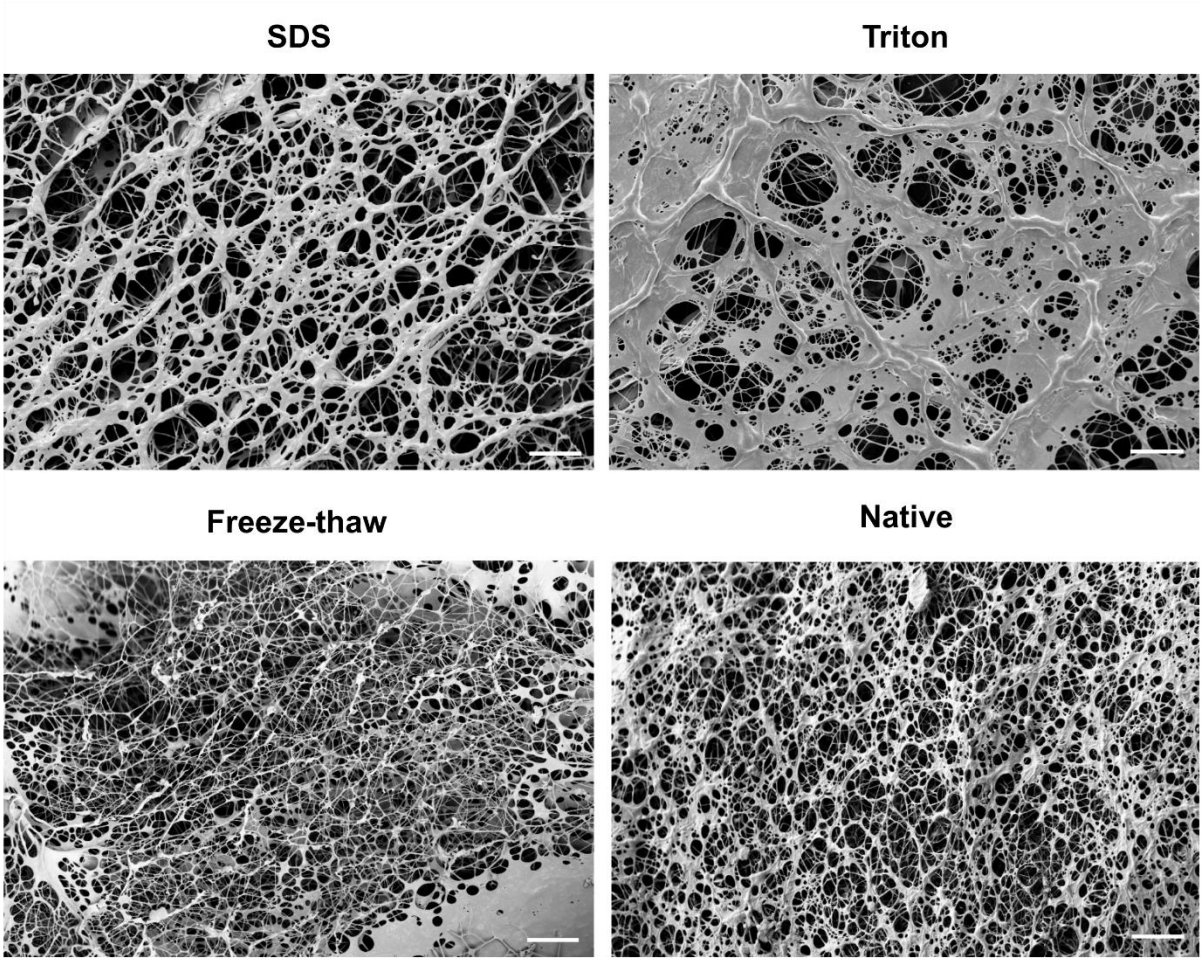

Figure 6-7. CryoSEM micrographs of ECM-derived hydrogels at ~1000x; scale bar = 10 µm.

6.3.6 Cytocompatibility

Human corneal stromal cells were embedded in the hydrogels to examine their cytocompatibility. Cell viability was assessed via calcein-acetoxymethyl ester and ethidium homodimer staining (Figure 6-8 A). After 1 day in culture, cells were highly viable in the Triton, freeze-thaw and native control hydrogel groups, while no viable cells were visible in the SDS treated group. Healthy cells presented an elongated morphology with small processes, indicating adhesion to the fibrillary architecture of the hydrogels. Over 5 days in culture, the hydrogels underwent significant contraction reflecting the ability of viable cells to actively attach and remodel the hydrogel (Figure 6-8 B-C). As expected from the viability assessment, the SDS hydrogel group did not undergo contraction. Hydrogels obtained from the SDS decellularization protocol were cytotoxic presumably due to inefficient washing after decellularization. To confirm this hypothesis the presence of detergent residues was determined using a methylene blue active substances (MBAS) assay, which is widely used in water quality control (George and White, 1999). This assay is based on the binding of the cations in methylene blue with the anions from the detergent that are extracted into the organic phase when in contact with chloroform. Methylene blue extraction confirmed the presence of SDS remnants in the hydrogel thus would explain their cytotoxicity (Figure 6-8 D).

6.3.7 *Ex vivo* testing

The cECM hydrogels obtained with the freeze-thawing method were used to fill a stromal defect on porcine corneas (Figure 6-9). After the defect was created (Figure 6-9 A), the acellular pre-gel solution was pipetted into it and allowed to gel *in situ* (Figure 6-9 B). Fluorescein staining after this procedure confirmed the absence of epithelium in the defect area (Figure 6-9 C), which was covered after 5 days of culture in the air-liquid interphase (Figure 6-9 D). Upon histological analysis, a one layer neo-epithelium was visible growing on the surface of the hydrogel, which was adhered to the underlying stroma (Figure 6-9 E).

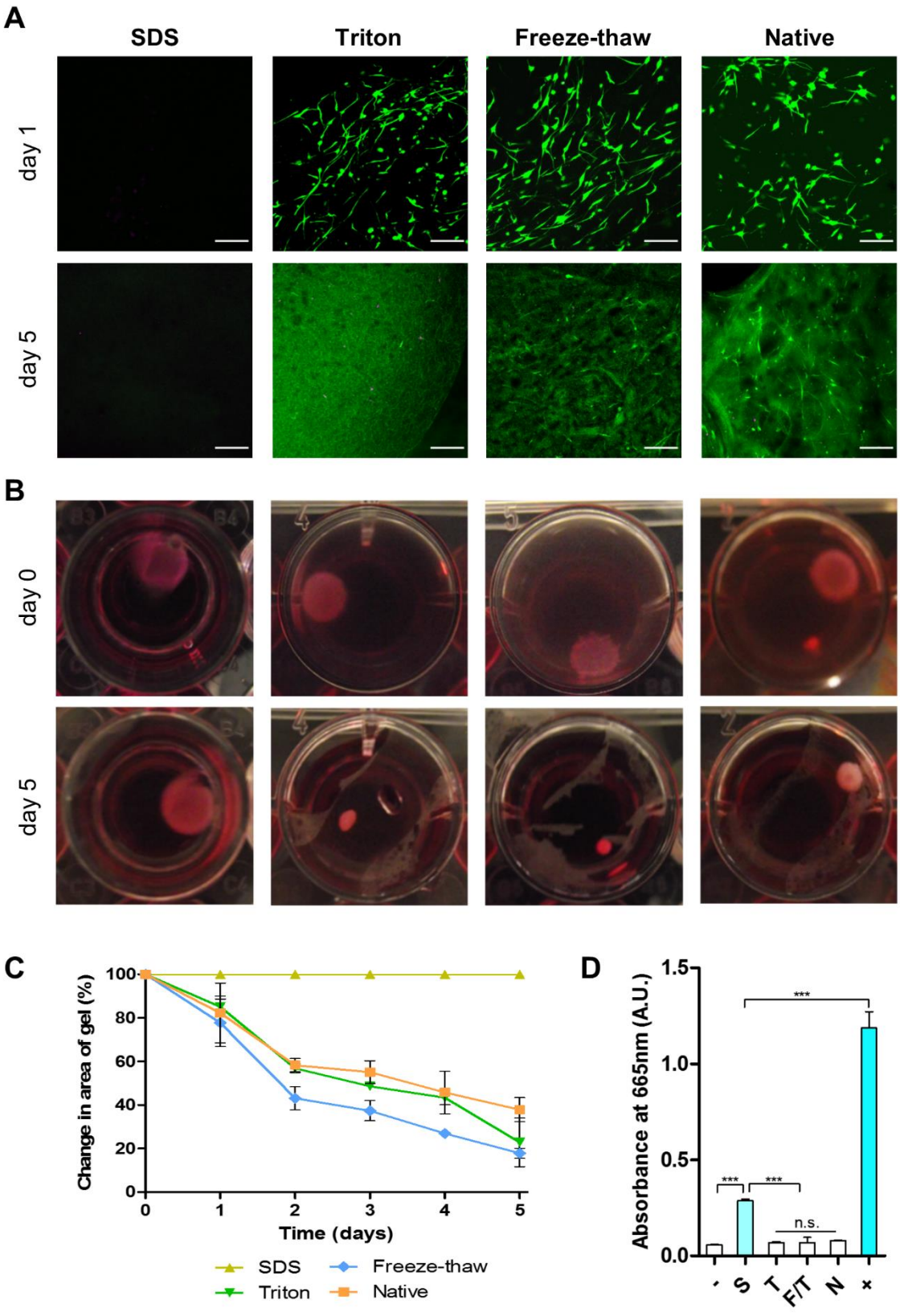

Figure 6-8. Cell activity in ECM-derived hydrogels: A) Cell viability assessment (green = live, magenta = dead, scale bar = 200 µm); B) macroscopic images of cell-laden hydrogels over time in culture; C) quantification of hydrogel area over time (n=3); D) quantification of methylene blue absorbance in the organic phase (n=4); * $p < 0.05$, ** $p < 0.01$, *** $p < 0.001$.

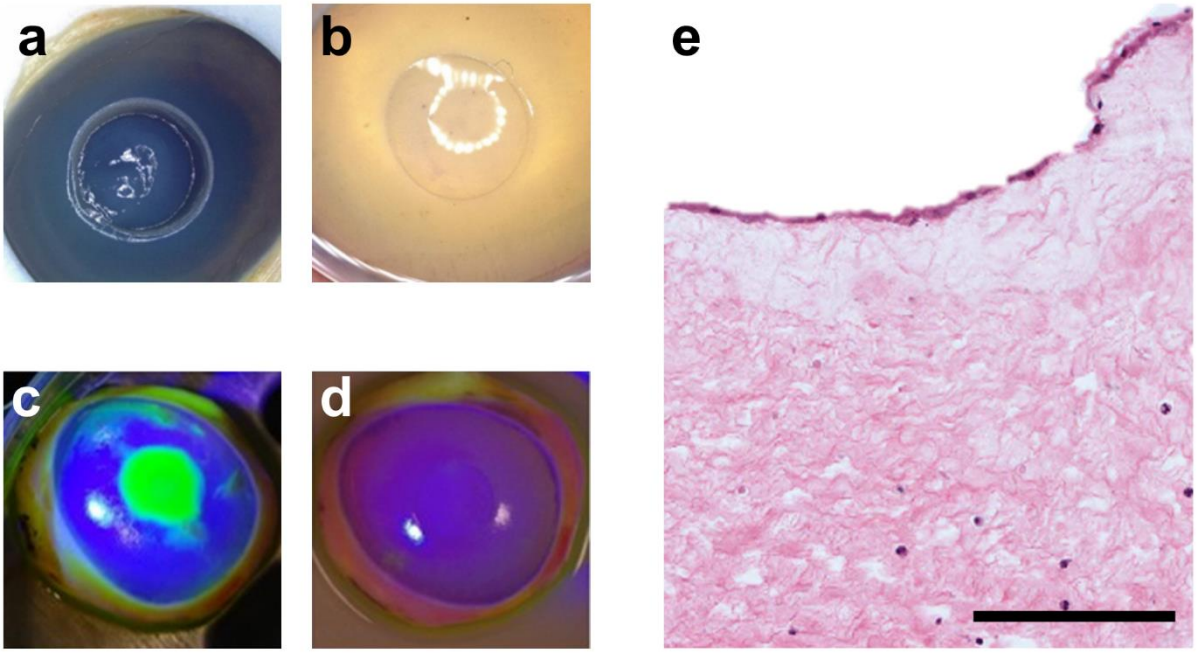

Figure 6-9. Cornea ECM-derived hydrogels for sutureless treatment of corneal defects. a) Stromal defect created, b) defect filled with cECM hydrogel, fluorescein staining at day 0, after filling the defect, d) fluorescein staining at day 5, and e) H&E staining at day 5 (scale bar = 150 µm).

6.4. Discussion

ECM-derived hydrogels offer great promise as biomaterials for tissue engineering as they can be delivered to the site in need in a minimally invasive manner, allow cell encapsulation prior to delivery, but can also allow for neighbouring cell recruitment. ECM hydrogel solutions have also been used as a bioink for 3D bioprinting several different tissues and organs (Kim et al., 2017; Lee et al., 2017; Pati et al., 2014). In this study, ECM-derived hydrogels were obtained from corneas decellularized using three different methods. All decellularization methods decreased DNA significantly and retained collagen and other ECM components. All hydrogels were highly transparent, with the freeze-thaw group showing the best optical properties. Gelation kinetics were affected by the decellularization method employed but not the rheological properties. Hydrogels presented a porous and fibrillary structure. Hydrogels were highly cytocompatible when Triton and freeze-thawing methods were used for decellularization, but cytocompatibility was compromised when using SDS as decellularization agent. This work highlights the influence that the decellularization process has on final properties of ECM-derived hydrogels.

One of the main benefits of using ECM-derived hydrogels is the ability to retain multiple ECM components that may not be present in other natural or synthetic hydrogels and therefore more closely mimics the native tissues. Composition analysis of the digested materials via SDS-PAGE confirmed the presence of multiple ECM components when compared to rat tail collagen which just consists of collagen I. Keratocan, a small leucine-rich proteoglycan almost exclusively found in the cornea, was detected in the ECM-derived hydrogels, irrespective of the decellularization method used. However, this study did show that the choice of decellularization technique is important with SDS decellularization retaining less sGAG than the other techniques tested. This removal of sGAG following decellularization has been previously reported for cornea (González-Andrades et al., 2011; Lynch et al., 2016b; Pang et al., 2010; Sasaki et al., 2009), cartilage (Elder et al., 2009; Pati et al., 2014), ligament (Gratzer et al., 2006) and adipose tissue (Pati et al., 2014). While this study demonstrated that the ECM composition was affected by the decellularization technique used, other techniques may be used to identify more specific tissue or organ ECM components such as mass spectrometry (DeQuach et al., 2010; Farnebo et al., 2014; Johnson et al., 2014; Odorico et al., 2018) or enzyme-linked immunosorbent assays (ELISA) (Jang et al., 2017; Kim et al., 2019b; Skardal et al., 2015).

One potential limitation with using ECM-derived hydrogels is that GAGs and various collagen types, such as collagen V have been shown to interfere in collagen I self-assembly *in vitro* (Birk et al., 1990; Brightman et al., 2000; Pins et al., 1997). *In vivo* small leucine-rich proteoglycans, such as keratocan and decorin in the cornea, play an important role in collagen fibrillogenesis, in terms of collagen assembly nucleation and linear and lateral fibril growth (Zhang et al., 2009). Therefore, the difference in gelation kinetics between the commercially available collagen I and the ECM-derived hydrogels can be explained by the presence of ECM components other than collagen I. Studies from ECM-derived hydrogels from other sources have reported a delay in fibrillogenesis (lag phase) similar to what was shown here. For example, hydrogels obtained from demineralized and decellularized bone showed a short lag phase of around 9 minutes (Sawkins et al., 2013), while myocardium ECM presented a long lag phase of 40 minutes (Johnson et al., 2011). Hydrogels obtained from urinary bladder matrix (Freytes et al., 2008), dermis (Wolf et al., 2012) and pancreas (Gaetani et al., 2018) presented lag periods in a similar range to the ones reported in this study, between 15 and 25 minutes. Furthermore, the presence of detergent remnants might have an influence in the increased

gelation time seen in SDS hydrogels. When we attempted to use concentrations above 0.1% SDS for decellularization, it was found that hydrogels could not be formed. This is in agreement with findings from Gaetani and colleagues who could not fabricate pancreas ECM-derived hydrogels when they used 1% SDS for decellularization (Gaetani et al., 2018).

Pre-gel solutions presented shear thinning characteristics, i.e. viscosity decreases as shear rate increases. Values presented here are in accordance to those reported for ECM-derived hydrogels from myocardium (Johnson et al., 2011), dermis (Wolf et al., 2012), urinary bladder matrix (Freytes et al., 2008) skeletal muscle (Ungerleider et al., 2015) and cornea (Kim et al., 2019b). This characteristic offers the potential for these gels to be used as an injectable biomaterial and for their use as bioinks in 3D bioprinting (Choi et al., 2016; Jang et al., 2017, 2016; Pati et al., 2015, 2014; Skardal et al., 2015). Gelation profiles seen with turbidimetric analysis were also obtained when using rheology. Despite being more concentrated than the rat-tail collagen hydrogels, the cornea ECM-derived hydrogels were softer. However, these values are in a similar range to the ones found in hydrogels derived from other tissues (Freytes et al., 2008; Sawkins et al., 2013). The values are lower than those reported for the storage and loss moduli of the native cornea, which are 2 kPa and 0.3 kPa, respectively (Hatami-Marbini, 2014). Additional steps such as cross-linking (Ahearne and Coyle, 2016) may be required to increase the modulus of the hydrogels to match the native corneas.

In this study, cryoSEM was used to investigate the ultrastructure of the hydrogels. This technique is believed to be better at retaining the hydrogel's structure compared to conventional SEM as the water present in the highly hydrated hydrogels is sublimated at extremely low temperatures (Schatten, 2013). The hydrogels obtained here were highly fibrillar and porous, which closely resembled the structure reported for ECM-derived hydrogels from other tissues, such as dermis (Wolf et al., 2012), myocardium (Johnson et al., 2011), demineralized bone (Sawkins et al., 2013) and small intestinal submucosa (Voytik-Harbin et al., 1998). These studies imaged the hydrogels using conventional SEM after glutaraldehyde fixation and critical point drying of the samples. Johnson and colleagues also described the presence of areas of higher fibre matrix density than others, which prevented implementation of automatized pore-size quantification (Johnson et al., 2011).

In the current study, standard gelation parameters where used that can influence the hydrogels properties if modified. Johnson and colleagues studied the effect of temperature, ionic strength, pH and ECM concentration on the fibril architecture, mechanical properties and gelation kinetics of myocardium ECM-derived hydrogels (Johnson et al., 2011). They showed that no hydrogels could be formed at 4 °C and 22 °C, while at 37 °C they obtained robust hydrogels. Fibre diameter was not influenced by any of the conditions studied. Similar to our results, the authors reported areas of increased fibre density visualized by SEM. The effect that reduction of ionic strength to 0.5x PBS was striking as it increased mechanical properties and sped up gelation. pH did not influence any of the analysed parameters. Increase in ECM concentration increased mechanical properties and viscosity as reported for urinary bladder matrix (Freytes et al., 2008), bone (Sawkins et al., 2013) and dermis (Wolf et al., 2012).

Furthermore, tissue origin plays an important role in hydrogel characteristics. It has been shown that porcine myocardium hydrogels retain more sGAG and have increased strength than healthy human myocardium hydrogels (Johnson et al., 2014). While using human tissues would ease the translation into the clinic as the issue of xenoimmunogenicity is avoided, sourcing healthy organs is difficult as these would be required for transplantation. However, for the cornea specifically, human corneas deemed unsuitable for transplantation due to low endothelial cell count, have the potential to be used to manufacture hydrogels. Decellularized porcine corneas have been used clinically as alternatives to donor grafts (M.-C. Zhang et al., 2015; Zheng et al., 2019), paving the path for other treatments based on ECM-derived materials.

Cells embedded within the hydrogels presented high viability and adopted a spindle morphology with multiple processes, indicating good adhesion to the fibres, except in the SDS group. Over the culturing period, the hydrogels contracted, as reported by Wolf and colleagues using dermal ECM-derived hydrogels (Wolf et al., 2012). This contraction effect was due to the traction forces exerted by the cells on the collagen fibrils. However, when cells died as in the SDS case, the hydrogels retained their shape and size. Depending on the application, the rate of contraction might limit the usefulness of these hydrogels without further cross-linking to strengthen them (Ahearne and Coyle, 2016) or using a cell culture condition that inhibits contractile behaviour (Miotto et al., 2019). Furthermore, contraction can also be inhibited when the hydrogel adheres to a material or is constrained at the edges (Ahearne et al., 2010). When the hydrogel adheres to the

tissue matrix, it will be less able to contract compared to a free-floating hydrogel in culture medium.

In this study, all steps were performed under sterile conditions so that no final sterilization method was required. However, for clinical purposes authorities may require terminal sterilization. It has been shown that common sterilization techniques such as electron beam, gamma irradiation or ethylene oxide inhibit gel formation when performed on the powder, but not when the lyophilized digest is treated (White et al., 2018). Furthermore, sterilizing the lyophilized digest could increase the likelihood of translation into the clinic as a ready-to-use product, whereby the clinician can rehydrate the lyophilize digest with a basic salt balanced solution and let the hydrogel form *in situ*.

There has been recently some focus in the corneal tissue engineering field towards the development of materials and scaffolds for a sutureless implantation. Methacrylated gelatin cross-linked with visible light has been reported, which passed all American Society for Testing and Materials (ASTM) standards for biological adhesives (Shirzaei Sani et al., 2019). In a similar *ex vivo* testing set-up to the one shown here, Koivusalo and colleagues showed the superiority of hyaluronic acid-dopamine hydrogels to their hyaluronic acid only counterpart to adhere to the stromal bed and deliver adipose-derived MSC for stromal regeneration (Koivusalo et al., 2019). The use of such materials could by-pass the need of sutures and the associated complications, and would not require high skilled personnel, particularly useful in remote areas with difficult access to healthcare.

In summary, it was demonstrated here the importance that the decellularization method has on the final characteristics of ECM-derived hydrogels using corneas as tissue model. Similar phenomena would be expected for hydrogels derived from the ECM of other tissues although the precise decellularization protocol should be specific to the tissue type. Therefore, it is recommended that researchers or companies involved in the development of ECM-derived hydrogels examine different decellularization techniques to find the optimal approach for preparing their hydrogels.

6.5. Concluding remarks

In this Chapter, the impact of decellularization method on the characteristics of cornea ECM-derived hydrogels was studied. The freeze-thawing method yielded the best hydrogels and potentially could be used as a sutureless technique to corneal defect

repair. Cornea ECM-derived hydrogels have been the third option of fabricating corneal substitutes described in this thesis.

CHAPTER 7

Discussion

7.1. Summary

The primary objective of this thesis was to develop alternatives to traditional corneal transplantation using a tissue engineering approach. Decellularized tissues were used as main biomaterial since it is the only biomaterial that resembles biochemically most the original tissue and, depending on the processing methods, can maintain the highly organized collagen micro and nanoarchitecture.

This Thesis started by trying to elucidate the role of media supplements to promote a keratocyte-like phenotype in serum-expanded stromal cells. In the first study (Chapter 3) several biochemical cues were investigated, and cell morphology, proliferation, phenotype and migration were analysed. Upon expansion with FBS, cells adopted a spindle shape, lost expression of keratocyte markers but did not express fibrotic markers. When serum was removed from the medium, cells presented some dendrites and recovered some expression of keratocyte markers. However, proliferation and migration were impeded. Addition of AA increased expression of keratocan, CD34 and collagen I. ITS and IGF-1 promoted cell proliferation, collagen I and CD34 expression, and migration. RA increased CD34 and keratocan expression. IBMX improved keratocan expression. PDGF-BB mainly had a pro-migratory effect and showed a fibroblastic phenotype, while FGF-2 promoted the maintenance of a fibroblastic phenotype despite the removal of serum. TGF-β1 and β3 increased α-SMA and collagen I expression and reduced migratory capacity of the cells. When the pro-keratocyte cues were supplemented in combination, a synergistic effect was seen on the up-regulation of CD34 and CD34, but downregulation of ALDH3A1 happened. From these results it was decided to use serum-free medium supplemented with AA and ITS for further experiments.

The second objective of this thesis was to repopulate whole decellularized corneas with stromal cells and evaluate their benefit in a rabbit anterior lamellar keratoplasty model. In Chapter 4 scaffolds were obtained by decellularizing porcine corneas and were recellularized *in vitro* with human stromal cells. In order to promote repopulation, cell-seeded scaffolds were cultured for 2 weeks in serum-containing medium. Thereafter, the

medium was switched to a serum-free supplemented with AA and ITS, to promote the recovery of an *in vivo*-like phenotype. While cells were not able to repopulate the deepest areas of the scaffolds, cells were able to migrate to some extent. The cells repopulating the scaffolds presented an *in vivo*-like phenotype. *In vitro* tests showed that epithelial cells could grow well on the surface of the scaffolds and that reinnervation after transplantation should be possible as seen by the sprouting of DRGs. Cell-free and recellularized scaffolds were implanted in an *in vivo* model of ALK. There seemed to be no major differences between the two groups, as all grafts were re-epithelialized and no grafts were rejected, but presented some neovascularization and some scar tissue. All scaffolds appeared to be highly repopulated with cells of varied phenotype.

Chapter 5 had the objective of exploring alternative methods to fabricate cornea-like tissues using decellularized corneas as starting materials to obtain highly cellular constructs in a rapid manner. To achieve this, porcine corneas were sliced into thin sheets which were then decellularized and air dried. These were used together with cell-laden collagen I hydrogels in a multi-layered fashion. Constructs presented high cell viability after 3 weeks in culture and cells had a keratocyte-like phenotype. Epithelial cells grew well on the surface. The constructs had sufficient strength to be sutured onto a porcine cornea in an *ex vivo* ALK model. When kept in culture, endogenous epithelial cells covered the constructs in 7 days.

To further expand on the use of decellularized tissues for corneal tissue engineering, I sought to solubilize corneal ECM to obtain hydrogels. The final objective of this thesis was to compare decellularization methods to obtain cornea ECM-derived hydrogels and their use as wound healing treatments. In Chapter 6, four decellularization methods were used and hydrogels produced which presented differences, mainly in gelation kinetics, transparency and cytocompatibility. Hydrogels obtained from the freeze-thawing method presented the best characteristics. Furthermore, their potential use for the treatment of corneal defects in a sutureless manner was explored in an *ex vivo* model, with promising early healing demonstrated by repopulation of epithelial cells.

The work presented in this thesis describes the fabrication of three different scaffolds for tissue engineering of corneal substitutes and the culture conditions needed for the recovery of keratocyte phenotype. These studies set the bases for future optimisation for their use in the clinic and palliate severe donor shortage.

7.2. Limitations and further remarks

Throughout this thesis human corneal stromal cells obtained via explant isolation cultured in serum-containing medium have been used. These cells lose their *in vivo* phenotype, and are essentially activated keratocytes or corneal fibroblasts, but it can be partially recovered, as seen in Chapter 3. It is important to note that experiments in this thesis were done with cells from a single donor. Therefore, age, gender and other parameters might also be important and results could vary. Cells isolated by collagenase digestion might present different characteristics, but this has not been addressed in this thesis. There is an important body of research describing the presence of corneal stromal stem cells, pioneered by Funderburgh. These cells are isolated as a side population, i.e. via FACS by Hoechst efflux through ABCG2 activity, from passage 4 collagenase-isolated cells cultured in a complex medium containing DMEM/MCDB-201, 2% FBS, EGF, PDGF-BB, ITS, leukemia inhibitory factor (LIF), linoleic acid–bovine serum albumin, AA and dexamethasone (Du et al., 2005). Studies have shown the increased capacity of these cells to secrete stromal-like ECM and better retention of keratocyte phenotype *in vitro*, and absence of inflammatory response and reduction of stromal haze *in vivo*, when compared to regular serum-expanded stromal cells (Basu et al., 2014; Hertsenberg et al., 2017; J. Wu et al., 2014; Wu et al., 2013). The isolation and characterization of their secretome has been recently reported, identifying extracellular vesicles as key players in the anti-scarring, anti-inflammatory and pro-regenerative effect of these cells (Shojaati et al., 2019). For personalized medicine, patient-specific stromal cells could be obtained from the contralateral eye if unaffected, in a similar way to the treatment for LSCD. However, if both eyes are affected, either allogenic cells should be used or an autogenic source found, such as adipose-derived MSC which have the ability to differentiate into a cell with some keratocyte characteristics (Arnalich-Montiel et al., 2008; Du et al., 2010; Espandar et al., 2012; Lynch and Ahearne, 2017; S. Zhang et al., 2013).

The ideal tissue source for corneal decellularization is human. While healthy corneas are usually transplanted to patients in need, some corneas are deemed unsuitable for transplantation due to low endothelial cell count or being positive for some viruses. In the case of low endothelial numbers, these corneas could potentially be repurposed for

decellularization (Wilson et al., 2016). In the case of infections, gamma irradiation could be used to eliminate the risk of bacterial, viral or fungal disease transmission (Utine et al., 2011). In addition, some studies have focused on the use of discarded tissue after small incision lenticule extraction (SMILE), a refractive technique for myopic treatment (Yam et al., 2016; Yin et al., 2016). While the use of human corneas is certainly one option, donor shortages remain an issue, thus alternative species have been explored. Due to their anatomical similarities to human cornea and their availability, porcine corneas have been the most extensively studied for decellularization. Pig corneas are slightly thicker than human but have similar mechanical characteristics (Zeng et al., 2001). In a recent study it was found that the porcine cornea had the highest similarity score to the human, compared to 13 other animals that could be used for decellularization, among them dog, cat, sheep, goat, cow, horse and rabbit (Sharifi et al., 2019). This score was calculated from amino acid sequence, isoelectric point and hydropathicity of the main ECM components found in the stroma. It is important to note that some immunogenic epitopes to humans are present in the porcine cornea, such as N-glycolylneuraminic acid (Neu5Gc) and Galactose-alpha- 1,3-galactose (α-Gal). This highlights the importance of applying a thorough decellularization process in order to avoid graft rejection.

SDS is extensively reported in the literature for its efficiency in cell removal. However, it can come in hand with cytotoxicity issues. As was seen in Chapter 6, the presence of residual SDS in the ECM rendered cytotoxic hydrogels. For the decellularization in Chapters 4 and 5, Triton-X100 was used as decellularizing agent but also to promote removal of SDS (Guyette et al., 2014). However, this effect might have been more effective as a washing step, rather than concomitant with SDS. While several cell types could attach and grow on the surface of the scaffolds and some infiltration was seen *in vitro*, remnants of SDS in the deeper areas of the scaffolds might be responsible for the limited repopulation. Quantification of SDS showed some residual SDS present in the scaffolds (Appendix Table A-1), but below what is reported to be toxic in the literature (Gratzer et al., 2006; Zvarova et al., 2016). By adding a 2 hour washing step with 0.5 mM $CaCl_2$, Friedriech and colleagues showed a 10-fold decrease of residual SDS compared to the same protocol omitting this step (Friedrich et al., 2018). This extra step had a tremendous impact when implanting *in vivo* as no fibrotic wound healing nor foreign body response was present, while in the higher SDS-containing scaffolds these

events happened. The presence of SDS residues could be an explanation for the limited success after *in vivo* implantation, regardless of prior *in vitro* recellularization.

Most *in vivo* studies have end-points spanning from 6 months to 24 months. Healing of the cornea is a slow process and while scarring can occur at initial time-points, this can spontaneously revert and heal properly (Medeiros et al., 2018). One could speculate that scaffold remodelling and recovery of transparency could be observed if the study had been longer.

In this thesis studies have been done over several scales, from simple *in vitro* experiments on tissue culture plastic, to *ex vivo* organ culture, to *in vivo* experimentation. Experiments on 2D do not offer the complexity of multi-cellular cross-talk, while *in vivo* testing is highly time and resource demanding. *Ex vivo* organ culture models are a great intermediate step to test materials developed in the lab for corneal tissue engineering applications. The first report of culturing human donor corneas unsuitable for transplantation in the air-liquid interphase was in 1991 (Richard et al., 1991). Some years later Foreman described a simple, yet effective method to study epithelial wound healing, by placing a cornea with corneo-scleral ring onto an agar/collagen plug. Many studies have based their *ex vivo* testing on this pioneer work (Deshpande et al., 2015; Evans et al., 2002; Pinnock et al., 2017; Xu et al., 2000). These models, unfortunately, cannot recapitulate the complexity of the immune system or of neovascularization.

7.3. Future directions

While this thesis has mainly focussed on the anterior cornea, many corneal diseases affect other layers in single, such as the epithelium or the endothelium. Some of the materials described here could be tested for the culture and transplantation of either cell type. ECM-derived hydrogels could be used to transplant limbal epithelial stem cells instead of fibrin gels as the current gold standard in cases of LSCD (Rama et al., 2010, 2001). Decellularized lenticules/sheets could be an excellent cell carrier for endothelial cells, but may need to be cut thinner. In a preliminary study, freshly isolated human endothelial cells were able to attach and were viable after 7 days when cultured on the posterior surface of decellularized porcine corneas (Appendix Figure A-11). Furthermore, ECM-derived hydrogels can be transformed into membranes by vitrification in a similar

way as done with collagen hydrogels (Calderón-Colón et al., 2012; Chae et al., 2015, 2014; McIntosh Ambrose et al., 2009) which could be used for epithelial and endothelial cell culture and transplantation.

To improve the results observed in Chapter 4, some actions could be done. As discussed earlier, longer experiments could give a better insight in success or failure in a more relevant way as the healing process of the cornea is slow. However, the scar tissue visible on the surface of the scaffolds could be triggered by repopulating epithelium in the absence of the basement membrane. Epithelial cells would eventually lay down their own basement membrane. Coating of the anterior surface of the scaffolds with one or more basement membrane components could alleviate the initial "shock" that epithelial cells experience. Gouveia and colleagues reported the use of compressed collagen I gels for LSCD treatment which was coated with laminin (Gouveia et al., 2019), as this is the most abundant non-collagenous protein in the epithelial basement membrane (Torricelli et al., 2013). The decellularization method used was very successful in cell removal, but came in hand with GAG removal. Glycoproteins and proteoglycans, such as laminins and perlecan (Torricelli et al., 2013), are highly present in the epithelial basement membrane and their disruption could have had an impact on the repopulating cells. Shafiq and colleagues have shown that SDS can disrupt the basement membrane of human corneas while decellularization with NaCl did not affect it (Shafiq et al., 2012). Therefore, future studies should investigate the use of alternative decellularizing methods.

The ECM-derived hydrogels described in Chapter 6 have the potential to be used as drug-delivery platforms. These can be small molecules or growth factors, such as insulin which showed improved keratocyte phenotype in Chapter 3. Several pathways would be interesting to target pharmacologically with such hydrogels. To prevent keratocyte to myofibroblast transformation TGF-β1 should be inhibited by blocking antibodies or antisense oligonucleotides (Cordeiro et al., 2003; Jester et al., 1997). Furthermore, the presence of small leucine-rich proteoglycans in these hydrogels could have an anti-scarring effect. Decorin binds to TGF-β1 and sequesters it, thereby blocking its effect (R. Mohan et al., 2011). As demonstrated by Hill and colleagues, corneal opacity was reduced in an infectious keratitis model with decorin-loaded gellan-based fluid gel eye drops (Hill et al., 2018). Another strategy would be to prevent neovascularization, which could be achieved by inhibiting VEGF, through antibodies or aptamers (Keating

and Jacobs, 2011), or by blocking the IL-1β pathway with corticosteroids, such as dexamethasone or bethamethasone.

Solubilized decellularized corneal ECM showed shear-thinning properties which make them an excellent candidate material for 3D bioprinting (Kim et al., 2019b). However, since the gelation time is rather long, a secondary cross-linking method or the mixing of this material with another one, generating an interpenetrating network, could increase the printing fidelity (Isaacson et al., 2018). Likewise, since the cornea is a curved tissue traditional in-air bioprinting can be challenging. Therefore, strategies such as the freeform reversible embedding of suspended hydrogels (FRESH), where the ink is extruded in a microbead bath that can be removed after gelation occurs, could be employed (Hinton et al., 2015; Lee et al., 2019).

The *ex vivo* organ culture used in this thesis could benefit from some further refinement. First, medium used should be optimized. The presence or absence of serum in the medium is likely to have an effect and could increase the scarring after creating the defect. Furthermore, supplementation of medium with dextran was used in one study but not in another. Dextran is a polysaccharide commonly used in organ culture of corneas for transplantation to reduce the oedema in submersion culture (Armitage, 2011). While not compared to non-supplemented medium, Yin and colleagues used dextran in their keratoconus model in *ex vivo* cultured corneas (Yin et al., 2019b). Another refinement would be the use of bioreactor systems to mimic blinking, and so keep the surface moist. A simple method would be to place the cultured corneas on a rocking system, which would move the medium over the surface of the cornea periodically. Such a system has been reported with striking differences between static and dynamic conditions (Deshpande et al., 2015). More sophisticated bioreactors appear in the literature which also take into account the culturing necessities of the endothelium (Schmid et al., 2018). These would allow for lengthy experiments in order to study slower wound healing processes such as stromal cell migration.

To bring the results obtained in this thesis closer to the clinic, some considerations need to be taken into account. First of all the incorporation or not of cells. When designing strategies for full thickness or endothelial therapies, cells must be transplanted in order for the therapy to succeed. However, for anterior corneal applications, cell-free approaches could be implemented. As seen in this thesis, it is still debatable if the delivery

of cells to the damaged cornea is a necessary. Materials based on decellularized matrices have been classified as “Medical Devices” which have different regulations than “Advanced Therapy Medicinal Products” if they include autologous or allogeneic cells, which are more stringent (Pellegrini et al., 2014; Webber et al., 2015). Another important parameter to take into consideration is the maintenance of sterility and/or terminal sterilization, through gamma-irradiation, for example. Dehydration in order to obtain a dry scaffold with prolonged shelf life would be an interesting factor to study. The decellularized sheets described in Chapter 5 were kept at room temperature for long periods of time without an evident degradation or difference in behaviour. As discussed in Chapter 6, the obtained hydrogels have the potential to be lyophilized before gelation and be rehydrated when needed, making them handy for initial point of care in situations where highly specialized ophthalmic personnel is unavailable. As with any other product, batch-to-batch differences need to be monitored.

CHAPTER 8
Conclusions

Overall the work from this thesis has led to the following conclusions:

- Keratocyte phenotype can be partially recovered after serum expansion via serum removal and supplementation with ascorbic acid and insulin-transferrin-selenium.
- Scaffolds obtained from decellularized porcine corneas were repopulated with phenotypically correct stromal cells. When implanted in a rabbit model of ALK, they integrated well but no benefit was observed when recellularized constructs were implanted compared to their acellular counterparts.
- Anterior corneal equivalents were fabricated by stacking sheets of decellularized tissues with cell-laden hydrogels. Cells in these constructs presented high cell viability and keratocyte-like phenotype. Epithelial cells attached and stratified. Constructs were robust to be sutured onto a porcine cornea in an ALK *ex vivo* model and tissue integration and re-epithelialization was observed.
- Cornea ECM-derived hydrogels were fabricated from corneas decellularized with different methods, which impacted in the gel characteristics. SDS decellularization rendered cytotoxic gels and gels obtained by freeze-thawing presented the best characteristics overall. These hydrogels were successfully used to fill a defect *in situ* on an *ex vivo* porcine cornea and supported host epithelial re-growth.

References

Abidin, F.Z., Gouveia, R.M., Connon, C.J., 2015. Application of retinoic acid improves form and function of tissue engineered corneal construct. Organogenesis 11, 122–136. https://doi.org/10.1080/15476278.2015.1093267

Aghamohammadzadeh, H., Newton, R.H., Meek, K.M., 2004. X-Ray Scattering Used to Map the Preferred Collagen Orientation in the Human Cornea and Limbus. Structure 12, 249–256. https://doi.org/10.1016/j.str.2004.01.002

Ahearne, M., Coyle, A., 2016. Application of UVA-riboflavin crosslinking to enhance the mechanical properties of extracellular matrix derived hydrogels. J. Mech. Behav. Biomed. Mater. 54, 259–267. https://doi.org/10.1016/j.jmbbm.2015.09.035

Ahearne, M., Liu, K.-K., El Haj, A.J., Then, K.Y., Rauz, S., Yang, Y., 2010. Online monitoring of the mechanical behavior of collagen hydrogels: Influence of corneal fibroblasts on elastic modulus. Tissue Eng. - Part C Methods 16. https://doi.org/10.1089/ten.tec.2008.0650

Ahearne, M., Lynch, A.P., 2015. Early Observation of Extracellular Matrix-Derived Hydrogels for Corneal Stroma Regeneration. Tissue Eng. Part C Methods 21, 1059–1069. https://doi.org/10.1089/ten.tec.2015.0008

Ahearne, M., Yang, Y., Then, K.Y., Liu, K.K., 2008. Non-destructive mechanical characterisation of UVA/riboflavin crosslinked collagen hydrogels. Br. J. Ophthalmol. 92, 268–271. https://doi.org/10.1136/bjo.2007.130104

Alaminos, M., Sánchez-Quevedo, M.D.C., Muñoz-Ávila, J.I., Serrano, D., Medialdea, S., Carreras, I., Campos, A., 2006. Construction of a complete rabbit cornea substitute using a fibrin-agarose scaffold. Investig. Ophthalmol. Vis. Sci. 47, 3311–3317. https://doi.org/10.1167/iovs.05-1647

Alió del Barrio, J.L., Chiesa, M., Garagorri, N., Garcia-Urquia, N., Fernandez-Delgado, J., Bataille, L., Rodriguez, A., Arnalich-Montiel, F., Zarnowski, T., Álvarez de Toledo, J.P., Alió, J.L., De Miguel, M.P., 2015. Acellular human corneal matrix sheets seeded with human adipose-derived mesenchymal stem cells integrate functionally in an experimental animal model. Exp. Eye Res. 132, 91–100. https://doi.org/10.1016/j.exer.2015.01.020

Alió del Barrio, J.L., El Zarif, M., Azaar, A., Makdissy, N., Khalil, C., Harb, W., El Achkar, I., Jawad, Z.A., de Miguel, M.P., Alió, J.L., 2018. Corneal Stroma Enhancement With Decellularized Stromal Laminas With or Without Stem Cell Recellularization for Advanced Keratoconus. Am. J. Ophthalmol. 186, 47–58. https://doi.org/10.1016/j.ajo.2017.10.026

Alió Del Barrio, J.L., El Zarif, M., De Miguel, M.P., Azaar, A., Makdissy, N., Harb, W., El Achkar, I., Arnalich-Montiel, F., Alió, J.L., 2017. Cellular Therapy with Human Autologous Adipose-Derived Adult Stem Cells for Advanced Keratoconus. Cornea 36, 952–960. https://doi.org/10.1097/ICO.0000000000001228

Allen, C.L., Clare, G., Stewart, E.A., Branch, M.J., McIntosh, O.D., Dadhwal, M., Dua, H.S., Hopkinson, A., 2013. Augmented dried versus cryopreserved amniotic membrane as an ocular surface dressing. PLoS One 8, e78441–e78441. https://doi.org/10.1371/journal.pone.0078441

Amano, S., Shimomura, N., Yokoo, S., Araki-Sasaki, K., Yamagami, S., 2008. Decellularizing corneal stroma using N2 gas. Mol. Vis. 14, 878–882.

Andrae, J., Gallini, R., Betsholtz, C., 2008. Role of platelet-derived growth factors in physiology and medicine. Genes Dev. 22, 1276–312. https://doi.org/10.1101/gad.1653708

Andresen, J.L., Ledet, T., Ehlers, N., 1997. Keratocyte migration and peptide growth factors: the effect of PDGF, bFGF, EGF, IGF-I, aFGF and TGF-beta on human keratocyte migration in a collagen gel. Curr Eye Res 16, 605–613. https://doi.org/10.1076/ceyr.16.6.605.5081

Armitage, W.J., 2011. Preservation of human cornea. Transfus. Med. Hemotherapy 38, 143–147. https://doi.org/10.1159/000326632

Arnalich-Montiel, F., Moratilla, A., Fuentes-Julián, S., Aparicio, V., Cadenas Martin, M., Peh, G., Mehta, J.S., Adnan, K., Porrua, L., Pérez-Sarriegui, A., De Miguel, M.P., 2019. Treatment of corneal endothelial damage in a rabbit model with a bioengineered graft using human decellularized corneal lamina and cultured human corneal endothelium. PLoS One 14, e0225480. https://doi.org/10.1371/journal.pone.0225480

Arnalich-Montiel, F., Pastor, S., Blazquez-Martinez, A., Fernandez-Delgado, J., Nistal, M., Alió, J.L., De Miguel, M.P., 2008. Adipose-Derived Stem Cells Are a Source for Cell Therapy of the Corneal Stroma. Stem Cells 26, 570–579. https://doi.org/10.1634/stemcells.2007-0653

Assouline, M., Chew, S.J., Thompson, H.W., Beuerman, R.W., 1992. Effect of growth factors on collagen lattice contraction by human keratocytes. Invest. Ophthalmol. Vis. Sci. 33, 1742–55.

Baptista, P.M., Siddiqui, M.M., Lozier, G., Rodriguez, S.R., Atala, A., Soker, S., 2011. The use of whole organ decellularization for the generation of a vascularized liver organoid. Hepatology 53, 604–617. https://doi.org/10.1002/hep.24067

Barakat, O., Abbasi, S., Rodriguez, G., Rios, J., Wood, R.P., Ozaki, C., Holley, L.S., Gauthier, P.K., 2012. Use of Decellularized Porcine Liver for Engineering Humanized Liver Organ. J. Surg. Res. 173, e11–e25. https://doi.org/10.1016/J.JSS.2011.09.033

Bartels, M.C., Doxiadis, I.I.N., Colen, T.P., Beekhuis, W.H., 2003. Long-term outcome in high-risk corneal transplantation and the influence of HLA-A and HLA-B matching. Cornea 22, 552–556. https://doi.org/10.1097/00003226-200308000-00013

Basu, S., Hertsenberg, A.J., Funderburgh, M.L., Burrow, M.K., Mann, M.M., Du, Y., Lathrop, K.L., Syed-Picard, F.N., Adams, S.M., Birk, D.E., Funderburgh, J.L., 2014. Human limbal biopsy-derived stromal stem cells prevent corneal scarring. Sci. Transl. Med. 6, 266ra172-266ra172. https://doi.org/10.1126/scitranslmed.3009644

Basu, S., Sureka, S.P., Shanbhag, S.S., Kethiri, A.R., Singh, V., Sangwan, V.S., 2016. Simple Limbal Epithelial Transplantation: Long-Term Clinical Outcomes in 125 Cases of Unilateral Chronic Ocular Surface Burns. Ophthalmology 123, 1000–1010. https://doi.org/10.1016/j.ophtha.2015.12.042

Bayyoud, T., Thaler, S., Hofmann, J., Maurus, C., Spitzer, M.S., Bartz-Schmidt, K.U., Szurman, P., Yoeruek, E., 2012. Decellularized Bovine Corneal Posterior Lamellae as Carrier Matrix for Cultivated Human Corneal Endothelial Cells. Curr. Eye Res. 37, 179–186. https://doi.org/10.3109/02713683.2011.644382

Beales, M.P., Funderburgh, J.L., Jester, J. V., Hassell, J.R., 1999. Proteoglycan synthesis by bovine keratocytes and corneal fibroblasts: Maintenance of the keratocyte phenotype in culture. Investig. Ophthalmol. Vis. Sci. 40, 1658–1663.

Berryhill, B.L., Kader, R., Kane, B.P., Birk, D.E., Feng, J., Hassell, J.R., 2002. Partial restoration of the keratocyte phenotype to bovine keratocytes made fibroblastic by serum. Investig. Ophthalmol. Vis. Sci. 43, 3416–3421.

Birk, D.E., Fitch, J.M., Babiarz, J.P., Doane, K.J., Linsenmayer, T.F., 1990. Collagen fibrillogenesis in vitro: interaction of types I and V collagen regulates fibril diameter. J. Cell Sci. 95.

Birk, D.E., Fitch, J.M., Linsenmayer, T.F., 1986. Organization of collagen types I and V in the embryonic chicken cornea. Invest. Ophthalmol. Vis. Sci. 27, 1470–7. https://doi.org/10.1073/pnas.81.9.2791

Bonanno, J.A., 2012. Molecular mechanisms underlying the corneal endothelial pump. Exp. Eye Res. 95, 2–7. https://doi.org/10.1016/j.exer.2011.06.004

Booth, A.J., Hadley, R., Cornett, A.M., Dreffs, A.A., Matthes, S.A., Tsui, J.L., Weiss, K., Horowitz, J.C., Fiore, V.F., Barker, T.H., Moore, B.B., Martinez, F.J., Niklason, L.E., White, E.S., 2012. Acellular Normal and Fibrotic Human Lung Matrices as a Culture System for *In Vitro* Investigation. Am. J. Respir. Crit. Care Med. 186, 866–876. https://doi.org/10.1164/rccm.201204-0754OC

Borderie, V.M., Mourra, N., Laroche, L., 1999. Influence of fetal calf serum, fibroblast growth factors, and hepatocyte growth factor on three-dimensional cultures of human keratocytes in collagen gel matrix. Graefe's Arch. Clin. Exp. Ophthalmol. 237, 861–9. https://doi.org/10.1007/s004170050324

Boulze Pankert, M., Goyer, B., Zaguia, F., Bareille, M., Perron, M.C., Liu, X., Cameron, J.D., Proulx, S., Brunette, I., 2014. Biocompatibility and functionality of a tissue-engineered living corneal stroma transplanted in the feline eye. Invest. Ophthalmol. Vis. Sci. 55, 6908–6920. https://doi.org/10.1167/iovs.14-14720

Bray, L.J., George, K. a., Hutmacher, D.W., Chirila, T. V., Harkin, D.G., 2012. A dual-layer silk fibroin scaffold for reconstructing the human corneal limbus. Biomaterials 33, 3529–3538. https://doi.org/10.1016/j.biomaterials.2012.01.045

Brightman, A.O., Rajwa, B.P., Sturgis, J.E., McCallister, M.E., Robinson, J.P., Voytik-Harbin, S.L., 2000. Time-lapse confocal reflection microscopy of collagen fibrillogenesis and extracellular matrix assembly in vitro. Biopolymers 54, 222–234. https://doi.org/10.1002/1097-0282(200009)54:3<222::AID-BIP80>3.0.CO;2-K

Brown, B.N., Chung, W.L., Almarza, A.J., Pavlick, M.D., Reppas, S.N., Ochs, M.W., Russell, A.J., Badylak, S.F., 2012. Inductive, Scaffold-Based, Regenerative Medicine Approach to Reconstruction of the Temporomandibular Joint Disk. J. Oral Maxillofac. Surg. 70, 2656–2668. https://doi.org/10.1016/j.joms.2011.12.030

Bueno, J.M., Gualda, E.J., Giakoumaki, A., Pérez-Merino, P., Marcos, S., Artal, P., 2011. Multiphoton microscopy of ex vivo corneas after collagen cross-linking. Investig. Ophthalmol. Vis. Sci. 52, 5325–5331. https://doi.org/10.1167/iovs.11-7184

Buznyk, O., Pasyechnikova, N., Islam, M.M., Iakymenko, S., Fagerholm, P., Griffith, M., 2015. Bioengineered Corneas Grafted as Alternatives to Human Donor Corneas in Three High-Risk Patients. Clin. Transl. Sci. 8, 558–562. https://doi.org/10.1111/cts.12293

Calderón-Colón, X., Xia, Z., Breidenich, J.L., Mulreany, D.G., Guo, Q., Uy, O.M., Tiffany, J.E., Freund, D.E., McCally, R.L., Schein, O.D., Elisseeff, J.H., Trexler, M.M., 2012. Structure and properties of collagen vitrigel membranes for ocular repair and regeneration applications. Biomaterials 33, 8286–8295. https://doi.org/10.1016/j.biomaterials.2012.07.062

Castro, N., Gillespie, S.R., Bernstein, A.M., 2019. Ex Vivo Corneal Organ Culture Model for Wound Healing Studies. J. Vis. Exp. 1–11. https://doi.org/10.3791/58562

Chae, J.J., McIntosh Ambrose, W., Espinoza, F.A., Mulreany, D.G., Ng, S., Takezawa, T., Trexler, M.M., Schein, O.D., Chuck, R.S., Elisseeff, J.H., 2015. Regeneration of corneal epithelium utilizing a collagen vitrigel membrane in rabbit models for corneal stromal wound and limbal stem cell deficiency. Acta Ophthalmol. 93, e57–e66. https://doi.org/10.1111/aos.12503

Chae, J.J., Mulreany, D.G., Guo, Q., Lu, Q., Choi, J.S., Strehin, I., Espinoza, F.A., Schein, O., Trexler, M.M., Bower, K.S., Elisseeff, J.H., 2014. Application of a Collagen-Based Membrane and Chondroitin Sulfate-Based Hydrogel Adhesive for the Potential Repair of Severe Ocular Surface Injuries. Mil. Med. 179, 686–694. https://doi.org/10.7205/MILMED-D-13-00360

Chaimov, D., Baruch, L., Krishtul, S., Meivar-levy, I., Ferber, S., Machluf, M., 2017. Innovative encapsulation platform based on pancreatic extracellular matrix achieve substantial insulin delivery. J. Control. Release 257, 91–101. https://doi.org/10.1016/j.jconrel.2016.07.045

Chakravarti, S., Stallings, R.L., SundarRaj, N., Cornuet, P.K., Hassell, J.R., 1995. Primary structure of human lumican (keratan sulfate proteoglycan) and localization of the gene (lum) to chromosome 12q21.3-q22. Genomics. https://doi.org/10.1006/geno.1995.1080

Che, X., Wu, H., Jia, C., Sun, H., Ou, S., Wang, J., Jeyalatha, M.V., He, X., Yu, J., Zuo, C., Liu, Z., Li, W., 2019. A Novel Tissue-Engineered Corneal Stromal Equivalent Based on Amniotic Membrane and Keratocytes. Investig. Opthalmology Vis. Sci. 60, 517. https://doi.org/10.1167/iovs.18-24869

Chen, J., Guerriero, E., Sado, Y., Sundarraj, N., 2009. Rho-mediated regulation of TGF-beta1-and FGF-2-induced activation of corneal stromal keratocytes. Investig. Ophthalmol. Vis. Sci. 50, 3662–3670. https://doi.org/10.1167/iovs.08-3276

Chen, J., Wong-Chong, J., SundarRaj, N., 2011. FGF-2- and TGF-β1-induced downregulation of lumican and keratocan in activated corneal keratocytes by JNK signaling pathway. Investig. Ophthalmol. Vis. Sci. 52, 8957–8964. https://doi.org/10.1167/iovs.11-8078

Chen, R.-N., Ho, H.-O., Tsai, Y.-T., Sheu, M.-T., 2004. Process development of an acellular dermal matrix (ADM) for biomedical applications. Biomaterials 25, 2679–86.

Chew, H.F., Ayres, B.D., Hammersmith, K.M., Rapuano, C.J., Laibson, P.R., Myers, J.S., Jin, Y.-P., Cohen, E.J., 2009. Boston keratoprosthesis outcomes and complications. Cornea 28, 989–996. https://doi.org/10.1097/ICO.0b013e3181a186dc

Choi, J.S., Williams, J.K., Greven, M., Walter, K.A., Laber, P.W., Khang, G., Soker, S., 2010. Bioengineering endothelialized neo-corneas using donor-derived corneal endothelial cells and decellularized corneal stroma. Biomaterials 31, 6738–6745. https://doi.org/10.1016/j.biomaterials.2010.05.020

Choi, Y.J., Kim, T.G., Jeong, J., Yi, H.G., Park, J.W., Hwang, W., Cho, D.W., 2016. 3D Cell Printing of Functional Skeletal Muscle Constructs Using Skeletal Muscle-Derived Bioink. Adv. Healthc. Mater. 5, 2636–2645. https://doi.org/10.1002/adhm.201600483

Cordeiro, M.F., Mead, A., Ali, R.R., Alexander, R. a, Murray, S., Chen, C., York-Defalco, C., Dean, N.M., Schultz, G.S., Khaw, P.T., 2003. Novel antisense oligonucleotides targeting TGF-beta inhibit in vivo scarring and improve surgical outcome. Gene Ther. 10, 59–71. https://doi.org/10.1038/sj.gt.3301865

Corpuz, L.M., Funderburgh, J.L., Funderburgh, M.L., Bottomley, G.S., Prakash, S., Conrad, G.W., 1996. Molecular Cloning and Tissue Distribution of Keratocan. J. Biol. Chem. 271, 9759–9763. https://doi.org/10.1074/jbc.271.16.9759

Courtman, D.W., Pereira, C.A., Kashef, V., McComb, D., Lee, J.M., Wilson, G.J., 1994. Development of a pericardial acellular matrix biomaterial: Biochemical and mechanical effects of cell extraction. J. Biomed. Mater. Res. 28, 655–666. https://doi.org/10.1002/jbm.820280602

Crapo, P.M., Gilbert, T.W., Badylak, S.F., 2011. An overview of tissue and whole organ decellularization processes. Biomaterials 32, 3233–3243. https://doi.org/10.1016/j.biomaterials.2011.01.057

Crawford, G.J., 2016. The development and results of an artificial cornea: AlphaCor^{TM}, in: Biomaterials and Regenerative Medicine in Ophthalmology: Second Edition.

Cyranoski, D., 2019. Woman is first to receive cornea made from 'reprogrammed' stem cells. Nature. https://doi.org/10.1038/d41586-019-02597-2

Dai, Y., Chen, Jiansu, Li, H., Li, S., Chen, Jian, Ding, Y., Wu, J., Wang, C., Tan, M., 2012. Characterizing the Effects of VPA, VC and RCCS on Rabbit Keratocytes onto Decellularized Bovine Cornea. PLoS One 7, 1–10. https://doi.org/10.1371/journal.pone.0050114

Darwish, T., Brahma, A., Efron, N., O'Donnell, C., 2007. Subbasal nerve regeneration after penetrating keratoplasty. Cornea 26, 935–940. https://doi.org/10.1097/ICO.0b013e3180de493f

DelMonte, D.W., Kim, T., 2011. Anatomy and physiology of the cornea and related structures. J Cataract Refract Surg 37, 588–598. https://doi.org/10.1016/j.jcrs.2010.12.037

DeQuach, J.A., Mezzano, V., Miglani, A., Lange, S., Keller, G.M., Sheikh, F., Christman, K.L., 2010. Simple and High Yielding Method for Preparing Tissue Specific Extracellular Matrix Coatings for Cell Culture. PLoS One 5, e13039. https://doi.org/10.1371/journal.pone.0013039

Deshpande, P., Ortega, I., Sefat, F., Sangwan, V.S., Green, N., Claeyssens, F., MacNeil, S., 2015. Rocking Media Over Ex Vivo Corneas Improves This Model and Allows the Study of the Effect of Proinflammatory Cytokines on Wound Healing. Invest. Ophthalmol. Vis. Sci. 56, 1553–1561. https://doi.org/10.1167/iovs.14-15308

Diao, J., Pang, X., Qiu, Y., Miao, Y., Yu, M., Fan, T., 2015. Construction of a human corneal stromal equivalent with non-transfected human corneal stromal cells and acellular porcine corneal stromata. Exp. Eye Res. 132, 216–244. https://doi.org/10.1016/j.exer.2015.01.015

Dikstein, S., Maurice, D.M., 1972. Metabolic Basis To Fluid Pump in Cornea. J. Physiol. 221, 29-.

Dong, M., Zhao, L., Wang, F., Hu, X., Li, H., Liu, T., Zhou, Q., Shi, W., 2019. Rapid porcine corneal decellularization through the use of sodium N-lauroyl glutamate and supernuclease. J. Tissue Eng. 10, 204173141987587. https://doi.org/10.1177/2041731419875876

Du, L., Wu, X., 2011. Development and characterization of a full-thickness acellular porcine cornea matrix for tissue engineering. Artif. Organs 35, 691–705. https://doi.org/10.1111/j.1525-1594.2010.01174.x

Du, L., Wu, X., Pang, K., Yang, Y., 2011. Histological evaluation and biomechanical characterisation of an acellular porcine cornea scaffold. Br. J. Ophthalmol. 95, 410–4. https://doi.org/10.1136/bjo.2008.142539

Du, Y., Funderburgh, M.L., Mann, M.M., SundarRaj, N., Funderburgh, J.L., 2005. Multipotent stem cells in human corneal stroma. Stem Cells 23, 1266–75. https://doi.org/10.1634/stemcells.2004-0256

Du, Y., Roh, D.S., Funderburgh, M.L., Mann, M.M., Marra, K.G., Rubin, J.P., Li, X., Funderburgh, J.L., 2010. Adipose-derived stem cells differentiate to keratocytes in vitro. Mol. Vis. 16, 2680–9.

Dua, H.S., Saini, J.S., Azuara-Blanco, A., Gupta, P., 2000. Limbal stem cell deficiency: concept, aetiology, clinical presentation, diagnosis and management. Indian J. Ophthalmol. 48, 83–92.

Edgar, L., Altamimi, A., García Sánchez, M., Tamburrinia, R., Asthana, A., Gazia, C., Orlando, G., 2018. Utility of extracellular matrix powders in tissue engineering. Organogenesis 14, 172–186. https://doi.org/10.1080/15476278.2018.1503771

Elder, B.D., Eleswarapu, S. V., Athanasiou, K.A., 2009. Extraction techniques for the decellularization of tissue engineered articular cartilage constructs. Biomaterials 30, 3749–3756. https://doi.org/10.1016/j.biomaterials.2009.03.050

Engel, H., Kao, S.W., Larson, J., Uriel, S., Jiang, B., Brey, E., Cheng, M.H., 2015. Investigation of Dermis-derived hydrogels for wound healing applications. Biomed. J. 38, 58–64. https://doi.org/10.4103/2319-4170.132899

Espana, E.M., He, H., Kawakita, T., Di Pascuale, M.A., Raju, V.K., Liu, C.Y., Tseng, S.C.G., 2003. Human Keratocytes Cultured on Amniotic Membrane Stroma Preserve Morphology and Express Keratocan. Investig. Ophthalmol. Vis. Sci. 44, 5136–5141. https://doi.org/10.1167/iovs.03-0484

Espandar, L., Bunnell, B., Wang, G.Y., Gregory, P., McBride, C., Moshirfar, M., 2012. Adipose-Derived Stem Cells on Hyaluronic Acid–Derived Scaffold. Arch. Ophthalmol. 130, 202. https://doi.org/10.1001/archopthalmol.2011.1398

Espandar, L., Carlson, A.N., 2013. Lamellar Keratoplasty: A Literature Review. J. Ophthalmol. 2013. https://doi.org/10.1155/2013/894319

Estrada, J.L., Martens, G., Li, P., Adams, A., Newell, K.A., Ford, M.L., Butler, J.R., Sidner, R., Tector, M., Tector, J., 2015. Evaluation of human and non-human primate antibody binding to pig cells lacking GGTA1/CMAH/β4GalNT2 genes. Xenotransplantation 22, 194–202. https://doi.org/10.1111/xen.12161

Etheredge, L., Kane, B.P., Hassell, J.R., 2009. The effect of growth factor signaling on keratocytes in vitro and its relationship to the phases of stromal wound repair. Invest. Ophthalmol. Vis. Sci. 50, 3128–36. https://doi.org/10.1167/iovs.08-3077

Etheredge, L., Kane, B.P., Valkov, N., Adams, S., Birk, D.E., Hassell, J.R., 2010. Enhanced cell accumulation and collagen processing by keratocytes cultured under agarose and in media containing IGF-I, TGF-β or PDGF. Matrix Biol. 29, 519–24. https://doi.org/10.1016/j.matbio.2010.05.003

Evans, M.D.M., McFarland, G.A., Xie, R.Z., Taylor, S., Wilkie, J.S., Chaouk, H., 2002. The use of corneal organ culture in biocompatibility studies. Biomaterials 23, 1359–1367. https://doi.org/10.1016/S0142-9612(01)00255-1

Fagerholm, P., Lagali, N., Merrett, K., Jackson, W.B., Munger, R., Liu, Y., Polarek, J.W., Söderqvist, M., Griffith, M., 2010. A biosynthetic alternative to human donor tissue for inducing corneal regeneration: 24-month follow-up of a phase 1 clinical study. Sci. Transl. Med. 2, 46ra61. https://doi.org/10.1126/scitranslmed.3001022

Fagerholm, P., Lagali, N., Ong, J.A., Merrett, K., Jackson, W.B., Polarek, J.W., Suuronen, E.J., Liu, Y., Brunette, I., Griffith, M., 2014. Stable corneal regeneration four years after implantation of a cell-free recombinant human collagen scaffold. Biomaterials 35, 2420–2427. https://doi.org/10.1016/j.biomaterials.2013.11.079

Faraj, L.A., Said, D.G., Al-Aqaba, M., Otri, A.M., Dua, H.S., 2016. Clinical evaluation and characterisation of corneal vascularisation. Br. J. Ophthalmol. 100, 315–322. https://doi.org/10.1136/bjophthalmol-2015-306686

Farndale, R.W., Sayers, C.A., Barrett, A.J., 1982. A direct spectrophotometric microassay for sulfated glycosaminoglycans in cartilage cultures. Connect. Tissue Res. 9, 247–8.

Farnebo, S., Woon, C.Y.L., Schmitt, T., Joubert, L.-M., Kim, M., Pham, H., Chang, J., 2014. Design and Characterization of an Injectable Tendon Hydrogel: A Novel Scaffold for Guided Tissue Regeneration in the Musculoskeletal System. Tissue Eng. Part A 20, 1550–1561. https://doi.org/10.1089/ten.tea.2013.0207

Feng, Y., Wang, W., 2015. In vivo confocal microscopic observation of lamellar corneal transplantation in the rabbit using xenogenic acellular corneal scaffolds as a substitute. Chin. Med. J. (Engl). 128, 933–40. https://doi.org/10.4103/0366-6999.154301

Fernández-Pérez, J., Ahearne, M., 2019. Influence of Biochemical Cues in Human Corneal Stromal Cell Phenotype. Curr. Eye Res. 44, 135–146. https://doi.org/10.1080/02713683.2018.1536216

Fernández-Pérez, J., Binner, M., Werner, C., Bray, L.J., 2017. Limbal stromal cells derived from porcine tissue demonstrate mesenchymal characteristics in vitro. Sci. Rep. 7, 6377. https://doi.org/10.1038/s41598-017-06898-2

Fini, M.E., 1999. Keratocyte and fibroblast phenotypes in the repairing cornea. Prog. Retin. Eye Res. 18, 529–551. https://doi.org/10.1016/S1350-9462(98)00033-0

Fini, M.E., Girard, M.T., Matsubara, M., 1992. Collagenolytic/gelatinolytic enzymes in corneal wound healing. Acta Ophthalmol. Suppl. (Oxf.). 26–33.

Fini, M.E., Stramer, B.M., 2005. How the cornea heals: cornea-specific repair mechanisms affecting surgical outcomes. Cornea 24, S2–S11. https://doi.org/10.1097/01.ico.0000178743.06340.2c

Flaxman, S.R., Bourne, R.R.A., Resnikoff, S., Ackland, P., Braithwaite, T., Cicinelli, M. V., Das, A., Jonas, J.B., Keeffe, J., Kempen, J., Leasher, J., Limburg, H., Naidoo, K., Pesudovs, K., Silvester, A., Stevens, G.A., Tahhan, N., Wong, T., Taylor, H., Arditi, A., Barkana, Y., Bozkurt, B., Bron, A., Budenz, D., Cai, F., Casson, R., Chakravarthy, U., Choi, J., Congdon, N., Dana, R., Dandona, R., Dandona, L., Dekaris, I., Del Monte, M., Deva, J., Dreer, L., Ellwein, L., Frazier, M., Frick, K., Friedman, D., Furtado, J., Gao, H., Gazzard, G., George, R., Gichuhi, S., Gonzalez, V., Hammond, B., Hartnett, M.E., He, M., Hejtmancik, J., Hirai, F., Huang, J., Ingram, A., Javitt, J., Joslin, C., Khairallah, M., Khanna, R., Kim, J., Lambrou, G., Lansingh, V.C., Lanzetta, P., Lim, J., Mansouri, K., Mathew, A., Morse, A., Munoz, B., Musch, D., Nangia, V., Palaiou, M., Parodi, M.B., Pena, F.Y., Peto, T., Quigley, H., Raju, M., Ramulu, P., Reza, D., Robin, A., Rossetti, L., Saaddine, J., Sandar, M., Serle, J., Shen, T., Shetty, R., Sieving, P., Silva, J.C., Sitorus, R.S., Stambolian, D., Tejedor, J., Tielsch, J., Tsilimbaris, M., van Meurs, J., Varma, R., Virgili, G., Wang, Y.X., Wang, N.L., West, S., Wiedemann, P., Wormald, R., Zheng, Y., 2017. Global causes of blindness and distance vision impairment 1990–2020: a systematic review and meta-analysis. Lancet Glob. Heal. 5, e1221–e1234. https://doi.org/10.1016/S2214-109X(17)30393-5

Foster, J.W., Gouveia, R.M., Connon, C.J., 2015. Low-glucose enhances keratocyte-characteristic phenotype from corneal stromal cells in serum-free conditions. Sci. Rep. 5, 10839. https://doi.org/10.1038/srep10839

Frantz, C., Stewart, K.M., Weaver, V.M., 2010. The extracellular matrix at a glance. J. Cell Sci. 123, 4195–4200. https://doi.org/10.1242/jcs.023820

Freytes, D.O., Martin, J., Velankar, S.S., Lee, A.S., Badylak, S.F., 2008. Preparation and rheological characterization of a gel form of the porcine urinary bladder matrix. Biomaterials 29, 1630–1637. https://doi.org/10.1016/j.biomaterials.2007.12.014

Friedrich, E.E., Lanier, S.T., Niknam-Bienia, S., Arenas, G.A., Rajendran, D., Wertheim, J.A., Galiano, R.D., 2018. Residual sodium dodecyl sulfate in decellularized muscle matrices leads to fibroblast activation in vitro and foreign body response in vivo. J. Tissue Eng. Regen. Med. 12, e1704–e1715. https://doi.org/10.1002/term.2604

Fu, Y., Fan, X., Chen, P., Shao, C., Lu, W., 2010. Reconstruction of a tissue-engineered cornea with porcine

corneal acellular matrix as the scaffold. Cells Tissues Organs 191, 193–202. https://doi.org/10.1159/000235680

Funamoto, S., Nam, K., Kimura, T., Murakoshi, A., Hashimoto, Y., Niwaya, K., Kitamura, S., Fujisato, T., Kishida, A., 2010. The use of high-hydrostatic pressure treatment to decellularize blood vessels. Biomaterials 31, 3590–3595. https://doi.org/10.1016/J.BIOMATERIALS.2010.01.073

Gaetani, R., Aude, S., DeMaddalena, L.L., Strassle, H., Dzieciatkowska, M., Wortham, M., Bender, R.H.F., Nguyen-Ngoc, K.-V., Schmid-Schöenbein, G.W., George, S.C., Hughes, C.C.W., Sander, M., Hansen, K.C., Christman, K.L., 2018. Evaluation of Different Decellularization Protocols on the Generation of Pancreas-Derived Hydrogels. Tissue Eng. Part C Methods 24, 697–708. https://doi.org/10.1089/ten.tec.2018.0180

Gain, P., Jullienne, R., He, Z., Aldossary, M., Acquart, S., Cognasse, F., Thuret, G., 2016. Global Survey of Corneal Transplantation and Eye Banking. JAMA Ophthalmol. 134, 167. https://doi.org/10.1001/jamaophthalmol.2015.4776

Gallego-Muñoz, P., Ibares-Frías, L., Lorenzo, E., Marcos, S., Perèz-Merino, P., Bekesi, N., Kochevar, I.E., Martínez-García, M.C., 2017a. Corneal wound repair after rose bengal and green light crosslinking: Clinical and histologic study. Investig. Ophthalmol. Vis. Sci. 58, 3471–3480. https://doi.org/10.1167/iovs.16-21365

Gallego-Muñoz, P., Ibares-Frías, L., Valsero-Blanco, M.C., Cantalapiedra-Rodriguez, R., Merayo-Lloves, J., Martínez-García, M.C., 2017b. Effects of TGFβ1, PDGF-BB, and bFGF, on human corneal fibroblasts proliferation and differentiation during stromal repair. Cytokine 96, 94–101. https://doi.org/10.1016/j.cyto.2017.03.011

Ganger, A., Tandon, R., Vanathi, M., Sagar, P., 2016. Superficial anterior lamellar keratoplasty (salk) for trauma-induced post refractive surgery corneal opacity. J. Ophthalmic Vis. Res. 11, 326–328. https://doi.org/10.4103/2008-322X.188394

George, A.L., White, G.F., 1999. Optimization Of The Methylene Blue Assay For Anionic Surfactants Added To Estuarine And Marine Water, Environmental Toxicology and Chemistry.

Ghezzi, C.E., Marelli, B., Omenetto, F.G., Funderburgh, J.L., Kaplan, D.L., 2017. 3D functional corneal stromal tissue equivalent based on corneal stromal stem cells and multi-layered silk film architecture. PLoS One 12, 1–18. https://doi.org/10.1371/journal.pone.0169504

Ghezzi, C.E., Rnjak-Kovacina, J., Kaplan, D.L., 2015. Corneal tissue engineering: recent advances and future perspectives. Tissue Eng. Part B. Rev. 21, 278–87. https://doi.org/10.1089/ten.TEB.2014.0397

Gilbert, T.W., Wognum, S., Joyce, E.M., Freytes, D.O., Sacks, M.S., Badylak, S.F., 2008. Collagen fiber alignment and biaxial mechanical behavior of porcine urinary bladder derived extracellular matrix. Biomaterials 29, 4775–4782. https://doi.org/10.1016/j.biomaterials.2008.08.022

Gilpin, S.E., Guyette, J.P., Gonzalez, G., Ren, X., Asara, J.M., Mathisen, D.J., Vacanti, J.P., Ott, H.C., 2014. Perfusion decellularization of human and porcine lungs: Bringing the matrix to clinical scale. J. Hear. Lung Transplant. 33, 298–308. https://doi.org/10.1016/J.HEALUN.2013.10.030

Girard, M.T., Matsubara, M., Kublin, C., Tessier, M.J., Cintron, C., Fini, M.E., 1993. Stromal fibroblasts synthesize collagenase and stromelysin during long-term tissue remodeling. J. Cell Sci. 1001–11.

Goh, S.-K., Bertera, S., Olsen, P., Candiello, J.E., Halfter, W., Uechi, G., Balasubramani, M., Johnson, S.A., Sicari, B.M., Kollar, E., Badylak, S.F., Banerjee, I., 2013. Perfusion-decellularized pancreas as a natural 3D scaffold for pancreatic tissue and whole organ engineering. Biomaterials 34, 6760–6772. https://doi.org/10.1016/J.BIOMATERIALS.2013.05.066

Gong, Y.Y., Xue, J.X., Zhang, W.J., Zhou, G.D., Liu, W., Cao, Y., 2011. A sandwich model for engineering cartilage with acellular cartilage sheets and chondrocytes. Biomaterials 32, 2265–2273. https://doi.org/10.1016/j.biomaterials.2010.11.078

González-Andrades, M., de la Cruz Cardona, J., Ionescu, A.M., Campos, A., Perez, M. del M., Alaminos, M., 2011. Generation of bioengineered corneas with decellularized xenografts and human keratocytes. Investig. Ophthalmol. Vis. Sci. 52, 215–220. https://doi.org/10.1167/iovs.09-4773

Gouveia, R.M., Castelletto, V., Hamley, I.W., Connon, C.J., 2015. New Self-Assembling Multifunctional Templates for the Biofabrication and Controlled Self-Release of Cultured Tissue. Tissue Eng. Part A 00, 1–14. https://doi.org/10.1089/ten.TEA.2014.0671

Gouveia, R.M., Connon, C.J., 2013. The Effects of Retinoic Acid on Human Corneal Stromal Keratocytes Cultured In Vitro Under Serum-Free Conditions. Investig. Opthalmology Vis. Sci. 54, 7483. https://doi.org/10.1167/iovs.13-13092

Gouveia, R.M., González-Andrades, E., Cardona, J.C., González-Gallardo, M. del C., Ionescu, A.M., Garzón, I., Alaminos, M., González-Andrades, M., Connon, C.J., 2017. Controlling the 3D architecture of Self-Lifting Auto-generated Tissue Equivalents (SLATEs) for optimized corneal graft composition and stability. Biomaterials 121, 205–219. https://doi.org/10.1016/j.biomaterials.2016.12.023

Gouveia, R.M., Lepert, G., Gupta, S., Mohan, R.R., Paterson, C., Connon, C.J., 2019. Assessment of corneal substrate biomechanics and its effect on epithelial stem cell maintenance and differentiation. Nat. Commun. 10, 1–17. https://doi.org/10.1038/s41467-019-09331-6

Grant, M.B., Khaw, P.T., Schultz, G.S., Adams, J.L., Shimizu, R.W., 1992. Effects of epidermal growth factor, fibroblast growth factor, and transforming growth factor-beta on corneal cell chemotaxis. Invest Ophthalmol Vis Sci 33, 3292–3301.

Gratzer, P.F., Harrison, R.D., Woods, T., 2006. Matrix Alteration and Not Residual Sodium Dodecyl Sulfate Cytotoxicity Affects the Cellular Repopulation of a Decellularized Matrix. Tissue Eng. 12, 2975–2983. https://doi.org/10.1089/ten.2006.12.ft-234

Griffith, M., Alarcon, E.I., Brunette, I., 2016. Regenerative approaches for the cornea. J. Intern. Med. 280, 276–286. https://doi.org/10.1111/joim.12502

Grobe, G.M., Reichl, S., 2013. Characterization of vitamin C-induced cell sheets formed from primary and immortalized human corneal stromal cells for tissue engineering applications. Cells. Tissues. Organs 197, 1–15. https://doi.org/10.1159/000346172

Guerriero, E., Chen, J., Sado, Y., Mohan, R.R., Wilson, S.E., Funderburgh, J.L., SundarRaj, N., 2007. Loss of Alpha3(IV) collagen expression associated with corneal keratocyte activation. Investig. Ophthalmol. Vis. Sci. 48, 627–635. https://doi.org/10.1167/iovs.06-0635

Gui, L., Chan, S.A., Breuer, C.K., Niklason, L.E., 2010. Novel utilization of serum in tissue decellularization. Tissue Eng. Part C. Methods 16, 173–84. https://doi.org/10.1089/ten.TEC.2009.0120

Guler, S., Aslan, B., Hosseinian, P., Aydin, H.M., 2017. Supercritical Carbon Dioxide-Assisted Decellularization of Aorta and Cornea. Tissue Eng. Part C Methods 23, 540–547. https://doi.org/10.1089/ten.tec.2017.0090

Guo, X.Q., Hutcheon, A.E.K., Melotti, S.A., Zieske, J.D., Trinkaus-Randall, V., Ruberti, J.W., 2007. Morphologic Characterization of Organized Extracellular Matrix Deposition by Ascorbic Acid–Stimulated Human Corneal Fibroblasts. Investig. Opthalmology Vis. Sci. 48, 4050. https://doi.org/10.1167/iovs.06-1216

Gutierrez-Aranda, I., Ramos-Mejia, V., Bueno, C., Munoz-Lopez, M., Real, P.J., Mácia, A., Sanchez, L., Ligero, G., Garcia-Parez, J.L., Menendez, P., 2010. Human induced pluripotent stem cells develop teratoma more efficiently and faster than human embryonic stem cells regardless the site of injection. Stem Cells 28, 1568–70. https://doi.org/10.1002/stem.471

Guyette, J.P., Gilpin, S.E., Charest, J.M., Tapias, L.F., Ren, X., Ott, H.C., 2014. Perfusion decellularization of whole organs. Nat. Protoc. 9, 1451–1468. https://doi.org/10.1038/nprot.2014.097

Gwon, A., 2008. The Rabbit in Cataract/IOL Surgery, Animal Models in Eye Research. https://doi.org/10.1016/B978-0-12-374169-1.00013-8

Haeusler, R.A., McGraw, T.E., Accili, D., 2017. Biochemical and cellular properties of insulin receptor signalling. Nat. Rev. Mol. Cell Biol. 19, 31–44. https://doi.org/10.1038/nrm.2017.89

Han, E., Chen, S.S., Klisch, S.M., Sah, R.L., 2011. Contribution of proteoglycan osmotic swelling pressure

to the compressive properties of articular cartilage. Biophys. J. 101, 916–924. https://doi.org/10.1016/j.bpj.2011.07.006

Hashimoto, Y., Funamoto, S., Sasaki, S., Honda, T., Hattori, S., Nam, K., Kimura, T., Mochizuki, M., Fujisato, T., Kobayashi, H., Kishida, A., 2010. Preparation and characterization of decellularized cornea using high-hydrostatic pressurization for corneal tissue engineering. Biomaterials 31, 3941–3948. https://doi.org/10.1016/j.biomaterials.2010.01.122

Hashimoto, Y., Funamoto, S., Sasaki, S., Negishi, J., Hattori, S., Honda, T., Kimura, T., Kobayashi, H., Kishida, A., 2019. Re-epithelialization and remodeling of decellularized corneal matrix in a rabbit corneal epithelial wound model. Mater. Sci. Eng. C 102, 238–246. https://doi.org/10.1016/j.msec.2019.04.024

Hashimoto, Y., Funamoto, S., Sasaki, S., Negishi, J., Honda, T., Hattori, S., Nam, K., Kimura, T., Mochizuki, M., Kobayashi, H., Kishida, A., 2015. Corneal Regeneration by Deep Anterior Lamellar Keratoplasty (DALK) Using Decellularized Corneal Matrix. PLoS One 10, e0131989. https://doi.org/10.1371/journal.pone.0131989

Hashimoto, Y., Hattori, S., Sasaki, S., Honda, T., Kimura, T., Funamoto, S., Kobayashi, H., Kishida, A., 2016. Ultrastructural analysis of the decellularized cornea after interlamellar keratoplasty and microkeratome-assisted anterior lamellar keratoplasty in a rabbit model. Sci. Rep. 6, 27734. https://doi.org/10.1038/srep27734

Hassell, J.R., Kane, B.P., Etheredge, L., Valkov, N., Birk, D.E., 2008. Increased stromal extracellular matrix synthesis and assembly by insulin activated bovine keratocytes cultured under agarose. Exp. Eye Res. 87, 604–11. https://doi.org/10.1016/j.exer.2008.09.010

Hatami-Marbini, H., 2014. Viscoelastic shear properties of the corneal stroma. J. Biomech. 47, 723–728. https://doi.org/10.1016/J.JBIOMECH.2013.11.019

Hayashi, R., Ishikawa, Y., Ito, M., Kageyama, T., Takashiba, K., Fujioka, T., Tsujikawa, M., Miyoshi, H., Yamato, M., Nakamura, Y., Nishida, K., 2012. Generation of Corneal Epithelial Cells from Induced Pluripotent Stem Cells Derived from Human Dermal Fibroblast and Corneal Limbal Epithelium. PLoS One 7, e45435. https://doi.org/10.1371/journal.pone.0045435

He, Z., Forest, F., Bernard, A., Gauthier, A.-S., Montard, R., Peoc'h, M., Jumelle, C., Courrier, E., Perrache, C., Gain, P., Thuret, G., 2016. Cutting and Decellularization of Multiple Corneal Stromal Lamellae for the Bioengineering of Endothelial Grafts. Investig. Opthalmology Vis. Sci. 57, 6639. https://doi.org/10.1167/iovs.16-20256

Heldin, C.H., Westermark, B., 1999. Mechanism of action and in vivo role of platelet-derived growth factor. Physiol. Rev. 79, 1283–316. https://doi.org/10.1146/annurev.ph.57.030195.001501

Hertsenberg, A.J., Shojaati, G., Funderburgh, M.L., Mann, M.M., Du, Y., Funderburgh, J.L., 2017. Corneal stromal stem cells reduce corneal scarring by mediating neutrophil infiltration after wounding. PLoS One 12, 1–16. https://doi.org/10.1371/journal.pone.0171712

Hicks, C.R., Crawford, G.J., Dart, J.K.G., Grabner, G., Holland, E.J., Stulting, R.D., Tan, D.T.H., Bulsara, M., 2006. AlphaCor: Clinical outcomes. Cornea 25, 1034–1042. https://doi.org/10.1097/01.ico.0000229982.23334.6b

Hill, L.J., Moakes, R.J.A., Vareechon, C., Butt, G., Ng, A., Brock, K., Chouhan, G., Vincent, R.C., Abbondante, S., Williams, R.L., Barnes, N.M., Pearlman, E., Wallace, G.R., Rauz, S., Logan, A., Grover, L.M., 2018. Sustained release of decorin to the surface of the eye enables scarless corneal regeneration. npj Regen. Med. 3, 23. https://doi.org/10.1038/s41536-018-0061-4

Hinton, T.J., Jallerat, Q., Palchesko, R.N., Park, J.H., Grodzicki, M.S., Shue, H.J., Ramadan, M.H., Hudson, A.R., Feinberg, A.W., 2015. Three-dimensional printing of complex biological structures by freeform reversible embedding of suspended hydrogels. Sci. Adv. 1. https://doi.org/10.1126/sciadv.1500758

Hjortdal, J., Pedersen, I.B., Bak-Nielsen, S., Ivarsen, A., 2013. Graft rejection and graft failure after penetrating keratoplasty or posterior lamellar keratoplasty for fuchs endothelial dystrophy. Cornea 32. https://doi.org/10.1097/ICO.0b013e3182687ff3

Hong, H., Huh, M.-I., Park, S.M., Lee, K., Kim, H.K., Kim, D.S., 2018. Decellularized corneal lenticule

embedded compressed collagen: toward a suturable collagenous construct for limbal reconstruction. Biofabrication 10, 045001. https://doi.org/10.1088/1758-5090/aad1a4

Hong, H., Kim, H., Han, S.J., Jang, J., Kim, H.K., Cho, D.-W., Kim, D.S., 2019. Compressed collagen intermixed with cornea-derived decellularized extracellular matrix providing mechanical and biochemical niches for corneal stroma analogue. Mater. Sci. Eng. C 103, 109837. https://doi.org/10.1016/j.msec.2019.109837

Hoppenreijs, V.P.T., Pels, E., Vrensen, G.F.J.M., Felten, P.C., Treffers, W.F., 1993. Platelet-derived growth factor: Receptor expression in corneas and effects on corneal cells. Investig. Ophthalmol. Vis. Sci. 34, 637–649.

Hu, X., Lui, W., Cui, L., Wang, M., Cao, Y., 2006. Tissue Engineering of Nearly Transparent Corneal Stroma. Tissue Eng. 11, 1710–1717. https://doi.org/10.1089/ten.2005.11.1710

Huang, C., Jacobson, K., Schaller, M.D., 2004. MAP kinases and cell migration. J. Cell Sci. 117, 4619–28. https://doi.org/10.1242/jcs.01481

Huang, Y.H., Tseng, F.W., Chang, W.H., Peng, I.C., Hsieh, D.J., Wu, S.W., Yeh, M.L., 2017. Preparation of acellular scaffold for corneal tissue engineering by supercritical carbon dioxide extraction technology. Acta Biomater. 58, 238–243. https://doi.org/10.1016/j.actbio.2017.05.060

Huh, M.-I., Lee, K.-P., Kim, J., Yi, S., Park, B.-U., Kim, H.K., 2018. Generation of Femtosecond Laser-Cut Decellularized Corneal Lenticule Using Hypotonic Trypsin-EDTA Solution for Corneal Tissue Engineering. J. Ophthalmol. 2018, 1–12. https://doi.org/10.1155/2018/2590536

Hurmeric, V., Yoo, S.H., Mutlu, F.M., 2012. Optical coherence tomography in cornea and refractive surgery. Expert Rev. Ophthalmol. 7, 241–250. https://doi.org/10.1586/eop.12.28

Ide, C., Tohyama, K., Yokota, R., Nitatori, T., Onodera, S., 1983. Schwann cell basal lamina and nerve regeneration. Brain Res. 288, 61–75. https://doi.org/10.1016/0006-8993(83)90081-1

Ignat'eva, N.Y., Danilov, N.A., Averkiev, S. V., Obrezkova, M. V., Lunin, V. V., Sobol', E.N., 2007. Determination of hydroxyproline in tissues and the evaluation of the collagen content of the tissues. J. Anal. Chem. 62, 51–57. https://doi.org/10.1134/S106193480701011X

Isaacson, A., Swioklo, S., Connon, C.J., 2018. 3D bioprinting of a corneal stroma equivalent. Exp. Eye Res. 173, 188–193. https://doi.org/10.1016/j.exer.2018.05.010

Islam, M.M., Buznyk, O., Reddy, J.C., Pasyechnikova, N., Alarcon, E.I., Hayes, S., Lewis, P., Fagerholm, P., He, C., Iakymenko, S., Liu, W., Meek, K.M., Sangwan, V.S., Griffith, M., 2018. Biomaterials-enabled cornea regeneration in patients at high risk for rejection of donor tissue transplantation. npj Regen. Med. 3, 2. https://doi.org/10.1038/s41536-017-0038-8

Jang, J., Kim, T.G., Kim, B.S., Kim, S.W., Kwon, S.M., Cho, D.W., 2016. Tailoring mechanical properties of decellularized extracellular matrix bioink by vitamin B2-induced photo-crosslinking. Acta Biomater. 33, 88–95. https://doi.org/10.1016/j.actbio.2016.01.013

Jang, J., Park, H.J., Kim, Seok Won, Kim, H., Park, J.Y., Na, S.J., Kim, H.J., Park, M.N., Choi, S.H., Park, S.H., Kim, Sung Won, Kwon, S.M., Kim, P.J., Cho, D.W., 2017. 3D printed complex tissue construct using stem cell-laden decellularized extracellular matrix bioinks for cardiac repair. Biomaterials 112, 264–274. https://doi.org/10.1016/j.biomaterials.2016.10.026

Jangamreddy, J.R., Haagdorens, M.K.C., Mirazul Islam, M., Lewis, P., Samanta, A., Fagerholm, P., Liszka, A., Ljunggren, M.K., Buznyk, O., Alarcon, E.I., Zakaria, N., Meek, K.M., Griffith, M., 2018. Short peptide analogs as alternatives to collagen in pro-regenerative corneal implants. Acta Biomater. 69, 120–130. https://doi.org/10.1016/j.actbio.2018.01.011

Jeng, B.H., 2014. Advances in Medical and Surgical Cornea, Essentials in Ophthalmology. Springer Berlin Heidelberg, Berlin, Heidelberg. https://doi.org/10.1007/978-3-662-44888-5

Jester, J. V., Barry-Lane, P., Cavanagh, H.D., Petroll, W.M., 1996. Induction of -Smooth Muscle Actin Expression and Myofibroblast Transformation in Cultured Corneal Keratocytes. Cornea.

Jester, J. V., Barry-Lane, P.A., Petroll, W.M., Olsen, D.R., Cavanagh, H.D., 1997. Inhibition of corneal fibrosis by topical application of blocking antibodies to TGF(β) in the rabbit. Cornea.

https://doi.org/10.1097/00003226-199703000-00010

Jester, J. V., Ho-Chang, J., 2003. Modulation of cultured corneal keratocyte phenotype by growth factors/cytokines control in vitro contractility and extracellular matrix contraction. Exp. Eye Res. 77, 581–592. https://doi.org/10.1016/S0014-4835(03)00188-X

Jester, J. V., Huang, J., Møller-Pedersen, T., Sax, C.M., Kays, W.T., Cavanagh, H.D., Petroll, W.M., Piatigorsky, J., 1999. The cellular basis of corneal transparency: evidence for "corneal crystallins." J. Cell Sci. 112 (Pt 5, 613–622.

Jiménez, C., Portela, R.A., Mellado, M., Rodríguez-Frade, J.M., Collard, J., Serrano, A., Martínez-A, C., Avila, J., Carrera, A.C., 2000. Role of the PI3K regulatory subunit in the control of actin organization and cell migration. J. Cell Biol. 151, 249–62. https://doi.org/10.1083/JCB.151.2.249

Jirá, N., Rozsival, P., Burova, M., Kalfertova, M., 2011. AlphaCor artificial cornea: clinical outcome. Eye 25, 1138–1146. https://doi.org/10.1038/eye.2011.122

Johnson, T.D., DeQuach, J.A., Gaetani, R., Ungerleider, J., Elhag, D., Nigam, V., Behfar, A., Christman, K.L., 2014. Human versus porcine tissue sourcing for an injectable myocardial matrix hydrogel. Biomater. Sci. 2, 735–744. https://doi.org/10.1039/C3BM60283D

Johnson, T.D., Lin, S.Y., Christman, K.L., 2011. Tailoring material properties of a nanofibrous extracellular matrix derived hydrogel. Nanotechnology 22. https://doi.org/10.1088/0957-4484/22/49/494015

Joyce, N.C., Meklir, B., Joyce, S.J., Zieske, J.D., 1996a. Cell cycle protein expression and proliferative status in human corneal cells. Invest. Ophthalmol. Vis. Sci. 37, 645–55.

Joyce, N.C., Navon, S.E., Roy, S., Zieske, J.D., 1996b. Expression of cell cycle-associated proteins in human and rabbit corneal endothelium in situ. Invest. Ophthalmol. Vis. Sci. 37, 1566–75.

Joyce, N.C., Zieske, J.D., 1997. Transforming growth factor-beta receptor expression in human cornea. Invest. Ophthalmol. Vis. Sci. 38, 1922–8.

Ju, C., Gao, L., Wu, X., Pang, K., 2012a. A human corneal endothelium equivalent constructed with acellular porcine corneal matrix. Indian J. Med. Res. 135, 887–894.

Ju, C., Gao, L., Wu, X., Pang, K., 2012b. A human corneal endothelium equivalent constructed with acellular porcine corneal matrix. Indian J. Med. Res. 135, 887–94.

Kafienah, W., Sims, T.J., 2004. Biochemical methods for the analysis of tissue-engineered cartilage. Methods Mol. Biol. 238, 217–30.

Kajbafzadeh, A.-M., Javan-Farazmand, N., Monajemzadeh, M., Baghayee, A., 2013. Determining the Optimal Decellularization and Sterilization Protocol for Preparing a Tissue Scaffold of a Human-Sized Liver Tissue. Tissue Eng. Part C Methods 19, 642–651. https://doi.org/10.1089/ten.tec.2012.0334

Kamiyama, K., Iguchi, I., Wang, X., Imanishi, J., 1998. Effects of PDGF on the Migration of Rabbit Corneal Fibroblasts and Epithelial Cells. Cornea 17, 315–325.

Karamichos, D., Funderburgh, M.L., Hutcheon, A.E.K., Zieske, J.D., Du, Y., Wu, J., Funderburgh, J.L., 2014a. A role for topographic cues in the organization of collagenous matrix by corneal fibroblasts and stem cells. PLoS One 9, e86260. https://doi.org/10.1371/journal.pone.0086260

Karamichos, D., Hutcheon, A.E.K., Zieske, J.D., 2014b. Reversal of fibrosis by TGF-β3 in a 3D in vitro model. Exp. Eye Res. 124, 31–36. https://doi.org/10.1016/j.exer.2014.04.020

Karamichos, D., Hutcheon, A.E.K., Zieske, J.D., 2011a. Transforming growth factor-β3 regulates assembly of a non-fibrotic matrix in a 3D corneal model. J. Tissue Eng. Regen. Med. 5, 228–238. https://doi.org/10.1002/term

Karamichos, D., Hutcheon, A.E.K., Zieske, J.D., 2011b. Transforming growth factor beta 3 regulates assembly of a non-fibrotic matrix in a 3D corneal model. J Tissue Eng Regen Med 5, 228–238. https://doi.org/10.1002/term.429.Transforming

Karamichos, D., Rich, C.B., Zareian, R., Hutcheon, A.E.K., Ruberti, J.W., Trinkaus-Randall, V., Zieske,

J.D., 2013. TGF-β3 Stimulates Stromal Matrix Assembly by Human Corneal Keratocyte-Like Cells. Investig. Opthalmology Vis. Sci. 54, 6612. https://doi.org/10.1167/iovs.13-12861

Keane, T.J., Londono, R., Turner, N.J., Badylak, S.F., 2012. Consequences of ineffective decellularization of biologic scaffolds on the host response. Biomaterials 33, 1771–1781. https://doi.org/10.1016/j.biomaterials.2011.10.054

Keating, A.M., Jacobs, D.S., 2011. Anti-VEGF treatment of corneal neovascularization. Ocul. Surf. https://doi.org/10.1016/S1542-0124(11)70035-0

Kenney, M.C., Shih, L.M., Labermeir, U., Satterfield, D., 1986. Modulation of rabbit keratocyte production of collagen, sulfated glycosaminoglycans and fibronectin by retinol and retinoic acid. Biochim. Biopyisica Acta 889, 156–162.

Kim, A., Lakshman, N., Karamichos, D., Petroll, W.M., 2010. Growth Factor Regulation of Corneal Keratocyte Differentiation and Migration in Compressed Collagen Matrices. Investig. Opthalmology Vis. Sci. 51, 864. https://doi.org/10.1167/iovs.09-4200

Kim, B.S., Kim, H., Gao, G., Jang, J., Cho, D.W., 2017. Decellularized extracellular matrix: A step towards the next generation source for bioink manufacturing. Biofabrication 9. https://doi.org/10.1088/1758-5090/aa7e98

Kim, H., Jang, J., Park, J., Lee, K.-P., Lee, S., Lee, D.-M., Kim, K.H., Kim, H.K., Cho, D.-W., 2019a. Shear-induced alignment of collagen fibrils using 3D cell printing for corneal stroma tissue engineering. Biofabrication 11, 035017. https://doi.org/10.1088/1758-5090/ab1a8b

Kim, H., Park, M.-N., Kim, J., Jang, J., Kim, H.-K., Cho, D.-W., 2019b. Characterization of cornea-specific bioink: high transparency, improved in vivo safety. J. Tissue Eng. 10, 204173141882338. https://doi.org/10.1177/2041731418823382

Kim, J.I., Kim, J.Y., Park, C.H., 2018. Fabrication of transparent hemispherical 3D nanofibrous scaffolds with radially aligned patterns via a novel electrospinning method. Sci. Rep. 8, 1–13. https://doi.org/10.1038/s41598-018-21618-0

Kim, M.K., Hara, H., 2015. Current status of corneal xenotransplantation. Int. J. Surg. 23, 255–260. https://doi.org/10.1016/j.ijsu.2015.07.685

Kim, W.-J., Mohan, Rahul R, Mohan, Rajiv R, Wilson, S.E., 1999. Effect of PDGF, IL-la, and BMP2/4 on Corneal Fibroblast Chemotaxis: Expression of the Platelet- Derived Growth Factor System in the Cornea. Investig. Ophthalmol. Vis. Sci. 40, 1364–1372.

Koivusalo, L., Kauppila, M., Samanta, S., Parihar, V.S., Ilmarinen, T., Miettinen, S., Oommen, O.P., Skottman, H., 2019. Tissue adhesive hyaluronic acid hydrogels for sutureless stem cell delivery and regeneration of corneal epithelium and stroma. Biomaterials 225, 119516. https://doi.org/10.1016/j.biomaterials.2019.119516

Kolli, S., Ahmad, S., Mudhar, H.S., Meeny, A., Lako, M., Figueiredo, F.C., 2014. Successful Application of Ex Vivo Expanded Human Autologous Oral Mucosal Epithelium for the Treatment of Total Bilateral Limbal Stem Cell Deficiency. Stem Cells 32, 2135–2146. https://doi.org/10.1002/stem.1694

Koulikovska, M., Rafat, M., Petrovski, G., Veréb, Z., Akhtar, S., Fagerholm, P., Lagali, N., 2015. Enhanced regeneration of corneal tissue via a bioengineered collagen construct implanted by a nondisruptive surgical technique. Tissue Eng. Part A 21, 1116–30. https://doi.org/10.1089/ten.TEA.2014.0562

Kruper, G.J., VandeGriend, Z.P., Lin, H.-S., Zuliani, G.F., 2013. Salvage of Failed Local and Regional Flaps with Porcine Urinary Bladder Extracellular Matrix Aided Tissue Regeneration. Case Rep. Otolaryngol. 2013, 1–5. https://doi.org/10.1155/2013/917183

Kureshi, A.K., Dziasko, M. a., Funderburgh, J.L., Daniels, J.T., 2015. Human corneal stromal stem cells support limbal epithelial cells cultured on RAFT tissue equivalents. Sci. Rep. 5, 16186. https://doi.org/10.1038/srep16186

Lagali, N., Bourghardt, B., Germundsson, J., Eden, U., Danyali, R., Rinaldo, M., Fagerholm, P., 2013a. Laser-Scanning in vivo Confocal Microscopy of the Cornea: Imaging and Analysis Methods for Preclinical and Clinical Applications, in: Confocal Laser Microscopy - Principles and Applications

in Medicine, Biology, and the Food Sciences. InTech. https://doi.org/10.5772/55216

Lagali, N., Griffith, M., Fagerholm, P., 2013b. In Vivo Confocal Microscopy of the Cornea to Assess Tissue Regenerative Response After Biomaterial Implantation in Humans, in: Wright, B., Connon, C.J. (Eds.), Corneal Regenerative Medicine, Methods in Molecular Biology. Humana Press, Totowa, NJ, pp. 211–223. https://doi.org/10.1007/978-1-62703-432-6

Lakshman, N., Petroll, W.M., 2012. Growth factor regulation of corneal keratocyte mechanical phenotypes in 3-D collagen matrices. Invest. Ophthalmol. Vis. Sci. 53, 1077–86. https://doi.org/10.1167/iovs.11-8609

LeCheminant, J., Field, C., 2012. Porcine urinary bladder matrix: a retrospective study and establishment of protocol. J. Wound Care 21, 476–482. https://doi.org/10.12968/jowc.2012.21.10.476

Lee, A., Hudson, A.R., Shiwarski, D.J., Tashman, J.W., Hinton, T.J., Yerneni, S., Bliley, J.M., Campbell, P.G., Feinberg, A.W., 2019. 3D bioprinting of collagen to rebuild components of the human heart. Science (80-.). 365, 482–487. https://doi.org/10.1126/science.aav9051

Lee, H., Han, W., Kim, H., Ha, D.-H., Jang, J., Kim, B.S., Cho, D.-W., 2017. Development of Liver Decellularized Extracellular Matrix Bioink for Three-Dimensional Cell Printing-Based Liver Tissue Engineering. Biomacromolecules 18, 1229–1237. https://doi.org/10.1021/acs.biomac.6b01908

Lee, R.E., Davison, P.F., 1984. The collagens of the developing bovine cornea. Exp. Eye Res. 39, 639–652. https://doi.org/10.1016/0014-4835(84)90063-0

LeRoith, D., Roberts, C.T., 2003. The insulin-like growth factor system and cancer. Cancer Lett. 195, 127–37.

Levis, H.J., Brown, R.A., Daniels, J.T., 2010. Plastic compressed collagen as a biomimetic substrate for human limbal epithelial cell culture. Biomaterials 31, 7726–7737. https://doi.org/10.1016/j.biomaterials.2010.07.012

Li, N., Wang, X., Wan, P., Huang, M., Wu, Z., Liang, X., Liu, Y., Ge, J., Huang, J., Wang, Z., 2011. Tectonic lamellar keratoplasty with acellular corneal stroma in high-risk corneal transplantation. Mol. Vis. 17, 1909–1917. https://doi.org/208 [pii]

Li, Q., Wang, H., Dai, Z., Cao, Y., Jin, C., 2017. Preparation and Biomechanical Properties of an Acellular Porcine Corneal Stroma. Cornea 36, 1343–1351. https://doi.org/10.1097/ICO.0000000000001319

Li, S., Deng, Y., Tian, B., Huang, H., Zhang, H., Yang, R., Zhong, J., Wang, B., Peng, L., Yuan, J., 2019. Healing characteristics of acellular porcine corneal stroma following therapeutic keratoplasty. Xenotransplantation 1–8. https://doi.org/10.1111/xen.12566

Li, W., Hayashida, Y., Chen, Y.T., Tseng, S.C.G., 2007. Niche regulation of corneal epithelial stem cells at the limbus. Cell Res. 17, 26–36. https://doi.org/10.1038/sj.cr.7310137

Li, W., Vergnes, J.P., Cornuet, P.K., Hassell, J.R., 1992. cDNA clone to chick corneal chondroitin/dermatan sulfate proteoglycan reveals identity to decorin. Arch. Biochem. Biophys. 296, 190–197. https://doi.org/10.1016/0003-9861(92)90562-B

Lin, C.-Y., Liu, T.-Y., Chen, Mei-Hsiu, Sun, J.-S., Chen, Ming-Hong, 2016. An injectable extracellular matrix for the reconstruction of epidural fat and the prevention of epidural fibrosis. Biomed. Mater. 11, 035010. https://doi.org/10.1088/1748-6041/11/3/035010

Lin, H., Wang, T., Li, T., Chang, Y., Sheu, M.-T., Huang, Y.-Y., Liu, D.-Z., 2019. Development of Decellularized Cornea by Organic Acid Treatment for Corneal Regeneration. Tissue Eng. Part A 25, 652–662. https://doi.org/10.1089/ten.tea.2018.0162

Lin, X.-C., Hui, Y.-N., Wang, Y.-S., Meng, H., Zhang, Y.-J., Jin, Y., 2008. Lamellar keratoplasty with a graft of lyophilized acellular porcine corneal stroma in the rabbit. Vet. Ophthalmol. 11, 61–66. https://doi.org/10.1111/j.1463-5224.2008.00601.x

Lin, Y., Zheng, Q., Hua, S., Meng, Y., Chen, W., Wang, Y., 2017. Cross-linked decellularized porcine corneal graft for treating fungal keratitis. Sci. Rep. 7, 9955. https://doi.org/10.1038/s41598-017-08207-3

Liu, W., Deng, C., McLaughlin, C.R., Fagerholm, P., Lagali, N.S., Heyne, B., Scaiano, J.C., Watsky, M.A., Kato, Y., Munger, R., Shinozaki, N., Li, F., Griffith, M., 2009. Collagen–phosphorylcholine interpenetrating network hydrogels as corneal substitutes. Biomaterials 30, 1551–1559. https://doi.org/10.1016/J.BIOMATERIALS.2008.11.022

Liu, W., Merrett, K., Griffith, M., Fagerholm, P., Dravida, S., Heyne, B., Scaiano, J.C., Watsky, M.A., Shinozaki, N., Lagali, N., Munger, R., Li, F., 2008. Recombinant human collagen for tissue engineered corneal substitutes. Biomaterials 29, 1147–1158. https://doi.org/10.1016/j.biomaterials.2007.11.011

Liu, X., Zhu, X., Wu, J., Wu, Z., Yin, Y., XH, X., Su, X., B, K., SY, P., H, Y., Y, C., N, A., SL, M., 2016. Acellular ostrich corneal stroma used as scaffold for construction of tissue-engineered cornea. Int. J. Ophthalmol. 325–331. https://doi.org/10.18240/ijo.2016.03.01

Long, C.J., Roth, M.R., Tasheva, E.S., Funderburgh, M.L., Smit, R., Conrad, G.W., Funderburgh, J.L., 2000. Fibroblast Growth Factor-2 Promotes Keratan Sulfate Proteoglycan Expression by Keratocytes in Vitro. J. Biol. Chem. 275, 13918–13923.

Lu, Y., Yao, Q.K., Feng, B., Yan, C.X., Zhu, M.Y., Chen, J.Z., Fu, W., Fu, Y., 2015. Characterization of a Hydrogel Derived from Decellularized Corneal Extracellular Matrix. J. Biomater. Tissue Eng. 5, 951–960. https://doi.org/10.1166/jbt.2015.1410

Luo, H., Lu, Y., Wu, T., Zhang, M., Zhang, Y.J., Jin, Y., 2013. Construction of tissue-engineered cornea composed of amniotic epithelial cells and acellular porcine cornea for treating corneal alkali burn. Biomaterials 34, 6748–6759. https://doi.org/10.1016/j.biomaterials.2013.05.045

Lynch, A.P., Ahearne, M., 2017. Retinoic Acid Enhances the Differentiation of Adipose-Derived Stem Cells to Keratocytes In Vitro. Transl. Vis. Sci. Technol. 6, 6. https://doi.org/10.1167/tvst.6.1.6

Lynch, A.P., Ahearne, M., 2013. Strategies for developing decellularized corneal scaffolds. Exp. Eye Res. 108, 42–47. https://doi.org/10.1016/j.exer.2012.12.012

Lynch, A.P., O'Sullivan, F., Ahearne, M., 2016a. The effect of growth factor supplementation on corneal stromal cell phenotype in vitro using a serum-free media. Exp. Eye Res. 151, 26–37. https://doi.org/10.1016/j.exer.2016.07.015

Lynch, A.P., Wilson, S.L., Ahearne, M., 2016b. Dextran Preserves Native Corneal Structure During Decellularization. Tissue Eng. Part C Methods 22, 561–572. https://doi.org/10.1089/ten.tec.2016.0017

Lyons, B.L., Schwarz, R.I., 1984. Ascorbate stimulation of PAT cells causes an increase in transcription rates and a decrease in degradation rates of procollagen mRNA. Nucleic Acids Res. 12, 2569–2579. https://doi.org/10.1093/nar/12.5.2569

Ma, X.Y., Zhang, Y., Zhu, D., Lu, Y., Zhou, G., Liu, W., Cao, Y., Zhang, W.J., 2015. Corneal Stroma Regeneration with Acellular Corneal Stroma Sheets and Keratocytes in a Rabbit Model. PLoS One 10, 1–13. https://doi.org/10.1371/journal.pone.0132705

Maenz, M., Morcos, M., Ritter, T., 2011. A comprehensive flow-cytometric analysis of graft infiltrating lymphocytes, draining lymph nodes and serum during the rejection phase in a fully allogeneic rat cornea transplant model. Mol. Vis. 17, 420–429.

Magno, V., Friedrichs, J., Weber, H.M., Prewitz, M.C., Tsurkan, M. V., Werner, C., 2017. Macromolecular crowding for tailoring tissue-derived fibrillated matrices. Acta Biomater. 55, 109–119. https://doi.org/10.1016/j.actbio.2017.04.018

Maltseva, O., Folger, P., Zekaria, D., Petridou, S., Masur, S.K., 2001. Fibroblast growth factor reversal of the corneal myofibroblast phenotype. Invest Ophthalmol. Vis. Sci. 42, 2490–5.

Mase, V.J., Hsu, J.R., Wolf, S.E., Wenke, J.C., Baer, D.G., Owens, J., Badylak, S.F., Walters, T.J., 2010. Clinical Application of an Acellular Biologic Scaffold for Surgical Repair of a Large, Traumatic Quadriceps Femoris Muscle Defect. Orthopedics 33, 511. https://doi.org/10.3928/01477447-20100526-24

Massie, I., Kureshi, A.K., Schrader, S., Shortt, A.J., Daniels, J.T., 2015. Optimization of optical and

mechanical properties of real architecture for 3-dimensional tissue equivalents: Towards treatment of limbal epithelial stem cell deficiency. Acta Biomater. 24, 241–250. https://doi.org/10.1016/j.actbio.2015.06.007

Masur, S.K., Dewal, H.S., Dinh, T.T., Erenburg, I., Petridou, S., 1996. Myofibroblasts differentiate from fibroblasts when plated at low density. Proc. Natl. Acad. Sci. U. S. A. 93, 4219–23. https://doi.org/10.1073/pnas.93.9.4219

Mathapati, S., Galla, S., Sankaranarayanan, K., Verma, R.S., Cherian, K.M., Guhathakurta, S., 2010. Qualitative and quantitative detection of sodium deoxycholic acid in decellularized tissue. Indian J. Thorac. Cardiovasc. Surg. 26, 129–131. https://doi.org/10.1007/s12055-010-0016-x

Matsubara, M., Girard, M.T., Kublin, C.L., Cintron, C., Fini, M.E., 1991a. Differential roles for two gelatinolytic enzymes of the matrix metalloproteinase family in the remodelling cornea. Dev. Biol. 147, 425–39.

Matsubara, M., Zieske, J.D., Fini, M.E., 1991b. Mechanism of basement membrane dissolution preceding corneal ulceration. Invest. Ophthalmol. Vis. Sci. 32, 3221–37.

Matthyssen, S., Van den Bogerd, B., Dhubhghaill, S.N., Koppen, C., Zakaria, N., 2018. Corneal regeneration: A review of stromal replacements. Acta Biomater. 69, 31–41. https://doi.org/10.1016/j.actbio.2018.01.023

McFetridge, P.S., Daniel, J.W., Bodamyali, T., Horrocks, M., Chaudhuri, J.B., 2004. Preparation of porcine carotid arteries for vascular tissue engineering applications. J. Biomed. Mater. Res. 70A, 224–234. https://doi.org/10.1002/jbm.a.30060

McIntosh Ambrose, W., Salahuddin, A., So, S., Ng, S., Ponce Márquez, S., Takezawa, T., Schein, O., Elisseeff, J.H., 2009. Collagen vitrigel membranes for the in vitro reconstruction of separate corneal epithelial, stromal, and endothelial cell layers. J. Biomed. Mater. Res. Part B Appl. Biomater. 90B, 818–831. https://doi.org/10.1002/jbm.b.31351

Medeiros, C.S., Marino, G.K., Santhiago, M.R., Wilson, S.E., 2018. The corneal basement membranes and stromal fibrosis. Investig. Ophthalmol. Vis. Sci. 59, 4044–4053. https://doi.org/10.1167/iovs.18-24428

Mikhailova, A., Ilmarinen, T., Uusitalo, H., Skottman, H., 2014. Small-molecule induction promotes corneal epithelial cell differentiation from human induced pluripotent stem cells. Stem Cell Reports 2, 219–231. https://doi.org/10.1016/j.stemcr.2013.12.014

Miotto, M., Gouveia, R.M., Ionescu, A.M., Figueiredo, F., Hamley, I.W., Connon, C.J., 2019. 4D Corneal Tissue Engineering: Achieving Time-Dependent Tissue Self-Curvature through Localized Control of Cell Actuators. Adv. Funct. Mater. 29, 1807334. https://doi.org/10.1002/adfm.201807334

Mohan, Rahul R., Hutcheon, A.E.K., Choi, R., Hong, J., Lee, J., Mohan, Rajiv R., Ambrósio, R., Zieske, J.D., Wilson, S.E., 2003. Apoptosis, necrosis, proliferation, and myofibroblast generation in the stroma following LASIK and PRK. Exp. Eye Res. 76, 71–87. https://doi.org/10.1016/S0014-4835(02)00251-8

Moser, P.T., Ott, H.C., 2014. Recellularization of organs. Curr. Opin. Organ Transplant. 19, 603–609. https://doi.org/10.1097/MOT.0000000000000131

Murab, S., Ghosh, S., 2016. Impact of osmoregulatory agents on the recovery of collagen conformation in decellularized corneas. Biomed. Mater. 11. https://doi.org/10.1088/1748-6041/11/6/065005

Murphy, N., Lynch, K., Lohan, P., Treacy, O., Ritter, T., 2016. Mesenchymal stem cell therapy to promote corneal allograft survival: Current status and pathway to clinical translation. Curr. Opin. Organ Transplant. 21, 559–567. https://doi.org/10.1097/MOT.0000000000000360

Musselmann, K., Kane, B.P., Alexandrou, B., Hassell, J.R., 2006. Stimulation of collagen synthesis by insulin and proteoglycan accumulation by ascorbate in bovine keratocytes in vitro. Investig. Ophthalmol. Vis. Sci. 47, 5260–5266. https://doi.org/10.1167/iovs.06-0612

Nagata, S., Hanayama, R., Kawane, K., 2010. Autoimmunity and the Clearance of Dead Cells. Cell 140, 619–630. https://doi.org/10.1016/j.cell.2010.02.014

Nakayama, K.H., Batchelder, C.A., Lee, C.I., Tarantal, A.F., 2010. Decellularized rhesus monkey kidney as a three-dimensional scaffold for renal tissue engineering. Tissue Eng. Part A 16, 2207–16. https://doi.org/10.1089/ten.tea.2009.0602

Nara, S., Chameettachal, S., Midha, S., Murab, S., Ghosh, S., 2016. Preservation of biomacromolecular composition and ultrastructure of a decellularized cornea using a perfusion bioreactor. RSC Adv. 6, 2225–2240. https://doi.org/10.1039/C5RA20745B

Naylor, R.W., McGhee, C.N.J., Cowan, C.A., Davidson, A.J., Holm, T.M., Sherwin, T., 2016. Derivation of Corneal Keratocyte-Like Cells from Human Induced Pluripotent Stem Cells. PLoS One 11, e0165464. https://doi.org/10.1371/journal.pone.0165464

Netto, M. V., Mohan, R.R., Sinha, S., Sharma, A., Dupps, W., Wilson, S.E., 2006. Stromal haze, myofibroblasts, and surface irregularity after PRK. Exp. Eye Res. 82, 788–797. https://doi.org/10.1016/j.exer.2005.09.021

Nichols, J.E., Niles, J., Riddle, M., Vargas, G., Schilagard, T., Ma, L., Edward, K., La Francesca, S., Sakamoto, J., Vega, S., Ogadegbe, M., Mlcak, R., Deyo, D., Woodson, L., McQuitty, C., Lick, S., Beckles, D., Melo, E., Cortiella, J., 2013. Production and Assessment of Decellularized Pig and Human Lung Scaffolds. Tissue Eng. Part A 19, 2045–2062. https://doi.org/10.1089/ten.tea.2012.0250

Nishida, K., Kinoshita, S., Yokoi, N., Kaneda, M., Hashimoto, K., Yamamoto, S., 1994. Immunohistochemical localization of transforming growth factor-beta 1, -beta 2, and -beta 3 latency-associated peptide in human cornea. Invest. Ophthalmol. Vis. Sci. 35, 3289–94.

Nishida, K., Yamato, M., Hayashida, Y., Watanabe, K., Yamamoto, K., Adachi, E., Nagai, S., Kikuchi, A., Maeda, N., Watanabe, H., Okano, T., Tano, Y., 2004. Corneal Reconstruction with Tissue-Engineered Cell Sheets Composed of Autologous Oral Mucosal Epithelium. N. Engl. J. Med. 351, 1187–1196. https://doi.org/10.1056/NEJMoa040455

Niu, D., Wei, H.-J., Lin, L., George, H., Wang, T., Lee, I.-H., Zhao, H.-Y., Wang, Y., Kan, Y., Shrock, E., Lesha, E., Wang, G., Luo, Y., Qing, Y., Jiao, D., Zhao, H., Zhou, X., Wang, S., Wei, H., Güell, M., Church, G.M., Yang, L., 2017. Inactivation of porcine endogenous retrovirus in pigs using CRISPR-Cas9. Science (80-.). 357, 1303–1307. https://doi.org/10.1126/science.aan4187

O'Neill, J.D., Anfang, R., Anandappa, A., Costa, J., Javidfar, J., Wobma, H.M., Singh, G., Freytes, D.O., Bacchetta, M.D., Sonett, J.R., Vunjak-Novakovic, G., 2013. Decellularization of Human and Porcine Lung Tissues for Pulmonary Tissue Engineering. Ann. Thorac. Surg. 96, 1046–1056. https://doi.org/10.1016/J.ATHORACSUR.2013.04.022

Odorico, J.S., Ma, F., Burlingham, W.J., Li, X., Sackett, S.D., Zhou, Y., Maguire, R.M., Brown, M.E., Tremmel, D.M., O'Brien, C., Feeney, A.K., Li, L., 2018. Extracellular matrix scaffold and hydrogel derived from decellularized and delipidized human pancreas. Sci. Rep. 8, 1–16. https://doi.org/10.1038/s41598-018-28857-1

Oh, J.Y., Kim, M.K., Lee, H.J., Ko, J.H., Wee, W.R., Lee, J.H., 2009. Processing Porcine Cornea for Biomedical Applications. Tissue Eng. Part C Methods 15, 635–645. https://doi.org/10.1089/ten.tec.2009.0022

Orlando, G., Booth, C., Wang, Z., Totonelli, G., Ross, C.L., Moran, E., Salvatori, M., Maghsoudlou, P., Turmaine, M., Delario, G., Al-Shraideh, Y., Farooq, U., Farney, A.C., Rogers, J., Iskandar, S.S., Burns, A., Marini, F.C., De Coppi, P., Stratta, R.J., Soker, S., 2013. Discarded human kidneys as a source of ECM scaffold for kidney regeneration technologies. Biomaterials 34, 5915–5925. https://doi.org/10.1016/J.BIOMATERIALS.2013.04.033

Ott, H.C., Matthiesen, T.S., Goh, S.-K., Black, L.D., Kren, S.M., Netoff, T.I., Taylor, D.A., 2008. Perfusion-decellularized matrix: using nature's platform to engineer a bioartificial heart. Nat. Med. 14, 213–221. https://doi.org/10.1038/nm1684

Pang, K., Du, L., Wu, X., 2010. A rabbit anterior cornea replacement derived from acellular porcine cornea matrix, epithelial cells and keratocytes. Biomaterials 31, 7257–7265. https://doi.org/10.1016/j.biomaterials.2010.05.066

Parekh, M., Ahmad, S., Ruzza, A., Ferrari, S., 2017. Human Corneal Endothelial Cell Cultivation From

Old Donor Corneas With Forced Attachment. Sci. Rep. 7, 142. https://doi.org/10.1038/s41598-017-00209-5

Parsons, W.J., Ramkumar, V., Stiles, G.L., 1988. Isobutylmethylxanthine stimulates adenylate cyclase by blocking the inhibitory regulatory protein, Gi. Mol. Pharmacol. 34.

Pascolini, D., Mariotti, S.P., 2012. Global estimates of visual impairment: 2010. Br. J. Ophthalmol. 96, 614–618. https://doi.org/10.1136/bjophthalmol-2011-300539

Pati, F., Ha, D.H., Jang, J., Han, H.H., Rhie, J.W., Cho, D.W., 2015. Biomimetic 3D tissue printing for soft tissue regeneration. Biomaterials 62, 164–175. https://doi.org/10.1016/j.biomaterials.2015.05.043

Pati, F., Jang, J., Ha, D.H., Won Kim, S., Rhie, J.W., Shim, J.H., Kim, D.H., Cho, D.W., 2014. Printing three-dimensional tissue analogues with decellularized extracellular matrix bioink. Nat. Commun. 5, 1–11. https://doi.org/10.1038/ncomms4935

Peh, G.S.L., Toh, K.P., Wu, F.Y., Tan, D.T., Mehta, J.S., 2011. Cultivation of human corneal endothelial cells isolated from paired donor corneas. PLoS One 6. https://doi.org/10.1371/journal.pone.0028310

Pellegata, A.F., Adelaide Asnaghi, M., Zonta, S., Zerbini, G., Mantero, S., 2012. A novel device for the automatic decellularization of biological tissues. Int. J. Artif. Organs 35, 191–198. https://doi.org/10.5301/ijao.5000079

Pellegrini, G., Rama, P., Di Rocco, A., Panaras, A., De Luca, M., 2014. Concise review: Hurdles in a successful example of limbal stem cell-based regenerative medicine. Stem Cells 32, 26–34. https://doi.org/10.1002/stem.1517

Petersen, T.H., Calle, E.A., Zhao, L., Lee, E.J., Gui, L., Raredon, M.B., Gavrilov, K., Yi, T., Zhuang, Z.W., Breuer, C., Herzog, E., Niklason, L.E., 2010. Tissue-Engineered Lungs for in Vivo Implantation. Science (80-.). 329, 538–541. https://doi.org/10.1126/SCIENCE.1189345

Phu, D., Orwin, E.J., 2009. Characterizing the effects of aligned collagen fibers and ascorbic acid derivatives on behavior of rabbit corneal fibroblasts. Proc. 31st Annu. Int. Conf. IEEE Eng. Med. Biol. Soc. Eng. Futur. Biomed. EMBC 2009 4242–4245. https://doi.org/10.1109/IEMBS.2009.5332702

Pinnock, A., Shivshetty, N., Roy, S., Rimmer, S., Douglas, I., MacNeil, S., Garg, P., 2017. Ex vivo rabbit and human corneas as models for bacterial and fungal keratitis. Graefes Arch. Clin. Exp. Ophthalmol. 255, 333–342. https://doi.org/10.1007/s00417-016-3546-0

Pins, G.D., Christiansen, D.L., Patel, R., Silver, F.H., 1997. Self-assembly of collagen fibers. Influence of fibrillar alignment and decorin on mechanical properties. Biophys. J. 73, 2164–2172. https://doi.org/10.1016/S0006-3495(97)78247-X

Ponce Márquez, S., Martínez, V.S., McIntosh Ambrose, W., Wang, J., Gantxegui, N.G., Schein, O.D., Elisseeff, J.H., 2009. Decellularization of bovine corneas for tissue engineering applications. Acta Biomater. 5, 1839–47. https://doi.org/10.1016/j.actbio.2009.02.011

Pot, S.A., Liliensiek, S.J., Myrna, K.E., Bentley, E., Jester, J. V., Nealey, P.F., Murphy, C.J., 2010. Nanoscale topography-induced modulation of fundamental cell behaviors of rabbit corneal keratocytes, fibroblasts, and myofibroblasts. Investig. Ophthalmol. Vis. Sci. 51, 1373–1381. https://doi.org/10.1167/iovs.09-4074

Price, A.P., Godin, L.M., Domek, A., Cotter, T., D'Cunha, J., Taylor, D.A., Panoskaltsis-Mortari, A., 2015. Automated Decellularization of Intact, Human-Sized Lungs for Tissue Engineering. Tissue Eng. Part C Methods 21, 94–103. https://doi.org/10.1089/ten.tec.2013.0756

Proulx, S., Audet, C., Uwamaliya, J. d'Arc, Deschambeault, A., Carrier, P., Giasson, C.J., Brunette, I., Germain, L., 2009. Tissue engineering of feline corneal endothelium using a devitalized human cornea as carrier. Tissue Eng. Part A 15, 1709–18. https://doi.org/10.1089/ten.tea.2008.0208

R. Mohan, R., C.K. Tovey, J., Gupta, R., Sharma, A., Tandon, A., 2011. Decorin Biology, Expression, Function and Therapy in the Cornea. Curr. Mol. Med. 11, 110–128. https://doi.org/10.2174/156652411794859241

Rafat, M., Li, F., Fagerholm, P., Lagali, N., Watsky, M.A., Munger, R., Matsuura, T., Griffith, M., 2008.

PEG-stabilized carbodiimide crosslinked collagen-chitosan hydrogels for corneal tissue engineering. Biomaterials 29, 3960–3972. https://doi.org/10.1016/j.biomaterials.2008.06.017

Rahman, S., Griffin, M., Naik, A., Szarko, M., Butler, P.E.M., 2018. Optimising the decellularization of human elastic cartilage with trypsin for future use in ear reconstruction. Sci. Rep. 8, 3097. https://doi.org/10.1038/s41598-018-20592-x

Rama, P., Bonini, S., Lambiase, A., Golisano, O., Paterna, P., De Luca, M., Pellegrini, G., 2001. Autologous fibrin-cultured limbal stem cells permanently restore the corneal surface of patients with total limbal stem cell deficiency. Transplantation 72, 1478–1485. https://doi.org/10.1097/00007890-200111150-00002

Rama, P., Matuska, S., Paganoni, G., Spinelli, A., De Luca, M., Pellegrini, G., 2010. Limbal stem-cell therapy and long-term corneal regeneration. N. Engl. J. Med. 363, 147–155. https://doi.org/10.1056/NEJMoa0905955

Ramboer, E., De Craene, B., De Kock, J., Vanhaecke, T., Berx, G., Rogiers, V., Vinken, M., 2014. Strategies for immortalization of primary hepatocytes. J. Hepatol. 61, 925–43. https://doi.org/10.1016/j.jhep.2014.05.046

Reinhard, T. (Thomas), Larkin, D.F.P., 2006. Cornea and external eye disease. Springer.

Rheinwald, J.G., Green, H., 1977. Epidermal growth factor and the multiplication of cultured human epidermal keratinocytes. Nature 265, 421–424. https://doi.org/10.1038/265421a0

Rheinwald, J.G., Green, H., 1975. Serial cultivation of strains of human epidermal keratinocytes in defined clonal and serum-free culture. J Invest Dermatol 6, 331–344.

Richard, N.R., Anderson, J.A., Weiss, J.L., Binder, P.S., 1991. Air/liquid corneal organ culture: a light microscopic study. Curr. Eye Res. 10, 739–749.

Richter, A., Slowik, C., Somodi, S., Vick, H.P., Guthoff, R., 1996. Corneal reinnervation following penetrating keratoplasty--correlation of esthesiometry and confocal microscopy. Ger. J. Ophthalmol. 5, 513–7.

Rønnov-Jessen, L., Petersen, O.W., 1996. A function for filamentous α-smooth muscle actin: Retardation of motility in fibroblasts. J. Cell Biol. 134, 67–80. https://doi.org/10.1083/jcb.134.1.67

Saegusa, J., Yamaji, S., Ieguchi, K., Wu, C.-Y., Lam, K.S., Liu, F.-T., Takada, Y.K., Takada, Y., 2009. The direct binding of insulin-like growth factor-1 (IGF-1) to integrin alphavbeta3 is involved in IGF-1 signaling. J. Biol. Chem. 284, 24106–14. https://doi.org/10.1074/jbc.M109.013201

Saika, S., 1993. Ascorbic acid and proliferation of cultured rabbit keratocytes. Cornea 12, 191–8.

Saika, S., Kanagawa, R., Uenoyama, K., Hiroi, K., Hiraoka, J., 1991. L-ascorbic acid 2-phosphate, a phosphate derivative of L-ascorbic acid, enhances the growth of cultured rabbit keratocytes. Graefe's Arch. Clin. Exp. Ophthalmol. = Albr. von Graefes Arch. für Klin. und Exp. Ophthalmol. 229, 79–83.

Saika, S., Uenoyama, K., Hiroi, K., Ooshima, A., 1992. L-ascorbic acid 2-phosphate enhances the production of type I and type III collagen peptides in cultured rabbit keratocytes. Ophthalmic Res. 24, 68–72.

Saldin, L.T., Cramer, M.C., Velankar, S.S., White, L.J., Badylak, S.F., 2017. Extracellular matrix hydrogels from decellularized tissues: Structure and function. Acta Biomater. 49, 1–15. https://doi.org/10.1016/j.actbio.2016.11.068

Saltiel, A.R., Kahn, C.R., 2001. Insulin signalling and the regulation of glucose and lipid metabolism. Nature 414, 799–806. https://doi.org/10.1038/414799a

Sangwan, V.S., Basu, S., MacNeil, S., Balasubramanian, D., 2012. Simple limbal epithelial transplantation (SLET): a novel surgical technique for the treatment of unilateral limbal stem cell deficiency. Br. J. Ophthalmol. 96, 931 LP – 934. https://doi.org/10.1136/bjophthalmol-2011-301164

Santoso, E.G., Yoshida, K., Hirota, Y., Aizawa, M., Yoshino, O., Kishida, A., Osuga, Y., Saito, S., Ushida, T., Furukawa, K.S., 2014. Application of Detergents or High Hydrostatic Pressure as Decellularization Processes in Uterine Tissues and Their Subsequent Effects on In Vivo Uterine

Regeneration in Murine Models. PLoS One 9, e103201. https://doi.org/10.1371/journal.pone.0103201

Sarenac, T., Trapecar, M., Gradisnik, L., Rupnik, M.S., Pahor, D., 2016. Single-cell analysis reveals IGF-1 potentiation of inhibition of the TGF-β/Smad pathway of fibrosis in human keratocytes in vitro. Sci. Rep. 6, 34373. https://doi.org/10.1038/srep34373

Sasaki, S., Funamoto, S., Hashimoto, Y., Kimura, T., Honda, T., Hattori, S., Kobayashi, H., Kishida, A., Mochizuki, M., 2009. In vivo evaluation of a novel scaffold for artificial corneas prepared by using ultrahigh hydrostatic pressure to decellularize porcine corneas. Mol. Vis. 15, 2022–2028. https://doi.org/10.1007/s10856-005-6689-9

Sawada, K., Terada, D., Yamaoka, T., Kitamura, S., Fujisato, T., 2008. Cell removal with supercritical carbon dioxide for acellular artificial tissue. J. Chem. Technol. Biotechnol. 83, 943–949. https://doi.org/10.1002/jctb.1899

Sawkins, M.J., Bowen, W., Dhadda, P., Markides, H., Sidney, L.E., Taylor, A.J., Rose, F.R.A.J., Badylak, S.F., Shakesheff, K.M., White, L.J., 2013. Hydrogels derived from demineralized and decellularized bone extracellular matrix. Acta Biomater. 9, 7865–7873. https://doi.org/10.1016/J.ACTBIO.2013.04.029

Scarritt, M., Murdock, M., Badylak, S.F., 2019. Biologic Scaffolds Composed of Extracellular Matrix for Regenerative Medicine, Principles of Regenerative Medicine. Elsevier Inc. https://doi.org/10.1016/B978-0-12-809880-6.00035-7

Schatten, H., 2013. Scanning electron microscopy for the life sciences. Cambridge University Press.

Schmid, R., Tarau, I.S., Rossi, A., Leonhardt, S., Schwarz, T., Schuerlein, S., Lotz, C., Hansmann, J., 2018. In Vivo-Like Culture Conditions in a Bioreactor Facilitate Improved Tissue Quality in Corneal Storage. Biotechnol. J. 13, 1–7. https://doi.org/10.1002/biot.201700344

Schorderet, D., 2015. Corneal Dystrophies, 1st ed, Molecular Biology of Eye Disease. Elsevier Inc. https://doi.org/10.1016/bs.pmbts.2015.04.004

Sengyoku, H., Tsuchiya, T., Obata, T., Doi, R., Hashimoto, Y., Ishii, M., Sakai, H., Matsuo, N., Taniguchi, D., Suematsu, T., Lawn, M., Matsumoto, K., Miyazaki, T., Nagayasu, T., 2018. Sodium hydroxide based non-detergent decellularizing solution for rat lung. Organogenesis 14, 94–106. https://doi.org/10.1080/15476278.2018.1462432

Seo, Y., Jung, Y., Kim, S.H., 2018. Decellularized heart ECM hydrogel using supercritical carbon dioxide for improved angiogenesis. Acta Biomater. 67, 270–281. https://doi.org/10.1016/J.ACTBIO.2017.11.046

Shafiq, M.A., Gemeinhart, R.A., Yue, B.Y.J.T., Djalilian, A.R., 2012. Decellularized Human Cornea for Reconstructing the Corneal Epithelium and Anterior Stroma. Tissue Eng. Part C Methods 18, 340–348. https://doi.org/10.1089/ten.tec.2011.0072

Shafiq, M.A., Milani, B.Y., Djalilian, A.R., 2014. In Vivo Evaluation of a Decellularized Limbal Graft for Limbal Reconstruction. Int. J. Tissue Eng. 2014, 1–6. https://doi.org/10.1155/2014/754245

Shao, Y., Tang, J., Zhou, Y., Qu, Y., He, H., Liu, Q., Tan, G., Li, W., Liu, Z., 2015. A novel method in preparation of acellular porcine corneal stroma tissue for lamellar keratoplasty. Am. J. Transl. Res. 7, 2612–29. https://doi.org/10.3980/j.issn.2222-3959.2012.04.02

Shao, Y., Yu, Y., Pei, C.-G., Zhou, Q., Liu, Q.-P., Tan, G., Li, J.-M., Gao, G.-P., Yang, L., 2012. Evaluation of novel decellularizing corneal stroma for cornea tissue engineering applications. Int. J. Ophthalmol. 5, 415–8. https://doi.org/10.3980/j.issn.2222-3959.2012.04.02

Sharifi, R., Yang, Y., Adibnia, Y., Dohlman, C.H., Chodosh, J., González-Andrades, M., 2019. Finding an Optimal Corneal Xenograft Using Comparative Analysis of Corneal Matrix Proteins Across Species. Sci. Rep. 9, 1876. https://doi.org/10.1038/s41598-018-38342-4

Shi, M., Zhu, J., Wang, R., Chen, X., Mi, L., Walz, T., Springer, T.A., 2011. Latent TGF-β structure and activation. Nature 474, 343–9. https://doi.org/10.1038/nature10152

Shi, W., Zhou, Q., Gao, H., Li, S., Dong, M., Wang, T., Jia, Y., Dong, C., Wang, X., Guo, Z., Zhao, L., Hu,

X., Xie, L., 2019. Protectively Decellularized Porcine Cornea versus Human Donor Cornea for Lamellar Transplantation. Adv. Funct. Mater. 29, 1902491. https://doi.org/10.1002/adfm.201902491

Shi, Y., Bikkuzin, T., Song, Z., Jin, X., Jin, H., Li, X., Zhang, H., 2017. Comprehensive evaluation of decellularized porcine corneal after clinical transplantation. Xenotransplantation 24, 1–7. https://doi.org/10.1111/xen.12338

Shirzaei Sani, E., Kheirkhah, A., Rana, D., Sun, Z., Foulsham, W., Sheikhi, A., Khademhosseini, A., Dana, R., Annabi, N., 2019. Sutureless repair of corneal injuries using naturally derived bioadhesive hydrogels. Sci. Adv. 5, eaav1281. https://doi.org/10.1126/sciadv.aav1281

Shojaati, G., Khandaker, I., Funderburgh, M.L., Mann, M.M., Basu, R., Stolz, D.B., Geary, M.L., Dos Santos, A., Deng, S.X., Funderburgh, J.L., 2019. Mesenchymal Stem Cells Reduce Corneal Fibrosis and Inflammation Via Extracellular Vesicle-Mediated Delivery of miRNA. Stem Cells Transl. Med. 1–10. https://doi.org/10.1002/sctm.18-0297

Shtein, R.M., Kelley, K.H., Musch, D.C., Sugar, A., Mian, S.I., 2012. In vivo confocal microscopic evaluation of corneal wound healing after femtosecond laser-assisted keratoplasty. Ophthalmic Surg. Lasers Imaging 43, 205–213. https://doi.org/10.3928/15428877-20120209-01

Sidney, L.E., Hopkinson, A., 2016. Corneal keratocyte transition to mesenchymal stem cell phenotype and reversal using serum-free medium supplemented with FGF-2, TGF-ß3 and retinoic acid. J. Tissue Eng. Regen. Med. 4. https://doi.org/10.1002/term.2316

Singelyn, J.M., DeQuach, J.A., Seif-Naraghi, S.B., Littlefield, R.B., Schup-Magoffin, P.J., Christman, K.L., 2009. Naturally derived myocardial matrix as an injectable scaffold for cardiac tissue engineering. Biomaterials 30, 5409–5416. https://doi.org/10.1016/j.biomaterials.2009.06.045

Skardal, A., Devarasetty, M., Kang, H.W., Mead, I., Bishop, C., Shupe, T., Lee, S.J., Jackson, J., Yoo, J., Soker, S., Atala, A., 2015. A hydrogel bioink toolkit for mimicking native tissue biochemical and mechanical properties in bioprinted tissue constructs. Acta Biomater. 25, 24–34. https://doi.org/10.1016/j.actbio.2015.07.030

Soh, Y.Q., Peh, G.S.L., Mehta, J.S., 2017. Translational issues for human corneal endothelial tissue engineering. J. Tissue Eng. Regen. Med. 11, 2425–2442. https://doi.org/10.1002/term.2131

Sorkio, A., Koch, L., Koivusalo, L., Deiwick, A., Miettinen, S., Chichkov, B., Skottman, H., 2018. Human stem cell based corneal tissue mimicking structures using laser-assisted 3D bioprinting and functional bioinks. Biomaterials 171, 57–71. https://doi.org/10.1016/j.biomaterials.2018.04.034

Srikumaran, D., Munoz, B., Aldave, A.J., Aquavella, J. V., Hannush, S.B., Schultze, R., Belin, M., Akpek, E.K., 2014. Long-term Outcomes of Boston Type 1 Keratoprosthesis Implantation. Ophthalmology 121, 2159–2164. https://doi.org/10.1016/j.ophtha.2014.05.030

Sriram, S., Tran, J.A., Guo, X., Hutcheon, A.E.K., Lei, H., Zieske, J.D., 2017. PDGFR a Is a Key Regulator of T1 and T3's Differential Effect on SMA Expression in Human Corneal Fibroblasts. Invest. Ophthalmol. Vis. Sci. 58, 1179–1186. https://doi.org/10.1167/iovs.16-20016

Stone, N., Meister, A., 1962. Function of ascorbic acid in the conversion of proline to collagen hydroxyproline. Nature 194, 555–557. https://doi.org/10.1038/194555a0

Stramer, B.M., Zieske, J.D., Jung, J.C., Austin, J.S., Fini, M.E., 2003. Molecular mechanisms controlling the fibrotic repair phenotype in cornea: Implications for surgical outcomes. Investig. Ophthalmol. Vis. Sci. 44, 4237–4246. https://doi.org/10.1167/iovs.02-1188

Tajima, S., Pinnell, S.R., 1982. Regulation of collagen synthesis by ascorbic acid increases type I procollagen mRNA. Biochem. Biophys. Res. Commun. 106, 632–637.

Tan, D.T.H., Dart, J.K.G., Holland, E.J., Kinoshita, S., 2012. Corneal transplantation. Lancet 379, 1749–1761. https://doi.org/10.1016/S0140-6736(12)60437-1

Tan, X.W., Hartman, L., Tan, K.P., Poh, R., Myung, D., Zheng, L.L., Waters, D., Noolandi, J., Beuerman, R.W., Frank, C.W., Ta, C.N., Tan, D.T., Mehta, J.S., 2013. In vivo biocompatibility of two PEG/PAA interpenetrating polymer networks as corneal inlays following deep stromal pocket implantation. J. Mater. Sci. Mater. Med. 24, 967–977. https://doi.org/10.1007/s10856-012-4848-3

Tervo, K., Van Setten, G.B., Beuerman, R.W., Virtanen, I., Tarkkanen, A., Tervo, T., 1991. Expression of tenascin and cellular fibronectin in the rabbit cornea after anterior keratectomy: Immunohistochemical study of wound healing dynamics. Investig. Ophthalmol. Vis. Sci. 32, 2912–2918.

Tonsomboon, K., Oyen, M.L., 2013. Composite electrospun gelatin fiber-alginate gel scaffolds for mechanically robust tissue engineered cornea. J. Mech. Behav. Biomed. Mater. 21, 185–194. https://doi.org/10.1016/j.jmbbm.2013.03.001

Torricelli, A.A.M., Santhanam, A., Wu, J., Singh, V., Wilson, S.E., 2016. The corneal fibrosis response to epithelial-stromal injury. Exp. Eye Res. 142, 110–118. https://doi.org/10.1016/j.exer.2014.09.012

Torricelli, A.A.M., Singh, V., Santhiago, M.R., Wilson, S.E., 2013. The corneal epithelial basement membrane: Structure, function, and disease. Investig. Ophthalmol. Vis. Sci. 54, 6390–6400. https://doi.org/10.1167/iovs.13-12547

Toti, P., Tosi, G.M., Traversi, C., Schürfeld, K., Cardone, C., Caporossi, A., 2002. CD-34 stromal expression pattern in normal and altered human corneas. Ophthalmology 109, 1167–1171. https://doi.org/10.1016/S0161-6420(02)01042-4

Treacy, O., O'Flynn, L., Ryan, A.E., Morcos, M., Lohan, P., Schu, S., Wilk, M., Fahy, G., Griffin, M.D., Nosov, M., Ritter, T., 2014. Mesenchymal Stem Cell Therapy Promotes Corneal Allograft Survival in Rats by Local and Systemic Immunomodulation. Am. J. Transplant. 14, 2023–2036. https://doi.org/10.1111/ajt.12828

Tukmachev, D., Forostyak, S., Koci, Z., Zaviskova, K., Vackova, I., Vyborny, K., Sandvig, I., Sandvig, A., Medberry, C.J., Badylak, S.F., Sykova, E., Kubinova, S., 2016. Injectable Extracellular Matrix Hydrogels as Scaffolds for Spinal Cord Injury Repair. Tissue Eng. - Part A 22, 306–317. https://doi.org/10.1089/ten.tea.2015.0422

Ungerleider, J.L., Johnson, T.D., Rao, N., Christman, K.L., 2015. Fabrication and characterization of injectable hydrogels derived from decellularized skeletal and cardiac muscle. Methods 84, 53–59. https://doi.org/10.1016/j.ymeth.2015.03.024

Utine, C.A., Tzu, J.H., Akpek, E.K., 2011. Lamellar Keratoplasty Using Gamma-Irradiated Corneal Lenticules. Am. J. Ophthalmol. 151, 170-174.e1. https://doi.org/10.1016/j.ajo.2010.08.007

Utomo, L., Pleumeekers, M.M., Nimeskern, L., Nürnberger, S., Stok, K.S., Hildner, F., van Osch, G.J.V.M., 2015. Preparation and characterization of a decellularized cartilage scaffold for ear cartilage reconstruction. Biomed. Mater. 10, 015010. https://doi.org/10.1088/1748-6041/10/1/015010

Uygun, B.E., Soto-Gutierrez, A., Yagi, H., Izamis, M.-L., Guzzardi, M.A., Shulman, C., Milwid, J., Kobayashi, N., Tilles, A., Berthiaume, F., Hertl, M., Nahmias, Y., Yarmush, M.L., Uygun, K., 2010. Organ reengineering through development of a transplantable recellularized liver graft using decellularized liver matrix. Nat. Med. 16, 814–820. https://doi.org/10.1038/nm.2170

Uzunalli, G., Soran, Z., Erkal, T.S., Dagdas, Y.S., Dinc, E., Hondur, A.M., Bilgihan, K., Aydin, B., Guler, M.O., Tekinay, A.B., 2014. Bioactive self-assembled peptide nanofibers for corneal stroma regeneration. Acta Biomater. 10, 1156–1166. https://doi.org/10.1016/j.actbio.2013.12.002

Van den Bogerd, B., Ní Dhubhghaill, S., Zakaria, N., 2018. Characterizing human decellularized crystalline lens capsules as a scaffold for corneal endothelial tissue engineering. J. Tissue Eng. Regen. Med. 12, e2020–e2028. https://doi.org/10.1002/term.2633

van Steenberghe, M., Schubert, T., Gerelli, S., Bouzin, C., Guiot, Y., Xhema, D., Bollen, X., Abdelhamid, K., Gianello, P., 2018. Porcine pulmonary valve decellularization with NaOH-based vs detergent process: preliminary in vitro and in vivo assessments. J. Cardiothorac. Surg. 13, 34. https://doi.org/10.1186/s13019-018-0720-y

Vattulainen, M., Ilmarinen, T., Koivusalo, L., Viiri, K., Hongisto, H., Skottman, H., 2019. Modulation of Wnt/BMP pathways during corneal differentiation of hPSC maintains ABCG2-positive LSC population that demonstrates increased regenerative potential. Stem Cell Res. Ther. 10, 236. https://doi.org/10.1186/s13287-019-1354-2

Vesaluoma, M., Teppo, A.M., Grönhagen-Riska, C., Tervo, T., 1997. Platelet-derived growth factor-BB

(PDGF-BB) in tear fluid: a potential modulator of corneal wound healing following photorefractive keratectomy. Curr. Eye Res. 16, 825–31.

Voytik-Harbin, S.L., Brightman, A.O., Waisner, B.Z., Robinson, J.P., Lamar, C.H., 1998. Small Intestinal Submucosa: A Tissue-Derived Extracellular Matrix That Promotes Tissue-Specific Growth and Differentiation of Cells *in Vitro*. Tissue Eng. 4, 157–174. https://doi.org/10.1089/ten.1998.4.157

Wagoner, M.D., Bohrer, L.R., Aldrich, B.T., Greiner, M.A., Mullins, R.F., Worthington, K.S., Tucker, B.A., Wiley, L.A., 2018. Feeder-free differentiation of cells exhibiting characteristics of corneal endothelium from human induced pluripotent stem cells. Biol. Open 7, bio032102. https://doi.org/10.1242/bio.032102

Wang, J.Y., Liou, A., Ren, Z.H., Zhang, L., Brown, B.N., Cui, X.T., Badylak, S.F., Cai, Y.N., Guan, Y.Q., Leak, R.K., Chen, J., Ji, X., Chen, L., 2013. Neurorestorative effect of urinary bladder matrix-mediated neural stem cell transplantation following traumatic brain injury in rats. CNS Neurol. Disord. Drug Targets 12, 413–425.

Wang, R., Ruan, M., Zhang, R., Chen, L., Li, X., Fang, B., Li, C., Ren, X., Liu, J., Xiong, Q., Zhang, L., Jin, Y., Li, L., Li, R., Wang, Y., Yang, H., Dai, Y., 2018. Antigenicity of tissues and organs from GGTA1/CMAH/b4GalNT2 triple gene knockout pigs. J. Biomed. Res. 0, 1–9. https://doi.org/10.7555/JBR.32.20180018

Wang, S., Ghezzi, C.E., Gomes, R., Pollard, R.E., Funderburgh, J.L., Kaplan, D.L., 2017. In vitro 3D corneal tissue model with epithelium, stroma, and innervation. Biomaterials 112, 1–9. https://doi.org/10.1016/j.biomaterials.2016.09.030

Wang, X., Xu, H., Huang, Y., Gu, S., Jiang, J.X., 2016. Coupling Effect of Water and Proteoglycans on the in Situ Toughness of Bone. J. Bone Miner. Res. 31, 1026–1029. https://doi.org/10.1002/jbmr.2774

Webber, M.J., Khan, O.F., Sydlik, S.A., Tang, B.C., Langer, R., 2015. A Perspective on the Clinical Translation of Scaffolds for Tissue Engineering. Ann. Biomed. Eng. 43, 641–656. https://doi.org/10.1007/s10439-014-1104-7

Wehmeyer, J.L., Natesan, S., Christy, R.J., 2015. Development of a Sterile Amniotic Membrane Tissue Graft Using Supercritical Carbon Dioxide. Tissue Eng. Part C. Methods 21, 649–59. https://doi.org/10.1089/ten.TEC.2014.0304

Welch, M.P., Odland, G.F., Clark, R.A., 1990. Temporal relationships of F-actin bundle formation, collagen and fibronectin matrix assembly, and fibronectin receptor expression to wound contraction. J. Cell Biol. 110, 133–45.

West-Mays, J.A., Cook, J.R., Sadow, P.M., Mullady, D.K., Bargagna-mohan, P., Strissel, K.J., Fini, M.E., 1999. Differential Inhibition of Collagenase and Interleukin- l a Gene Expression in Cultured Corneal Fibroblasts by TGF-b, Dexamethasone, and Retinoic Acid. Investig. Ophthalmol. Vis. Sci. 40, 887–896.

Whitcher, J.P., Srinivasan, M., Upadhyay, M.P., 2001. Corneal blindness : a global perspective. Bull. World Health Organ. 79, 214–221.

White, L.J., Keane, T.J., Smoulder, A., Zhang, L., Castleton, A.A., Reing, J.E., Turner, N.J., Dearth, C.L., Badylak, S.F., 2018. The impact of sterilization upon extracellular matrix hydrogel structure and function. J. Immunol. Regen. Med. 2, 11–20. https://doi.org/10.1016/j.regen.2018.04.001

Wilson, S.E., He, Y.G., Lloyd, S.A., 1992. EGF, EGF receptor, basic FGF, TGF beta-1, and IL-1 alpha mRNA in human corneal epithelial cells and stromal fibroblasts. Invest. Ophthalmol. Vis. Sci. 33, 1756–1765.

Wilson, S.E., Kim, W.J., 1998. Keratocyte apoptosis: Implications on corneal wound healing, tissue organization, and disease. Investig. Ophthalmol. Vis. Sci. 39, 220–221.

Wilson, S.E., Mohan, Rahul R, Mohan, Rajiv R, Ambrósio, R., Hong, J., Lee, J., 2001. The corneal wound healing response: Cytokine-mediated interaction of the epithelium, stroma, and inflammatory cells. Prog. Retin. Eye Res. 20, 625–637. https://doi.org/10.1016/S1350-9462(01)00008-8

Wilson, S.L., Sidney, L.E., Dunphy, S.E., Dua, H.S., Hopkinson, A., 2016. Corneal Decellularization: A

Method of Recycling Unsuitable Donor Tissue for Clinical Translation? Curr. Eye Res. 41, 769–782. https://doi.org/10.3109/02713683.2015.1062114

Wilson, S.L., Sidney, L.E., Dunphy, S.E., Dua, H.S., Hopkinson, A., 2015. Corneal Decellularization: A Method of Recycling Unsuitable Donor Tissue for Clinical Translation? Curr. Eye Res. 3683, 1–14. https://doi.org/10.3109/02713683.2015.1062114

Wilson, S.L., Sidney, L.E., Dunphy, S.E., Rose, J.B., Hopkinson, A., 2013. Keeping an eye on decellularized corneas: a review of methods, characterization and applications. J. Funct. Biomater. 4, 114–61. https://doi.org/10.3390/jfb4030114

Wilson, S.L., Wimpenny, I., Ahearne, M., Rauz, S., El Haj, A.J., Yang, Y., 2012. Chemical and topographical effects on cell differentiation and matrix elasticity in a corneal stromal layer model. Adv. Funct. Mater. 22. https://doi.org/10.1002/adfm.201200655

Wolf, M.T., Daly, K.A., Brennan-Pierce, E.P., Johnson, S.A., Carruthers, C.A., D'Amore, A., Nagarkar, S.P., Velankar, S.S., Badylak, S.F., 2012. A hydrogel derived from decellularized dermal extracellular matrix. Biomaterials 33, 7028–7038. https://doi.org/10.1016/j.biomaterials.2012.06.051

Wu, J., Du, Y., Mann, M.M., Funderburgh, J.L., Wagner, W.R., 2014. Corneal stromal stem cells versus corneal fibroblasts in generating structurally appropriate corneal stromal tissue. Exp. Eye Res. 120, 71–81. https://doi.org/10.1016/j.exer.2014.01.005

Wu, J., Du, Y., Mann, M.M., Yang, E., Funderburgh, J.L., Wagner, W.R., 2013. Bioengineering organized, multilamellar human corneal stromal tissue by growth factor supplementation on highly aligned synthetic substrates. Tissue Eng. Part A 19, 2063–75. https://doi.org/10.1089/ten.TEA.2012.0545

Wu, Z., Zhou, Q., Duan, Haoyun, Wang, X., Xiao, J., Duan, Hucheng, Li, N., Li, C., Wan, P., Liu, Y., Song, Y., Zhou, C., Huang, Z., Wang, Z., 2014. Reconstruction of auto-tissue-engineered lamellar cornea by dynamic culture for transplantation: A rabbit model. PLoS One 9. https://doi.org/10.1371/journal.pone.0093012

Wu, Z., Zhou, Y., Li, N., Huang, M., Duan, H., Ge, J., Xiang, P., Wang, Z., 2009. The use of phospholipase A2 to prepare acellular porcine corneal stroma as a tissue engineering scaffold. Biomaterials 30, 3513–3522. https://doi.org/10.1016/j.biomaterials.2009.03.003

Xiao, J., Duan, H., Liu, Z., Wu, Z., Lan, Y., Zhang, W., Li, C., Chen, F., Zhou, Q., Wang, X., Huang, J., Wang, Z., 2011. Construction of the recellularized corneal stroma using porous acellular corneal scaffold. Biomaterials 32, 6962–6971. https://doi.org/10.1016/j.biomaterials.2011.05.084

Xu, B., Song, Z., Fan, T., 2017. Construction of Anterior Hemi-Corneal Equivalents Using Nontransfected Human Corneal Cells and Transplantation in Dog Models. Artif. Organs 41, 1004–1016. https://doi.org/10.1111/aor.12878

Xu, J., 1996. Receptor Specificity of the Fibroblast Growth Factor Family. J. Biol. Chem. 271, 15292–15297. https://doi.org/10.1074/jbc.271.25.15292

Xu, K.P., Li, X.F., Yu, F.S.X., 2000. Corneal organ culture model for assessing epithelial responses to surfactants. Toxicol. Sci. 58, 306–314. https://doi.org/10.1093/toxsci/58.2.306

Xu, Y.-G., Xu, Y.-S., Huang, C., Feng, Y., Li, Y., Wang, W., 2008. Development of a rabbit corneal equivalent using an acellular corneal matrix of a porcine substrate. Mol. Vis. 14, 2180–9.

Xu, Z.-Z., Li, Z.-J., Du, L.-X., Li, J., Wang, L.-Y., 2013. Using bovine pituitary extract to increase proliferation of keratocytes and maintain their phenotype in vitro. Int. J. Ophthalmol. 6, 758–765. https://doi.org/10.3980/j.issn.2222-3959.2013.06.04

Yagi, H., Fukumitsu, K., Fukuda, K., Kitago, M., Shinoda, M., Obara, H., Itano, O., Kawachi, S., Tanabe, M., Coudriet, G.M., Piganelli, J.D., Gilbert, T.W., Soto-Gutierrez, A., Kitagawa, Y., 2013. Human-scale whole-organ bioengineering for liver transplantation: A regenerative medicine approach. Cell Transplant. 22, 231–242. https://doi.org/10.3727/096368912X654939

Yam, G.H.-F., Williams, G.P., Setiawan, M., Yusoff, N.Z.B.M., Lee, X., Htoon, H.M., Zhou, L., Fuest, M., Mehta, J.S., 2017. Nerve regeneration by human corneal stromal keratocytes and stromal fibroblasts. Sci. Rep. 7, 45396. https://doi.org/10.1038/srep45396

Yam, G.H.-F., Yusoff, N.Z.B.M., Goh, T.-W., Setiawan, M., Lee, X.-W., Liu, Y.-C., Mehta, J.S., 2016. Decellularization of human stromal refractive lenticules for corneal tissue engineering. Sci. Rep. 6, 26339. https://doi.org/10.1038/srep26339

Yanai, R., Yamada, N., Kugimiya, N., Inui, M., Nishida, T., 2002. Mitogenic and antiapoptotic effects of various growth factors on human corneal fibroblasts. Invest. Ophthalmol. Vis. Sci. 43, 2122–6.

Yin, H., Lu, Q., Wang, X., Majumdar, S., Jun, A.S., Stark, W.J., Grant, M.P., Elisseeff, J.H., 2019a. Tissue-derived microparticles reduce inflammation and fibrosis in cornea wounds. Acta Biomater. 85, 192–202. https://doi.org/10.1016/j.actbio.2018.12.027

Yin, H., Qiu, P., Wu, F., Zhang, W., Teng, W., Qin, Z., Li, C., Zhou, J., Fang, Z., Tang, Q., Fu, Q., Ma, J., Yang, Y., 2016. Construction of a Corneal Stromal Equivalent with SMILE-Derived Lenticules and Fibrin Glue. Sci. Rep. 6, 33848. https://doi.org/10.1038/srep33848

Yin, H., Wang, X., Majumdar, S., Sohn, J., Kim, B., Stark, W., Elisseeff, J.H., 2019b. Tissue-Derived Biological Particles Restore Cornea Properties in an Enzyme-Mediated Corneal Ectatic Model. Bioengineering 6, 90. https://doi.org/10.3390/bioengineering6040090

Yin, X.-T., Tajfirouz, D.A., Stuart, P.M., 2014. Murine Corneal Transplantation: A Model to Study the Most Common Form of Solid Organ Transplantation. J. Vis. Exp. e51830–e51830. https://doi.org/10.3791/51830

Yoeruek, E., Bayyoud, T., Maurus, C., Hofmann, J., Spitzer, M.S., Bartz-Schmidt, K.U., Szurman, P., 2012a. Decellularization of porcine corneas and repopulation with human corneal cells for tissue-engineered xenografts. Acta Ophthalmol. 90, 125–131. https://doi.org/10.1111/j.1755-3768.2011.02261.x

Yoeruek, E., Bayyoud, T., Maurus, C., Hofmann, J., Spitzer, M.S., Bartz-Schmidt, K.U., Szurman, P., 2012b. Reconstruction of corneal stroma with decellularized porcine xenografts in a rabbit model. Acta Ophthalmol. 90, 206–210. https://doi.org/10.1111/j.1755-3768.2011.02300.x

Zeng, Y., Yang, J., Huang, K., Lee, Z., Lee, X., 2001. A comparison of biomechanical properties between human and porcine cornea. J. Biomech. 34, 533–537. https://doi.org/10.1016/S0021-9290(00)00219-0

Zhang, C., Nie, X., Hu, D., Liu, Y., Deng, Z., Dong, R., Zhang, Y., Jin, Y., 2007. Survival and integration of tissue-engineered corneal stroma in a model of corneal ulcer. Cell Tissue Res. 329, 249–257. https://doi.org/10.1007/s00441-007-0419-1

Zhang, G., Chen, S., Goldoni, S., Calder, B.W., Simpson, H.C., Owens, R.T., McQuillan, D.J., Young, M.F., Iozzo, R. V, Birk, D.E., 2009. Genetic evidence for the coordinated regulation of collagen fibrillogenesis in the cornea by decorin and biglycan. J. Biol. Chem. 284, 8888–97. https://doi.org/10.1074/jbc.M806590200

Zhang, J., Zhang, C.-W., Du, L.-Q., Wu, X.-Y., 2016. Acellular porcine corneal matrix as a carrier scaffold for cultivating human corneal epithelial cells and fibroblasts in vitro. Int. J. Ophthalmol. 9, 1–8. https://doi.org/10.18240/ijo.2016.01.01

Zhang, L., Zhang, F., Weng, Z., Brown, B.N., Yan, H., Ma, X.M., Vosler, P.S., Badylak, S.F., Dixon, C.E., Cui, X.T., Chen, J., 2013. Effect of an inductive hydrogel composed of urinary bladder matrix upon functional recovery following traumatic brain injury. Tissue Eng. Part A 19, 1909–18. https://doi.org/10.1089/ten.TEA.2012.0622

Zhang, M.-C., Liu, X., Jin, Y., Jiang, D.-L., Wei, X.-S., Xie, H.-T., 2015. Lamellar Keratoplasty Treatment of Fungal Corneal Ulcers With Acellular Porcine Corneal Stroma. Am. J. Transplant. 15, 1068–1075. https://doi.org/10.1111/ajt.13096

Zhang, R., Wang, Y., Chen, L., Wang, R., Li, C., Li, X., Fang, B., Ren, X., Ruan, M., Liu, J., Xiong, Q., Zhang, L., Jin, Y., Zhang, M., Liu, X., Li, L., Chen, Q., Pan, D., Li, R., Cooper, D.K.C., Yang, H., Dai, Y., 2018. Reducing immunoreactivity of porcine bioprosthetic heart valves by genetically-deleting three major glycan antigens, GGTA1/β4GalNT2/CMAH. Acta Biomater. 72, 196–205. https://doi.org/10.1016/j.actbio.2018.03.055

Zhang, S., Espandar, L., Imhof, K.M.P., Bunnell, B.A., 2013. Differentiation of Human Adipose-derived

Stem Cells along the Keratocyte Lineage In vitro. J. Clin. Exp. Ophthalmol. 04, 270. https://doi.org/10.4172/2155-9570.1000270

Zhang, Z., Niu, G., Choi, J.S., Giegengack, M., Atala, A., Soker, S., 2015. Bioengineered multilayered human corneas from discarded human corneal tissue. Biomed. Mater. 10, 035012. https://doi.org/10.1088/1748-6041/10/3/035012

Zheng, J., Huang, X., Zhang, Y., Wang, Y., Qin, Q., Lin, L., Jin, X., Lam, C., Zhang, J., 2019. Short-term results of acellular porcine corneal stroma keratoplasty for herpes simplex keratitis. Xenotransplantation 26, e12509. https://doi.org/10.1111/xen.12509

Zheng, X., Zhang, D., Li, S., Zhang, J., Zheng, J., Du, L., Gao, J., 2018. An Experimental Study of Femto-Laser in Assisting Xenograft Acellular Cornea Matrix Lens Transplantation. Med. Sci. Monit. 24, 5208–5215. https://doi.org/10.12659/MSM.909294

Zhou, Y., Wu, Z., Ge, J., Wan, P., Li, N., Xiang, P., Gao, Q., Wang, Z., 2011. Development and characterization of acellular porcine corneal matrix using sodium dodecylsulfate. Cornea 30, 73–82. https://doi.org/10.1097/ICO.0b013e3181dc8184

Zhu, X., Beuerman, R.W., Chan-Park, M.B.E., Cheng, Z., Ang, L.P.K., Tan, D.T.H., 2006. Enhancement of the mechanical and biological properties of a biomembrane for tissue engineering the ocular surface. Ann. Acad. Med. Singapore 35, 210–214.

Zilic, L., Wilshaw, S.-P., Haycock, J.W., 2016. Decellularisation and histological characterisation of porcine peripheral nerves. Biotechnol. Bioeng. 113, 2041–53. https://doi.org/10.1002/bit.25964

Zvarova, B., Uhl, F.E., Uriarte, J.J., Borg, Z.D., Coffey, A.L., Bonenfant, N.R., Weiss, D.J., Wagner, D.E., 2016. Residual Detergent Detection Method for Nondestructive Cytocompatibility Evaluation of Decellularized Whole Lung Scaffolds. Tissue Eng. Part C Methods 22, 418–428. https://doi.org/10.1089/ten.tec.2015.0439

Appendix

A. Recellularization methods

Several methods were used to recellularize the decellularized porcine corneas with expanded human corneal stromal cells.

Method 1 (Figure A-2 A): embedding of decellularized porcine corneas in cell-laden collagen gels. 0.1 $x10^6$ cells were embedded in each gel which was cast over the scaffold in a 24-well plate. 3.5 mg/ml gels were fabricated according to manufacturer's guidelines.

Method 2 (Figure A-2 B): Another method was to place a Teflon disk on the bottom of the plate or cover the bottom of the well with agarose to avoid cells adhering to the tissue culture plastic and therefore promote cell adhesion on the scaffold. 0.1 $x10^6$ cells were seeded on top of the scaffolds using a volume of 10-20 µl, let attach for 30 minutes in a humidified incubator at 37 °C, scaffolds were then flipped and procedure repeated, and finally submerged in medium containing 0.3 $x10^6$ cells.

Method 3 (Figure A-2 C): a 1 ml syringe attached to an insulin needle (29G, Terumo®, Belgium) was loaded with cell suspension (1 $x10^6$ cells/ml). Two injections per scaffold were performed introducing around 100 µl of cells. Typically, medium would "spill out".

Samples were wax embed, sliced and stained with DAPI to visualize cell nuclei. The distance from the edge was measured and was demonstrated that Method 3 was the most successful.

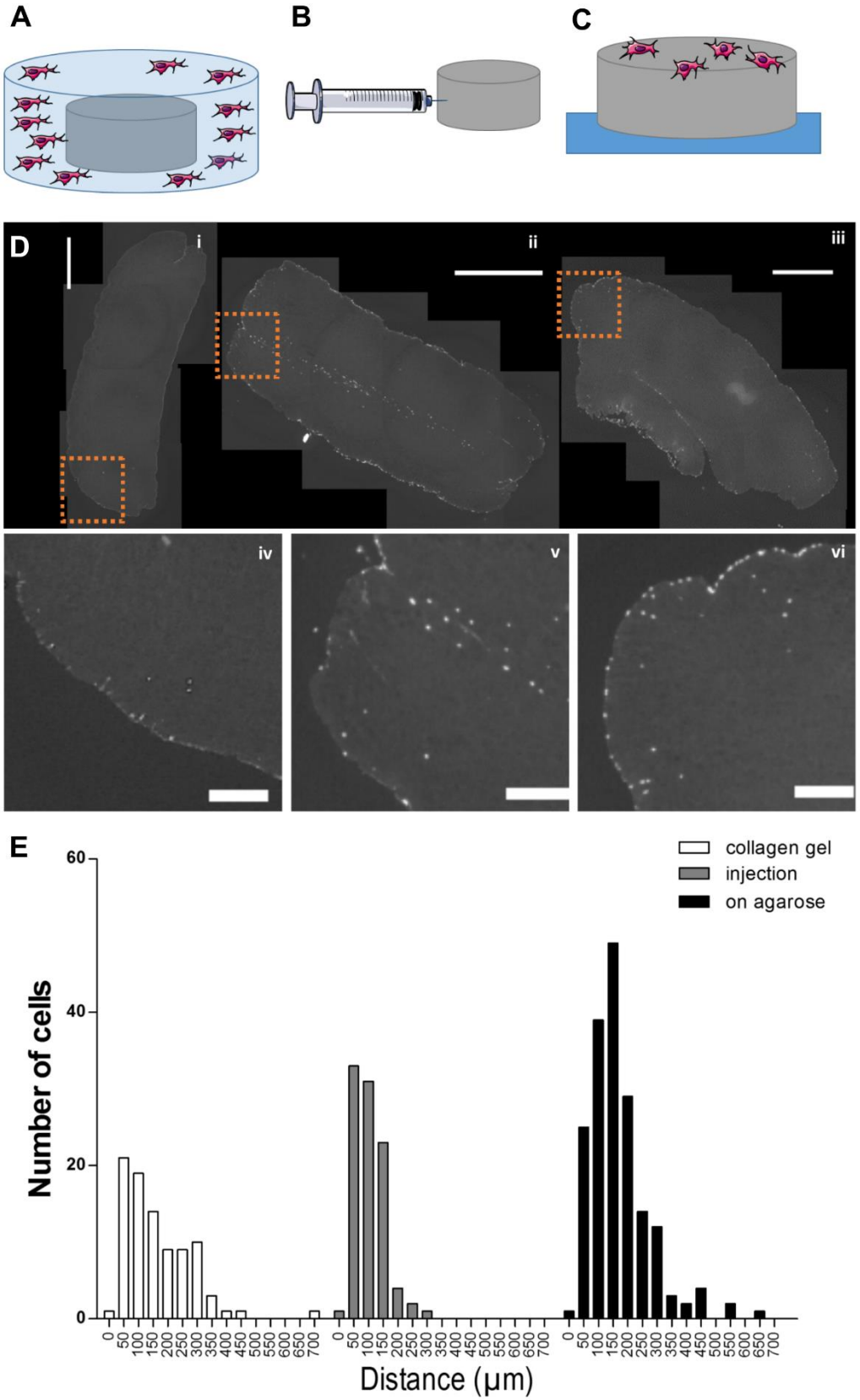

Figure A-8-1. Recellularization of decellularized porcine corneas with human corneal stromal-derived cells. Schematics of each method: A) collagen gel method, B) cell injection and C) cell seeding on non-adherent surfaces D) Representative images of recellularized corneas after slicing and staining with DAPI (top row) and close ups (bottom row): collagen gel method (i and iv), cell injection (ii and v) and cell seeding on non-adherent surfaces (iii and vi). Scale bar = 1 mm (i-iii) and 200 µm (iv-vi). E) Quantification of migration inside the scaffold.

B. Histology and immunostaining of *in vivo* samples

The following figures show a representative image of each individual sample of a rabbit cornea 3 months post-implantation, either recellularized *in vitro* (left) or non-recellularized (right), from Chapter 4.

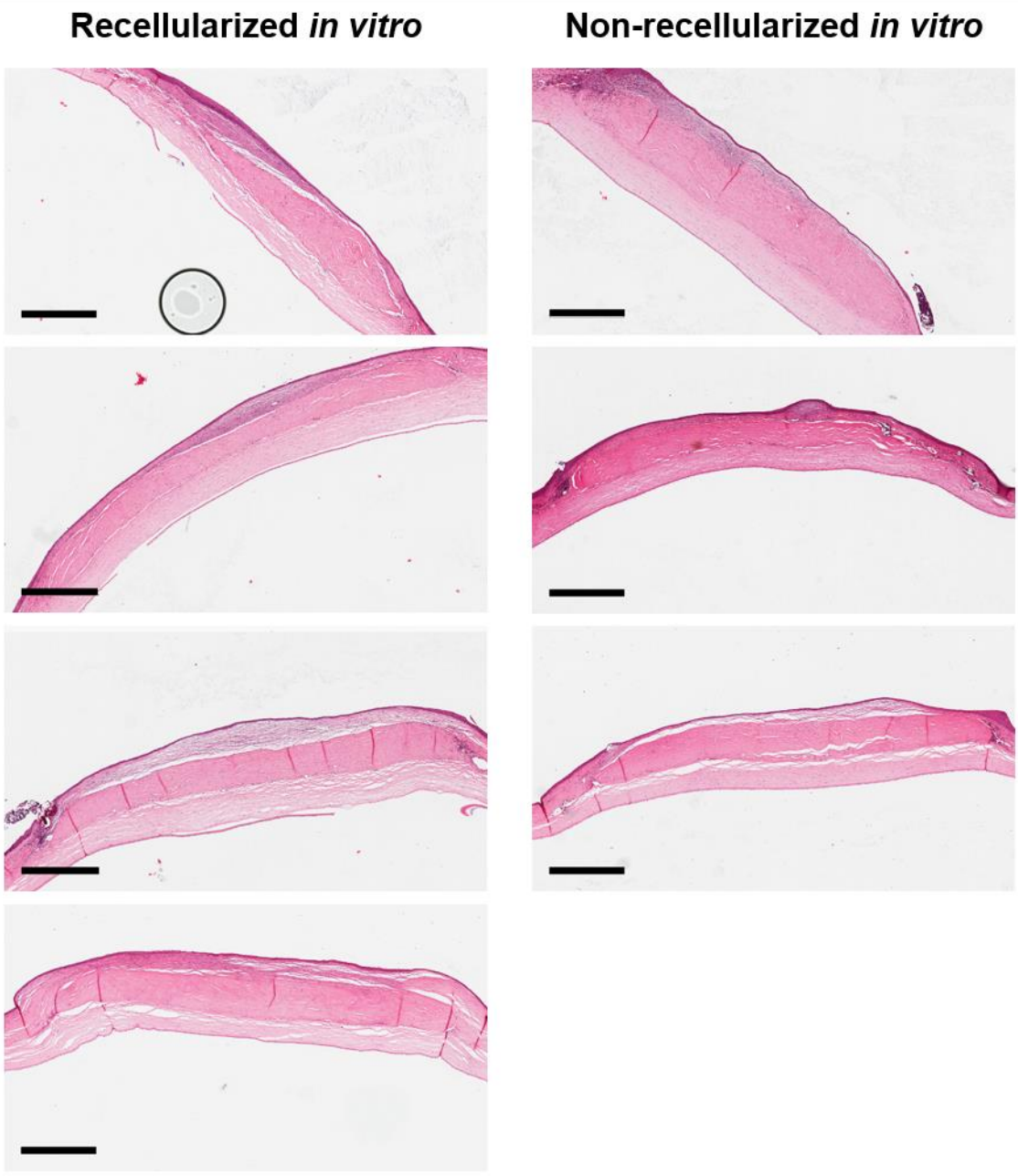

Figure A-8-2. H&E staining of the implanted scaffolds 3 months post-surgery (scale bar = 700 µm).

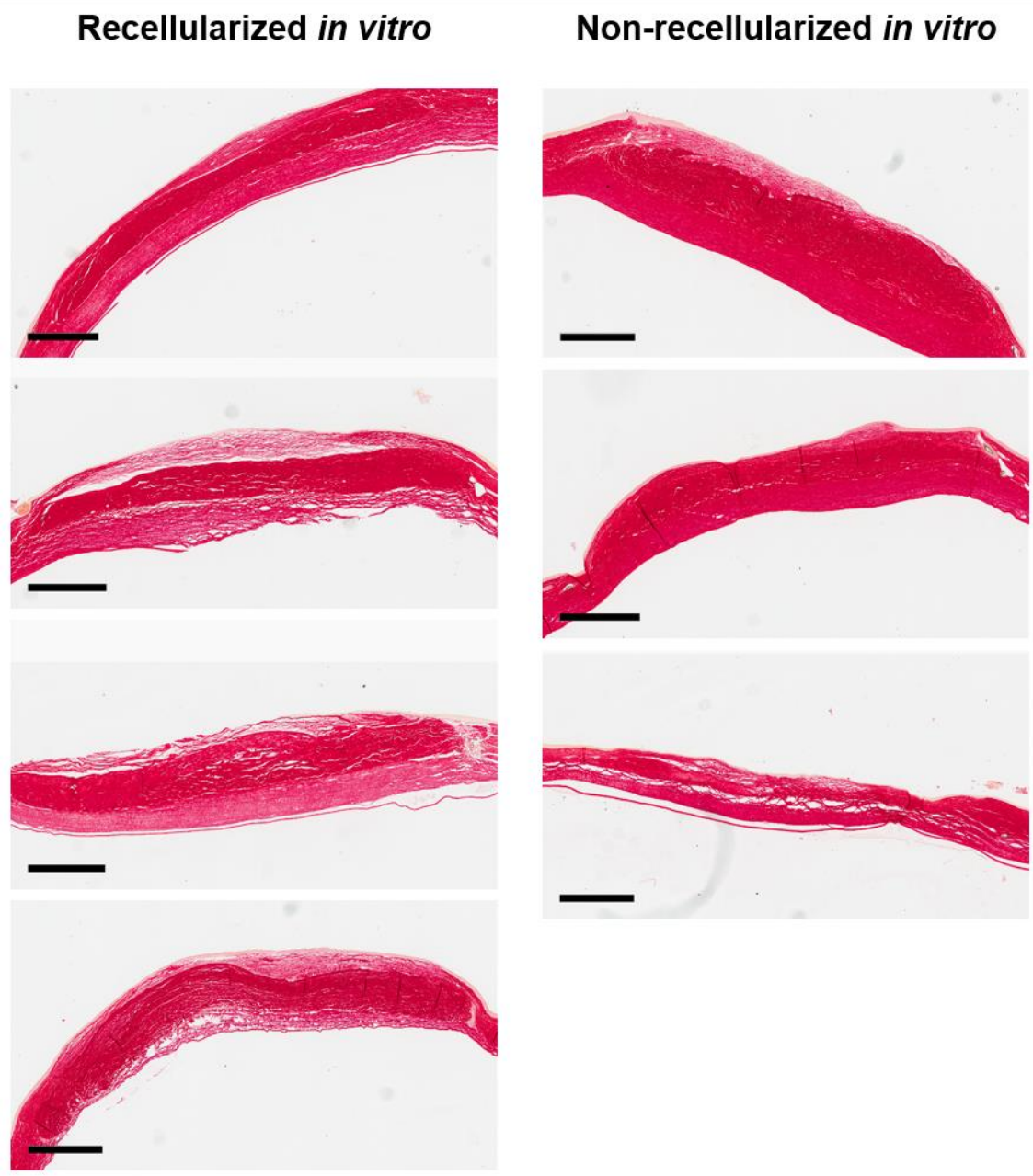

Figure A-8-3. Picrosirius red staining of the implanted scaffolds 3 months post-surgery (scale bar = 700 µm).

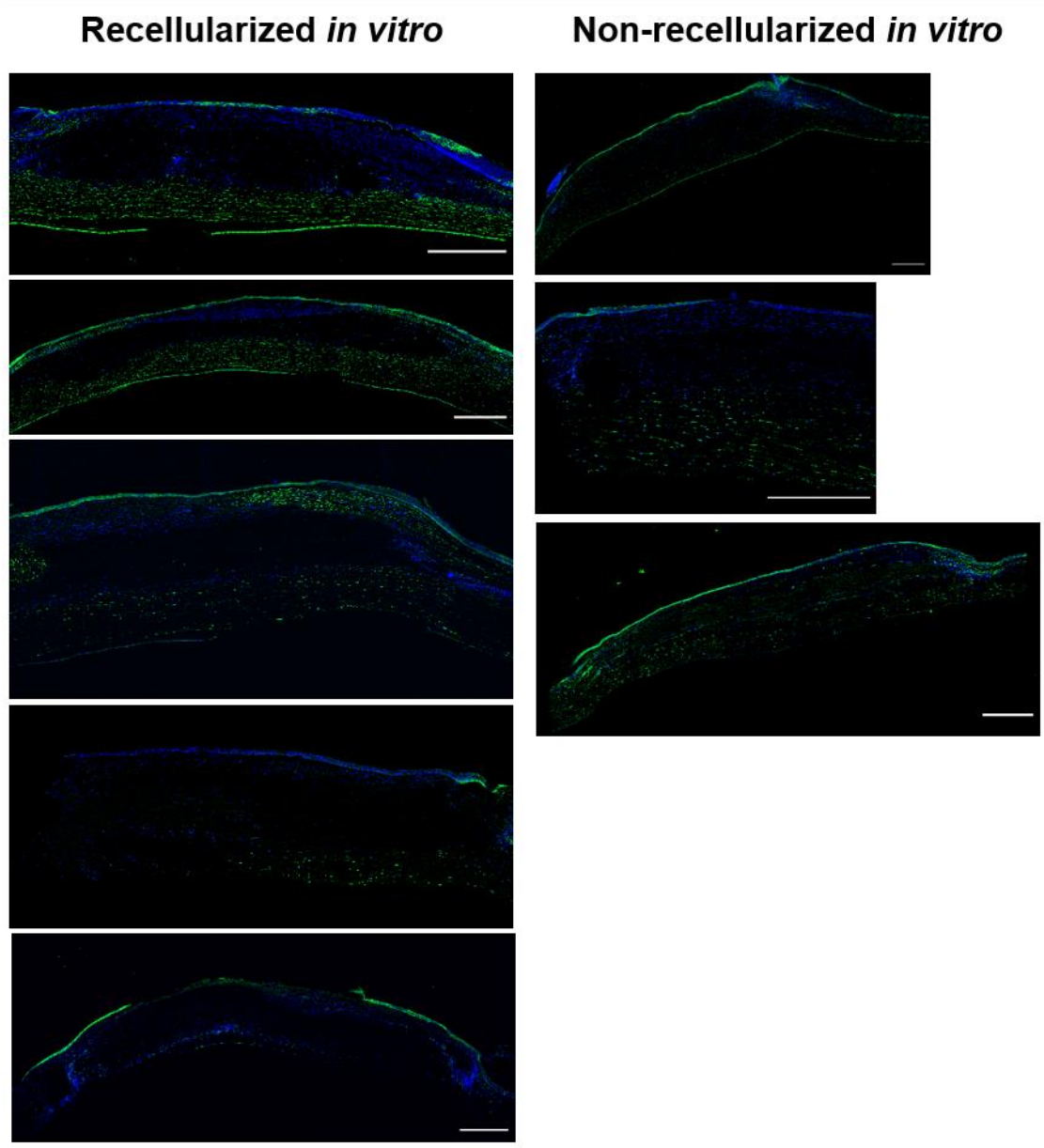

Figure A-8-4. Immunostaining against ALDH1A1 of the implanted scaffolds 3 months post-surgery (scale bar = 500 μm).

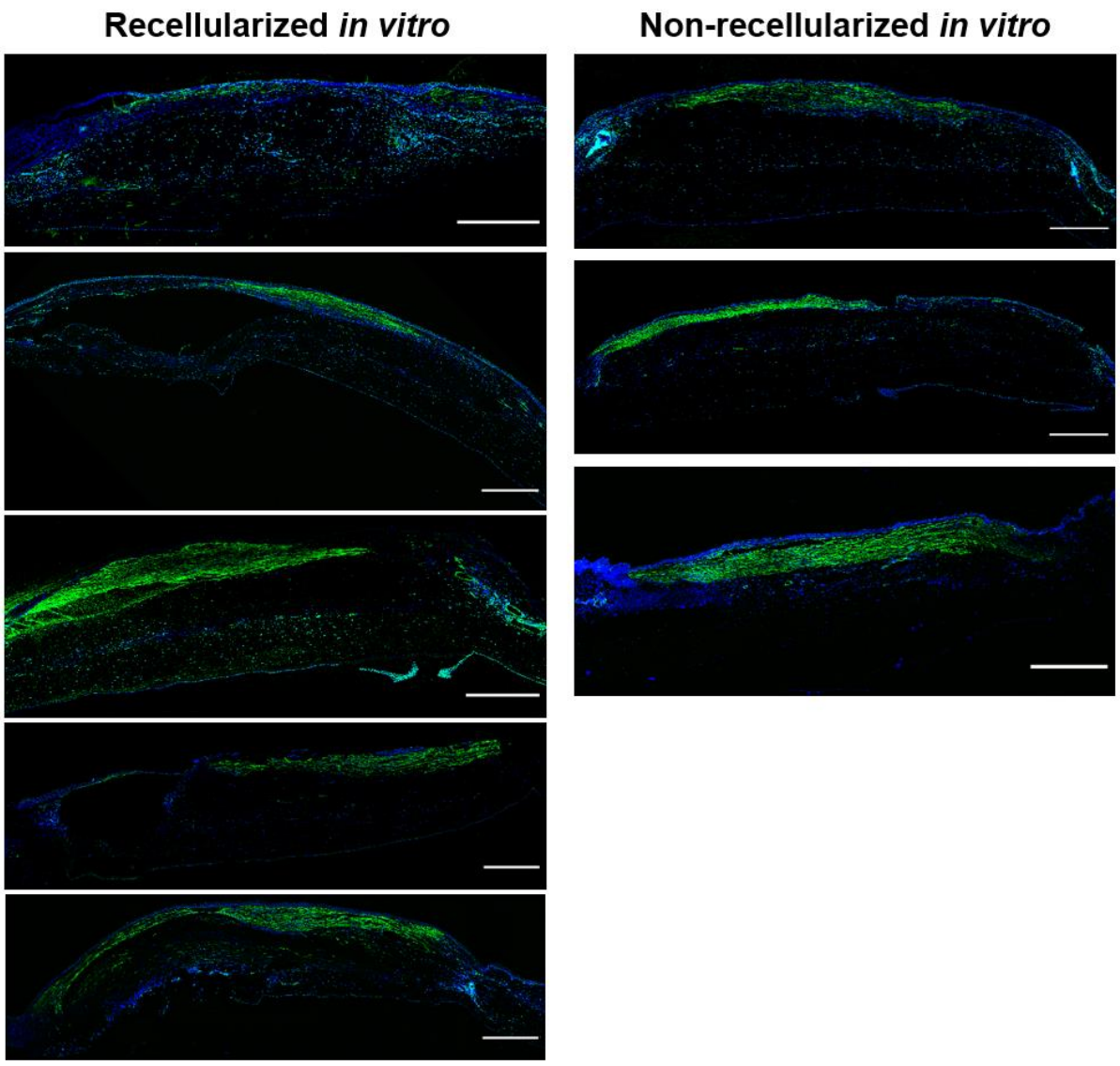

Figure A-8-5. Immunostaining against α-SMA of the implanted scaffolds 3 months post-surgery (scale bar = 500 μm).

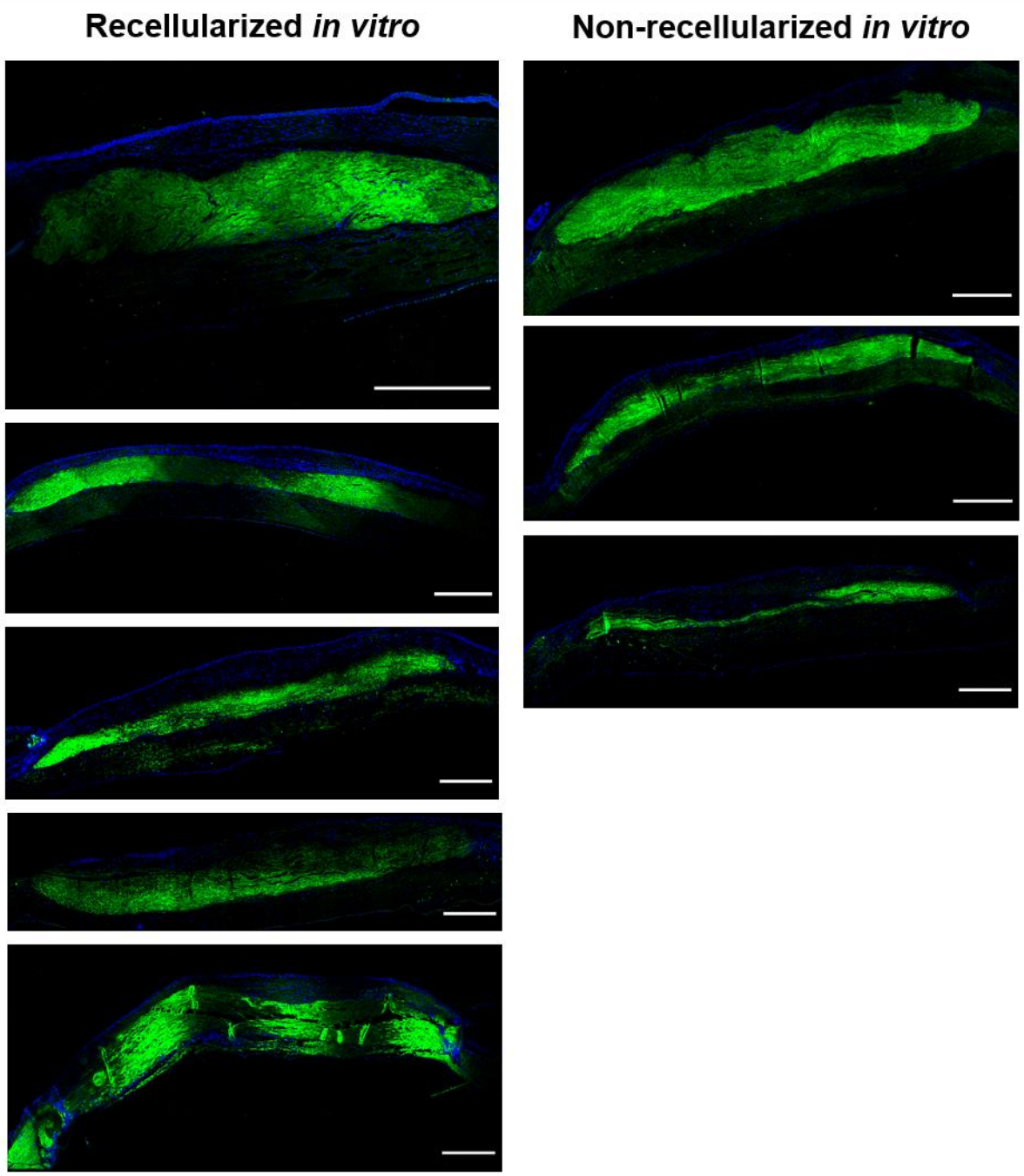

Figure A-8-6. Immunostaining against collagen I of the implanted scaffolds 3 months post-surgery (scale bar = 500 µm).

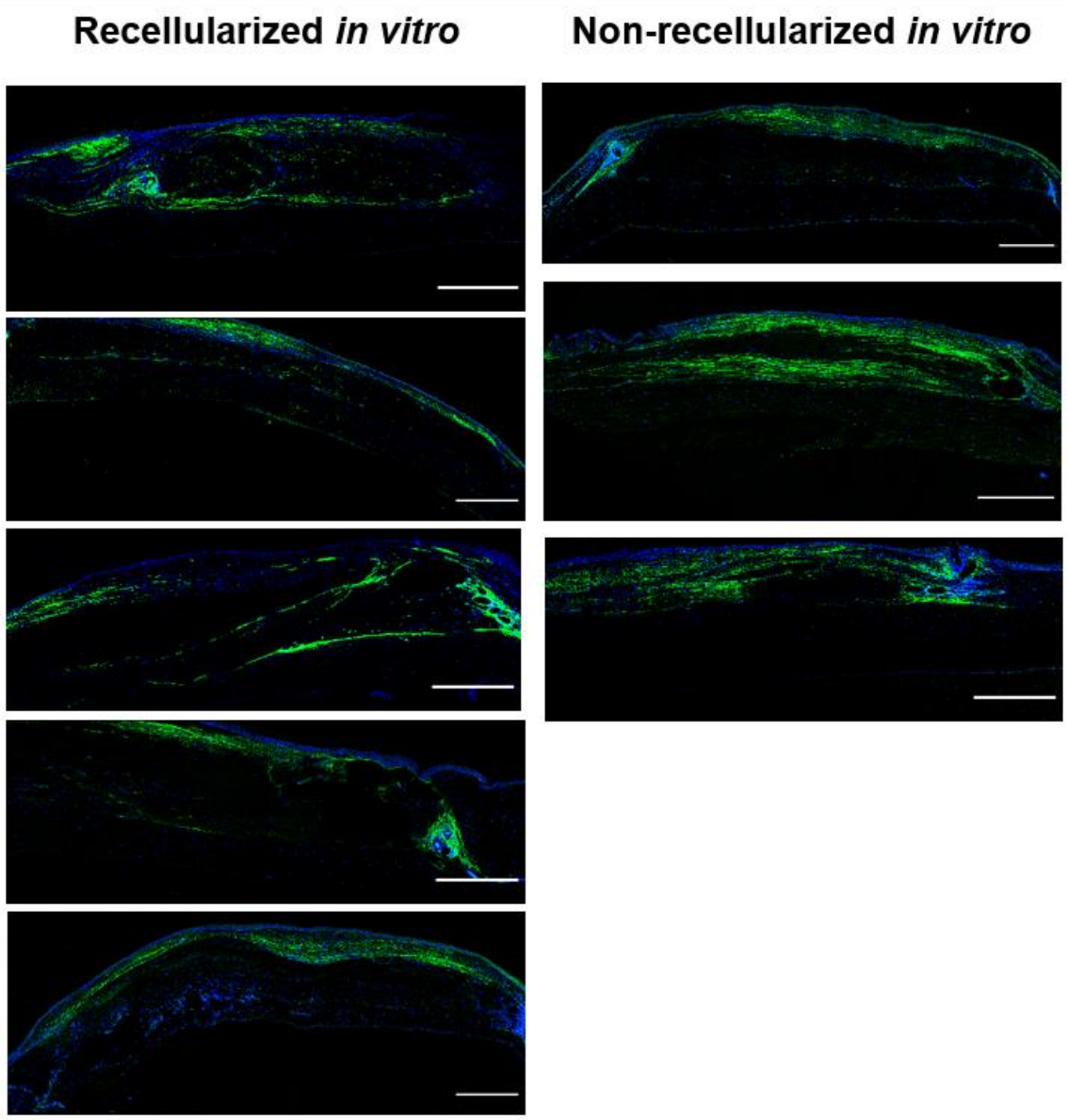

Figure A-8-7. Immunostaining against collagen III of the implanted scaffolds 3 months post-surgery (scale bar = 500 µm).

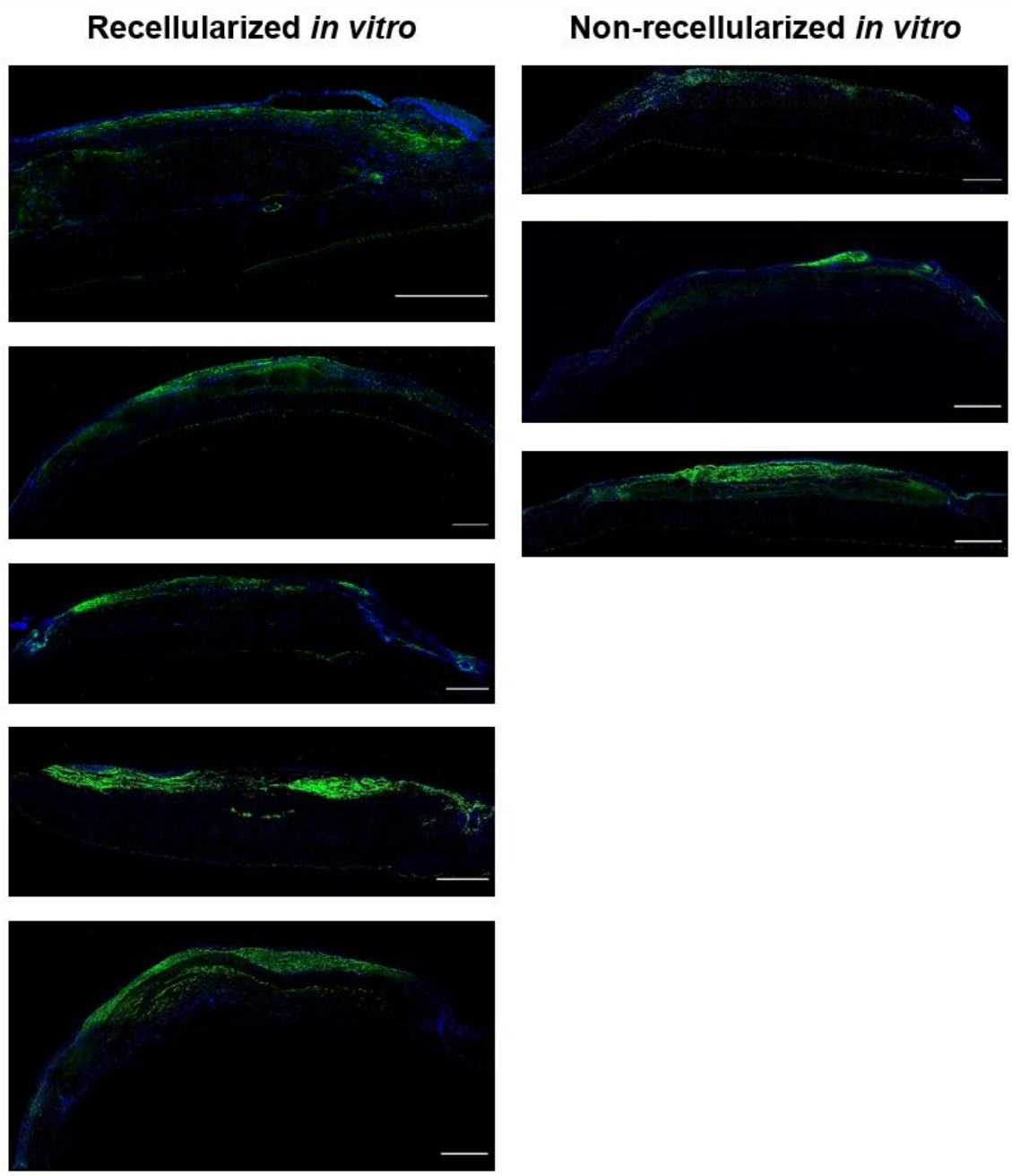

Figure A-8-8. Immunostaining against fibronectin of the implanted scaffolds 3 months post-surgery (scale bar = 500 µm).

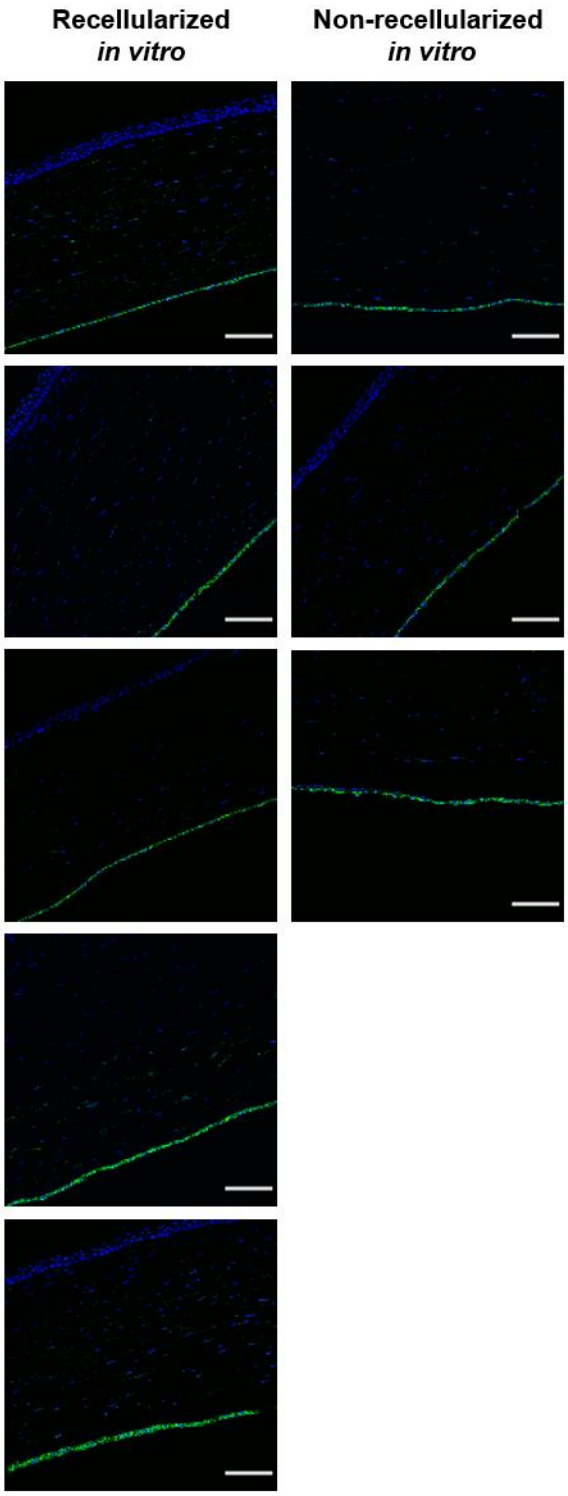

Figure A-8-9. Immunostaining against aquaporin 1 of the implanted scaffolds 3 months post-surgery (scale bar = 100 μm).

C. Quantification of residual SDS in scaffolds

MBAS assay was performed with some modifications from previously described methods. A methylene blue (Sigma-Aldrich) solution was prepared in water to a final concentration of 250 µg/ml. Freeze-dried scaffolds were weighed and rehydrated with 1 ml of distilled water and vortexed thoroughly for 1 minute. The scaffolds were macerated at room temperature for six hours and vortexed throughout. 250 µl of this supernatant was mixed with 250 µl methylene blue solution and vortexed. Then 1 ml of chloroform was added, vortexed 3 times for 30 seconds and centrifuged for 1 minute using a benchtop centrifuge. Serial dilutions from a 0.5% SDS solution were made and the process above performed on them to obtain a standard curve. A negative control was obtained using 250 µl distilled water. The absorbance of the bottom phase was measured at 665nm using a plate reader (BioTekTM Synergy HTX).

Table A-1. Residual SDS present in scaffolds measured by Methylene blue active substances (MBAS) assay.

% SDS (w/v)	µg SDS/mg tissue
0.0015 ± 0.00068	6.61 ± 0.93

D. Preliminary studies with endothelial cells

The use of decellularized porcine corneas as carriers for endothelial cells was investigated during a short stay at the Fondazione Banca degli Occhi del Veneto Onlus (Venice, Italy) financed by a Short Term Scientific Mission Scholarship from COST Action (BM1302). Endothelial cells were isolated from research graded human corneas as previously described (Parekh et al., 2017; Peh et al., 2011), by incubating the stripped Descemet's membrane in collagenase 1. These were directly seeded on the posterior surface of decellularized porcine corneas and cultured for 3 weeks. After the culturing period samples were stained for cell viability (Calcein-AM and Hoechst 33342) and imaged, they were then fixed in 4 % PFA, cryosectioned and stained with DAPI. Round, not yet attached cells could be seen immediately after seeding, while cells attached and spread after two days in culture (Figure A-11 A). Cultured cells showed high cell viability after 7 days in culture (Figure A-11 B). Using standard histology techniques, cell nuclei could be seen forming a monolayer on the surface of the scaffold (Figure A-11 C).

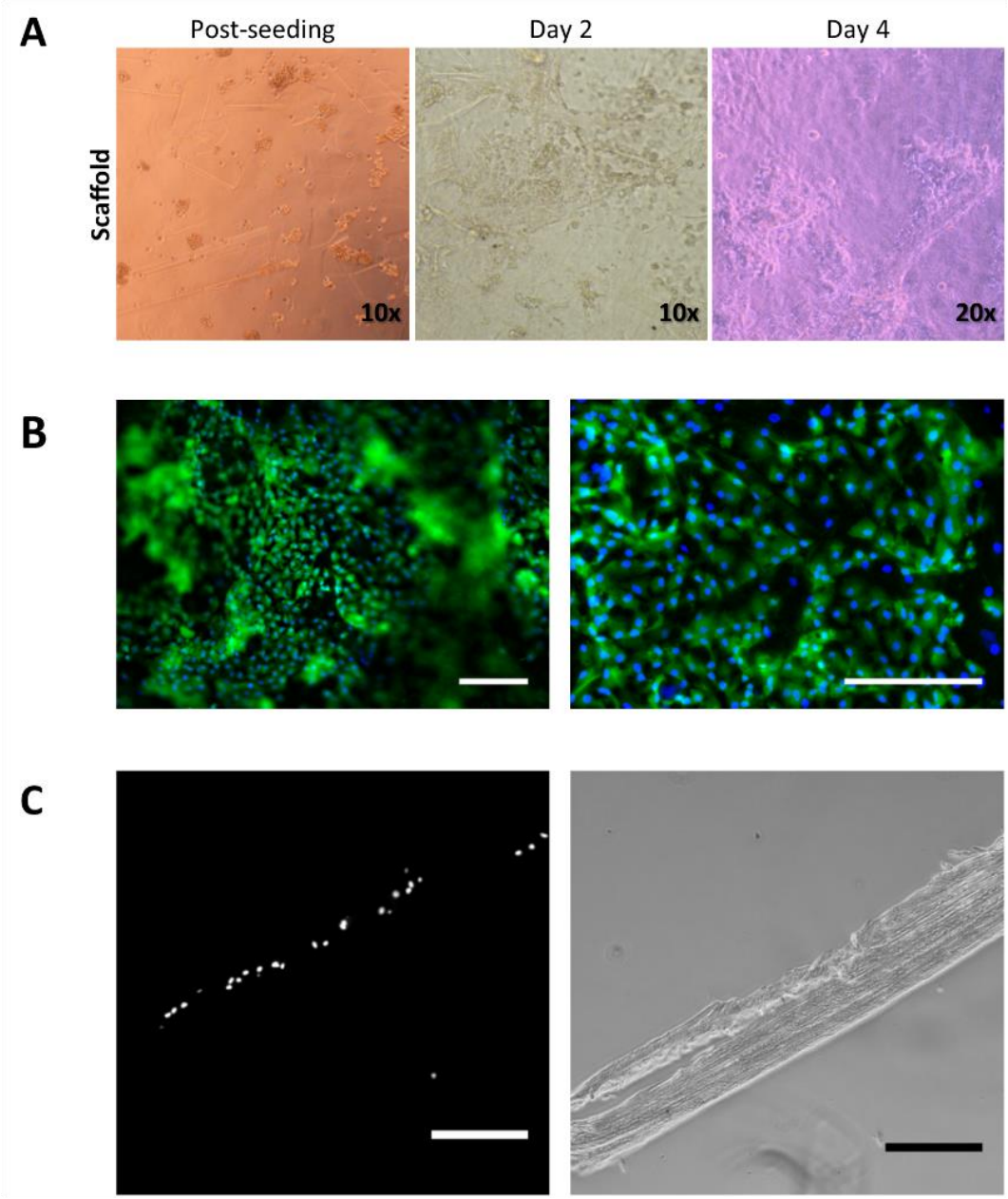

Figure A-8-10. Endothelial cells on scaffolds. A) Bright field images, B) Life-dead imaging after 7 days in culture, C) DAPI staining and bright field imaging of cryosections of samples cultured for 7 days (scale bar = 200 µm).

Methods 171 (2020) 86–96

Contents lists available at ScienceDirect

Methods

journal homepage: www.elsevier.com/locate/ymeth

Decellularization and recellularization of cornea: Progress towards a donor alternative

Julia Fernández-Pérez[a,b], Mark Ahearne[a,b,*]

[a] Dept of Mechanical and Manufacturing Engineering, School of Engineering, Trinity College Dublin, University of Dublin, Ireland
[b] Trinity Centre for Biomedical Engineering, Trinity Biomedical Science Institute, Trinity College Dublin, University of Dublin, Ireland

ARTICLE INFO

Keywords:
Decellularization
Cornea
Tissue engineering
Keratoplasty
Eye

ABSTRACT

The global shortage of donor corneas for transplantation has led to corneal bioengineering being investigated as a method to generate transplantable tissues. Decellularized corneas are among the most promising materials for engineering corneal tissue since they replicate the complex structure and composition of real corneas. Decellularization is a process that aims to remove cells from organs or tissues resulting in a cell-free scaffold consisting of the tissues extracellular matrix. Here different decellularization techniques are described, including physical, chemical and biological methods. Analytical techniques to confirm decellularization efficiency are also discussed. Different cell sources for the recellularization of the three layers of the cornea, recellularization methods used in the literature and techniques used to assess the outcome of the implantation of such scaffolds are examined. Studies involving the application of decellularized corneas in animal models and human clinical studies are discussed. Finally, challenges for this technology are explored involving scalability, automatization and regulatory affairs.

1. Introduction

The cornea is the outer most structure of the eye. It is comprised of three main cellularized layers, the epithelium, the stroma, and the endothelium. The corneal epithelium consists of stratified epithelial cells whose main function is to act as a barrier to protect the inner corneal layers [1]. Limbal epithelial stem cells that reside in the Palisades of Vogt, between the sclera and the cornea, replenish the epithelial cell population [2]. The stroma is the thickest part of the cornea and is comprised of extracellular matrix (ECM) populated by keratocytes and consisting of collagen type I and lesser amounts of collagen type V, glycosaminoglycans (GAGs) and proteoglycans, such as decorin, lumican and keratocan [3–7]. The endothelium consists of a monolayer of hexagonal cells with limited regenerative capabilities. These cells pump fluids from the stroma to the aqueous humour to maintain water homeostasis and are responsible for transporting nutrients to the avascular cornea [8,9].

It is estimated that 10 million people worldwide have bilateral corneal blindness [10]. Severe cases can only be treated by a corneal transplant, or keratoplasty. Despite cornea being an immune privileged organ due to its avascular nature, corneal transplants can undergo graft rejection, which is the most common cause of transplant failure for corneas [11,12]. In a recent global survey it was determined that there is only one cornea available for every 70 needed, which highlights the severe donor shortage of such a tissue [13]. It is for these reasons that there has been a lot of interest in corneal bioengineering as an approach to generate transplantable tissues.

Tissue bioengineering aims to overcome donation shortages and immune rejection by fabricating organs in the lab with patient-specific cells. Traditional tissue engineering is based on the interplay between cells, the fabrication of biocompatible scaffolds and the application of external stimuli including mechanical, chemical or biological stimuli. In the field of corneal tissue engineering, multiple biomaterials are being investigated [14]. Collagen-based materials are the most common as collagen is the most abundant component of the corneal stroma. These have been fabricated as highly-hydrated hydrogels [15,16], plastically compressed matrices [17,18] and membranes by vitrification [19]. Other natural polymers such as chitosan [20,21], silk fibroin [22–24], fibrin [25,26] and self-assembling peptides [27] have also been investigated. 3D bioprinting, a revolutionary technique, has also been used to fabricate corneas using bioinks [28,29]. While these studies have produced some promising results, these materials lack the biochemical composition of the real cornea and fail to replicate the cornea fibril arrangements and ECM architecture. Techniques such as 3D bioprinting [28,29] or electrospinning [30,31] have the potential to generate scaffolds with similar shape and structure to real cornea but these

* Corresponding author at: Dept of Mechanical and Manufacturing Engineering, School of Engineering, Trinity College Dublin, University of Dublin, Ireland.
E-mail address: ahearnm@tcd.ie (M. Ahearne).

https://doi.org/10.1016/j.ymeth.2019.05.009
Received 12 February 2019; Received in revised form 9 May 2019; Accepted 10 May 2019
Available online 22 May 2019

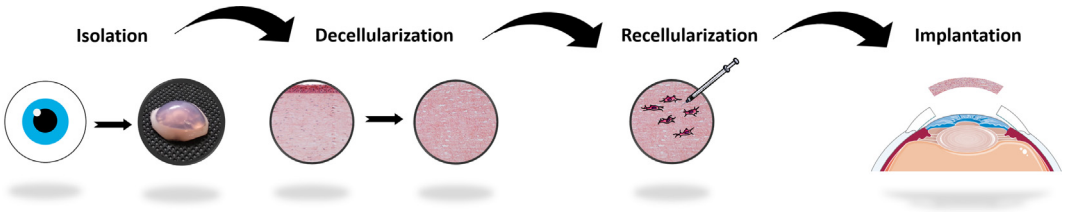

Fig. 1. General workflow for the use of decellularized corneas as donor alternatives.

still do not replicate the composition. Hydrogels derived from corneal ECM have also been developed that maintain much of the cornea's ECM but often lack its fibril organization [32–34]. Scaffold-free approaches where cells secrete their own ECM and create a tissue *in vitro* have been reported too [35–37] but these are costly and take months to obtain. Therefore the use of decellularized corneas as a scaffold for corneal engineering is attractive since both the fibril architecture and corneal composition can be accurately mimicked. The process involves isolating the donor tissue, removing cells, adding new healthy cells and implanting into a patient (Fig. 1).

2. Decellularization of the corneas

Decellularization is a process that aims to remove cells from organs or tissues resulting in a cell-free scaffold consisting of the tissue's own ECM. Cell removal reduces graft rejection by depleting the scaffolds from major histocompatibility complexes. Insufficient decellularization has been shown to illicit polarization of macrophages to an M1-phenotype *in vivo* and *in vitro* [38]. Furthermore, cellular components that have not been removed can be bound by immunoglobulins and complement proteins which will activate macrophages and B lymphocytes [39]. In the last decade a wide range of organs have been decellularized including heart [40,41], kidney [42], liver [43–45], lung [46–49] or pancreas [50]. In this section different techniques used to remove cells and cellular components from the cornea will be explored. All decellularization techniques can be categorized into three types of methods: physical, chemical and biological methods. A summary of these methods can be found in Table 1. However, it should be noted that most decellularization protocols combine several methods and techniques.

Table 1
Summary of the decellularization methods reviewed.

Decellularization methods	Refs.
Physical methods	
Agitation	n.a.
Freeze-thawing	[34,53–56]
Electrophoresis	[57,58]
High hydrostatic pressure	[59–61]
Supercritical CO_2	[61,62]
Lyophilization	[67–69]
Chemical agents	
Sodium dodecyl sulphate (SDS)	[69–75]
Sodium deoxycholate	[55,76]
Triton X-100	[77–81]
Peracetic acid	[85]
Formic acid	[86]
Ammonium hydroxide	[77,87]
Sodium chloride (hypertonic)	[53,65,73,81,90–94]
Ethylenediaminetetraacetic acid (EDTA)	[53,75,80]
Biological agents	
Trypsin	[53,68,80,97–98]
Dispase	[53,80,92,96]
Phospholipase A_2	[67,99–101]
Human serum	[57,58]
Nucleases (DNAse and RNAse)	[55,72,76,103–106]

2.1. Physical methods

Some form of mechanical agitation is present in most decellularization protocols and mostly carried out using orbital shakers or rotators to promote the flow of decellularizing agents through the ECM. For example, Nara and colleagues have described the use of a direct perfusion chamber that applied detergents in a continuous unidirectional flow [51]. The use of automatized devices that allow both mechanical agitation and fluid exchange, such as the one described by Pellegata and colleagues to decellularize blood vessels, offers great promise to speed up the process and ensure sterility [52].

A simple method of decellularization is using repeated freeze-thaw cycles where cells are lysed due to the formation of ice crystals. This is usually followed by rinsing or the addition of another decellularization method to ensure removal of cell debris [34,53–56]. Temperatures used for the freeze-thawing cycles range from −20 °C to −197 °C with the use of liquid nitrogen. Another method is the use of electrophoresis, which has been reported in the literature as a final step to remove debris [57,58] but is not a widespread method. The use of high hydrostatic pressure has been shown to reduce DNA and maintain glycosaminoglycan (GAG) levels in decellularized porcine corneas [59–61]. This method is not used commonly as the equipment needed is expensive [62]. Li and colleagues have recently reported on the use of ultrasound in conjunction with freeze-thawing and nucleases for the decellularization of porcine corneas [56].

Decellularization using supercritical CO_2 was first used by Sawada and colleagues for vascular tissues [63]. This technique is based on the high permeability and transfer rate characteristic of supercritical fluids. Carbon dioxide can be used as a critical fluid under moderate conditions (T_C = 32 °C, P_C = 7.38 MPa) and after the procedure there are no remnants as the gas can diffuse out easily. Bovine [64] and porcine corneas [65] have also been recently decellularized using this method with good initial results. Furthermore, this technique can be used to sterilize the tissue simultaneously [66].

While not strictly a decellularization method, lyophilisation has been used by researchers to obtain more porous scaffolds as water in the decellularized cornea becomes frozen and then removed by sublimation once a vacuum is applied. With this approach the repopulation by neighbouring cells is thought to increase although the process would likely disrupt the cornea's collagen architecture [67–69].

2.2. Chemical agents

The use of detergents is the most common method for corneal decellularization. The most widely used is the ionic detergent sodium dodecyl sulphate (SDS) [69–75]. While extremely effective, SDS can disrupt the ECM as it is a denaturing agent. Therefore other milder detergents are being explored such as sodium deoxycholate [55,76]. Non-ionic detergents, such as Triton X-100, are less effective but in turn less disruptive [77–81]. Zwitteronic detergents have characteristics of ionic detergents, as they have positive and negative functional groups, and non-ionic detergents, as their net charge is zero. However, these detergents have been used unsuccessfully for cornea decellularization [78].

Organic acids have also been used to decellularize corneas.

Peracetic acid has widely been used to decellularize and terminally sterilize urinary bladder and small intestine submucosa by the Badylak lab [82–84], and Ponce Márquez reported the use of it for the cornea with suboptimal results [85]. Mild acids commonly found in nature, such as acetic, formic and citric acids, have been recently employed for porcine cornea decellularization. Formic acid at a 30% concentration showed the best results in terms of DNA removal, and sulfated GAG (sGAG) and collagen retention [86]. Bases are less used than acids and only ammonium hydroxide appears in the literature for corneal decellularization [77,87] while sodium hydroxide has been used to decellularize lungs and heart valves [88,89].

Hypertonic solutions, especially sodium chloride at concentrations of 1.5 or 2 M, have been used by multiple research groups with positive outcomes in terms of transparency, cell removal and retention of ECM components [53,65,73,81,90–94]. When combined with a washing step using 0.2% Triton X-100 the best results were achieved [81,94].

Other chemicals used to decellularize corneas include alcohols, such as ethanol, and chelating agents, such as Ethylenediaminetetraacetic acid (EDTA). Ponce Márquez and colleagues used 75% ethanol following a protocol originally described to decellularize arteries [85,95]. EDTA is commonly used in conjunction with trypsin as it helps disrupt cell–cell interactions by sequestering calcium present in cadherin junctions [53,75,80].

2.3. Biological agents

Several enzymes have been used in the literature to decellularize corneas. Trypsin and Dispase II are cell dissociating proteins commonly used for cell isolation. If used for longer periods or at higher concentrations, they can result in cell lysis [53,68,80,92,96–98]. Phospholipase A_2 (PLA_2) is an esterase that breaks the phospholipids present in the cell membrane and has been shown to remove cell components successfully with minimal ECM disruption [67,99–101]. Another biological agent is human serum which has been used to decellularize blood vessels [102] and corneas alongside the use of electrophoresis [57,58]. Most studies include an additional step of incubation with nucleases to assist with the degradation of DNA released following cell lysis [55,72,76,103–106].

2.4. Confirmation of decellularization

There is no current consensus to validate the success of a decellularization protocol. In general, the decellularization procedure should remove exogenous cells, and cell debris, including DNA, RNA and other cell remnants such as mitochondria, while minimally disrupting the ECM. To verify the removal of nuclei and cellular components three parameters should be examined [107]. The first parameter involves staining with Haematoxylin and Eosin (H&E) and/or 4′,6-diamidino-2-phenylindole (DAPI) to demonstrate absence of intact cell nuclei. Next dsDNA is quantified via Hoechst 33,342 binding or via PicoGreen™ (Invitrogen) assay. This should give values of below 50 ng of dsDNA per mg of dry weight [108]. Finally the maximum length of DNA remnants should be 200 bp determined via agarose gel electrophoresis [39,108].

While these parameters will determine the presence of cellular components, it is important that the decellularization process also maintains the cornea's structure, composition and transparency to allow the scaffold to retain its function. ECM can be analysed using standard histological stains such as Picrosirius Red, to stain collagen fibers, or Alcian Blue, to visualize GAGs. These parameters can also be quantified using biochemical assays such as hydroxyproline reagent to quantify collagen [109,110] or dimethylmethylene blue assay to quantify GAGs [111]. Immunohistochemistry can be used to identify specific ECM components such as the type of collagen present or specific proteoglycans and GAGs. Second harmonic generation imaging can be used as a non-destructive technique to give information on collagen fiber orientation and identify damage to the collagen during decellularization [112]. Electron microscopy offers a great deal of ultrastructure detail, especially in the cornea where the precise arrangement of collagen bundles determines the optical properties of the tissue. Both SEM and TEM require highly specialized and expensive equipment, only available in big universities and research centres.

Unlike most other tissues and organs, the transparency of scaffolds is an important parameter that needs to be considered for corneal tissue engineering. The optical characteristics of decellularized corneal scaffolds can be easily quantified using a simple spectrophotometer (or plate reader). The absorbance at different wavelengths in the visual spectrum of light provides information on the clarity or opacity of a scaffold. The mechanical properties of decellularized cornea also need to be sufficient to allow suturing and withstand any applied forces. Minimizing disruption to the ECM during decellularization should allow the mechanical characteristics of the cornea to be maintained. Furthermore, the use of osmoregulators such as dextran or glycerol can aid on palliating swelling and thus recovering transparency and increasing tissue stiffness and strength [104,113].

2.5. Species used for corneal decellularization

Porcine corneas have been the most extensively studied for decellularization mainly due to their availability and anatomical similarities with the human cornea. However, porcine cells present several epitopes that are extremely immunogenic to humans such as Galactose-alpha-1,3-galactose (α-Gal) and N-glycolylneuraminic acid (Neu5Gc). Insufficient cell removal could elicit an immune response that could lead to graft rejection. It is therefore recommended to perform immunostaining against these epitopes to ensure their absence in the scaffolds. As reviewed by Kim and Hara [114], the thickness of the porcine cornea varies greatly with age and breed, which highlights the need of standardisation. By breeding animals specifically for organ decellularization and transplantation in quarantined animal facilities, heterogeneity from batches can be monitored and brought to a minimum. In addition, with the advent of genetic engineering, pure xenogenic transplantation could become a reality, with the use of so-called "humanized" pigs. Two main hurdles have to be overcome in order to use pig corneas for transplantation as if they were human: the removal of multiple xenoreactive cell surface molecules and porcine endogenous retroviruses (PERV). The use of CRISPR-Cas9 has been shown to be successful in obtaining triple knockout strains of pigs lacking GGTA1, CMAH, and β4GalNT2, genes important for the presence of immunogenic surface glycans [115–117]. This same genome editing technique has been used to remove PERVs *in vitro* to obtain PERV-inactivated pigs [118]. Other species that have been used to fabricate decellularized corneal scaffolds include cat [101], ostrich [119], bovine [85,120] goat [51] or dog [121].

Human corneas have been used in decellularization experiments [72–74,87]. While the use of human tissue does not have to face the same challenges of xenogenic tissues, the availability of such tissues is scarce. However, corneas deemed unsuitable for corneal transplantation due to low endothelial cell count could be used to obtain decellularized scaffolds [122]. Furthermore, recent studies have focused on the use of discarded tissue after refractive surgeries as an alternative source [73,123]. In this case, thinner tissues are decellularized which facilitate the removal of cellular components, compared to whole corneas.

2.6. Optimal parameters for decellularization

It is difficult to determine the optimal technique for decellularizing cornea due to the different researchers obtaining differing results despite using similar protocols. A number of papers have directly compared different decellularization techniques on cornea to determine the optimal technique. Shafiq et al., (2011) compared several different techniques and found that a combination of sodium chloride and

nucleases was the best option for removing cellular components while still supporting the growth of new cells [103]. Wilson et al., (2016) compared hyperionic, ionic and non-ionic detergents and concluded that increasing the efficiency of cell removal led to increased ECM damage [91]. For this reason it is still difficult to identify one specific methods that is closer to use in clinical practice.

In addition to the decellularization efficiency of these techniques, issues associated with gaining regulatory approval for clinical translation of corneas subjected to each technique has to be considered. For example, the use of detergents and nucleases may provide a barrier to the cornea's clinical use since there is a risk that any residual chemical could have a negative effect post-implantation. Non-chemical techniques may be more beneficial for gaining clinical approval but can be more expensive to operate.

3. Recellularization of the cornea

Once the removal of exogenous cells has been confirmed, it may be beneficial to repopulate these matrices with human cells to generate a viable cornea. The origin of the cells used for scaffold recellularization is an important issue to take into account. For every cell type found in the cornea, there are several potential sources of cells that can be used for recellularization (Table 2), with benefits and drawbacks associated to each of them. There are reports of decellularized matrices being repopulated using immortalized cell lines [55,76,93] and while such cell types are acceptable for *in vitro* studies as a proof of concept, these should not be acceptable for transplantation. Cells modified to be passaged *ad infinitum* pose the risk of tumour formation [124]. Therefore, it is advisable to only use primary cultivated cells. This requires the initial isolation of cells from the patient or donor, further expansion in the laboratory, seeding of these cells onto the scaffold, culture/maturation of the newly cellularized organ and implantation into the patient. Recellularization of perfused organs such as the heart or the lungs have used the endogenous vasculature to reintroduce cells [125], however the cornea, being an avascular organ, relatively thin and containing 3 different cell types needs to be recellularized using other approaches.

3.1. Stroma

For the repopulation of the corneal stroma, autologous corneal stromal cells can be obtained from a small biopsy from the contralateral eye. Since these cells are from the patient, they are less likely to illicit an immune response. If both eyes are compromised, alternatives have to be found. Since the cornea is avascular, it is often considered to be an "immune privileged" organ so allogenic cells could be used with less risk of rejection compared to other organs. Alternatively a number of studies have examined the use of autogenic cells but from an extraocular source. Since keratocytes originate from the neural crest mesenchyme, other mesenchymal tissues have the potential to be differentiated into keratocytes. Mesenchymal stem cells derived from adipose tissues have been successfully induced to express corneal keratocyte markers such as ALDH3A1, keratocan, lumican and decorin [126–130]. Adipose-derived MSC have been used clinically as a cell therapy without a scaffolding material [131] and seeded onto decellularized human corneal stroma sheets [74]. The differentiation of induced pluripotent stem cells (iPSC) into keratocyte-like cells has been reported in the literature [132]. iPSCs were differentiated into neural crest cells and cultured on cadaveric human corneas into which the cells migrated and adopted a similar phenotype to keratocytes. This technique offers the opportunity for autogenic cell transplantation. There have been reports of oncogenic transformation of iPSCs [133] so the use of such cells for the treatment of low risk corneal diseases might not be recommended.

The stroma is the thickest layer of the cornea consisting of densely packed collagen fibrils. This structure makes it difficult for cells to penetrate and recellularize after decellularization. One approach to overcome this problem is to inject cells directly into the stroma, however the optimal procedure for doing this is unclear. Cell seeding densities, volume per injection and number of injections vary between publications with values for the final injected volume ranging from 12 µl in 2 µl injections [76] to 1 full ml in a single injection [69,79,134]. In addition, during decellularization tissues swell significantly making it difficult to inject more liquid [104]. The number of cells seeded ranges in the literature from only 1200 and 4500 cells per construct [55,76] up to $1x10^5$, $4x10^5$ and $5x10^5$ cells [79,103,134]. It is noteworthy that in multiple publications the final number of seeded cells is difficult to determine [72,75]. Furthermore, injections can disrupt the stromal fibril architecture and result in permanent damage [125].

The simplest method to recellularize the stroma is to seed cells directly on the surface of the decellularized scaffold. This approach relies on the capacity of the cells to migrate into deeper regions of the stroma. González-Andrades and colleagues showed repopulation of NaCl-decellularized porcine corneas with human keratocytes which were distributed similarly to the native counterparts [92]. More recently, Alió del Barrio *et al.* reported recellularization of 120 µm thick decellularized laminas with adipose-derived MSCs for 24 h before implantation [74]. The authors did not shown the distribution of these cells on the scaffold. In addition, freeze-drying have been use to induce the formation of pores to increase the depth that cells can penetrate and repopulated the corneas *in vitro* [69].

While not commonly used for cornea, there are reports of bioreactors being used to aid in repopulating decellularized corneas with cells or as a culture method after initial seeding. Fu and colleagues used a magnetic stirrer to keep the construct in suspension during the culture period [79]. The use of a rotary cell culture system for repopulating purposes has also been described in the literature, whereby the cells are encouraged to colonize the scaffold as they cannot attach elsewhere [135]. A more sophisticated bioreactor system has been reported for the repopulation of the epithelium which mimicked and *in vivo* air–liquid interface [100].

Another strategy is to recellularize the scaffolds *in situ* during transplantation. Ma and colleagues describe a method by which cells were seeded on thin sheets of decellularized porcine cornea as they were being placed on the bed of a lamellar keratoplasty [90]. The procedure was repeated so that five layers had been deposited. When compared to the sheets without cells or a thicker acellular tissue, the recellularized sheets showed better results in terms of transparency and overall transplant success.

3.2. Epithelium

The corneal epithelium is constantly undergoing renewal from limbal derived stem cells [2]. If the limbus is damaged and the stem cells are lost, the patient can develop Limbal Stem Cell Deficiency (LSCD), resulting in conjunctivalization and neovascularization of the

Table 2
Potential cell sources for cornea recellularization.

Cornea layer and cell source	Refs.
Epithelium	
Limbal stem cells from unaffected contralateral eye biopsy	[137]
Oral mucosa	[138,139]
iPSCs	[140]
Stroma	
Keratocytes/Corneal Fibroblasts	[55,76,90,92,103]
Adipose-derived MSC	[74,126–129,131]
iPSCs	[132]
Endothelium	
Human endothelial cells	[77]
Human immortalized endothelial cells	[93]
iPSCs	[144]

Table 3
Summary of *in vivo* studies using decellularized corneas (SDS: sodium dodecyl sulfate, SDC: sodium deoxycholate, ALK: anterior lamellar keratoplasty, Y: recellularized, N: not recellularized).

Origin of cornea	Decell type	Details of decell	Surgical procedure	Recipient species	Cells (Y/N)	Details about cells	Refs.
Porcine	Physical	Nitrogen gas	Intrastromal pocket	Rabbit	N	–	[148]
Porcine	Chemical + Physical	SDS + sodium orthovanadate	ALK	Rabbit	Y	Human immortalized stromal cells injected and cultured for 3 days prior to implantation	[55]
Porcine	Chemical + Biological	Triton, Dispase + Trypsin	Intrastromal pocket	Rabbit	N	–	[80]
Porcine	Physical	High hydrostatic pressure	Intrastromal pocket	Rabbit	N	–	[60]
Porcine	Chemical	SDS	Intrastromal pocket	Rabbit	N	–	[69]
Porcine	Chemical	SDS	Intrastromal pocket	Rabbit	N	–	[70]
Porcine	Chemical	Phospholipase A2	Interlamellar keratoplasty	Rabbit	N	–	[67]
Porcine	Chemical	SDS	Intrastromal pocket	Rabbit	N	–	[71]
Porcine	Chemical	SDS	Intrastromal pocket	Rabbit	N	–	[105]
Porcine	Chemical	NaCl + Triton X-100	Intrastromal pocket and ALK	Rabbit	Y	Rabbit amniotic epithelial cells for ALK cultured for 1 week before implantation	[81]
Human	Chemical	SDS	Intrastromal pocket	Rabbit	Y	Adipose-derived MSC injected into the stroma and cultured 5 days before implantation	[72]
Porcine	Physical	High hydrostatic pressure	ALK	Rabbit	N	–	[106]
Porcine	Chemical	NaCl	Intrastromal pocket	Rabbit	Y	Keratocytes in suspension sandwiched between sheets of decellularized tissue during surgery	[90]
Human	Chemical	SDS	Intrastromal pocket	Rabbit	N	–	[73]
Porcine	Physical	High hydrostatic pressure	Intrastromal pocket	Rabbit	N	–	[59]
Porcine	Chemical	SDC + sodium orthovanadate	ALK	Dog	Y	Human epithelial and stromal cells	[76]
Human	Chemical	SDS	Intrastromal pocket (advanced keratoconus)	Human	Y	Human adipose-derived MSC cultured for 24 h prior to implantation	[74]
Porcine	Physical	High hydrostatic pressure	Intrastromal pocket	Rabbit	N	–	[61]
Porcine	Chemical	NaCl + Triton X-100	ALK (fungal ulcers)	Human	N	–	[94]
Porcine	Biological	Phospholipase A2	ALK	Rabbit	N	–	[99]
Cat	Chemical + Biological	Phospholipase A2 + SDC	Tectonic ALK	Rabbit	N	–	[101]
Porcine	Chemical	Glycerol + EDC/NHS crosslinking	ALK in infectious keratitis model	Rabbit	N	–	[164]
Porcine	Biological + Physical	Human serum + electrophoresis	Intrastromal pocket	Rabbit	N	–	[57]
Porcine	Biological + Physical + Chemical	Trypsin + freeze-thawing + NaOH	ALK	Rabbit	N	–	[68]
Porcine	Chemical	NaCl + Triton X-100	ALK (herpes simplex keratitis)	Human	N	–	[163]

cornea [136]. If the contralateral eye is not affected, a small biopsy can be taken and limbal stem cells can be isolated and expanded. These cells can then be transplanted onto the diseased cornea and replenish the stem cell niche [137]. If both eyes are affected, allogenic cells or cells from the same patient but from an extraocular source, such as the oral mucosa, can be used [138,139]. An alternative autogenic cell source are iPSCs differentiated into limbal epithelial stem cell-like cells [140].

Decellularized corneas have been repopulated *in vitro* with epithelial cells, which rapidly attach and form a multi-layered epithelium, typically expressing cytokeratin 3 and 12 [69,80,134]. Better results have been reported when using a construct based on a decellularized porcine cornea repopulated with stromal and epithelial cells compared to the acellular construct in a one year anterior corneal transplant model in dogs [76]. However, in this study a group with only stromal cells was not included and the implanted cells were not labelled, therefore the healthy epithelium was probably from the host. It is noteworthy, however, that results in the literature are inconclusive as to *in vitro* re-epithelialization of decellularized matrices before implantation in defects of the central cornea. Luo and colleagues seeded amniotic epithelial cells onto decellularized scaffolds and implanted them into an alkali burn rabbit model [81]. When compared to an acellular scaffold, the pre-epithelialized construct was accepted better, probably due to the anti-angiogenic and anti-inflammatory factors secreted by the amniotic epithelial cells.

3.3. Endothelium

Corneal endothelial cells do not proliferate *in vivo* as they are arrested in the G_1 phase [141,142]. *In vitro*, however, endothelial cells can be isolated and expanded, and seeded onto carrier materials for transplantation. Multiple studies have investigated the optimization of culture conditions to promote proliferation and avoid endothelial-to-mesenchymal transition [143]. The use of these cells relies on donor corneas and can only be done with allogenic cells. As for keratocytes and epithelial cells, human corneal endothelial-like cells have been obtained from iPSCs that could potentially be used for implantation [144].

Attempts have been made to use decellularized corneas as carriers for endothelial cell transplantation [54,77,80,93,145,146]. Choi and colleagues decellularized 110 μm-thick sections of human corneas with Triton X-100 and NH_4OH and seeded them with human endothelial cells for 14 days [77]. The constructs expressed zonula occludens-1 (ZO-1), gap junction protein connexin-43 and Na^+/K^+-ATPase, markers of mature and functional corneal endothelium. Another study obtained decellularized sections using a femtosecond laser, seeded an endothelial cell-line and performed an *ex vivo* transplantation, demonstrating the potential for translation into the clinic [93]. An alternative approach has been to use trypsin-decellularized crystalline lens capsules as it is a tissue usually discarded during cataract surgeries [147].

3.4. Further remarks

While one would think that *in vitro* recellularization prior to implantation would be essential for positive outcome, there are several examples where the implantation of an acellular cornea has been successful [60,65,148,68,69,71,73,80,94,99,106]. Most of these studies evaluate their success in terms of low immune reaction, little or no vascularization and transparency recovery. It is important to note that the surgical procedure in these studies was an intrastromal pocket or an anterior lamellar keratoplasty, i.e. the endothelium remained undamaged. The repopulation of the acellular graft by host stromal cells is usually only assessed by simple histological staining and claims of infiltrating keratocytes are often inconclusive. Generally the epithelium is able to grow over the scaffolds with no major differences to the control, especially at the longer time-points. Other studies, however, show better results when comparing cell-containing scaffolds versus their acellular counterparts [55,72,76,81,90]. More studies need to be done to determine the necessity of recellularization, although eliminating the need for cells makes its potential translation to the clinic easier, with reduced costs and decreased risk of infection and disease transmission.

4. *In vivo* studies

While there has been considerable *in vitro* research undertaken to demonstrate the potential of decellularized and recellularized corneas as an alternative donor corneas for keratoplasties, the ultimate goal is to translate this research into the clinic to benefit patients. Prior to their use with patients, the cornea need to be tested in animal models *in vivo* to evaluate the host response to the implants. Following the successful outcome of animal models, a number of studies have recently entered clinical trials. This section will focus on the progress of decellularized corneas as transplants with the most up-to-date results of animal experiments and clinical data. A summary of *in vivo* studies undertaken is shown in Table 3.

4.1. Techniques used to assess outcome

Multiple techniques are used in *in vivo* experiments to assess the progress of an implant. These can be mainly divided into two groups: non-disruptive techniques used during the experiment and while the animal or patient is still alive, and terminal techniques, performed after the sacrifice of the animal (or in case of failure and the patient is re-transplanted).

Most of the techniques used during experiments to assess the implanted decellularized corneas are the same of those routinely by ophthalmologists after a real corneal transplant. Intraocular pressure (IOP) is routinely measured using a tonometer since increased IOP post transplantation can lead to glaucoma. Slit lamp biomicroscopy can be used to evaluate the thickness and transparency of the cornea. Optical coherence tomography (OCT) can also be used to measure thickness for all the cornea and obtain a pachymetric map, i.e. a topographical map [149]. To assess health of the epithelium, the anterior surface is stained with fluorescein and imaged using blue light. Areas of debrided or damaged epithelium will appear fluorescent. Other parameters such as neovascularization, inflammation, infection are usually determined visually by trained personnel using a grading scheme [150]. A technique that is becoming popular in the recent times is laser scanning *in vivo* confocal microscopy. As it is a contact technique, in patients it is done under local topical anaesthesia while in animal models it is performed under total anaesthesia. This method allows the visualization with high resolution at all depths of the cornea without the aid of any enhancing contrast agents. It is the only technique that can be used to quantify nerve regeneration [151,152].

Terminal techniques require the excision of the cornea. Despite being quite an old technique, histological staining with H&E provides useful information about the implant. This technique can assess epithelial health by allowing the number of cell layers and their morphology to be visualized, quantifying the repopulation of the implant by the surrounding stromal cells and identifying the presence of inflammatory cells in addition to examining other parameters. Other standard histological stains can also provide information about the ECM composition, such as Alcian Blue for GAGs and Picrosirius Red for collagens. Another method to obtain more information on the corneas is immunohistochemistry. The phenotype of quiescent keratocytes can be determined by positive staining of crystalline protein aldehyde dehydrogenase 3A1 (ALDH3A1) or transmembrane phosphoglycoprotein CD34. Presence of myofibroblasts, typical of fibrosis, can be detected by positive staining for alpha smooth muscle actin (α-SMA). Blood vessels can be identified staining for Platelet endothelial cell adhesion molecule (PECAM-1), also known as CD31, or for von Willebrand factor (vWF). The presence of Integrin alpha M ($\alpha_M\beta_2$), also known as CD11b,

is a hallmark of the activity of the innate immune system. The fate of implanted cells can be determined by several different methods. Cells can be fluorescently labelled before implantation and this staining is still visible even after 12 weeks, as reported by Alió del Barrio and colleagues [72]. Another approach is to stain for species-specific markers when implanting cells from one species into a recipient of a different species. An example of this is the human nuclear antigen, which is located in human nucleoli but not in rodent nucleoli. The possibility of implanted cells undergoing apoptosis can be determined by the Terminal deoxynucleotidyl transferase dUTP nick end labeling (TUNEL) assay which detects DNA fragmentation. On the other hand, proliferating cells can be detected by Bromodeoxyuridine (BrdU) labelling one hour prior to animal sacrifice. Cells synthesising new DNA will incorporate this synthetic nucleoside which can be detected with specific antibodies. By using electron microscopy more detailed information about the arrangement of the collagen fibrils can be obtained. Serial block face-scanning electron microscopy (SBF-SEM) and 3D reconstruction of the sections allows the visualization of cell distribution and lamellae arrangement with great resolution [153]. X-ray scattering is another method to analyse the structure of the cornea and the orientation of fibrillar collagens [154].

4.2. Selection of animal models

The most common used animal model in research is the mouse. This is due to the relative low cost, short gestation period, large litter size and overall ease of housing. Furthermore, the abundance of genetically defined strains offers the possibility of studying immune responses in a mechanistic way [155]. However, the size of the mouse ocular globe is rather small, hence it is rarely used for corneal studies. Rat models have been developed to study corneal rejection and immunomodulation with cell therapy, such as MSCs infusion [156–158]. Shafiq and colleagues have described the use of decellularized human cornea as a limbal graft in a rat laser induced limbal injury model [159].

While corneal transplants can be performed using mice and rats as experimental animal models, they are difficult surgeries and poorly model human corneas. For this reason, the rabbit remains the most commonly used animal model for corneal studies [160]. Rabbit eyes have a very similar anatomy to human eyes and are big enough to be operated with standard human surgical techniques. As a proof of concept many early studies using decellularized corneal tissue for transplantation were used in intrastromal pocket surgeries [60,61,148,69–73,80,90,105]. This technique can give a good insight into the immune response generated by the scaffold and some information about the neighbouring cells' behaviour and migration into the implanted matrix. However, these surgeries are not routinely performed in the clinic, so for a more translational approach anterior or deep anterior lamellar keratoplasties are more suitable. One of the first experiments in rabbits using decellularized corneal tissues was performed by Wu and colleagues in 2009 [99]. They reported the use of PLA_2 decellularized porcine corneas on an anterior lamellar keratoplasty model in rabbits. The acellular grafts were re-epithelialized in one week, transparency recovered in less than 3 months and with no presence of neovascularization. Luo and colleagues decellularized corneas using 2 M NaCl and seeded amniotic epithelial cells [81]. Tissue-engineered constructs implanted in rabbits showed better integration and transparency than the acellular counterparts. Detergent decellularized corneas were implanted intrastromally with no major signs of rejection or neovascularization and recovering transparency before 6 months post-implantation [69]. Hashimoto and colleagues decellularized porcine corneas with high hydrostatic pressure and implanted them in a deep anterior lamellar keratoplasty model [106]. Scaffolds integrated completely into the host cornea, recovered transparency and showed no signs of inflammation or neovascularization. Re-epithelialization was slow and some keratocytes migrated into the scaffold. Porcine corneas decellularized using supercritical carbon dioxide have shown very promising results after grafting into rabbits [65]. Transparency was achieved within 2 weeks and epithelium re-grew in a month. While these studies demonstrate the promise of decellularized corneas for use in transplantations, differences in the regenerative capacities of rabbit and human corneas should also be considered.

In addition to rabbits, other species have been used as animal models for corneal transplantation such as mini-pigs [161,162], cats [37] and dogs [76]. However, only one study has used the dog as a model for implantation of decellularized matrices as an alternative to human cadaveric donor corneas. Porcine corneas were decellularized using sodium deoxycholate and sodium orthovanadate and seeded with stromal and epithelial cells. Constructs were implanted in dogs and followed during a one year period. Recellularized scaffolds showed improved re-innervation, epithelial integrity and central corneal thickness.

4.3. Human studies

Despite being a recent approach, clinical studies have been carried out with decellularized corneal tissues. Alió del Barrio and colleagues recently reported the use of thin sections (laminas) of decellularized human corneas as intrastromal implants for advanced keratoconus patients [74]. Some of the laminas where seeded with autologous adipose-derived MSCs. Initial reports show improved visual acuity, corneal shape and topography, and patients recovered normal corneal thickness. The implanted tissue remained visible with OCT after 6 months and some signs of recellularization by host keratocytes detected by confocal biomicroscopy. The authors identified no positive effect from the recellularized tissues versus the acellular tissues.

Chinese company China Regenerative Medicine International Limited (CRMI) was granted a medical device registration certificate by the China Food and Drug Administration (CFDA) in 2015. Their product consists of a porcine cornea decellularized with 2 M NaCl, washed with 0.2% Triton X-100, dehydrated with glycerol, and irradiated with Co^{60} to ensure sterility [81]. In a first study in 2015, Zhang and colleagues reported the outcome of 47 patients with fungal corneal ulcers treated with such product [94]. Another short-term study using this product has been reported for the treatment of herpes simplex keratitis with generally positive results, albeit some patients needing re-grafting of human allograft transplantation due to scaffold dissolution [163]. Irritation and neovascularization scores improved as did the transparency of the graft, originally hazy. While more than 1000 scaffolds have been implanted, no long term follow up studies have been published and it is still to be determined if this product would be suitable for corneal diseases other than fungal infections.

Being a relatively new field, there is still much research and optimization needed before these corneas can be accepted as valid alternatives to real corneas for keratoplasty. Most of the decellularization techniques discussed can only be done in small batches, at a laboratory scale. Efforts are required to automate the optimized decellularization protocols under sterile conditions at a larger scale. Furthermore, an international consensus is required to assess the quality of these scaffolds in terms of xenogenic or allogenic cell removal and ECM preservation. It would be beneficial to identify the most appropriate cell source for specific corneal transplants and how best to deliver these cells to recellularize the scaffolds. Good manufacturing practices (GMP) should be ensured in all steps and correct storage and transportation organized in a similar fashion as in current eye banking. If recellularization is not necessary for a specific application, then off-the-shelf scaffolds can be developed. In all cases, these alternative scaffolds should show similar if not improved efficacy to keratoplasties.

5. Conclusions

While multiples issues still have to be overcome in the field of corneal decellularization, such as identifying the optimal

decellularization and recellularization protocols (if required) and assessing their performance *in vivo* in patients, decellularization research has advanced substantially in recent years. Decellularized corneas have enormous potential to be used as alternatives to traditional donor corneas and could help alleviate the shortage of donor corneas suitable for transplantation worldwide.

Acknowledgements

The research is supported by funding from the European Research Council (ERC) under the European Union's Horizon 2020 research and innovation program (grant agreement no. 637460) and from Science Foundation Ireland (15/ERC/3269).

References

[1] D.W. DelMonte, T. Kim, Anatomy and physiology of the cornea and related structures, J. Cataract. Refract. Surg. 37 (2011) 588–598, https://doi.org/10.1016/j.jcrs.2010.12.037.
[2] W. Li, Y. Hayashida, Y.T. Chen, S.C.G. Tseng, Niche regulation of corneal epithelial stem cells at the limbus, Cell Res. 17 (2007) 26–36, https://doi.org/10.1038/sj.cr.7310137.
[3] R.E. Lee, P.F. Davison, The collagens of the developing bovine cornea, Exp. Eye Res. 39 (1984) 639–652, https://doi.org/10.1016/0014-4835(84)90063-0.
[4] D.E. Birk, J.M. Fitch, T.F. Linsenmayer, Organization of collagen types I and V in the embryonic chicken cornea, Invest. Ophthalmol. Vis. Sci. 27 (1986) 1470–1477, https://doi.org/10.1073/pnas.81.9.2791.
[5] W. Li, J.P. Vergnes, P.K. Cornuet, J.R. Hassell, cDNA clone to chick corneal chondroitin/dermatan sulfate proteoglycan reveals identity to decorin, Arch. Biochem. Biophys. 296 (1992) 190–197, https://doi.org/10.1016/0003-9861(92)90562-B.
[6] Shukti Chakravarti, Raymond L. Stallings, Nirmala SundarRaj, Pamela K. Cornuet, John R. Hassell, Primary Structure of Human Lumican (Keratan Sulfate Proteoglycan) and Localization of the Gene (LUM) to Chromosome 12q21.3-q22, Genomics 27 (3) (1995) 481–488, https://doi.org/10.1006/geno.1995.1080.
[7] L.M. Corpuz, J.L. Funderburgh, M.L. Funderburgh, G.S. Bottomley, S. Prakash, G.W. Conrad, Molecular cloning and tissue distribution of keratocan, J. Biol. Chem. 271 (1996) 9759–9763, https://doi.org/10.1074/jbc.271.16.9759.
[8] J.A. Bonanno, Molecular mechanisms underlying the corneal endothelial pump, Exp. Eye Res. 95 (2012) 2–7, https://doi.org/10.1016/j.exer.2011.06.004.
[9] S. Dikstein, D.M. Maurice, Metabolic basis to fluid pump in cornea, J. Physiol. 221 (1972) 29-.
[10] D. Pascolini, S.P. Mariotti, Global estimates of visual impairment: 2010, Br. J. Ophthalmol. 96 (2012) 614–618, https://doi.org/10.1136/bjophthalmol-2011-300539.
[11] M. Taravella, W.G. Gensheimer, Corneal graft rejection, EMedicine (2016).
[12] D.T.H. Tan, J.K.G. Dart, E.J. Holland, S. Kinoshita, Corneal transplantation, Lancet 379 (2012) 1749–1761, https://doi.org/10.1016/S0140-6736(12)60437-1.
[13] P. Gain, R. Jullienne, Z. He, M. Aldossary, S. Acquart, F. Cognasse, G. Thuret, Global survey of corneal transplantation and eye banking, JAMA Ophthalmol. 134 (2016) 167–173, https://doi.org/10.1001/jamaophthalmol.2015.4776.
[14] S. Matthyssen, B. Van den Bogerd, S.N. Dhubhghaill, C. Koppen, N. Zakaria, Corneal regeneration: a review of stromal replacements, Acta Biomater. 69 (2018) 31–41, https://doi.org/10.1016/j.actbio.2018.01.023.
[15] W. Liu, K. Merrett, M. Griffith, P. Fagerholm, S. Dravida, B. Heyne, J.C. Scaiano, M.A. Watsky, N. Shinozaki, N. Lagali, R. Munger, F. Li, Recombinant human collagen for tissue engineered corneal substitutes, Biomaterials 29 (2008) 1147–1158, https://doi.org/10.1016/j.biomaterials.2007.11.011.
[16] P. Fagerholm, N.S. Lagali, K. Merrett, W.B. Jackson, R. Munger, Y. Liu, J.W. Polarek, M. Soderqvist, M. Griffith, A biosynthetic alternative to human donor tissue for inducing corneal regeneration: 24-month follow-up of a phase 1 clinical study, Sci. Transl. Med. 2 (2010) 46ra61, https://doi.org/10.1126/scitranslmed.3001022.
[17] A.K. Kureshi, M.a. Dziasko, J.L. Funderburgh, J.T. Daniels, Human corneal stromal stem cells support limbal epithelial cells cultured on RAFT tissue equivalents, Sci. Rep. 5 (2015) 16186, https://doi.org/10.1038/srep16186.
[18] H.J. Levis, R.A. Brown, J.T. Daniels, Plastic compressed collagen as a biomimetic substrate for human limbal epithelial cell culture, Biomaterials 31 (2010) 7726–7737, https://doi.org/10.1016/j.biomaterials.2010.07.012.
[19] W. McIntosh Ambrose, A. Salahuddin, S. So, S. Ng, S. Ponce Márquez, T. Takezawa, O. Schein, J.H. Elisseeff, Collagen vitrigel membranes for the in vitro reconstruction of separate corneal epithelial, stromal, and endothelial cell layers, J. Biomed. Mater. Res. Part B Appl. Biomater. 90B (2009) 818–831, https://doi.org/10.1002/jbm.b.31351.
[20] M. Rafat, F. Li, P. Fagerholm, N. Lagali, M.A. Watsky, R. Munger, T. Matsuura, M. Griffith, PEG-stabilized carbodiimide crosslinked collagen-chitosan hydrogels for corneal tissue engineering, Biomaterials 29 (2008) 3960–3972, https://doi.org/10.1016/j.biomaterials.2008.06.017.
[21] X. Zhu, R.W. Beuerman, M.B.E. Chan-Park, Z. Cheng, L.P.K. Ang, D.T.H. Tan, Enhancement of the mechanical and biological properties of a biomembrane for tissue engineering the ocular surface, Ann. Acad. Med. Singapore. 35 (2006) 210–214.
[22] L.J. Bray, K.a. George, D.W. Hutmacher, T.V. Chirila, D.G. Harkin, A dual-layer silk fibroin scaffold for reconstructing the human corneal limbus, Biomaterials 33 (2012) 3529–3538, https://doi.org/10.1016/j.biomaterials.2012.01.045.
[23] J. Fernández-Pérez, M. Binner, C. Werner, L.J. Bray, Limbal stromal cells derived from porcine tissue demonstrate mesenchymal characteristics in vitro, Sci. Rep. (2017) 1–28, https://doi.org/10.1038/s41598-017-06898-2.
[24] S. Wang, C.E. Ghezzi, R. Gomes, R.E. Pollard, J.L. Funderburgh, D.L. Kaplan, In vitro 3D corneal tissue model with epithelium, stroma, and innervation, Biomaterials. 112 (2017) 1–9, https://doi.org/10.1016/j.biomaterials.2016.09.030.
[25] M. Alaminos, M.D.C. Sánchez-Quevedo, J.I. Muñoz-Ávila, D. Serrano, S. Medialdea, I. Carreras, A. Campos, Construction of a complete rabbit cornea substitute using a fibrin-agarose scaffold, Investig. Ophthalmol. Vis. Sci. 47 (2006) 3311–3317, https://doi.org/10.1167/iovs.05-1647.
[26] P. Rama, S. Bonini, A. Lambiase, O. Golisano, P. Paterna, M. De Luca, G. Pellegrini, Autologous fibrin-cultured limbal stem cells permanently restore the corneal surface of patients with total limbal stem cell deficiency, Transplantation 72 (2001) 1478–1485.
[27] G. Uzunalli, Z. Soran, T.S. Erkal, Y.S. Dagdas, E. Dinc, A.M. Hondur, K. Bilgihan, B. Aydin, M.O. Guler, A.B. Tekinay, Bioactive self-assembled peptide nanofibers for corneal stroma regeneration, Acta Biomater. 10 (2014) 1156–1166, https://doi.org/10.1016/j.actbio.2013.12.002.
[28] A. Sorkio, L. Koch, L. Koivusalo, A. Deiwick, S. Miettinen, B. Chichkov, H. Skottman, Human stem cell based corneal tissue mimicking structures using laser-assisted 3D bioprinting and functional bioinks, Biomaterials 171 (2018) 57–71, https://doi.org/10.1016/j.biomaterials.2018.04.034.
[29] A. Isaacson, S. Swioklo, C.J. Connon, 3D bioprinting of a corneal stroma equivalent, Exp. Eye Res. 173 (2018) 188–193, https://doi.org/10.1016/j.exer.2018.05.010.
[30] S.L. Wilson, I. Wimpenny, M. Ahearne, S. Rauz, A.J. El Haj, Y. Yang, Chemical and topographical effects on cell differentiation and matrix elasticity in a corneal stromal layer model, Adv. Funct. Mater. 22 (2012) 3641–3649, https://doi.org/10.1002/adfm.201200655.
[31] K. Tonsomboon, M.L. Oyen, Composite electrospun gelatin fiber-alginate gel scaffolds for mechanically robust tissue engineered cornea, J. Mech. Behav. Biomed. Mater. 21 (2013) 185–194, https://doi.org/10.1016/j.jmbbm.2013.03.001.
[32] H. Kim, M.-N. Park, J. Kim, J. Jang, H.-K. Kim, D.-W. Cho, Characterization of cornea-specific bioink: high transparency, improved in vivo safety, J. Tissue Eng. 10 (2019), https://doi.org/10.1177/2041731418823382 204173141882338.
[33] M. Ahearne, A. Coyle, Application of UVA-riboflavin crosslinking to enhance the mechanical properties of extracellular matrix derived hydrogels, J. Mech. Behav. Biomed. Mater. 54 (2016) 259–267, https://doi.org/10.1016/j.jmbbm.2015.09.035.
[34] M. Ahearne, A.P. Lynch, Early observation of extracellular matrix-derived hydrogels for corneal stroma regeneration, Tissue Eng. Part C Methods 21 (2015) 1059–1069, https://doi.org/10.1089/ten.tec.2015.0008.
[35] X.Q. Guo, A.E.K. Hutcheon, S.A. Melotti, J.D. Zieske, V. Trinkaus-Randall, J.W. Ruberti, Morphologic characterization of organized extracellular matrix deposition by ascorbic acid-stimulated human corneal fibroblasts, Investig. Opthalmol. Vis. Sci. 48 (2007) 4050, https://doi.org/10.1167/iovs.06-1216.
[36] Ricardo M. Gouveia, Elena González-Andrades, Juan C. Cardona, Carmen González-Gallardo, Ana M. Ionescu, Ingrid Garzon, Miguel Alaminos, Miguel González-Andrades, Che J. Connon, Controlling the 3D architecture of Self-Lifting Auto-generated Tissue Equivalents (SLATEs) for optimized corneal graft composition and stability, Biomaterials 121 (2017) 205–219, https://doi.org/10.1016/j.biomaterials.2016.12.023.
[37] M. Boulze Pankert, B. Goyer, F. Zaguia, M. Bareille, M.C. Perron, X. Liu, J.D. Cameron, S. Proulx, I. Brunette, Biocompatibility and functionality of a tissue-engineered living corneal stroma transplanted in the feline eye, Invest. Ophthalmol. Vis. Sci. 55 (2014) 6908–6920, https://doi.org/10.1167/iovs.14-14720.
[38] T.J. Keane, R. Londono, N.J. Turner, S.F. Badylak, Consequences of ineffective decellularization of biologic scaffolds on the host response, Biomaterials 33 (2012) 1771–1781, https://doi.org/10.1016/j.biomaterials.2011.10.054.
[39] S. Nagata, R. Hanayama, K. Kawane, Autoimmunity and the clearance of dead cells, Cell 140 (2010) 619–630, https://doi.org/10.1016/j.cell.2010.02.014.
[40] H.C. Ott, T.S. Matthiesen, S.-K. Goh, L.D. Black, S.M. Kren, T.I. Netoff, D.A. Taylor, Perfusion-decellularized matrix: using nature's platform to engineer a bioartificial heart, Nat. Med. 14 (2008) 213–221, https://doi.org/10.1038/nm1684.
[41] J.P. Guyette, S.E. Gilpin, J.M. Charest, L.F. Tapias, X. Ren, H.C. Ott, Perfusion decellularization of whole organs, Nat. Protoc. 9 (2014) 1451–1468, https://doi.org/10.1038/nprot.2014.097.
[42] G. Orlando, C. Booth, Z. Wang, G. Totonelli, C.L. Ross, E. Moran, M. Salvatori, P. Maghsoudlou, M. Turmaine, G. Delario, Y. Al-Shraideh, U. Farooq, A.C. Farney, J. Rogers, S.S. Iskandar, A. Burns, F.C. Marini, P. De Coppi, R.J. Stratta, S. Soker, Discarded human kidneys as a source of ECM scaffold for kidney regeneration technologies, Biomaterials 34 (2013) 5915–5925, https://doi.org/10.1016/J.BIOMATERIALS.2013.04.033.
[43] H. Yagi, K. Fukumitsu, K. Fukuda, M. Kitago, M. Shinoda, H. Obara, O. Itano, S. Kawachi, M. Tanabe, G.M. Coudriet, J.D. Piganelli, T.W. Gilbert, A. Soto-Gutierrez, Y. Kitagawa, Human-scale whole-organ bioengineering for liver transplantation: a regenerative medicine approach, Cell Transplant. 22 (2013) 231–242, https://doi.org/10.3727/096368912X654939.
[44] O. Barakat, S. Abbasi, G. Rodriguez, J. Rios, R.P. Wood, C. Ozaki, L.S. Holley,

P.K. Gauthier, Use of decellularized porcine liver for engineering humanized liver organ, J. Surg. Res. 173 (2012) e11–e25, https://doi.org/10.1016/J.JSS.2011.09.033.
[45] A.-M. Kajbafzadeh, N. Javan-Farazmand, M. Monajemzadeh, A. Baghayee, Determining the optimal decellularization and sterilization protocol for preparing a tissue scaffold of a human-sized liver tissue, Tissue Eng. Part C Methods. 19 (2013) 642–651, https://doi.org/10.1089/ten.tec.2012.0334.
[46] S.E. Gilpin, J.P. Guyette, G. Gonzalez, X. Ren, J.M. Asara, D.J. Mathisen, J.P. Vacanti, H.C. Ott, Perfusion decellularization of human and porcine lungs: Bringing the matrix to clinical scale, J. Hear. Lung Transplant. 33 (2014) 298–308, https://doi.org/10.1016/J.HEALUN.2013.10.030.
[47] J.E. Nichols, J. Niles, M. Riddle, G. Vargas, T. Schilagard, L. Ma, K. Edward, S. La Francesca, J. Sakamoto, S. Vega, M. Ogadegbe, R. Mlcak, D. Deyo, L. Woodson, C. McQuitty, S. Lick, D. Beckles, E. Melo, J. Cortiella, Production and assessment of decellularized pig and human lung scaffolds, Tissue Eng. Part A 19 (2013) 2045–2062, https://doi.org/10.1089/ten.tea.2012.0250.
[48] J.D. O'Neill, R. Anfang, A. Anandappa, J. Costa, J. Javidfar, H.M. Wobma, G. Singh, D.O. Freytes, M.D. Bacchetta, J.R. Sonett, G. Vunjak-Novakovic, Decellularization of human and porcine lung tissues for pulmonary tissue engineering, Ann. Thorac. Surg. 96 (2013) 1046–1056, https://doi.org/10.1016/J.ATHORACSUR.2013.04.022.
[49] A.J. Booth, R. Hadley, A.M. Cornett, A.A. Dreffs, S.A. Matthes, J.L. Tsui, K. Weiss, J.C. Horowitz, V.F. Fiore, T.H. Barker, B.B. Moore, F.J. Martinez, L.E. Niklason, E.S. White, Acellular normal and fibrotic human lung matrices as a culture system for *in vitro* investigation, Am. J. Respir. Crit. Care Med. 186 (2012) 866–876, https://doi.org/10.1164/rccm.201204-0754OC.
[50] S.-K. Goh, S. Bertera, P. Olsen, J.E. Candiello, W. Halfter, G. Uechi, M. Balasubramani, S.A. Johnson, B.M. Sicari, E. Kollar, S.F. Badylak, I. Banerjee, Perfusion-decellularized pancreas as a natural 3D scaffold for pancreatic tissue and whole organ engineering, Biomaterials 34 (2013) 6760–6772, https://doi.org/10.1016/J.BIOMATERIALS.2013.05.066.
[51] S. Nara, S. Chameettachal, S. Midha, S. Murab, S. Ghosh, Preservation of biomacromolecular composition and ultrastructure of a decellularized cornea using a perfusion bioreactor, RSC Adv. 6 (2016) 2225–2240, https://doi.org/10.1039/C5RA20745B.
[52] A.F. Pellegata, M. Adelaide Asnaghi, S. Zonta, G. Zerbini, S. Mantero, A novel device for the automatic decellularization of biological tissues, Int. J. Artif. Organs. 35 (2012) 191–198, https://doi.org/10.5301/ijao.5000079.
[53] J.Y. Oh, M.K. Kim, H.J. Lee, J.H. Ko, W.R. Wee, J.H. Lee, Processing porcine cornea for biomedical applications, TISSUE Eng. Part C. 15 (2009) 635–645, https://doi.org/10.1089/ten.tec.2009.0022.
[54] S. Proulx, C. Audet, J. d'Arc Uwamaliya, A. Deschambeault, P. Carrier, C.J. Giasson, I. Brunette, L. Germain, Tissue engineering of feline corneal endothelium using a devitalized human cornea as carrier, Tissue Eng. Part A. 15 (2009) 1709–1718, https://doi.org/10.1089/ten.tea.2008.0208.
[55] J. Diao, X. Pang, Y. Qiu, Y. Miao, M. Yu, T. Fan, Construction of a human corneal stromal equivalent with non-transfected human corneal stromal cells and acellular porcine corneal stromata, Exp. Eye Res. 132 (2015) 216–244, https://doi.org/10.1016/j.exer.2015.01.015.
[56] Q. Li, H. Wang, Z. Dai, Y. Cao, C. Jin, Preparation and biomechanical properties of an acellular porcine corneal stroma, Cornea (2017), https://doi.org/10.1097/ICO.0000000000001319.
[57] Y. Shao, J. Tang, Y. Zhou, Y. Qu, H. He, Q. Liu, G. Tan, W. Li, Z. Liu, A novel method in preparation of acellular porcine corneal stroma tissue for lamellar keratoplasty, Am. J. Transl. Res. 7 (2015) 2612–2629, https://doi.org/10.3980/j.issn.2222-3959.2012.04.02.
[58] Y. Shao, Y. Yu, C.-G. Pei, Q. Zhou, Q.-P. Liu, G. Tan, J.-M. Li, G.-P. Gao, L. Yang, Evaluation of novel decellularizing corneal stroma for cornea tissue engineering applications, Int. J. Ophthalmol. 5 (2012) 415–418, https://doi.org/10.3980/j.issn.2222-3959.2012.04.02.
[59] Y. Hashimoto, S. Hattori, S. Sasaki, T. Honda, T. Kimura, S. Funamoto, H. Kobayashi, A. Kishida, Ultrastructural analysis of the decellularized cornea after interlamellar keratoplasty and microkeratome-assisted anterior lamellar keratoplasty in a rabbit model, Sci. Rep. 6 (2016) 27734, https://doi.org/10.1038/srep27734.
[60] S. Sasaki, S. Funamoto, Y. Hashimoto, T. Kimura, T. Honda, S. Hattori, H. Kobayashi, A. Kishida, M. Mochizuki, In vivo evaluation of a novel scaffold for artificial corneas prepared by using ultrahigh hydrostatic pressure to decellularize porcine corneas, Mol. Vis. 15 (2009) 2022–2028, https://doi.org/10.1007/s10856-005-6689-9.
[61] Y. Hashimoto, S. Funamoto, S. Sasaki, T. Honda, S. Hattori, K. Nam, T. Kimura, M. Mochizuki, T. Fujisato, H. Kobayashi, A. Kishida, Preparation and characterization of decellularized cornea using high-hydrostatic pressurization for corneal tissue engineering, Biomaterials (2010), https://doi.org/10.1016/j.biomaterials.2010.01.122.
[62] A.P. Lynch, M. Ahearne, Strategies for developing decellularized corneal scaffolds, Exp. Eye Res. 108 (2013) 42–47, https://doi.org/10.1016/j.exer.2012.12.012.
[63] K. Sawada, D. Terada, T. Yamaoka, S. Kitamura, T. Fujisato, Cell removal with supercritical carbon dioxide for acellular artificial tissue, J. Chem. Technol. Biotechnol. 83 (2008) 943–949, https://doi.org/10.1002/jctb.1899.
[64] S. Guler, B. Aslan, P. Hosseinian, H.M. Aydin, Supercritical carbon dioxide-assisted decellularization of aorta and cornea, Tissue Eng. Part C Methods. 23 (2017) 540–547, https://doi.org/10.1089/ten.tec.2017.0090.
[65] Y.H. Huang, F.W. Tseng, W.H. Chang, I.C. Peng, D.J. Hsieh, S.W. Wu, M.L. Yeh, Preparation of acellular scaffold for corneal tissue engineering by supercritical carbon dioxide extraction technology, Acta Biomater. 58 (2017) 238–243, https://doi.org/10.1016/j.actbio.2017.05.060.
[66] J.L. Wehmeyer, S. Natesan, R.J. Christy, Development of a sterile amniotic membrane tissue graft using supercritical carbon dioxide, Tissue Eng. Part C. Methods. 21 (2015) 649–659, https://doi.org/10.1089/ten.TEC.2014.0304.
[67] J. Xiao, H. Duan, Z. Liu, Z. Wu, Y. Lan, W. Zhang, C. Li, F. Chen, Q. Zhou, X. Wang, J. Huang, Z. Wang, Construction of the recellularized corneal stroma using porous acellular corneal scaffold, Biomaterials 32 (2011) 6962–6971, https://doi.org/10.1016/j.biomaterials.2011.05.084.
[68] X.C. Lin, Y.N. Hui, Y.S. Wang, H. Meng, Y.J. Zhang, Y. Jin, Lamellar keratoplasty with a graft of lyophilized acellular porcine corneal stroma in the rabbit, Vet. Ophthalmol. 11 (2008) 61–66, https://doi.org/10.1111/j.1463-5224.2008.00601.x.
[69] K. Pang, L. Du, X. Wu, A rabbit anterior cornea replacement derived from acellular porcine cornea matrix, epithelial cells and keratocytes, Biomaterials 31 (2010) 7257–7265, https://doi.org/10.1016/j.biomaterials.2010.05.066.
[70] L. Du, X. Wu, Development and characterization of a full-thickness acellular porcine cornea matrix for tissue engineering, Artif. Organs. 35 (2011) 691–705, https://doi.org/10.1111/j.1525-1594.2010.01174.x.
[71] Y. Zhou, Z. Wu, J. Ge, P. Wan, N. Li, P. Xiang, Q. Gao, Z. Wang, Development and characterization of acellular porcine corneal matrix using sodium dodecylsulfate, Cornea 30 (2011) 73–82, https://doi.org/10.1097/ICO.0b013e3181dc8184.
[72] J.L. Alió del Barrio, M. Chiesa, N. Garagorri, N. Garcia-Urquia, J. Fernandez-Delgado, L. Bataille, A. Rodriguez, F. Arnalich-Montiel, T. Zarnowski, J.P. Álvarez de Toledo, J.L. Alió, M.P. De Miguel, Acellular human corneal matrix sheets seeded with human adipose-derived mesenchymal stem cells integrate functionally in an experimental animal model, Exp. Eye Res. 132 (2015) 91–100, https://doi.org/10.1016/j.exer.2015.01.020.
[73] G.H.-F. Yam, N.Z.B.M. Yusoff, T.W. Goh, M. Setiawan, X.W. Lee, Y.C. Liu, J.S. Mehta, Decellularization of human stromal refractive lenticules for corneal tissue engineering, Sci. Rep. 6 (2016) 1–11, https://doi.org/10.1038/srep26339.
[74] J.L. Alió del Barrio, M. El Zarif, A. Azaar, N. Makdissy, C. Khalil, W. Harb, I. El Achkar, Z.A. Jawad, M.P. de Miguel, J.L. Alió, Corneal stroma enhancement with decellularized stromal laminas with or without stem cell recellularization for advanced keratoconus, Am. J. Ophthalmol. 186 (2018) 47–58, https://doi.org/10.1016/j.ajo.2017.10.026.
[75] E. Yoeruek, T. Bayyoud, C. Maurus, J. Hofmann, M.S. Spitzer, K.U. Bartz-Schmidt, P. Szurman, Decellularization of porcine corneas and repopulation with human corneal cells for tissue-engineered xenografts, Acta Ophthalmol. 90 (2012) 125–131, https://doi.org/10.1111/j.1755-3768.2011.02261.x.
[76] B. Xu, Z. Song, T. Fan, Construction of anterior hemi-corneal equivalents using nontransfected human corneal cells and transplantation in dog models, Artif. Organs. 00 (2017), https://doi.org/10.1111/aor.12878.
[77] J.S. Choi, J.K. Williams, M. Greven, K.A. Walter, P.W. Laber, G. Khang, S. Soker, Bioengineering endothelialized neo-corneas using donor-derived corneal endothelial cells and decellularized corneal stroma, Biomaterials 31 (2010) 6738–6745, https://doi.org/10.1016/j.biomaterials.2010.05.020.
[78] L. Du, X. Wu, K. Pang, Y. Yang, Histological evaluation and biomechanical characterisation of an acellular porcine cornea scaffold, Br. J. Ophthalmol. 95 (2011) 410–414, https://doi.org/10.1136/bjo.2008.142539.
[79] Y. Fu, X. Fan, P. Chen, C. Shao, W. Lu, Reconstruction of a tissue-engineered cornea with porcine corneal acellular matrix as the scaffold, Cells Tissues Organs. 191 (2010) 193–202, https://doi.org/10.1159/000235680.
[80] Y.-G. Xu, Y.-S. Xu, C. Huang, Y. Feng, Y. Li, W. Wang, Development of a rabbit corneal equivalent using an acellular corneal matrix of a porcine substrate, Mol. Vis. 14 (2008) 2180–2189.
[81] H. Luo, Y. Lu, T. Wu, M. Zhang, Y.J. Zhang, Y. Jin, Construction of tissue-engineered cornea composed of amniotic epithelial cells and acellular porcine cornea for treating corneal alkali burn, Biomaterials 34 (2013) 6748–6759, https://doi.org/10.1016/j.biomaterials.2013.05.045.
[82] D.O. Freytes, J. Martin, S.S. Velankar, A.S. Lee, S.F. Badylak, Preparation and rheological characterization of a gel form of the porcine urinary bladder matrix, Biomaterials 29 (2008) 1630–1637, https://doi.org/10.1016/j.biomaterials.2007.12.014.
[83] T.W. Gilbert, S. Wognum, E.M. Joyce, D.O. Freytes, M.S. Sacks, S.F. Badylak, Collagen fiber alignment and biaxial mechanical behavior of porcine urinary bladder derived extracellular matrix, Biomaterials 29 (2008) 4775–4782, https://doi.org/10.1016/j.biomaterials.2008.08.022.
[84] V.J. Mase, J.R. Hsu, S.E. Wolf, J.C. Wenke, D.G. Baer, J. Owens, S.F. Badylak, T.J. Walters, Clinical application of an acellular biologic scaffold for surgical repair of a large, traumatic quadriceps femoris muscle defect, Orthopedics 33 (2010) 511, https://doi.org/10.3928/01477447-20100526-24.
[85] S. Ponce Márquez, V.S. Martínez, W. McIntosh Ambrose, J. Wang, N.G. Gantxegui, O.D. Schein, J.H. Elisseeff, Decellularization of bovine corneas for tissue engineering applications, Acta Biomater. 5 (2009) 1839–1847, https://doi.org/10.1016/j.actbio.2009.02.011.
[86] H. Lin, T. Wang, T. Li, Y. Chang, M.T. Sheu, Y.-Y. Huang, D.-Z. Liu, Development of decellularized cornea by organic acid treatment for corneal regeneration, Tissue Eng. Part A. In press (2018), https://doi.org/10.1089/ten.TEA.2018.0162.
[87] Z. Zhang, G. Niu, J.S. Choi, M. Giegengack, A. Atala, S. Soker, Bioengineered multilayered human corneas from discarded human corneal tissue, 035012, Biomed. Mater. 10 (2015), https://doi.org/10.1088/1748-6041/10/3/035012.
[88] H. Sengyoku, T. Tsuchiya, T. Obata, R. Doi, Y. Hashimoto, M. Ishii, H. Sakai, N. Matsuo, D. Taniguchi, T. Suematsu, M. Lawn, K. Matsumoto, T. Miyazaki, T. Nagayasu, Sodium hydroxide based non-detergent decellularizing solution for rat lung, Organogenesis 14 (2018) 94–106, https://doi.org/10.1080/15476278.2018.1462432.

[89] M. van Steenberghe, T. Schubert, S. Gerelli, C. Bouzin, Y. Guiot, D. Xhema, X. Bollen, K. Abdelhamid, P. Gianello, Porcine pulmonary valve decellularization with NaOH-based vs detergent process: preliminary in vitro and in vivo assessments, J. Cardiothorac. Surg. 13 (2018) 34, https://doi.org/10.1186/s13019-018-0720-y.
[90] X.Y. Ma, Y. Zhang, D. Zhu, Y. Lu, G. Zhou, W. Liu, Y. Cao, W.J. Zhang, Corneal stroma regeneration with acellular corneal stroma sheets and keratocytes in a rabbit model, PLoS One 10 (2015) 1–13, https://doi.org/10.1371/journal.pone.0132705.
[91] S.L. Wilson, L.E. Sidney, S.E. Dunphy, H.S. Dua, A. Hopkinson, Corneal decellularization: a method of recycling unsuitable donor tissue for clinical translation? Curr. Eye Res. (2016), https://doi.org/10.3109/02713683.2015.1062114.
[92] M. Gonzalez-Andrades, J. de la Cruz Cardona, A.M. Ionescu, A. Campos, M. del Mar Perez, M. Alamino, Generation of bioengineered corneas with decellularized xenografts and human keratocytes, Investig. Ophthalmol. Vis. Sci. (2011), https://doi.org/10.1167/iovs.09-4773.
[93] Z. He, F. Forest, A. Bernard, A.S. Gauthier, R. Montard, M. Peoc'h, C. Jumelle, E. Courrier, C. Perrache, P. Gain, G. Thuret, Cutting and decellularization of multiple corneal stromal lamellae for the bioengineering of endothelial grafts, Investig. Ophthalmol. Vis. Sci. 57 (2016) 6639–6651, https://doi.org/10.1167/iovs.16-20256.
[94] M.-C.M. Zhang, X. Liu, Y. Jin, D.-L. Jiang, X.-S. Wei, H.-T. Xie, Lamellar keratoplasty treatment of fungal corneal ulcers with acellular porcine corneal stroma, Am. J. Transplant. 15 (2015) 1068–1075, https://doi.org/10.1111/ajt.13096.
[95] P.S. McFetridge, J.W. Daniel, T. Bodamyali, M. Horrocks, J.B. Chaudhuri, Preparation of porcine carotid arteries for vascular tissue engineering applications, J. Biomed. Mater. Res. 70A (2004) 224–234, https://doi.org/10.1002/jbm.a.30060.
[96] C. Zhang, X. Nie, D. Hu, Y. Liu, Z. Deng, R. Dong, Y. Zhang, Y. Jin, Survival and integration of tissue-engineered corneal stroma in a model of corneal ulcer, Cell Tissue Res. 329 (2007) 249–257, https://doi.org/10.1007/s00441-007-0419-1.
[97] M.-I. Huh, K.-P. Lee, J. Kim, S. Yi, B.-U. Park, H.K. Kim, Generation of femtosecond laser-cut decellularized corneal lenticule using hypotonic trypsin-EDTA solution for corneal tissue engineering, J. Ophthalmol. 2018 (2018), https://doi.org/10.1155/2018/2590536.
[98] H. Hong, M.-I. Huh, S.M. Park, K. Lee, H.K. Kim, D.S. Kim, Decellularized corneal lenticule embedded compressed collagen: Toward a suturable collagenous construct for limbal reconstruction, Biofabrication. (2018), https://doi.org/10.1088/1758-5090/aad1a4.
[99] Z. Wu, Y. Zhou, N. Li, M. Huang, H. Duan, J. Ge, P. Xiang, Z. Wang, The use of phospholipase A2 to prepare acellular porcine corneal stroma as a tissue engineering scaffold, Biomaterials 30 (2009) 3513–3522, https://doi.org/10.1016/j.biomaterials.2009.03.003.
[100] Z. Wu, Q. Zhou, H. Duan, X. Wang, J. Xiao, H. Duan, N. Li, C. Li, P. Wan, Y. Liu, Y. Song, C. Zhou, Z. Huang, Z. Wang, Reconstruction of auto-tissue-engineered lamellar cornea by dynamic culture for transplantation: a rabbit model, PLoS One 9 (2014), https://doi.org/10.1371/journal.pone.0093012.
[101] N. Li, X. Wang, P. Wan, M. Huang, Z. Wu, X. Liang, Y. Liu, J. Ge, J. Huang, Z. Wang, Tectonic lamellar keratoplasty with acellular corneal stroma in high-risk corneal transplantation, Mol. Vis. 17 (2011) 1909–1917 208 [pii].
[102] L. Gui, S.A. Chan, C.K. Breuer, L.E. Niklason, Novel utilization of serum in tissue decellularization, Tissue Eng. Part C. Methods. 16 (2010) 173–184, https://doi.org/10.1089/ten.TEC.2009.0120.
[103] M.A. Shafiq, R.A. Gemeinhart, B.Y.J.T. Yue, A.R. Djalilian, Decellularized human cornea for reconstructing the corneal epithelium and anterior stroma, Tissue Eng. Part C Methods. 18 (2012) 340–348, https://doi.org/10.1089/ten.tec.2011.0072.
[104] A.P. Lynch, S.L. Wilson, M. Ahearne, Dextran preserves native corneal structure during decellularization, Tissue Eng. Part C Methods. 22 (2016) 561–572, https://doi.org/10.1089/ten.tec.2016.0017.
[105] E. Yoeruek, T. Bayyoud, C. Maurus, J. Hofmann, M.S. Spitzer, K.U. Bartz-Schmidt, P. Szurman, Reconstruction of corneal stroma with decellularized porcine xenografts in a rabbit model, Acta Ophthalmol. 90 (2012) 206–210, https://doi.org/10.1111/j.1755-3768.2011.02300.x.
[106] Y. Hashimoto, S. Funamoto, S. Sasaki, J. Negishi, T. Honda, S. Hattori, K. Nam, T. Kimura, M. Mochizuki, H. Kobayashi, A. Kishida, Corneal regeneration by deep anterior lamellar keratoplasty (DALK) using decellularized corneal matrix, PLoS One 10 (2015) 1–10, https://doi.org/10.1371/journal.pone.0131989.
[107] M. Scarritt, M. Murdock, S.F. Badylak, Biologic scaffolds composed of extracellular matrix for regenerative medicine, Elsevier Inc., 2019 doi: 10.1016/B978-0-12-809880-6.00035-7.
[108] P.M. Crapo, T.W. Gilbert, S.F. Badylak, An overview of tissue and whole organ decellularization processes, Biomaterials 32 (2011) 3233–3243, https://doi.org/10.1016/j.biomaterials.2011.01.057.
[109] W. Kafienah, T.J. Sims, Biochemical methods for the analysis of tissue-engineered cartilage, Methods Mol. Biol. 238 (2004) 217–230.
[110] N.Y. Ignat'eva, N.A. Danilov, S.V. Averkiev, M.V. Obrezkova, V.V. Lunin, E.N. Sobol, Determination of hydroxyproline in tissues and the evaluation of the collagen content of the tissues, J. Anal. Chem. 62 (2007) 51–57, https://doi.org/10.1134/S106193480701011X.
[111] R.W. Farndale, C.A. Sayers, A.J. Barrett, A direct spectrophotometric microassay for sulfated glycosaminoglycans in cartilage cultures, Connect. Tissue Res. 9 (1982) 247–248.
[112] J.M. Bueno, E.J. Gualda, A. Giakoumaki, P. Pérez-Merino, S. Marcos, P. Artal, Multiphoton microscopy of ex vivo corneas after collagen cross-linking, Investig. Ophthalmol. Vis. Sci. 52 (2011) 5325–5331, https://doi.org/10.1167/iovs.11-7184.
[113] S. Murab, S. Ghosh, Impact of osmoregulatory agents on the recovery of collagen conformation in decellularized corneas, Biomed. Mater. 11 (2016), https://doi.org/10.1088/1748-6041/11/6/065005.
[114] M.K. Kim, H. Hara, Current status of corneal xenotransplantation, Int. J. Surg. 23 (2015) 255–260, https://doi.org/10.1016/j.ijsu.2015.07.685.
[115] R. Wang, M. Ruan, R. Zhang, L. Chen, X. Li, B. Fang, C. Li, X. Ren, J. Liu, Q. Xiong, L. Zhang, Y. Jin, L. Li, R. Li, Y. Wang, H. Yang, Y. Dai, Antigenicity of tissues and organs from GGTA1/CMAH/b4GalNT2 triple gene knockout pigs, J. Biomed. Res. (2018) 1–9, https://doi.org/10.7555/JBR.32.20180018.
[116] R. Zhang, Y. Wang, L. Chen, R. Wang, C. Li, X. Li, B. Fang, X. Ren, M. Ruan, J. Liu, Q. Xiong, L. Zhang, Y. Jin, M. Zhang, X. Liu, L. Li, Q. Chen, D. Pan, R. Li, D.K.C. Cooper, H. Yang, Y. Dai, Reducing immunoreactivity of porcine bioprosthetic heart valves by genetically-deleting three major glycan antigens, GGTA1/β4GalNT2/CMAH, Acta Biomater. 72 (2018) 196–205, https://doi.org/10.1016/j.actbio.2018.03.055.
[117] J.L. Estrada, G. Martens, P. Li, A. Adams, K.A. Newell, M.L. Ford, J.R. Butler, R. Sidner, M. Tector, J. Tector, Evaluation of human and non-human primate antibody binding to pig cells lacking GGTA1/CMAH/β4GalNT2 genes, Xenotransplantation 22 (2015) 194–202, https://doi.org/10.1111/xen.12161.
[118] Dong Niu, Hong-Jiang Wei, Lin Lin, Haydy George, Tao Wang, I-Hsiu Lee, Hong-Ye Zhao, Yong Wang, Yinan Kan, Ellen Shrock, Emal Lesha, Gang Wang, Yonglun Luo, Yubo Qing, Deling Jiao, Heng Zhao, Xiaoyang Zhou, Shouqi Wang, Hong Wei, Marc Güell, George M. Church, Luhan Yang, Inactivation of porcine endogenous retrovirus in pigs using CRISPR-Cas9, Science 357 (6357) (2017) 1303–1307, https://doi.org/10.1126/science:aan4187.
[119] X.N. Liu, X.P. Zhu, J. Wu, Z.J. Wu, Y. Yin, X.H. Xiao, X. Su, B. Kong, S.Y. Pan, H. Yang, Y. Cheng, N. An, S.L. Mi, Acellular ostrich corneal stroma used as scaffold for construction of tissue-engineered cornea, Int. J. Ophthalmol. (2016) 325–331, https://doi.org/10.18240/ijo.2016.03.01.
[120] X. Zheng, D. Zhang, S. Li, J. Zhang, J. Zheng, L. Du, J. Gao, An Experimental study of femto-laser in assisting xenograft acellular cornea matrix lens transplantation, Med. Sci. Monit. 24 (2018) 5208–5215, https://doi.org/10.12659/MSM.909294.
[121] Y. Feng, W. Wang, In vivo confocal microscopic observation of lamellar corneal transplantation in the rabbit using xenogenic acellular corneal scaffolds as a substitute, Chin. Med. J. (Engl) 128 (2015) 933–940, https://doi.org/10.4103/0366-6999.154301.
[122] S.L. Wilson, L.E. Sidney, S.E. Dunphy, J.B. Rose, A. Hopkinson, Keeping an eye on decellularized corneas: a review of methods, characterization and applications, J. Funct. Biomater. 4 (2013) 114–161, https://doi.org/10.3390/jfb4030114.
[123] H. Yin, P. Qiu, F. Wu, W. Zhang, W. Teng, Z. Qin, C. Li, J. Zhou, Z. Fang, Q. Tang, Q. Fu, J. Ma, Y. Yang, Construction of a corneal stromal equivalent with SMILE-derived lenticules and fibrin glue, Sci. Rep. 6 (2016) 33848, https://doi.org/10.1038/srep33848.
[124] E. Ramboer, B. De Craene, J. De Kock, T. Vanhaecke, G. Berx, V. Rogiers, M. Vinken, Strategies for immortalization of primary hepatocytes, J. Hepatol. 61 (2014) 925–943, https://doi.org/10.1016/j.jhep.2014.05.046.
[125] P.T. Moser, H.C. Ott, Recellularization of organs, Curr. Opin. Organ Transplant. 19 (2014) 603–609, https://doi.org/10.1097/MOT.0000000000000131.
[126] A.P. Lynch, M. Ahearne, Retinoic acid enhances the differentiation of adipose-derived stem cells to keratocytes in vitro, Transl. Vis. Sci. Technol. 6 (2017) 6, https://doi.org/10.1167/tvst.6.1.6.
[127] Y. Du, D.S. Roh, M.L. Funderburgh, M.M. Mann, K.G. Marra, J.P. Rubin, X. Li, J.L. Funderburgh, Adipose-derived stem cells differentiate to keratocytes in vitro, Mol. Vis. 16 (2010) 2680–2689.
[128] F. Arnalich-Montiel, S. Pastor, A. Blazquez-Martinez, J. Fernandez-Delgado, M. Nistal, J.L. Alió, M.P. De Miguel, Adipose-derived stem cells are a source for cell therapy of the corneal stroma, Stem Cells 26 (2008) 570–579, https://doi.org/10.1634/stemcells.2007-0653.
[129] L. Espandar, B. Bunnell, G.Y. Wang, P. Gregory, C. McBride, M. Moshirfar, Adipose-derived stem cells on hyaluronic acid-derived scaffold, Arch. Ophthalmol. 130 (2012) 202, https://doi.org/10.1001/archopthalmol.2011.1398.
[130] S. Zhang, L. Espandar, K.M.P. Imhof, B.A. Bunnell, Differentiation of human adipose-derived stem cells along the keratocyte lineage In vitro, J. Clin. Exp. Ophthalmol. 04 (2013) 270, https://doi.org/10.4172/2155-9570.1000270.
[131] J.L. Alió Del Barrio, M. El Zarif, M.P. De Miguel, A. Azaar, N. Makdissy, W. Harb, I. El Achkar, F. Arnalich-Montiel, J.L. Alió, Cellular therapy with human autologous adipose-derived adult stem cells for advanced keratoconus, Cornea 36 (2017) 952–960, https://doi.org/10.1097/ICO.0000000000001228.
[132] R.W. Naylor, C.N.J. McGhee, C.A. Cowan, A.J. Davidson, T.M. Holm, T. Sherwin, Derivation of corneal keratocyte-like cells from human induced pluripotent stem cells, e0165464, PLoS One. 11 (2016), https://doi.org/10.1371/journal.pone.0165464.
[133] I. Gutierrez-Aranda, V. Ramos-Mejia, C. Bueno, M. Munoz-Lopez, P.J. Real, A. Mácia, L. Sanchez, G. Ligero, J.L. Garcia-Parez, P. Menendez, Human induced pluripotent stem cells develop teratoma more efficiently and faster than human embryonic stem cells regardless the site of injection, Stem Cells. 28 (2010) 1568–1570, https://doi.org/10.1002/stem.471.
[134] J. Zhang, C.-W. Zhang, L.-Q. Du, X.-Y. Wu, Acellular porcine corneal matrix as a carrier scaffold for cultivating human corneal epithelial cells and fibroblasts in vitro, Int. J. Ophthalmol. 9 (2016) 1–8, https://doi.org/10.18240/ijo.2016.01.01.
[135] Y. Dai, J. Chen, H. Li, S. Li, J. Chen, Y. Ding, J. Wu, C. Wang, M. Tan, Characterizing the effects of VPA, VC and RCCS on rabbit keratocytes onto decellularized bovine cornea, PLoS One 7 (2012) 1–10, https://doi.org/10.1371/journal.pone.0050114.
[136] H.S. Dua, J.S. Saini, A. Azuara-Blanco, P. Gupta, Limbal stem cell deficiency: concept, aetiology, clinical presentation, diagnosis and management, Indian J.

Ophthalmol. 48 (2000) 83–92.
[137] P. Rama, S. Matuska, G. Paganoni, A. Spinelli, M. De Luca, G. Pellegrini, Limbal stem-cell therapy and long-term corneal regeneration, N. Engl. J. Med. 363 (2010) 147–155, https://doi.org/10.1056/NEJMoa0905955.
[138] K. Nishida, M. Yamato, Y. Hayashida, K. Watanabe, K. Yamamoto, E. Adachi, S. Nagai, A. Kikuchi, N. Maeda, H. Watanabe, T. Okano, Y. Tano, Corneal reconstruction with tissue-engineered cell sheets composed of autologous oral mucosal epithelium, N. Engl. J. Med. 351 (2004) 1187–1196, https://doi.org/10.1056/NEJMoa040455.
[139] S. Kolli, S. Ahmad, H.S. Mudhar, A. Meeny, M. Lako, F.C. Figueiredo, Successful application of Ex Vivo expanded human autologous oral mucosal epithelium for the treatment of total bilateral limbal stem cell deficiency, Stem Cells. 32 (2014) 2135–2146, https://doi.org/10.1002/stem.1694.
[140] A. Mikhailova, T. Ilmarinen, H. Uusitalo, H. Skottman, Small-molecule induction promotes corneal epithelial cell differentiation from human induced pluripotent stem cells, Stem Cell Rep. 2 (2014) 219–231, https://doi.org/10.1016/j.stemcr.2013.12.014.
[141] N.C. Joyce, S.E. Navon, S. Roy, J.D. Zieske, Expression of cell cycle-associated proteins in human and rabbit corneal endothelium in situ, Invest. Ophthalmol. Vis. Sci. 37 (1996) 1566–1575.
[142] N.C. Joyce, B. Meklir, S.J. Joyce, J.D. Zieske, Cell cycle protein expression and proliferative status in human corneal cells, Invest. Ophthalmol. Vis. Sci. 37 (1996) 645–655.
[143] Y.Q. Soh, G.S.L. Peh, J.S. Mehta, Translational issues for human corneal endothelial tissue engineering, J. Tissue Eng. Regen. Med. 11 (2017) 2425–2442, https://doi.org/10.1002/term.2131.
[144] M.D. Wagoner, L.R. Bohrer, B.T. Aldrich, M.A. Greiner, R.F. Mullins, K.S. Worthington, B.A. Tucker, L.A. Wiley, Feeder-free differentiation of cells exhibiting characteristics of corneal endothelium from human induced pluripotent stem cells, Biol. Open. 7 (2018) bio032102, https://doi.org/10.1242/bio.032102.
[145] C. Ju, L. Gao, X. Wu, K. Pang, A human corneal endothelium equivalent constructed with acellular porcine corneal matrix, Indian J. Med. Res. 135 (2012) 887–894.
[146] T. Bayyoud, S. Thaler, J. Hofmann, C. Maurus, M.S. Spitzer, K.U. Bartz-Schmidt, P. Szurman, E. Yoeruek, Decellularized bovine corneal posterior lamellae as carrier matrix for cultivated human corneal endothelial cells, Curr. Eye Res. 37 (2012) 179–186, https://doi.org/10.3109/02713683.2011.644382.
[147] B. Van den Bogerd, S. Ní Dhubhghaill, N. Zakaria, Characterizing human decellularized crystalline lens capsules as a scaffold for corneal endothelial tissue engineering, J. Tissue Eng. Regen. Med. 12 (2018) e2020–e2028, https://doi.org/10.1002/term.2633.
[148] S. Amano, N. Shimomura, S. Yokoo, K. Araki-Sasaki, S. Yamagami, Decellularizing corneal stroma using N2 gas, Mol. Vis. 14 (2008) 878–882.
[149] V. Hurmeric, S.H. Yoo, F.M. Mutlu, Optical coherence tomography in cornea and refractive surgery, Expert Rev. Ophthalmol. 7 (2012) 241–250, https://doi.org/10.1586/eop.12.28.
[150] L.A. Faraj, D.G. Said, M. Al-Aqaba, A.M. Otri, H.S. Dua, Clinical evaluation and characterisation of corneal vascularisation, Br. J. Ophthalmol. 100 (2016) 315–322, https://doi.org/10.1136/bjophthalmol-2015-306686.
[151] N. Lagali, B. Bourghardt, J. Germundsson, U. Eden, R. Danyali, M. Rinaldo, P. Fagerholm, Laser-Scanning in vivo Confocal Microscopy of the Cornea: Imaging and Analysis Methods for Preclinical and Clinical Applications, in: Confocal Laser Microsc. - Princ. Appl. Med. Biol. Food Sci., InTech, 2013. doi: 10.5772/55216.
[152] N. Lagali M. Griffith P. Fagerholm In, in: B. Wright, C.J. Connon (Eds.), Corneal Regen. Med., Vivo Confocal Microscopy of the Cornea to Assess Tissue Regenerative Response After Biomaterial Implantation in Humans 2013 Humana Press Totowa, NJ pp. 211–223. doi: 10.1007/978-1-62703-432-6.
[153] M.M. Islam, O. Buznyk, J.C. Reddy, N. Pasyechnikova, E.I. Alarcon, S. Hayes, P. Lewis, P. Fagerholm, C. He, S. Iakymenko, W. Liu, K.M. Meek, V.S. Sangwan, M. Griffith, Biomaterials-enabled cornea regeneration in patients at high risk for rejection of donor tissue transplantation, Npj Regen. Med. 3 (2018) 2, https://doi.org/10.1038/s41536-017-0038-8.
[154] H. Aghamohammadzadeh, R.H. Newton, K.M. Meek, X-Ray scattering used to map the preferred collagen orientation in the human cornea and limbus, Structure 12 (2004) 249–256, https://doi.org/10.1016/j.str.2004.01.002.
[155] X.-T. Yin, D.A. Tajfirouz, P.M. Stuart, Murine corneal transplantation: a model to study the most common form of solid organ transplantation, e51830–e51830, J. Vis. Exp. (2014), https://doi.org/10.3791/51830.
[156] O. Treacy, L. O'Flynn, A.E. Ryan, M. Morcos, P. Lohan, S. Schu, M. Wilk, G. Fahy, M.D. Griffin, M. Nosov, T. Ritter, Mesenchymal stem cell therapy promotes corneal allograft survival in rats by local and systemic immunomodulation, Am. J. Transplant. 14 (2014) 2023–2036, https://doi.org/10.1111/ajt.12828.
[157] N. Murphy, K. Lynch, P. Lohan, O. Treacy, T. Ritter, Mesenchymal stem cell therapy to promote corneal allograft survival: current status and pathway to clinical translation, Curr. Opin. Organ Transplant. 21 (2016) 559–567, https://doi.org/10.1097/MOT.0000000000000360.
[158] M. Maenz, M. Morcos, T. Ritter, A comprehensive flow-cytometric analysis of graft infiltrating lymphocytes, draining lymph nodes and serum during the rejection phase in a fully allogeneic rat cornea transplant model, Mol. Vis. 17 (2011) 420–429.
[159] M.A. Shafiq, B.Y. Milani, A.R. Djalilian, In vivo evaluation of a decellularized limbal graft for limbal reconstruction, Int. J. Tissue Eng. 2014 (2014) 1–6, https://doi.org/10.1155/2014/754245.
[160] A. Gwon, The Rabbit in Cataract/IOL Surgery (2008), https://doi.org/10.1016/B978-0-12-374169-1.00013-8.
[161] W. Liu, C. Deng, C.R. McLaughlin, P. Fagerholm, N.S. Lagali, B. Heyne, J.C. Scaiano, M.A. Watsky, Y. Kato, R. Munger, N. Shinozaki, F. Li, M. Griffith, Collagen–phosphorylcholine interpenetrating network hydrogels as corneal substitutes, Biomaterials 30 (2009) 1551–1559, https://doi.org/10.1016/J.BIOMATERIALS.2008.11.022.
[162] J.R. Jangamreddy, M.K.C. Haagdorens, M. Mirazul Islam, P. Lewis, A. Samanta, P. Fagerholm, A. Liszka, M.K. Ljunggren, O. Buznyk, E.I. Alarcon, N. Zakaria, K.M. Meek, M. Griffith, Short peptide analogs as alternatives to collagen in pro-regenerative corneal implants, Acta Biomater. 69 (2018) 120–130, https://doi.org/10.1016/j.actbio.2018.01.011.
[163] J. Zheng, X. Huang, Y. Zhang, Y. Wang, Q. Qin, L. Lin, X. Jin, C. Lam, J. Zhang, Short-term results of acellular porcine corneal stroma keratoplasty for herpes simplex keratitis, Xenotransplantation (2019), https://doi.org/10.1111/xen.12509.
[164] Y. Lin, Q. Zheng, S. Hua, Y. Meng, W. Chen, Y. Wang, Cross-linked decellularized porcine corneal graft for treating fungal keratitis, Sci. Rep. 7 (2017) 1–11, https://doi.org/10.1038/s41598-017-08207-3.

ADVANCED FUNCTIONAL MATERIALS
www.afm-journal.de

Designing Scaffolds for Corneal Regeneration

Mark Ahearne, Julia Fernández-Pérez, Sophia Masterton, Peter W. Madden, and Promita Bhattacharjee*

Corneal blindness is one of the most common causes of vision loss worldwide, affecting millions of people. To treat these patients, researchers have been examining different approaches to engineer corneal scaffolds suitable for transplantation. Scaffolds have been developed to replace part or all of the cornea depending on the patient requirements. Both acellular and cell-seeded scaffolds have been tested in animal models. Materials that have been under investigation for manufacturing scaffolds include collagen, silk fibroin, amniotic membrane, decellularized cornea, fibrin, chitosan, gelatin, agarose, alginate, and hyaluronic acid in addition to several synthetic polymers. Different combinations of materials, fiber crosslinking techniques, and incorporation of bioactive molecules have also been examined. Factors such as the physical properties, cytocompatibility, degradation behavior, and optical characteristics have to be considered when selecting a suitable scaffold material. Recent advancements in materials fabrication techniques such as bioprinting, electrospinning, and different collagen alignment techniques, allow scaffolds to be generated that more accurately mimic the structure of the corneal stroma. A number of scaffolds have commenced clinical trials to determine their suitability for corneal regeneration.

1. Introduction

The cornea is a transparent, multilayered component of the ocular surface whose primary function is to focus light onto the lens where it is directed toward the retina. Each distinct layer of the cornea differs in composition, structure, function, and the type of cells resident (**Figure 1**). The epithelium is the outer layer of the cornea and consists of stratified epithelial cells that are replenished from stem cells located in limbal crypts along the corneal-conjunctival boundary.[1] These cells form a barrier that allows the diffusion of oxygen and essential nutrients from the tear film but prevents pathogens and debris penetrating into the eye. The Bowman's layer along with a basement membrane are acellular collagenous layers that separate the epithelium from the stroma. The Bowman's layer has a high stiffness[2] but poor regenerative properties after injury. The stroma, which constitutes 90% of the total corneal thickness, comprises a highly structured orthogonal arrangement of small, evenly spaced collagen fibrils, 31–34 nm in diameter[3] and surrounded by other collagens and proteoglycans. The stroma contains neural crest derived cells called keratocytes that maintain the tissue's homeostasis and can be activated upon injury. The Descemet's membrane connects the endothelium to the posterior side of the stroma. The inner layer of the cornea is the endothelium and consists of a single layer of endothelial cells whose primary function is regulating the hydration of the whole cornea. Damage to this layer results in swelling and impairment of vision. The overall thickness of the cornea is ≈0.53 mm at the center, increasing to 0.71 mm closer to the edge.[4]

Damage to the cornea's cells or extracellular matrix (ECM) resulting from medical conditions or physical damage can lead to impaired vision. For many indications, a corneal transplant is required to preserve or improve the patient's sight. Corneal transplants have a high success rate relative to other tissues and organs partially due to the absence of vascular and lymphatic vessels in the cornea reducing the chances of immune rejection.[5] However, globally there is a shortage of donor corneas suitable for transplantation for a variety of reasons including lack of awareness about donations, lack of facilities in some countries to remove and store corneas and not all corneas being suitable for donation.[6] For these reasons there has been considerable interest in the need to develop alternative treatment strategies.

One alternative to transplanting corneas is to use a keratoprosthesis. These devices replace the cornea with a transparent polymer and enable the full or partial restoration of vision. The most commonly used keratoprosthesis is the Boston keratoprosthesis, although, despite its success in improving vision for many patients, several complications are associated with these implants including an increased risk of glaucoma,[7] endophthalmitis,[8]

Prof. M. Ahearne, J. Fernández-Pérez, S. Masterton, Dr. P. W. Madden, Dr. P. Bhattacharjee
Trinity Centre for Biomedical Engineering
Trinity Biomedical Sciences Institute
Trinity College Dublin
The University of Dublin
Dublin 2, Ireland
E-mail: ahearnm@tcd.ie

Prof. M. Ahearne, J. Fernández-Pérez, S. Masterton, Dr. P. W. Madden, Dr. P. Bhattacharjee
Department of Mechanical and Manufacturing Engineering
School of Engineering
Trinity College Dublin
The University of Dublin
Dublin 2, Ireland

The ORCID identification number(s) for the author(s) of this article can be found under https://doi.org/10.1002/adfm.201908996.

DOI: 10.1002/adfm.201908996

retroprosthetic membrane formation,[9] and corneal melt.[10] Other keratoprosthesis include the AlphaCor and the osteo-odonto keratoprosthesis, although these too have many limitations. Currently, keratoprostheses are normally only used in cases where the patient is unable to sustain a corneal transplant and this is the only option to regain some vision.

Tissue engineering approaches offer a different solution to the lack of donor corneas available for transplantation. Most engineered tissues are fabricated using a top-down approach by combining cells with a biomaterial-based scaffold to replicate the real tissue. Unlike keratoprostheses that contain no cells, in principle, tissue engineered corneas can adapt to biological and biophysical cues in a similar manner to native corneas. Tissue engineering is still relatively new, the concept was first investigated in the early 1990's,[11] hence there is considerable research still continuing into its development and application. Two key factors in determining the potential of an engineered tissue to accurately mimic native tissue is the type of material used to fabricate the scaffold and how the scaffold is manufactured. A number of recent review papers and book chapters have focused on different types of scaffolds for corneal tissue engineering including stromal scaffolds,[12] nanomaterial scaffolds,[13] decellularized scaffolds,[14] and bioprinted scaffolds.[15] Here, we provide a more comprehensive overview of corneal scaffolds to repair or replace the different layers of the cornea. In addition, a systematic process for designing corneal scaffolds has been outlined. Several important factors that need to be considered before designing corneal scaffolds are discussed, different biomaterials that can be used to generate scaffolds suitable for engineering cornea are evaluated and several advanced fabrication techniques and novel scaffold designs are considered. Finally, a future perspective is provided discussing where corneal tissue engineering might be heading.

2. Design Considerations

It is often beneficial to outline a clear design process prior to the commencement of any design project. An example of how such a process could be applied to designing corneal scaffolds is shown in **Table 1**. First, it is important to ask what is the problem that we are trying to solve and whether a scaffold is necessary. For cornea, the problem is a lack of healthy donor tissue to replace part or all of a damaged or diseased cornea. While scaffold free approaches to this problem have some merit, scaffolds provide a useful artificial matrix to allow a tissue to form. Once the problem is understood, a thorough review of literature and patents should commence to determine the progress made in addressing this problem, the limitations with other approaches and potentially identify new solutions. Next, the specific user and material requirements of the scaffolds need to be defined. Using this information, a prototype should be designed, fabricated, and assessed physically and biochemically. These steps should be repeated until a scaffold that fulfills all the user requirements has been developed. Finally, it is important to consider the regulatory approval process early in the design process. It may be advantageous to use materials and fabrication processes that have already undergone approval for other applications.

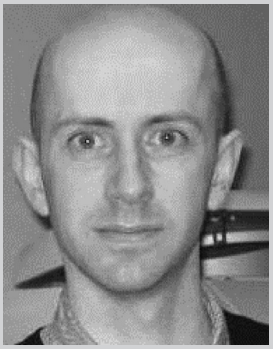

Mark Ahearne is Assistant Professor in Biomedical Engineering at Trinity College Dublin, The University of Dublin. He received a B.E. in Mechanical Engineering from the University of Limerick in 2001, an M.Sc. in Cell and Tissue Engineering from Keele University in 2003, and a Ph.D. in Biomedical Engineering from Keele University in 2007. He subsequently worked as a research fellow at Keele University and Trinity College Dublin before being appointed to his current position in 2015. His research interests include corneal regeneration, tissue engineering, biomaterials, and ocular mechanobiology.

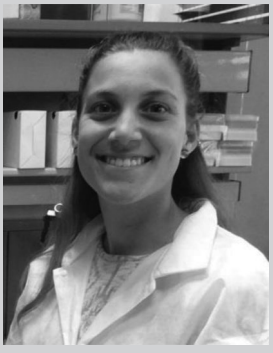

Julia Fernández-Pérez is a Ph.D. student at the Trinity Center for Biomedical Engineering at Trinity College Dublin. She received a B.Sc. in Human Biology from Pompeu Fabra University in Barcelona. She graduated from the Technical University of Dresden, where she obtained her M.Sc. in Molecular Bioengineering. She is currently developing alternatives to traditional corneal transplantation using tissue engineering approaches, focusing on the use of decellularized matrices.

Sophia Masterton is a Ph.D. candidate at Trinity Centre for Biomedical Engineering focusing on corneal epithelium mechanobiology. She obtained her M.Sc. degree from Trinity College Dublin in 2014 in Molecular Medicine and her B.Sc. in Biochemistry from University College Dublin. Her research interests include the mechanical regulation of the corneal epithelium with a focus on how this affects stem cell maintenance. Her current work is examining shear stress regulation of corneal epithelial cells and deciphering the role of mechanical regulatory mechanisms in the corneal epithelium.

2.1. Surgical Application

One of the first factors to consider when designing a scaffold for corneal regeneration is how it will be applied. Depending on the type of injury or medical condition that a patient

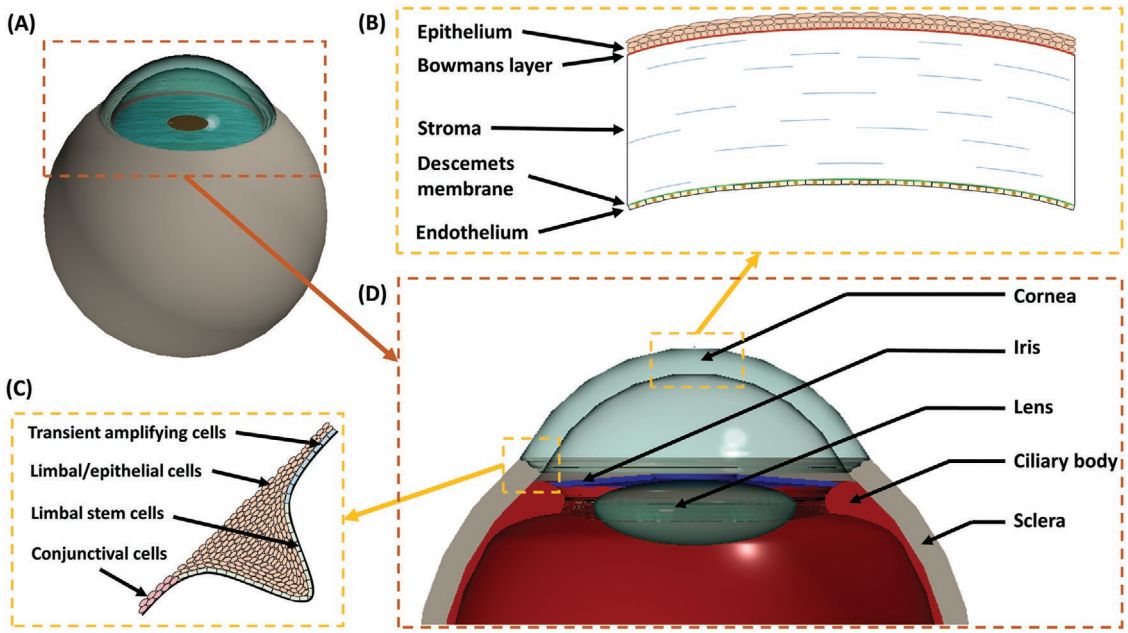

Figure 1. Schematic representations of A) the human eye with the cornea visible on the anterior surface; B) cross-section of part of the cornea showing the different layers present; C) cross-section of a limbal crypt with the different cell types; D) cross-section of the anterior segments of the eye.

suffered, several different types of surgeries or keratoplasties can be used to restore vision (**Table 2**). Traditionally, penetrating keratoplasty (PKP) involves the removal of the full thickness of the central cornea, leaving only a small rim of tissue near the limbal interface (**Figure 2**). A donated cornea is then positioned in the space left by the patient's cornea and sutured in place. While PKP is still relatively common, alternative procedures that require specific layers of the cornea to be transplanted such as anterior lamellar keratoplasty (ALK), deep anterior lamellar keratoplasty (DALK), Descemet's membrane endothelial keratoplasty (DMEK), and Descemet's stripping endothelial keratoplasty (DSEK) have become increasingly popular. Between 2005 and 2014, the percentage of keratoplasties in United States that were PKP fell from 95% to 42%[16] with similar trends found in other countries.[17] Transplantation of limbal tissue (LT) has also become more popular in recent years as a method of treating conditions that result in limbal stem cell deficiencies.

Table 1. Design process for developing corneal scaffolds.

Design process	Application to cornea
Define problem	A lack of corneal tissue suitable for keratoplasties
Research current solutions	Keratoprosthesis, stem cells, tissue engineering, etc.
Define user requirement	For patient: to restore and maintain vision without pain or medical complications For surgeon: easy to handle and suture For industry: cost, market size, and scalability
Specify material requirement	Biocompatibility, cell adhesion, regulation of cell behavior, degradation, mechanical properties, transparency, etc.
Design prototype	Select suitable material, fabrication process, sterilization technique, etc.
Evaluate design	In vitro using appropriate cells in culture, in vivo using animal model; both physical and biological properties need to be considered
Optimization	Use findings of previous steps to modify and improve the scaffold design
Seek regulatory approval	Interact with regulatory bodies early to discuss the feasibility of clinical translating design to treat patients

The type of surgery that is required has a significant influence on the type of scaffold required. For procedures such as LT or DMEK, a thin, flexible, and permeable film capable of supporting the cells is ideal. For DMEK, the film would also need to allow it to be rolled up to enable its insertion under the cornea and it should degrade without the release of any cytotoxic or inflammatory constituents. For surgeries involving replacement of the stroma, a thicker 3D scaffold capable of containing cells would be needed.

2.2. Cells

Once the type of keratoplasty is known, the next decision is to determine if it is necessary to culture cells in the scaffold prior to transplantation or to design the scaffold to allow the patient's own cells to repopulate it in vivo post-transplantation. In cases where there is a lack of endothelial cells, it will be necessary to culture cells on the scaffold prior to transplantation as corneal endothelial cells have poor proliferative capacity due to being arrested in the G1 phase of the cell cycle[18] and just implanting a biomaterial without cells would likely be of little benefit. Similarly, for patients with limbal stem cell deficiencies, cells are required to repopulate the limbal region of the eye. Acellular biomaterials could be used to deliver specific biomolecules to accelerate regeneration and repair, with amniotic membranes

Table 2. Types of corneal surgery and clinical indications.

Surgery	Abbreviation	Layers needed	Possible indications
Penetrating keratoplasty	PKP	Full thickness cornea	Severe keratoconus with damage to endothelium
Anterior lamellar keratoplasty	ALK	Epithelium, Bowmans layer, partial stroma	Keratoconus, anterior scarring
Deep anterior lamellar keratoplasty	DALK	Epithelium, Bowmans layer, most of the stroma	Keratoconus
Descemets membrane endothelial keratoplasty	DMEK	Endothelium, Descemets membrane	Bullous keratopathy, Fuchs dystrophy
Descemets stripping endothelial keratoplasty	DSEK	Endothelium, Descemets membrane, partial stroma	Bullous keratopathy, Fuchs dystrophy
Limbal transplant	LT	Limbus	Limbal stem cell deficiency, Stephen-Johnson syndrome, aniridia

currently used in this way to deliver molecules capable of inhibiting inflammation, scarring, and angiogenesis.[19]

Different reports have investigated the use of cell seeded and acellular scaffolds to replace the stroma, although few studies have undertaken direct comparisons between the two. To promote cell infiltration of acellular scaffolds post-transplantation, the scaffolds need to be sufficiently porous to allow cells to enter[20] or contain extracellular matrix proteins that the cells can degrade or remodel.[21] Topographical cues such as aligned fibers may also be used to guide cells into a scaffold.[22] Biochemical cues could also be incorporated into the scaffold to promote a chemotactic response and increase cell infiltration and proliferation.[23] However, it should be noted that cells from rabbit and human corneas behave quite differently to each other[24] and the size, thickness, and mechanical behavior of rabbit corneas also differs to human,[25] therefore the rabbit data may not be directly translatable to humans.

Should it be decided that scaffolds are to be seeded with cells prior to transplantation, the source and phenotype of the cells has to be considered. The three main cell types in the cornea (epithelial, stromal, and endothelial) all have different challenges associated with their culture and application. Limbal derived epithelial cells can be contaminated by stromal cells quite easily and normally require a feeder layer to allow their expansion in culture. Stromal cells become fibroblastic in the presence of serum but are slow to proliferate in serum free conditions. One approach to overcome this limitation is to expand the cells in serum and then switch to a supplemented serum free medium that allows the partial restoration of the cell phenotype.[26] Endothelial cells are particularly difficult to culture particularly as most donors as quite old and their cells no longer support proliferation.

While autologous cells may reduce the risk of rejection, these can be difficult to obtain from the patient's own cornea in sufficient quantities due to the probable lack of healthy tissue. Some studies have taken limbal cells from the patient's healthy eye, expanded these cells in vitro, and transferred them to the damaged eye using a scaffold.[27] Cells can also be isolated from other tissues in the body or other sources and used to populate scaffolds for corneal stromal regeneration. Bone marrow derived mesenchymal stem cells (BMSCs),[28] adipose derived stem cells (ASCs),[29] and embryonic stem cells (ESCs)[30] and umbilical cord stem cells (USCs)[31] have all been shown to be capable of differentiating toward a keratocyte lineage when cultured under specific biochemical conditions. However, a recent study by Dos Santos et al. showed that corneal derived stem cells were better at developing a keratocyte lineage and were less inflammatory compared to BMSCs, ASCs, and USCs.[32] In addition, it has recently been suggested that MSCs are not truly stem cells when in the body but rather they just release molecules to support and regulate the existing cell populations after implantation.[33] Induced pluripotent stem cells (iPSCs) have also been suggested as an alternative source of stem cells and have been shown to be capable of inducing epithelial, keratocyte, and endothelial phenotypes although challenges such as genetic variability and unwanted differentiation remain to be overcome.[34]

An alternative to using a scaffold is to culture cells over a prolonged period and allow the cells to generate new tissue using a "bottom-up approach" rather than a "top-down approach."

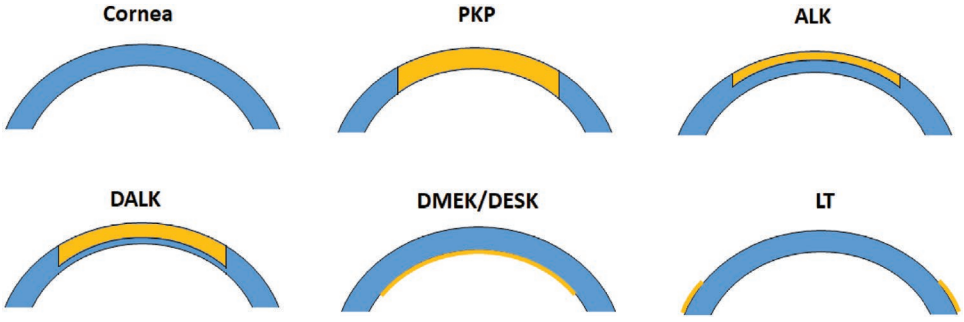

Figure 2. Schematic representation of the different types of keratoplasty. The blue section represents the original cornea and yellow represents the transplanted cells or tissue (PKP = penetrating keratoplasty, ALK = anterior lamellar keratoplasty, DALK = deep anterior lamellar keratoplasty, DMEK = Descemets membrane endothelial keratoplasty; Descemets stripping endothelial keratoplasty, LT = limbal transplant).

This technique has been shown to be capable of generating stromal tissue with good transparency and a fibril organization and matrix composition similar to that found in the native corneal stoma.[35] The stroma formed is also capable of supporting epithelium and endothelium formation. The main limitations with this approach are the time taken to culture sufficient number of cells and the limited thickness of the stromal tissue with reports suggesting a culture time of 4–5 weeks to generate 50 µm thick stroma. Research by the Zeugolis lab has shown that the stromal tissue formation process by cells can be accelerated using macromolecular crowding, a technique that reduces the amount of procollagen being washed away in the cell culture medium.[36] A simple method of overcoming the issues with thickness could potentially be resolved by stacking multiple stromal sheets,[37] although the success of the implant would be dependent on how well the layers integrate with each other. The integration of the layers is particularly important for PKP and DLKP where multiple layers would be required and there is a danger of slippage between layers leading to degradation. The self-assembly of cells has also been used to generate epithelium on a temperature responsive carrier material that allows the detachment of the cells from the material without the need for enzymes.[38] Since the focus of this paper is on corneal scaffold design, the proceeding sections will concentrate on scaffold-based solutions rather than the bottom-up approach.

2.3. Scaffold Physical Properties

To determine the suitability of a scaffold for corneal regeneration or replacement, it is important to understand how cells will interact with the scaffold both in vitro and in vivo. Factors such as cell adhesion, morphology, migration, proliferation, and extracellular matrix production are all influenced by the physical and chemical properties of the scaffold. Several studies have shown that the stiffness of a material can influence the phenotype of many different cell types including corneal epithelial cells,[39] limbal derived stem cells,[40] corneal stromal cells,[41] and corneal endothelial cells.[42] For stromal derived cells, culture on a low stiffness appears to reduce transforming growth factor β1 (TGF-β1) induced myofibroblastic differentiation.[41a,43]

In addition to affecting how cells behave, mechanical properties of the scaffolds are also important for functional reasons. The scaffolds must be sufficiently stiff and strong to be able to withstand suturing without tearing and withstand physiological forces applied to it postimplantation such as intraocular pressure, eyelid motion, and tear film motion.[44] If the scaffold is insufficiently stiff or strong, it could undergo deformation or failure, respectively. The scaffold stiffness should also not be too high, as this would reduce its ability to deform in the same way as the surrounding tissue when under stress and potentially lead to a mismatch in strain. The viscoelastic characteristics of cornea also have to be considered as these influence the behavior of the cornea under load.[45] Ideally, the scaffold mechanical properties should match the native corneas as close as possible. Young's modulus and tensile strength of cornea varying considerable between publications (modulus ≈100 kPa to 57 MPa; strength ≈3–6 MPa) due to the tissue anisotropy, different testing mechanisms and donor variability.[46] Corneal permeability (≈2.2×10^{-18} m^4 N^{-1} s^{-1}[47]) is another factor that is often overlooked when designing scaffolds but is vital for allowing nutrients and gases into the central cornea.

Another factor that will influence how cells behave is the structure of the scaffolds. In vivo corneal stromal cells reside between layers of aligned collagen fibrils. To examine how these cells response in vitro to such topographical cues, channels with widths and depths in the micrometer and nanometer ranges have been used. Aligned substrates were found to increase corneal stromal cell alignment, direct cell migration and promote a keratocyte phenotype.[48] Similarly, channels that mimic the nanostructure of the corneal basement membrane,[49] have been shown to affect corneal epithelial cells elongation, adhesion, proliferation, and gene expression.[48d,50] Scaffolds have also been developed to study the effect of topographical cues on corneal cells in a 3D environment since this is more physiologically relevant. Wilson et al. showed that incorporating aligned nanofibers into a hydrogel increased expression of keratocyte specific genes and reduced expression of myofibroblastic genes.[51] In addition to surface topography, it has recently been shown that surface curvature can also influence the orientation and phenotype of corneal stromal and epithelial cells.[52]

In addition to the scaffold affecting how the cells behave, reciprocally, cells can remodel the scaffold through the application of strain and the release of enzymes and extracellular matrix molecules.[53] It is therefore important that the scaffold supports the cells to remodel it into a tissue that resembles real cornea. Ideally, as the scaffold degrades ECM molecules should replace the structure without compromising its integrity or functionality. Generation of aligned collagen fibrils in the stroma while remodeling is important for corneal transparency and may be assisted by initially aligning the scaffold in a similar pattern. For example, low concentration collagen hydrogels seeded with corneal fibroblasts undergo contraction and form an opaque sphere unless tethered to a support structure such as a ring.[53] Factors such as seeding density, culture media composition, biomaterial degradation resistance, material concentration in hydrogels, porosity, and structure can be optimized to control the remodeling process. Some scaffolds may be designed to avoid remodeling and degradation and instead provide a stable implant that does not change over time. While this has some advantages, including lower risk of uncontrolled degradation and reduced susceptibility to donor/patient variability over long time periods, these implants would likely fail due to the lack of regeneration occurring. Hence, scaffolds that support remodeling and regeneration have more potential as corneal substitutes.

The phenotype of the cells is another important factor, particularly for stromal remodeling with quiescent keratocytes being noncontractile and producing minimal matrix components, while myofibroblasts are highly contractile and produce different proteins and matrix metalloproteinases (MMPs).[54]

The biocompatibility of the scaffold is important to ensure that it survives after implantation. The materials used to fabricate the scaffolds and their degradation products need to be noncytotoxic and not induce a host immune response. Keratoplasties are often considered to be immune privileged since there are no blood or lymphatic vessels in the cornea. However, despite having a lower

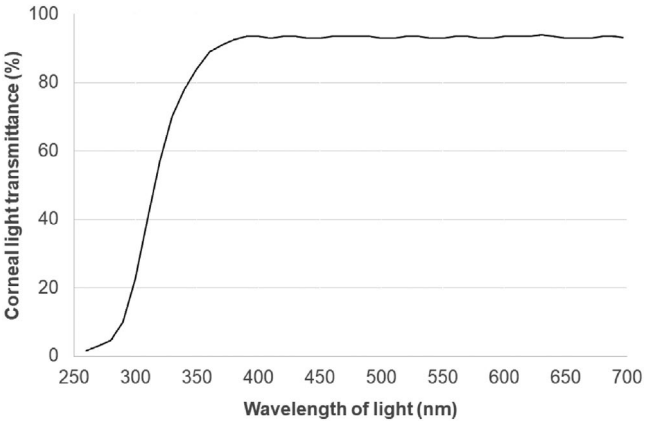

Figure 3. Image showing the transmittance of light through a cornea across different wavelengths.

immune rejection rate than many other tissues and organs, the implanted cornea can still illicit an immune response and undergo rejection. The risk of immune rejection increases with regrafts due to the initial severing of nerves leading to the loss of anterior chamber-associated immune deviation.[55]

2.4. Optical Properties

Another factor that needs to be considered when developing scaffolds for corneal regeneration is that the scaffolds need to have similar light transmittance characteristics to the real cornea. The cornea allows light from the visible light spectrum (wavelength 400–780 nm) to pass through while limiting light in the ultraviolet (UV) spectrum (less than 400 nm) as shown (**Figure 3**). The ability of UV light to pass though the cornea differs between the central and peripheral regions[56] and UV exposure can result in damage to the retina.[57] In addition, the cornea needs to be able to focus light through the lens into the retina. An improper curvature of the cornea (such as with astigmatism) can result in light not being focused correctly and lead to reduced vision.

The transparency of the cornea is dependent on its collagen fibril structure. The corneal stroma consists of small, aligned collagen fibrils with regular spacing between fibrils.[3] This highly organized arrangement is believed to be vital to allow light to pass between the fibrils since any disruption of this organization due to injury or disease results in a reduction in transparency.[58] The cells in the stroma also play a role in allowing visible light through the cornea. Crystalline proteins found in the cytoplasm such as ALDH1A1 and ALDH3A1 reduce the ability of keratocytes to scatter light.[59] When these cells are activated, the presence of these proteins is reduced and the cells disrupt the passage of light.

3. Materials Selection

3.1. Collagen

Collagen type I is the most abundant protein in the cornea with lesser amounts of other collagens also present.[3,60] Collagen forms a triple helix molecule containing repeating units of the amino acids glycine, proline, and hydroxyproline. In total, collagen constitutes ≈70% of the dry weight of the cornea.[61] For this reason, collagen has been a popular choice of material to manufacture scaffolds that mimic the native cornea's composition. Some of the earliest attempts at engineering corneal tissue used collagen scaffolds and hydrogels. For example, Germain et al. used collagen to engineer the anterior segment of the cornea.[62] Orwin and Hubel described the development of a collagen sponge that could support the growth of corneal epithelial, stromal, and endothelial cells.[63] However, despite these promising early studies, a number of challenges were evident including poor mechanical properties (Young's modulus of collagen sponge ≈95–370 Pa[47a]) and scaffolds not mimicking the stroma's native fibril organization. Numerous studies have since explored different methods of overcoming these issues and used collagen as their primary material for fabricating corneal scaffolds (summarized in **Table 3**).

Many collagen scaffolds have inferior mechanical properties and degradation resistance when compared to the native tissue.[78a] This is often due to a lower density of collagen being used to generate a scaffold compared to the collagen density in

Table 3. Summary of collagen-based scaffolds.

Application	Scaffold material	Tested in vivo	Refs.
Epithelial	Rat collagen I	No	[64]
Epithelial	Bovine collagen I	No	[61,65]
Epithelial	Bovine collagen I	Rabbit	[66]
Epithelial	Recombinant human collagen III	No	[67]
Epithelial	Recombinant human collagen III	Mini-pig and rabbit	[68]
Epithelial	Porcine collagen I + GAG	No	[69]
Epithelial and stroma	Porcine collagen I	Rabbit	[70]
Epithelial and stroma	Rat collagen I	Rabbit	[71]
Epithelial and stroma	Bovine collagen I	Rabbit	[72]
Epithelial and stroma	Bovine collagen I	Dog	[73]
Epithelial, stroma, and endothelium	Rat collagen I + GAG	No	[74]
Epithelial, stroma, and endothelium	Bovine collagen I	No	[63]
Stroma	Rat collagen I	No	[53,75]
Stroma	Rat collagen I	Rabbit	[76]
Stroma	Rat collagen I + PA	No	[77]
Stroma	Bovine collagen I	No	[47a,78]
Stroma	Bovine collagen I	Pig	[79]
Stroma	Porcine collagen I	Guinea pig	[80]
Stroma	Recombinant human collagen I and III	Mini-pig	[81]
Stroma	Recombinant human collagen III	No	[82]
Stroma	Recombinant human collagen III	Human	[83]
Endothelium	Rat collagen I	No	[84]
Endothelium	Bovine collagen I	Rabbit	[85]
Endothelium	Porcine collagen I	Rabbit	[86]
Endothelium	Human collagen I	Rabbit	[87]

real cornea and a lack of crosslinks between collagen fibers in the scaffolds. To overcome this problem, different crosslinking treatments have been explored. Chemical crosslinking by glutaraldehyde, 1-ethyl-3-(3-dimethyl aminopropyl) carbodiimide hydrochloride (EDC) and multifunctional dendrimers have been shown to significantly increase the modulus and strength of collagen-based scaffolds (Young's modulus increased to 1.4 MPa after dendrimer crosslinking).[61] The main limitation with these treatments is that these chemicals are cytotoxic so crosslinking can only be done on acellular scaffolds. Genipin has been suggested as a less cytotoxic alternative to crosslinking with glutaraldehyde,[88] however at the concentrations needed to significantly increase mechanical properties, it results in collagen scaffolds turning a dark blue color.[89] Crosslinking collagen with UVA light in the presence of riboflavin has been shown to increase the modulus of collagen hydrogels seeded with corneal stromal cells. This approach also led to a reduction in cell viability, albeit some viable cell remain after the treatment.[90] The addition of peptide amphiphiles (PAs) to collagen has been shown to control contraction to enable a curvature to be generated.[77]

Different types of collagen scaffolds have been developed for corneal tissue engineering including hydrogels, films and sponges. Collagen hydrogels usually have a very high water content (up to 99.7% v/v) but unlike many other hydrophilic hydrogels that are incompressible, the water content of collagen hydrogels can be reduced under compression, thus allowing the collagen concentration and hydrogel stiffness to be controlled.[91] Collagen films can be used to expand and transplant epithelial or endothelial cells[72,84b] or can be stacked to form multiple layers that mimic the stroma.[75b] Collagen sponges tend to have poor transparency compared to films or hydrogels and are believed to promote a myofibroblastic phenotype in stromal derived cells.[78c]

The source of collagen plays an important role in dictating the scaffold's physical and biological properties. Collagen used for manufacturing corneal scaffolds is usually derived from animal tissues such as bovine or porcine skin or rat-tail or porcine tendon. The species and tissue from which the collagen is taken can affect the final physical properties of the scaffolds.[92] The amino acids in collagen can vary between different species, which in turn affects the collagens overall characteristics.[93] The modulus of collagen hydrogel scaffolds has also been shown to be dependent on the age of the animal from which the collagen is derived.[94] Recently alternative sources to animal tissue have been investigated due to the potential risk of cross species disease transmission. Human derived collagen from bone chips has also been used for corneal tissue engineering, although the supply of such tissue is more limited than using animal derived collagen.[87] As a potentially safer alternative to animal collagen, recombinant human like collagen can be manufactured from specific plants, bacteria, and yeast cells.[95] This approach reduces the potential of disease transmission and should improve the consistency of the collagen produced since there are no donor variations. Transgenic animals may also be modified to secrete human like collagen in milk or other fluids.[96]

In addition to the collagen source, the type of collagen needs to be considered when producing a corneal scaffold. While the majority of studies have used type I collagen since this is the most widely available and the most abundant collagen in the stroma, other studies have focused on different types of collagen to generate scaffolds. For example, recombinant collagen type III has been shown to be suitable for manufacturing artificial stroma with similar optical properties and structure to the native stroma.[82] Merrett et al. and Lagali et al. found that type I and type III recombinant collagen scaffolds had similar physical properties to the corneal stroma and produced a similar cell response when used as a stromal replacement.[81] Clinical data suggests that recombinant collagen III implants remain stable and transparent for several years without inducing any negative side effects and could be used to treat patients with severe corneal damage.[83]

Collagen scaffolds can be processed in a number of different ways to give very different properties. One type of collagen scaffold that has been under investigation for corneal tissue engineering is referred to as a vitrigel.[97] This is a collagen hydrogel that has been vitrified and then rehydrated. Vitrification involves the slow dehydration of the hydrogel at a predetermined temperature to form a rigid glassy material. The result is a mechanically strong and stable material with good optical properties.[98] Vitrigels have been used to grow and transplant corneal epithelium[66] and endothelium[86] in animal models. More recently, the material has been used to manufacture ocular permeability and irritancy assays to assess the safety of chemical and pharmaceutical products.[99] One potential limitation with this material is that it is unclear how well corneal stromal cells migrate into the vitrigel, which might limit its applications as a stromal replacement.

One alternative approach to generating collagen scaffolds with aligned fibers and low immunogenicity is to use fish scales. Scales from the tilapia have been decellularized and decalcified to leave an organized, biocompatible collagen type I matrix.[100] These scaffolds have been tested intrastromally in vivo using rats[101] and rabbits.[100a,102] In these studies, the scaffolds were acellular upon implantation so it is not clear if they can be populated with keratocytes in vitro prior to implantation. While scales from tilapia have been the most extensively studied, scales from other species of fish have also been used to produce collagen scaffolds.[103] Fish scale derived scaffolds have also been used for culturing human corneal endothelial cells, however further modification of structure and surface chemistry is required before considering it as a potential cell carrier for endothelial cells.[104]

3.2. Silk Fibroin

Silk fibroin is a protein that has become a biomaterial of considerable interest for corneal tissue engineering and regeneration over recent years due to its biocompatibility, biodegradability, mechanical strength, transparency, and ability to be used in a wide variety of forms including hydrogels, sheets, fibers, and sponges as well as forming various nanomaterial structures.[105] Several silk products have been clinically approved for use in Europe and North America including silk sutures, silk dressings, and surgical meshes. A summary of studies involving the application of silk fibroin for corneal regeneration is shown (**Table 4**).

Table 4. Summary of silk fibroin scaffolds.

Application	Scaffold material	Tested in vivo	Refs.
Epithelial	*Bombyx mori*	No	[106]
Epithelial	*Bombyx mori* or *Antheraea pernyi*	No	[107]
Epithelial	*Bombyx mori* and RGD peptides or PDL	No	[108]
Epithelial	*Bombyx mori* and PEG	Rabbit	[109]
Epithelial and stroma	*Bombyx mori*	No	[110]
Epithelial and stroma	*Antheraea mylitta*	Rabbit	[111]
Epithelial and stroma	*Bombyx mori* and chitosan	Rabbit	[112]
Epithelial and stroma	*Bombyx mori* and collagen	Rabbit	[113]
Stroma	*Bombyx mori*	No	[114]
Stroma	*Bombyx mori*	Rabbit	[115]
Stroma	*Bombyx mori* and RGD peptides	No	[116]
Stroma	*Bombyx mori* and chitosan	Rabbit	[117]
Stroma	*Bombyx mori* and RGD peptides	Rabbit	[118]
Stroma	*Bombyx mori*, retinoic acid, and riboflavin	No	[119]
Endothelium	*Bombyx mori*	No	[120]
Endothelium	*Bombyx mori*	Rabbit	[121]
Endothelium	*Bombyx mori* and aloe vera	Rabbit	[122]
Endothelium	*Bombyx mori* and PLLA/PCL	No	[123]
Endothelium	*Bombyx mori* and collagen	No	[124]
Endothelium	*Bombyx mori* and beta-carotene	No	[125]
Endothelium	*Bombyx mori* and glycerol	No	[126]

Silk fibroin derived from *Bombyx mori* cocoons has been the most extensively evaluated for use in engineering cornea. These silkworms are commonly used to produce silk for clothes, hence the cocoons are much cheaper than other sources. Hogerheyde et al. explored the use of silk fibroin derived from *Antheraea pernyi* cocoons for culturing and transplanting corneal epithelial cells but found the material to be less transparent and more brittle than *B. mori* fibroin.[107] Hazra et al. examined the use of *Antheraea mylitta* cocoons to isolate fibroin for corneal regeneration.[111] This study showed that *A. mylitta* derived fibroin was transparent, supported cell growth, and was nonimmunogenic when implanted into the corneal stroma of rabbits. However, the study did not compare the fibroin directly to *B. mori* fibroin so it is unclear if *A. mylitta* fibroin has any additional benefits or limitations. One benefit might be that *A. mylitta* fibroin is chemically different from *B. mori* and contains arginyl-glycyl-aspartic acid (RGD) peptides that enhance cell adhesion.[127] Silk fibroin isolated from other sources such as spider silk has to date not been examined for corneal tissue engineering or regeneration.

Several studies have modified *B. mori* silk fibroin by adding other molecules to alter its chemical properties and how it interacts with cells. For example, several studies have added RGD peptides to improve cell adhesion and spreading on fibroin. However, Jia et al. found that the addition of RGD to fibroin led to an increase in hydrophobicity and therefore suggested the addition of poly-D-lysine (PDL) to fibroin as an alternative approach to improve cell adhesion.[108] Silk fibroin has also been blended with other biomaterials such as collagen or chitosan[112,117] to improve cell attachment and proliferation. Crosslinking silk fibroin films using riboflavin and UVA light has been shown improve their adhesion to the ocular surface.[106g] Bioactive molecules, such as retinoic acid, have also been incorporated into silk fibroin to regulate the phenotype of corneal stromal cells.[119]

Silk fibroin provides a useful substrate to incorporate topographical cues that can deliberately influence cell behavior. As stated previously, microgrooves and nanogrooves have been shown to direct cell migration and affect cell phenotype. These patterns can be imprinted onto silk fibroin using lithography or casting techniques. Patterned silk fibroin has been used to examine the influence of topographical channels on epithelial cell phenotype,[50a] epithelial migration,[106e] limbal cell adhesion and cytoskeletal organization,[106d] and limbal cell differentiation.[128] Stromal stem cells and fibroblasts have also been cultured on pattern silk fibroin films and stacked to generate a stromal equivalent.[114e]

Silk fibroin films have been shown to act as a useful carrier of corneal epithelial and limbal cells due to their permeability, transparency, strength, and thickness. In several studies, silk fibroin has been combined with other materials (such as polyethylene glycol (PEG) or RGD peptides) to enhance cell adhesion. Changes to the surface topography have also been shown to enhance the adhesion of limbal cells,[106d] promote migration in a specific direction,[106e] and regulate the cell's phenotype.[50a]

The high Young's modulus (6–8 GPa[129]), flexibility, and ability to form thin films make silk fibroin a particularly attractive material for engineering corneal endothelial grafts. Madden et al. were one of the first groups to demonstrate that corneal endothelial cells could be cultured on silk fibroin films and maintain their cellular morphology.[120] Similar silk fibroin films seeded with rabbit endothelial cells have been successfully transplanted in vivo using rabbits.[121] No inflammation or immune rejection was detected and the grafts completely integrated with surrounding corneal tissue 6 weeks after implantation. Other studies have combined silk fibroin with other materials or chemicals such as lysophosphatidic acid,[130] aloe vera,[122] glycerol,[126] β-carotene,[125] poly-ε-caprolactone (PCL) or poly-L-lactic acid (PLLA),[123] and collagen[124] to manufacture films suitable for generating an endothelial graft. The most common reasons for combining silk with other materials was to improve cell adhesion, cell proliferation, and Na^+/K^+ adenosine triphosphatase (ATPase) pump function. For example, 4 weeks after implantation into rabbits, silk fibroin films combined with aloe vera appeared to have superior cell retention and more tight junctions between cells compared to films without aloe vera.[122]

A number of studies have used silk fibroin to generate in vitro models of the cornea to study cell behavior, assess ocular

toxicity or model disease. Wang et al. developed a model to study nerve regeneration into a cornea.[110b] Several layers of silk fibroin were seeded with corneal stromal cells and combined using a collagen hydrogel. This portion of the construct was then covered with epithelial cells. Dorsal root ganglion neurons were then encapsulated in a silk sponge along the outer rim of the construct and the nerve growth into the central construct was monitored via immunofluorescent staining. Using a similar model, Deardorff et al. developed a diabetic corneal neuropathy model to study the effect of increases in glucose on corneal nerves.[131]

In addition to fibroin, silk also contains a protein called sericin that is usually discarded as a waste product during the fibroin extraction process. During the degumming process of silk cocoons, small peptides of sericin can be obtained. The fraction of sericin extracted differs depending on the extraction method used.[132] Urea extraction resulted in water-soluble fractions while fractions obtained using other extraction methods tended to form hydrocolloids.[133] However, to prevent degradation of the protein, Chirila et al. have suggested a slow, mild extraction process.[134] Purified sericin has been used to increase the corneal wound healing rate in rats.[135] The rate of wound healing was restricted by addition of an ERK inhibitor, implying that sericin is responsible for phosphorylation of ERK1/2. In a separate study, when compared to silk fibroin, sericin and sericin-fibroin composites had inferior mechanical strength and stiffness but enhanced adhesion of corneal limbal cells.[136] One limitation with using sericin is its cytotoxicity, although this appears to be dependent on the extraction process. For example, the cytotoxicity of sericin extracted using urea was found to be significantly higher compared to other extraction methods.[133] In contrast, other studies have found that sericin is immunologically inert[137] and potentially anti-inflammatory due to its antiproliferative effects.[138]

3.3. Amniotic Membrane

One of the most commonly used natural biopolymers for corneal regeneration is the amniotic membrane isolated from placentas following caesarean section. It has been used for a variety of ophthalmological applications including the treatment of corneal burns and persistent epithelial defects.[139] The tissue has also been used as a carrier for ex vivo expansion of limbal epithelial cells or grafted directly onto the cornea where it can integrate with the host tissue.[140] The feasibility of using amniotic membranes for transplantation of endothelial cells has also been explored.[141] The anti-inflammatory properties as well as high biocompatibility make amniotic membrane an attractive natural biopolymer for regenerating the corneal surface. However, limitations including availability of tissue, donor variability, uncontrolled degradation and issues associated with the improper storage and processing of membranes has led to an increased demand for alternative biomaterials to treat defects of the corneal epithelium.[44] The mechanical strength of the membranes can be improved by the incorporation of a nanofiber mesh as a support scaffold.[142] To overcome storage limitations, the membranes can be freeze-dried and then rehydrated by a surgeon just before surgery.[143]

3.4. Natural Biopolymers

In addition to silk fibroin, collagen, and amniotic membrane, several other natural biopolymers have been explored for use in corneal regeneration. Many of these natural biopolymers have attractive properties including good biocompatibility, low immunogenicity, noncytotoxic degradation products, easily modified degradation rate in a biological system, and overall availability of materials.[144] A table summarizing the different natural biopolymers that have been used for fabricating corneal scaffolds is shown below (**Table 5**).

3.4.1. Gelatin

Gelatin is a natural protein derived from the hydrolysis of collagen and has been used in many tissue engineering applications including the cornea.[165] Among the properties that make gelatin an attractive material include its biocompatibility, low cost, and low immunogenicity.[166] However, gelatin lacks

Table 5. Summary of natural biopolymer scaffolds.

Application	Scaffold material	Tested in vivo	Refs.
Epithelial	Gelatin + collagen I + hyaluronic acid	No	[145]
Epithelial	Gelatin + chitosan	No	[146]
Epithelial	Gelatin + chitosan + hyaluronic acid	Rabbit	[147]
Epithelial	Alginate	No	[148]
Epithelial	Hyaluronic acid	No	[149]
Epithelial and stroma	GelMA	Rabbit	[150]
Epithelial and stroma	Hyaluronic acid	No	[151]
Epithelial and stroma	Fibrin + agarose	Human	[152]
Epithelial, stroma, and endothelium	Fibrin + agarose	Rabbit	[153]
Stroma	Gelatin	Rabbit	[154]
Stroma	Gelatin + GAG	Rabbit	[155]
Stroma	Gelatin + collagen I	No	[156]
Stroma	GelMA	No	[157]
Stroma	Fibrin + fibronectin	No	[158]
Stroma	Alginate	No	[159]
Endothelium	Gelatin	No	[160]
Endothelium	Gelatin	Rabbit	[161]
Endothelium	GelMA	Rabbit	[162]
Endothelium	Hyaluronic acid	No	[163]
Endothelium	Hyaluronic acid	Rabbit	[164]

thermal stability[167] and undergoes degradation quickly unless chemically crosslinked or combined with another material. The most common methods of crosslinking gelatin involve using carbodiimide (EDC) and *N*-hydroxysuccinimide (NHS)[145,155b,156] or glutaraldehyde, although other methods have also been examined.[166] Alternatively, gelatin can be chemically modified using methacrylic anhydride to form GelMA, a material that can undergo crosslinking via exposure to UVA light.[168] Unlike most chemical crosslinking processes that are cytotoxic, the main advantage of using GelMA is that the cells can be mixed into the material prior to crosslinking. GelMA has been used to engineer stromal scaffolds,[157] endothelial sheets,[162] and as a corneal bioadhesive.[169] Gelatin has also been combined with other materials to improve its mechanical properties, cell response and degradation rate including collagen, chitosan, chondroitin sulfate, and hyaluronic acid.[145–147,155b,156]

Due to its isoelectric point allowing a polyion complex to be formed, gelatin has been used as delivery vehicle for growth factors or other biomolecules.[170] Isoelectric point and pH can vary depending on the source of gelatin and how it is processed so it is important to select a suitable type of gelatin for a particular application.[161b] In one study, ascorbic acid was incorporated into gelatin in the form of a cryogel for corneal stroma engineering.[154b] Ascorbic acid is known to increase cell proliferation, enhance collagen deposition, and regulate the phenotype of keratocytes.[26a,171] An alkali burn animal model was used to demonstrate that intrastromal implantation of the constructs improved matrix regeneration, transparency, and decreased corneal damage.

Gelatin has been used to fabricate sheets for culturing and transplanting endothelial cells.[160,161] When compared to atelocollagen sheets, gelatin displayed greater transparency, mechanical properties, and permeability for endothelial cell transplantation.[160] Normal expression of functional endothelial phenotypic markers was observed on gelatin hydrogels. This study suggested that gelatin hydrogel sheets could be used for the transportation of corneal endothelial cells during transplantation.

In addition to using gelatin as a scaffold for engineering cornea or a sheet for transplanting cells, it can be used to manufacture bioadhesive hydrogels to be used for sealing and repairing cornea following injury without the need for sutures.[169,172] A chemically modified, UV crosslinkable gelatin based material called GelCORE has been developed that mimics native corneal stiffness, is highly adhesive, cytocompatible, and biodegradable. In vivo data showed that this hydrogel was able to seal corneal defects without the need for sutures and promoted re-epithelialization of the corneal surface.[169]

3.4.2. Fibrin

Fibrin is produced by combining fibrinogen and thrombin and has been used as an alternative to suturing for keratoplasties. Fibrin has also been used to transplant limbal tissue with the aim of decreasing operative time, improving patient comfort, and increasing the ease of technique for surgeons.[173] However, an in vitro study showed that the use of fibrin on explants significantly delayed corneal epithelial migration by acting as a physical barrier and should therefore be used with care to ensure the glue does not wrap around the explant.[174] Recently, fibrin has been used in the form of a glue for sealing corneal wounds and leaks that have persisted after surgery as well as damage caused by trauma.[175] The fibrin glue could be injected into the anterior chamber to seal any leaks postoperatively. However, the small number of cases used in this study as well as alternative interventions that are simpler and just as effective limits its use in this manner. A similar study used fibrin tissue glue to treat complex epithelial ingrowth after LASIK surgery.[176] After removal of epithelial ingrowth with adjunctive fibrin glue, the recurrence of ingrowth was absent in 91.7% of eyes and visual acuity improved.

Fibrin combined with agarose has been used to engineer cornea.[152a,153,177] The presence of agarose mechanically stabilized the hydrogel, improved transparency, and slowed degradation. The hydrogel is able to support the growth of corneal epithelial, stromal, and endothelial cells.[153] Clinical trials are ongoing to examine the safety and feasibility of using this material for anterior lamellar keratoplasty.[152]

Fibrin combined with fibronectin has been used to form an interconnected network similar to those seen during in vivo wound healing.[158] In a collagen matrix, corneal fibroblasts move independently whereas the fibrin matrix induces an interconnected, collective mode of cell spreading that was aided by fibronectin patterning.

3.4.3. Chitosan

Chitosan is a polysaccharide derived from chitin obtained from crustaceans. This material has been used to generate scaffolds for a variety of tissues due to its biocompatibility, antimicrobial and anti-inflammatory properties, and nontoxic biodegradability.[178] However, chitosan scaffolds have poor mechanical properties and they can degrade quickly, although the degradation rate can be modified.[179] Chitosan is more commonly used in combination with other materials when being used to develop scaffolds for engineering cornea. For example, chitosan has been combined with gelatin alone or gelatin and hyaluronic acid to generate sheets for culturing and transplanting limbal and epithelial cells.[146,147] Chitosan has also been combined with silk fibroin to generate a corneal stromal substitute.[112,117]

3.4.4. Alginate

Alginate is a natural biopolymer derived from seaweed that has been used for several medical and biological applications including tissue engineering, drug delivery, and cell encapsulation.[180] It consists of *b*-D-mannuronic and *a*-L-guluronic acid chains, the ratio of which influences the material's physical properties.[181] A hydrogel can be formed by dissolving sodium alginate powder and exposing it to a source of calcium (e.g., calcium chloride) that allows the sodium ions to be replaced by calcium ions. Since alginate lacks cell adhesion sites, the material needs to be modified or combined with other materials for corneal applications. For example, alginate has been used with gelatin nanofibers to generate a corneal stromal scaffold.[159]

The addition of nanofibers to the alginate hydrogel enhanced its mechanical properties and resulted in a Young's modulus similar to native cornea. Oxidized alginate has also been used to support the culture corneal epithelial cells.[148] The stability and lack of binding sites in alginate have limited the number of studies that have used this material for engineering cornea.

3.4.5. Hyaluronic Acid

Hyaluronic acid or hyaluronan is a nonsulfated glycosaminoglycan (GAG) found in several tissues and has previously been used for cartilage repairs and skin regeneration[182] but has also been used as a scaffold for engineering cornea. Koivusalo et al. demonstrated using a porcine organ culture model that modified hyaluronic acid based hydrogels seeded with adipose derived stem cells could be used to repair damaged cornea without the need for sutures.[151] Hyaluronic acid has also been suggested as a suitable xeno-free substrate for culturing corneal epithelial cells[149] and as a potential carrier for endothelial cells.[163,164] Despite some promising results, one potential limiting factor with using hyaluronic acid for corneal tissue regeneration is that the material has been associated with lymphangiogenesis in the limbus, although this requires further study.[183]

3.5. Decellularized Cornea

Organ decellularization consists of removing cells and their debris to obtain an acellular scaffold composed of just the organ's ECM. By removing the cells, major histocompatibility complexes are depleted thus reducing the risk of graft rejection. The main advantage of using decellularized corneas is that the obtained scaffold should be biochemically identical to original tissue. Furthermore, the exquisite collagen arrangement in the corneal stroma can be maintained, which is difficult to replicate using other biomaterials. The scaffolds should remain sterile throughout the decellularization process although terminal sterilization via gamma irradiation is often used to ensure sterility.[184] In a recent study, researchers have demonstrated that gamma irradiation does not significantly disturb the architecture of the ECM.[185] As with many materials, batch-to-batch variability can be expected due to donor variability. It is also important to ensure the corneas have been sufficiently decellularized. Macrophage polarization toward an M1-phenotype has been observed in vitro and in vivo when decellularization is incomplete.[186] B lymphocyte activation may also occur, as well as binding of immunoglobulins and complement proteins to residual cell components.[187]

A wide range of methods have been described to decellularize organs. In general, these methods can be divided into physical, chemical, and biological methods (**Table 6**). Most decellularization methods are based on a combination of different methods. Physical methods include agitation, freeze-thawing,[188] high hydrostatic pressure,[189] or supercritical CO_2.[190] Chemical agents include detergents, such as sodium dodecyl sulphate (SDS),[191] sodium deoxycholate (SDC),[184f,188b] Triton X-100,[192] or lauroyl glutamate;[193] organic acids, such as peracetic acid[194] or formic acid;[195] bases, such as ammonium

Table 6. Summary of decellularized cornea studies.

Application	Scaffold species	Primary decellularization technique	Tested in vivo	Refs.
Epithelium	Human	Biological	Rabbit	[212]
Epithelium	Porcine	Biological	Rabbit	[230]
Epithelium	Human	Chemical	Rat	[231]
Stroma	Porcine	Biological	Rabbit	[184b]
Stroma	Porcine	Chemical	Dog	[184f]
Stroma	Human	Biological	Rabbit	[198b]
Stroma	Porcine	Physical	No	[225b]
Stroma	Bovine	Chemical	No	[232]
Stroma	Bovine	Physical	No	[190b]
Stroma	Human	Chemical	Human	[210]
Stroma	Human	Chemical	Rabbit	[201a]
Stroma	Porcine	Biological	Rabbit	[184e,199]
Stroma	Porcine	Chemical	Human	[184c,213]
Stroma	Porcine	Chemical	Nonhuman primate	[233]
Stroma	Porcine	Physical	Rabbit	[234]
Stroma	Human	Chemical	Rabbit	[205a]
Stroma	Porcine	Chemical	Rabbit	[228]
Stroma	Porcine	Chemical	No	[229]
Endothelium	Human	Chemical	No	[192a]
Endothelium	Human	Chemical	No	[208]
Endothelium	Human	Physical	Cat	[188c]

hydroxide;[192a,196] and hypertonic solutions, mainly 1.5–2 M sodium chloride.[188a,192b,197] Biological methods used include commonly used cell dissociating agents, such as trypsin and dispase II;[188a,198] other catalytic enzymes, such as phospholipase A2;[184e,199] human serum;[200] and nucleases, such as DNAses and RNAses.[184f,188b,201] Each of these methods presents strengths and limitations, which have been highlighted previously.[202] The main limitations with specific decellularization techniques may include insufficient removal of cells and DNA, loss of ECM components, disruption of the stromal matrix organization, and residual chemical agents remaining in the scaffold and affecting its biocompatibility. For this reason, optimization of the process is required.

Another factor that needs to be considered is the species from which the corneas are obtained. The ideal tissue source for corneal decellularization is human. While healthy corneas are usually transplanted to patients in need, some corneas are deemed unsuitable for transplantation due to low endothelial cell count or being positive for some viruses. In the case of low endothelial numbers, these corneas could potentially be repurposed for decellularization.[203] In the case of infections, gamma irradiation could be used to eliminate the risk of bacterial, viral or fungal disease transmission.[204] In addition, some studies have focused on the use of discarded tissue after small incision lenticule extraction (SMILE), a refractive technique for myopic treatment.[205] While the use of human corneas is certainly one option, donor shortages remain an issue, thus alternative species have been explored.

Due to their anatomical similarities to human cornea and their availability, porcine corneas have been the most extensively studied for decellularization. Pig corneas are slightly thicker than human but have similar mechanical characteristics.[206] In a recent study, it was found that the porcine cornea had the highest similarity score to the human, compared to 13 other animals that could be used for decellularization, among them were dog, cat, sheep, goat, cow, horse, and rabbit.[207] This score was calculated from amino acid sequence, isoelectric point, and hydropathicity of the main ECM components found in the stroma. It is important to note that some immunogenic epitopes to humans are present in the porcine cornea, such as *N*-glycolylneuraminic acid (Neu5Gc) and galactose-alpha-1,3-galactose (α-Gal). This highlights the importance of applying a thorough decellularization process in order to avoid graft rejection.

Corneas can be decellularized as a whole or can be cut to a certain thickness by manual dissection or using a femtosecond laser-assisted cutting machine prior to decellularizatio n.[198b,208] In some cases, researchers have opted to recellularize the scaffolds prior to implantation. For the recellularization of the stroma, the thickest layer of the cornea, the most common strategies have been injection[184f,188b,191a,209] or simple seeding on the surface.[191a,197,210] Injection can introduce cells into deeper areas of the tissue but can also result in fibril disruption. Seeding cells on the surface requires the cells to migrate into the densely packed collagen stroma. Seeding is more commonly used for the recellularization of the epithelium or endothelium since these cells are not required to migrate into the tissue, only to form a layer on the corneas anterior and posterior surfaces, respectively.

To evaluate decellularized corneal scaffolds, many studies have implanted them intrastromally by creating an intrastromal pocket and filling it with the scaffold. This approach provides some insight in the ability of the scaffold to integrate and elicit or inhibit strong immune responses. Recovery of transparency can also be assessed with this approach. Anterior lamellar keratoplasty is a more clinically useful model and provides information on the ability of the epithelium to regenerate on the surface of the scaffold. In a study by Xu et al., in vitro recellularized scaffolds with epithelial and stromal cells were shown to be beneficial in an ALK model in dogs.[184f] Other studies have shown that scaffolds without an epithelium still provided a good substrate for endogenous cells to repopulate the surface.[184b,e,211]

There have been a few novel approaches to generating corneal scaffolds that combine decellularization with other material fabrication techniques. For example, one approach has been to embed a decellularized lenticule in a compressed collagen I hydrogel to improve the hydrogel's mechanical properties, susceptibility to degradation and suturability, while maintaining its excellent cytocompatibility in an limbal epithelial stem cells deficiency model in rabbits.[212] Decellularized corneas have also been studied as carriers for the transplantation of endothelial cells.[192a,208] He et al. decellularized cornea lamellae obtained by femtosecond laser using different methods and found 1% SDS with DNAse to be optimal.[208] The lamellae were then recellularized with an endothelial cell line that adhered and formed a tight endothelium expressing Na^+/K^+ ATPase and tight junctions. While the reports are promising, the Descemet's membrane was not present. The hypothesis is however, that the implanted cells will lay down their own Descemet's membrane over time.

Despite being a relatively young field, findings from in vitro and animal experiments have been translated to the clinic. There has been one study in human where thin sections of human corneas were decellularized and implanted into patients with keratoconus to increase their stromal thickness and delay the need for transplantation.[210] Some patients received sections recellularized with ASCs but there was no significant benefit when compared to cell-free sections. Furthermore, Chinese company AiNear Corneal Engineering Co., Ltd. has a product based on dehydrated decellularized porcine corneas. It has been used to treat patients with fungal keratitis and herpes simplex keratitis, conditions that have a high risk of graft rejection. Overall, reports of the use of this product have been positive.[184c,213] These scaffolds have recently been improved by controlling ionic and colloid osmotic pressure, thus reducing swelling and loss of transparency. This led to earlier improved visual acuity in patients with corneal ulcers, from bacterial, fungal or unknown origin.[193a] Other researchers have bypassed the decrease in transparency during decellularization by immersing the scaffolds in glycerol to further lyophilize them for storage.[214]

Hydrogels have been obtained from the solubilization of ECM by decellularizing tissues or organs, lyophilizing the remaining ECM, grinding this into a powder, and digesting in a suitable solution such as acidic pepsin or acetic acid. By neutralizing the pH of the solution and raising the temperature to 37 °C, fibrillation is induced. Hydrogels following this method

have been obtained from many organs including urinary bladder matrix,[215] dermis,[216] pancreas,[217] myocardium,[218] skeletal muscle,[218b] demineralized bone,[219] small intestinal submucosa,[220] liver,[221] cartilage,[222] tendon,[223] adipose tissue,[222] and kidney.[224] This approach allows for the injection of these hydrogels into the diseased site due to their shear thinning properties and opens the door for their use in 3D bioprinting. Hydrogels obtained from decellularized corneas have been reported in the literature[225] and were first described by our group.[225b] Since these hydrogels are mechanically weak, postgelation crosslinking can be used to improve stiffness and strength. For example, using a UVA-riboflavin crosslinking technique, similar to the technique used clinically on patients suffering from keratoconus, has been shown to significant increase the modulus of corneal ECM hydrogels.[225c] The decellularization technique used also needs to be considered as this can have a significant effect on the hydrogel's final physical and biological characteristics.[226] Kim et al. recently reported using decellularized cornea ECM for 3D bioprinting which resulted in a more transparent construct compared to using type I collagen.[225a]

ECM particles have been incorporated into different biomaterials to generate scaffolds for several different types of tissue. The ECM is used to provide biochemical cues and support biological functions rather than construct a 3D environment.[227] Recently tissue-derived microparticles from the lymph nodes, cartilage, and cornea were compared for their potential to improve corneal wound healing.[228] In vitro these particles decreased TNFα and MMP9 expression by keratocytes induced by exogenous IL-1β. In vivo experiments were performed using the lymph node particles as they showed better effects on epithelial and conjunctival cells. The particles were applied on an anterior lamellar keratoplasty model in a rabbit using fibrin glue as a carrier. In a subsequent study, the particles were applied to an ex vivo model of keratoconus, obtained by weakening the stroma with Chondroitinase ABC.[229] The treatment improved mechanical properties, increased collagen fibril density, and promoted the expression of several keratocyte markers.

3.6. Synthetic Polymers

All the previously described polymers are derived from natural sources. Synthetically produced polymers have also been used for designing corneal scaffolds. Many polymers such as PCL and PLLA that have been used as scaffolds to engineer other tissues are normally considered unsuitable for cornea due to the lack of transparency, although they could be used to mechanically support other polymers. Polyvinyl-alcohol (PVA) is one transparent synthetic polymer that also has been shown to have good biocompatibility and good mechanical strength.[235] To enhance cell adhesion and the bioactivity of the material, PVA has been combined with natural materials like cellulose, amniotic membrane, and collagen to generate scaffolds for corneal tissue engineering.[236] PEG is another synthetic polymer that has been used in corneal scaffolds. PEG hydrogels have good biocompatibility, permeability, and transparency making them a potentially suitable material to replace cornea. More commonly, PEG is combined with another material to generate a corneal scaffold. Islam et al. reported conjugating a collagen-like peptide to PEG to generate a transparent hydrogel capable of promoting cell infiltration and nerve growth in vivo in a stromal mini-pig model.[237]

4. Fabrication Processes

4.1. Bioprinting

Bioprinting is an additive manufacturing technique that involves printing both cells and materials with the aim of generating viable, 3D tissues and organs.[238] By printing layer upon layer of material, complex geometries to deal with patient specific problems can be achieved. There are a number of different techniques that can be used to bioprint tissues including extrusion, inkjet printing, laser assisted printing, and stereolithography (**Figure 4**), the advantages and limitations associated with each of these have been highlighted previously.[239]

There have been several different approaches to bioprint cornea and corneal components. One of the first reported uses of corneal derived cells in a bioprinted construct involved human corneal epithelial cells bioprinted inside alginate-gelatin-collagen based bioink.[240] Despite the high cell viability and the cells positive staining for the epithelial marker cytokeratin 3, the transparency of the final construct was poor. Corneal stromal constructs containing keratocytes have been bioprinted using various bioinks including alginate with methacrylated collagen,[241] agarose blended with collagen,[242] and corneal extracellular matrix.[225a,243] Rather than using the conventional extrusion based bioprinting technique, Sorkio et al. used laser induced forward transfer to bioprint the anterior segment of the cornea. They used ESCs and laminin to fabricate the epithelium and ASCs and collagen to fabricate the stroma.[244]

While bioprinting has many advantages over other construct manufacturing techniques such as automation, reproducibility, and ability to print specific shapes, there are a number of limitations when the technique is applied to fabricating cornea. The main limitation associated with many of the bioprinted corneal constructs is their poor optical properties compared to real corneal tissue. While the bioink material being printed is usually transparent, the surface of the final printed construct is often rough resulting in an uneven refraction of light as it passes though the construct. This is a limitation of the printing process itself since to generate a curvature by printing flat layers, each printed layer needs to be slightly offset from the previous layer. The problem can be partially overcome by printing cylindrical rather than hemispherical corneal constructs although this introduces a new problem since the construct will probably differ in shape to the tissue it is replacing.[245] Another potential limitation with bioprinting is the difficulty to replicate the collagen fibril organization found in the stroma. To overcome this problem, Kim et al. utilized the shear flow properties of the bioink during printing to direct fibrils in the desired orientations.[243] The collagen fibrils in the bioink aligned in the direction that the needle was moving. Cells in these aligned constructs presented increased expression of keratocyte markers keratocan and ALDH.

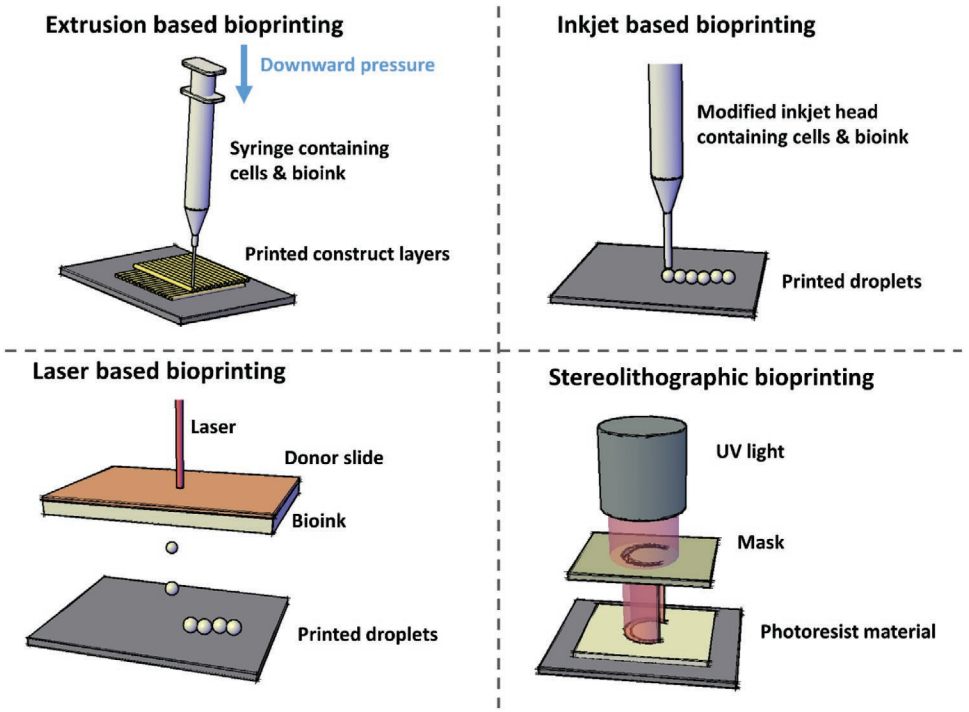

Figure 4. Schematic representation of different bioprinting techniques including extrusion-based bioprinting, inkjet bioprinting, laser-based bioprinting, and stereolithographic bioprinting.

4.2. Electrospinning

Electrospinning is another materials fabrication technique that can be used to generate scaffolds.[246] In most cases, the scaffold material is dissolved in a solvent and extruded through a needle under a high electrostatic charge. This charge affects the surface tension of the solution leading to a thin jet being pulled toward a grounded or negatively charged collector. The solvent evaporates as the jet is moving toward the collector, resulting in the formation of micro- or nanofibers. This process is particularly attractive for generating corneal scaffolds since the fibers generated can theoretically mimic the collagen fibrils present in the stroma.

The type of collector used is vital to controlling the orientation of fibers produced during electrospinning. Examples of different types of collectors are shown (**Figure 5**). To replicate the corneal stroma, aligned sheets of fibers need to be produced and these sheets arrange in orthogonally orientated layers. Flat plate collectors are the most commonly used collectors for electrospinning but these result in fibers arranged in a random configuration. Rotating mandrels can be used to obtain more aligned fibers. As the mandrel rotates, the fibers are pulled around it resulting in a layer of fibers orientated around the cylinder. These can be detached and used to manufacture scaffolds. An alternative technique to produce aligned fibers is to use two parallel plates with sharp metallic edges. As the fibers are produced, they move between the two edges leading to the formation of aligned fibers. The fibers can be removed from the collector using cellulose frames that adhere to be fibers, allowing their orientation to remain fixed.[22b,51] Radially aligned fibers can be produced using a cup and pin collector where the fibers align between the pin and outer circular ring (or cup).[247] To obtain orthogonally orientated fibers a negatively charged collector connected to four separate posts can be used.[247] The negative charge switches between the two horizontal posts and the two vertical posts at a specified rate. When the horizontal posts are charged the fibers are attached toward these and aligned horizontally between them. When the charge is switched to the vertical posts, fibers align vertically. This approach allows multiple layers of fibers to be formed with different orientations.

Several different materials have been used to generate electrospun scaffolds for corneal tissue engineering. Synthetic polymers such as PCL, PLLA, polymethyl methacrylate (PMMA), poly-L-D-lactic acid (PLDLA), polylactic-*co*-glycolic acid (PLGA), polyglycerol sebacate (PGS), and polyethyleneglycol diacrylate (PEGDA) have been investigated to determine their suitability for fabricating electrospun corneal scaffolds.[51,232,248] These materials have better strength and degradation resistance than many natural polymers, however in most cases the materials lack transparency; therefore, sufficient spacing is required between fibers to allow light to pass through. Rather than generating full thickness corneal scaffolds, synthetic polymers are more suitable for generating thin electrospun sheets for epithelial[248b,d] or endothelial[248a] transplantation, as an alternative to amniotic membranes[249] or as mechanical support for a stromal hydrogel material.[51] Natural polymers including gelatin and collagen have been investigated for use in generating scaffolds for corneal regeneration.[250] In the case of collagen, care needs to be taken in selecting a suitable solvent since many solvents result in denaturation of the collagen's triple helix molecule, resulting in the formation of gelatin.[159,251]

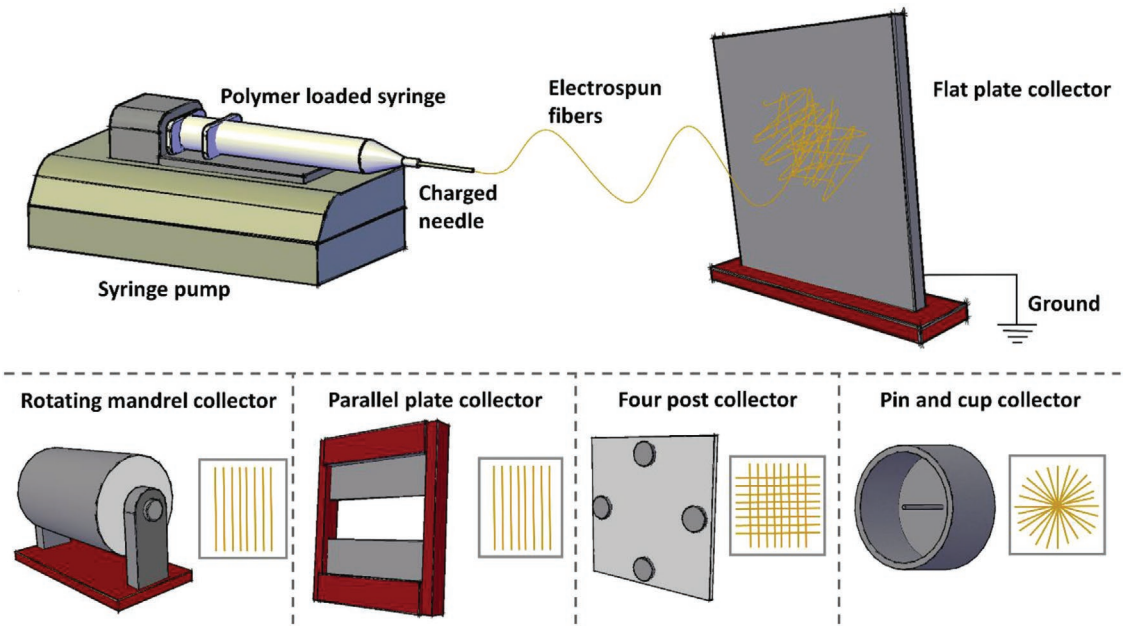

Figure 5. Schematic representation of the electrospinning process, examples of different types of collector, and the orientation of fibers produced using those collectors.

The main limitation with using electrospun natural polymers are their poor mechanical properties that make them more likely to be damaged during transplantation and difficult to handle. Several studies have combined natural and synthetic polymers to find an optimal combination of transparency, biocompatibility, and strength. Examples include combining PVA with collagen,[235a] PCL with collagen,[252] PLLA with gelatin,[253] and PLLA and PCL with silk fibroin.[123]

One issue with producing scaffolds using electrospinning is how to keep the fibers together. The individual fibers produced during electrospinning are not crosslinked to each other so often an alternative method is needed to form a stable scaffold. One simple method is to encapsulate the fibers in a hydrogel. Wilson et al. demonstrated that aligned PLDLA fibers seeded with corneal fibroblasts could be encapsulated using a collagen hydrogel.[51] Similarly, Tonsomboon and Oyen encapsulated gelatin fibers in an alginate hydrogel.[159]

Recently, there has been increasing interest in melt electrospinning.[254] Rather than using solvents to dissolve the polymer, in melt electrospinning the polymer is heated into its viscous phase to allow it to be extruded through the needle. This process allows better control of the fiber architecture compared to solvent-based electrospinning, however the fibers formed are generally larger in diameter and the range of materials that can be used is more limited. Despite the potential of the technique to engineer various tissues and organs[255] and generate scaffolds that modulate cell behavior,[256] there have been no reports on its use for corneal applications.

There are a number of limitations associated with using electrospinning to generate corneal scaffolds. One of the main difficulties is trying to spin fibers that are similar in size to the collagen fibrils found in the stroma, ≈36 nm in diameter.[257] The spacing between fibers is also difficult to control and is vital for maintaining corneal transparency. The pore size between fibers also needs to be considered, as this would need to be sufficiently large to allow cells to penetrate into the scaffold. Since most solvents used for electrospinning are cytotoxic, it is necessary to prove that no residual solvent remains before the scaffolds could be with patients. Electrospun scaffolds can also be fragile and difficult to handle which is a challenge if the scaffold needs to be implanted and sutured.

4.3. Mechanical Manipulation

One of the main limitations associated with many of the collagen and ECM-based hydrogels used for corneal regeneration is that they lack the collagen density and organization needed to mimic the cornea ECM physical properties in vivo. Collagen hydrogels have been shown to be easily remodeled by corneal stromal cells resulting in their contraction.[53] In addition, the low collagen density lead to inferior mechanical properties compared to native corneal tissue.[75a] To overcome the limitations, a number of processing techniques have been developed that involve the application of either compressive or tensile forces.

Plastic compression is a simple technique that can be used to increase the density of collagen hydrogels.[91a,258] It involves placing the hydrogel under an applied load that results in water being absorbed from the hydrogel, thus leading to a 100–200-fold increase in collagen density[91b] (**Figure 6**A). A more recent variation of the technique involves using an absorber to remove water without a load needing to be applied[259] (Figure 6B). Cells encapsulated within the hydrogels remain viable despite the force applied to their surrounding matrix. The result is a thin collagen structure that appears similar to many soft tissues. This technique has been used to generate corneal epithelial,[64a] stromal, and endothelial[260] constructs. These scaffolds displayed good biocompatibility when inserted into a rabbit

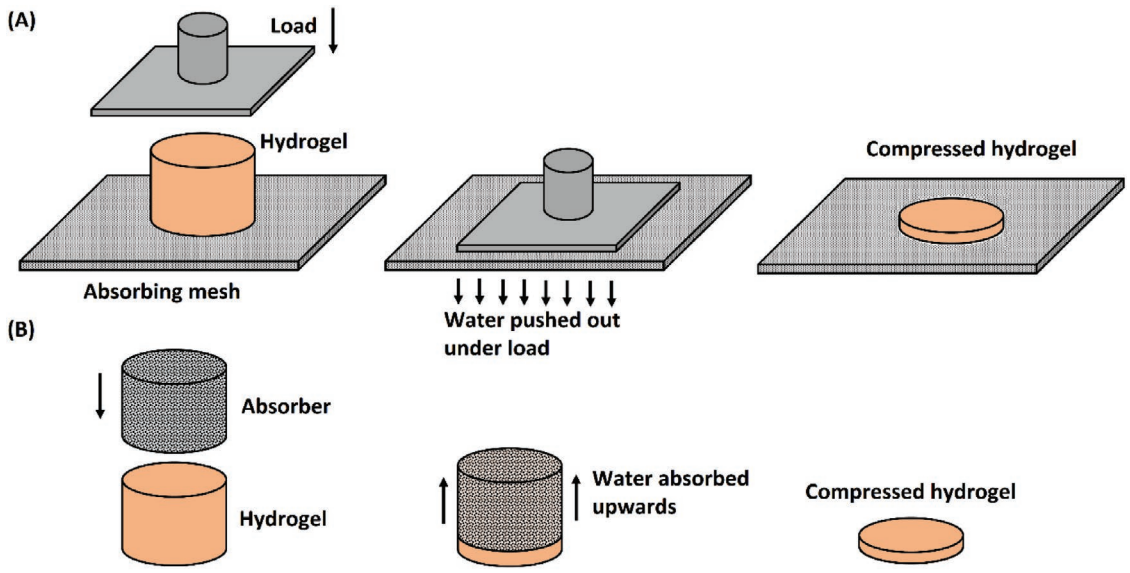

Figure 6. Schematic representation showing plastic compression of a collagen hydrogel A) by the application of a load and B) by the application of an absorber.

stromal pocket.[76] To improve transparency and reduce fibril diameter, Hong et al. used different mixtures of type I collagen and decellularized cornea ECM.[261] To improve the integration of the scaffolds into the stroma, Rafat et al. combined plastically compressed collagen with a porous outer collagen skirt to generate an artificial stromal implant whose inner core was transparent and whose outer skirt could be used to transport cells or drugs.[70b] Kong et al. obtained a similar result by plastically compressing collagen onto electrospun PLGA to generate a physical support around the edge of the construct.[262] Plastic compression has also been applied to generate biomimetic niches for limbal derived stem cells by preparing the collagen on a micropatterned surface.[263]

Plastic compression allows for collagen to be aligned in one plane only. Several methods have been investigated to induce the alignment of collagen in scaffolds and hydrogels (**Figure 7**). Static tensile strain or stretch of collagen hydrogels has been shown to result in collagen fibers orientating in parallel to the strain direction.[264] The application of cyclical strain may also be used to align collagen perpendicular to the strain direction,[265] although this would also lead to mechanotransduction and alter the phenotype of any cells present.[266] It has previously been shown that corneal stromal cells respond to localized strains by altering focal adhesion to minimize strain effect on the cells.[41b] For cell-seeded collagen hydrogels, tethering the hydrogel at opposite ends would result in contraction and alignment of the hydrogel,[267] however, generating a sheet of material using this technique is challenging. Alternatively, the direction of flow can be manipulated to result in collagen alignment prior to gelation of these hydrogels.[268] Finally, the negative diamagnetic anisotropy of collagen allows it to be aligned when subjected to a high magnetic field.[71,269] While these techniques allow for alignment of collagen in one direction, multiple layers of aligned collagen sheets would need to be stacked to mimic the stromal fibril architecture.

Another approach to both compacting and aligning collagen to increase its density is by applying an electrochemical fabrication method.[78b] Based on the principles of isoelectric focusing, this approach works by placing a collagen solution in an electric field where a pH gradient in the collagen causes positively charged collagen molecules to align at the positive end of the field and negatively charged molecules at the negative end. The electric charge repels the collagen molecules thus leading to compaction of the hydrogel. The result was a stable, transparent hydrogel that supports the culture of keratocytes.

5. Future Trends and Considerations

A comprehensive overview of the different design considerations, materials, and processing techniques used for engineering corneal scaffolds has been provided. While each scaffold material has specific advantages and limitations, collagen-based scaffolds and decellularized ECM appear to show the most promise since they more accurately mimic the corneal stroma's native composition. While amniotic membranes are still the gold standard for epithelial regeneration, collagen films loaded with specific biochemical reagents could be manufactured to mimic the amniotic membranes without the drawback of donor variability or limited supply. For the endothelium, silk fibroin appears to have the most potential due to its ability to form thin, strong films that support endothelial growth. Fabrication processes such as electrospinning and bioprinting will need to undergo significant improvements before they are capable of manufacturing corneal scaffolds suitable for kertoplasty. Several corneal scaffolds are currently undergoing clinical trials so the next few years could see these therapies becoming more readily available to patients suffering corneal blindness.

There are many tissue engineering and regenerative strategies under investigation for other tissues and organs that

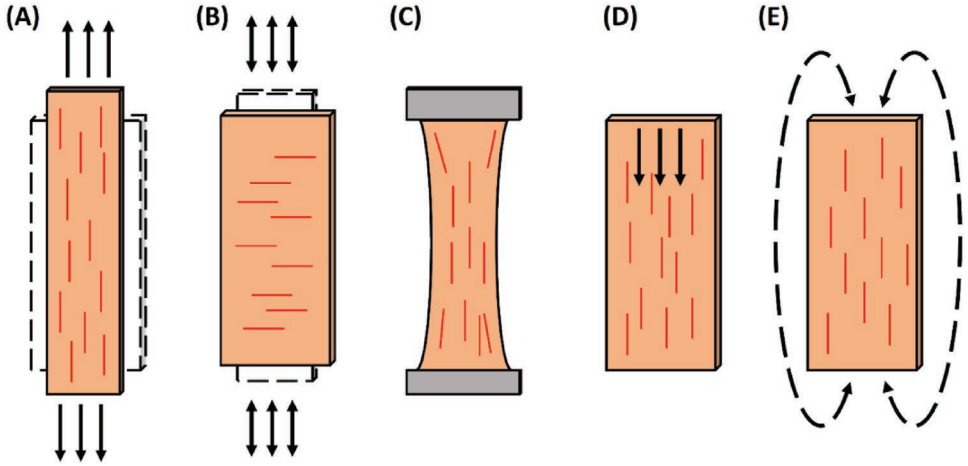

Figure 7. Schematic representation showing different methods of inducing collagen alignment: A) static tensile stretch; B) cyclic tensile stretch; C) tethering at opposite ends to allow contraction by cells; D) shear-induced alignment via flow; E) magnetic field alignment. Arrows represent direction of strain/flow/flux; red lines represent collagen orientation.

could potentially be applied to generate "smart" corneal scaffolds. One of the more promising are gene-activate scaffolds that can transfect cells using viral vectors or nanoparticles.[270] Extensive research has been conducted to use this approach to fabricate scaffold to enhance bone repair,[271] in addition to regenerating other tissues such as cartilage[272] and skin.[273] While the use of gene therapies to treat damaged or diseased corneas has been examined,[274] the use of scaffolds to delivery genes to the cornea remains unexplored. Scaffold designed to inhibit inflammation or infection are also been explored for other tissues.[275] Despite the corneas immune prevalent status, many cornea transplants eventually undergo rejection due to inflammation or neovascularization,[276] therefore there is potential for anti-inflammatory corneal scaffolds to be developed for high-risk patients.

One of the biggest challenges facing researchers is translating their research from the lab to the clinic. In most developed countries, scaffolds need to undergo extensive testing and adhere to rigorous regulatory guidelines prior to use in clinical trials. This is particularly the case for cell-seeded scaffolds. This has led to a recent trend by some researchers to trial their therapies in developing countries where regulations are less strict. While this may speed up the development of new therapies, it does raise ethical concerns. If a therapy is not deemed safe enough to be tested in richer countries, why is it safe to use in poorer countries?

In addition to the clinical translation of corneal scaffolds, their commercial value has to be considered. Due to the high costs associated with developing and manufacturing cell-based therapies, cell free scaffolds for replacing the stroma will appear to be more attractive to produce for companies than cell-seeded scaffolds. Cell free scaffolds also have a longer shelf life and do not require storage under cell culture conditions. For epithelial damage or limbal stem cell deficiencies, cells are required for repair and regeneration. While it is more challenging to get this to market, one example of a cell-based therapy that has successfully undergone regulatory approval and commercialization is Holoclar, a cell-based treatment involving the expansion of limbal derived stem cells in vitro and recently received approval from the European Medicines Agency, to treat limbal deficiency due to burns.[277]

In summary, while great progress has been made in developing scaffold for corneal tissue engineering and regeneration, a number of challenges remain in translating current research to the clinic. The success or failure of on-going clinical trials will have a significant impact on the ability of future therapies to treat patients.

Acknowledgements

The research leading to these results received funding from the European Research Council (ERC) under the European Union's Horizon 2020 Research and Innovation Program (grant agreement no. 637460) and from Science Foundation Ireland (15/ERC/3269).

Conflict of Interest

The authors declare no conflict of interest.

Keywords

biomaterials, cornea, hydrogels, scaffolds, tissue engineering

Received: October 30, 2019
Revised: January 8, 2020
Published online:

[1] a) H. S. Dua, V. A. Shanmuganathan, A. O. Powell-Richards, P. J. Tighe, A. Joseph, *Brit. J. Ophthalmol.* **2005**, *89*, 529; b) A. M. H. Yeung, U. Schloetzer-Schrehardt, B. Kulkarni, N. L. Tint, A. Hopkinson, H. S. Dua, *Arch. Ophthalmol.* **2008**, *126*, 665.

[2] a) J. A. Last, S. J. Liliensiek, P. F. Nealey, C. J. Murphy, *J. Struct. Biol.* **2009**, *167*, 19; b) J. A. Last, S. M. Thomasy, C. R. Croasdale, P. Russell, C. J. Murphy, *Micron* **2012**, *43*, 1293.

[3] K. M. Meek, *Biophys. Rev.* **2009**, *1*, 83.
[4] E. L. Martola, J. L. Baum, *Arch. Ophthalmol.* **1968**, *79*, 28.
[5] a) T. B. Abud, A. Di Zazzo, A. Kheirkhah, R. Dana, *J. Ophthalmic Vision Res.* **2017**, *12*, 81; b) W. Zhong, M. Montana, S. M. Santosa, I. D. Isjwara, Y. H. Huang, K. Y. Han, C. O'Neil, A. Wang, M. S. Cortina, J. de la Cruz, Q. Zhou, M. I. Rosenblatt, J. H. Chang, D. T. Azar, *Surv. Ophthalmol.* **2018**, *63*, 453; c) A. W. Taylor, *Front. Immunol.* **2016**, *7*, 37.
[6] a) V. Romano, M. Dinsdale, S. Kaye, *Lancet* **2019**, *102*, 306; b) P. Gain, R. Jullienne, Z. He, M. Aldossary, S. Acquart, F. Cognasse, G. Thuret, *JAMA Ophthalmol.* **2016**, *134*, 167; c) A. M. Williams, K. W. Muir, *Clin. Ophthalmol.* **2018**, *12*, 1049.
[7] A. Crnej, E. I. Paschalis, B. Salvador-Culla, A. Tauber, B. Drnovsek-Olup, L. Q. Shen, C. H. Dohlman, *Cornea* **2014**, *33*, 349.
[8] a) M. Nouri, H. Terada, E. C. Alfonso, C. S. Foster, M. L. Durand, C. H. Dohlman, *Arch. Ophthalmol.* **2001**, *119*, 484; b) I. Behlau, K. V. Martin, J. N. Martin, E. N. Naumova, J. J. Cadorette, J. T. Sforza, R. Pineda, C. H. Dohlman, *Acta Ophthalmol.* **2014**, *92*, e546.
[9] R. K. Talati, J. A. Hallak, F. I. Karas, J. de la Cruz, M. S. Cortina, *Cornea* **2018**, *37*, 145.
[10] S. Bouhout, M. C. Robert, S. Deli, M. Harissi-Dagher, *Ocul. Immunol. Inflammation* **2018**, *26*, 693.
[11] a) C. A. Vacanti, J. P. Vacanti, *Surg. Technol. Int.* **1991**, *I*, 43; b) R. Langer, J. P. Vacanti, *Science* **1993**, *260*, 920.
[12] a) S. Matthyssen, B. Van den Bogerd, S. N. Dhubhghaill, C. Koppen, N. Zakaria, *Acta Biomater.* **2018**, *69*, 31; b) N. Lagali, *Curr. Eye Res.* **2019**, https://doi.org/10.1080/02713683.2019.16638741.
[13] V. J. Wicklein, B. B. Singer, T. Scheibel, S. Salehi, in *Nanoengineered Biomaterials for Regenerative Medicine* (Eds: M. Mozafari, J. Rajadas, D. Kaplan), Elsevier, Amsterdam **2019**, Ch. 17, p. 379.
[14] A. Isidan, S. Liu, P. Li, M. Lashmet, L. J. Smith, H. Hara, D. K. C. Cooper, B. Ekser, *Xenotransplantation* **2019**, *26*, e12564.
[15] B. Zhang, Q. Xue, J. Li, L. Ma, Y. Yao, H. Ye, Z. Cui, H. Yang, *Med. Eng. Phys.* **2019**, *71*, 68.
[16] C. Y. Park, J. K. Lee, P. K. Gore, C. Y. Lim, R. S. Chuck, *Ophthalmology* **2015**, *122*, 2432.
[17] a) T. Rock, J. Landenberger, M. Bramkamp, K. U. Bartz-Schmidt, D. Rock, *Ann. Transplant.* **2017**, *22*, 749; b) U. de Sanctis, C. Alovisi, L. Bauchiero, G. Caramello, G. Girotto, C. Panico, L. Vinai, F. Genzano, A. Amoroso, F. Grignolo, *Int. J. Ophthalmol.* **2016**, *9*, 48; c) D. J. Coster, M. T. Lowe, M. C. Keane, K. A. Williams, Australian Corneal Graft Registry Contributors, *Ophthalmology* **2014**; d) E. Flockerzi, P. Maier, D. Bohringer, H. Reinshagen, F. Kruse, C. Cursiefen, T. Reinhard, G. Geerling, N. Torun, B. Seitz, G. K. R. Contr, *Am. J. Ophthalmol.* **2018**, *188*, 91.
[18] a) N. C. Joyce, S. E. Navon, S. Roy, J. D. Zieske, *Invest. Ophthalmol. Visual Sci.* **1996**, *37*, 1566; b) N. C. Joyce, D. L. Harris, *Mol. Vision* **2010**, *16*, 897; c) N. C. Joyce, *Prog. Retinal Eye Res.* **2003**, *22*, 359.
[19] J. Liu, H. Sheha, Y. Fu, L. Liang, S. C. Tseng, *Expert Rev. Ophthalmol.* **2010**, *5*, 645.
[20] C. M. Murphy, M. G. Haugh, F. J. O'Brien, *Biomaterials* **2010**, *31*, 461.
[21] V. Quaranta, *J. Cell Biol.* **2000**, *149*, 1167.
[22] a) P. Sharma, C. Ng, A. Jana, A. Padhi, P. Szymanski, J. S. H. Lee, B. Behkam, A. S. Nain, *Mol. Biol. Cell* **2017**, *28*, 2579; b) Y. Yang, I. Wimpenny, M. Ahearne, *Nanomedicine* **2011**, *7*, 131; c) C. M. Chen, J. C. Tang, Y. Gu, L. L. Liu, X. Z. Liu, L. F. Deng, C. Martins, B. Sarmento, W. G. Cui, L. Chen, *Adv. Funct. Mater.* **2019**, *29*, 1970024.
[23] a) V. Agrawal, S. A. Johnson, J. Reing, L. Zhang, S. Tottey, G. Wang, K. K. Hirschi, S. Braunhut, L. J. Gudas, S. F. Badylak, *Proc. Natl. Acad. Sci. USA* **2010**, *107*, 3351; b) S. A. DeLong, J. J. Moon, J. L. West, *Biomaterials* **2005**, *26*, 3227.
[24] a) J. V. Jester, A. Budge, S. Fisher, J. Y. Huang, *Invest. Ophthalmol. Visual Sci.* **2005**, *46*, 2369; b) D. L. Van Horn, D. D. Sendele, S. Seideman, P. J. Buco, *Invest. Ophthalmol. Visual Sci.* **1977**, *16*, 597.
[25] a) M. A. Watsky, M. M. Jablonski, H. F. Edelhauser, *Curr. Eye Res.* **1988**, *7*, 483; b) B. Jue, D. M. Maurice, *J. Biomech.* **1986**, *19*, 847.
[26] a) J. Fernandez-Perez, M. Ahearne, *Curr. Eye Res.* **2019**, *44*, 135; b) A. P. Lynch, F. O'sullivan, M. Ahearne, *Exp. Eye Res.* **2016**, *151*, 26.
[27] J. D. M. Campbell, S. Ahmad, A. Agrawal, C. Bienek, A. Atkinson, N. W. A. Mcgowan, S. Kaye, S. Mantry, K. Ramaesh, A. Glover, J. Pelly, C. MacRury, M. MacDonald, E. Hargreaves, J. Barry, J. Drain, B. Cuthbertson, L. Nerurkar, I. Downing, A. R. Fraser, M. L. Turner, B. Dhillon, *Stem Cells Transl. Med.* **2019**, *8*, 323.
[28] a) S. H. Park, K. W. Kim, Y. S. Chun, J. C. Kim, *Exp. Eye Res.* **2012**, *101*, 16; b) H. S. Liu, J. H. Zhang, C. Y. Liu, Y. Hayashi, W. W. Y. Kao, *J. Cell. Mol. Med.* **2012**, *16*, 1114.
[29] a) S. Zhang, L. Espandar, K. M. Imhof, B. A. Bunnell, *J. Clin. Exp. Ophthalmol.* **2013**, *4*, 11435; b) M. Ahearne, J. Lysaght, A. P. Lynch, *Cell Regener.* **2014**, *3*, 3:13; c) Y. Du, D. S. Roh, M. L. Funderburgh, M. M. Mann, K. G. Marra, J. P. Rubin, X. Li, J. L. Funderburgh, *Mol. Vision* **2010**, *16*, 2680.
[30] a) A. A. Chan, A. J. Hertsenberg, M. L. Funderburgh, M. M. Mann, Y. Q. Du, K. A. Davoli, J. D. Mich-Basso, L. Yang, J. L. Funderburgh, *PLoS One* **2013**, *8*, 56831; b) Q. Zhu, M. M. Li, C. Yan, Q. Q. Lu, S. H. Wei, R. Gao, M. F. Yu, Y. Zou, G. Sriram, H. J. Tong, W. Hunziker, C. J. Seneviratne, Z. Y. Gong, B. R. Olsen, T. Cao, *Biotechnol. J.* **2017**, *12*, 1700067.
[31] D. Karamichos, C. B. Rich, A. E. Hutcheon, R. Ren, B. Saitta, V. Trinkaus-Randall, J. D. Zieske, *J. Funct. Biomater.* **2011**, *2*, 213.
[32] A. Dos Santos, A. Balayan, M. L. Funderburgh, J. Ngo, J. L. Funderburgh, S. X. Deng, *Invest. Ophthalmol. Visual Sci.* **2019**, *60*, 3013.
[33] a) A. I. Caplan, *Stem Cells Transl. Med.* **2017**, *6*, 1445; b) T. S. de Windt, L. A. Vonk, D. B. F. Saris, *Stem Cells Transl. Med.* **2017**, *6*, 1747.
[34] K. Chakrabarty, R. Shetty, A. Ghosh, *Stem Cell Res. Ther.* **2018**, *9*, 287.
[35] a) C. Couture, K. Zaniolo, P. Carrier, J. Lake, J. Patenaude, L. Germain, S. L. Guérin, *Biomaterials* **2016**, *78*, 86; b) S. Proulx, J. d'Arc Uwamaliya, P. Carrier, A. Deschambeault, C. Audet, C. J. Giasson, S. L. Guérin, F. A. Auger, L. Germain, *Mol. Vision* **2010**, *16*, 2192; c) D. Karamichos, X. Q. Guo, A. E. Hutcheon, J. D. Zieske, *Invest. Ophthalmol. Visual Sci.* **2010**, *51*, 1382; d) R. Ren, A. E. Hutcheon, X. Q. Guo, N. Saeidi, S. A. Melotti, J. W. Ruberti, J. D. Zieske, V. Trinkaus-Randall, *Dev. Dyn.* **2008**, *237*, 2705; e) X. Q. Guo, A. E. K. Hutcheon, S. A. Melotti, J. D. Zieske, V. Trinkaus-Randall, J. W. Ruberti, *Invest. Ophthalmol. Visual Sci.* **2007**, *48*, 4050; f) T. B. McKay, D. Karamichos, A. E. K. Hutcheon, X. Guo, J. D. Zieske, *Bioengineering* **2019**, *6*, 110. g) R. M. Gouveia, V. Castelletto, I. W. Hamley, C. J. Connon, *Tissue Eng., Part A* **2015**, *21*, 1772.
[36] a) P. Kumar, A. Pandit, D. Zeugolis, *Adv. Mater.* **2016**, *28*, 5381; b) P. Kumar, A. Satyam, X. Fan, Y. Rochev, B. J. Rodriguez, A. Gorelov, L. Joshi, M. Raghunath, A. Pandit, D. I. Zeugolis, *Tissue Eng., Part C* **2015**, *21*, 660.
[37] R. M. Gouveia, E. Gonzalez-Andrades, J. C. Cardona, C. Gonzalez-Gallardo, A. M. Ionescu, I. Garzon, M. Alaminos, M. Gonzalez-Andrades, C. J. Connon, *Biomaterials* **2017**, *121*, 205.
[38] K. Nishida, M. Yamato, Y. Hayashida, K. Watanabe, N. Maeda, H. Watanabe, K. Yamamoto, S. Nagai, A. Kikuchi, Y. Tano, T. Okano, *Transplantation* **2004**, *77*, 379.

[39] a) S. Molladavoodi, H. J. Kwon, J. Medley, M. Gorbet, *Acta Biomater.* **2015**, *11*, 324; b) S. Masterton, M. Ahearne, *R. Soc. Open Sci.* **2019**, *6*, 191796.
[40] a) R. R. Jones, I. W. Hamley, C. J. Connon, *Stem Cell Res.* **2012**, *8*, 403; b) R. M. Gouveia, G. Lepert, S. Gupta, R. R. Mohan, C. Paterson, C. J. Connon, *Nat. Commun.* **2019**, *10*, 1496; c) R. M. Gouveia, F. Vajda, J. A. Wibowo, F. Figueiredo, C. J. Connon, *Cells* **2019**, *8*, 347.
[41] a) B. Dreier, S. M. Thomasy, R. Mendonsa, V. K. Raghunathan, P. Russell, C. J. Murphy, *Invest. Ophthalmol. Visual Sci.* **2013**, *54*, 5901; b) W. M. Petroll, M. Vishwanath, L. Ma, *Invest. Ophthalmol. Visual Sci.* **2004**, *45*, 3466; c) D. Karamichos, N. Lakshman, W. M. Petroll, *Invest. Ophthalmol. Visual Sci.* **2007**, *48*, 5030.
[42] R. N. Palchesko, K. L. Lathrop, J. L. Funderburgh, A. W. Feinberg, *Sci. Rep.* **2015**, *5*, 7955.
[43] S. M. Thomasy, V. K. Raghunathan, H. Miyagi, A. T. Evashenk, J. C. Sermeno, G. K. Tripp, J. T. Morgan, C. J. Murphy, *Exp. Eye Res.* **2018**, *170*, 101.
[44] S. Masterton, M. Ahearne, *Exp. Eye Res.* **2018**, *177*, 122.
[45] a) M. Ahearne, Y. Yang, K. Y. Then, K. K. Liu, *Ann. Biomed. Eng.* **2007**, *35*, 1608; b) D. H. Glass, C. J. Roberts, A. S. Litsky, P. A. Weber, *Invest. Ophthalmol. Visual Sci.* **2008**, *49*, 3919; c) S. Kling, N. Bekesi, C. Dorronsoro, D. Pascual, S. Marcos, *PLoS One* **2014**, *9*, e104904.
[46] a) N. Garcia-Porta, P. Fernandes, A. Queiros, J. Salgado-Borges, M. Parafita-Mato, J. M. Gonzalez-Meijome, *ISRN Ophthalmol.* **2014**, *2014*, 724546; b) B. J. Blackburn, M. W. Jenkins, A. M. Rollins, W. J. Dupps, *Front. Bioeng. Biotechnol.* **2019**, *7*, 66; c) F. Boschetti, V. Triacca, L. Spinelli, A. Pandolfi, *J. Biomech. Eng.* **2012**, *134*, 031003.
[47] a) M. L. Borene, V. H. Barocas, A. Hubel, *Ann. Biomed. Eng.* **2004**, *32*, 274; b) A. Edwards, M. R. Prausnitz, *AIChE J.* **1998**, *44*, 214.
[48] a) K. Y. Then, Y. Yang, M. Ahearne, A. J. El Haj, *Curr. Eye Res.* **2011**, *36*, 88; b) S. Koo, S. J. Ahn, H. Zhang, J. C. Wang, E. K. F. Yim, *Cell Mol. Bioeng.* **2011**, *4*, 399; c) A. I. Teixeira, P. F. Nealey, C. J. Murphy, *J. Biomed. Mater. Res.* **2004**, *71A*, 369; d) S. J. Liliensiek, S. Campbell, P. F. Nealey, C. J. Murphy, *J. Biomed. Mater. Res., Part A* **2006**, *79A*, 185.
[49] G. A. Abrams, S. S. Schaus, S. L. Goodman, P. F. Nealey, C. J. Murphy, *Cornea* **2000**, *19*, 57.
[50] a) K. B. Kang, B. D. Lawrence, X. R. Gao, Y. C. Luo, Q. Zhou, A. H. Liu, V. H. Guaiquil, M. I. Rosenblatt, *Invest. Ophthalmol. Visual Sci.* **2017**, *58*, 6388; b) A. I. Teixeira, G. A. Abrams, P. J. Bertics, C. J. Murphy, P. F. Nealey, *J. Cell Sci.* **2003**, *116*, 1881.
[51] S. L. Wilson, I. Wimpenny, M. Ahearne, S. Rauz, A. J. El Haj, Y. Yang, *Adv. Funct. Mater.* **2012**, *22*, 3641.
[52] R. M. Gouveia, E. Koudouna, J. Jester, F. Figueiredo, C. J. Connon, *Adv. Biosyst.* **2017**, *1*, 1700135.
[53] M. Ahearne, K. K. Liu, A. J. El Haj, K. Y. Then, S. Rauz, Y. Yang, *Tissue Eng., Part C* **2010**, *16*, 319.
[54] K. E. Myrna, S. A. Pot, C. J. Murphy, *Vet. Ophthalmol.* **2009**, *12*, 25.
[55] a) J. Mo, S. Neelam, J. Mellon, J. R. Brown, J. Y. Niederkorn, *Invest. Ophthalmol. Visual Sci.* **2017**, *58*, 137; b) S. Neelam, J. Mellon, A. Wilkerson, J. Y. Niederkorn, *Invest. Ophthalmol. Visual Sci.* **2018**, *59*, 4738.
[56] J. Doutch, A. J. Quantock, V. A. Smith, K. M. Meek, *Biophys. J.* **2008**, *95*, 5092.
[57] R. D. Glickman, *Eye Contact Lens: Sci. Clin. Pract.* **2011**, *37*, 196.
[58] a) D. M. Maurice, *J. Physiol.* **1957**, *136*, 263; b) G. B. Benedek, *Appl. Opt.* **1971**, *10*, 459; c) K. M. Meek, C. Knupp, *Prog. Retinal Eye Res.* **2015**, *49*, 1.
[59] a) J. V. Jester, *Semin. Cell Dev. Biol.* **2008**, *19*, 82; b) J. V. Jester, T. Moller-Pedersen, J. Y. Huang, C. M. Sax, W. T. Kays, H. D. Cavangh, W. M. Petroll, J. Piatigorsky, *J. Cell Sci.* **1999**, *112*, 613.
[60] L. Robert, J. M. Legeais, A. M. Robert, G. Renard, *Pathol. Biol.* **2001**, *49*, 353.
[61] X. Duan, H. Sheardown, *Biomaterials* **2006**, *27*, 4608.
[62] L. Germain, F. A. Auger, E. Grandbois, R. Guignard, M. Giasson, H. Boisjoly, S. L. Guerin, *Pathobiology* **1999**, *67*, 140.
[63] E. J. Orwin, A. Hubel, *Tissue Eng.* **2000**, *6*, 307.
[64] a) S. Mi, B. Chen, B. Wright, C. J. Connon, *J. Biomed. Mater. Res., Part A* **2010**, *95A*, 447; b) Q. Ke, X. Wang, Q. Gao, Z. Wu, P. Wan, W. Zhan, J. Ge, Z. Wang, *J. Tissue Eng. Regener. Med.* **2011**, *5*, 138.
[65] X. Duan, C. McLaughlin, M. Griffith, H. Sheardown, *Biomaterials* **2007**, *28*, 78.
[66] J. J. Chae, W. M. Ambrose, F. A. Espinoza, D. G. Mulreany, S. Ng, T. Takezawa, M. M. Trexler, O. D. Schein, R. S. Chuck, J. H. Elisseeff, *Acta Ophthalmol.* **2015**, *93*, e57.
[67] a) S. Dravida, S. Gaddipati, M. Griffith, K. Merrett, S. Lakshmi Madhira, V. S. Sangwan, G. K. Vemuganti, *J. Tissue Eng. Regener. Med.* **2008**, *2*, 263; b) M. M. Islam, V. Cepla, C. L. He, J. Edin, T. Rakickas, K. Kobuch, Z. Ruzele, W. B. Jackson, M. Rafat, C. P. Lohmann, R. Valiokas, M. Griffith, *Acta Biomater.* **2015**, *12*, 70.
[68] W. G. Liu, C. Deng, C. R. McLaughlin, P. Fagerholm, N. S. Lagali, B. Heyne, J. C. Scaiano, M. A. Watsky, Y. Kato, R. Munger, N. Shinozaki, F. F. Li, M. Griffith, *Biomaterials* **2009**, *30*, 1551.
[69] C. Deng, F. Li, J. M. Hackett, S. H. Chaudhry, F. N. Toll, B. Toye, W. Hodge, M. Griffith, *Acta Biomater.* **2010**, *6*, 187.
[70] a) M. Koulikovska, M. Rafat, G. Petrovski, Z. Vereb, S. Akhtar, P. Fagerholm, N. Lagali, *Tissue Eng., Part A* **2015**, *21*, 1116; b) M. Rafat, M. Xeroudaki, M. Koulikovska, P. Sherrell, F. Groth, P. Fagerholm, N. Lagali, *Biomaterials* **2016**, *83*, 142.
[71] N. Builles, H. Janin-Manificat, M. Malbouyres, V. Justin, M. R. Rovere, G. Pellegrini, J. Torbet, D. J. S. Hulmes, C. Burillon, O. Damour, F. Ruggiero, *Biomaterials* **2010**, *31*, 8313.
[72] Y. Liu, X. Liu, M. H. Wu, P. H. Ji, H. L. Lv, L. H. Deng, *Int. J. Biol. Macromol.* **2019**, *121*, 233.
[73] E. Bentley, C. J. Murphy, F. Li, D. J. Carlsson, M. Griffith, *Cornea* **2010**, *29*, 910.
[74] N. E. Vrana, N. Builles, V. Justin, J. Bednarz, G. Pellegrini, B. Ferrari, O. Damour, D. J. Hulmes, V. Hasirci, *Invest. Ophthalmol. Visual Sci.* **2008**, *49*, 5325.
[75] a) M. Ahearne, S. L. Wilson, K. K. Liu, S. Rauz, A. J. El Haj, Y. Yang, *Exp. Eye Res.* **2010**, *91*, 584; b) C. Kilic, A. Girotti, C. Rodriguez-Cabello, V. Hasirci, *Biomater. Sci.* **2014**, *2*, 318.
[76] X. Xiao, S. Pan, X. Liu, X. Zhu, C. J. Connon, J. Wu, S. Mi, *J. Biomed. Mater. Res., Part A* **2014**, *102*, 1782.
[77] M. Miotto, R. M. Gouveia, A. M. Ionescu, F. Figueiredo, I. W. Hamley, C. J. Connon, *Adv. Funct. Mater.* **2019**, *29*, 1807334.
[78] a) E. J. Orwin, M. L. Borene, A. Hubel, *J. Biomech. Eng.* **2003**, *125*, 439; b) V. Kishore, R. Iyer, A. Frandsen, T. U. Nguyen, *Biomed. Mater.* **2016**, *11*, 055008; c) R. A. Crabb, E. P. Chau, D. M. Decoteau, A. Hubel, *Ann. Biomed. Eng.* **2006**, *34*, 1615.
[79] F. Li, M. Griffith, Z. Li, S. Tanodekaew, H. Sheardown, M. Hakim, D. J. Carlsson, *Biomaterials* **2005**, *26*, 3093.
[80] C. R. McLaughlin, M. C. Acosta, C. Luna, W. Liu, C. Belmonte, M. Griffith, J. Gallar, *Biomaterials* **2010**, *31*, 2770.
[81] a) K. Merrett, P. Fagerholm, C. R. McLaughlin, S. Dravida, N. Lagali, N. Shinozaki, M. A. Watsky, R. Munger, Y. Kato, F. F. Li, C. J. Marmo, M. Griffith, *Invest. Ophthalmol. Visual Sci.* **2008**, *49*, 3887; b) N. Lagali, M. Griffith, P. Fagerholm, K. Merrett, M. Huynh, R. Munger, *Invest. Ophthalmol. Visual Sci.* **2008**, *49*, 3895.
[82] S. Hayes, P. Lewis, M. M. Islam, J. Doutch, T. Sorensen, T. White, M. Griffith, K. M. Meek, *Acta Biomater.* **2015**, *25*, 121.

[83] a) P. Fagerholm, N. S. Lagali, J. A. Ong, K. Merrett, W. B. Jackson, J. W. Polarek, E. J. Suuronen, Y. Liu, I. Brunette, M. Griffith, *Biomaterials* **2014**, *35*, 2420; b) P. Fagerholm, N. S. Lagali, K. Merrett, W. B. Jackson, R. Munger, Y. Liu, J. W. Polarek, M. Soderqvist, M. Griffith, *Sci. Transl. Med.* **2010**, *2*, 46ra61; c) P. Fagerholm, N. S. Lagali, D. J. Carlsson, K. Merrett, M. Griffith, *Clin. Transl. Sci.* **2009**, *2*, 162; d) J. A. Ong, E. Auvinet, K. J. Forget, N. Lagali, P. Fagerholm, M. Griffith, J. Meunier, I. Brunette, *Invest. Ophthalmol. Visual Sci.* **2016**, *57*, 2355; e) O. Buznyk, N. Pasyechnikova, M. M. Islam, S. Iakymenko, P. Fagerholm, M. Griffith, *Clin. Transl. Sci.* **2015**, *8*, 558.

[84] a) Y. J. Cen, Y. Feng, *Chin. Med. J.* **2018**, *131*, 1710; b) R. N. Palchesko, J. L. Funderburgh, A. W. Feinberg, *Adv. Healthcare Mater.* **2016**, *5*, 2942.

[85] T. Mimura, S. Yamagami, S. Yokoo, T. Usui, K. Tanaka, S. Hattori, S. Irie, K. Miyata, M. Araie, S. Amano, *Invest. Ophthalmol. Visual Sci.* **2004**, *45*, 2992.

[86] J. Yoshida, S. Yokoo, A. Oshikata-Miyazaki, S. Amano, T. Takezawa, S. Yamagami, *Curr. Eye Res.* **2017**, *42*, 1420.

[87] N. Vazquez, M. Chacon, C. A. Rodriguez-Barrientos, J. Merayo-Lloves, M. Naveiras, B. Baamonde, J. F. Alfonso, I. Zambrano-Andazol, A. C. Riestra, A. Meana, *PLoS One* **2016**, *11*, e0167578.

[88] M. Y. Avila, V. A. Gerena, J. L. Navia, *Mol. Vision* **2012**, *18*, 1068.

[89] Y. S. Kwon, E. S. Lim, H. M. Kim, Y. C. Hwang, K. W. Lee, K. S. Min, *J. Endod.* **2015**, *41*, 501.

[90] M. Ahearne, Y. Yang, K. Y. Then, K. K. Liu, *Brit. J. Ophthalmol.* **2008**, *92*, 268.

[91] a) R. A. Brown, M. Wiseman, C. B. Chuo, U. Cheema, S. N. Nazhat, *Adv. Funct. Mater.* **2005**, *15*, 1762; b) U. Cheema, R. A. Brown, *Adv. Wound Care* **2013**, *2*, 176.

[92] E. E. Antoine, P. P. Vlachos, M. N. Rylander, *Tissue Eng., Part B* **2014**, *20*, 683.

[93] E. Davison-Kotler, W. S. Marshall, E. Garcia-Gareta, *Bioengineering* **2019**, *6*, 56.

[94] S. L. Wilson, M. Guilbert, J. Sule-Suso, J. Torbet, P. Jeannesson, G. D. Sockalingum, Y. Yang, *FASEB J.* **2014**, *28*, 14.

[95] a) J. A. Werkmeister, J. A. Ramshaw, *Biomed. Mater.* **2012**, *7*, 012002; b) S. Browne, D. I. Zeugolis, A. Pandit, *Tissue Eng., Part A* **2013**, *19*, 1491; c) B. An, D. L. Kaplan, B. Brodsky, *Front. Chem.* **2014**, *2*, 40.

[96] L. M. Houdebine, *Comp. Immunol., Microbiol. Infect. Dis.* **2009**, *32*, 107.

[97] T. Takezawa, K. Ozaki, A. Nitani, C. Takabayashi, T. Shimo-Oka, *Cell Transplant.* **2004**, *13*, 463.

[98] X. Calderon-Colon, Z. Xia, J. L. Breidenich, D. G. Mulreany, Q. Guo, O. M. Uy, J. E. Tiffany, D. E. Freund, R. L. McCally, O. D. Schein, J. H. Elisseeff, M. M. Trexler, *Biomaterials* **2012**, *33*, 8286.

[99] a) H. Yamaguchi, T. Takezawa, *Drug Metab. Dispos.* **2018**, *46*, 1684; b) H. Yamaguchi, H. Kojima, T. Takezawa, *J. Appl. Toxicol.* **2016**, *36*, 1025.

[100] a) T. H. van Essen, L. van Zijl, T. Possemiers, A. A. Mulder, S. J. Zwart, C. H. Chou, C. C. Lin, H. J. Lai, G. P. M. Luyten, M. J. Tassignon, N. Zakaria, A. El Ghalbzouri, M. J. Jager, *Biomaterials* **2016**, *81*, 36; b) C. C. Lin, R. Ritch, S. M. Lin, M. H. Ni, Y. C. Chang, Y. L. Lu, H. J. Lai, F. H. Lin, *Eur. Cells Mater.* **2010**, *19*, 50.

[101] T. H. van Essen, C. C. Lin, A. K. Hussain, S. Maas, H. J. Lai, H. Linnartz, T. J. T. P. van den Berg, D. C. F. Salvatori, G. P. M. Luyten, M. J. Jager, *Invest. Ophthalmol. Visual Sci.* **2013**, *54*, 3224.

[102] F. Yuan, L. Y. Wang, C. C. Lin, C. H. Chou, L. Li, *J. Ophthalmol.* **2014**, *2014*, 914542.

[103] S. Krishnan, S. Sekar, M. F. Katheem, S. Krishnakumar, T. P. Sastry, *Artif. Organs* **2012**, *36*, 829.

[104] M. Parekh, B. Van den Bogerd, N. Zakaria, D. Ponzin, S. Ferrari, *Stem Cells Int.* **2018**, *2018*, 8146834.

[105] a) N. Kasoju, U. Bora, *Adv. Healthcare Mater.* **2012**, *1*, 393; b) Y. Wang, J. Guo, L. Zhou, C. Ye, F. G. Omenetto, D. L. Kaplan, S. J. Ling, *Adv. Funct. Mater.* **2018**, *28*, 1805305.

[106] a) T. Chirila, Z. Barnard, Zainuddin, D. G. Harkin, I. R. Schwab, L. Hirst, *Tissue Eng., Part A* **2008**, *14*, 1203; b) L. J. Bray, K. A. George, S. L. Ainscough, D. W. Hutmacher, T. V. Chirila, D. G. Harkin, *Biomaterials* **2011**, *32*, 5086; c) J. Liu, B. D. Lawrence, A. Liu, I. R. Schwab, L. A. Oliveira, M. I. Rosenblatt, *Invest. Ophthalmol. Visual Sci.* **2012**, *53*, 4130; d) B. D. Lawrence, Z. Pan, A. Liu, D. L. Kaplan, M. I. Rosenblatt, *Acta Biomater.* **2012**, *8*, 3732; e) B. D. Lawrence, Z. Pan, M. I. Rosenblatt, *PLoS One* **2012**, *7*, 50190; f) E. Biazar, A. Baradaran-Rafii, S. Heidari-keshel, S. Tavakolifard, *J. Biomater. Sci., Polym. Ed.* **2015**, *26*, 1139; g) M. B. Applegate, B. P. Partlow, J. Coburn, B. Marelli, C. Pirie, R. Pineda, D. L. Kaplan, F. G. Omenetto, *Adv. Mater.* **2016**, *28*, 2417.

[107] T. A. Hogerheyde, S. Suzuki, S. A. Stephenson, N. A. Richardson, T. V. Chirila, D. G. Harkin, L. J. Bray, *Biomed. Mater.* **2014**, *9*, 025016.

[108] L. Jia, C. E. Ghezzi, D. L. Kaplan, *J. Biomed. Mater. Res., Part B* **2016**, *104*, 431.

[109] Y. Li, Y. Yang, L. Yang, Y. Zeng, X. Gao, H. Xu, *Stem Cell Res. Ther.* **2017**, *8*, 256.

[110] a) L. J. Bray, K. A. George, D. W. Hutmacher, T. V. Chirila, D. G. Harkin, *Biomaterials* **2012**, *33*, 3529; b) S. Wang, C. E. Ghezzi, R. Gomes, R. E. Pollard, J. L. Funderburgh, D. L. Kaplan, *Biomaterials* **2017**, *112*, 1; c) E. A. Gosselin, T. Torregrosa, C. E. Ghezzi, A. C. Mendelsohn, R. Gomes, J. L. Funderburgh, D. L. Kaplan, *J. Tissue Eng. Regener. Med.* **2018**, *12*, 285.

[111] S. Hazra, S. Nandi, D. Naskar, R. Guha, S. Chowdhury, N. Pradhan, S. C. Kundu, A. Konar, *Sci. Rep.* **2016**, *6*, 21840.

[112] L. Guan, H. Y. Ge, X. L. Tang, S. Su, P. Tian, N. Xiao, H. Zhang, L. Zhang, P. Liu, *Cells Tissues Organs* **2013**, *198*, 190.

[113] K. Long, Y. Liu, W. C. Li, L. Wang, S. Liu, Y. J. Wang, Z. C. Wang, L. Ren, *J. Biomed. Mater. Res., Part A* **2015**, *103*, 1159.

[114] a) B. D. Lawrence, J. K. Marchant, M. A. Pindrus, F. G. Omenetto, D. L. Kaplan, *Biomaterials* **2009**, *30*, 1299; b) E. S. Gil, S. H. Park, J. Marchant, F. Omenetto, D. L. Kaplan, *Macromol. Biosci.* **2010**, *10*, 664; c) M. C. Lee, D. K. Kim, O. J. Lee, J. H. Kim, H. W. Ju, J. M. Lee, B. M. Moon, H. J. Park, D. W. Kim, S. H. Kim, C. H. Park, *J. Biomed. Mater. Res., Part B* **2016**, *104*, 508; d) W. Zhang, J. L. Chen, L. J. Backman, A. D. Malm, P. Danielson, *Adv. Healthcare Mater.* **2017**, *6*, 1601238; e) C. E. Ghezzi, B. Marelli, F. G. Omenetto, J. L. Funderburgh, D. L. Kaplan, *PLoS One* **2017**, *12*, 0169504.

[115] C. E. Ghezzi, L. Wang, I. Behlau, J. Rnjak-Kovacina, S. Wang, M. H. Goldstein, J. Liu, J. K. Marchant, M. I. Rosenblatt, D. L. Kaplan, *J. Appl. Biomater. Funct. Mater.* **2016**, *14*, 266.

[116] a) E. S. Gil, B. B. Mandal, S. H. Park, J. K. Marchant, F. G. Omenetto, D. L. Kaplan, *Biomaterials* **2010**, *31*, 8953; b) J. Wu, J. Rnjak-Kovacina, Y. Du, M. L. Funderburgh, D. L. Kaplan, J. L. Funderburgh, *Biomaterials* **2014**, *35*, 3744.

[117] L. N. Guan, P. Tian, H. Y. Ge, X. L. Tang, H. Zhang, L. L. Du, P. Liu, *J. Mol. Histol.* **2013**, *44*, 609.

[118] L. Wang, R. Ma, G. Du, H. Guo, Y. Huang, *J. Biomed. Mater. Res., Part B* **2015**, *103*, 204.

[119] P. Bhattacharjee, J. Fernandez-Perez, M. Ahearne, *Mater. Sci. Eng., C* **2019**, *105*, 110093.

[120] P. W. Madden, J. N. X. Lai, K. A. George, T. Giovenco, D. G. Harkin, T. V. Chirila, *Biomaterials* **2011**, *32*, 4076.

[121] N. Vazquez, C. A. Rodriguez-Barrientos, S. D. Aznar-Cervantes, M. Chacon, J. L. Cenis, A. C. Riestra, R. M. Sanchez-Avila, M. Persinal, A. Brea-Pastor, L. F. V. Cueto, A. Meana, J. Merayo-Lloves, *Invest. Ophthalmol. Visual Sci.* **2017**, *58*, 3357.

[122] D. K. Kim, B. R. Sim, G. Khang, *ACS Appl. Mater. Interfaces* **2016**, *8*, 15160.

[123] J. Chen, C. Yan, M. Y. Zhu, Q. K. Yao, C. Y. Shao, W. J. Lu, J. Wang, X. M. Mo, P. Gu, Y. Fu, X. Q. Fan, *Int. J. Nanomed.* **2015**, *10*, 3337.
[124] E. Y. Kim, N. Tripathy, S. A. Cho, C. K. Joo, D. Lee, G. Khang, *Colloids Surf., B* **2015**, *136*, 394.
[125] D. K. Kim, B. R. Sim, J. I. Kim, G. Khang, *Colloids Surf., B* **2018**, *164*, 340.
[126] J. E. Song, B. R. Sim, Y. S. Jeon, H. S. Kim, E. Y. Shin, C. Carlomagno, G. Khang, *J. Biomater. Sci., Polym. Ed.* **2019**, *30*, 263.
[127] G. H. Darshan, D. Kong, J. Gautrot, S. Vootla, *Sci. Rep.* **2017**, *7*, 10344.
[128] K. B. Kang, B. D. Lawrence, X. R. Gao, V. H. Guaiquil, A. Liu, M. I. Rosenblatt, *Sci. Rep.* **2019**, *9*, 1507.
[129] C. Y. Jiang, X. Y. Wang, R. Gunawidjaja, Y. H. Lin, M. K. Gupta, D. L. Kaplan, R. R. Naik, V. V. Tsukruk, *Adv. Funct. Mater.* **2007**, *17*, 2229.
[130] J. H. Choi, H. Jeon, J. E. Song, J. M. Oliveira, R. L. Reis, G. Khang, *Nanomaterials* **2018**, *8*, 290.
[131] P. M. Deardorff, T. B. McKay, S. Wang, C. E. Ghezzi, D. M. Cairns, R. D. Abbott, J. L. Funderburgh, K. R. Kenyon, D. L. Kaplan, *Sci. Rep.* **2018**, *8*, 17294.
[132] P. Aramwit, T. Siritientong, T. Srichana, *Waste Manage. Res.* **2012**, *30*, 217.
[133] P. Aramwit, S. Kanokpanont, T. Nakpheng, T. Srichana, *Int. J. Mol. Sci.* **2010**, *11*, 2200.
[134] T. V. Chirila, S. Suzuki, N. C. McKirdy, *Prog. Biomater.* **2016**, *5*, 135.
[135] a) N. Nagai, Y. Fukuoka, M. Ishii, H. Otake, T. Yamamoto, A. Taga, N. Okamoto, Y. Shimomura, *Int. J. Mol. Sci.* **2018**, *19*, 1123; b) N. Nagai, T. Murao, Y. Ito, N. Okamoto, M. Sasaki, *Biol. Pharm. Bull.* **2009**, *32*, 933.
[136] T. V. Chirila, S. Suzuki, L. J. Bray, N. L. Barnett, D. G. Harkin, *Prog. Biomater.* **2013**, *2*, 14.
[137] B. Panilaitis, G. H. Altman, J. Chen, H. J. Jin, V. Karageorgiou, D. L. Kaplan, *Biomaterials* **2003**, *24*, 3079.
[138] T. Chlapanidas, S. Farago, G. Lucconi, S. Perteghella, M. Galuzzi, M. Mantelli, M. A. Avanzini, M. C. Tosca, M. Marazzi, D. Vigo, M. L. Torre, M. Faustini, *Int. J. Biol. Macromol.* **2013**, *58*, 47.
[139] D. Meller, M. Pauklin, H. Thomasen, H. Westekemper, K.-P. Steuhl, *Dtsch. Aerztebl. Int.* **2011**, *108*, 243.
[140] K. Jirsova, G. L. A. Jones, *Cell Tissue Banking* **2017**, *18*, 193.
[141] Y. Ishino, Y. Sano, T. Nakamura, C. J. Connon, H. Rigby, N. J. Fullwood, S. Kinoshita, *Invest. Ophthalmol. Visual Sci.* **2004**, *45*, 800.
[142] Z. Zhou, D. Long, C. C. Hsu, H. Liu, L. Chen, B. Slavin, H. Lin, X. Li, J. Tang, S. Yiu, S. Tuffaha, H. Q. Mao, *Acta Biomater.* **2019**, *97*, 310.
[143] C. L. Allen, G. Clare, E. A. Stewart, M. J. Branch, O. D. McIntosh, M. Dadhwal, H. S. Dua, A. Hopkinson, *PLoS One* **2013**, *8*, 78441.
[144] W. L. Stoppel, C. E. Ghezzi, S. L. McNamara, L. D. Black 3rd, D. L. Kaplan, *Ann. Biomed. Eng.* **2015**, *43*, 657.
[145] Y. Liu, L. Ren, Y. J. Wang, *Mater. Sci. Eng., C* **2013**, *33*, 196.
[146] A. de la Mata, T. Nieto-Miguel, M. Lopez-Paniagua, S. Galindo, M. R. Aguilar, L. Garcia-Fernandez, S. Gonzalo, B. Vazquez, J. S. Roman, R. M. Corrales, M. Calonge, *J. Mater. Sci.: Mater. Med.* **2013**, *24*, 2819.
[147] W. H. Xu, Z. Y. Wang, Y. Liu, L. P. Wang, Z. W. Jiang, T. Li, W. H. Zhang, Y. Liang, *Carbohydr. Polym.* **2018**, *192*, 240.
[148] B. Wright, P. A. De Bank, K. A. Luetchford, F. R. Acosta, C. J. Connon, *J. Biomed. Mater. Res., Part A* **2014**, *102*, 3393.
[149] D. Chen, Y. Qu, X. Hua, L. Zhang, Z. Liu, S. C. Pflugfelder, D. Q. Li, *Eye* **2017**, *31*, 962.
[150] E. S. Sani, A. Kheirkhah, D. Rana, Z. M. Sun, W. Foulsham, A. Sheikhi, A. Khademhosseini, R. Dana, N. Annabi, *Sci. Adv.* **2019**, *5*, 1281.
[151] a) L. Koivusalo, M. Kauppila, S. Samanta, V. S. Parihar, T. Ilmarinen, S. Miettinen, O. P. Oommen, H. Skottman, *Biomaterials* **2019**, *225*, 119516; b) L. Koivusalo, J. Karvinen, E. Sorsa, I. Jonkkari, J. Valiaho, P. Kallio, T. Ilmarinen, S. Miettinen, H. Skottman, M. Kellomaki, *Mater. Sci. Eng., C* **2018**, *85*, 68.
[152] a) L. Rico-Sanchez, I. Garzon, M. Gonzalez-Andrades, A. Ruiz-Garcia, M. Punzano, A. Lizana-Moreno, J. I. Munoz-Avila, M. C. Sanchez-Quevedo, J. Martinez-Atienza, L. Lopez-Navas, R. Sanchez-Pernaute, R. I. Oruezabal, S. Medialdea, M. D. C. Gonzalez-Gallardo, G. Carmona, S. Sanbonmatsu-Gamez, M. Perez, P. Jimenez, N. Cuende, A. Campos, M. Alaminos, *J. Tissue Eng. Regener. Med.* **2019**, *13*, 2142; b) M. Gonzalez-Andrades, R. Mata, M. D. C. Gonzalez-Gallardo, S. Medialdea, S. Arias-Santiago, J. Martinez-Atienza, A. Ruiz-Garcia, L. Perez-Fajardo, A. Lizana-Moreno, I. Garzon, A. Campos, M. Alaminos, G. Carmona, N. Cuende, *BMJ Open* **2017**, *7*, 016487.
[153] M. Alaminos, M. Del Carmen Sanchez-Quevedo, J. I. Munoz-Avila, D. Serrano, S. Medialdea, I. Carreras, A. Campos, *Invest. Ophthalmol. Visual Sci.* **2006**, *47*, 3311.
[154] a) T. Mimura, S. Amano, S. Yokoo, S. Uchida, S. Yamagami, T. Usui, Y. Kimura, Y. Tabata, *Mol. Vision* **2008**, *14*, 1819; b) L.-J. Luo, J.-Y. Lai, S.-F. Chou, Y.-J. Hsueh, D. H.-K. Ma, *Acta Biomater.* **2018**, *65*, 123.
[155] a) J. Y. Lai, Y. T. Li, C. H. Cho, T. C. Yu, *Int. J. Nanomed.* **2012**, *7*, 1101; b) J. Y. Lai, *Int. J. Mol. Sci.* **2013**, *14*, 2036.
[156] H. Goodarzi, K. Jadidi, S. Pourmotabed, E. Sharifi, H. Aghamollaei, *Int. J. Biol. Macromol.* **2019**, *126*, 620.
[157] C. K. Bektas, V. Hasirci, *J. Tissue Eng. Regener. Med.* **2018**, *12*, 1899.
[158] M. Miron-Mendoza, E. Graham, S. Manohar, W. M. Petroll, *Matrix Biol.* **2017**, *64*, 69.
[159] K. Tonsomboon, M. L. Oyen, *J. Mech. Behav. Biomed. Mater.* **2013**, *21*, 185.
[160] R. Watanabe, R. Hayashi, Y. Kimura, Y. Tanaka, T. Kageyama, S. Hara, Y. Tabata, K. Nishida, *Tissue Eng., Part A* **2011**, *17*, 2213.
[161] a) J. Y. Lai, D. H. K. Ma, M. H. Lai, Y. T. Li, R. J. Chang, L. M. Chen, *PLoS One* **2013**, *8*, 54058; b) J. Y. Lai, P. L. Lu, K. H. Chen, Y. Tabata, G. H. Hsiue, *Biomacromolecules* **2006**, *7*, 1836; c) J. Y. Lai, K. H. Chen, G. H. Hsiue, *Transplantation* **2007**, *84*, 1222; d) G. H. Hsiue, J. Y. Lai, K. H. Chen, W. M. Hsu, *Transplantation* **2006**, *81*, 473.
[162] M. Rizwan, G. S. L. Peh, H. P. Ang, N. C. Lwin, K. Adnan, J. S. Mehta, W. S. Tan, E. K. F. Yim, *Biomaterials* **2017**, *120*, 139.
[163] P. L. Lu, J. Y. Lai, D. H. K. Ma, G. H. Hsiue, *J. Biomater. Sci., Polym. Ed.* **2008**, *19*, 1.
[164] J. Y. Lai, H. Y. Cheng, D. H. K. Ma, *PLoS One* **2015**, *10*, 0136067.
[165] M. C. Echave, L. Saenz del Burgo, J. L. Pedraz, G. Orive, *Curr. Pharm. Des.* **2017**, *23*, 3567.
[166] B. J. Rose, S. Pacelli, J. A. Haj, S. H. Dua, A. Hopkinson, J. L. White, R. F. Rose, *Materials* **2014**, *7*, 3106.
[167] M. Y. Sun, X. T. Sun, Z. Y. Wang, S. Y. Guo, G. J. Yu, H. Z. Yang, *Polymers* **2018**, *10*, 1290.
[168] A. I. Van den Bulcke, B. Bogdanov, N. De Rooze, E. H. Schacht, M. Cornelissen, H. Berghmans, *Biomacromolecules* **2000**, *1*, 31.
[169] E. Shirzaei Sani, A. Kheirkhah, D. Rana, Z. Sun, W. Foulsham, A. Sheikhi, A. Khademhosseini, R. Dana, N. Annabi, *Sci. Adv.* **2019**, *5*, 1281.
[170] a) M. Ahearne, C. T. Buckley, D. J. Kelly, *Biotechnol. Appl. Biochem.* **2011**, *58*, 345; b) M. Ahearne, D. J. Kelly, *Biomed. Mater.* **2013**, *8*, 035004.
[171] K. Musselmann, B. Kane, B. Alexandrou, J. R. Hassell, *Invest. Ophthalmol. Visual Sci.* **2006**, *47*, 5260.
[172] S. Guhan, S. L. Peng, H. Janbatian, S. Saadeh, S. Greenstein, F. Al Bahrani, A. Fadlallah, T. C. Yeh, S. A. Melki, *Brit. J. Ophthalmol.* **2018**, *102*, 1328.

[173] a) N. Nassiri, H. K. Pandya, A. R. Djalilian, *Arch. Ophthalmol.* **2011**, *129*, 218; b) B. Sonmez, U. Beden, *Cornea* **2011**, *30*, 296; c) J. D. Welder, H. K. Pandya, N. Nassiri, A. R. Djalilian, *Ophthalmic Surg., Lasers, Imaging* **2012**, *43*, 323.
[174] A. M. Yeung, L. A. Faraj, O. D. McIntosh, V. K. Dhillon, H. S. Dua, *Eye* **2016**, *30*, 1389.
[175] C. Scalcione, D. Ortiz-Vaquerizas, D. G. Said, H. S. Dua, *Eye* **2018**, *32*, 463.
[176] L. Y. Chen, J. S. Kung, E. E. Manche, *Eye Contact Lens: Sci. Clin. Pract.* **2018**, *44*, S210.
[177] a) A. M. Ionescu, M. Alaminos, J. D. Cardona, J. D. G. L. Duran, M. Gonzalez-Andrades, R. Ghinea, A. Campos, E. Hita, M. D. Perez, *J. Mech. Behav. Biomed. Mater.* **2011**, *4*, 1963; b) I. Garzon, M. A. Martin-Piedra, C. Alfonso-Rodriguez, M. Gonzalez-Andrades, V. Carriel, C. Martinez-Gomez, A. Campos, M. Alaminos, *Invest. Ophthalmol. Visual Sci.* **2014**, *55*, 4073; c) A. M. Ionescu, J. de la Cruz Cardona, M. Gonzalez-Andrades, M. Alaminos, A. Campos, E. Hita, M. del Mar Perez, *Cornea* **2010**, *29*, 895.
[178] a) F. Croisier, C. Jerome, *Eur. Polym. J.* **2013**, *49*, 780; b) C.-H. Kim, S. J. Park, D. H. Yang, H. J. Chun, in *Novel Biomaterials for Regenerative Medicine* (Eds: H. J. Chun, K. Park, C.-H. Kim, G. Khang), Springer, Singapore **2018**, p. 475.
[179] a) P. Kumar, B. S. Dehiya, A. Sindhu, *Int. Nano Lett.* **2017**, *7*, 285; b) T. Freier, H. S. Koh, K. Kazazian, M. S. Shoichet, *Biomaterials* **2005**, *26*, 5872.
[180] a) K. Y. Lee, D. J. Mooney, *Prog. Polym. Sci.* **2012**, *37*, 106; b) M. Szekalska, A. Pucilowska, E. Szymanska, P. Ciosek, K. Winnicka, *Int. J. Poly. Sci.* **2016**, *2016*, 7697031.
[181] M. Ahearne, Y. Yang, A. J. El Haj, K. Y. Then, K. K. Liu, *J. R. Soc., Interface* **2005**, *2*, 455.
[182] a) W. Y. Chen, G. Abatangelo, *Wound Repair Regener.* **1999**, *7*, 79; b) K. R. Kirker, Y. Luo, J. H. Nielson, J. Shelby, G. D. Prestwich, *Biomaterials* **2002**, *23*, 3661; c) L. A. Solchaga, J. E. Dennis, V. M. Goldberg, A. I. Caplan, *J. Orthop. Res.* **1999**, *17*, 205; d) I. L. Kim, R. L. Mauck, J. A. Burdick, *Biomaterials* **2011**, *32*, 8771.
[183] M. X. Sun, S. Puri, K. N. Mutoji, Y. M. Coulson-Thomas, V. C. Hascall, D. G. Jackson, T. F. Gesteira, V. J. Coulson-Thomas, *Invest. Ophthalmol. Visual Sci.* **2019**, *60*, 1050.
[184] a) Q. Li, H. Wang, Z. Dai, Y. Cao, C. Jin, *Cornea* **2017**, *36*, 1343; b) X. C. Lin, Y. N. Hui, Y. S. Wang, H. Meng, Y. J. Zhang, Y. Jin, *Vet. Ophthalmol.* **2008**, *11*, 61; c) M. C. Zhang, X. Liu, Y. Jin, D. L. Jiang, X. S. Wei, H. T. Xie, *Am. J. Transplant.* **2015**, *15*, 1068; d) Y. Lin, Q. Zheng, S. Hua, Y. Meng, W. Chen, Y. Wang, *Sci. Rep.* **2017**, *7*, 9955; e) Z. Wu, Y. Zhou, N. Li, M. Huang, H. Duan, J. Ge, P. Xiang, Z. Wang, *Biomaterials* **2009**, *30*, 3513; f) B. Xu, Z. Song, T. Fan, *Artif. Organs* **2017**, *41*, 1004.
[185] M. M. Islam, R. Sharifi, S. Mamodaly, R. Islam, D. Nahra, D. B. Abusamra, P. C. Hui, Y. Adibnia, M. Goulamaly, E. I. Paschalis, A. Cruzat, J. Kong, P. H. Nilsson, P. Argueso, T. E. Mollnes, J. Chodosh, C. H. Dohlman, M. Gonzalez-Andrades, *Acta Biomater.* **2019**, *96*, 330.
[186] T. J. Keane, R. Londono, N. J. Turner, S. F. Badylak, *Biomaterials* **2012**, *33*, 1771.
[187] S. Nagata, R. Hanayama, K. Kawane, *Cell* **2010**, *140*, 619.
[188] a) J. Y. Oh, M. K. Kim, H. J. Lee, J. H. Ko, W. R. Wee, J. H. Lee, *Tissue Eng., Part C* **2009**, *15*, 635; b) J. M. Diao, X. Pang, Y. Qiu, Y. Miao, M. M. Yu, T. J. Fan, *Exp. Eye Res.* **2015**, *132*, 216; c) S. Proulx, T. Bensaoula, O. Nada, C. Audet, J. d'Arc Uwamaliya, A. Devaux, G. Allaire, L. Germain, I. Brunette, *Invest. Ophthalmol. Visual Sci.* **2009**, *50*, 2686.
[189] a) S. Sasaki, S. Funamoto, Y. Hashimoto, T. Kimura, T. Honda, S. Hattori, H. Kobayashi, A. Kishida, M. Mochizuki, *Mol. Vision* **2009**, *15*, 2022; b) Y. Hashimoto, S. Funamoto, S. Sasaki, T. Honda, S. Hattori, K. Nam, T. Kimura, M. Mochizuki, T. Fujisato, H. Kobayashi, A. Kishida, *Biomaterials* **2010**, *31*, 3941.
[190] a) Y. H. Huang, F. W. Tseng, W. H. Chang, I. C. Peng, D. J. Hsieh, S. W. Wu, M. L. Yeh, *Acta Biomater.* **2017**, *58*, 238; b) S. Guler, B. Aslan, P. Hosseinian, H. M. Aydin, *Tissue Eng., Part C* **2017**, *23*, 540.
[191] a) K. Pang, L. Du, X. Wu, *Biomaterials* **2010**, *31*, 7257; b) L. Du, X. Wu, *Artif. Organs* **2011**, *35*, 691; c) Y. Zhou, Z. Wu, J. Ge, P. Wan, N. Li, P. Xiang, Q. Gao, Z. Wang, *Cornea* **2011**, *30*, 73.
[192] a) J. S. Choi, J. K. Williams, M. Greven, K. A. Walter, P. W. Laber, G. Khang, S. Soker, *Biomaterials* **2010**, *31*, 6738; b) H. Luo, Y. Lu, T. Wu, M. Zhang, Y. Zhang, Y. Jin, *Biomaterials* **2013**, *34*, 6748.
[193] a) W. Shi, Q. Zhou, H. Gao, S. Li, M. Dong, T. Wang, Y. Jia, C. Dong, X. Wang, Z. Guo, L. Zhao, X. Hu, L. Xie, *Adv. Funct. Mater.* **2019**, *29*, 1902491; b) M. Dong, L. Zhao, F. Wang, X. Hu, H. Li, T. Liu, Q. Zhou, W. Shi, *J. Tissue Eng.* **2019**, *10*, 2041731419875876.
[194] S. Ponce Marquez, V. S. Martinez, W. McIntosh Ambrose, J. Wang, N. G. Gantxegui, O. Schein, J. Elisseeff, *Acta Biomater.* **2009**, *5*, 1839.
[195] H. J. Lin, T. J. Wang, T. W. Li, Y. Y. Chang, M. T. Sheu, Y. Y. Huang, D. Z. Liu, *Tissue Eng., Part A* **2019**, *25*, 652.
[196] Z. Zhang, G. Niu, J. S. Choi, M. Giegengack, A. Atala, S. Soker, *Biomed. Mater.* **2015**, *10*, 035012.
[197] M. Gonzalez-Andrades, J. de la Cruz Cardona, A. M. Ionescu, A. Campos, M. Del Mar Perez, M. Alaminos, *Invest. Ophthalmol. Visual Sci.* **2011**, *52*, 215.
[198] a) Y. G. Xu, Y. S. Xu, C. Huang, Y. Feng, Y. Li, W. Wang, *Mol. Vision* **2008**, *14*, 2180; b) M. I. Huh, K. P. Lee, J. Kim, S. Yi, B. U. Park, H. K. Kim, *J. Ophthalmol.* **2018**, *2018*, 2590536.
[199] J. Xiao, H. Duan, Z. Liu, Z. Wu, Y. Lan, W. Zhang, C. Li, F. Chen, Q. Zhou, X. Wang, J. Huang, Z. Wang, *Biomaterials* **2011**, *32*, 6962.
[200] Y. Shao, J. Tang, Y. Zhou, Y. Qu, H. He, Q. Liu, G. Tan, W. Li, Z. Liu, *Am. J. Transl. Res.* **2015**, *7*, 2612.
[201] a) J. L. Alio del Barrio, M. Chiesa, N. Garagorri, N. Garcia-Urquia, J. Fernandez-Delgado, L. Bataille, A. Rodriguez, F. Arnalich-Montiel, T. Zarnowski, J. P. Alvarez de Toledo, J. L. Alio, M. P. De Miguel, *Exp. Eye Res.* **2015**, *132*, 91; b) A. P. Lynch, S. L. Wilson, M. Ahearne, *Tissue Eng., Part C* **2016**, *22*, 561.
[202] a) J. Fernandez-Perez, M. Ahearne, *Methods* **2019**, *171*, 86; b) S. L. Wilson, L. E. Sidney, S. E. Dunphy, J. B. Rose, A. Hopkinson, *J. Funct. Biomater.* **2013**, *4*, 114.
[203] S. L. Wilson, L. E. Sidney, S. E. Dunphy, H. S. Dua, A. Hopkinson, *Curr. Eye Res.* **2016**, *41*, 769.
[204] C. A. Utine, J. H. Tzu, E. K. Akpek, *Am. J. Ophthalmol.* **2011**, *151*, 170.
[205] a) G. H. Yam, N. Z. Yusoff, T. W. Goh, M. Setiawan, X. W. Lee, Y. C. Liu, J. S. Mehta, *Sci. Rep.* **2016**, *6*, 26339; b) H. Yin, P. Qiu, F. Wu, W. Zhang, W. Teng, Z. Qin, C. Li, J. Zhou, Z. Fang, Q. Tang, Q. Fu, J. Ma, Y. Yang, *Sci. Rep.* **2016**, *6*, 33848.
[206] Y. Zeng, J. Yang, K. Huang, Z. Lee, X. Lee, *J. Biomech.* **2001**, *34*, 533.
[207] R. Sharifi, Y. Yang, Y. Adibnia, C. H. Dohlman, J. Chodosh, M. Gonzalez-Andrades, *Sci. Rep.* **2019**, *9*, 1876.
[208] Z. He, F. Forest, A. Bernard, A. S. Gauthier, R. Montard, M. Peoc'h, C. Jumelle, E. Courrier, C. Perrache, P. Gain, G. Thuret, *Invest. Ophthalmol. Visual Sci.* **2016**, *57*, 6639.
[209] a) Y. Fu, X. Fan, P. Chen, C. Shao, W. Lu, *Cells Tissues Organs* **2010**, *191*, 193; b) J. Zhang, C. W. Zhang, L. Q. Du, X. Y. Wu, *Int. J. Ophthalmol.* **2016**, *9*, 1; c) M. A. Shafiq, R. A. Gemeinhart, B. Y. Yue, A. R. Djalilian, *Tissue Eng., Part C* **2012**, *18*, 340.
[210] J. L. Alio Del Barrio, M. El Zarif, A. Azaar, N. Makdissy, C. Khalil, W. Harb, I. El Achkar, Z. A. Jawad, M. P. de Miguel, J. L. Alio, *Am. J. Ophthalmol.* **2018**, *186*, 47.
[211] Y. Hashimoto, S. Funamoto, S. Sasaki, J. Negishi, T. Honda, S. Hattori, K. Nam, T. Kimura, M. Mochizuki, H. Kobayashi, A. Kishida, *PLoS One* **2015**, *10*, 0131989.

[212] H. Hong, M. I. Huh, S. M. Park, K. P. Lee, H. K. Kim, D. S. Kim, *Biofabrication* **2018**, *10*, 045001.
[213] J. Zheng, X. Huang, Y. Zhang, Y. Wang, Q. Qin, L. Lin, X. Jin, C. Lam, J. Zhang, *Xenotransplantation* **2019**, *26*, 12509.
[214] M.-R. Rovere, C. Ouilhon, D. Salmon, M. Haftek, O. Damour, C. Auxenfans, *Cell Tissue Banking* **2019**, *20*, 49.
[215] D. O. Freytes, J. Martin, S. S. Velankar, A. S. Lee, S. F. Badylak, *Biomaterials* **2008**, *29*, 1630.
[216] M. T. Wolf, K. A. Daly, E. P. Brennan-Pierce, S. A. Johnson, C. A. Carruthers, A. D'Amore, S. P. Nagarkar, S. S. Velankar, S. F. Badylak, *Biomaterials* **2012**, *33*, 7028.
[217] a) R. Gaetani, S. Aouad, L. L. Demaddalena, H. Straessle, M. Dzieciatkowska, M. Wortham, H. R. Bender, K. V. Nguyen-Ngoc, G. W. Schmid-Schoenbein, S. C. George, C. C. W. Hughes, M. Sander, K. C. Hansen, K. L. Christman, *Tissue Eng., Part C* **2018**, *24*, 697; b) S. D. Sackett, D. M. Tremmel, F. Ma, A. K. Feeney, R. M. Maguire, M. E. Brown, Y. Zhou, X. Li, C. O'Brien, L. Li, W. J. Burlingham, J. S. Odorico, *Sci. Rep.* **2018**, *8*, 10452.
[218] a) T. D. Johnson, S. Y. Lin, K. L. Christman, *Nanotechnology* **2011**, *22*, 494015; b) J. L. Ungerleider, T. D. Johnson, N. Rao, K. L. Christman, *Methods* **2015**, *84*, 53.
[219] M. J. Sawkins, W. Bowen, P. Dhadda, H. Markides, L. E. Sidney, A. J. Taylor, F. R. Rose, S. F. Badylak, K. M. Shakesheff, L. J. White, *Acta Biomater.* **2013**, *9*, 7865.
[220] S. L. Voytik-Harbin, A. O. Brightman, B. Z. Waisner, J. P. Robinson, C. H. Lamar, *Tissue Eng.* **1998**, *4*, 157.
[221] H. Lee, W. Han, H. Kim, D.-H. Ha, J. Jang, B. S. Kim, D.-W. Cho, *Biomacromolecules* **2017**, *18*, 1229.
[222] F. Pati, J. Jang, D. H. Ha, S. Won Kim, J. W. Rhie, J. H. Shim, D. H. Kim, D. W. Cho, *Nat. Commun.* **2014**, *5*, 3935.
[223] S. Farnebo, C. Y. Woon, T. Schmitt, L. M. Joubert, M. Kim, H. Pham, J. Chang, *Tissue Eng., Part A* **2014**, *20*, 1550.
[224] V. Magno, J. Friedrichs, H. M. Weber, M. C. Prewitz, M. V. Tsurkan, C. Werner, *Acta Biomater.* **2017**, *55*, 109.
[225] a) H. Kim, M.-N. Park, J. Kim, J. Jang, H.-K. Kim, D.-W. Cho, *J. Tissue Eng.* **2019**, *10*, 2041731418823382; b) M. Ahearne, A. P. Lynch, *Tissue Eng., Part C* **2015**, *21*, 1059; c) M. Ahearne, A. Coyle, *J. Mech. Behav. Biomed. Mater.* **2016**, *54*, 259; d) Y. Lu, Q. K. Yao, B. Feng, C. X. Yan, M. Y. Zhu, J. Z. Chen, W. Fu, Y. Fu, *J. Biomater. Tissue Eng.* **2015**, *5*, 951.
[226] J. Fernandez-Perez, M. Ahearne, *Sci. Rep.* **2019**, *9*, 14933.
[227] a) L. Edgar, A. Altamimi, M. García Sánchez, R. Tamburrinia, A. Asthana, C. Gazia, G. Orlando, *Organogenesis* **2018**, *14*, 172; b) J. LeCheminant, C. Field, *J. Wound Care* **2012**, *21*, 476; c) G. J. Kruper, Z. P. Vandegriend, H. S. Lin, G. F. Zuliani, *Case Rep. Otolaryngol.* **2013**, *2013*, 917183; d) B. N. Brown, W. L. Chung, A. J. Almarza, M. D. Pavlick, S. N. Reppas, M. W. Ochs, A. J. Russell, S. F. Badylak, *J. Oral Maxillofac. Surg.* **2012**, *70*, 2656.
[228] H. Yin, Q. Lu, X. Wang, S. Majumdar, A. S. Jun, W. J. Stark, M. P. Grant, J. H. Elisseeff, *Acta Biomater.* **2019**, *85*, 192.
[229] H. Yin, X. Wang, S. Majumdar, J. Sohn, B. J. Kim, W. Stark, J. H. Elisseeff, *Bioengineering* **2019**, *6*, 90.
[230] M. Huang, N. Li, Z. Wu, P. Wan, X. Liang, W. Zhang, X. Wang, C. Li, J. Xiao, Q. Zhou, Z. Liu, Z. Wang, *Biomaterials* **2011**, *32*, 7812.
[231] M. A. Shafiq, B. Y. Milani, A. R. Djalilian, *Int. J. Tissue Eng.* **2014**, *2014*, 754245.
[232] B. Aslan, S. Guler, A. Tevlek, H. M. Aydin, *J. Biomed. Mater. Res., Part B* **2018**, *106*, 2157.
[233] Y. C. Liu, E. P. W. Teo, H. P. Ang, X. Y. Seah, N. C. Lwin, G. H. F. Yam, J. S. Mehta, *Sci. Rep.* **2018**, *8*, 1831.
[234] S. Amano, N. Shimomura, S. Yokoo, K. Araki-Sasaki, S. Yamagami, *Mol. Vision* **2008**, *14*, 878.
[235] a) Z. J. Wu, B. Kong, R. Liu, W. Sun, S. L. Mi, *Nanomaterials* **2018**, *8*, 124; b) Y. Uchino, S. Shimmura, H. Miyashita, T. Taguchi, H. Kobayashi, J. Shirnazaki, J. Tanaka, K. Tsubota, *J. Biomed. Mater. Res., Part B* **2007**, *81B*, 201.
[236] G. K. Tummala, T. Joffre, V. R. Lopes, A. Liszka, O. Buznyk, N. Ferraz, C. Persson, M. Griffith, A. Mihranyan, *ACS Biomater. Sci. Eng.* **2016**, *2*, 2072.
[237] M. M. Islam, M. Griffith, K. Merrett, in *Methods in Molecular Biology*, Vol. *1014* (Eds: B. Wright, C. J. Connon), Humana Press, Totowa, NJ **2013**, p. 157.
[238] a) S. V. Murphy, A. Atala, *Nat. Biotechnol.* **2014**, *32*, 773; b) D. B. Kolesky, R. L. Truby, A. S. Gladman, T. A. Busbee, K. A. Homan, J. A. Lewis, *Adv. Mater.* **2014**, *26*, 3124; c) S. B. Ozler, E. Bakirci, C. Kucukgul, B. Koc, *J. Biomed. Mater. Res., Part B* **2017**, *105*, 2530; d) M. Kesti, C. Eberhardt, G. Pagliccia, D. Kenkel, D. Grande, A. Boss, M. Zenobi-Wong, *Adv. Funct. Mater.* **2015**, *25*, 7406.
[239] a) I. Donderwinkel, J. C. M. van Hest, N. R. Cameron, *Polym. Chem.* **2017**, *8*, 4451; b) D. A. Foyt, M. D. A. Norman, T. T. L. Yu, E. Gentleman, *Adv. Healthcare Mater.* **2018**, *7*, 1700939; c) S. L. Francis, C. Di Bella, G. G. Wallace, P. F. M. Choong, *Front. Surg.* **2018**, *5*, 70.
[240] Z. Wu, X. Su, Y. Xu, B. Kong, W. Sun, S. Mi, *Sci. Rep.* **2016**, *6*, 24474.
[241] A. Isaacson, S. Swioklo, C. J. Connon, *Exp. Eye Res.* **2018**, *173*, 188.
[242] D. F. D. Campos, M. Rohde, M. Ross, P. Anvari, A. Blaeser, M. Vogt, C. Panfil, G. H. F. Yam, J. S. Mehta, H. Fischer, P. Walter, M. Fuest, *J. Biomed. Mater. Res., Part A* **2019**, *107*, 1945.
[243] H. Kim, J. Jang, J. Park, K. P. Lee, S. Lee, D. M. Lee, K. H. Kim, H. K. Kim, D. W. Cho, *Biofabrication* **2019**, *11*, 035017;
[244] A. Sorkio, L. Koch, L. Koivusalo, A. Deiwick, S. Miettinen, B. Chichkov, H. Skottman, *Biomaterials* **2018**, *171*, 57.
[245] J. Park, K. P. Lee, H. Kim, S. Park, R. E. Wijesinghe, J. Lee, S. Han, S. Lee, P. Kim, D. W. Cho, J. Jang, H. K. Kim, M. Jeon, J. Kim, *J. Biophotonics* **2019**, *12*, 201900098.
[246] a) D. H. Reneker, I. Chun, *Nanotechnology* **1996**, *7*, 216; b) T. J. Sill, H. A. von Recum, *Biomaterials* **2008**, *29*, 1989; c) D. Li, Y. N. Xia, *Adv. Mater.* **2004**, *16*, 1151.
[247] J. Fernández-Pérez, K. E. Kador, A. P. Lynch, M. Ahearne, *Mater. Sci. Eng., C* **2020**, *108*, 110415.
[248] a) M. Kruse, P. Walter, B. Bauer, S. Rutten, K. Schaefer, N. Plange, T. Gries, S. Jockenhoevel, M. Fuest, *Curr. Eye Res.* **2018**, *43*, 1; b) S. Sharma, S. Mohanty, D. Gupta, M. Jassal, A. K. Agrawal, R. Tandon, *Mol. Vision* **2011**, *17*, 2898; c) S. Sharma, D. Gupta, S. Mohanty, M. Jassal, A. K. Agrawal, R. Tandon, *Invest. Ophthalmol. Visual Sci.* **2014**, *55*, 899; d) P. Deshpande, R. McKean, K. A. Blackwood, R. A. Senior, A. Ogunbanjo, A. J. Ryan, S. MacNeil, *Regener. Med.* **2010**, *5*, 395; e) P. Stafiej, F. Kung, D. Thieme, M. Czugala, F. E. Kruse, D. W. Schubert, T. A. Fuchsluger, *Mater. Sci. Eng., C* **2017**, *71*, 764; f) I. Ortega, A. J. Ryan, P. Deshpande, S. MacNeil, F. Claeyssens, *Acta Biomater.* **2013**, *9*, 5511; g) I. Ortega, F. Sefat, P. Deshpande, T. Paterson, C. Ramachandran, A. J. Ryan, S. MacNeil, F. Claeyssens, *J. Visualized Exp.* **2014**, *91*, 51826; h) S. Salehi, M. Czugala, P. Stafiej, M. Fathi, T. Bahners, J. S. Gutmann, B. B. Singer, T. A. Fuchsluger, *Acta Biomater.* **2017**, *50*, 370.
[249] C. Ramachandran, V. S. Sangwan, I. Ortega, U. Bhatnagar, S. M. A. Mulla, R. McKean, S. MacNeil, *Brit. J. Ophthalmol.* **2019**, *103*, 286.
[250] a) L. S. Wray, E. J. Orwin, *Tissue Eng., Part A* **2009**, *15*, 1463; b) D. Phu, L. S. Wray, R. V. Warren, R. C. Haskell, E. J. Orwin, *Tissue Eng., Part A* **2011**, *17*, 799.
[251] a) D. I. Zeugolis, S. T. Khew, E. S. Yew, A. K. Ekaputra, Y. W. Tong, L. Y. Yung, D. W. Hutmacher, C. Sheppard, M. Raghunath, *Biomaterials* **2008**, *29*, 2293; b) B. Dong, O. Arnoult, M. E. Smith, G. E. Wnek, *Macromol. Rapid Commun.* **2009**, *30*, 539;

c) A. Elamparithi, A. M. Punnoose, S. Kuruvilla, *Artif. Cells, Nanomed., Biotechnol.* **2016**, *44*, 1318.
[252] J. I. Kim, J. Y. Kim, C. H. Park, *Sci. Rep.* **2018**, *8*, 3424.
[253] a) C. Zhang, J. H. Wen, J. Yan, Y. B. Kao, Z. Q. Ni, X. J. Cui, H. Y. Wang, *RSC Adv.* **2015**, *5*, 12123; b) J. Yan, L. H. Qiang, Y. Gao, X. J. Cui, H. Y. Zhou, S. L. Zhong, Q. Wang, H. Y. Wang, *J. Biomed. Mater. Res., Part A* **2012**, *100A*, 527.
[254] T. D. Brown, P. D. Dalton, D. W. Hutmacher, *Adv. Mater.* **2011**, *23*, 5651.
[255] a) M. Castilho, D. Feyen, M. Flandes-Iparraguirre, G. Hochleitner, J. Groll, P. A. F. Doevendans, T. Vermonden, K. Ito, J. P. G. Sluijter, J. Malda, *Adv. Healthcare Mater.* **2017**, *6*, 1700311; b) B. L. Farrugia, T. D. Brown, Z. Upton, D. W. Hutmacher, P. D. Dalton, T. R. Dargaville, *Biofabrication* **2013**, *5*, 025001; c) O. Bas, E. M. De-Juan-Pardo, M. P. Chhaya, F. M. Wunner, J. E. Jeon, T. J. Klein, D. W. Hutmacher, *Eur. Polym. J.* **2015**, *72*, 451; d) M. L. Muerza-Cascante, A. Shokoohmand, K. Khosrotehrani, D. Haylock, P. D. Dalton, D. W. Hutmacher, D. Loessner, *Acta Biomater.* **2017**, *52*, 145.
[256] K. F. Eichholz, D. A. Hoey, *Acta Biomater.* **2018**, *75*, 140.
[257] D. F. Holmes, C. J. Gilpin, C. Baldock, U. Ziese, A. J. Koster, K. E. Kadler, *Proc. Natl. Acad. Sci. USA* **2001**, *98*, 7307.
[258] E. Hadjipanayi, M. Ananta, M. Binkowski, I. Streeter, Z. Lu, Z. F. Cui, R. A. Brown, V. Mudera, *J. Tissue Eng. Regener. Med.* **2011**, *5*, 505.
[259] H. J. Levis, A. K. Kureshi, I. Massie, L. Morgan, A. J. Vernon, J. T. Daniels, *J. Funct. Biomater.* **2015**, *6*, 50.
[260] H. J. Levis, G. S. L. Peh, K. P. Toh, R. Poh, A. J. Shortt, R. A. L. Drake, J. S. Mehta, J. T. Daniels, *PLoS One* **2012**, *7*, 50993.
[261] H. Hong, H. Kim, S. J. Han, J. Jang, H. K. Kim, D.-W. Cho, D. S. Kim, *Mater. Sci. Eng., C* **2019**, *103*, 109837.
[262] B. Kong, W. Sun, G. S. Chen, S. Tang, M. Li, Z. W. Shao, S. L. Mi, *Sci. Rep.* **2017**, *7*, 970.
[263] a) H. J. Levis, I. Massie, M. A. Dziasko, A. Kaasi, J. T. Daniels, *Biomaterials* **2013**, *34*, 8860; b) H. J. Levis, J. Menzel-Severing, R. A. Drake, J. T. Daniels, *Curr. Eye Res.* **2013**, *38*, 41.
[264] a) D. Vader, A. Kabla, D. Weitz, L. Mahadevan, *PLoS One* **2009**, *4*, 5902; b) K. M. Riching, B. L. Cox, M. R. Salick, C. Pehlke, A. S. Riching, S. M. Ponik, B. R. Bass, W. C. Crone, Y. Jiang, A. M. Weaver, K. W. Eliceiri, P. J. Keely, *Biophys. J.* **2014**, *107*, 2546.
[265] E. Nam, W. C. Lee, S. Takeuchi, *Macromol. Biosci.* **2016**, *16*, 995.
[266] a) N. Wang, J. P. Butler, D. E. Ingber, *Science* **1993**, *260*, 1124; b) R. Kaunas, P. Nguyen, S. Usami, S. Chien, *Proc. Natl. Acad. Sci. USA* **2005**, *102*, 15895; c) M. Chiquet, L. Gelman, R. Lutz, S. Maier, *Biochim. Biophys. Acta, Mol. Cell Res.* **2009**, *1793*, 911.
[267] M. Ahearne, P. O. Bagnaninchi, Y. Yang, A. J. El Haj, *J. Tissue Eng. Regener. Med.* **2008**, *2*, 521.
[268] a) C. He, T. Ye, W. Teng, Z. Fang, W. S. Ruan, G. Liu, H. Chen, J. Sun, L. Hui, F. Sheng, D. Pan, C. Yang, Y. Zheng, M. B. Luo, K. Yao, B. Wang, *ACS Nano* **2019**, *13*, 1910; b) N. Saeidi, E. A. Sander, R. Zareian, J. W. Ruberti, *Acta Biomater.* **2011**, *7*, 2437.
[269] a) D. L. Worcester, *Proc. Natl. Acad. Sci. USA* **1978**, *75*, 5475; b) J. Torbet, M. C. Ronziere, *Biochem. J.* **1984**, *219*, 1057; c) J. Torbet, M. Malbouyres, N. Builles, V. Justin, M. Roulet, O. Damour, A. Oldberg, F. Ruggiero, D. J. Hulmes, *Biomaterials* **2007**, *28*, 4268.
[270] R. M. Raftery, E. G. Tierney, C. M. Curtin, S. A. Cryan, F. J. O'Brien, *J. Controlled Release* **2015**, *210*, 84.
[271] a) H. Lin, Y. Tang, K. Sun, J. W. Xue, W. F. Yin, B. Wang, R. Tuan, *Mol. Ther.* **2016**, *24*, S209; b) E. G. Tierney, G. P. Duffy, A. J. Hibbitts, S. A. Cryan, F. J. O'Brien, *J. Controlled Release* **2012**, *158*, 304; c) A. McMillan, M. K. Nguyen, T. Gonzalez-Fernandez, P. L. Ge, X. H. Yu, W. L. Murphy, D. J. Kelly, E. Alsberg, *Biomaterials* **2018**, *161*, 240; d) R. M. Raftery, D. P. Walsh, I. M. Castano, A. Heise, G. P. Duffy, S. A. Cryan, F. J. O'Brien, *Adv. Mater.* **2016**, *28*, 5447; e) C. M. Curtin, G. M. Cunniffe, F. G. Lyons, K. Bessho, G. R. Dickson, G. P. Duffy, F. J. O'Brien, *Adv. Mater.* **2012**, *24*, 749.
[272] H. J. Diao, J. L. Wang, C. Shen, S. H. Xia, T. Guo, L. Dong, C. Y. Zhang, J. N. Chen, J. N. Zhao, J. F. Zhang, *Tissue Eng., Part A* **2009**, *15*, 2687.
[273] A. K. Reckhenrich, U. Hopfner, F. Krotz, Z. Y. Zhang, C. Koch, M. Kremer, H. G. Machens, C. Plank, J. T. Egana, *Biomaterials* **2011**, *32*, 1996.
[274] a) R. R. Mohan, J. T. Rodier, A. Sharma, *Ocul. Surf.* **2013**, *11*, 150; b) J. Torrecilla, A. del Pozo-Rodriguez, M. Vicente-Pascual, M. A. Solinis, A. Rodriguez-Gascon, *Exp. Eye Res.* **2018**, *176*, 130; c) S. Gupta, J. T. Rodier, A. Sharma, E. A. Giuliano, P. R. Sinha, N. P. Hesemann, A. Ghosh, R. R. Mohan, *PLoS One* **2017**, *12*, 0172928.
[275] a) E. Lih, W. Park, K. W. Park, S. Y. Chun, H. Kim, Y. K. Joung, T. G. Kwon, J. A. Hubbell, D. K. Han, *ACS Cent. Sci.* **2019**, *5*, 458; b) A. Zakeri Siavashani, J. Mohammadi, K. Maniura-Weber, B. Senturk, J. Nourmohammadi, B. Sadeghi, L. Huber, M. Rottmar, *Biomater. Sci.* **2019**, *8*, 148; c) J. Y. Kim, S. Y. Chun, S. H. Lee, E. Lih, J. Kim, D. H. Kim, Y. S. Ha, J. W. Chung, J. N. Lee, B. S. Kim, H. T. Kim, E. S. Yoo, D. K. Han, T. G. Kwon, B. I. Jang, *Tissue Eng. Regener. Med.* **2018**, *15*, 381; d) L. Zhang, Z. Cao, T. Bai, L. Carr, J. R. Ella-Menye, C. Irvin, B. D. Ratner, S. Jiang, *Nat. Biotechnol.* **2013**, *31*, 553.
[276] a) D. J. Coster, C. F. Jessup, K. A. Williams, *Eye* **2009**, *23*, 1894; b) Y. Qazi, P. Hamrah, *J. Clin. Cell Immunol.* **2013**, *2013*, 006; c) D. Hos, M. Matthaei, F. Bock, K. Maruyama, M. Notara, T. Clahsen, Y. Hou, V. N. H. Le, A. C. Salabarria, J. Horstmann, B. O. Bachmann, C. Cursiefen, *Prog. Retinal Eye Res.* **2019**, *73*, 100768.
[277] a) G. Pellegrini, D. Ardigo, G. Milazzo, G. Iotti, P. Guatelli, D. Pelosi, M. De Luca, *Stem Cells Transl. Med.* **2018**, *7*, 146; b) G. Pellegrini, P. Rama, S. Matuska, A. Lambiase, S. Bonini, A. Pocobelli, R. G. Colabelli, L. Spadea, R. Fasciani, E. Balestrazzi, P. Vinciguerra, P. Rosetta, A. Tortori, M. Nardi, G. Gabbriellini, C. E. Traverso, C. Macaluso, L. Losi, A. Percesepe, B. Venturi, F. Corradini, A. Panaras, A. Di Rocco, P. Guatelli, M. De Luca, *Regener. Med.* **2013**, *8*, 553; c) P. Rama, S. Matuska, G. Paganoni, A. Spinelli, M. De Luca, G. Pellegrini, *N. Engl. J. Med.* **2010**, *363*, 147.

Current Eye Research

ISSN: 0271-3683 (Print) 1460-2202 (Online) Journal homepage: https://www.tandfonline.com/loi/icey20

Influence of Biochemical Cues in Human Corneal Stromal Cell Phenotype

Julia Fernández-Pérez & Mark Ahearne

To cite this article: Julia Fernández-Pérez & Mark Ahearne (2019) Influence of Biochemical Cues in Human Corneal Stromal Cell Phenotype, Current Eye Research, 44:2, 135-146, DOI: 10.1080/02713683.2018.1536216

To link to this article: https://doi.org/10.1080/02713683.2018.1536216

Accepted author version posted online: 18 Oct 2018.
Published online: 29 Oct 2018.

CURRENT EYE RESEARCH
2019, VOL. 44, NO. 2, 135–146
https://doi.org/10.1080/02713683.2018.1536216

Taylor & Francis
Taylor & Francis Group

Influence of Biochemical Cues in Human Corneal Stromal Cell Phenotype

Julia Fernández-Pérez[a,b] and Mark Ahearne[a,b]

[a]Department of Mechanical and Manufacturing Engineering, School of Engineering, Trinity College Dublin, University of Dublin, Dublin, Ireland; [b]Trinity Centre for Bioengineering, Trinity Biomedical Science Institute, Trinity College Dublin, University of Dublin, Dublin, Ireland

ABSTRACT

Purpose: To identify biochemical cues that could promote a keratocyte-like phenotype in human corneal stromal cells that had become fibroblastic when expanded in serum-supplemented media while also examining the effect on cell proliferation and migration.

Methods: Proliferation was assessed by PrestoBlue™, morphology was monitored by phase contrast microscopy, phenotype was analyzed by real-time polymerase chain reaction (qPCR), immunochemistry and flow cytometry, and migration was studied with a scratch assay.

Results: Ascorbic Acid (AA), Retinoic Acid (RA), Insulin-Transferrin-Selenium (ITS), Insulin-like Growth Factor 1 (IGF-1) and 3-isobutyl-1-methylxanthine (IBMX) promoted a dendritic morphology, increased the expression of keratocyte markers, such as keratocan, aldehyde dehydrogenase 3 family member A1 (ALDH3A1) and CD34, and prevented myofibroblast differentiation, while in some cases increasing proliferation. Transforming Growth Factor beta 1 (TGF-β1) and 3 (TGF-β3) promoted the differentiation toward myofibroblasts, with increased expression of α-SMA. Fibroblast Growth Factor 2 (FGF-2) supported a fibroblastic phenotype while Platelet-Derived Growth Factor Homodimer B (PDGF-BB) induced a pro-migratory fibroblastic phenotype. A combination of all the pro-keratocyte factors was also compared to the serum-free only, which significantly increased CD34 and keratocan expression.

Conclusions: Partially recovery towards a quiescent keratocyte-like phenotype was achieved by the removal of serum and the addition of AA, IGF-1, RA, ITS and IBMX to a basal medium. These findings can be used to develop cell-based corneal therapies and to study corneal diseases *in vitro*.

ARTICLE HISTORY
Received 14 December 2017
Revised 26 September 2018
Accepted 10 October 2018

KEYWORDS
Keratocytes; corneal fibroblasts; myofibroblasts; biochemical cues; growth factors

Introduction

Corneal diseases and injuries are among the most prevalent causes of blindness and affect more than 45 million people worldwide, only being surpassed by cataracts.[1,2] While minor injuries to the cornea can heal quickly, deeper or more severe injuries can lead to scar formation and corneal haze. The main treatment offered to patients with corneal blindness is keratoplasty. However, due to the high demand for this procedure, the need of donor corneal tissue has increased and has resulted in donor shortage in several countries.[3–5] For this reason alternatives to donor allografts are being developed such as cell-based therapies and tissue engineering strategies.[6,7]

To successfully develop new cell-based therapies, a suitable cell source is required. For injuries or diseases affecting the corneal stroma, keratocytes, the main cell type in the stroma that has characteristics associated with mesenchymal stromal cells, are the logical choice of cells for corneal regeneration. To obtain a large enough number of stromal cells required for cell-based therapies or tissue engineering, the cells must be expanded *in vitro* normally using serum-supplemented media. When keratocytes are exposed to serum, they become fibroblastic recapitulating the *in vivo* process of wound healing. Upon serum activation there is a change in morphology from a dendritic shape to an elongated spindle morphology and markers associated with the native keratocyte phenotype such as crystalline ALDH3A1 and keratin sulphate proteoglycans such as keratocan are lost.[8] When treated with Transforming Growth Factor β1 (TGF-β1) corneal fibroblasts transition to a myofibroblast phenotype, becoming larger and expressing alpha smooth muscle actin (α-SMA). These two distinct phenotypes are fairly easy to obtain *in vitro* from isolated corneal stromal cells via the supplementation of medium with fetal bovine serum (FBS) for fibroblasts and addition of TGF-β1 for myofibroblasts. Although some studies have reported a partial reversal to a keratocyte-like phenotype using serum-free media,[9–12] there is still a lack of information on how individual media supplements such as vitamins or growth factors affect this process.

The aim of this study was to examine the effect of several biochemical reagents, ranging from small molecules to proteins, on the phenotype and activity of serum-expanded human corneal stromal cells when switched to a serum-free media. By doing this, the role of individual biochemical cues on the ability to restore a keratocyte phenotype *in vitro* can be examined.

CONTACT Mark Ahearne ahearnm@tcd.ie Trinity Centre for Bioengineering, Trinity Biomedical,Sciences Institute, Trinity College Dublin, University of Dublin, Dublin, Ireland

Color versions of one or more of the figures in the article can be found online at www.tandfonline.com/icey.

Material and methods

Cell isolation

Cells were isolated from the healthy donor's corneal-scleral ring remaining after a corneal transplant in accordance with the Declaration of Helsinki. The corneal-scleral rings were rinsed with sterile phosphate buffered saline (PBS) and the sclera, epithelium and endothelium were carefully removed using a scalpel blade. After a brief wash with sterile PBS, the corneal stroma was diced into small pieces, transferred into 25 cm^2 culture flasks and let attach to the plastic. Media consisting of low-glucose Dulbecco's Modified Eagle Medium (DMEM, Hyclone) supplemented with 10% Fetal Bovine Serum, (FBS, Gibco) and 2% Penicillin/Streptomycin (Pen/Strep, Invitrogen) was added and the stromal pieces were cultured at 37°C and 5% CO_2 in a humidified incubator. Media was changed regularly until cells had migrated from the tissue and reached 80–90% confluence, then they were passaged to allow further expansion. Cells in this study were used at passage 4 from cryopreserved expanded cells.

Cell culture conditions

Cells were harvested and seeded at 10,000 cells per cm^2 using low-glucose DMEM + 10% FBS and let attach overnight. The following day media was switched to DMEM/F12 (glucose concentration: 3.15 mg/ml, Hyclone) for a 3 day serum-starvation period, after which one of the following biochemical factors was added with the following concentrations: 100 µg/ml ascorbic acid (AA, Sigma); 0.1 µM retinoic acid (RA, Sigma); 10 ng/ml fibroblast growth factor 2 (FGF-2, R&D); 50 ng/ml platelet derived growth factor BB (PDGF-BB, Preprotech); 50 ng/ml Insulin-like Growth Factor 1 (IGF-1, ProSpec); 10 ng/ml transforming growth factor β1 (TGF-β1, ProSpec); 0.1 ng/ml transforming growth factor β3 (TGF-β3, R&D); 1x insulin-transferrin-selenium (ITS, Gibco) and 10^{-5} M 3-isobutyl-1-methylxanthine (IBMX, Sigma). Control groups were cells cultured in serum-free DMEM/F12 only and cells cultured in DMEM/F12 supplemented with 10% FBS. Medium was changed every 2 days for culture periods of 1, 7 and 14 days. Images of the cells were recorded over the culture period using an Olympus IX83 microscope (Tokyo, Japan).

Metabolic activity

Metabolic activity was assessed by the PrestoBlue assay (Invitrogen) following the manufacturer's instructions. 96-well plates were seeded separately for each time-point (day 1, 3, 7 and 14). Media was removed and 100 µl PrestoBlue working solution (1x from a 10x stock) was added and incubated at 37°C for 1 h. The plates were analyzed on a plate reader (BioTek™ Synergy HTX, Vermont, USA) by measuring the absorbance at 570 nm and 600 nm. Metabolic activity was calculated relative to the serum-free medium condition.

Gene expression

RNA from cultures was isolated using Trizol, according to the manufacturer's instructions (Invitrogen). Briefly, 1 ml of Trizol was added to the monolayer and a cell scrapper was used to detach the cells. 200 µl of chloroform was added, vortexed and centrifuged at 12 000 g at 4°C. The supernatant was transferred to a new RNAse-free tube to which the same volume of isopropanol and 4 µl of Glycoblue (Applied Biosystems) were added. After an overnight incubation at −20°C, tubes were centrifuged at 12 000 g for 15 min at 4°C. The supernatant was discarded and 1 ml 70% ethanol was added and vortexed to wash the pellet. After a second centrifugation step of 12 000 g for 15 min at 4°C, the ethanol was removed, the pellet was air dried and dissolved in 11 µl of RNAse-free water. RNA yield and purity was quantified using a NanoDrop-1000 (ThermoFisher).

A high capacity cDNA reverse transcription kit (Invitrogen) was used to reverse transcribe 500 ng of RNA using a thermocycler. Real-time PCR of the resultant cDNA was performed using TaqMan gene expression assay primers and TaqMan Universal Master Mix II (all Applied Biosystems). The primers examined were glyceraldehyde-3-phosphate dehydrogenase (*GAPDH*, Hs02758991_g1), aldehyde dehydrogenase 3A1 (*ALDH3A1*, Hs00964880_m1), alpha smooth muscle actin (*ACTA2*, Hs00426835_g1), keratocan (*KERA*; Hs00559942_m1) and collagen 1a1 (*COL1*; Hs00164004_m1). Each gene of interest was normalized against *GAPDH* using the ΔΔCt method. Calculated values were expressed as a power of $2^{-\Delta\Delta Ct}$. For this study, all values were normalized to the serum-free controls at each time-point.

Immunochemistry

Cells were fixed with 4% Paraformaldehyde (PFA) for 15 min, followed by three washes with PBS and stored at 4°C until further staining. Blocking and permeabilization were carried out in a single step using 2% FBS and 0.5% Triton X-100 diluted in PBS for 30 min at room temperature, followed by three washing steps with PBS. Primary antibodies were incubated overnight at 4°C. Concentrations were used as follows: ALDH3A1 (Abcam) 1:250, keratocan (Santa Cruz) 1:100, α-SMA (Abcam) 1:250. After three washes with PBS, samples were incubated with the secondary antibody and phalloidin-rhodamine for 1 h at room temperature. Samples were washed three times with PBS and incubated for 10 min with DAPI. Images were obtained using an Olympus IX83 microscope.

Flow cytometry

Cell phenotype was further assessed by flow cytometry. Data was acquired using an LSRFortessa (BD Biosciences) flow cytometer and then analyzed using FlowJo software (Tree Star Inc., Oregon, USA). Cells were trypsinized and resuspended in 150 µl of 2% FBS in PBS and 50 µl of cell suspension was used for the staining. 1 µl of each of the following

fluorophore-coupled antibodies was added to the cell suspension: CD34-allophycocyanin (APC), CD44-eFluor450, CD45-fluorescein isothiocyanate (FITC), CD73-PerCP-eFluor710, CD90-phycoerythrin (PE) and CD105-PE-Cy7 (all eBiosciences), and the final volume was adjusted to 100 µl (so that antibodies were used at 1:100 dilution). Samples were vortexed and incubated at 4°C for a minimum of 30 min. Unstained controls were treated the same way. Compensation beads (eBiosciences) were stained with each fluorophore-coupled antibody. Two washing steps were performed to remove unbound antibodies. The remaining pellet was resuspended in 300 µl of buffer and 5 µl of propidium iodide was added to recognize and exclude dead cells.

Wound healing assay

To assess the influence of biochemical cues in migration of human corneal keratocyte-like cells a scratch assay was performed. Cells were seeded in 6-well plates at a density of 10 000 cells per cm^2 in expansion media, which was changed regularly until confluent. Cells were then serum-starved using DMEM/F12 for 3 days. A "scratch" was applied to the monolayer with a 200 µl pipette tip, which resulted in a cell-free area. Cells were then cultured in media containing each of the molecules to be tested, having two controls: one serum-free only and one containing 10% FBS. Cells were imaged on the same area every day for 7 days using phase contrast imaging in an inverted microscope (Olympus IX83) coupled to a digital camera. The cell-free area at each time-point was calculated using ImageJ (NIH) by finding the edges, adjusting the threshold, binarizing the images and selecting the cell-free areas with the tracing tool. The wound closure was calculated using the following formula:

$$\frac{\text{cell free area } t_0 - \text{cell free area } t_x}{\text{cell free area } t_0} \times 100$$

Statistics analysis

All experiments were performed three times using a minimum of three replicates, unless otherwise stated. Statistical analyses were performed using GraphPad Prism Software 5.0 (GraphPad Software, Inc. La Jolla, CA, USA). All data are presented as the mean ± SD. To determine statistical significance one-way ANOVA with Dunnet post-hoc analyses were performed. Differences were considered to be statistically significant at $p \leq 0.05$.

Results

Effect of biochemical cues on cell proliferation

Metabolic activity under the induction of each biochemical cue was analyzed using the PrestoBlue® assay and used as an estimate for cell proliferation (Figure 1). The addition of FBS to the medium had a remarkable effect on proliferation, increasing 591% ± 131% (average ± SD) at day 7 compared to the serum-free control. TGF-β1 increased proliferation significantly from day 3 onwards, achieving values of 199% ± 29% by day 14. A similar trend was observed when cells were treated with TGF-β3, which increased proliferation at day 7 (164% ± 31%) and day 14 (203% ± 74%). IGF-1 increased proliferation significantly at day 3 (136% ± 19%) and day 7 (144% ± 25%) but then the effect appeared to stagnate. ITS promoted proliferation after one (156% ± 20%) and 2 weeks in culture (181% ± 94%). The rest of treatments did not have a positive nor negative effect on cell metabolic activity when compared to the serum-free control.

Effect of biochemical cues on cell morphology

Removal of serum from the medium had an effect on cell morphology, with the cells becoming smaller and the appearance of dendrites (Figure 2). This morphology resembles that of quiescent keratocytes *in vivo*. More cells adopt this morphology upon the addition of IGF-1, AA, RA, ITS or IBMX. The addition of PDGF-BB induced the cells to cluster and adopt a very elongated spindle shape. FGF-2 maintained a fibroblastic-like morphology, with very few sparse cells having processes. TGF-β1 and TGF-β3 induced cells to adopt a spread-out shape with some cells becoming polygonal and stress fibers visible. Cells cultured with FBS maintained a spindle shape.

Effect of biochemical cues on cell phenotype

Removal of serum from the medium led to an increased expression of keratocyte markers ALDH3A1 and keratocan when compared to cells cultured in serum-supplemented media (Figure 3). None of the biochemical reagents had a significantly positive effect on *ALDH3A1* expression when compared to the serum-free control. TGF-β1, PDGF-BB and FBS down-regulated the expression of this gene. The expression of keratocan was significantly up-regulated upon treatment with AA and IBMX after 14 days of induction (3.82 ± 1.87 and 3.99 ± 4.58, respectively; average ± SD). RA, ITS and IGF-1 also up-regulated this marker, but to a limited extent ($p > 0.05$). FGF-2, PDGF-BB, TGF-β1 and TGF-β3 did not have a significant effect, while FBS down-regulated the expression of keratocan. Expression of collagen type I (*COL1*) was increased significantly at time-point day 1 with the addition of IGF-1, TGF-β1 and TGF-β3 (1.74 ± 0.28, 1.54 ± 0.34, 1.73 ± 0.11, respectively; average ± SD). At later time-points only AA and ITS increased significantly this gene's expression (3.82 ± 0.20, 3.00 ± 0.44, respectively; average ± SD). TGF-β1 up-regulated significantly the expression of *ACTA2* at all time-points tested (8.74 ± 2.29 at day 1, 7.55 ± 2.46 at day 7 and 4.33 ± 1.87 at day 14; average ± SD). TGF-β3 had the same effect as TGF-β1, with very similar fold changes compared with the serum-free control (8.42 ± 4.78 at day 1, 4.36 ± 3.43 at day 7 and 3.26 ± 2.14 at day 14; average ± SD). Levels of myofibroblastic marker *ACTA2* did not change much over time, for all other treatments.

Expression of these markers was further analyzed with immunochemistry. While expression of ALDH3A1 was down-regulated at the mRNA level, staining showed positive cells in some conditions. Cells with a dendritic morphology

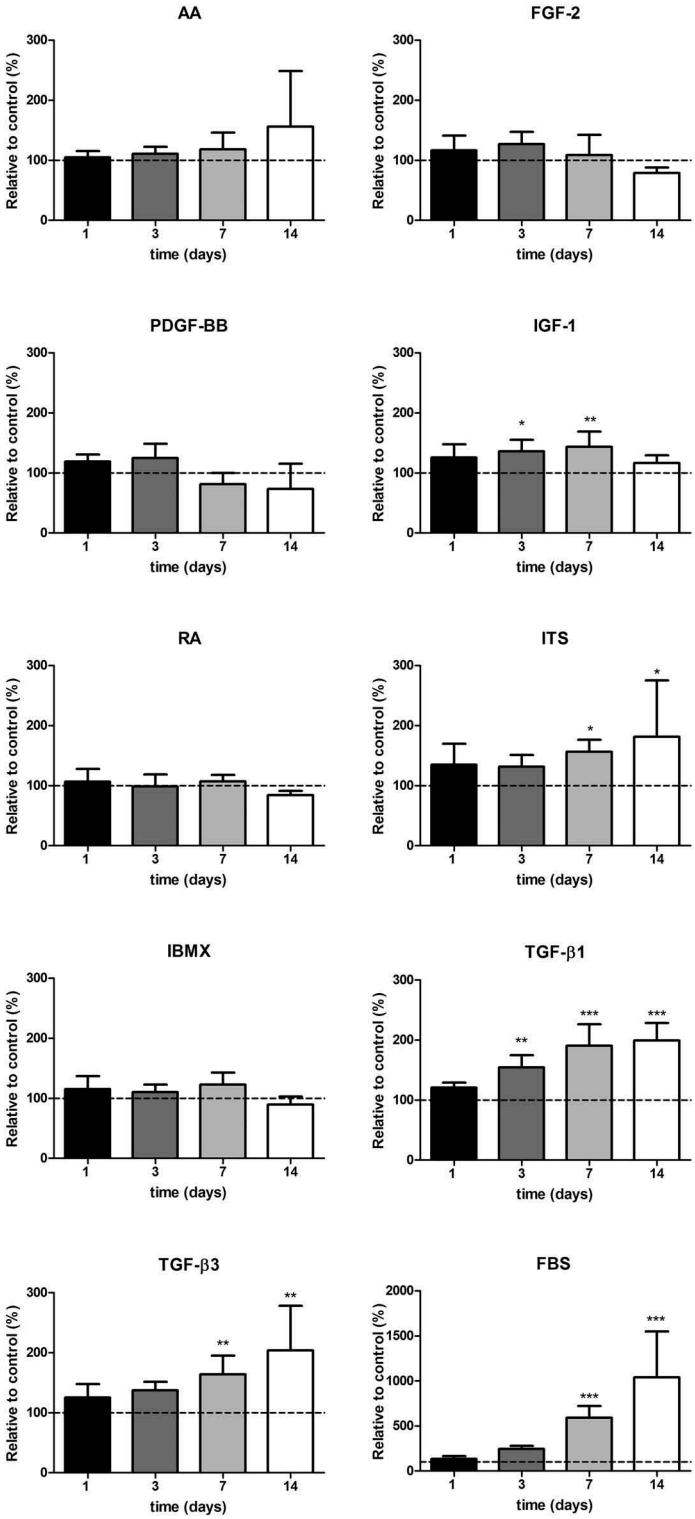

Figure 1. Effect of treatment on proliferation of human corneal stromal-derived cells ($n = 6$). Dotted line indicated control. *o $p < 0.05$, ** $p < 0.01$, *** $p < 0.001$.

showed more intense staining, especially when treated with ITS, IGF-1, IBMX, RA and in the serum-free control. Very low staining was seen in cultures treated with PDGF-BB, FBS, TGF-β1 and TGF-β3 (Figure 4a). Immunostaining of keratocan showed faint cytosolic staining in all conditions. When cells were treated with IGF-1, IBMX, ITS and RA, bright perinuclear staining was observed (Figure 4b). However, keratocan is a keratin sulphated proteoglycan that is deposited as ECM, hence was probably washed away during cell feedings. Expression of α-SMA correlated with expression of its gene *ACTA2*. Bright α-SMA stress fibers can be observed in cells treated with TGF-β1 and TGF-β3. Very sparse α-SMA$^+$ cells were seen in treatments with AA and ITS (Figure 4c).

After 7 and 14 days in culture, cell surface markers were analyzed and quantified by flow cytometry (Table 1). Typical

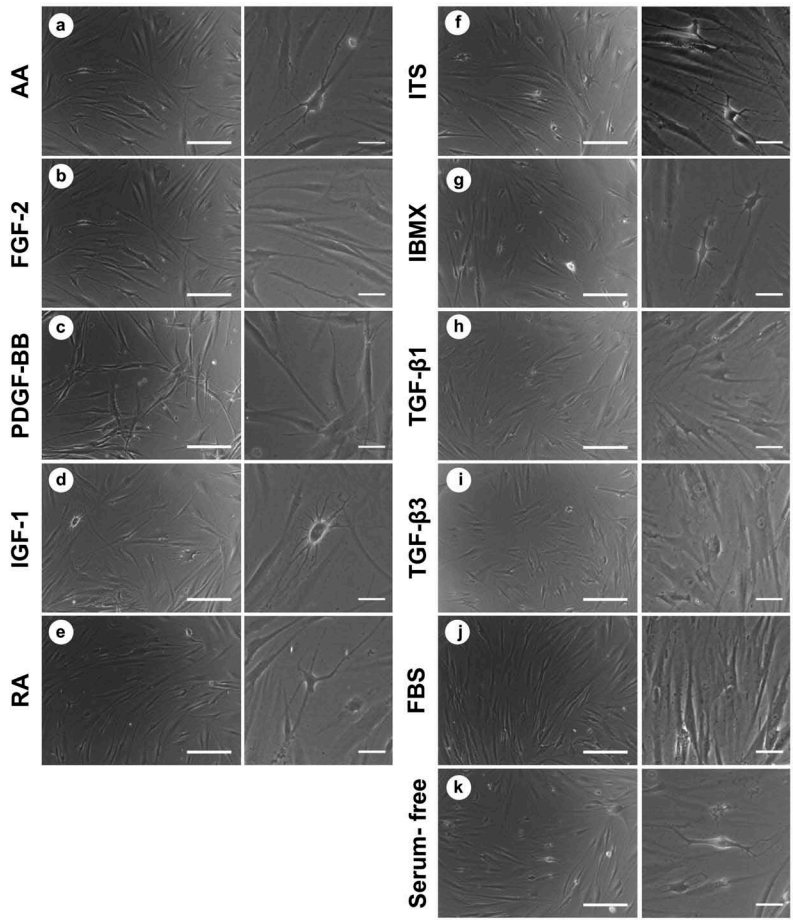

Figure 2. Morphology of cultured cells under the induction of studied biochemical cues after 14 days in culture: (a) ascorbic acid; (b) FGF-2; (c) PDGF-BB; (d) IGF-1; (e) retinoic acid; (f) insulin-transferrin-selenium; (g) IBMX; (h) TGF-β1; (I) TGF-β3; (J) foetal bovine serum; (k) serum-free control. Low magnification scale bar = 200 μm, high magnification scale bar = 50 μm.

markers used for the identification of mesenchymal stromal cells were employed. CD34 was found to change the most for each treatment. After 7 days of treatment, the serum-free controls presented 9.13% of the population positive for this marker, while treatment with AA, IBMX, IGF-1, ITS and RA increased this percentage considerably (14.03, 10.81, 9.52, 13.55 and 31.75%, respectively). This trend was maintained and increased after 14 days. However, only treatment with RA increased the $CD34^+$ population significantly. Other biochemical cues led to a reduction in the percentage of positive CD34 cells by day 7 (FBS: 0.08%, PDGF-BB: 0.47%, TGF-β1: 1.62% and TGF-β3: 2.09%) and day 14 (FBS: 1.47%, PDGF-BB: 1.49%, TGF-β1: 5.15% and TGF-β3: 5.03%). CD73 remained > 90% positive and was only reduced when treated with FBS and PDGF-BB (78.23% and 86.90%, respectively at day 7). After 14 days in culture, this marker remained positive (> 90%) in all conditions. CD90 was > 95% positive in all conditions, and most conditions induced an expression of > 99%. Expression of CD90 remained positive after 14 days (> 90%). Expression of CD105 also remained positive (> 88%) at culture time 7 days and 14 days. CD45 was < 2% in all conditions at day 7 and < 3.5% at day 14. CD44 was highly expressed (> 95% positive) in all conditions at day 7 without any noticeable difference among groups and remained positive after 14 days of treatment.

Effect of biochemical cues on wound healing ability

The influence of biochemical cues on the ability of wound healing was studied with a scratch assay (Figure 5). Seven days after the scratch was performed, only cells fed with serum-supplemented medium (100% ± 0%; average ± SD) or medium with PDGF-BB were able to fully close the wound gap (93% ± 3%; average ± SD). Supplementation with IGF-1 and ITS increased the closing of the scratch significantly when compared to the serum-free control (73% ± 8% and 69% ± 8%, respectively; average ± SD). Addition of AA, FGF-2 and IBMX slightly increased cell migration but not significantly. RA, TGF-β1 and TGF-β3 reduced cell migration to some extent. Only PDGF-BB can be described to have a positive migration effect as the wound closure is only due to cell migration since this growth factor had little effect on cell proliferation.

Combinatorial effect of pro-keratocyte cues

A final experiment was conducted in which the cues that showed a promotion of the keratocyte phenotype were used in combination with the basal medium and compared to serum-free conditions. Cells cultured for 2 weeks in medium containing AA, ITS, RA and IBMX presented a higher

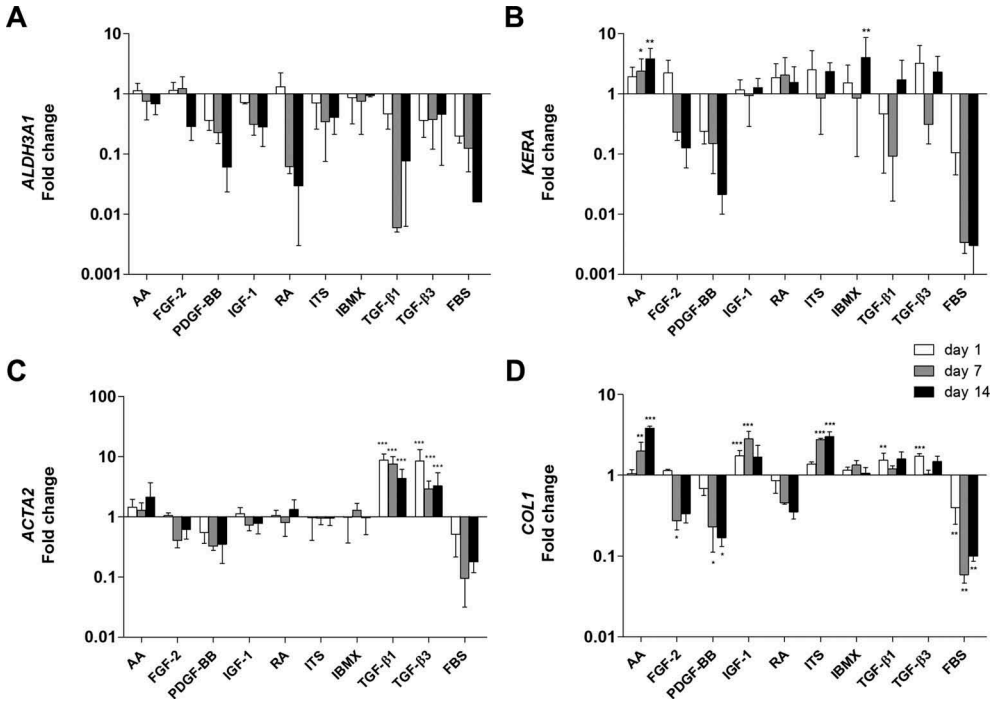

Figure 3. Effect of tested treatments on the expression of a) ALDH3A1, b) KERA, c) ACTA2 and d) COL1 as determined by qPCR relative to serum-free control at each time-point (n = 5–10). p^* < 0.05, p^{**} < 0.01, p^{***} < 0.001.

number of dendritic cells, $CD34^+$ population was highly increased and keratocan gene expression was particularly up-regulated. However, expression of ALDH3A1 was down-regulated and expression of COL1 did not increase. α-SMA remained negative at the gene and protein level. Cells were positive for CD44, CD90 and CD105 and negative for CD45 in both media conditions, while CD73 decreased slightly, yet significantly. These results are depicted in Figure 6.

Discussion

Understanding the effect of different biochemical cues on cultured human corneal stromal cells is key to understanding their physiological and pathological behavior. A deep knowledge of cell culture conditions is essential when developing *in vitro* models of corneal diseases, as well as developing cell-based therapies and tissue engineering corneal substitutes. Here a thorough study of how human corneal stromal-derived cells, initially expanded in serum-containing medium, react to a range of biochemical cues under serum-free conditions is presented. A summary showing the overall effect of each cue on the cell behavior is shown in Table 2.

Expansion of corneal stromal cells in FBS is known to result in a fibroblastic phenotype.[13] While alternatives to FBS, such as bovine pituitary extract, show a lot of promise as an approach for expanding keratocytes while maintaining the native phenotype,[14] most researchers still use FBS in the expansion phase. When compared to cells where FBS was removed, the cells in FBS proliferated rapidly, maintained a spindle morphology, and displayed low levels of keratocan and ALDH3A1 at both mRNA and the protein level as reported previously by other researchers.[15,16] Despite the activated nature, the cells did not differentiate into myofibroblasts as very little α-SMA could be detected, either at the mRNA or the protein level. Similar results have been shown in our group and in others, especially when seeded at high densities.[10,17–19] MSC markers were expressed in the same pattern as the serum-free control, except no increase in CD34 was observed. Cells treated with FBS closed fully the wound in the scratch assay, although this could be due to proliferation.

Both AA and RA are antioxidant vitamins commonly used as culture media supplements to support cell growth. In this study both regents supported a dendritic morphology, had little effect on cell proliferation, inhibited α-SMA formation and promoted an increase in keratocan gene expression although only AA was statistically significant. The findings for AA agree with previous studies that show increased keratocan expression[20] and no significant change in MSC markers[12] associated with this molecule. There are conflicting reports on the effect of AA on proliferation with both increases in proliferation or no alterations in cell number having been shown.[20,21] It has long been known that AA stabilizes the triple helix of collagen as it is a co-substrate of peptidyl-prolyl hydroxylase which converts proline into hydroxyproline.[22] In this study AA increased expression of COL1 gene, similar as reported for other cell types such as skin fibroblasts and avian tendon cells.[23,24] RA has also been associated with both increases and decreases in cell number although this is dependent on the concentration of RA used.[25,26] RA has also been associated with increases in the expression of keratocyte markers in both ordinary cell culture[25] and in collagen hydrogels.[27] RA had a significant effect in increasing the $CD34^+$ population, while not modifying the expression of the other MSC markers, in a similar way as reported by Sidney and Hopkinson.[12] The observed reduction in migration of cells treated with RA also matches previous findings that used keratocytes[25] and adipose-

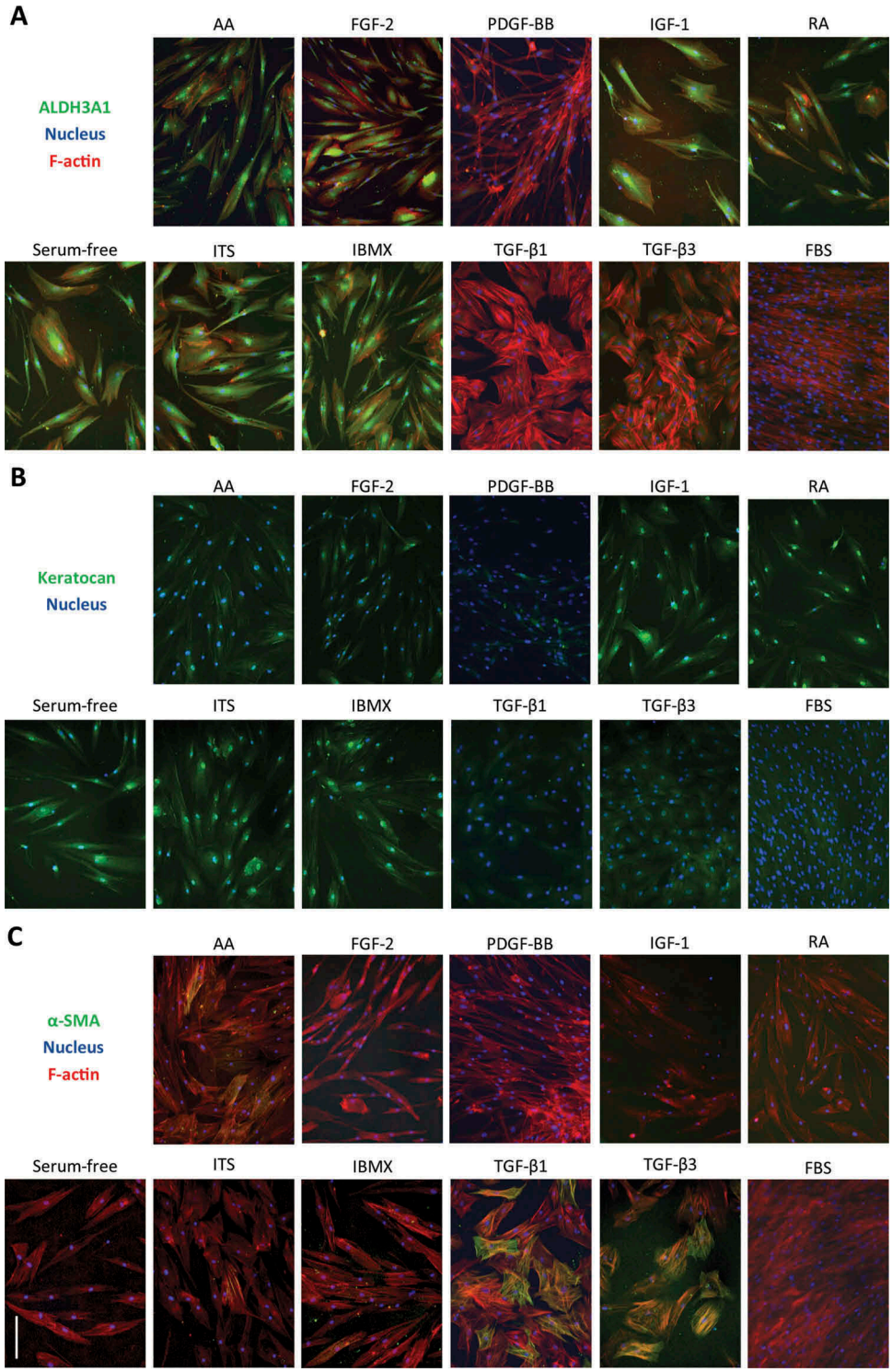

Figure 4. Effect of biochemical cues on the expression of markers determined by immunofluorescence after 14 days of treatment. a) ALDH3A1 (green), nuclei (blue) and F-actin (red). b) Keratocan (green), nuclei (blue). c)α-SMA (green), nuclei (blue) and F-actin (red). Scale bar = 200 μm.

derived stem cells in a keratocyte differentiation medium.[28] Gouveia and Connon showed that promoter regions of keratocyte marker genes did not have RARE sequences, and therefore RA should signal via alternative pathways. However, the gene encoding for CD34 has an enhancer region (GeneHancer identifier GH01I207846) with RARα binding domains which could explain the increase in $CD34^+$ cells when treated with RA. These results indicate that both AA and RA may assist in inducing a partial restoration of the keratocyte phenotype.

FGF-2 did not have a significant effect on cell proliferation, contrary to some reports in the literature[29,30] although these studies used media formulations containing additional supplements. However, our FGF-2 proliferation data did agree with findings that used bovine keratocytes.[31] FGF-2 did not

Table 1. Cell surface marker expression after 7 and 14 days of treatment ($n = 4$).

DAY 7	CD34	CD44	CD45	CD73	CD90	CD105
Serum-free	9.13% ± 0.05	95.15% ± 0.03	1.21% ± 0.01	92.05% ± 0.04	97.98% ± 0.02	88.20% ± 0.04
AA	14.03% ± 0.10	97.60% ± 0.03	0.79% ± 0.01	91.93% ± 0.06	99.10% ± 0.01	90.23% ± 0.08
FGF-2	8.09% ± 0.08	98.58% ± 0.01	1.48% ± 0.01	95.15% ± 0.03	99.50% ± 0.01	93.13% ± 0.05
PDGF-BB	0.47% ± 0.01	97.58% ± 0.04	0.68% ± 0.01	86.90% ± 0.07	98.50% ± 0.02	89.60% ± 0.06
IGF-1	9.52% ± 0.03	98.43% ± 0.01	0.80% ± 0.01	91.00% ± 0.06	99.03% ± 0.01	95.20% ± 0.03
RA	31.75% ± 0.08 (***)	98.23% ± 0.01	0.91% ± 0.01	93.58% ± 0.05	99.40% ± 0.00	92.75% ± 0.04
ITS	13.55% ± 0.07	98.83% ± 0.01	1.58% ± 0.02	91.15% ± 0.08	99.30% ± 0.01	95.95% ± 0.02
IBMX	10.81% ± 0.05	98.18% ± 0.01	1.21% ± 0.01	89.58% ± 0.12	99.48% ± 0.01	88.43% ± 0.11
TGF-β1	1.62% ± 0.02	98.43% ± 0.01	0.39% ± 0.00	90.83% ± 0.06	99.58% ± 0.00	93.48% ± 0.04
TGF-β3	2.09% ± 0.02	97.83% ± 0.01	0.43% ± 0.00	90.90% ± 0.06	99.68% ± 0.00	92.50% ± 0.03
FBS	0.08% ± 0.00	97.95% ± 0.02	0.05% ± 0.00	78.23% ± 0.03	96.78% ± 0.03	89.65% ± 0.14
DAY 14	CD34	CD44	CD45	CD73	CD90	CD105
Serum-free	11.39% ± 0.10	95.83% ± 0.04	1.36% ± 0.02	96.70% ± 0.03	96.55% ± 0.03	94.83% ± 0.04
AA	20.08% ± 0.11	94.85% ± 0.07	1.19% ± 0.02	94.75% ± 0.06	95.60% ± 0.07	92.98% ± 0.08
FGF-2	12.11% ± 0.13	96.48% ± 0.05	2.31% ± 0.02	96.23% ± 0.04	94.38% ± 0.05	91.48% ± 0.06
PDGF-BB	1.49% ± 0.02	95.53% ± 0.05	3.02% ± 0.03	94.60% ± 0.03	92.73% ± 0.06	81.68% ± 0.13
IGF-1	15.10% ± 0.09	96.33% ± 0.04	2.76% ± 0.03	97.00% ± 0.03	97.30% ± 0.03	96.55% ± 0.04
RA	35.35% ± 0.14	94.33% ± 0.07	3.16% ± 0.03	94.70% ± 0.07	95.08% ± 0.07	92.43% ± 0.08
ITS	13.67% ± 0.10	90.45% ± 0.15	1.51% ± 0.01	90.70% ± 0.14	91.23% ± 0.15	90.45% ± 0.14
IBMX	12.42% ± 0.09	94.00% ± 0.09	1.86% ± 0.02	94.73% ± 0.08	94.75% ± 0.08	92.35% ± 0.09
TGF-β1	5.15% ± 0.06	87.93% ± 0.16	0.55% ± 0.01	96.20% ± 0.03	89.28% ± 0.16	84.63% ± 0.16
TGF-β3	5.03% ± 0.09	96.23% ± 0.06	0.51% ± 0.01	95.70% ± 0.04	96.80% ± 0.05	94.27% ± 0.04
FBS	1.47% ± 0.03	97.40% ± 0.03	0.12% ± 0.00	93.63% ± 0.01	95.60% ± 0.03	94.30% ± 0.04

Data shown as average ± standard deviation. ***$p < 0.001$.

have an effect in changing cell morphology after serum-starvation as cells maintained their spindle shape, similar to some previously reported studies.[32] Expression of ALDH3A1, keratocan and α-SMA were not up-regulated. It has been postulated that the reduced expression of keratan sulfate proteoglycans such as Lumican or Keratocan by FGF-2 is mediated by the Rho and JNK pathways.[33,34] Furthermore, FGF-2 supplementation led to a reduction in the number of $CD34^+$ cells. The loss of CD34 in the cornea is associated with keratoconus where cells also become more fibroblastic.[35] Overall these findings suggest that FGF-2 induces a fibroblastic phenotype of cultured stromal cells.

PDGF-BB did not promote cell proliferation in this study, conflicting with some published research. However, in those studies the media used was supplemented with 0.5% FBS[36] or 2% FBS.[37] In the current study, cells treated with PDGF-BB show a fibroblastic-like shape but with a more elongated cell body than when treated with FBS, a similar finding to that previously described.[32] However, when cells treated with PDGF-BB were embedded in compressed collagen gels they presented branching processes indicating that the physical surroundings may play a role in how the cells react to the growth factor.[38] In our study, expression of keratocyte markers was down-regulated, while no upregulation of myofibroblastic markers was detected. As seen with FGF-2, treatment with PDGF-BB also reduced the number of $CD34^+$ cells. This growth factor also displayed a strong chemotactic effect as has been previously demonstrated in 2D using Boyden chambers-[39] and in 3D compressed collagen gels.[38] It is believed that PDGF influences cell migration via Erk, which phosphorylates FAK and paxillin regulating dynamics of focal adhesions.[40] Decrease in actin stress fibers can me mediated by N-WASP after downstream signaling via PI3K and Cdc42, a Rho GTPase.[41] Hence we can conclude that PDGF-BB promotes a motile fibroblastic phenotype.

In this study the roles of IGF-1 and ITS supplementation were examined. Insulin is a commonly used cell culture supplement that regulates the uptake of glucose and amino acids. Insulin binds to insulin receptor (INSR) through the alpha subunit, which produces a conformational change that will induce the phosphorylation of tyrosine residues in the beta subunit of the insulin receptor. This triggers a downstream signaling cascade through the MAPK pathway, inducing cell proliferation, and through the PI3K/Akt pathway leading to cell growth, and lipid, glycogen and protein synthesis.[42–44] IGF-1 led to an early positive increase in cell proliferation, a dendritic morphology, increases in keratocan gene expression, ALDH3A1 staining and $CD34^+$ cells. Etheredge and colleagues reported no effect on corneal fibroblast proliferation at a concentration of 10 ng/ml, while Yanai and colleagues showed increase in proliferation and inhibition of apoptosis at 305 nM, which corresponds to 2 μg/ml.[31,45] Maintenance of a dendritic morphology in rabbit stromal cells when treated with IGF-1 has also previously been shown.[32] ITS had a positive effect in cell survival similar to that seen by other authors,[20] promoted a dendritic morphology with multiple processes and led to a significant increase in *COL1* gene expression, ALDH3A1 immunofluorescence and more $CD34^+$ cells. Similar to IGF-1, ITS promoted the closure of the wound in the scratch assay but the increase in proliferation renders the chemotactic effect elusive. No upregulation of *ACTA2* or expression of α-SMA was detected for either IGF-1 or ITS. In fact, recent studies suggest that IGF-1 inhibits fibrosis initiated by TGF-β.[46] Taking these findings together, it can be said that both IGF-1 and ITS partially induce a quiescent keratocyte phenotype.

IBMX is a competitive non-selective inhibitor of phosphodiesterase that raises intracellular cAMP levels, which activate protein kinase A, phosphorylating in turn cAMP response element-binding proteins (CREB) in the nucleus which act

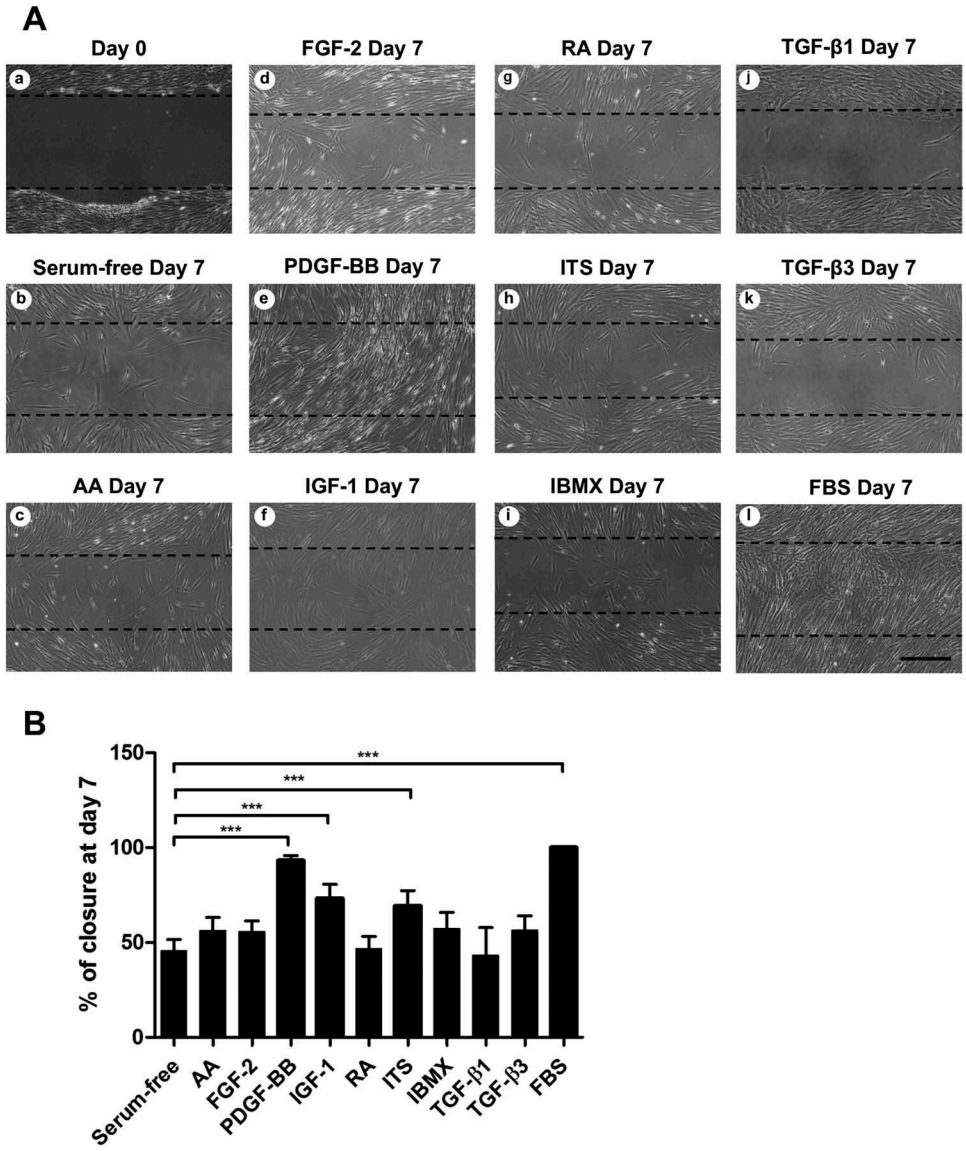

Figure 5. Effect of tested biochemical cues on cell migration. a) Phase contrast micrographs of wound closure at day 0 and day 7. Dashed line represents scratch at day 0. Scale bar = 200 μm. b) Quantification of wound closure by day 7 (n = 6); $p^{***} < 0.001$.

as transcription factors.[47] Researchers have used IBMX to emulate the effects of low glucose conditions.[48] Upon treatment with IBMX, cells with multiple dendrite-like structures were observed similar to that reported previously.[48] A significant increase in keratocan gene expression was observed and bright perinuclear staining was observed for this marker. The increase of this marker could be due the presence of CRE sequences in the promoter of this gene.[48] ALH3A1 was highly expressed in cells with processes, similar to observations by Foster and colleagues for ALDH1.[48] These authors reported an increase of CD34 at the transcriptional level, while our study showed an increase in the $CD34^{+}$ population via flow cytometry. IBMX did not induce changes in any other MSC markers and did not show a chemotactic effect. The addition of this chemical did not influence expression of *COL1* or *ACTA2*. This data indicates that treatment with IBMX promoted the restoration of a keratocyte-like phenotype.

Both TGF-β1 and TGF-β3 had a similar effect on all the parameters examined in this study, particularly the upregulation and immunochemical staining of α-SMA, a known myofibroblast marker. It has previously been well established that TGF-β1 induces a myofibroblastic phenotype.[30–32,49,50] Transcription of α-SMA is induced by the translocation to the nucleus of phosphorylated Smad2/3/4 complex. These proteins are activated by ALK5, which is phosphorylated by TGFβ Receptor I and II upon ligand binding.[51] Fibroblasts expressing α-SMA display a retarded motility using a scratch assay[52] which coincides with the current findings where α-SMA positive cells were unable to bridge the gap during the scratch assay. In fact, the edge of the wound was always clear and straight, and the whole front would move together, suggesting that any apparent migration was due to cell proliferation. Despite an initial upregulation of *COL1* by both TGFs, at later time-points the expression was similar to that of the serum-free control. The effect of TGF-β3 in this study was interesting since it contradicts some other studies that suggest TGF-β3 has an antifibrotic effect.[53,54] One possible explanation is that the authors used a self-assembled culture, medium

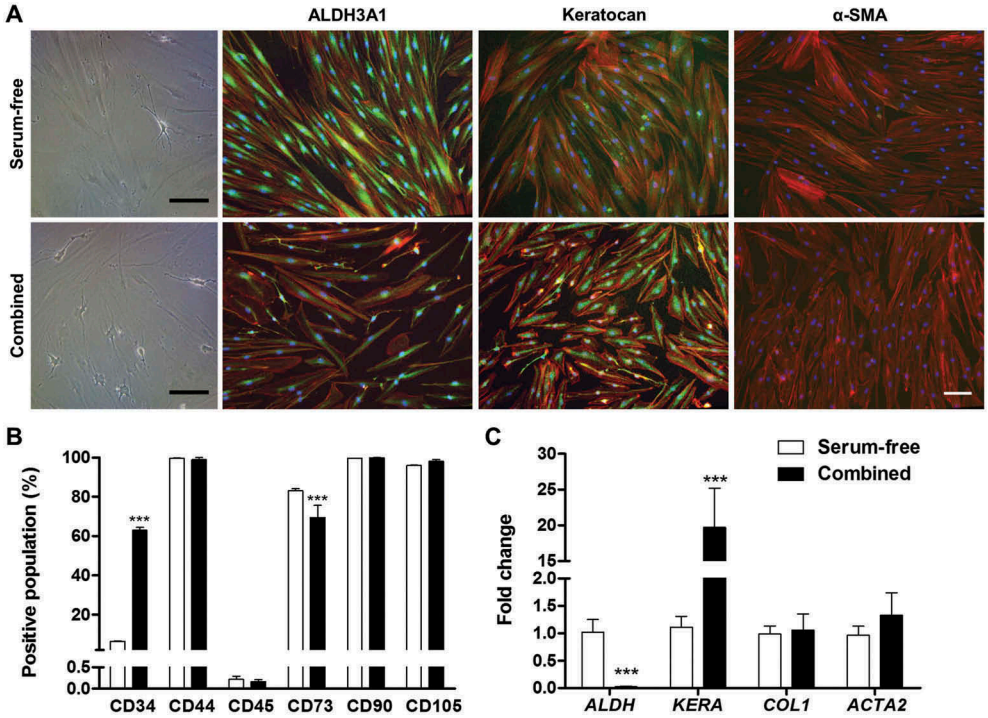

Figure 6. Effect of combined pro-keratocyte cues. a) Bright field images and immunofluorescence against ALDH3A1, Keratocan and α-SMA (all green, F-actin is shown in red and nuclei in blue). Scale bar = 100 μm. b) Flow cytometry profiling of cells cultured in serum-free medium or with the combination of pro-keratocyte cues (n = 3). c) Gene expression of cells cultured in serum-free medium or with the combination of pro-keratocyte cues (n = 6). p *** < 0.001.

Table 2. Summary of results from this study.

Reagent	Proliferation	Morphology	Phenotype	Migration	Final cell type
AA	/	Dendritic	General expression of keratocyte markers (significant upregulation of keratocan). No α-SMA	/	Keratocyte-like
FGF-2	/	Spindle	No upregulation of keratocyte markers. No α-SMA	/	Fibroblast (activated keratocyte)
PDGF-BB	/	Elongated spindle	No upregulation of keratocyte markers. No α-SMA	+	Fibroblast (activated keratocyte)
IGF-1	+	Dendritic	General expression of keratocyte markers. No α-SMA	+	Keratocyte-like
RA	/	Dendritic	General expression of keratocyte markers (significant increase of $CD34^+$ cells). No α-SMA	-	Keratocyte-like
ITS	+	Dendritic	General expression of keratocyte markers. No α-SMA	+	Keratocyte-like
IBMX	/	Dendritic	General expression of keratocyte markers (significant upregulation of keratocan). No α-SMA	/	Keratocyte-like
TGF-β1	+	Spread and polygonal	No expression of keratocyte markers. Significant upregulation of α-SMA	-	Myofibroblast
TGF-β3	+	Spread and polygonal	No expression of keratocyte markers. Significant upregulation of α-SMA	-	Myofibroblast
FBS	+	Spindle	Down-regulation of keratocyte markers. No α-SMA	+	Fibroblast (activated keratocyte)

+: positive effect; -: negative effect; /: no effect.

containing 10% FBS and AA and cultured their cells for 4 weeks, hence multiple factors may be contributing to the cell behavior. Sidney and Hopkinson showed that TGF-β3 led to lower levels of ALDH3A1 and vimentin and higher levels α-SMA gene expression when compared to cells cultured under serum and growth factor free conditions.[12] Another study recently showed positive α-SMA staining resulting from the addition of TGF-β3 although the amount of staining was significantly less than at the same concentration of TGF-β1[55] From our results it would appear that both TGF-β1 and TGF-β3 promote a myofibroblastic phenotype.

When AA, ITS, RA and IBMX were used in combination, keratocyte markers CD34 and keratocan were up-regulated, while ALDH3A1 was down-regulated and COL1 remained unchanged. Since RA individually decreased these two markers one could speculate that RA is the main reagent responsible and that the other cues could not synergistically overcome this.

As discussed throughout, multiple signaling pathways are involved after supplementation with the factors studied here. Although outside of this study's scope, investigating the expression of some of the key down-stream proteins is key to understanding the mechanisms of keratocyte activation and return to quiescence. The use of advanced molecular techniques with high-throughput potential, such as microarrays, would be extremely beneficial for this. By understanding

influence of these signaling pathways, better control of the cell phenotype could be achieved.

This study reveals once more the importance of biochemical cues to promote the reversal of activated keratocytes toward a quiescent keratocyte phenotype *in vitro*. However, biochemical supplementation of the medium is unlikely to lead to a full phenotype reversal. Other environmental cues such as substrate stiffness, material topography and 3D culture play an important role as multiple studies have demonstrated.[10,11,56] Furthermore, factors such as the donor's age and health, the number of population doublings of the cells and the time in culture are among other variables that need to be considered. Since tissue remodeling and wound healing are long lasting processes in the corneal stroma[57], it is therefore logical to suspect that phenotype reversal *in vitro* can only be achieved after longer culture periods.

From this study we can conclude that human corneal stromal-derived cells originally expanded in serum-containing medium can partially recover a quiescent keratocyte-like phenotype by the removal of serum and the addition of AA, IGF-1, RA, ITS and IBMX to a basal medium. The keratocyte-like phenotype was demonstrated by a dendritic morphology and upregulation of keratocyte markers such as keratocan, ALDH3A1, COL1 and CD34. These findings are important for the optimization of culture conditions to enable the expansion of stromal derived cells for regenerative therapies and tissue engineering.

Acknowledgments

The authors would like to thank Dr Barry Moran for the support in the flow cytometry experiments.

Disclosure statement

No potential conflict of interest was reported by the authors.

Funding

The research leading to these results has received funding from the European Research Council (ERC) under the European Union's Horizon 2020 research and innovation program (grant agreement no. 637460) and from Science Foundation Ireland (15/ERC/3269).

References

1. Whitcher JP, Srinivasan M, Upadhyay MP. Corneal blindness: a global perspective. Bull World Health Organ. 2001;79(3):214–21. doi:10.1111/ceo.12330.
2. Pascolini D, Mariotti SP. Global estimates of visual impairment: 2010. Br J Ophthalmol. 2012;96(5):614–18. doi:10.1136/bjophthalmol-2011-300539.
3. Rasouli M, Caraiscos VB, Slomovic AR. Efficacy of routine notification and request on reducing corneal transplantation wait times in Canada. Can J Ophthalmol. 2009;44(1):31–35. doi:10.3129/i08-187.
4. Reinhard T, Böhringer D, Bogen A, Sundmacher R. The transplantation law: a chance to overcome the shortage of corneal grafts in Germany? Transplant Proc. 2002;34(4):1322–24. doi:10.1016/s0041-1345(02)02783-5.
5. de By TM. Shortage in the face of plenty: improving the allocation of corneas for transplantation. Dev Ophthalmol. 2003;36:56–61. doi:10.1159/000067656.
6. Griffith M, Alarcon EI, Brunette I. Regenerative approaches for the cornea. J Intern Med. 2016;280(3):276–86. doi:10.1111/joim.12502.
7. Ghezzi CE, Rnjak-Kovacina J, Kaplan DL. Corneal tissue engineering: recent advances and future perspectives. Tissue Eng Part B Rev. 2015;21(3):278–87. doi:10.1089/ten.teb.2014.0397.
8. Jester JV, Huang J, Møller-Pedersen T, Sax CM, Kays WT, Cavanagh HD, Petroll WM, Piatigorsky J. The cellular basis of corneal transparency: evidence for "corneal crystallins.". J Cell Sci. 1999;112:613–22.
9. Berryhill BL, Kader R, Kane BP, Birk DE, Feng J, Hassell JR. Partial restoration of the keratocyte phenotype to bovine keratocytes made fibroblastic by serum. Invest Ophthalmol Vis Sci. 2002;43:3416–21.
10. Lynch AP, O'Sullivan F, Ahearne M. The effect of growth factor supplementation on corneal stromal cell phenotype in vitro using a serum-free media. Exp Eye Res. 2016;151:26–37. doi:10.1016/j.exer.2016.07.015.
11. Wilson SL, Wimpenny I, Ahearne M, Rauz S, El Haj AJ, Yang Y. Chemical and topographical effects on cell differentiation and matrix elasticity in a corneal stromal layer model. Adv Funct Mater. 2012;22(17):3641–49. doi:10.1002/adfm.201200655.
12. Sidney LE, Hopkinson A. Corneal keratocyte transition to mesenchymal stem cell phenotype and reversal using serum-free medium supplemented with FGF-2, TGF-ß3 and retinoic acid. J Tissue Eng Regen Med. 2016;12(1):e203–15. doi:10.1002/term.2316.
13. Fini ME. Keratocyte and fibroblast phenotypes in the repairing cornea. Prog Retin Eye Res. 1999;18(4):529–51. doi:10.1016/S1350-9462(98)00033-0.
14. Xu -Z-Z, Li Z-J, Du L-X, Li J, Wang L-Y. Using bovine pituitary extract to increase proliferation of keratocytes and maintain their phenotype in vitro. Int J Ophthalmol. 2013;6:758–65.
15. Beales MP, Funderburgh JL, Jester JV, Hassell JR. Proteoglycan synthesis by bovine keratocytes and corneal fibroblasts: maintenance of the keratocyte phenotype in culture. Invest Ophthalmol Vis Sci. 1999;40:1658–63.
16. Espana EM, He H, Kawakita T, Di Pascuale MA, Raju VK, Liu CY, Tseng SC. Human keratocytes cultured on amniotic membrane stroma preserve morphology and express keratocan. Invest Ophthalmol Vis Sci. 2003;44(12):5136–41. doi:10.1167/iovs.03-0484.
17. Masur SK, Dewal HS, Dinh TT, Erenburg I, Petridou S. Myofibroblasts differentiate from fibroblasts when plated at low density. Proc Natl Acad Sci USA. 1996;93(9):4219–23. doi:10.1073/pnas.93.9.4219.
18. Pot SA, Liliensiek SJ, Myrna KE, Bentley E, Jester JV, Nealey PF, Murphy CJ. Nanoscale topography-induced modulation of fundamental cell behaviors of rabbit corneal keratocytes, fibroblasts, and myofibroblasts. Invest Ophthalmol Vis Sci. 2010;51(3):1373–81. doi:10.1167/iovs.09-4074.
19. Guerriero E, Chen J, Sado Y, Mohan RR, Wilson SE, Funderburgh JL, SundarRaj N. Loss of alpha3(IV) collagen expression associated with corneal keratocyte activation. Invest Ophthalmol Vis Sci. 2007;48(2):627–35. doi:10.1167/iovs.06-0635.
20. Musselmann K, Kane BP, Alexandrou B, Hassell JR. Stimulation of collagen synthesis by insulin and proteoglycan accumulation by ascorbate in bovine keratocytes in vitro. Invest Ophthalmol Vis Sci. 2006;47(12):5260–66. doi:10.1167/iovs.06-0612.
21. Saika S, Kanagawa R, Uenoyama K, Hiroi K, Hiraoka J. L-ascorbic acid 2-phosphate, a phosphate derivative of L-ascorbic acid, enhances the growth of cultured rabbit keratocytes. Graefe's Arch Clin Exp Ophthalmol. 1991;229(1):79–83. doi:10.1007/bf00172267.
22. Stone N, Meister A. Function of ascorbic acid in the conversion of proline to collagen hydroxyproline. Nature. 1962;194(4828):555–57. doi:10.1038/194555a0.
23. Tajima S, Pinnell SR. Regulation of collagen synthesis by ascorbic acid increases type I procollagen mRNA. Biochem Biophys Res Commun. 1982;106(2):632–37. doi:10.1016/0006-291X(82)91157-3.
24. Lyons BL, Schwarz RI. Ascorbate stimulation of PAT cells causes an increase in transcription rates and a decrease in degradation

rates of procollagen mRNA. Nucleic Acids Res. 1984;12(5):2569–79. doi:10.1093/nar/12.5.2569.
25. Gouveia RM, Connon CJ. The effects of retinoic acid on human corneal stromal keratocytes cultured in vitro under serum-free conditions. Invest Opthalmol Vis Sci. 2013;54(12):7483. doi:10.1167/iovs.13-13092.
26. Kenney MC, Shih LM, Labermeir U, Satterfield D. Modulation of rabbit keratocyte production of collagen, sulfated glycosaminoglycans and fibronectin by retinol and retinoic acid. Biochim Biophys Acta. 1986;889:156–62. doi:10.1016/0167-4889(86)90099-6.
27. Abidin FZ, Gouveia RM, Connon CJ. Application of retinoic acid improves form and function of tissue engineered corneal construct. Organogenesis. 2015;11(3):122–36. doi:10.1080/15476278.2015.1093267.
28. Lynch AP, Ahearne M. Retinoic acid enhances the differentiation of adipose-derived stem cells to keratocytes in vitro. Trans Vis Sci Technol. 2017;6(1):6. doi:10.1167/tvst.6.1.6.
29. Long CJ, Roth MR, Tasheva ES, Funderburgh ML, Smit R, Conrad GW, Funderburgh JL. Fibroblast growth factor-2 promotes keratan sulfate proteoglycan expression by keratocytes in vitro. J Biol Chem. 2000;275(18):13918–23. doi:10.1074/jbc.275.18.13918.
30. Jester JV, Barry-Lane P, Cavanagh HD, Petroll WM. Induction of smooth muscle actin expression and myofibroblast transformation in cultured corneal keratocytes. Cornea. 1996;505–16. doi:10.1097/00003226-199609000-00011.
31. Etheredge L, Kane BP, Hassell JR. The effect of growth factor signaling on keratocytes in vitro and its relationship to the phases of stromal wound repair. Invest Ophthalmol Vis Sci. 2009;50(7):3128–36. doi:10.1167/iovs.08-3077.
32. Jester JV, Ho-Chang J. Modulation of cultured corneal keratocyte phenotype by growth factors/cytokines control in vitro contractility and extracellular matrix contraction. Exp Eye Res. 2003;77(5):581–92. doi:10.1016/s0014-4835(03)00188-x.
33. Chen J, Guerriero E, Sado Y, Sundarraj N. Rho-mediated regulation of TGF-beta1-and FGF-2-induced activation of corneal stromal keratocytes. Invest Ophthalmol Vis Sci. 2009;50(8):3662–70. doi:10.1167/iovs.08-3276.
34. Chen J, Wong-Chong J, SundarRaj N. FGF-2- and TGF-β1-induced downregulation of lumican and keratocan in activated corneal keratocytes by JNK signaling pathway. Invest Ophthalmol Vis Sci. 2011;52(12):8957–64. doi:10.1167/iovs.11-8078.
35. Toti P, Tosi GM, Traversi C, Schürfeld K, Cardone C, Caporossi A. CD-34 stromal expression pattern in normal and altered human corneas. Ophthalmology. 2002;109(6):1167–71. doi:10.1016/s0161-6420(02)01042-4.
36. Kim W-J, Mohan RR, Mohan RR, Wilson SE. Effect of PDGF, IL-la, and BMP2/4 on corneal fibroblast chemotaxis: expression of the platelet derived growth factor system in the cornea. Invest Ophthalmol Vis Sci. 1999;40:1364–72.
37. Hoppenreijs VPT, Pels E, Vrensen GFJM, Felten PC, Treffers WF. Platelet-derived growth factor: receptor expression in corneas and effects on corneal cells. Invest Ophthalmol Vis Sci. 1993;34:637–49.
38. Kim A, Lakshman N, Karamichos D, Petroll WM. Growth factor regulation of corneal keratocyte differentiation and migration in compressed collagen matrices. Invest Ophthalmol Vis Sci. 2010;51(2):864. doi:10.1167/iovs.09-4200.
39. Kamiyama K, Iguchi I, Wang X, Imanishi J. Effects of PDGF on the migration of rabbit corneal fibroblasts and epithelial cells. Cornea. 1998;17(3):315–25. doi:10.1097/00003226-199805000-00013.
40. Huang C, Jacobson K, Schaller MD. MAP kinases and cell migration. J Cell Sci. 2004;117:4619–28. doi:10.1242/jcs.01481.
41. Jiménez C, Portela RA, Mellado M, Rodríguez-Frade JM, Collard J, Serrano A, Martínez AC, Avila J, Carrera AC. Role of the PI3K regulatory subunit in the control of actin organization and cell migration. J Cell Biol. 2000;151(2):249–62. doi:10.1083/jcb.151.2.249.
42. Saltiel AR, Kahn CR. Insulin signalling and the regulation of glucose and lipid metabolism. Nature. 2001;414(6865):799–806. doi:10.1038/414799a.
43. LeRoith D, Roberts CT. The insulin-like growth factor system and cancer. Cancer Lett. 2003;195(2):127–37. doi:10.1016/s0304-3835(03)00159-9.
44. Haeusler RA, McGraw TE, Accili D. Biochemical and cellular properties of insulin receptor signalling. Nat Rev Mol Cell Biol. 2017;19(1):31–44. doi:10.1038/nrm.2017.89.
45. Yanai R, Yamada N, Kugimiya N, Inui M, Nishida T. Mitogenic and antiapoptotic effects of various growth factors on human corneal fibroblasts. Invest Ophthalmol Vis Sci. 2002;43:2122–26.
46. Sarenac T, Trapecar M, Gradisnik L, Rupnik MS, Pahor D. Single-cell analysis reveals IGF-1 potentiation of inhibition of the TGF-β/Smad pathway of fibrosis in human keratocytes in vitro. Sci Rep. 2016;6(1):34373. doi:10.1038/srep34373.
47. Parsons WJ, Ramkumar V, Stiles GL. Isobutylmethylxanthine stimulates adenylate cyclase by blocking the inhibitory regulatory protein, Gi. Mol Pharmacol. 1988;34:37–41.
48. Foster JW, Gouveia RM, Connon CJ. Low-glucose enhances keratocyte-characteristic phenotype from corneal stromal cells in serum-free conditions. Sci Rep. 2015;5:10839. doi:10.1038/srep10839.
49. Andresen JL, Ledet T, Ehlers N. Keratocyte migration and peptide growth factors: the effect of PDGF, bFGF, EGF, IGF-I, aFGF and TGF-beta on human keratocyte migration in a collagen gel. Curr Eye Res. 1997;16(6):605–13. doi:10.1076/ceyr.16.6.605.5081.
50. West-Mays JA, Cook JR, Sadow PM, Mullady DK, Bargagna-Mohan P, Strissel KJ, Fini ME. Differential inhibition of collagenase and interleukin-l a gene expression in cultured corneal fibroblasts by TGF-b, dexamethasone, and retinoic acid. Invest Ophthalmol Vis Sci. 1999;40:887–96.
51. Massagué J, Wotton D. Transcriptional control by the TGF-beta/Smad signaling system. The EMBO Journal. 2000;19(8):1745–1754. doi:10.1093/emboj/19.8.1745.
52. Rønnov-Jessen L, Petersen OW. A function for filamentous α-smooth muscle actin: retardation of motility in fibroblasts. J Cell Biol. 1996;134(1):67–80. doi:10.1083/jcb.134.1.67.
53. Karamichos D, Hutcheon AEK, Zieske JD. Reversal of fibrosis by TGF-β3 in a 3D in vitro model. Exp Eye Res. 2014;124:31–36. doi:10.1016/j.exer.2014.04.020.
54. Karamichos D, Hutcheon AEK, Zieske JD. Transforming growth factor-β3 regulates assembly of a non-fibrotic matrix in a 3D corneal model. J Tissue Eng Regen Med. 2011;5:228–38. doi:10.1016/j.exer.2014.04.020.
55. Sriram S, Tran JA, Guo X, Hutcheon AEK, Lei H, Zieske JD. PDGFR a is a key regulator of T1 and T3's differential effect on SMA expression in human corneal fibroblasts. Invest Ophthalmol Vis Sci. 2017;58:1179–86. doi:10.1167/iovs.16-20016.
56. Lakshman N, Petroll WM. Growth factor regulation of corneal keratocyte mechanical phenotypes in 3-D collagen matrices. Invest Ophthalmol Vis Sci. 2012;53(3):1077–86. doi:10.1167/iovs.11-8609.
57. Wilson SE, Mohan RR, Mohan RR, Ambrósio R, Hong J, Lee J. The corneal wound healing response: cytokine-mediated interaction of the epithelium, stroma, and inflammatory cells. Prog Retin Eye Res. 2001;20(5):625–37. doi:10.1016/S1350-9462(01)00008-8.

TISSUE ENGINEERING: Part A
Volume 00, Number 00, 2020
Mary Ann Liebert, Inc.
DOI: 10.1089/ten.tea.2020.0019

termis
Tissue Engineering
& Regenerative Medicine
International Society

Engineering a Corneal Stromal Equivalent Using a Novel Multilayered Fabrication Assembly Technique*

Julia Fernández-Pérez, MSc,[1,2] Peter W. Madden, PhD,[1,2] and Mark Ahearne, PhD[1,2]

To overcome the serious shortage of donor corneas for transplantation, alternatives based on tissue engineering need to be developed. Decellularized corneas are one potential alternative, but their densely packed collagen architecture inhibits recellularization *in vitro*. Therefore, a new rapid method of recellularizing these constructs to ensure high cellularity throughout the collagen scaffold is needed. In this study, we developed a novel method for fabricating corneal constructs by using decellularized porcine corneal sheets assembled using a bottom-up approach by layering multiple sheets between cell-laden collagen I hydrogel.

Corneal lenticules were cut from porcine corneas by cryosectioning, then decellularized with detergents and air-dried for storage as sheets. Human corneal stromal cells were encapsulated in collagen I hydrogel and cast between the dried sheets. Constructs were cultured in serum-free medium supplemented with ascorbic acid and insulin for 2 weeks. Epithelial cells were then seeded on the surface and cultured for an additional week. Transparency, cell viability, and phenotype were analyzed by qPCR, histology, and immunofluorescence. Constructs without epithelial cells were sutured onto an *ex vivo* porcine cornea and cultured for 1 week.

Lenticules were successfully decellularized, achieving dsDNA values of 13 ± 1.2 ng/mg dry tissue, and were more resistant to degradation than the collagen I hydrogels. Constructs maintained high cell viability with a keratocyte-like phenotype with upregulation of keratocan, decorin, lumican, collagen I, ALDH3A1, and CD34 and the corneal epithelial cells stratified with a cobblestone morphology. The construct was amenable to surgical handling and no tearing occurred during suturing. After 7 days *ex vivo*, constructs were covered by a neoepithelium from the host porcine cells and integration into the host stroma was observed.

This study describes a novel approach toward fabricating anterior corneal substitutes in a simple and rapid manner, obtaining mature and suturable constructs using only tissue-derived materials.

Keywords: cornea, tissue engineering, decellularization, keratocyte, lenticules

Impact Statement

New strategies are needed to face the important worldwide shortage of donor tissues for corneal transplantation. This study describes a novel approach based on decellularized sheets of porcine cornea interspaced with cell-laden collagen I hydrogels. These constructs matured into a transplantable tissue.

Introduction

Several diseases affecting the cornea can lead to blindness and require a corneal transplant to regain sight. Supply of human donor tissue is limited and it is estimated that only 1 cornea is available for every 70 needed,[1] highlighting the critical shortage. There is a clear necessity for alternative approaches with tissue engineering being one method of potentially generating transplantable tissue.

Among the promising materials under consideration for fabricating the cornea is decellularized animal tissue. This comprises of the extracellular matrix (ECM) of the cornea

[1]Department of Mechanical and Manufacturing Engineering, School of Engineering, Trinity College Dublin, University of Dublin, Dublin, Ireland.
[2]Trinity Center for Biomedical Engineering, Trinity Biomedical Science Institute, Trinity College Dublin, University of Dublin, Dublin, Ireland.
*Part of this study has been presented at the 2019 Annual Meeting of the Association for Vision and Ophthalmology (ARVO). The abstract is published in Investigative Ophthalmology and Visual Science 60 (9), 4124–4124.

without any donor cells present to provide a scaffold for cell growth. Decellularized porcine corneas have been transplanted into humans in cases of infectious ulcers with encouraging results.[2,3] However, these acellular scaffolds are composed of densely packed collagen lamellae, and thus recellularization is difficult, making it slow, both *in vitro*[4] and *in vivo*.[5]

In attempts to improve recellularization, human lenticules extracted during myopia correction surgeries have been attached together using a fibrin glue hydrogel to prepare a decellularized scaffold.[6] Although the decellularized lenticules did populate with a small number of cells, the phenotype of these was not characterized.

In another study, thin sheets of decellularized porcine cornea were seeded with stromal cells and multiple layers implanted intrastromally.[7] After 6 months, the corneas had the same thickness as unoperated eyes and some cells were visible between engrafted sheets. Thus, the first study showed the feasibility of binding the decellularized lenticules without using cells, and the second showed the possibility of recellularizing each layer before implantation. The combination of both approaches where cells are embedded in the hydrogel has not been explored previously and sets the basis for this study. This novel approach would allow cells to be incorporated directly into the decellularized cornea while still binding the different layers together.

The aim of this study was therefore to develop a corneal substitute by using sheets of decellularized porcine cornea interspersed with cell-laden collagen hydrogels. The use of collagen rather than fibrin is more physiologically relevant since the cornea is primarily made up of collagen fibrils. These constructs presented high transparency, easy handling after fabrication, high viability, and *in vivo*-like phenotype after a culture period of 3 weeks. Furthermore, constructs containing both stromal and epithelial cells were fabricated, and remained viable when sutured into an *ex vivo* model of anterior lamellar keratoplasty (ALK).

Materials and Methods

Fabrication of acellular matrix sheets

Porcine eyes were obtained within 24 h from abattoir death. After trimming and under sterile conditions, the eye globes were washed twice with phosphate-buffered saline (PBS), immersed in 2% iodine solution (Videne®, Ecolab, Belgium) for 4 min under gentle agitation, and then rinsed three times with PBS for 2 min. The central corneal button from each eye was excised using a 10 mm biopsy punch. Corneal buttons were embedded in optimal cutting temperature medium (OCT; Thermo-Scientific, Ireland), snap-frozen in liquid nitrogen, and cryosectioned on a cryostat (Leica, Germany) to obtain 60-μm-thick slices. Slices were washed in PBS to remove OCT and then transferred into a decellularization solution of 0.5% (w/v) sodium dodecyl sulfate (SDS) and 1% (v/v) Triton X-100 (both Sigma-Aldrich, Ireland) in distilled water for 24 h at room temperature.

To promote penetration of the solution and removal of debris, this and further processing was carried out on an orbital shaker. The samples were treated with 10 U/mL of RNAse and DNAse in 10 mM $MgCl_2$ solution for 1 h at 37°C (all Sigma), then decontaminated by washing in PBS supplemented with 100 U/mL penicillin, 100 mg/mL streptomycin (both Gibco, Ireland), and 250 ng/mL amphotericin B (Sigma) for another 24 h at room temperature, followed by washing in sterile distilled water three times.

The acellular sheets were air dried in a sterile biohazard cabinet and stored in a sealed container at room temperature until use. Native, decellularized and decellularized, dehydrated and rehydrated sheets were fixed in 4% paraformaldehyde for 15 min at room temperature. They were then embedded in paraffin wax and sectioned on a microtome (Leica). Slides were deparaffinized, rehydrated, and coverslipped using 4′,6-diamidino-2-phenylindole (DAPI)-containing aqueous mounting medium (Sigma). Slides were imaged with an epifluorescence microscope (Olympus IX83). The thickness of the sheets was measured in ImageJ from those images ($n = 20–30$). Additionally, the macroscopic appearance and transparency of the dried acellular sheets was assessed by placing them over printed text.

DNA content

Native and decellularized porcine cornea sheets were freeze dried and digested in 3.88 U/mL of papain solution rotating at 60°C for 18 h. DNA content was then quantified using a Quant-iT™ PicoGreen® dsDNA Kit (Invitrogen, Ireland) following the manufacturer's instructions. The plates were read using a spectrophotometer (BioTek™ Synergy HTX) using 480 nm excitation wavelength and 520 nm emission wavelength.

Degradation test

In vitro enzymatic digestion was performed to determine the resistance to biodegradation. Single decellularized sheets and 100 μL collagen gels (cast as described later) were tested by being incubated with 1 mL 20 U/mL collagenase I (Gibco) in PBS at 37°C. Photographs were taken periodically, before the supernatant was collected and fresh collagenase solution added. Collagen content in the supernatant was quantified by measuring the hydroxyproline content through a dimethylaminobenzaldehyde (DMBA) assay.[8]

Briefly, 200 μL of supernatant at each time point was digested with 12 M HCl for 18 h at 110°C. These samples were then allowed to evaporate for 48 h at 50°C in a fume hood. After evaporation, the dry samples were resuspended in deionized water and incubated for 20 min at room temperature with Chloramine T and an oxidizing buffer. DMBA reagent was added and incubated for 20 min at 60°C. After cooling, the reactants were read at 570 nm in a plate reader (BioTek Synergy HTX).

Cell culture

Human corneal stromal cells were isolated from the corneal/scleral ring remaining after a corneal transplant in accordance with the Declaration of Helsinki. The corneal/scleral rings were rinsed with sterile PBS and the epithelium and endothelium were carefully removed using a scalpel blade. After a brief wash with sterile PBS, the corneal stroma was diced into small pieces and transferred into a 25-cm^2 culture flask. Media consisted of low-glucose Dulbecco's modified Eagle's medium (DMEM; HyClone, Dublin, Ireland) supplemented with 10% fetal bovine serum and 100 U/mL Penicillin/Streptomycin (Gibco). The stromal pieces were cultured at 37°C and 5% CO_2 in a humidified incubator.

Media were changed regularly until the cells had migrated from the tissue and reached 80–90% confluence before being passaged to allow further expansion. The cells were cryopreserved and used at passage 4.

Human telomerase-immortalized corneal epithelial cells (hTCEpi, Evercyte, Austria) were expanded and cultured using keratinocyte growth medium (PromoCell, Germany), following the manufacturer's instructions.

Construction of an engineered corneal stroma

Collagen hydrogels were prepared from rat tail collagen I (Corning, New York) as previously described.[9] A 3.5 mg/mL solution was prepared from stock, salt concentration adjusted using 10×PBS and pH raised to neutral by addition of 1 N NaOH. After this neutralization, 10,000 cells/μL gel were embedded in the solution. Twenty-five microliters of solution was deposited on a decellularized corneal sheet and a second sheet placed on top. This process was repeated until there were four gels and five sheets. This construct was then incubated for 30 min at 37°C in a humidified incubator, before being submerged in a media of DMEM/F12 (1:1; HyClone) supplemented with 1×insulin/transferrin/selenium (Gibco) and 100 μg/mL L-ascorbic acid-2-phosphate (Sigma). This medium was chosen as it has been shown to promote a keratocyte-like phenotype.[10] Constructs were fed every second day for 3 weeks.

A total of 50.000 hTCEpi cells were seeded on the construct after 2 weeks and cultured for another week in Keratinocyte growth medium.

Cell viability

Constructs were incubated with 2 μM Calcein-AM and 4 μM EthD-1 (Biotium, San Francisco, California, USA) for 1 h at 37°C in a humidified incubator. Samples were washed three times in PBS and imaged by laser scanning confocal imaging (Leica SP8, Germany).

Transparency and light transmittance

The macroscopic appearance of the constructs was assessed by placing them over printed text. Additionally, light transmittance through the constructs after 3 weeks of culture was quantified by measuring the absorbance of light at different wavelengths ranging from 300 to 700 nm that pass through each sample using a microplate reader (BioTek Synergy HTX, Winooski, Vermont, USA). The absorbance of light passing through ultrapure water was used as a control to represent 100% transmittance and this absorbance reading was subtracted from the measured absorbance of each sample to give the change in absorbance due to the sample being present (A). The transmittance of light was calculated using the following formula as described elsewhere[11]:

$$Transmittance\,(\%) = \frac{1}{10^{A}} \times 100$$

Quantitative polymerase chain reaction

RNA from constructs was extracted using TRIzol, following the manufacturer's instructions (Invitrogen). To increase lysis and release of the genetic material, samples were triturated using a tissue homogenizer (IKA T10 basic, Germany). Chloroform was added, the samples were vortexed, and then centrifuged for 15 min at 12,000 *g* at 4°C. The supernatant was transferred into a new tube and an equal volume of isopropanol added, along with 3 μL of GlycoBlue™ (Invitrogen) to improve precipitation. Samples were kept overnight at −20°C and then centrifuged at 12,000 *g* for 15 min at 4°C. The supernatant was discarded and 70% ethanol in RNAse-free water used to wash the pellet. Samples were centrifuged again, and the supernatant removed before the pellets were air dried. The pellets were dissolved in RNAse-free water and RNA yield and purity quantified using a NanoDrop-1000 (Thermo Scientific). All steps were performed on ice.

RNA was converted into cDNA using the High-Capacity cDNA Reverse Transcription Kit (Invitrogen). Real-time polymerase chain reaction was performed using TaqMan Universal Master Mix II and the following TaqMan primers: glyceraldehyde-3-phosphate dehydrogenase (GAPDH, Hs02758991_g1), aldehyde dehydrogenase 3A1 (ALDH3A1, Hs00964880_m1), alpha smooth muscle actin (α-SMA) (ACTA2, Hs00426835_g1), keratocan (KERA; Hs005 59942_m1), collagen 1a1 (COL1; Hs00164004_m1), lumican (LUM, Hs00929860_m1), decorin (DCN, Hs0075 4870_s1), and CD34 (Hs00990732_m1). The genes of interest were normalized against GAPDH using the ΔΔCt method. Calculated values were expressed as a power of $2^{-\Delta\Delta Ct}$. For this study, all values were normalized to the serum-expanded cells.

Histological analysis and immunohistochemistry

After culture, samples were fixed with 4% paraformaldehyde for 15 min at room temperature. They were then embedded in paraffin wax and sectioned on a microtome (Leica). Routine Hematoxylin and Eosin (H&E), Alcian Blue, and Picrosirius Red staining were performed.

Slides were stained for 4 min with Harris Hematoxylin (Sigma), followed by a 10-min wash with running tap water, 30 s in acid alcohol, and further tap water for 5 min. Counterstaining was 2 min with Eosin Y (Sigma). Alcian Blue was used to assess sulfated glycoaminoglycans (sGAG) content; 1% Alcian Blue 8GX (Sigma) in 0.1 M HCl was applied for 5 min, followed by three, 30-s washes in deionized water. Picrosirius Red was used to assess collagen distribution; slides were immersed in Sirius Red (Sigma) in a saturated aqueous solution of picric acid for 1 h followed by 1 min in 0.5% acetic acid. After staining, all slides were dehydrated and coverslips attached using DPX mountant (Sigma).

For immunofluorescent staining, slides were rehydrated followed by an antigen-retrieval step. Samples were first blocked with 1% bovine serum albumin (BSA) and 10% donkey serum in 0.5% Triton X-100 for 1 h at room temperature. The following primary antibodies were used and incubated overnight at 4°C: Collagen I, Decorin, Keratocan, ALDH3A1, Lumican, CD34, and α-SMA. After incubation, three, 5-min washes with 1% BSA in PBS were performed to remove the unbound antibody. Secondary antibody was then incubated for 1 h at room temperature followed by again washing three times for 5 min with 1% BSA in PBS. Coverslips were attached using DAPI-containing aqueous mounting medium (Sigma). Slides were imaged using laser scanning confocal microscopy (Leica SP8). Table 1 contains

Table 1. Antibodies and Antigen Retrieval Methods for Immunofluorescent Staining

Primary antibody	*Catalogue number (brand)*	*Dilution*	*Antigen retrieval method*	*Secondary antibody (dilution)*
ALDH3A1	Ab76976 (Abcam)	1:200	Heat-mediated citrate buffer pH 6 (30 min at 95°C)	Donkey anti-rabbit-AlexaFluor® 488 (1:200)
α-SMA	Ab7817 (Abcam)	1:100	Heat-mediated citrate buffer pH 6 (30 min at 95°C)	Goat anti-mouse AlexaFluor 488 (1:200)
Keratocan	HPA039321 (Atlas Antibodies)	1:50	Heat-mediated citrate buffer pH 6 (30 min at 95°C)	Donkey anti-rabbit-AlexaFluor 488 (1:200)
CD34	Ab81289 (Abcam)	1:250	Heat-mediated citrate buffer pH 6 (30 min at 95°C)	Donkey anti-rabbit-AlexaFluor 488 (1:200)
Decorin	Ab189364 (Abcam)	1:133	Heat-mediated citrate buffer pH 6 (30 min at 95°C)	Rabbit anti-goat-AlexaFluor 594 (1:200)
Lumican	Ab168348 (Abcam)	1:100	Heat-mediated citrate buffer pH 6 (30 min at 95°C)	Donkey anti-rabbit-AlexaFluor 488 (1:200)
Collagen I	Ab90395 (Abcam)	1:400	Enzymatic-mediated 0.25 U/mL Chondroitinase ABC (1 h at 37°C)	Donkey anti-mouse AlexaFluor 488 (1.5:200)

α-SMA, alpha smooth muscle actin.

details of the immunofluorescent staining procedure. Secondary antibody only staining was performed as negative control.

Constructs containing epithelial and stromal cells were fixed for 15 min in 4% paraformaldehyde, permeabilized with 0.5% Triton X-100 during 10 min at room temperature, and subsequently stained with 0.5 μg/mL Phalloidin-TRITC (Sigma) and 1 μg/mL DAPI (Sigma) for 1 h protected from light. Samples were then imaged using laser scanning confocal microscopy (Leica SP8). They were further processed for wax embedding and H&E staining, as previously described.

Implantation of constructs onto an ex vivo *porcine cornea*

Porcine eyes were obtained within 24 h from abattoir death. A 6-mm-diameter defect of approximately half of the depth of the cornea was made using a trephine. Lamellar dissection was performed using a blunt crescent knife (Beaver-Visitec International, UK). Constructs after 3 weeks of culture (without epithelial cells) were sutured in place with 4 or 8, 10–0 nylon sutures. The corneas were resected with 5 mm of scleral rim and placed onto a hemispherical agarose mold (2% agarose w/v). Corneas were cultured for 7 days in a humidified chamber in 4 mL of serum-free DMEM/F12, supplemented with 4% dextran (MW 450,000–650,000, Sigma) to limit swelling. The medium was added to the level of the limbus, leaving the cornea at the air/liquid interface. Medium was changed daily, with three drops added onto the corneal surface to limit drying.

To determine re-epithelialization from the host tissue fluorescein staining was performed. Four–five drops of 1% fluorescein sodium salt (Sigma) in PBS solution were added

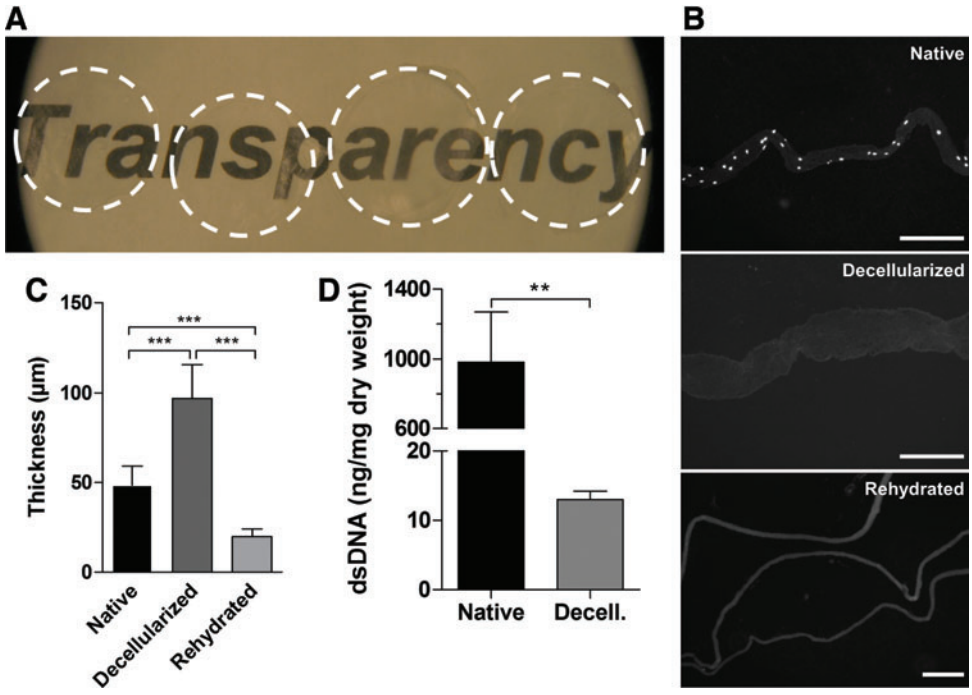

FIG. 1. Characterization of decellularized sheets. **(A)** Macroscopic appearance of the dried acellular sheets, showing high transparency. **(B)** DAPI staining of a native sheet, a sheet after decellularization, and three sheets after dehydration and rehydration, showing the absence of cell nuclei after decellularization (scale bar = 200 μm). **(C)** Thickness measurements of sheets: native, after decellularization, and after dehydration and rehydration. **(D)** dsDNA quantification of native and decellularized sheets. $^{**}p \leq 0.001$, $^{***}p \leq 0.0001$. DAPI, 4′,6-diamidino-2-phenylindole. Color images are available online.

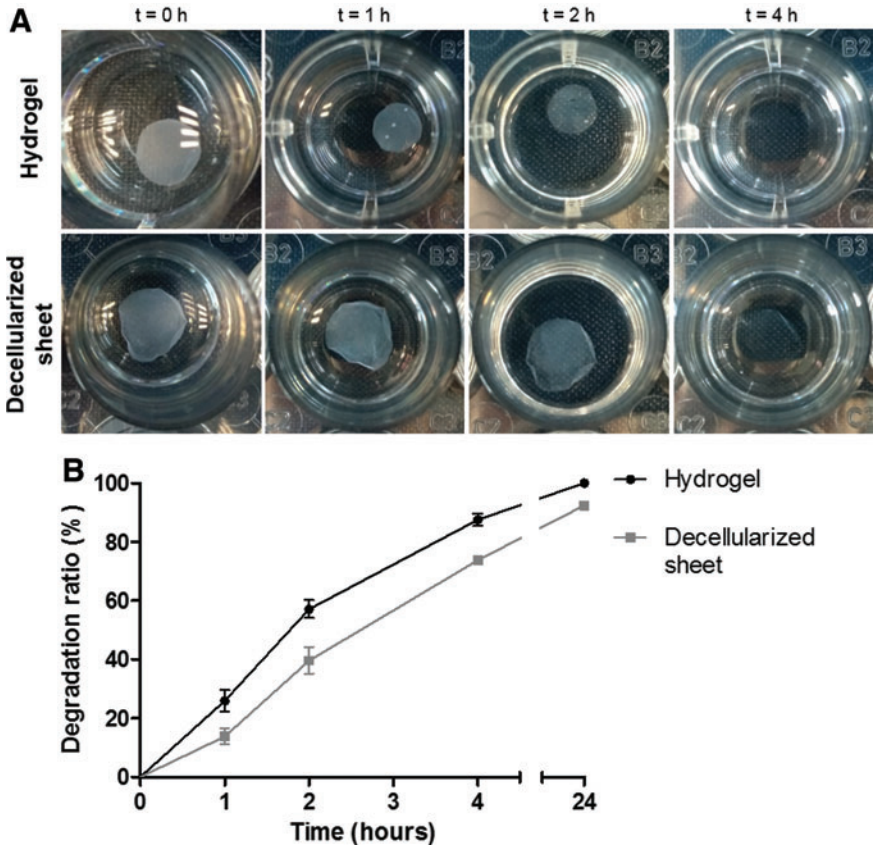

FIG. 2. Resistance to biodegradation. **(A)** Macroscopic visualization and **(B)** quantitative analysis of degradation. Color images are available online.

to cover the surface of the corneas, after 1 min of incubation at room temperature, sterile PBS was used to wash the corneas until no more dye was visibly leaching. In the dark, samples were exposed to blue light from a handheld slit lamp (15090—PSL, Reichert) and imaged with a cell phone. This was performed at 2 and 7 days after implantation. After culture, corneas were fixed overnight in formalin and processed for wax embedding and H&E staining, as previously described.

Statistical analysis

All experiments were performed three times with a minimum of three replicates. Unpaired two-tailed t-test and two-way analysis of variance were employed, and statistical significance accepted at a level of $p < 0.05$.

Results

Characterization of decellularized sheets

The decellularized sheets obtained were highly transparent (Fig. 1A). Sections stained with DAPI presented no cell nuclei after decellularization (Fig. 1B). Thickness measurements showed that the decellularization procedure had a swelling effect on the sections and that, when sections were air dried and rehydrated, they did not recover their original thickness (Fig. 1C). Quantification of dsDNA showed successful decellularization, with significantly lower levels of DNA remnants than the native tissue (Fig. 1D). Native sheets had 982.8 ± 286 ng/mg of DNA per dry tissue (average ± standard deviation), while decellularized sheets presented 13 ± 1.2 ng/mg of DNA per dry tissue (average ± standard deviation).

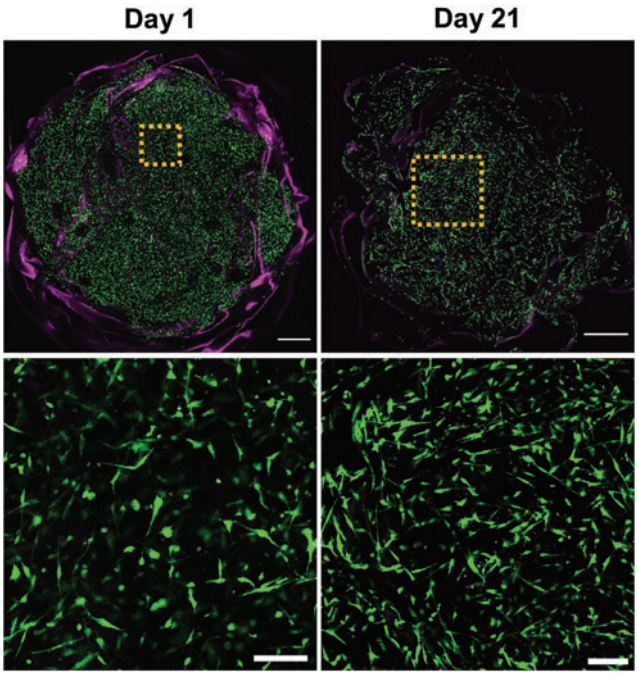

FIG. 3. Cell viability in constructs after fabrication and after 3 weeks in culture (live = *green*, dead = magenta. *Bottom row* insert from *top row* at higher magnification. Top scale bar = 1 mm, *bottom* scale bar = 200 μm). Color images are available online.

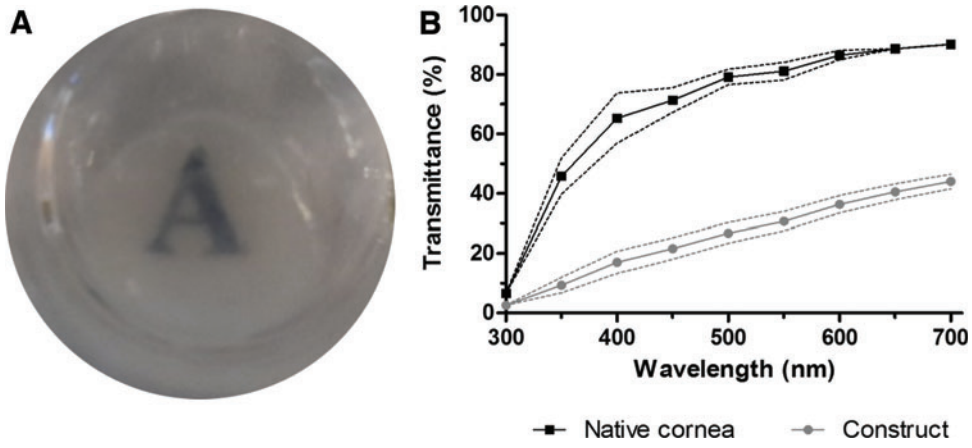

FIG. 4. Macroscopic appearance of constructs after 3 weeks of culture **(A)** and quantification of light transmittance **(B)**. Color images are available online.

Degradation was slower in the decellularized sheets than the collagen hydrogels. After 4 h of incubation in collagenase solution, hydrogels appeared to completely degrade, while decellularized sheets were still visible (Fig. 2A). Even after 24 h, remnants of the sheets were still present. When quantified (Fig. 2B), 57% of the hydrogels was degraded by 2 h, 87% by 4 h, and 100% after 24 h. In comparison, 39%, 73%, and 92% of the decellularized sheets were degraded after 2, 4, and 24 h, respectively. After 48 h, sheets had degraded completely.

Corneal stromal equivalent viability and transparency

Tissue constructs were obtained by stacking dried sheets between cell-laden collagen hydrogels. Human corneal stromal cells remained viable in the constructs throughout the culturing period, even in serum-deprived conditions (Fig. 3). After 1 day in culture, some cell spreading could be detected within the scaffold. After the whole 3-week culture period, most cells displayed an elongated morphology with visible processes. Furthermore, even in this short period, constructs had acceptable optical properties when assessed macroscopically (Fig. 4A). When quantified, they allowed less light transmittance than the native cornea, but did allow >40% of transmittance in the longer wavelengths of the visible spectrum (Fig. 4B).

Corneal stromal equivalent cell phenotype

Characteristic markers of corneal stromal ECM and corneal stromal cell phenotype were analyzed by quantitative polymerase chain reaction (qPCR) (Fig. 5). Keratocyte markers

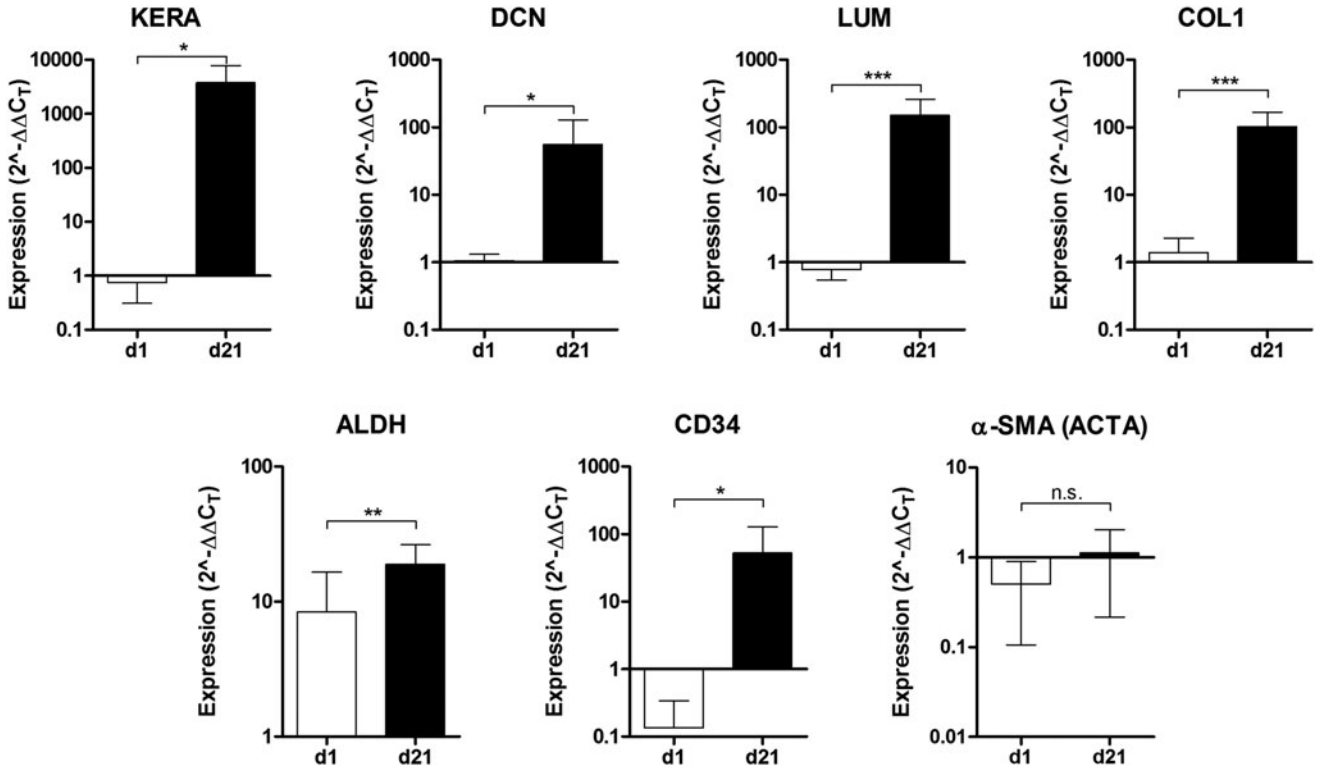

FIG. 5. Phenotypic analysis of stromal cells in the constructs by qPCR at day 1 and 21 of culture. Relative expression of keratocan (KERA), decorin (DCN), lumican (LUM), collagen I (COL1), ALDH3A1, CD34, and α-SMA (ACTA). $*p \leq 0.05$, $**p \leq 0.001$, $***p \leq 0.0001$. α-SMA, alpha smooth muscle actin; qPCR, quantitative polymerase chain reaction.

ALDH3A1 and CD34 were significantly upregulated as the time in serum-free conditions increased. All ECM components analyzed were also highly upregulated. Typical small leucine-rich proteoglycans, keratocan, lumican, and decorin that are found in the corneal stroma, were expressed significantly higher. The expression of collagen I, the most common collagen in the corneal stroma, was significantly upregulated. Furthermore, the fibrotic marker α-SMA was not significantly upregulated.

Constructs were further analyzed through histology and immunohistochemistry (Fig. 6). The thickness of the constructs decreased significantly during the culturing period, from 245.2 ± 66.50 μm to 187.9 ± 27.44 μm, presumably due to the cells remodeling the collagen hydrogel. Constructs presented cells distributed evenly in all hydrogel layers, as seen by H&E staining (Fig. 6A). Picrosirius Red staining for collagen showed differential staining in the hydrogel portion and the decellularized sheets (Fig. 6B). Despite the loss of sGAG during decellularization, upon subsequent culture, cells produced their own ECM in the hydrogel sections (Fig. 6C).

Immunohistostaining corroborated the results obtained from qPCR with constructs staining positive for ALDH3A1, CD34, keratocan, lumican, decorin, and collagen I, whereas α-SMA remained negative (Fig. 6D).

Epithelial cell growth on corneal stromal equivalents

Corneal epithelial cells were cultured on the top layer of the constructs (Fig. 7). A coculture was successfully obtained using this method with stromal cells detected in the middle and lower layers. Epithelial cells had attached to the construct surface and formed a tight epithelium presenting a typical cobblestone morphology (Fig. 7E). Some degree of stratification was visible in H&E-stained sections (Fig. 7F, G).

Implantation of corneal stromal equivalent in an ex vivo *anterior lamellar keratoplasty model*

Constructs were successfully implanted onto porcine corneas in an *ex vivo* ALK model (Fig. 8). Constructs were amenable to surgical handling and suturing without tearing (Fig. 8A). Fluorescein staining is commonly used to assess corneal epithelial wounds. If the staining is positive (yellow), it indicates an area with damaged or absent epithelium (barrier function compromised); whereas a negative staining is an indication of a healthy epithelium as its barrier does not allow the penetration of the dye.

In this study, positive staining was seen on the constructs after 2 days of implantation, while the presence of only small islands of positive fluorescein staining at day 7 indicated that

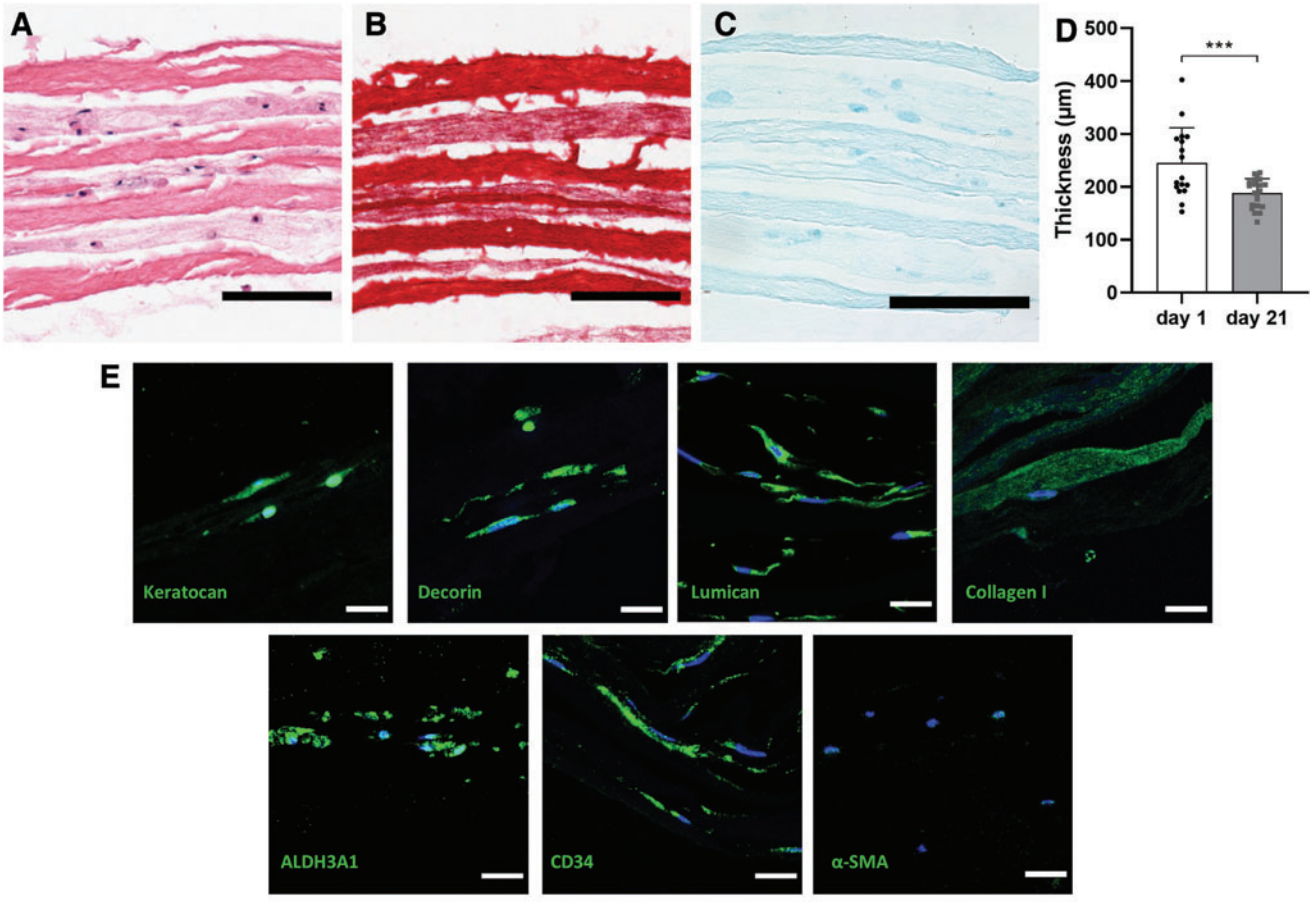

FIG. 6. Histological examination of constructs at day 21, staining with **(A)** H&E (s = sheet, h = hydrogel), **(B)** Picrosirius Red, and **(C)** Alcian Blue (scale bar = 100 μm). **(D)** Thickness measurements of constructs at day 1 and 21. **(E)** Immunohistofluorescent staining of Keratocan, Lumican, Decorin, Collagen I, ALDH3A1, CD34, and α-SMA (*green*), and cell nuclei (*blue*), scale bar = 20 μm. H&E, Hematoxylin and Eosin. Color images are available online.

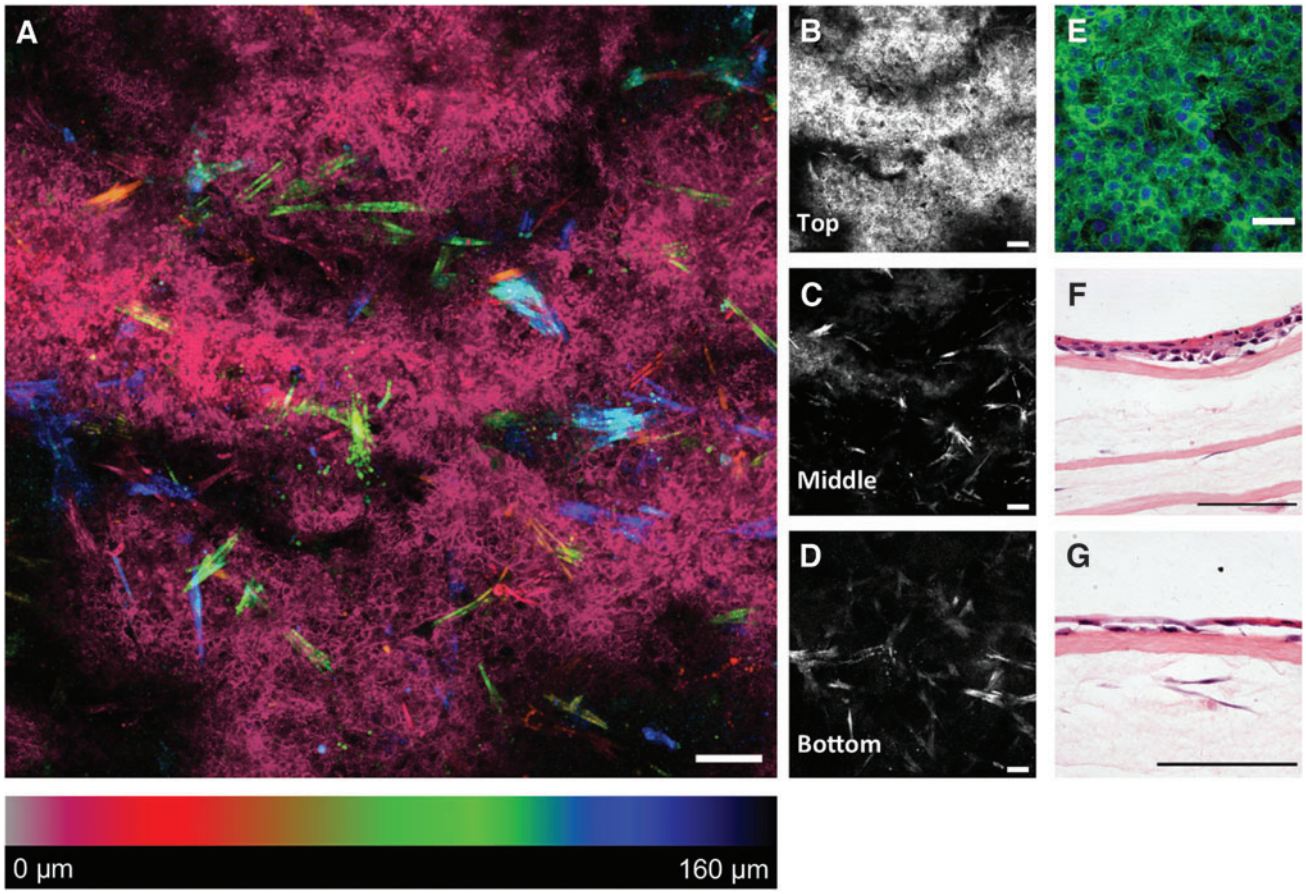

FIG. 7. Anterior cornea constructs with epithelium. **(A)** Depth color-coded Z-stack, cells at the surface (epithelium) appear *pink/red*, whereas stromal cells in deeper areas appear from *orange* to *blue*; **(B–D)** single images of the Z-stack (scale bar = 100 μm); **(E)** higher magnification of the epithelium F-actin (*green*) and nuclei (*blue*), scale bar = 10 μm; **(F, G)** H&E-stained sections show a degree of epithelial stratification (scale bar = 100 μm). Color images are available online.

neighboring epithelial cells colonized the surface of the scaffold (Fig. 8B). Histological analysis through H&E showed good integration of the construct onto the host bed and at its periphery, while the surface was covered in a neoepithelium (Fig. 8C).

Discussion

To overcome the severe worldwide shortage of donor corneal tissue for transplantation, tissue engineering approaches are being developed. In this study, a multilayered construct fabricated with decellularized cornea sheets and cell-laden collagen hydrogels is described. These corneal stroma tissue equivalents presented high cell viability, transparency, expression of stromal cell markers, and supported epithelial regeneration.

Decellularization of the stromal sheets was successful, with values of dsDNA remaining well below the recommended maximum concentration of 50 ng/mg of dry tissue to minimize adverse host reactions.[12] While a shorter decellularization protocol to that previously described was used in this study, levels of DNA were lower.[13] This is probably due to the thinner tissue allowing improved penetration of the detergents.

Swelling occurred during the decellularization process, which has been previously reported.[14–18] Once the endothelium is damaged or removed, the cornea swells. Furthermore, SDS is an aliphatic molecule and it binds to proteins by its hydrophobic domain that results in increased negative charge, which attracts water and leads to swelling.[19] To counteract this, osmoregulators, such as dextran,[13,20] glycerol,[20] gelatin, and sodium chloride[21] can be used to reduce swelling. Unsurprisingly, dehydration resulted in a reduction in thickness, however, the thickness only partially recovered upon rehydration. This could be attributed to the loss of sGAG during the decellularization process that would normally attract water molecules into the tissue.[22,23]

In this study, the sheets were dehydrated by air drying in a laminar flow hood and did not fully recover their thickness after rehydration. This would lead to a denser collagen network than found in the native tissue.

Alternative dehydration techniques such as freeze drying or critical point drying could be used but these also introduce new limitations. While freeze drying has been previously used to obtain dried sheets of decellularized cartilage,[24] preliminary investigations by our group using stromal sheets showed that freeze drying did not affect the thickness but inhibited the transmission of light through the tissue. Critical point drying was not used as it could lead to degradation of the ECM following exposure to ethanol. The addition of a protecting agent to limit shrinkage was not

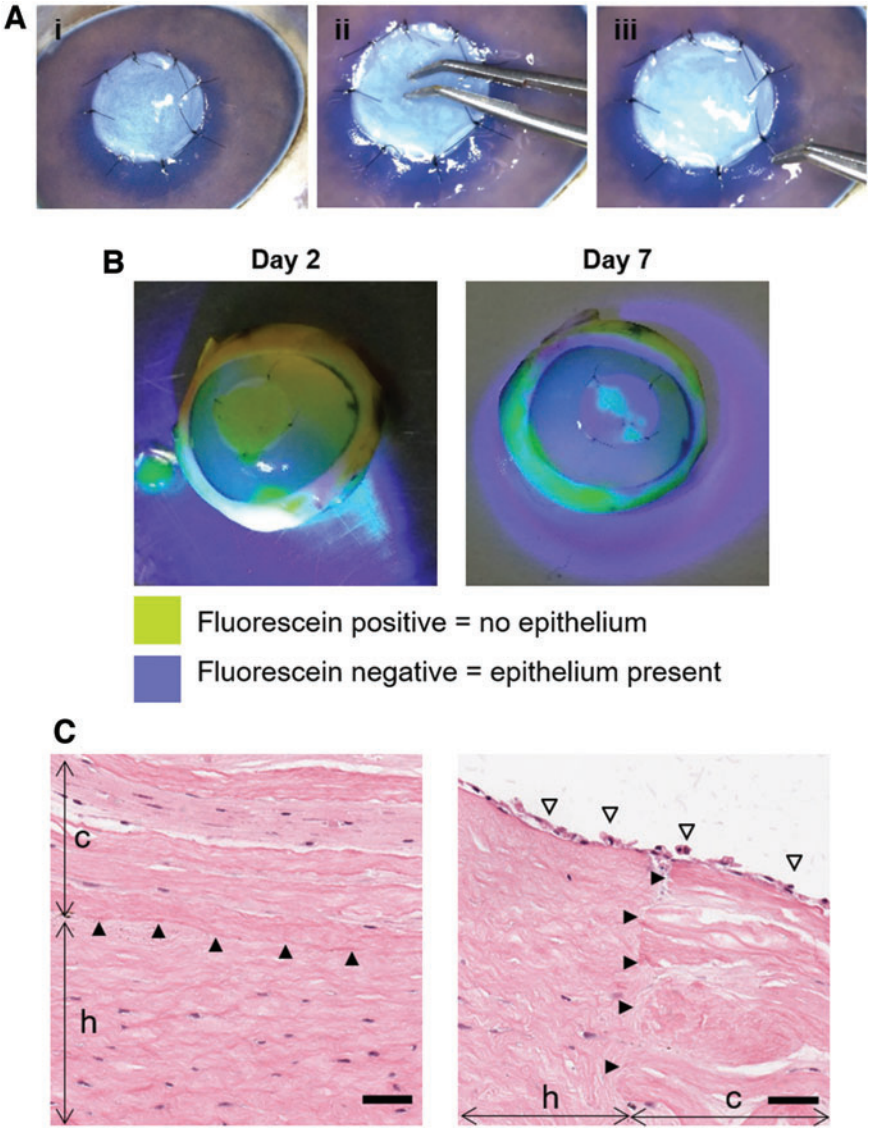

FIG. 8. Implantation of constructs without epithelium onto an *ex vivo* porcine cornea. **(A)** Surgical procedure: (i) implant sutured in place using 10-0 nylon sutures, (ii) pressing onto the implant to show strength of construct and suture points and (iii) pulling of sutures to demonstrate construct does not tear. **(B)** Fluorescein staining of operated porcine corneas after implantation and culture. **(C)** H&E analysis of implanted constructs, showing good integration of construct (c) with the host (h) (*arrowheads*) at the center and the edge of the construct. Epithelium (*empty arrowheads*) from the host has grown onto the construct (scale bar = 50 μm). Color images are available online.

explored in this study, but could potentially assist in controlling the sheet thickness.[25] While other researchers have used freshly decellularized lenticules,[6,26,27] in this study, dried lenticules were used because of their ease in handling, room temperature storage, and possibility of terminal sterilization, such as gamma irradiation.

We hypothesized that cell delivery through a gel would be a gentle, but effective, way to allow the inclusion of cells at all depths. Collagen I was chosen since it is the primary type of collagen found in the corneal stroma.[28] Our approach showed homogeneous cell distribution throughout the construct. In addition, the collagen hydrogel proved to be an excellent binding agent of the dehydrated decellularized sheets, which were attracted by the moisture of the hydrogel.

The use of the decellularized sheets provided stability to the construct, making it more robust and easier to handle than a gel alone. Hong *et al.* reported a carrier for limbal epithelial stem cells based on embedding a single sheet of decellularized human cornea in a collagen gel that was further plastically compressed.[29] With this approach they increased the suturability and resistance to biodegradation of the construct.

In our study, the sheets resisted degradation more than the hydrogels, giving an advantage for the strength and retention of an implant. Furthermore, when corneal stromal cells are embedded in collagen gel alone and cultured under free-floating conditions, they contract greatly.[30] By removing the serum from the medium, this phenomenon can be diminished,[30] but the present study shows that contraction can be controlled by anchoring the collagen gel to a stronger material,[31] in this case, the decellularized sheets. The differences in construct thickness reported during the culture period could indicate remodeling or compaction of the collagen hydrogel, conferring the constructs more mechanical stability. Moreover, additional crosslinking, such as UV-riboflavin, genipin, or transglutaminase, could further improve mechanical properties.

Layer-by-layer is an approach that has been used for stromal replacement constructs, since it aims to replicate the lamellar structure of the corneal stroma. Wilson *et al.* fabricated a stromal model by orthogonal stacking of layers of cell-seeded, aligned, electrospun PLDLA mesh, using collagen gel to bind them together.[32] Ghezzi *et al.* reported

constructs based on orthogonally stacked cell-seeded patterned silk films, without the aid of any binding material.[33] Che *et al*. have recently described the fabrication of stromal equivalents by stacking cell-seeded ultrathin amniotic membrane.[34] In this case, an extended culture period of 8 weeks allowed the stromal cells to produce ECM to bind the layers. The constructs reported in our present study were fabricated with materials found in the native stroma, which might present advantages for clinical translation.

Decellularized porcine corneas have been used to treat patients suffering from corneal ulcers[2,3,21] showing the feasibility of employing xenogeneic material. The use of discarded tissue from myopia correction procedures is an option to use human material[6,27] as well as donated corneas unsuitable for transplantation due to low endothelial cell count, for example.[26]

In the present study, the keratocytes were primarily found in the gel. It is known that *in vivo* remodeling of thin decellularized stromal tissue is faster than that of thicker tissues.[7] 3 weeks of culture might not have been enough time to allow the cells to repopulate the sheets by migrating from the gels. However, the reduction in construct thickness observed can be an indication of cells remodeling the collagen hydrogel. It is necessary to remark that the nonrecovery of sheet thickness after dehydration could have led to collagen fiber compaction, which might make the sheets more dense and, therefore, more difficult for the cells to penetrate. Moreover, the culture conditions used in this study have been optimized for the recovery of a keratocyte phenotype and these cells are known to migrate slowly.[10]

We would, expect that given enough time, once the keratocytes have remodeled the collagen gel, they would migrate to the decellularized sheets as a suitable substrate. In the future, using corneal stromal stem cells (CSSCs) instead of corneal fibroblasts in serum-free conditions might improve the outcome further since CSSCs present a more keratocyte-like phenotype,[35] produce a more natural ECM[36] and possess antiscarring activity.[37] These cells have also been shown to support limbal epithelial stem cells in a compressed collagen I stromal model.[38]

Several studies have developed hydrogels as corneal substitutes, which required implantation using overlying sutures as they are not sufficiently strong to be implanted using running sutures[39–42] or relied on the use of fibrin glue.[43] Alternative strategies such as the one reported by Hong *et al.* increased suturability by embedding a decellularized human corneal lenticule in a compressed collagen gel.[29] These authors also report the fabrication of anterior stromal equivalents by embedding keratocytes in a plastically compressed gel, composed of a collagen I and decellularized corneal ECM mixture, with epithelial cells on the surface.[44] In the approach we took, stacking the decellularized sheets with the normally unsuturable collagen gels provided a construct that could be sutured with conventional interrupted 10-0 sutures.

Constructs at the time of implantation had a thickness of $\sim 190\,\mu m$, suitable for ALK and superficial ALK. These procedures are employed to treat anterior stromal defects, such as scarring, opacification, or ulceration resulting from infection, inflammation, trauma, or inadequate healing after surgical refractive procedures.[45,46] Patients suffering from lattice, granular, or Reis/Bückler corneal dystrophies could also benefit from the use of these constructs.[45,46] If thicker or thinner constructs would be needed, more or less layers, respectively, should be stacked when fabricating the constructs.

The optical properties of the presented constructs were suboptimal. However, studies report a recovery of transparency upon implantation, once the hydration state of the construct matches the native rather dehydrated nature.[18,47] Furthermore, decellularized cornea ECM-derived hydrogels could be employed in future studies since these are more transparent than rat tail collagen hydrogels.[48]

Decellularized stromal lenticules similar to the ones described in this study have been used to culture corneal endothelial cells.[49–52] While not in the scope of this study, the constructs described could also be seeded with endothelial cells to obtain a full-thickness laboratory-grown corneal substitute.

In summary, the feasibility of fabricating an anterior cornea equivalent using only tissue-derived materials was demonstrated, with good cell viability, optical properties, and cell phenotype. These were assembled in a rapid process that allowed regular and dense cell distribution, independent of cell migration. These corneal substitutes show translatability since they can be sutured and support regeneration of the epithelium in an *ex vivo* model.

Disclosure Statement

No competing financial interests exist.

Funding Information

The research is supported by funding from the European Research Council (ERC) under the European Union's Horizon 2020 research and innovation program (grant agreement no. 637460) and from Science Foundation Ireland (15/ERC/3269). Human eye tissue was kindly supplied through the Tissue Bank of the Irish Blood Transfusion Service, Dublin, after appropriate consent.

References

1. Gain, P., Jullienne, R., He, Z., *et al.* Global survey of corneal transplantation and eye banking. JAMA Ophthalmol **134,** 167, 2016.
2. Zhang, M.-C., Liu, X., Jin, Y., Jiang, D.-L., Wei, X.-S., and Xie, H.-T. Lamellar keratoplasty treatment of fungal corneal ulcers with acellular porcine corneal stroma. Am J Transplant **15,** 1068, 2015.
3. Zheng, J., Huang, X., Zhang, Y., *et al.* Short-term results of acellular porcine corneal stroma keratoplasty for herpes simplex keratitis. Xenotransplantation **26,** e12509, 2019.
4. Xu, Y.-G., Xu, Y.-S., Huang, C., Feng, Y., Li, Y., and Wang, W. Development of a rabbit corneal equivalent using an acellular corneal matrix of a porcine substrate. Mol Vis **14,** 2180, 2008.
5. Li, S., Deng, Y., Tian, B., *et al.* Healing characteristics of acellular porcine corneal stroma following therapeutic keratoplasty. Xenotransplantation **27,** e12566, 2020.
6. Yin, H., Qiu, P., Wu, F., *et al.* Construction of a corneal stromal equivalent with SMILE-derived lenticules and fibrin glue. Sci Rep **6,** 33848, 2016.
7. Ma, X.Y., Zhang, Y., Zhu, D., *et al.* Corneal stroma regeneration with acellular corneal stroma sheets and keratocytes in a rabbit model. PLoS One **10,** 1, 2015.

8. Kafienah, W., and Sims, T.J. Biochemical methods for the analysis of tissue-engineered cartilage. Methods Mol Biol **238,** 217, 2004.
9. Ahearne, M., Yang, Y., Then, K.Y., and Liu, K.K. Non-destructive mechanical characterisation of UVA/riboflavin crosslinked collagen hydrogels. Br J Ophthalmol **92,** 268, 2008.
10. Fernández-Pérez, J., and Ahearne, M. Influence of biochemical cues in human corneal stromal cell phenotype. Curr Eye Res **44,** 135, 2019.
11. Kim, H., Park, M.-N., Kim, J., Jang, J., Kim, H.-K., and Cho, D.-W. Characterization of cornea-specific bioink: high transparency, improved in vivo safety. J Tissue Eng **10,** 204173141882338, 2019.
12. Crapo, P.M., Gilbert, T.W., and Badylak, S.F. An overview of tissue and whole organ decellularization processes. Biomaterials **32,** 3233, 2011.
13. Lynch, A.P., Wilson, S.L., and Ahearne, M. Dextran preserves native corneal structure during decellularization. Tissue Eng Part C Methods **22,** 561, 2016.
14. Dong, M., Zhao, L., Wang, F., *et al.* Rapid porcine corneal decellularization through the use of sodium N-lauroyl glutamate and supernuclease. J Tissue Eng **10,** 204173141987587, 2019.
15. Du, L., and Wu, X. Development and characterization of a full-thickness acellular porcine cornea matrix for tissue engineering. Artif Organs **35,** 691, 2011.
16. Lin, Y., Zheng, Q., Hua, S., Meng, Y., Chen, W., and Wang, Y. Cross-linked decellularized porcine corneal graft for treating fungal keratitis. Sci Rep **7,** 9955, 2017.
17. Pang, K., Du, L., and Wu, X. A rabbit anterior cornea replacement derived from acellular porcine cornea matrix, epithelial cells and keratocytes. Biomaterials **31,** 7257, 2010.
18. Wu, Z., Zhou, Y., Li, N., *et al.* The use of phospholipase A2 to prepare acellular porcine corneal stroma as a tissue engineering scaffold. Biomaterials **30,** 3513, 2009.
19. Courtman, D.W., Pereira, C.A., Kashef, V., McComb, D., Lee, J.M., and Wilson, G.J. Development of a pericardial acellular matrix biomaterial: biochemical and mechanical effects of cell extraction. J Biomed Mater Res **28,** 655, 1994.
20. Murab, S., and Ghosh, S. Impact of osmoregulatory agents on the recovery of collagen conformation in decellularized corneas. Biomed Mater **11,** 065005, 2016.
21. Shi, W., Zhou, Q., Gao, H., *et al.* Protectively decellularized porcine cornea versus human donor cornea for lamellar transplantation. Adv Funct Mater **29,** 1902491, 2019.
22. Wang, X., Xu, H., Huang, Y., Gu, S., and Jiang, J.X. Coupling effect of water and proteoglycans on the in situ toughness of bone. J Bone Miner Res **31,** 1026, 2016.
23. Han, E., Chen, S.S., Klisch, S.M., and Sah, R.L. Contribution of proteoglycan osmotic swelling pressure to the compressive properties of articular cartilage. Biophys J **101,** 916, 2011.
24. Gong, Y.Y., Xue, J.X., Zhang, W.J., Zhou, G.D., Liu, W., and Cao, Y. A sandwich model for engineering cartilage with acellular cartilage sheets and chondrocytes. Biomaterials **32,** 2265, 2011.
25. Allen, C.L., Clare, G., Stewart, E.A., *et al.* Augmented dried versus cryopreserved amniotic membrane as an ocular surface dressing. PLoS One **8,** e78441, 2013.
26. Alió del Barrio, J.L., El Zarif, M., Azaar, A., *et al.* Corneal stroma enhancement with decellularized stromal laminas with or without stem cell recellularization for advanced keratoconus. Am J Ophthalmol **186,** 47, 2018.
27. Yam, G.H.-F., Yusoff, N.Z.B.M., Goh, T.-W., *et al.* Decellularization of human stromal refractive lenticules for corneal tissue engineering. Sci Rep **6,** 26339, 2016.
28. Lee, R.E., and Davison, P.F. The collagens of the developing bovine cornea. Exp Eye Res **39,** 639, 1984.
29. Hong, H., Huh, M.-I., Park, S.M., Lee, K., Kim, H.K., and Kim, D.S. Decellularized corneal lenticule embedded compressed collagen: toward a suturable collagenous construct for limbal reconstruction. Biofabrication **10,** 045001, 2018.
30. Miotto, M., Gouveia, R.M., Ionescu, A.M., Figueiredo, F., Hamley, I.W., and Connon, C.J. 4D Corneal tissue engineering: achieving time-dependent tissue self-curvature through localized control of cell actuators. Adv Funct Mater **29,** 1807334, 2019.
31. Ahearne, M., Liu, K.-K., El Haj, A.J., Then, K.Y., Rauz, S., and Yang, Y. Online monitoring of the mechanical behavior of collagen hydrogels: influence of corneal fibroblasts on elastic modulus. Tissue Eng Part C Methods **16,** 319, 2010.
32. Wilson, S.L., Wimpenny, I., Ahearne, M., Rauz, S., El Haj, A.J., and Yang, Y. Chemical and topographical effects on cell differentiation and matrix elasticity in a corneal stromal layer model. Adv Funct Mater **22,** 3641, 2012.
33. Ghezzi, C.E., Marelli, B., Omenetto, F.G., Funderburgh, J.L., and Kaplan, D.L. 3D functional corneal stromal tissue equivalent based on corneal stromal stem cells and multilayered silk film architecture. PLoS One **12,** 1, 2017.
34. Che, X., Wu, H., Jia, C., *et al.* A novel tissue-engineered corneal stromal equivalent based on amniotic membrane and keratocytes. Investig Opthalmology Vis Sci. **60,** 517, 2019.
35. Wu, J., Du, Y., Mann, M.M., Funderburgh, J.L., and Wagner, W.R. Corneal stromal stem cells versus corneal fibroblasts in generating structurally appropriate corneal stromal tissue. Exp Eye Res **120,** 71, 2014.
36. Karamichos, D., Funderburgh, M.L., Hutcheon, A.E.K., *et al.* A role for topographic cues in the organization of collagenous matrix by corneal fibroblasts and stem cells. PLoS One **9,** e86260, 2014.
37. Basu, S., Hertsenberg, A.J., Funderburgh, M.L., *et al.* Human limbal biopsy-derived stromal stem cells prevent corneal scarring. Sci Transl Med **6,** 266ra172, 2014.
38. Kureshi, A.K., Dziasko, M.A., Funderburgh, J.L., and Daniels, J.T. Human corneal stromal stem cells support limbal epithelial cells cultured on RAFT tissue equivalents. Sci Rep **5,** 16186, 2015.
39. Rafat, M., Li, F., Fagerholm, P., *et al.* PEG-stabilized carbodiimide crosslinked collagen-chitosan hydrogels for corneal tissue engineering. Biomaterials **29,** 3960, 2008.
40. Liu, W., Deng, C., McLaughlin, C.R., *et al.* Collagen–phosphorylcholine interpenetrating network hydrogels as corneal substitutes. Biomaterials **30,** 1551, 2009.
41. Fagerholm, P., Lagali, N., Merrett, K., *et al.* A biosynthetic alternative to human donor tissue for inducing corneal regeneration: 24-month follow-up of a phase 1 clinical study. Sci Transl Med **2,** 46ra61, 2010.
42. Fagerholm, P., Lagali, N., Ong, J.A., *et al.* Stable corneal regeneration four years after implantation of a cell-free

recombinant human collagen scaffold. Biomaterials **35,** 2420, 2014.
43. Massie, I., Kureshi, A.K., Schrader, S., Shortt, A.J., and Daniels, J.T. Optimization of optical and mechanical properties of real architecture for 3-dimensional tissue equivalents: towards treatment of limbal epithelial stem cell deficiency. Acta Biomater **24,** 241, 2015.
44. Hong, H., Kim, H., Han, S.J., *et al.* Compressed collagen intermixed with cornea-derived decellularized extracellular matrix providing mechanical and biochemical niches for corneal stroma analogue. Mater Sci Eng C **103,** 109837, 2019.
45. Espandar, L., and Carlson, A.N. Lamellar keratoplasty: a literature review. J Ophthalmol **2013,** 2013, 894319.
46. Ganger, A., Tandon, R., Vanathi, M., and Sagar, P. Superficial anterior lamellar keratoplasty (salk) for trauma-induced post refractive surgery corneal opacity. J Ophthalmic Vis Res **11,** 326, 2016.
47. Hashimoto, Y., Funamoto, S., Sasaki, S., *et al.* Corneal regeneration by deep anterior lamellar keratoplasty (DALK) using decellularized corneal matrix. PLoS One **10,** e0131989, 2015.
48. Ahearne, M., and Lynch, A.P. Early observation of extracellular matrix-derived hydrogels for corneal stroma regeneration. Tissue Eng Part C Methods **21,** 1059, 2015.
49. He, Z., Forest, F., Bernard, A., *et al.* Cutting and decellularization of multiple corneal stromal lamellae for the bioengineering of endothelial grafts. Invest Ophthalmol Vis Sci **57,** 6639, 2016.
50. Choi, J.S., Williams, J.K., Greven, M., *et al.* Bioengineering endothelialized neo-corneas using donor-derived corneal endothelial cells and decellularized corneal stroma. Biomaterials **31,** 6738, 2010.
51. Ju, C., Gao, L., Wu, X., and Pang, K. A human corneal endothelium equivalent constructed with acellular porcine corneal matrix. Indian J Med Res **135,** 887, 2012.
52. Arnalich-Montiel, F., Moratilla, A., Fuentes-Julián, S., *et al.* Treatment of corneal endothelial damage in a rabbit model with a bioengineered graft using human decellularized corneal lamina and cultured human corneal endothelium. PLoS One **14,** e0225480, 2019.

Address correspondence to:
Mark Ahearne, PhD
Trinity Centre for Biomedical Engineering
Trinity Biomedical Science Institute
Trinity College Dublin
University of Dublin
Dublin D02 R590
Ireland

E-mail: ahearnm@tcd.ie

Received: January 23, 2020
Accepted: April 29, 2020
Online Publication Date: June 25, 2020

SCIENTIFIC REPORTS
nature research

Corrected: Author Correction

OPEN

The impact of decellularization methods on extracellular matrix derived hydrogels

Julia Fernández-Pérez[1,2] & Mark Ahearne[1,2*]

Tissue-derived decellularized biomaterials are ideal for tissue engineering applications as they mimic the biochemical composition of the native tissue. These materials can be used as hydrogels for cell encapsulation and delivery. The decellularization process can alter the composition of the extracellular matrix (ECM) and thus influence the hydrogels characteristics. The aim of this study was to examine the impact of decellularization protocols in ECM-derived hydrogels obtained from porcine corneas. Porcine corneas were isolated and decellularized with SDS, Triton X-100 or by freeze-thaw cycles. All decellularization methods decreased DNA significantly when measured by PicoGreen and visually assessed by the absence of cell nuclei. Collagen and other ECM components were highly retained, as quantified by hydroxyproline content and sGAG, by histological analysis and by SDS-PAGE. Hydrogels obtained by freeze-thaw decellularization were the most transparent. The method of decellularization impacted gelation kinetics assessed by turbidimetric analysis. All hydrogels showed a fibrillary and porous structure determined by cryoSEM. Human corneal stromal cells were embedded in the hydrogels to assess cytotoxicity. SDS decellularization rendered cytotoxic hydrogels, while the other decellularization methods produced highly cytocompatible hydrogels. Freeze-thaw decellularization produced hydrogels with the overall best properties.

The extracellular matrix (ECM) is primarily composed of structural and regulatory proteins and polysaccharides and is generated and maintained by cells. Many cellular functions, such as proliferation, migration or differentiation are regulated by the ECM[1]. Each organ and tissue is composed of a distinctive ECM, in its biochemical composition and structural organization. The properties of ECM are important in the fields of tissue engineering and regenerative medicine, which often aim to replicate the composition and structure of the ECM. By using synthetic or natural materials, three-dimensional scaffolds can be fabricated to repair or restore damaged organs and tissues.

One popular approach to generating scaffolds that try to imitate the tissues or organs ECM characteristics is to use decellularization. This technique involves the removal of cellular components from a tissue so that only the ECM remains. Many methods have been examined for performing decellularization and these can be divided into three main categories: physical, chemical and biological[2]. Physical methods include freeze-thawing cycles[3–6], high hydrostatic pressure[7–9] or supercritical CO_2[10–12]. Chemical agents can involve ionic detergents, such as sodium dodecyl sulphate (SDS)[13,14] or sodium deoxycholate[15]; non-ionic detergents, such as Triton X-100[16]; hypertonic or hypotonic salt solutions, such as sodium chloride[17,18]; and acids and bases, such as peracetic acid[19] or ammonium hydroxide[20]. Enzymes such as trypsin, dispase and phospholipase A2 have been used as biological methods for decellularization[21,22]. Furthermore, nucleases, such as DNAse, are used to promote the fragmentation of residual DNA into <200 bp fragments in order to minimize immunological responses[2]. Extensive research has been completed to optimize these decellularization procedures to allow for maximal cell removal and minimal ECM damage for each tissue/organ.

One difficulty associated with some decellularized tissues is their limited potential for recellularization. For many tissue-engineering applications, healthy cells need to be embedded into the ECM to generate a functional and viable tissue. To overcome this problem decellularized organs and tissues can be transformed into hydrogels that allow cells to be encapsulated throughout their structure. These hydrogels can then be used as injectables for minimally invasive delivery into irregular spaces[23–28] and for 3D printing of scaffolds[29–34]. Since the first

[1]Department of Mechanical and Manufacturing Engineering, School of Engineering, Trinity College Dublin, the University of Dublin, Dublin, Ireland. [2]Trinity Centre for Biomedical Engineering, Trinity Biomedical Science Institute, Trinity College Dublin, the University of Dublin, Dublin, Ireland. *email: ahearnm@tcd.ie

report of ECM-derived hydrogels in 1998[35], over 70 papers have appeared in the literature describing the use of ECM-derived hydrogels from a wide variety of organs[36]. ECM-derived hydrogels have been under investigation to treat several medical conditions. These include type 1 diabetes, where the hydrogel provided a matrix to delivery cells to the pancreas[27]; myocardial infarction by replacing damaged cardiac tissue[23], skin wounds[37], and keratoconus by using the ECM to 3D bioprint a corneal stromal substitute[38]. Despite the increasing interest in such hydrogels, the effect of different decellularization methods on the final hydrogel characteristics has not been widely studied.

The aim of this study was to examine the impact of three different decellularization protocols on ECM-derived hydrogels obtained from porcine corneas. Two detergent-based techniques (SDS and Triton X-100) and a freeze-thaw cycling technique were used to decellularize corneas and hydrogels were fabricated from the resulting ECM. The impact of these decellularization protocols were evaluated in terms of biochemical composition, transparency, gelation kinetics, mechanical properties and cytocompatibility.

Results

Biochemical characterization of decellularized material. The biochemical composition of the fabricated ECM hydrogels was analysed. PicoGreen was used to quantify DNA remnants, collagen content was measured by hydroxyproline quantification and sulphated glycosaminoglycans (sGAG) were quantified by dimethylmethylene blue assay (DMMB). All decellularization methods led to a significant reduction in DNA when compared to the non-decellularized control, i.e. hydrogels from native corneas (Fig. 1A). Collagen levels remained constant in all treatments (Fig. 1B). sGAG levels were maintained when decellularization was performed with Triton or the freeze-thaw methods, while SDS resulted in significant loss of sGAG (Fig. 1C). Furthermore, histological examination appeared to validate these results (Fig. 1D). Staining with haematoxylin & eosin confirmed the absence of cell nuclei after decellularization. Dense collagen was observed after picro-sirius red staining across all samples. Alcian blue staining showed the presence of sGAG in all hydrogels with a noticeable reduction in staining for the SDS treated group.

Further analysis of the composition of ECM-derived hydrogels was performed using SDS-PAGE and western blotting. SDS-PAGE showed the presence of collagen chains β, $\alpha 1$ and $\alpha 2$ for all conditions. Gamma chains were too heavy to be detected in a 7% polyacrylamide gel. Other lighter proteins were detected in the ECM-derived material lanes but not in a pure collagen type I control isolated from rat tail (Fig. 2). Immunodetection via western blot detected the presence of the corneal proteoglycan keratocan in all ECM-derived materials, independent of decellularization method, but not in rat tail derived collagen.

Light transmittance. Since ECM from cornea was used to fabricate the hydrogels in this study, it is necessary to examine the transparency of the hydrogels since this is required for corneal tissue engineering. Transparency was measured by quantifying the light absorbed by the material and from this calculating the amount of light transmitted through each sample. As seen in Fig. 3, all hydrogels allowed light to pass through them, although hydrogels decellularized using SDS and the native hydrogels were cloudier in appearance. Quantitatively, all hydrogels presented at least 50% light transmittance at the end of the visible spectrum. Hydrogels decellularized using the freeze-thaw method were the most transparent with transmittance values above 70%. These values are only slightly lower than full thickness porcine corneas.

Gelation kinetics. Gelation kinetics of ECM hydrogels were analysed by turbidimetric analysis. This technique is based on the increased in turbidity, and thus absorbance, experienced during collagen self-assembly. All samples presented a sigmoidal profile and gelled after a lag period or t_{lag} (Fig. 4). All treatments yielded hydrogels which started gelling after a longer lag phase than pure rat tail collagen (t_{lag} 7.93 ± 0.55 minutes). Freeze-thawing produced the earliest gelling material of all treatments (t_{lag} 16.43 ± 0.37 minutes), while SDS treated hydrogels took the longest to gel (t_{lag} 27.53 ± 1.36 minutes). However, there was no statistically significant difference between the different speeds at which the ECM-derived materials gelled. All values are displayed in Table 1.

Rheology of ECM hydrogels. Rheology was utilized to assess mechanical characteristics of the hydrogels. Increasing shear rates were used to calculate the viscosity at 15 °C, quite below gelling temperature. Shear thinning properties were observed in all pre-gel solutions, regardless of decellularization treatment (Fig. 5A). Storage modulus (G') and loss modulus (G'') were determined by following the gelation kinetics at 37 °C over time at a fixed frequency of 1 rad/s and 5% strain. All hydrogels had similar moduli values with no statistical significance among decellularization treatments (Fig. 5B). Only the Triton and the freeze-thaw groups were significantly weaker than the rat tail collagen hydrogels.

Evaluation of hydrogel ultrastructure. CryoSEM was employed to study the structure of the hydrogels in the least disruptive way. Samples were snap frozen in nitrogen, sublimated, freeze-fractured and coated for SEM imaging. SEM confirmed the porous and fibrillar structure of the hydrogels, without evident differences between treatments (Fig. 6). Some areas displayed inhomogeneity in the density of fibres.

Cytocompatibility. Human corneal stromal cells were embedded in the hydrogels to examine their cytocompatibility. Cell viability was assessed via calcein-acetoxymethyl ester and ethidium homodimer staining (Fig. 7A). After 1 day in culture, cells were highly viable in the Triton, freeze-thaw and native control hydrogel groups, while no viable cells were visible in the SDS treated group. Healthy cells presented an elongated morphology with small processes, indicating adhesion to the fibrillary architecture of the hydrogels. Over 5 days in culture, the hydrogels underwent significant contraction reflecting the ability of viable cells to actively attach and remodel the hydrogel (Fig. 7B,C). As expected from the viability assessment, the SDS hydrogel group did not undergo contraction. Hydrogels obtained from the SDS decellularization protocol were cytotoxic presumably

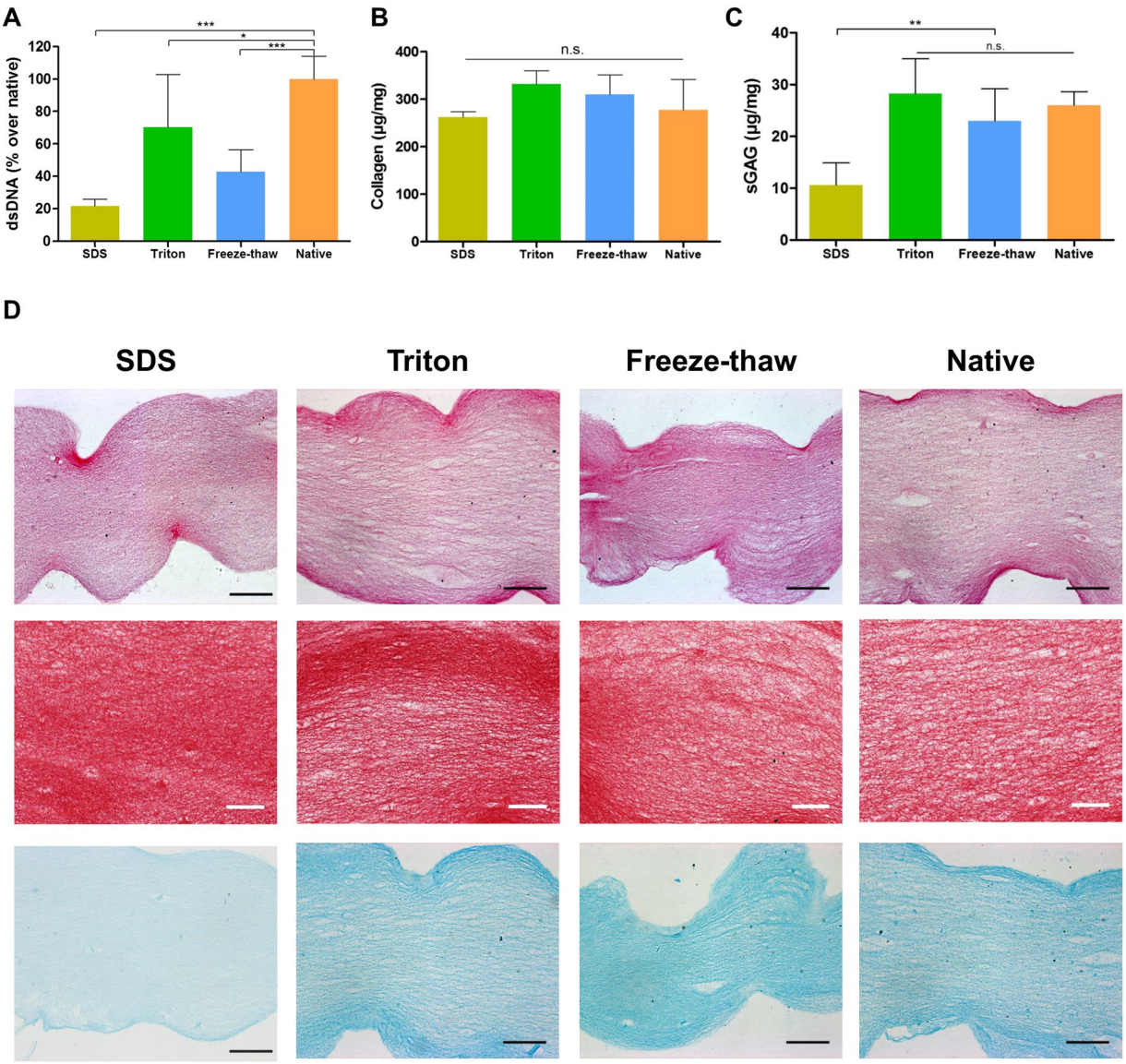

Figure 1. Evaluation of decellularization of ECM-derived hydrogels: (**A**) Quantification of dsDNA, (**B**) Collagen, and (**C**) sGAG; *$p < 0.05$, **$p < 0.01$, ***$p < 0.001$; (**D**) histological examination of hydrogels, stained with haematoxylin and eosin, picro-sirius red and Alcian blue; black scale bar = 100 µm, white scale bar = 50 µm.

due to inefficient washing after decellularization. To confirm this hypothesis the presence of detergent residues was determined using a methylene blue active substances (MBAS) assay, which is widely used in water quality control[39]. This assay is based on the binding of the cations in methylene blue with the anions from the detergent that are extracted into the organic phase when in contact with chloroform. Methylene blue extraction confirmed the presence of SDS remnants in the hydrogel thus would explain their cytotoxicity (Fig. 7D).

Discussion

ECM-derived hydrogels offer great promise as biomaterials for tissue engineering as they can be delivered to the site in need in a minimally invasive manner, allow cell encapsulation prior to delivery, but can also allow for neighbouring cell recruitment. ECM hydrogel solutions have also been used as a bioink for 3D bioprinting several different tissues and organs[29,40,41]. In this study, ECM-derived hydrogels were obtained from corneas decellularized using three different methods. All decellularization methods decreased DNA significantly and retained collagen and other ECM components. All hydrogels were highly transparent, with the freeze-thaw group showing the best optical properties. Gelation kinetics were affected by the decellularization method employed but not the rheological properties. Hydrogels presented a porous and fibrillary structure. Hydrogels were highly cytocompatible when Triton and freeze-thawing methods were used for decellularization, but cytocompatibility was compromised when using SDS as decellularization agent. This work highlights the influence that the decellularization process has on final properties of ECM-derived hydrogels.

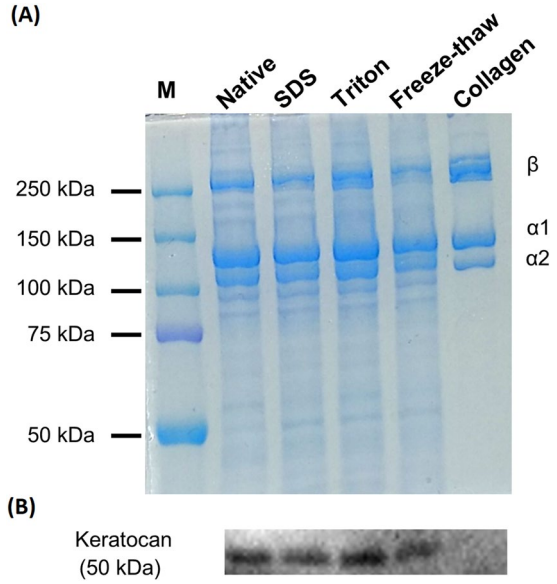

Figure 2. (**A**) Biochemical composition of ECM-derived hydrogels via SDS-PAGE (7%); (**B**) western blot against keratocan; M = molecular weight ladder.

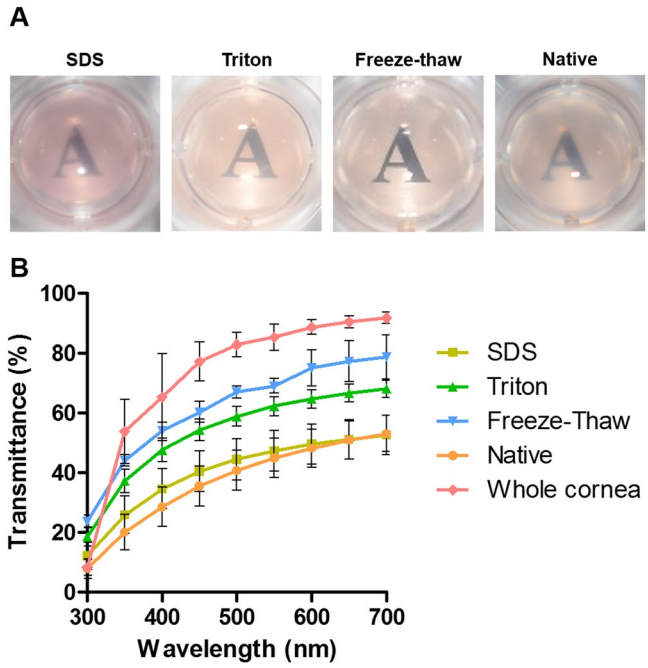

Figure 3. Transparency analysis of ECM-derived hydrogels: (**A**) Macroscopic appearance with hydrogels placed over printed text; (**B**) light transmittance quantification over the visible spectrum of light.

One of the main benefits of using ECM-derived hydrogels is the ability to retain multiple ECM components that may not be present in other natural or synthetic hydrogels and therefore more closely mimics the native tissues. Composition analysis of the digested materials via SDS-PAGE confirmed the presence of multiple ECM components when compared to rat tail collagen which just consists of collagen type I. Keratocan, a small leucine-rich proteoglycan almost exclusively found in the cornea, was detected in the ECM-derived hydrogels, irrespective of the decellularization method used. However, this study did show that the choice of decellularization technique is important with SDS decellularization retaining less sGAG than the other techniques tested. This removal of sGAG following decellularization has been previously reported for cornea[14,18,42,43], cartilage[29,44], ligament[45] and adipose tissue[29]. While this study demonstrated that the ECM composition was affected by the decellularization technique used, other techniques may be used to identify more specific tissue or organ ECM components such as mass spectrometry[46–49] or enzyme-linked immunosorbent assays (ELISA)[32,33,50].

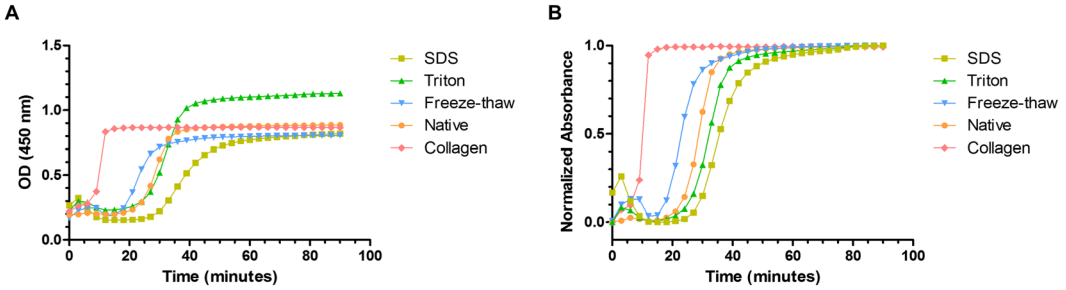

Figure 4. Gelation kinetics of ECM-derived hydrogels via turbidimetric analysis: (**A**) Raw values; (**B**) normalized data.

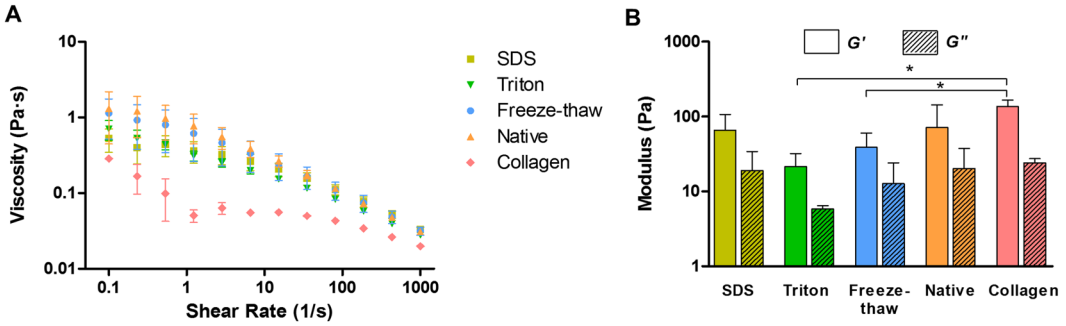

Figure 5. Rheology analysis of ECM-derived hydrogels: (**A**) Viscosity measurements at increasing shear rates; (**B**) storage modulus (G′) and loss modulus (G′); *$p < 0.05$.

Condition	*S*	$t_{1/2}$ *(min)*	t_{lag} *(min)*
SDS	0.061 (±0.006)	35.75 (±1.86)	27.53 (±1.36)
Triton	0.070 (±0.003)	32.14 (±0.33)	24.94 (±0.28)
Freeze-thaw	0.075 (±0.002)	23.11 (±0.35)	16.43 (±0.37)
Native	0.090 (±0.002)	28.04 (±1.51)	22.51 (±1.37)
Collagen	0.235 (±0.026)	10.08 (±0.33)	7.93 (±0.55)

Table 1. Turbidimetric analysis results of ECM-derived hydrogels. Average ± SD.

One potential limitation with using ECM-derived hydrogels is that GAGs and various collagen types, such as collagen type V have been shown to interfere in collagen type I self-assembly *in vitro*[51–53]. *In vivo* small leucine-rich proteoglycans, such as keratocan and decorin in the cornea, play an important role in collagen fibrillogenesis, in terms of collagen assembly nucleation and linear and lateral fibril growth[54]. Therefore, the difference in gelation kinetics between the commercially available collagen type I and the ECM-derived hydrogels can be explained by the presence of ECM components other than collagen type I. Studies from ECM-derived hydrogels from other sources have reported a delay in fibrillogenesis (lag phase) similar to what was shown here. For example, hydrogels obtained from demineralized and decellularized bone showed a short lag phase of around 9 minutes[55], while myocardium ECM presented a long lag phase of 40 minutes[56]. Hydrogels obtained from urinary bladder matrix[57], dermis[19] and pancreas[58] presented lag periods in a similar range to the ones reported in this study, between 15 and 25 minutes. Furthermore, the presence of detergent remnants might have an influence in the increased gelation time seen in SDS hydrogels. When we attempted to use concentrations above 0.1% SDS for decellularization, it was found that hydrogels could not be formed. This is in agreement with findings from Gaetani and colleagues who could not fabricate pancreas ECM-derived hydrogels when they used 1% SDS for decellularization[58].

Pre-gel solutions presented shear thinning characteristics, i.e. viscosity decreases as shear rate increases. Values presented here are in accordance to those reported for ECM-derived hydrogels from myocardium[56], dermis[19], urinary bladder matrix[57] skeletal muscle[24] and cornea[50]. This characteristic offers the potential for these gels to be used as an injectable biomaterial and for their use as bioinks in 3D bioprinting[29–34]. Gelation profiles seen with turbidimetric analysis were also obtained when using rheology. Despite being more concentrated than the rat tail collagen hydrogels, the cornea ECM-derived hydrogels were softer. However, these values are in a similar range to the ones found in hydrogels derived from other tissues[55,57]. The values are lower than those reported for

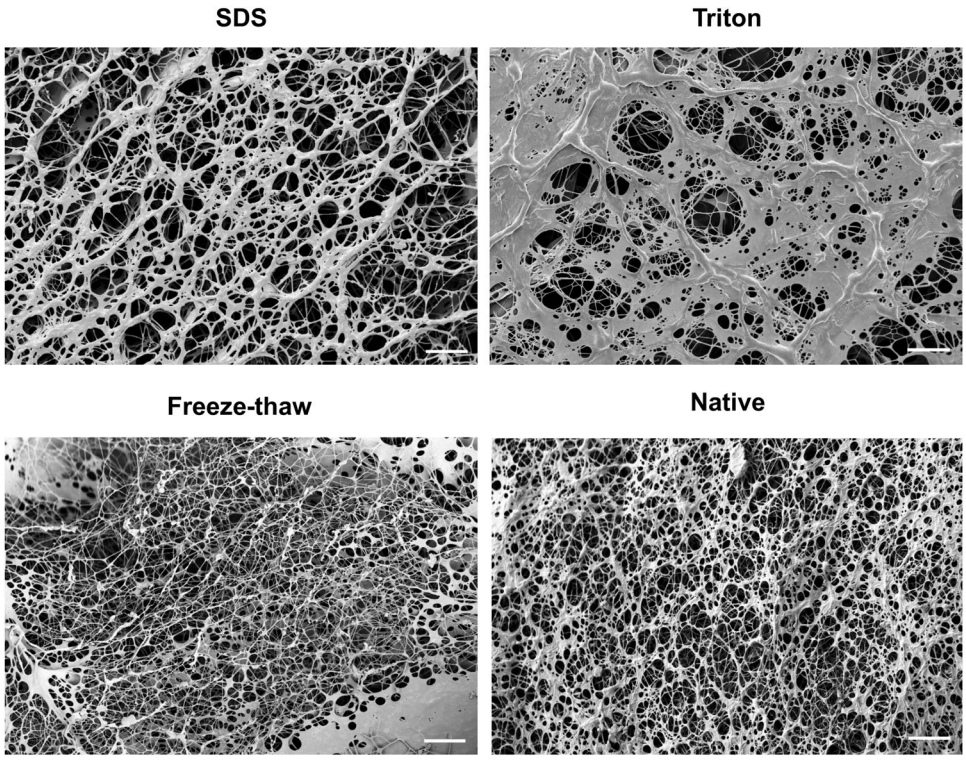

Figure 6. CryoSEM micrographs of ECM-derived hydrogels at ~1000x; scale bar = 10 µm.

the storage and loss moduli of the native cornea, which are 2 kPa and 0.3 kPa, respectively[59]. Additional steps such as cross-linking[60] may be required to increase the modulus of the hydrogels to match the native corneas.

In this study, cryoSEM was used to investigate the ultrastructure of the hydrogels. This technique is believed to be better at retaining the hydrogel's structure compared to conventional SEM as the water present in the highly hydrated hydrogels is sublimated at extremely low temperatures[61]. The hydrogels obtained here were highly fibrillar and porous, which closely resembled the structure reported for ECM-derived hydrogels from other tissues, such as dermis[19], myocardium[56], demineralized bone[55] and small intestinal submucosa[35]. These studies imaged the hydrogels using conventional SEM after glutaraldehyde fixation and critical point drying of the samples. Johnson and colleagues also described the presence of areas of higher fibre matrix density than others, which prevented implementation of automatized pore size quantification[56].

In the current study, standard gelation parameters where used that can influence the hydrogels properties if modified. Johnson and colleagues studied the effect of temperature, ionic strength, pH and ECM concentration on the fibril architecture, mechanical properties and gelation kinetics of myocardium ECM-derived hydrogels[56]. They showed that no hydrogels could be formed at 4 °C and 22 °C, while at 37 °C they obtained robust hydrogels. Fibre diameter was not influenced by any of the conditions studied. Similar to our results, the authors reported areas of increased fibre density visualized by SEM. The effect that reduction of ionic strength to 0.5x PBS was striking as it increased mechanical properties and sped up gelation. pH did not influence any of the analysed parameters. Increase in ECM concentration increased mechanical properties and viscosity as reported for urinary bladder matrix[57], bone[55] and dermis[19].

Furthermore, tissue origin plays an important role in hydrogel characteristics. It has been shown that porcine myocardium hydrogels retain more sGAG and have increased strength than healthy human myocardium hydrogels[49]. While using human tissues would ease the translation into the clinic as the issue of xenoimmunogenicity is avoided, sourcing healthy organs is difficult as these would be required for transplantation. However, for the cornea specifically, human corneas deemed unsuitable for transplantation due to low endothelial cell count, have the potential to be used to manufacture hydrogels. Decellularized porcine corneas have been used clinically as alternatives to donor grafts[62,63], paving the path for other treatments based on ECM-derived materials.

Cells embedded within the hydrogels presented high viability and adopted a spindle morphology with multiple processes, indicating good adhesion to the fibres, except in the SDS group. Over the culturing period, the hydrogels contracted, as reported by Wolf and colleagues using dermal ECM-derived hydrogels[19]. This contraction effect was due to the traction forces exerted by the cells on the collagen fibrils. However, when cells died as in the SDS case, the hydrogels retained their shape and size. Depending on the application, the rate of contraction might limit the usefulness of these hydrogels without further cross-linking to strengthen them[60] or using a cell culture condition that inhibits contractile behaviour[64,65]. Furthermore, contraction can also be inhibited when the hydrogel adheres to a material or is constrained at the edges[66]. When the hydrogel adheres to the tissue matrix, it will be less able to contract compared to a free-floating hydrogel in culture medium.

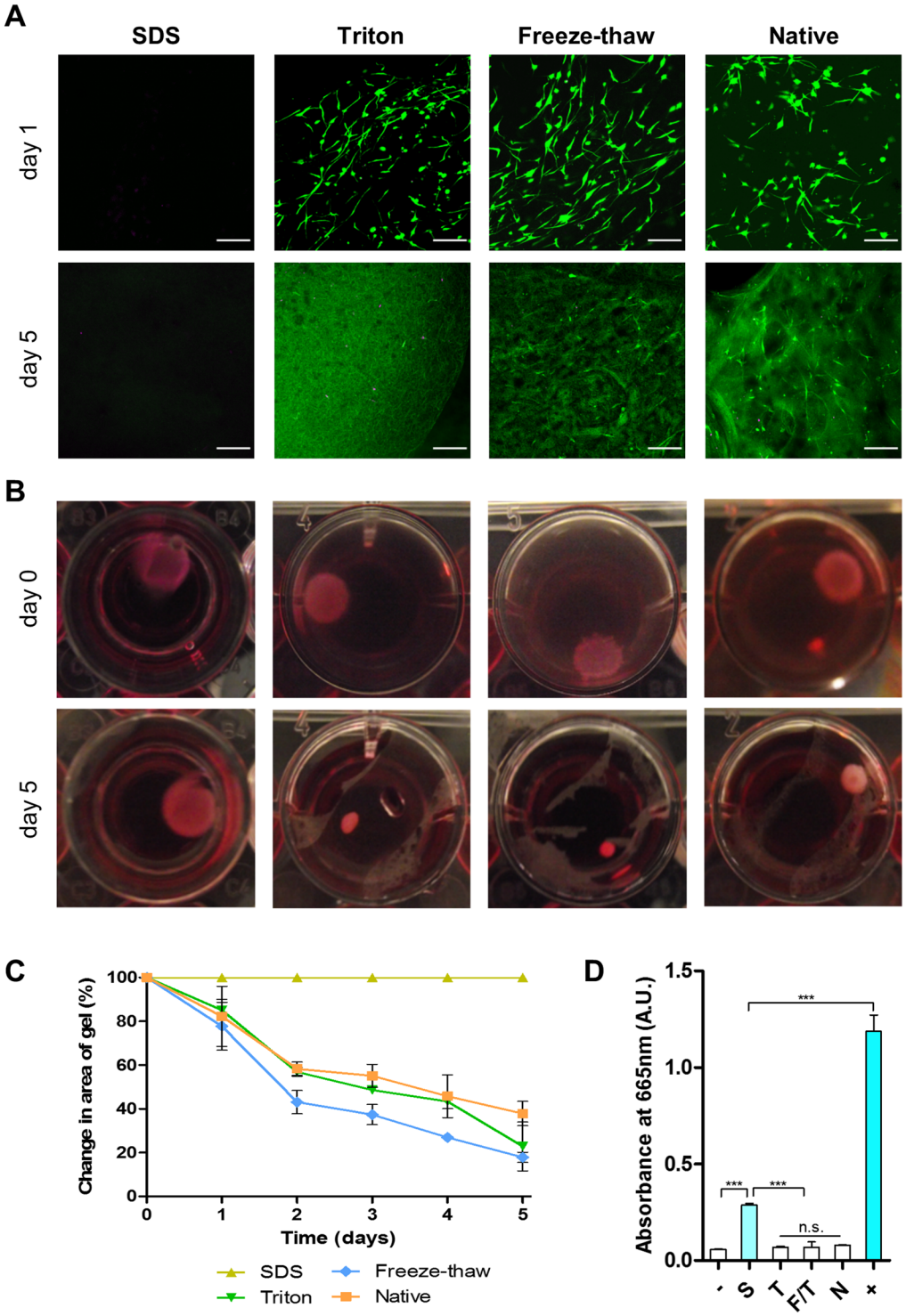

Figure 7. Cell activity in ECM-derived hydrogels: (**A**) Cell viability assessment (green = live, magenta = dead, scale bar = 200 µm); (**B**) macroscopic images of cell-laden hydrogels over time in culture; (**C**) quantification of hydrogel area over time; (**D**) quantification of methylene blue absorbance in the organic phase; *$p < 0.05$, **$p < 0.01$, ***$p < 0.001$.

In this study, all steps were performed under sterile conditions so that no final sterilization method was required. However, for clinical purposes authorities may require terminal sterilization. It has been shown that common sterilization techniques such as electron beam, gamma irradiation or ethylene oxide inhibit gel formation when performed on the powder, but not when the lyophilized digest is treated[12]. Furthermore, sterilizing the lyophilized digest could increase the likelihood of translation into the clinic as a ready-to-use product, whereby

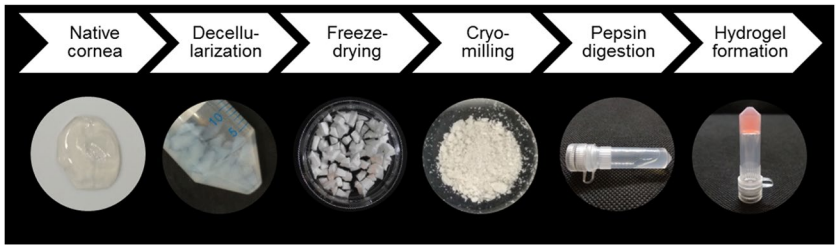

Figure 8. Main steps in the fabrication of cornea ECM-derived hydrogels.

the clinician can rehydrate the lyophilize digest with a basic salt balanced solution and let the hydrogel form *in situ*.

Future studies are required to assess the suitability of these hydrogels before they can be used for clinical applications. The hydrogels will need to be tested *in vivo* to evaluate the immunological response and ability to integrate with the surrounding tissue. The survival and functionality of the hydrogels would also need to be monitored. Should the hydrogel not induce any negative effects *in vivo* then the potential for hydrogels to replace damaged or diseased tissue could be explored using suitable animal models. For example in the cornea, the potential for ECM-derived hydrogels to replace tissue damaged due to trauma or diseases such as keratoconus could be explored. This is important due to a global shortage of donor corneas available for transplantation[67].

In summary, here we demonstrated the importance that the decellularization method has on the final characteristics of ECM-derived hydrogels using corneas as tissue model. Similar phenomena would be expected for hydrogels derived from the ECM of other tissues although the precise decellularization protocol should be specific to the tissue type. We would therefore recommend that researchers or companies involved in the development of ECM-derived hydrogels examine different decellularization techniques to find the optimal approach for preparing their hydrogels.

Materials and Methods

Decellularization of porcine corneas. Porcine ocular globes were obtained from a local slaughterhouse. The remaining pieces of flesh were removed and, under aseptic conditions, the eyes were immersed in 2% iodine solution (Videne, Ecolab, Belgium) in sterile phosphate buffer saline (PBS) for one minute, gently rocking throughout. The eyes were subsequently washed twice in sterile PBS and the central corneal button was excised using scissors and cut into small pieces (2 mm × 2 mm, approximately). Three decellularization methods were tested:

(a) SDS (anionic detergent): each corneal button was immersed in 3 ml of 0.1% (w/v) sodium dodecyl sulphate (SDS, Sigma-Aldrich) solution for 72 hours under rotation. Solution was exchanged every 24 hours.
(b) Triton (non-ionic detergent): each corneal button was immersed in 3 ml of 1% (v/v) Triton X-100 (Sigma-Aldrich) solution for 72 hours under rotation. Solution was exchanged every 24 hours.
(c) Freeze-thaw (mechanical procedure): each corneal button was immersed in 5 ml sterile deionized H_2O and placed in a −80 °C freezer for a minimum of 5 hours. Thereafter, they were let to thaw at room temperature. Once thawed, the solution was exchanged and the procedure repeated until 5 freeze-thaw cycles had been completed.

Afterwards, all corneas where subjected to a DNAse treatment for 1 hour at 37 °C under rotation. DNAse (Sigma-Aldrich) was used at a concentration of 10 U/ml prepared in 10 mM magnesium chloride buffer at pH 7.5. Corneas where extensively washed with sterile deionized water for 72 hours, with solution exchanged every 24 hours, under gentle rotation. Finally, decellularized corneas where dehydrated using a freeze drier and turned into powder by cryomilling (SPEX SamplePrep Freeze/Mill). Non-decellularized corneas were lyophilized and cryomilled to be used as controls (native).

Hydrogel formation. ECM hydrogels were prepared as previously described[68]. Briefly, ECM powder was dissolved in 1 mg/ml pepsin solution in 0.1 M hydrochloric acid at a concentration of 20 mg/ml and incubated for 72 hours at room temperature under slow rotation. Hydrogels were formed by neutralizing the solution with 1 N NaOH, balancing salt concentration using 10x PBS and incubating at 37 °C for one hour to induce fibrillation. Hydrogels had a final ECM concentration of 16 mg/ml. This process is depicted in Fig. 8. Rat tail collagen type 1 hydrogels were fabricated as described previously[68] and used as a control for some studies.

Biochemical quantification. Quantification of dsDNA, sGAG and collagen was performed after papain digestion of 100 µl hydrogels. DNA was quantified with the Quant-iT PicoGreen dsDNA Assay Kit (Invitrogen), following manufacturer's specifications. sGAG quantification was performed using dimethylmethylene blue dye-binding assay (Blyscan, Biocolor). Collagen content was inferred by measuring the content of hydroxyproline using a chloramine T assay[69,70].

Histology. Hydrogels were fixed in 4% paraformaldehyde and processed for wax embedding. 6 µm-thick slices of each sample were cut, attached to a glass slide, dewaxed, rehydrated and stained as follows. Haematoxylin & eosin was used to visualize any nuclei still present after decellularization. Slides were stained with Harris

Haematoxylin (Sigma-Aldrich) for 4 minutes, followed by a 10-minute wash with running tap water. Then slides were immersed in acid alcohol for 30 seconds and washed with tap water for 5 minutes. Finally, slides were stained with Eosin Y (Sigma-Aldrich) for 2 minutes. Picro-sirius red was used to assess collagen distribution. Slides were stained with Sirius Red (Sigma-Aldrich) in a saturated aqueous solution of picric acid for one hour and then for one minute in 0.5% acetic acid. Alcian blue was used to assess sGAG content. Slides were stained with 1% Alcian Blue 8GX (Sigma-Aldrich) in 0.1 M HCl for 5 minutes followed by three 30-second washes in dH_2O. After staining, all slides were dehydrated and coverslipped using DPX.

SDS-PAGE and western blot. 7.5% polyacrylamide gels were cast and loaded with 50 µg of sample mixed with Laemmli buffer (1:1) that was previously boiled for 5 minutes. Gels were run for 90 minutes at 120 V. Gels were then stained with GelCode (Thermo-Fisher) following manufacturer's directions. For western blot, 100 µg were loaded into precast 12% SDS-PAGE gels (Biorad) and run at 200 V for 45 minutes. Gels were transferred to a PVDF membrane using a semi-dry transfer system (Thermo-Fisher) with Pierce 1-step transfer buffer (Thermo-Fisher). The membrane was activated with methanol and then blocked overnight at 4 °C with 3% BSA. Primary antibody (keratocan, sc-66941, Santa Cruz) was used at a dilution of 1:200 in 3% BSA and incubated overnight at 4 °C. Three 5-minute washes with TBST were performed under agitation, and then the HRP-linked secondary antibody (A0545, Sigma-Aldrich) at a dilution of 1:1000 was incubated for an hour at room temperature. Another set of washing steps was carried out and then membranes were developed with Western Chemiluminescent HRP Substrate (Fisher Scientific). Membranes were imaged with GelDoc (Biorad).

Transparency. The macroscopic appearance and transparency of the gels was assessed by placing them over printed text. Subsequently, light transmittance was quantified. The absorbance of light at several wavelengths ranging from 350 to 700 nm was determined with a microplate reader (BioTek Synergy HTX). Deionized water was used as a baseline control. The transmittance of light was calculated using the following formula:

$$\%Transmittance = 10^{2-Absorbance}$$

Gelation kinetics. Gelation kinetics was determined via turbidimetric spectrophotometric analysis, as described elsewhere[57]. Briefly, 100 µl hydrogels were casted into 96-well plates at 4 °C and inserted in a plate reader pre-heated at 37 °C (BioTek Synergy HTX). Absorbance at 405 nm wavelength was measured every 3 minutes for 90 minutes. Absorbance values were normalized with the following formula:

$$NA = (A - A_0)/(A_{max} - A_0)$$

where NA is the normalized absorbance, A is the absorbance at any given time, A_0 is the initial absorbance and A_{max} is the maximal absorbance.

The lag phase (t_{lag}) was calculated by obtaining the linear portion of the curve and extrapolating the time value at which the normalized absorbance is 0. Similarly, $t_{1/2}$ was determined as the time at which the normalized absorbance is 0.5. The slope of the linear portion of the curve determined the gelation speed (S).

Rheology. All rheological experiments were performed using a MCR 102 rheometer (Anton Paar, Austria) equipped with temperature controlling systems and using a 25 mm diameter parallel plate. Viscosity of pre-gel solutions was measured by performing a frequency sweep, from 0.1 to 1000 Hz, at 5% strain at 15 °C. Viscosity constants can be found in Supplementary Table S1. Storage and loss moduli were calculated with fixed frequency of 1 rad/s and 5% strain. Pre-gel solutions were applied at 4 °C and left equilibrate during 10 minutes, after which temperature was raised to 37 °C to induce gelation. Measurements where stopped once G' values plateaued.

CryoSEM. Hydrogels were snap-frozen in nitrogen for 5 seconds, sublimated for 40 minutes at −100 °C and 10^{-5} Pa, freeze fractured and sputter coated with platinum for 20 seconds. These were then imaged with a scanning electron microscope at 5 kV (Ultra 2 Zeiss, Germany, with a Quorum Technologies CryoSEM Preparation System, UK).

Cell culture. Human corneal stromal cells were isolated and cultured as previously described in accordance with the Declaration of Helsinki[64]. The use of human cornea tissue with donor consent for isolating cells received ethical approval from the Trinity College Dublin, University of Dublin, School of Medicine Research Ethics Committee. 100,000 cells were embedded in each 100 µl hydrogel and cast in the wells of a 96-well plate. After gelation, hydrogels were released from the wells and transferred to 24-well plates. Constructs were fed every second day with low glucose DMEM (Hyclone) supplemented with 10% FBS, 100 U/ml Penicillin 100 µg/ml Streptomycin (both Gibco). Cell viability was assessed at day 1 and day 5 by staining the constructs with 2 µM calcein-acetoxymethyl ester and 4 µM ethidium homodimer-1 in PBS for 1 hour at 37 °C in a humidified incubator. Cells were then imaged via laser scanning confocal microscopy (Leica SP8). Furthermore, the shape of the hydrogels was monitored and images were taken daily over 5 days. The area of the hydrogels was calculated using Image J (NIH) and was plotted as the percentage of change of area with time.

Methylene blue active substances (MBAS) assay. MBAS assay was performed with some modifications from previously described methods[71]. A methylene blue (Sigma-Aldrich) solution was prepared in water to a final concentration of 250 µg/ml. 1 mg of cryomilled powder from each experimental group was mixed with 1 ml of distilled water and vortexed thoroughly for 1 minute and spun down for 30 seconds on a mini-centrifuge. 250 µl of this supernatant was mixed with 250 µl methylene blue solution and vortexed. Then 1 ml of chloroform was added, vortexed 3 times for 30 seconds and centrifuged for 1 minute using a benchtop centrifuge. A negative

control was obtained using 250 µl distilled water and a positive control using 250 µl of 0.5% SDS solution. A phase separation was evident in all tests and visually the SDS group had a blue coloration in the organic (bottom) phase. This was further quantified by measuring the absorbance of the bottom phase at 665 nm using a plate reader (BioTek Synergy HTX).

Statistics analysis. GraphPad Prism Software 5.0 (GraphPad Software, Inc. La Jolla, CA, USA) was used to perform statistical analyses. All data are presented as the mean ± SD. One-way ANOVA with Tuckey post-hoc analyses were performed to determine statistical significance. Differences were considered to be statistically significant at $p \leq 0.05$.

Received: 20 June 2019; Accepted: 28 August 2019;

Published online: 17 October 2019

References

1. Frantz, C., Stewart, K. M. & Weaver, V. M. The extracellular matrix at a glance. *J. Cell Sci.* **123**, 4195–4200 (2010).
2. Crapo, P. M., Gilbert, T. W. & Badylak, S. F. An overview of tissue and whole organ decellularization processes. *Biomaterials* **32**, 3233–3243 (2011).
3. Proulx, S. *et al*. Tissue engineering of feline corneal endothelium using a devitalized human cornea as carrier. *Tissue Eng. Part A* **15**, 1709–18 (2009).
4. Ide, C., Tohyama, K., Yokota, R., Nitatori, T. & Onodera, S. Schwann cell basal lamina and nerve regeneration. *Brain Res.* **288**, 61–75 (1983).
5. Utomo, L. *et al*. Preparation and characterization of a decellularized cartilage scaffold for ear cartilage reconstruction. *Biomed. Mater.* **10**, 015010 (2015).
6. Rahman, S., Griffin, M., Naik, A., Szarko, M. & Butler, P. E. M. Optimising the decellularization of human elastic cartilage with trypsin for future use in ear reconstruction. *Sci. Rep.* **8**, 3097 (2018).
7. Hashimoto, Y. *et al*. Ultrastructural analysis of the decellularized cornea after interlamellar keratoplasty and microkeratome-assisted anterior lamellar keratoplasty in a rabbit model. *Sci. Rep.* **6**, 27734 (2016).
8. Santoso, E. G. *et al*. Application of detergents or high hydrostatic pressure as decellularization processes in uterine tissues and their subsequent effects on *in vivo* uterine regeneration in murine models. *PLoS One* **9**, e103201 (2014).
9. Funamoto, S. *et al*. The use of high-hydrostatic pressure treatment to decellularize blood vessels. *Biomaterials* **31**, 3590–3595 (2010).
10. Guler, S., Aslan, B., Hosseinian, P. & Aydin, H. M. Supercritical carbon dioxide-assisted decellularization of aorta and cornea. *Tissue Eng. Part C Methods* **23**, 540–547 (2017).
11. Seo, Y., Jung, Y. & Kim, S. H. Decellularized heart ECM hydrogel using supercritical carbon dioxide for improved angiogenesis. *Acta Biomater.* **67**, 270–281 (2018).
12. White, L. J. *et al*. The impact of sterilization upon extracellular matrix hydrogel structure and function. *J. Immunol. Regen. Med.* **2**, 11–20 (2018).
13. Zilic, L. & Wilshaw, S.-P. & Haycock, J. W. Decellularisation and histological characterisation of porcine peripheral nerves. *Biotechnol. Bioeng.* **113**, 2041–53 (2016).
14. Lynch, A. P., Wilson, S. L. & Ahearne, M. Dextran preserves native corneal structure during decellularization. *Tissue Eng. Part C Methods* **22**, 561–572 (2016).
15. Price, A. P. *et al*. Automated decellularization of intact, human-sized lungs for tissue engineering. *Tissue Eng. Part C Methods* **21**, 94–103 (2015).
16. Choi, J. S. *et al*. Bioengineering endothelialized neo-corneas using donor-derived corneal endothelial cells and decellularized corneal stroma. *Biomaterials* **31**, 6738–6745 (2010).
17. Luo, H. *et al*. Construction of tissue-engineered cornea composed of amniotic epithelial cells and acellular porcine cornea for treating corneal alkali burn. *Biomaterials* **34**, 6748–6759 (2013).
18. González-Andrades, M. *et al*. Generation of bioengineered corneas with decellularized xenografts and human keratocytes. *Investig. Ophthalmol. Vis. Sci.* **52**, 215–220 (2011).
19. Wolf, M. T. *et al*. A hydrogel derived from decellularized dermal extracellular matrix. *Biomaterials* **33**, 7028–7038 (2012).
20. Baptista, P. M. *et al*. The use of whole organ decellularization for the generation of a vascularized liver organoid. *Hepatology* **53**, 604–617 (2011).
21. Chen, R.-N., Ho, H.-O., Tsai, Y.-T. & Sheu, M.-T. Process development of an acellular dermal matrix (ADM) for biomedical applications. *Biomaterials* **25**, 2679–86 (2004).
22. Wu, Z. *et al*. The use of phospholipase A2 to prepare acellular porcine corneal stroma as a tissue engineering scaffold. *Biomaterials* **30**, 3513–3522 (2009).
23. Singelyn, J. M. *et al*. Naturally derived myocardial matrix as an injectable scaffold for cardiac tissue engineering. *Biomaterials* **30**, 5409–5416 (2009).
24. Ungerleider, J. L., Johnson, T. D., Rao, N. & Christman, K. L. Fabrication and characterization of injectable hydrogels derived from decellularized skeletal and cardiac muscle. *Methods* **84**, 53–59 (2015).
25. Wang, J. Y. *et al*. Neurorestorative effect of urinary bladder matrix-mediated neural stem cell transplantation following traumatic brain injury in rats. *CNS Neurol. Disord. Drug Targets* **12**, 413–425 (2013).
26. Zhang, L. *et al*. Effect of an inductive hydrogel composed of urinary bladder matrix upon functional recovery following traumatic brain injury. *Tissue Eng. Part A* **19**, 1909–18 (2013).
27. Chaimov, D. *et al*. Innovative encapsulation platform based on pancreatic extracellular matrix achieve substantial insulin delivery. *J. Control. Release* **257**, 91–101 (2017).
28. Lin, C.-Y., Liu, T.-Y., Chen, M.-H., Sun, J.-S. & Chen, M.-H. An injectable extracellular matrix for the reconstruction of epidural fat and the prevention of epidural fibrosis. *Biomed. Mater.* **11**, 035010 (2016).
29. Pati, F. *et al*. Printing three-dimensional tissue analogues with decellularized extracellular matrix bioink. *Nat. Commun.* **5**, 1–11 (2014).
30. Pati, F. *et al*. Biomimetic 3D tissue printing for soft tissue regeneration. *Biomaterials* **62**, 164–175 (2015).
31. Jang, J. *et al*. Tailoring mechanical properties of decellularized extracellular matrix bioink by vitamin B2-induced photo-crosslinking. *Acta Biomater.* **33**, 88–95 (2016).
32. Jang, J. *et al*. 3D printed complex tissue construct using stem cell-laden decellularized extracellular matrix bioinks for cardiac repair. *Biomaterials* **112**, 264–274 (2017).
33. Skardal, A. *et al*. A hydrogel bioink toolkit for mimicking native tissue biochemical and mechanical properties in bioprinted tissue constructs. *Acta Biomater.* **25**, 24–34 (2015).

34. Choi, Y. J. *et al*. 3D cell printing of functional skeletal muscle constructs using skeletal muscle-derived bioink. *Adv. Healthc. Mater.* **5**, 2636–2645 (2016).
35. Voytik-Harbin, S. L., Brightman, A. O., Waisner, B. Z., Robinson, J. P. & Lamar, C. H. Small intestinal submucosa: a tissue-derived extracellular matrix that promotes tissue-specific growth and differentiation of cells *in vitro*. *Tissue Eng.* **4**, 157–174 (1998).
36. Saldin, L. T., Cramer, M. C., Velankar, S. S., White, L. J. & Badylak, S. F. Extracellular matrix hydrogels from decellularized tissues: Structure and function. *Acta Biomater.* **49**, 1–15 (2017).
37. Engel, H. *et al*. Investigation of Dermis-derived hydrogels for wound healing applications. *Biomed. J.* **38**, 58–64 (2015).
38. Kim, H. *et al*. Shear-induced alignment of collagen fibrils using 3D cell printing for corneal stroma tissue engineering. *Biofabrication* **11**, 035017 (2019).
39. George, A. L. & White, G. F. Optimization of the methylene blue assay for anionic surfactants added to estuarine and marine water. *Environmental Toxicology and Chemistry* **18**, (1999).
40. Lee, H. *et al*. Development of liver decellularized extracellular matrix bioink for three-dimensional cell printing-based liver tissue engineering. *Biomacromolecules* **18**, 1229–1237 (2017).
41. Kim, B. S., Kim, H., Gao, G., Jang, J. & Cho, D. W. Decellularized extracellular matrix: A step towards the next generation source for bioink manufacturing. *Biofabrication* **9**, (2017).
42. Pang, K., Du, L. & Wu, X. A rabbit anterior cornea replacement derived from acellular porcine cornea matrix, epithelial cells and keratocytes. *Biomaterials* **31**, 7257–7265 (2010).
43. Sasaki, S. *et al*. *In vivo* evaluation of a novel scaffold for artificial corneas prepared by using ultrahigh hydrostatic pressure to decellularize porcine corneas. *Mol. Vis.* **15**, 2022–2028 (2009).
44. Elder, B. D., Eleswarapu, S. V. & Athanasiou, K. A. Extraction techniques for the decellularization of tissue engineered articular cartilage constructs. *Biomaterials* **30**, 3749–3756 (2009).
45. Gratzer, P. F., Harrison, R. D. & Woods, T. Matrix alteration and not residual sodium dodecyl sulfate cytotoxicity affects the cellular repopulation of a decellularized matrix. *Tissue Eng.* 2975–2983, https://doi.org/10.1089/ten.2006.12.ft-234 (2006).
46. Odorico, J. S. *et al*. Extracellular matrix scaffold and hydrogel derived from decellularized and delipidized human pancreas. *Sci. Rep.* **8**, 1–16 (2018).
47. DeQuach, J. A. *et al*. Simple and high yielding method for preparing tissue specific extracellular matrix coatings for cell culture. *PLoS One* **5**, e13039 (2010).
48. Farnebo, S. *et al*. Design and characterization of an injectable tendon hydrogel: a novel scaffold for guided tissue regeneration in the musculoskeletal system. *Tissue Eng. Part A* **20**, 1550–1561 (2014).
49. Johnson, T. D. *et al*. Human versus porcine tissue sourcing for an injectable myocardial matrix hydrogel. *Biomater. Sci.* **2**, 735–744 (2014).
50. Kim, H. *et al*. Characterization of cornea-specific bioink: high transparency, improved *in vivo* safety. *J. Tissue Eng.* **10**, 1–12 (2019).
51. Birk, D. E., Fitch, J. M., Babiarz, J. P., Doane, K. J. & Linsenmayer, T. F. Collagen fibrillogenesis *in vitro*: interaction of types I and V collagen regulates fibril diameter. *J. Cell Sci.* **95**, (1990).
52. Pins, G. D., Christiansen, D. L., Patel, R. & Silver, F. H. Self-assembly of collagen fibers. Influence of fibrillar alignment and decorin on mechanical properties. *Biophys. J.* **73**, 2164–2172 (1997).
53. Brightman, A. O. *et al*. Time-lapse confocal reflection microscopy of collagen fibrillogenesis and extracellular matrix assembly *in vitro*. *Biopolymers* **54**, 222–234 (2000).
54. Zhang, G. *et al*. Genetic evidence for the coordinated regulation of collagen fibrillogenesis in the cornea by decorin and biglycan. *J. Biol. Chem.* **284**, 8888–97 (2009).
55. Sawkins, M. J. *et al*. Hydrogels derived from demineralized and decellularized bone extracellular matrix. *Acta Biomater.* **9**, 7865–7873 (2013).
56. Johnson, T. D., Lin, S. Y. & Christman, K. L. Tailoring material properties of a nanofibrous extracellular matrix derived hydrogel. *Nanotechnology* **22**, (2011).
57. Freytes, D. O., Martin, J., Velankar, S. S., Lee, A. S. & Badylak, S. F. Preparation and rheological characterization of a gel form of the porcine urinary bladder matrix. *Biomaterials* **29**, 1630–1637 (2008).
58. Gaetani, R. *et al*. Evaluation of different decellularization protocols on the generation of pancreas-derived hydrogels. *Tissue Eng. Part C Methods* **24**, 697–708 (2018).
59. Hatami-Marbini, H. Viscoelastic shear properties of the corneal stroma. *J. Biomech.* **47**, 723–728 (2014).
60. Ahearne, M. & Coyle, A. Application of UVA-riboflavin crosslinking to enhance the mechanical properties of extracellular matrix derived hydrogels. *J. Mech. Behav. Biomed. Mater.* **54**, 259–267 (2016).
61. Schatten, H. *Scanning electron microscopy for the life sciences*. (Cambridge University Press, 2013).
62. Zhang, M.-C. M. *et al*. Lamellar keratoplasty treatment of fungal corneal ulcers with acellular porcine corneal stroma. *Am. J. Transplant.* **15**, 1068–1075 (2015).
63. Zheng, J. *et al*. Short-term results of acellular porcine corneal stroma keratoplasty for herpes simplex keratitis. *Xenotransplantation* e12509 (2019).
64. Fernández-Pérez, J. & Ahearne, M. Influence of biochemical cues in human corneal stromal cell phenotype. *Curr. Eye Res.* **44**, 135–146 (2019).
65. Miotto, M. *et al*. 4D corneal tissue engineering: achieving time-dependent tissue self-curvature through localized control of cell actuators. *Adv. Funct. Mater.* **29**, 1807334 (2019).
66. Ahearne, M. *et al*. Online monitoring of the mechanical behavior of collagen hydrogels: Influence of corneal fibroblasts on elastic modulus. *Tissue Eng. - Part C Methods* **16**, (2010).
67. Gain, P. *et al*. Global survey of corneal transplantation and eye banking. *JAMA Ophthalmol.* **134**, 167 (2016).
68. Ahearne, M. & Lynch, A. P. Early observation of extracellular matrix-derived hydrogels for corneal stroma regeneration. *Tissue Eng. Part C Methods* **21**, 1059–1069 (2015).
69. Ignat'eva, N. Y. *et al*. Determination of hydroxyproline in tissues and the evaluation of the collagen content of the tissues. *J. Anal. Chem.* **62**, 51–57 (2007).
70. Kafienah, W. & Sims, T. J. Biochemical methods for the analysis of tissue-engineered cartilage. *Methods Mol. Biol.* **238**, 217–30 (2004).
71. Mathapati, S. *et al*. Qualitative and quantitative detection of sodium deoxycholic acid in decellularized tissue. *Indian J. Thorac. Cardiovasc. Surg.* **26**, 129–131 (2010).

Acknowledgements

The research leading to these results has received funding from the European Research Council (ERC) under the European Union's Horizon 2020 research and innovation program (grant agreement no. 637460) and from Science Foundation Ireland (15/ERC/3269).

Author contributions

J.F.P. designed and conducted experiments analysed data and wrote the manuscript. M.A. supervised the project and corrected the manuscript for publication.

Competing interests

The authors declare no competing interests.

Additional information

Supplementary information is available for this paper at https://doi.org/10.1038/s41598-019-49575-2.

Correspondence and requests for materials should be addressed to M.A.

Reprints and permissions information is available at www.nature.com/reprints.

Publisher's note Springer Nature remains neutral with regard to jurisdictional claims in published maps and institutional affiliations.